Springer Series in Materials Science 255

Annette Bussmann-Holder
Hugo Keller
Antonio Bianconi *Editors*

High-Tc Copper Oxide Superconductors and Related Novel Materials

Dedicated to Prof. K. A. Müller on the Occasion of his 90th Birthday

Springer

Springer Series in Materials Science

Volume 255

The Springer Series in Materials Science covers the complete spectrum of materials physics, including fundamental principles, physical properties, materials theory and design. Recognizing the increasing importance of materials science in future device technologies, the book titles in this series reflect the state-of-the-art in understanding and controlling the structure and properties of all important classes of materials.

More information about this series at http://www.springer.com/series/856

Annette Bussmann-Holder • Hugo Keller •
Antonio Bianconi
Editors

High-Tc Copper Oxide Superconductors and Related Novel Materials

Dedicated to Prof. K. A. Müller on the Occasion of his 90th Birthday

Springer

Editors
Annette Bussmann-Holder
Max-Planck-Institute for Solid State Research
Stuttgart, Germany

Hugo Keller
Physik-Institut
Universität Zürich Physik-Institut
Zürich, Switzerland

Antonio Bianconi
3RICMASS
Rome, Italy

ISSN 0933-033X ISSN 2196-2812 (electronic)
Springer Series in Materials Science
ISBN 978-3-319-52674-4 ISBN 978-3-319-52675-1 (eBook)
DOI 10.1007/978-3-319-52675-1

Library of Congress Control Number: 2017936954

Printed on acid-free paper

This Springer imprint is published by Springer Nature
The registered company is Springer International Publishing AG
The registered company address is: Gewerbestrasse 11, 6330 Cham, Switzerland

Foreword

Dear Alex,

10 years ago, we edited a book entitled "High T_c superconductors and transition metal oxides" in honor of your 80th birthday. We did not anticipate that there would be another chance to have a second edition now entitled "High T_c copper oxide superconductors and related materials" on the occasion of your 90th birthday. Again we invited friends, companions, colleagues, and former students of yours to contribute to this book and had a very positive resonance which is reflected in the new edition. Their contributions are unlimited with respect to the length and format, and we specifically welcomed them to not only submit purely scientific papers but also to commemorate personal interactions with you. Accordingly this volume comprises a broad spectrum ranging from wonderful memories to purely scientific contributions, reflecting partly your complex positive personality and your unconventional comprehensive approach to science.

During the last 10 years, you mentioned many times to both of us that not only the discovery of high-temperature superconductivity in cuprates was decisive for your career, but that all previous work would have been sufficient for you to quit science and commemorate a positive balance of your achievements. These have been multifold and mostly related to the pioneering work on ferroelectrics, critical phenomena and phase transitions, electron paramagnetic resonance, Jahn–Teller effect, polaron physics, granular superconductivity, and many more related topics. The most famous work before cuprates is certainly related to $SrTiO_3$ and perovskites which is still under intensive investigation and highly cited as groundbreaking advancement in the field. For illustration purposes, the citation history of a single paper by you ($SrTiO_3$: Intrinsic Quantum Paraelectric Below 4-K; KA MULLER, H. BURKARD, PHYSICAL REVIEW B **19**, 3593 (1979)) on $SrTiO_3$ is shown in Figure 1. The paper has been cited 981 times with an average citation rate 25.82 per year.

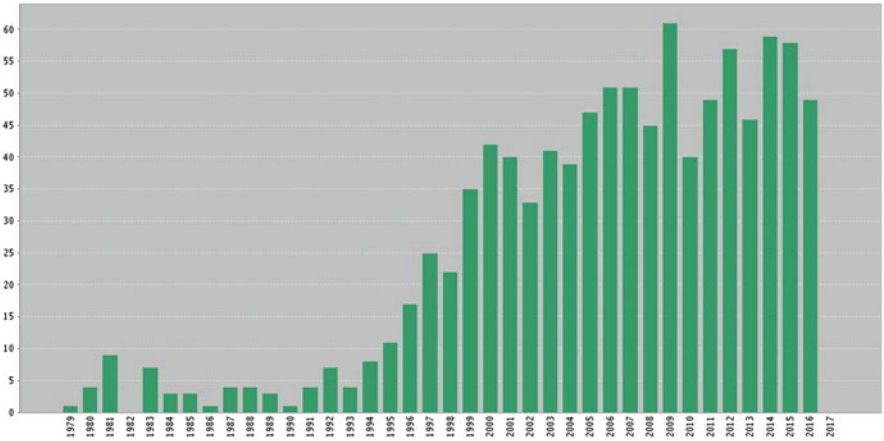

Since we have summarized these activities in the foreword of the previous volume, we look back here on the past ten years of your private and scientific life.

Your 80th birthday was celebrated with your family and close friends on the lake of Zug in a beautiful and picturesque environment. In spite of this positive start into a new decade, the future developed differently due to various health problems which forced you to reduce your travel activities in contrast to scientific ambitions. As soon as you were able to overcome these problems and recover to full health, you accepted various invitations to international conferences from which only the highlights are mentioned below.

In particular, it is important to emphasize your travel to the APS meeting in Dallas in 2011, where a special session was devoted to the 100th year discovery of superconductivity and the 25th anniversary of high-temperature superconductivity in cuprates. You gave a remarkable and outstanding presentation of your viewpoint on cuprates which is in contrast to some prominent common theoretical understanding. You did not bother to confront those with different opinions with arguments and your own comprehension of the physics of cuprates. This talk was well acknowledged by the audience and honored by standing ovations.

You decided to withdraw from presenting further scientific talks at international events and finalize your oral contributions by giving your last talk at the M^2S conference in Geneva in 2015. This conference series was initiated by Georg Bednorz and you in Interlaken in 1988 and became a famous platform in the field of superconductivity and magnetism. In Geneva, you emphasized once again in a very emphatic way your understanding of the physics of cuprates and the importance of polaron physics especially supported by numerous isotope experiments initiated by you. Your talk was appreciated by the frenetic applause by the audience.

During the last 10 years and keeping in mind your age of 80+, your scientific activity remained as active as in previous years and was inspired by innovative ideas and original experiments. While the focus was on cuprates, you also went

back to your former interests in ferroelectrics. Altogether, you published more than 25 papers in this period with emphasis on polaron and bipolaron formation and essential heterogeneity in cuprates and their relation to Fermi glass systems. Jahn–Teller physics, isotope effects, and coupled s+d-wave order parameters were another focus. An important achievement for the understanding of the dynamical properties of ferroelectrics was made by reinvestigating EPR data and concluding about the phase transition mechanism. This list is not complete but demonstrates already the diverse variety of your activities.

Both of us enjoyed and highly estimated your warm and thoughtful friendship and care which helped us enormously in recovering from personal problems. You adopted our difficulties as yours and tried to resolve those with us. However, and in spite of your advanced age, you also celebrated with us diverse anniversaries and contributed actively and in a dedicated manner to those. Your interests are not restricted to our persons only but extend to our families and their developments.

Scientifically, you were and are a permanent and fruitful source of inspiration for novel ideas and activities which is well reflected in our current common projects.

Dear Alex,

We warmly congratulate you to the 90th birthday and wish you many more happy and healthy years where we can further enjoy your deep friendship and energetic strong support.

Leute mit Mut und Charakter sind den anderen Leuten immer sehr unheimlich.
Damit das Mögliche entsteht, muss immer wieder das Unmögliche versucht werden.

People with courage and character are always scary to others.
For the possible to arise, the impossible has to be envoked.

Stuttgart, Germany
07.12.2016

Annette Bussmann-Holder
Hugo Keller

Contents

Chapter 1
Electronic Phase Separation and Electron–Phonon Coupling in Cuprate Superconductors

Andreas Bill, Vladimir Hizhnyakov, and Götz Seibold

Prologue

Immediately after the discovery of high-temperature superconductivity by Bednorz and Müller [1] late Ernst Sigmund and his group at the University of Stuttgart started to work on the problem how doping of charge carriers alters the electronic properties of the perovskite material. These efforts were supported by Vladimir Hizhnyakov from the University of Tartu, who together with Ernst Sigmund proposed an inhomogeneous doping mechanism for the cuprates in 1988 [2–5]. According to their picture the individual charge carriers form localized magnetic polarons in a fluctuating antiferromagnetic environment which then cluster together to form metallic regions (cf. Fig. 1.1). Above some critical doping a percolative network is realized, which then becomes superconducting. During these early days, such a scenario was viewed with scepticism by the high-T_c community, in particular because only few experiments supported some kind of electronic phase separation in the cuprates. By a lucky coincidence, Reinhard Kremer from the nearby Max-Planck institute in Stuttgart started thermal quenching experiments on lanthanum cuprates which strongly supported the formation of an electronically inhomogeneous state in these materials. Alex Müller, who had an established, close contact

A. Bill (✉)
Department of Physics and Astronomy, California State University Long Beach, Long Beach, CA 90840, USA
e-mail: abill@csulb.edu

V. Hizhnyakov
Institute of Physics, University of Tartu, 2400 Tartu, Estonia
e-mail: hizh@ut.ee

G. Seibold
Institut für Physik, BTU Cottbus-Senftenberg, PBox 101344, 03013 Cottbus, Germany
e-mail: seibold@b-tu.de

A. Bussmann-Holder et al. (eds.), *High-Tc Copper Oxide Superconductors and Related Novel Materials*, Springer Series in Materials Science 255,
DOI 10.1007/978-3-319-52675-1_1

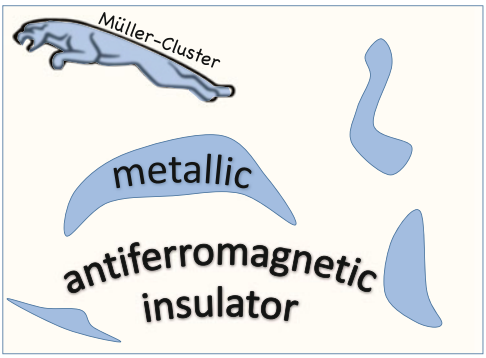

Fig. 1.1 Sketch of metallic cluster formation in an antiferromagnetic environment [2–5]. The structure of the *top left* cluster is likely the model of choice for Alex Müller

with Ernst Sigmund, became aware of these experiments and subsequently frequently visited the University and Max-Planck Institute in Stuttgart participating in discussions of the experimental data. These resulted in two publication in Zeitschrift für Physik [6, 7]. In this context his preferred car to drive from Zürich to Stuttgart has certainly influenced his own view on the structure of electronic inhomogeneities (Fig. 1.1). There is no doubt that Alex Müller's support and exchanges with the Stuttgart group gave substantial visibility to the work by Kremer, Hizhnyakov and Sigmund resulting in numerous presentations of their results at international conferences beginning of the 1990s. Moreover, a series of conferences on phase separation in high-temperature superconductors was initiated where the emerging evidences for electronic inhomogeneities in the cuprates was discussed.

In this contribution we discuss the relation of these early ideas of phase separation to the current experimental situation in cuprate superconductors and in particular focus on the long-range electron–phonon coupling promoted in such an electronically inhomogeneous environment and leading to a crucial contribution to the pairing mechanism.

Electronic Phase Separation in Cuprates: From Early Theories to Current Experiments

Electronic phase separation is a consequence of competing attractive and repulsive interactions and therefore may be closely related to superconductivity. This is one of the perspectives that has motivated early work on phase separation in high-temperature superconductors [8–10]. Another motivation was due to the fact that the phase separated electronic state may provide an electronic environment which is more supportive for the superconducting mechanism itself [2–5, 11].

Cuprate superconductors are correlated materials and the question how these correlations may trigger an electronically inhomogeneous state may be asked in essentially two different ways. One can start from the strongly overdoped

(essentially Fermi liquid like) regime and investigate the possibility of a phase separation instability upon lowering doping. This approach was followed by the Rome group [8] who initially studied phase separation in proximity of a charge-transfer instability within the three-band Hubbard model. In general, it was realized that the correlation induced reduction of the kinetic energy makes the system susceptible towards phase separation once a short range attractive interaction is incorporated in the Hamiltonian. The theory was subsequently extended by incorporating also long-range Coulomb interactions [9] into the model which led to the so-called 'frustrated phase separation' scenario. These long-range forces turn the phase separation instability into a 'Quantum Critical Point' (QCP) that separates the disordered regime from an ordered incommensurate charge-density-wave phase. With regard to the observation of charge-density wave phases in a large class of cuprate compounds (see below) the theory has been rather powerful in explaining various peculiar features of the phase diagram [12].

Magnetic interactions are the essential ingredient for the phase separation mechanism proposed by Emery and Kivelson [10] who argued on the basis of the tJ-model that a corresponding instability could be realized in doped antiferromagnets due to the competing kinetic and magnetic energies in the dilute and large doping regimes. Here, the loss in magnetic energy in the dilute hole regime is essentially given by the broken antiferromagnetic bonds $\sim J$ whereas the strongly doped (metallic) regime determines the gain in kinetic energy $\sim t$. Later the theory has also been extended to include long-range Coulomb forces [13]. It is interesting to note that with regard to the parameter regime $J/t < 1$ relevant for cuprates, Emery and Kivelson refer in their paper to earlier works by Visscher [14] and by Ioffe and Larkin [15], who on the basis of the Hubbard model showed, that a very low density of holes is unstable to phase separation with the hole-rich phase being ferromagnetic. This kind of ferromagnetic clustering is at the heart of the second kind of scenario proposed by Hizhnyakov and Sigmund [2–5] which does not rely on a thermodynamic phase separation instability but starts with the question how the individual holes arrange when doped into the CuO_2 plane. In the Sigmund-Hizhnyakov original proposal, a hole doped into the long-range antiferromagnetically ordered copper-oxygen plane and bound to its dopant ion, will locally distort the antiferromagnetic (AF) magnetic configuration. The resulting local entity has a ferromagnetic polarization and has initially been called a 'ferron' state [16, 17]. With increased doping the ferrons bind together and establish a granular system of nanoscale metallic regions (cf. Fig. 1.1) that percolates above a critical doping which was associated with the onset of T_c. The assumption of a 'ferron' (or 'spin-cluster') type state was initially motivated by purely energetic considerations and later substantiated with variational calculations of three-band Hubbard models [18–20]. These calculations showed the analogy of the 'ferron' with a strongly localized magnetic polaron. Figure 1.2a shows the charge and spin structure of two separated magnetic polarons within the CuO_2 plane obtained within the unrestricted Gutzwiller approximation [21]. The doped hole charge is mainly confined to the oxygen plaquette around the polaron center with a strongly reduced (and slightly ferromagnetically polarized) Cu moment. It is noteworthy that the

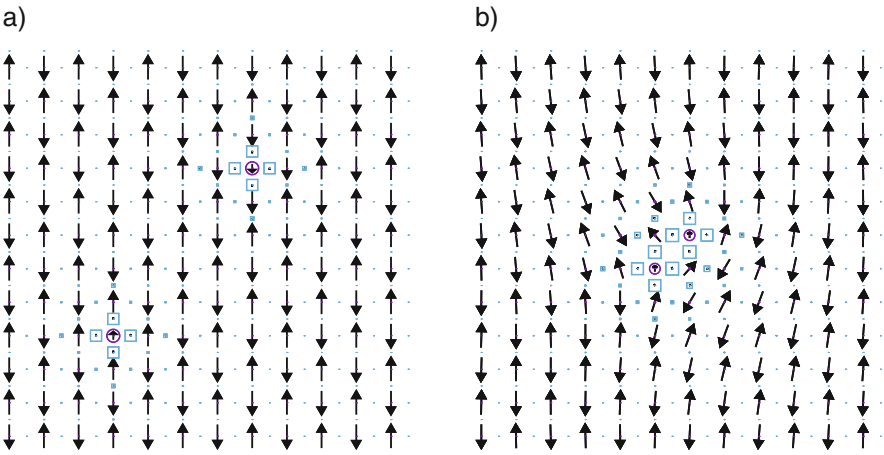

Fig. 1.2 Two-hole states in the copper-oxygen plane. (**a**) Two magnetic polarons; (**b**) vortex-antivortex pair. *Squares* (*circles*) indicate the distribution of doped hole charges on oxygen (copper) sites and *arrows* show the Cu spin structure. Both configurations have been obtained within the unrestricted Gutzwiller approximation [21] on a 12×12 system with 146 holes. Parameters of the three-band model are taken from [22]

superposition of such states within a configuration-interaction approach [23], leads to a dispersion relation for the spin-polaron similar to that obtained in the tJ-model for the single-hole state (e.g. [24]).

Localized magnetic polarons, bound to the dopant ions, may dominate the electronic properties in the very dilute regime. However, it turns out that the energetically most stable solution for two holes is a vortex-antivortex pair [21, 25] shown in Fig. 1.2b. The corresponding spin texture can be described by

$$S_i^x = S_0 \exp[i\boldsymbol{Q}\boldsymbol{r}] \cos(\phi_v - \phi_a), \tag{1.1}$$

$$S_i^y = S_0 \exp[i\boldsymbol{Q}\boldsymbol{r}] \sin(\phi_v - \phi_a), \tag{1.2}$$

where the phases ϕ_a, ϕ_v are determined by the centers of the vortex (v) and antivortex (a)

$$\tan\left(\phi_{v/a}\right) = \frac{y_i - y_{v/a}}{x_i - x_{v/a}},$$

which for the structure depicted in Fig. 1.2b are located on diagonally adjacent sites. It turns out that the interaction between the pairs is dominated by an anisotropic short-range core-core contribution which originates from the charge distribution of the localized holes. The percolative scenario described in [2–5] corresponds then to a head-to-tail aggregation of vortex-antivortex pairs that tend to form segments in such a way that only the vortex and the antivortex on the extremes contribute to the long range distortion of the magnetic structure. It has

been shown that a collection of such segments can induce a spiral distortion of the Cu spin configuration, the structure factor of which is in very good agreement with neutron scattering data of cuprate superconductors in the low doping regime, i.e. in the vicinity of the spin-glass phase [25]. Moreover, a recent Monte Carlo study has demonstrated as one lowers the temperature the segments condense first into a smectic state and then a Wigner crystal, both accompanied by inversion symmetry breaking [26]. An important ingredient in this theory is again the long-range part of the Coulomb interaction which limits the infinite proliferation of vortex-antivortex pairs and contributes to the effective interaction among the segments.

Early experiments which provide evidence for phase separation in cuprate superconductors have been discussed on several conferences on this issue and are published in [27–29]. One key aspect in this regard was the role of electronic and chemical phase separation. For $La_{2-x}CuO_{4+\delta}$ a chemical or structural phase separation was reported by Jorgensen et al. by powder neutron diffraction already in 1988 [30] followed by the observation of Kremer [6, 7] that the formation of the superconducting phase in this compound can be very effectively suppressed by rapid quenching from room temperature to temperatures below about 200 K. More recently it has been shown by scanning synchrotron radiation X-ray microdiffraction [31] that depending on thermal history, ordering of oxygen interstitials can occur in the La_2O_{2+y} spacer layers of La_2CuO_{4+y} which is characterized by a fractal distribution up to a maximum limiting size of 400 μM. Concerning the electronic contribution, evidence for charge segregation on a local scale first came from NMR [32] and NQR [33–35] experiments (cf. also P. G. Baranov and A. G. Badalyan as well as O. C. Hammel et al. in [28]).

Progress towards an understanding of the spatial structure of the inhomogeneous charge distribution was made in 1995 when Tranquada and collaborators observed a splitting of both spin and charge order peaks in $La_{1.48}Nd_{0.4}Sr_{0.12}CuO_4$ within elastic neutron scattering [36, 89]. The outcome of this experiment resembled similar data in the nickelates where both incommensurate antiferromagnetic (AF) order [37, 38] and the ordering of charges [38, 39] had been detected by neutron diffraction, electron and hard x-ray diffraction [88], respectively. In [38] it was shown that the magnetic ordering displays itself as an occurence of first and third harmonic Bragg peaks whereas the charge ordering is associated with second harmonic peaks. From this it was concluded that the doped holes arrange themselves in quasi-one-dimensional structures, called stripes, which simultaneously constitute antiphase domain walls for the AF order and coexist but also compete with superconductivity [90]. While the neutron scattering experiments only provide indirect evidence for charge ordering via the coupling to the lattice, bulk evidence for charge stripe order in the lanthanum cuprates has been found in $La_{1.875}Ba_{0.125}CuO_4$ [40] and $La_{1.8-x}Eu_{0.2}Sr_xCuO_4$ [41] by resonant x-ray scattering (RXS) experiments. The rapid improvement and development of this technique has meanwhile led to the detection of charge order in a large variety of cuprate compounds, including YBCO [42, 43], Bi2212 [44], and Bi2011 [45]. Moreover, for YBCO charge order has also been evidenced by high-energy x-rays [46] and quantum oscillations in both

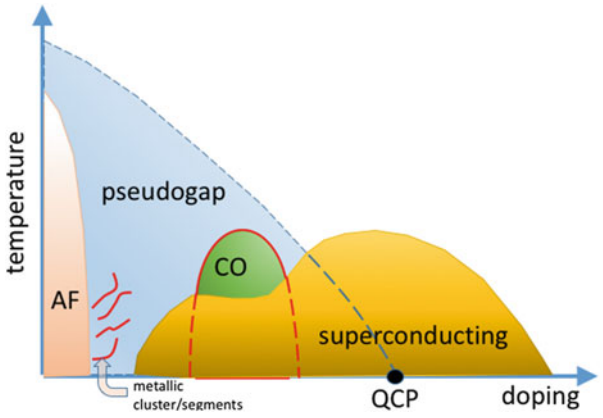

Fig. 1.3 Phase diagram of cuprate superconductors indicating the region where charge order (CO) has been experimentally established. On the low doping side the formation of metallic clusters [2, 6, 8, 9] or segments [33] can be viewed as precursor to CO. On the other hand, the instability towards CO at large doping is due to a Quantum Critical Point (QCP) which due to quantum fluctuation establishes long-range order only at a slightly lower doping [13, 16]

transport and thermodynamic experiments in magnetic fields [47–49] sufficient to suppress superconducting long-range order.

Figure 1.3 summarizes the generic phase diagram of cuprates including the charge ordered (CO) phase in the underdoped regime. The tendency of charge carriers to form quasi one-dimensional segments at low doping is indicated by the wiggly lines. In this regard the early theory by Sigmund and Hizhnyakov [2–5] and the 'frustrated phase separation' mechanism [9] provide a complementary description of the formation of quasi one-dimensional electronic inhomogeneities in high-T_c superconductors which approach the problem from the high- and low doping side, respectively.

Charge Inhomogeneities and Electron–Phonon Coupling

The inhomogeneous electronic structure discussed in the previous section affects electron–phonon interactions in an important way. It leads to an enhancement of the long-wavelength optical phonon contribution to the interaction between charge carriers. As is well known, the electron–phonon interaction with optical phonons is long-range and strong in insulators but screened out by the high-frequency plasmons in normal metals. In high-T_c superconductors the presence of local charge order implies the existence of regions with a local reduction of charge carrier concentration. In their vicinity the electric field associated with the long-wave optical phonon remains poorly screened, and the total screening of the interaction is reduced. This effect of inhomogeneities on the screening bears some resemblance with the reduction of screening caused by insulating granules in granular

superconductors. It was shown in this latter case that the reduction of screening implied an enhancement of the critical temperature in these systems [50].

An additional ingredient is the vertex which couples the charge carriers in the hole enriched regions to the long-wavelength optical phonons. This coupling is influenced by the strongly correlated character of the system which for certain phonons can sustain the vertex in the long-wavelength limit as discussed in the next subsection.

Enhancement of the Electron–Phonon Vertex Due to Correlation Effects in the Limit of Small Momentum Transfer

For the family of cuprate superconductors density functional theory (DFT) usually yields an electron–phonon coupling constant which is too small in order to explain the high transition temperatures of these materials [51]. This becomes even worse when the effect of electronic correlations is considered which are underestimated within the DFT method. Basically, correlations suppress the charge fluctuations and thus the scattering of electrons from phonons, which leads to a further reduction of the el-ph interaction (for a review cf. [52, 53]).

In terms of Hubbard type models the el-ph interaction is usually investigated for couplings that arise from an expansion of on-site energies in terms of some vibrational coordinates [52, 54–56] (so-called 'Holstein' coupling) so that in general both interactions, electronic and electron–phonon, are local or at least have a dominant local contribution. The interplay of el-el and el-ph interactions leads to a screening of the latter over the whole Brillouin zone which is most pronounced at large momenta [54, 57]. For sizeable correlations the maximum in the phonon self-energy is then shifted from the Peierls wave-vector to $q = 0$, which for strong electron lattice couplings eventually induces a phase separation instability (cf. previous section).

Here instead we discuss the influence of correlations on phonons which involve kinetic processes, i.e. modulations of the hopping integral. In cuprates, such couplings are believed to be of significance for the so-called breathing and buckling modes which correspond to in- and out-of plane motions of the oxygen atoms and which contribute most to the pairing interaction arising from phonons [58, 59]. In contrast to the Holstein-, local-type coupling correlations can enhance the electron–phonon vertex for small momentum transfer [60, 61] and therefore support the coupling to long wavelength optical phonons in an inhomogeneous electronic environment.

We study this issue within the time-dependent Gutzwiller approximation (TDGA) [62] that allows for the computation of charge- spin- and pair correlations for Hubbard-type models in very good agreement with exact diagonalization results [63–66]. The Gutzwiller approximation (GA) [67–69] corresponds to the energy functional of a Hubbard-type model

$$E^{GA} = \sum_{ij\sigma,\, i\neq j} t_{ij} z_{i\sigma} z_{j\sigma} \rho_{ji}^{\sigma} + U \sum_{i} D_i, \tag{1.3}$$

where D_i denotes the double occupancy at lattice site R_i and $\rho_{ji}^{\sigma} \equiv \left\langle c_{i\sigma}^{\dagger} c_{j\sigma} \right\rangle$ is the density matrix. Due to the factors $z_{i\sigma}(D, \rho)$ the GA has the structure of a renormalized mean-field theory, where the ground state energy has to be determined by minimizing the energy with respect to the variational double occupancy parameters D_i. For the half-filled single-band model this yields $4D = 1 - U/8|\varepsilon_0|$ (ε_0 being the ground state energy of the non-interacting system), i.e. D vanishes at the critical onsite repulsion $U_{BR} = 8|\varepsilon_0|$. This is the so-called Brinkman-Rice transition [70] above which particles localize. This can be viewed as an illustrative description of the Mott metal-insulator transition. The transitive electron–phonon coupling is then obtained by expansion of the hopping integral t_{ij} in terms of displacement coordinates Q_n^{α} ($\alpha = x, y, z$) which yields.

$$E^{el-ph} = \sum_{ij\sigma} g_{i\neq j}^{\alpha\beta} z_{i\sigma} z_{j\sigma} \left(Q_i^{\alpha} - Q_j^{\beta} \right) \rho_{ji}^{\sigma}. \tag{1.4}$$

The computation of the renormalized electron–phonon vertex requires the evaluation of the electron-hole excitations which are in turn dressed by all electronic interactions (cf. Fig. 1.4). This can be achieved by the TDGA which amounts to expand the energy functional Eq. (1.3) in terms of the local (ρ_q) and kinetic (T_q) density fluctuations up to quadratic order

$$E_{ee}^{(2)} = \frac{1}{2N} \sum_{q} \begin{pmatrix} \delta\rho_q \\ \delta T_q \end{pmatrix}^{\dagger} \begin{pmatrix} A_q & B_q \\ B_q & C_q \end{pmatrix} \begin{pmatrix} \delta\rho_{-q} \\ \delta T_{-q} \end{pmatrix}. \tag{1.5}$$

where A_q, B_q and C_q denote the local, local transitive, and pure transitive effective interactions among the Gutzwiller quasiparticles. Within a standard random phase approximation (RPA) one simply has $A_q = U/2$ and $B_q = C_q = 0$ (cf. Fig. 1.5). Here, however we also incorporate vertex corrections, in some sense similarly to the conserving approach by Vilk and Trembley [71].

Figure 1.5 shows the coupling elements of the effective transitive interaction as a function of U/t for two different charge carrier concentrations. At half-filling the local and transitive interactions are decoupled ($B_q = 0$) up to the Brinkman-Rice transition where the interaction between local density fluctuations diverges. On the other hand, the interaction between kinetic fluctuations turns out to be negative $C_q < 0$, i.e. these processes mediate an attraction which is maximum around U_{BR}. This attraction is at the heart of the correlation induced enhancement of the electron–phonon vertex for the transitive coupling Eq. (1.4). To demonstrate this feature one can compute analytically the static second order scattering amplitude (i.e. the effective interaction resulting from the exchange of one phonon, cf. Fig. 1.4b) for the one-dimensional, half-filled Su-Schrieffer-Heeger model

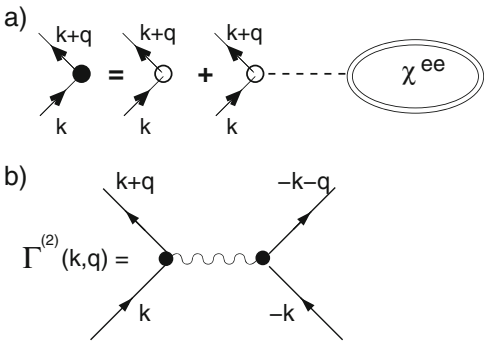

Fig. 1.4 (**a**) The renormalized electron–phonon vertex dressed by electron-hole excitations χ^{ee}. The *dashed line* represents electronic interactions. (**b**) Second order scattering amplitude. The *wavy line* represents the bare phonon propagator

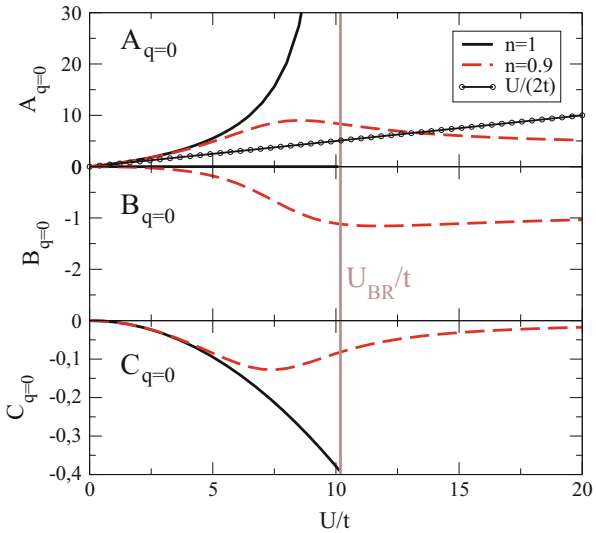

Fig. 1.5 The effective interactions between Gutzwiller quasiparticles, Eq. (1.5), for a single-band Hubbard model at half-filling (*solid*) and carrier concentration $n = 0.9$ (*dashed*). The *dots with thin solid line* is the effective interaction of the standard RPA approach. The *vertical line* near $U/t \sim 10$ indicates the Brinkman-Rice value for the critical onsite repulsion. The transitive coupling to optical modes show a correlation induced enhancement of the coupling constants, in the long wavelength limit

[72] supplemented with a local Hubbard repulsion U. For small momentum transfer one obtains

$$\Gamma_q^{(2)} = \frac{g^2}{4c} q \left[z_0^2 - C_q |e_0| \right]^2 \approx \frac{g^2}{4c} q \left[1 + 2u^2 \right] \tag{1.6}$$

where the approximation is obtained for small U/t. Here c denotes the sound velocity of the acoustic mode, $z_0^2 = 1 - u^2$ is the ground state renormalization factor and $u \equiv U/U_{BR}$. Without the term proportional to $\sim C_q$ in Eq. (1.6) the

scattering amplitude would be proportional to z_0^4. Thus, it would vanish at the Brinkman-Rice transition since in this limit the bare interaction Eq. (1.4) tends to zero. Interestingly, the vertex renormalization $\sim C_q$ can overcompensate this reduction and therefore induce an enhancement of $\Gamma_q^{(2)}$ with increasing U. On the other hand at large momentum transfer (short length scales) one finds a suppression of $\Gamma_q^{(2)}$ with U, similarly to the Hubbard-Holstein model [60, 61].

In the present model with one acoustic mode the correlation-induced enhancement is proportional to the momentum transfer q and therefore has minor impact at small q. It is therefore interesting to evaluate the correlation induced enhancement of $\Gamma_q^{(2)}$ for an optical mode, which has been accomplished in [61] for the A_{1g} and B_{1g} components of the so-called buckling mode in cuprate superconductors. For the case A_{1g} mode one finds an enhancement of the vertex with U for small momentum transfers around the antinodal regions of the Fermi surface. Concomitantly, the vertex is generally suppressed for the coupling to the B_{1g} component. Although the A_{1g} vertex is enhanced, its absolute magnitude is small around the antinodal regions. Therefore, this enhancement does not promote the superconducting pairing, which is obtained from an average over the whole Brillouin zone. On the other hand the enhancement can substantially support the coupling to long-range optical phonons which are unscreened in an inhomogeneous electronic environment as discussed in the next subsection.

Superconductivity Induced by Long Wavelength Optical Phonons

The previous sections demonstrated that the existence of electronic inhomogeneities and strong correlations-induced vertex corrections in the CuO_2 plane of high temperature superconductors bring about unconventional electron–phonon interactions. Due to imperfect screening, the long wavelength optical phonons can couple substantially to the charge carriers as evidenced e.g. by the renormalization of such modes in the superconducting state observed in Raman and infrared spectra [73–77]. The reduction of screening is also expressed in the structure of these materials. High temperature superconductors have layered structure and anisotropic transport properties. As a result, low energy electronic collective modes are present and the dynamic part of the screening plays an important role [78–81]. These modes have been shown to contribute constructively to superconductivity [79–81]. The anisotropic transport properties further reduce the screening along the direction perpendicular to the CuO_2 planes and the interaction to long wave optical phonons is therefore three dimensional. Noteworthy is also that the pairing interaction resulting from the coupling to these phonon modes leads to a well-defined $\mathbf{k}-$dependence of the order parameter, since the long range nature of the interaction leads to averaging over the smaller scale electronic inhomogeneities.

These considerations led Ernst Sigmund and Vladimir Hizhnyakov to propose that the pairing interaction responsible for the superconducting state is due to the mixing of states with close wave vectors through the long range optical phonons, and the resulting order parameter $\mathbf{k}-$dependence is determined by the density of states on the Fermi surface [11, 82, 83, 91]. In addition, the experimental observation of the $d-$wave symmetry of the order parameter is simply due to strong enough local Coulomb repulsion [84].

The unconventional interaction potential contribution to the BCS gap equation is caused by the long range coupling to A_{1g}, B_{1g} and B_{2g} modes and takes the form

$$V_{A_{1g}}\left(\mathbf{q}_{\parallel}\right) \simeq \frac{U_{A_{1g}}}{\kappa^2 + q_x^2 + q_y^2} \tag{1.7}$$

$$V_{B_{1g}}(\mathbf{k};\mathbf{q}) = \frac{U_{B_{1g}}}{\kappa_1^2 + q_x^2 + q_y^2}\left(\cos k_x - \cos k_y\right)^2. \tag{1.8}$$

with $\mathbf{q} = \mathbf{k} - \mathbf{k}^{'}$ and $\mathbf{k} = (k_x, k_y)$ is the wave-vector component *parallel* to the CuO_2 plane. The coupling to the B_{2g} mode is obtained from the expression for the B_{1g} mode but with a $\pi/4$ rotation of the $\mathbf{k}$ space basis. Because of this rotation, the contribution of the B_{2g} mode to Δ_{max} and T_c is negligible and essentially determined by the A_{1g} and B_{1g} mode contributions.

$U_{A_{1g}}$, $U_{B_{1g}}$ and κ were estimated in [84] and are of the order $U_{A_{1g},B_{1g}} \sim 0.01\,\text{eV}$ and $\kappa \sim 0.3$. These values are in agreement with the corresponding parameters used in [85–87] to describe the experimentally observed phonon renormalization caused by the superconducting transition.

Next to the unconventional long range contributions just described there are also short range contributions usually found in metals that come from the electron–phonon and Coulomb interactions. For the A_{1g}, B_{1g} and B_{2g} modes the pair potential takes the form [11, 82–84]

$$\bar{V}_{A_{1g}}(\mathbf{k};\mathbf{q}) \simeq -\frac{\bar{U}_{A_{1g}}\omega_{k;q}^2}{\omega_{k;q}^2 - (\omega_\nu + i\gamma_\nu)^2} \tag{1.9}$$

$$\bar{V}_{B_{1g}}(\mathbf{k};\mathbf{q}) \simeq -\frac{\bar{U}_{B_{1g}}\omega_\nu^2}{\omega_{\mathbf{k};\mathbf{q}}^2 - (\omega_\nu + i\gamma_\nu)^2}\left(\cos k_x - \cos k_y\right)^2, \tag{1.10}$$

where $\hbar\omega_{\mathbf{k},\mathbf{q}} \equiv \varepsilon_{\mathbf{k}+\mathbf{q}} - \varepsilon_{\mathbf{k}}$ and $\gamma_\nu \ll \omega_\nu$ is the damping rate of the phonon. Again, the B_{2g} contribution is obtained from the B_{1g} mode with a $\pi/4$ rotation. It was shown in [84] that the B_{2g} contribution to the superconducting order parameter is negligible. In contrast to the long range pair potentials, Eq. (1.7), the short range contributions are attractive or repulsive depending on whether $|\omega_{\mathbf{k},\mathbf{q}}|$ is small or large. It is worth pointing out that $\bar{V}_{A_{1g}} \to -\bar{U}_{A_{1g}}$ when $|\omega_{\mathbf{k},\mathbf{q}}| \gg \omega_\nu$, while $\bar{V}_{B_{1g}} \to 0$ in the same limit.

Using these long- and short range pair potential contributions, one can solve the BCS gap equation [84]. This leads to two main observations. First, the magnitude

Δ_{max} and anisotropy $\Delta(\mathbf{k})$ of the order parameter are determined by the coupling of electronic degrees of freedom to unconventional long range electron phonon interactions. For reasonable values of the parameters both are in excellent agreement with the experimentally determined order parameter. However, the order parameter has $s-$wave symmetry. Second, the symmetry of the order parameter ($d-$, $s-$wave, ...) is determined by the short range Coulomb repulsion term. Already a rather moderate value of the local repulsion term leads to the stabilization of the $d-$wave symmetry. We emphasize that in this model spin fluctuations are not the major motor for the superconducting state. Instead, the ineffective screening and associated long range interaction to optical phonons explains the presence of the superconducting state.

Conclusions

We have presented a presented a personal view on the physics of cuprates which has been strongly influenced by inspiring discussions with Alex Müller. In our opinion electronic inhomogeneities are a crucial ingredient in order to set up a consistent theory for the high-T_c superconductors as they prepare the ground for the efficiency of pairing interactions. Of course, the very early ideas in this regard were rather rough but, as we tried to outline in this chapter, already pointed in the right direction as suggested by the current experiments. We therefore appreciate that the community now largely accepts the existence of electronic inhomogeneities in the cuprates as Alex Müller has already done 25 years ago.

Acknowledgements In this contribution we have presented results and concepts obtained together with numerous collaborators during almost 30 years. We are especially grateful to K. A. Müller and E. Sigmund for countless discussions and illuminating conversations. This work was supported by Estonian Research Council (project IUT2-27) and European Union through the European Regional Development Fund (project 3.2.0101.11-0029). A.B. thanks the National Science Foundation for the support (DMR-13409341). G.S. acknowledges support from the DAAD and the DFG.

References

1. J.G. Bednorz, K.A. Müller, Z. Phys. B **64**, 189 (1986)
2. V. Hizhnyakov, E. Sigmund, Physica C **156**, 655 (1988)
3. V. Hizhnyakov, N. Kristoffel, E. Sigmund, Physica C **161**, 435 (1989)
4. V. Hizhnyakov, N. Kristoffel, E. Sigmund, Physica C **160**, 119 (1989)
5. V. Hizhnyakov, E. Sigmund, M. Schneider, Phys. Rev. B **44**, 795 (1991)
6. R. Kremer, E. Sigmund, V. Hizhnyakov, F. Hentsch, A. Simon, K.A. Müller, M. Mehring, Z. Phys. B **86**, 319 (1992)
7. R. Kremer, V. Hizhnyakov, E. Sigmund, A. Simon, K.A. Müller, Z. Physik B **94**, 17 (1993)
8. M. Grilli, R. Raimondi, C. Castellani, C. Di Castro, G. Kotliar, Phys. Rev. Lett. **67**, 259 (1991)

9. C. Castellani, C. Di Castro, M. Grilli, Phys. Rev. Lett. **75**, 4650 (1995)
10. V.J. Emery, S.A. Kivelson, H.Q. Lin, Phys. Rev. Lett. **64**, 475 (1990)
11. V. Hizhnyakov, E. Sigmund, Phys. Rev. B **53**, 5163 (1996)
12. S. Caprara, C. Di Castro, G. Seibold, M. Grilli, arXiv:1604.07852
13. U. Löw et al., Phys. Rev. Lett. **72**, 1918 (1994)
14. P.B. Visscher, Phys. Rev. B **10**, 943 (1974)
15. L.B. Ioffe, A.I. Larkin, Phys. Rev. B **37**, 5730 (1988)
16. E.L. Nagaev, Pisma Zh. Eksp. Teor. Fiz. **6**, 484 (1967)
17. E.L. Nagaev, Zh. Eksp. Teor. Fiz. **54**, 228 (1967)
18. G. Seibold, E. Sigmund, V. Hizhnyakov, Phys. Rev. B **48**, 7537 (1993)
19. D. Klemm, M. Letz, E. Sigmund, G. Zavt, Phys. Rev. B **50**, 7046 (1994)
20. G. Seibold, J. Seidel, E. Sigmund, Phys. Rev. B **53**, 5166 (1996)
21. G. Seibold, E. Sigmund, V. Hizhnyakov, Phys. Rev. B **57**, 6937 (1998)
22. A.K. McMahan, J.F. Annett, R.M. Martin, Phys. Rev. B **42**, 6268 (1990)
23. G. Seibold, Phys. Rev. B **77**, 235109 (2008)
24. G. Martinez, P. Horsch, Phys. Rev. B **44**, 317 (1991)
25. G. Seibold, M. Capati, C. Di Castro, M. Grilli, J. Lorenzana, Phys. Rev. B **87**, 035138 (2013)
26. M. Capati, S. Caprara, C. Di Castro, M. Grilli, G. Seibold, J. Lorenzana, Nat. Commun. **6**, 7691 (2015). doi:10.1038/ncomms8691
27. K. A. Müller, G. Benedek (eds.), *Proceedings of the First workshop on phase separation in cuprate superconductors* (World Scientific, Singapore, 1993)
28. E. Sigmund, K. A. Müller (eds.), *Proceedings of the Second workshop on phase separation in cuprate superconductors* (Springer, Berlin Heidelberg, 1994)
29. C. Di Castro, E. Sigmund (eds.), *Proceedings of the 3rd Workshop on Phase Separation, Electronic Inhomogeneitites and Related Mechanisms in High-T_c Superconductors*, J. Supercond. **9** (1996)
30. J.D. Jorgensen et al., Phys. Rev. B **38**, 1137 (1988)
31. M. Fratini et al., Nature **466**, 841 (2010)
32. J. Haase, C.P. Slichter, C.T. Milling, J. Supercond. **15**, 339 (2002)
33. S. Krämer, M. Mehring, Phys. Rev. Lett. **83**, 396 (1999)
34. G.B. Teitel'baum, B. Büchner, H. de Gronckel, Phys. Rev. Lett. **84**, 2949 (2000)
35. P.M. Singer, A.W. Hunt, T. Imai, Phys. Rev. Lett. **88**, 047602 (2002)
36. J.M. Tranquada, B.J. Sternlieb, J.D. Axe, Y. Nakamura, S. Uchida, Nature **375**, 56 (1995)
37. S.M. Hayden, G.H. Lander, J. Zarestky, P.J. Brown, C. Stassis, P. Metcalf, J.M. Honig, Phys. Rev. Lett. **68**, 1061 (1992)
38. J.M. Tranquada, D.J. Buttrey, V. Sachan, J.E. Lorenzo, Phys. Rev. Lett. **73**, 1003 (1994)
39. C.H. Chen, S.-W. Cheong, A.S. Cooper, Phys. Rev. Lett. **71**, 2461 (1993)
40. P. Abbamonte, A. Rusydi, S. Smadici, G.D. Gu, G.A. Sawatzky, D.L. Feng, Nat. Phys. **1**, 155 (2005)
41. J. Fink, E. Schierle, E. Weschke, J. Geck, D. Hawthorn, V. Soltwisch, H. Wadati, H.-H. Wu, Phys. Rev. B **79**, 100502 (2009)
42. G. Ghiringhelli et al., Science **337**, 821 (2012)
43. J. Chang et al., Nat. Phys. **8**, 871 (2012)
44. E.H. da Silva Neto et al., Science **343**, 393 (2014)
45. R. Comin et al., Science **343**, 390 (2014)
46. M. Hücker et al., Phys. Rev. B **90**, 054514 (2014)
47. N. Doiron-Leyraud et al., *Nature* **447**, 565 (2007)
48. S.E. Sebastian, N. Harrison, G.G. Lonzarich, Rep. Prog. Phys. **75**, 102501 (2012)
49. F. Laliberté et al., Nat. Commun. **2**, 432 (2011)
50. G. Deutscher, H. Fenichel, M. Gershenson, E. Grunbaum, Z. Ovadyahu, J. Low Temp. Phys. **10**, 213 (1973)
51. S.Y. Savrasov, O.K. Anderson, Phys. Rev. Lett. **77**, 4430 (1996)
52. O. Gunnarsson, O. Rösch, J. Phys. Condens. Matter **20**, 043201 (2008)

53. M. Capone, C. Castellani, M. Grilli, Adv. Condens. Matter Phys. **2010**, 920860 (2010)
54. M.L. Kulić, R. Zeyher, Phys. Rev. B **94**, 4395 (1993)
55. E. Koch, R. Zeyher, Phys. Rev. B **70**, 09410 (2004)
56. M. Mierzejewski, J. Zieliński, P. Entel, Phys. Rev. B **60**, 10442 (1999)
57. A. Di Ciolo, J. Lorenzana, M. Grilli, G. Seibold, Phys. Rev. B **79**, 085101 (2009)
58. R. Heid, K.-P. Bohnen, R. Zeyher, D. Manske, Phys. Rev. Lett. **100**, 137001 (2008)
59. R. Heid, R. Zeyher, D. Manske, K.-P. Bohnen, Phys. Rev. B **80**, 024507 (2009)
60. E. von Oelsen, A. Di Ciolo, J. Lorenzana, G. Seibold, M. Grilli, Phys. Rev. B **81**, 155116 (2010)
61. G. Seibold, M. Grilli, J. Lorenzana, Phys. Rev. B **83**, 174522 (2011)
62. G. Seibold, J. Lorenzana, Phys. Rev. Lett. **86**, 2605 (2001)
63. G. Seibold, F. Becca, J. Lorenzana, Phys. Rev. B **67**, 085108 (2003)
64. G. Seibold, F. Becca, P. Rubin, J. Lorenzana, Phys. Rev. B **69**, 155113 (2004)
65. G. Seibold, F. Becca, J. Lorenzana, Phys. Rev. Lett. **100**, 016405 (2008)
66. G. Seibold, F. Becca, J. Lorenzana, Phys. Rev. B **78**, 045114 (2008)
67. M.C. Gutzwiller, Phys. Rev. Lett. **10**, 159 (1963)
68. M.C. Gutzwiller, Phys. Rev. **134**, A923 (1964)
69. M.C. Gutzwiller, Phys. Rev. **137**, A1726 (1965)
70. W.F. Brinkman, T.M. Rice, Phys. Rev. B **2**, 4302 (1970)
71. Y.M. Vilk, A.-M.S. Temblay, J. Phys. I France **7**, 1309 (1997)
72. W.P. Su, J.R. Schrieffer, A.J. Heeger, Phys. Rev. Lett. **42**, 1698 (1979)
73. R.M. Macfarlane, H. Rosen, H. Seki, Solid State Commun. **63**, 831 (1987)
74. M. Kranz, H.J. Rosen, R.M. Macfarlane, V.Y. Lee, Phys. Rev. B **38**, 4992 (1988)
75. A. Wittlin, R. Liu, M. Cardona, L. Genzel, W. König, W. Bauhofer, H. Mattausch, A. Simon, F. Garcia-Alvarado, Solid State Commun. **64**, 477 (1987)
76. B. Friedl, C. Thomsen, M. Cardona, Phys. Rev. Lett. **65**, 915 (1990)
77. R. Zeyher, G. Zwicknagel, Z. Phys. B **78**, 175 (1990)
78. V.Z. Kresin, H. Morawitz, Phys. Rev. B **37**, 7854 (1988)
79. A. Bill, H. Morawitz, V.Z. Kresin, Phys. Rev. B **68**, 144519 (2003)
80. A. Bill, H. Morawitz, V.Z. Kresin, J. Low Temp. Phys. **117**, 283 (1999)
81. A. Bill, H. Morawitz, V.Z. Kresin, Phys. Rev. B **66**, 100501 (2002)
82. V. Hizhnyakov, E. Sigmund, J. Supercond. Proc. Est. Acad. Sci. Phys. Math. **9**, 335 (1996)
83. V. Hizhnyakov, Proc. Est. Acad. Sci., Chem. **43**, 185 (1994)
84. A. Bill, V. Hizhnyakov, D. Nevedrov, G. Seibold, E. Sigmund, Z. Phys. B **104**, 753 (1997)
85. A. Bill, V. Hizhnyakov, E. Sigmund, Phys. Rev. B **52**, 7637 (1995)
86. A. Bill, V. Hizhnyakov, E. Sigmund, J. Supercond. **10**, 493 (1996)
87. J. Maly, D.Z. Lin, K. Levin, Phys. Rev. B **53**, 6786 (1996)
88. A. Vigliante, M. von Zimmermann, J.R. Schneider, T. Frello, N.H. Andersen, J. Madsen, D.J. Buttrey, D. Gibbs, J.M. Tranquada, Phys. Rev. B **56**, 8248 (1997)
89. J.M. Tranquada, J.D. Axe, N. Ichikawa, Y. Nakamura, S. Uchida, B. Nachumi, Phys. Rev. B **54**, 7489 (1996)
90. J.M. Tranquada, J.D. Axe, N. Ichikawa, A.R. Moodenbaugh, Y. Nakamura, S. Uchida, Phys. Rev. Lett. **78**, 338 (1997)
91. E. Sigmund, A. Bill, V. Hizhnyakov, *Proceeding of the workshop on Anharmonic properties of high-T_c cuprates* (World Scientific, Singapore, 1995) ed. by D. Mihailovi'c, G. Ruani, E. Kaldis, K.A. Müller, p. 187

Chapter 2
The Search for Higher T_c in Houston

C.W. Chu

Dedicated to Alex Mueller, whose "important breakthrough in the discovery of superconductivity in ceramic materials" in 1986 has changed the world of superconductivity.

It is a great pleasure to be invited to join the chorus on this auspicious occasion to celebrate Professor K. Alex Mueller's 90th birthday by Professors Annette Bussman-Holder, Hugo Keller, and Antonio Bianconi. As a student in high temperature superconductivity, I am forever grateful to Professor Alex Mueller and Dr. Georg Bednorz "for their important breakthrough in the discovery of superconductivity in the ceramic materials" in 1986 as described in the citation of their 1987 Nobel Prize in Physics. It is this breakthrough discovery that has ushered in the explosion of research activities in high temperature superconductivity (HTS) and has provided immense excitement in HTS science and technology in the ensuing decades till now. Alex has not been resting on his laurels and has continued to search for the origin of the unusual high temperature superconductivity in cuprates.

My first encounter with Alex was through a phone conversation on December 10th, 1986, following my short note to him and Georg Bednorz a week earlier (Fig. 2.1). During the dog days of superconductivity in 1986 when federal funding diminished to a trickle, our work on BPBO did not lead to any T_c-jump above 13 K, although it did suggest that oxides with low density of states in the absence of d-electrons could be a possible candidate for higher T_c (as described in my proposal submitted to the National Science Foundation in summer 1986). However, the crucial turning point was the appearance of the paper by J. G. Bednorz and K. A. Mueller (BM)—"Possible high T_c superconductivity in the Ba−La−Cu−O system," *Z. Phys. B*. **64** (1986) [1]. In Fall 1986, I started hopping between Houston to take care of my lab and Washington, D.C., to serve as a program director of the

C.W. Chu (✉)
Department of Physics and Texas Center for Superconductivity, University of Houston, Houston, TX, USA
e-mail: cwchu@uh.edu

A. Bussmann-Holder et al. (eds.), *High-Tc Copper Oxide Superconductors and Related Novel Materials*, Springer Series in Materials Science 255,
DOI 10.1007/978-3-319-52675-1_2

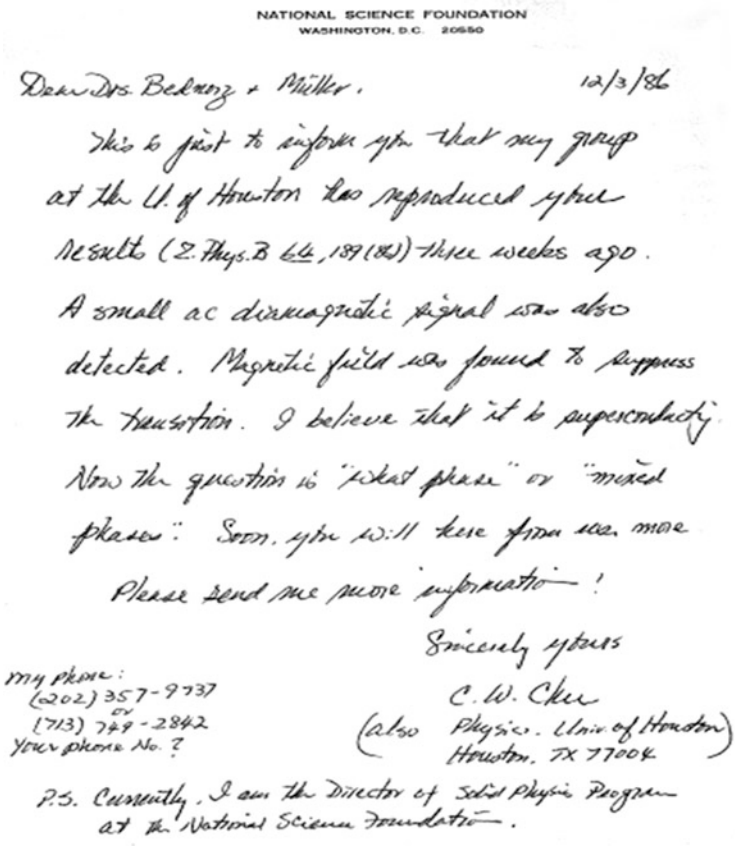

NATIONAL SCIENCE FOUNDATION
WASHINGTON, D.C. 20550

Dear Drs. Bednorz + Müller, 12/3/86

This is just to inform you that my group at the U. of Houston has reproduced your results (Z. Phys. B 64, 189 (86)) three weeks ago. A small ac diamagnetic signal was also detected. Magnetic field was found to suppress the transition. I believe that it is superconductivity. Now the question is "what phase" or "mixed phases". Soon, you will here from us more. Please send me more information!

Sincerely yours

my phone:
(202) 357-9737
or
(713) 749-2842
Your phone No. ?

C. W. Chu
(also Physics. Univ of Houston
Houston, TX 77004)

P.S. Currently, I am the Director of Solid Physic Program at the National Science Foundation.

Fig. 2.1 Provided by Georg Bednorz at the 1997 March APS Meeting in Denver

National Science Foundation (NSF), using the federal flex-time scheme and depending on the goodwill of the managements at both the NSF and the University of Houston. I was extremely excited to read the BM paper on November 8 in my lab and felt that we should be able to do better with our experience in oxides. Initially, their paper did not attract the attention it deserved due to the many false alarms of high T_c previously reported, and its modest title did not help either. The first order of business at the time for us was to reproduce their results. We did this very quickly, which made our group Thanksgiving party that year extra special. To share the excitement, I dropped BM a note on December 3, 1986, as shown in Fig. 2.1. A week later Alex called me from Zurich to thank me. Instead, I thanked him for pointing out a new direction of cuprates for us for higher T_c. We briefly touched on the importance of faith in discovery. By this time, we had also had some interesting preliminary results on La–Ba–Cu–O at ambient and high pressure and therefore I mentioned to him that I was full of confidence for a T_c of 77 K, as was also communicated to my friend, Wei-kan Chu, then at University of North Carolina,

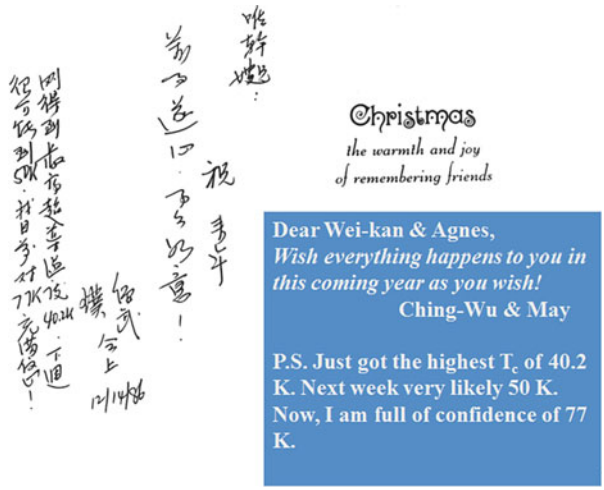

Fig. 2.2 A Xmas greeting from C. W. Chu to Wei-kan Chu on December 14, 1986, with translation

shown in the Christmas card in Fig. 2.2. Later, at the 1987 APS March Meeting, Alex confessed to me that he had thought at the time that I was over-optimistic. The rest is the exciting history of high temperature superconductivity.

Indeed, in the last three decades, great progress has been made in all areas of HTS research and development: materials, science, and technology. For example, more than 250 stable compounds of cuprates and iron-based pnictides and chalcogenides have been discovered with T_c up to 134 and 164 K in $HgBa_2Ca_2Cu_3O_7$ at ambient and 32 GPa, respectively (not to mention the most recently reported unstable hydrogen-rich molecular compounds with a T_c up to 203 K under ultrahigh pressures above 200 GPa, to be discussed later); many new unusual phenomena have been observed in these compounds; the electronic, phononic, and magnetic spectra have been determined in many of these compounds; various theoretical models have been proposed to account for the observations; kilometer-long HTS ribbons have been fabricated with respectably high J_c; and many prototypes of HTS devices have been successfully constructed and demonstrated with performance better than their non-superconducting counterparts. Unfortunately, to date there exists no theoretical HTS model that is commonly accepted, and commercially viable HTS devices are yet to be made available.

We believe that the most effective way to provide relief to the above impasse is to increase the superconducting material space with higher T_c preferably above room temperature, higher J_c via anisotropy reduction, and a greater number of material and structural types through the discovery of novel compounds. In view of the complexity of the existing HTS materials, a holistic multidisciplinary enlightened empirical approach has been proposed to achieve novel HTS with higher T_c [2].

It is therefore not surprising to find that the search for novel superconducting materials with higher T_c has been an important integral part of superconductivity research ever since its discovery, as shown in Fig. 2.3. Over the years, the search has lured many great minds and at the same time humbled many. In this

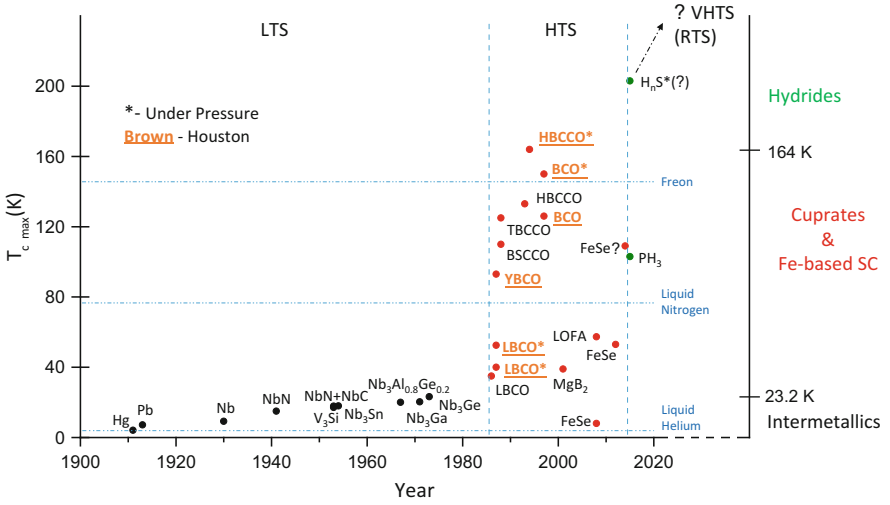

Fig. 2.3 $T_{c\ max}$-evolution with time

congratulatory note, I would like to briefly describe and comment on some of our ongoing efforts at Houston in the search for higher T_c. A few examples follow (details of some have been reported elsewhere):

Interface-Induced Superconductivity

Cuprate superconductors with a T_c above 77 K, the liquid nitrogen boiling point, share a common layered structure with multiple block subsystems: an active subsystem, where certain interactions promote charge-carrier pairing, and a charge reservoir subsystem to offer carriers to the former subsystem without introducing defects, similar to that which occurs in a semiconducting superlattice structure. As a consequence, many cuprates, especially those with high T_cs, show high anisotropy, or quasi 2D-like features. Excitations with different energy scales are believed to provide the glue for superconducting electron-pairings, although a commonly accepted nature of such excitations for the high T_c is yet to emerge. One way that has long been proposed to achieve enhanced T_cs is to take advantage of artificially or naturally assembled interfaces, where soft phonons and/or excitons may occur. In fact, the discovery of the layered cuprate HTS and the great advancement in molecular beam epitaxy growth of perfect thin films have revived the interest in, and accelerated the search for, the interfacial effect in the artificially assembled composite layered compound systems. In addition, naturally assembled metal/semiconductor

interfaces have been demonstrated in the BSCCO single crystalline samples by the observation of the Shapiro steps in a microwave environment [3].

Although the idea to achieve high T_c via interfaces is not new, the first serious model analysis was not made until 1973 when Allender, Bray, and Bardeen (ABB) examined the effect of metal/semiconductor interfaces on superconductivity [4]. They found an impressive T_c-enhancement effect when the stringent conditions on the interfaces are met. Many experiments were inspired by the prediction. An excellent recent article [5] has summarized numerous experiments that display enhanced superconductivity in artificially formed layered compound systems between two different non-superconducting, one superconducting (sc) and one non-superconducting (nsc), or two different superconducting materials. For instance, superconductivity has been observed in heterostructures of PbTe(nsc)/YbS(nsc) up to 6 K, in Al(sc)/Al_2O_3(nsc) up to 6 K vs. 1.2 K in bulk Al, and in (La, Sr)$_2CuO_4$(nsc)/La_2CuO_4(nsc) up to 52 K, all suggesting a rather large T_c-enhancement effect. Although the exact nature of the enhancement remains unclear, exotic interfacial effects that may facilitate the exchange of excitons have been implied.

The alkaline-earth iron arsenide $CaFe_2As_2$ (Ca122) is the parent compound of a large superconductor family. The superconductivity of many compounds in this family seems to be rather unusual. The most unusual observation is the non-bulk superconductivity up to 49 K induced in Ca122 at ambient pressure by slight Ca-replacement with a rare-earth element, La, Ce, Pr, or Nd [6, 7]. A systematic study on the slightly rare-earth doped Ca122 suggests that the above non-bulk superconductivity detected may be associated with the naturally occurring interfaces associated with defects in the samples [8]. However, direct evidence remains elusive due to complications involved in doping and pressure. As for the superconductivity in undoped Ca122, the situation is even more confusing. Filamentary superconductivity up to ~10 K has been detected sporadically under ambient pressure [9]. Although the related superconducting volume-fraction is much higher only under non-hydrostatic pressure, the origin of the superconductivity remains an open issue. The complications associated with the delicate pressure environment, however, seem to prevent a comprehensive experimental verification.

Later studies show that the complex phase-evolution under pressure can be reproduced through heat treatment [10, 11], which may offer a reproducible, controllable, and reversible environment in which many characterization techniques can be applied to explore the issue, if similar superconductivity can be induced. This motivates our studies. We found [12] that Ca122 quenched from 850 °C or above has a tetragonal structure at room temperature (P_1 phase), but transforms to a collapsed-tetragonal phase with a 10% shorter *c* lattice parameter below T_{cT}, the T-cT transition temperature [13]. No magnetic ordering is detected over the whole temperature range. The furnace-cooled Ca122 single crystals, on the other hand, exhibit a tetragonal structure at room temperature with a slightly longer *c* (P_2 phase). On cooling, they undergo a tetragonal-to-orthorhombic transition (T-O) at T_N, closely related to the spin-density-waves transition, to an antiferromagnetic phase. The two transitions, *i.e.* T-cT in P_1 and T-O in P_2, carry with them

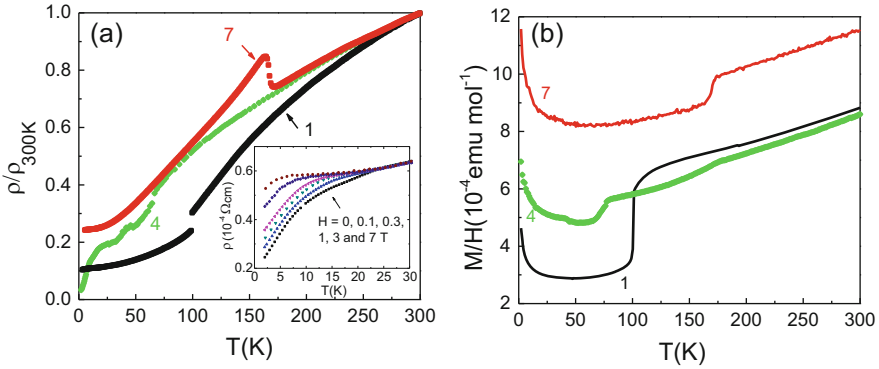

Fig. 2.4 #1—P_1 phase (quenched from 850 °C); #4—mixed phase (sc, annealed at 350 °C for 12 h); #7—P_2 phase (annealed at 350 °C for >16 h). From K. Zhao et al., PNAS 113, 12968 (2016)

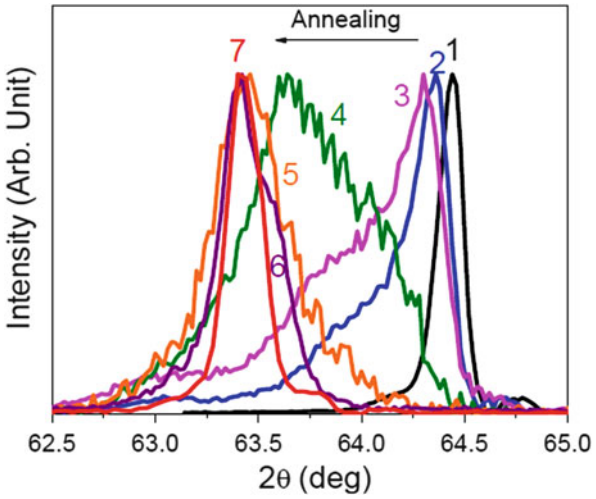

Fig. 2.5 XRD for different annealing times at 350 °C. From K. Zhao et al., PNAS 113, 12968 (2016)

distinct resistive and magnetic signatures at T_{cT} and T_N, respectively, making their detection rather easy (Fig. 2.4). We found that neither the P_1 nor the P_2 phase is superconducting down to 2 K. However, through low temperature annealing at 350 °C for different periods of time t, the P_1-phase transforms progressively to the P_2-phase as evidenced from the XRD results exhibited in Fig. 2.5, showing the mixing of two phases in random-stacking without the appearance of a third phase, in agreement with our XRD-simulation. Superconductivity with an almost constant onset $T_c \sim 25$ K appears when the two phases coexist and the superconducting volume fraction scales with the volume of the phase mixture, as displayed in Fig. 2.6, in agreement with the suggestion of interface-induced superconductivity.

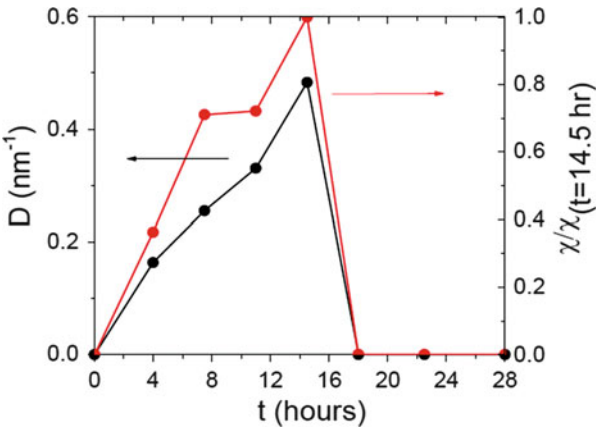

Fig. 2.6 Superconducting volume fraction. From K. Zhao et al., PNAS 113, 12968 (2016)

In summary, superconductivity with an almost constant T_c of ~25 K can be reversibly induced in the mixed phase region of two non-superconducting phases P_1 and P_2 in undoped Ca122 by low temperature annealing at 350 °C for different time periods. The XRD data analysis demonstrates that the superconducting samples consist of randomly stacked layers of P_1 and P_2. The superconductivity volume fraction scales qualitatively with the interface density deduced from the XRD-data. The significant role of interfaces in the 25 K superconductivity is clearly in evidence. Comparison with previous high pressure studies and the small screening volume fraction, however, suggest that a simple strain effect cannot account for the observations. The above observation in undoped Ca122 single crystals represents the most direct evidence for interface-induced superconductivity to date. Similar effect is being explored in other compounds both macroscopically and microscopically. The possible effect of strain during phase mixing will also be further examined.

Layered Cuprate Superconductors with a T_c Above 164 K

Layered cuprate superconductors have dominated the HTS field of study since their discovery. Great efforts have been devoted to the enhancement of their T_c via chemical and/or physical means. Indeed, by controlling these two knobs, T_c has been optimized for each compound or compound family. For example, the peak T_c of the three major cuprate families that superconduct above the liquid nitrogen boiling point, HBCCO [14], BSCCO [15], and YBCO [16], has been observed at 134 or 164 K, 115 or 136 K, and 90 or 92 K at ambient or high pressure, respectively. In spite of the many different models proposed, the general dome-shape of T_c-variation with the alteration of the chemical and/or physical parameter appears to be the norm. For example, T_c of a cuprate has been found to follow the universal hole-concentration quadratically [17] and to follow the pressure applied

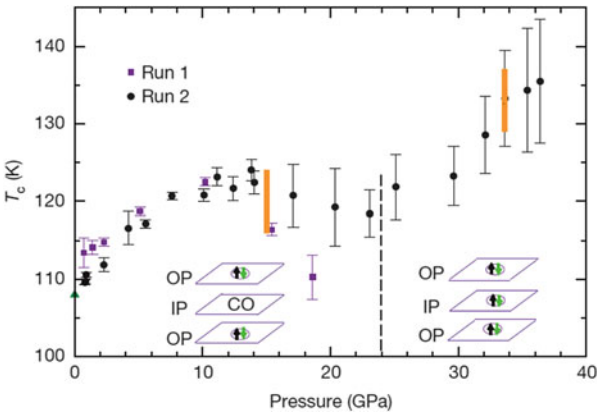

Fig. 2.7 From X. J. Chen et al., Nature 466, 950 (2010), Fig. 3

in a similar fashion. In other words, T_c goes up through a maximum and comes back down with chemical dopant or physical pressure applied. Some colleagues even turn philosophical by saying that whatever goes up will come down. This implies that a simple electronic rigid band is in operation within certain ranges of doping and pressure. If this is strictly the case, any attempt to raise the T_c via these means without changing the band structure would appear to be futile. However, the situation can be rather different if a certain kind of electronic transition can be induced by doping and/or pressurizing without triggering the catastrophic collapse of the crystal. Examination of the existing high pressure data on cuprate high temperature superconductors up to 30s GPa by us and others indeed suggests such a possibility to raise the T_c to above the current record of 164 K.

High pressure investigations have been made on the three optimally doped representative members of the families, but only up to 30s GPa, i.e. $Bi_2Sr_2Ca_2Cu_3O_{10}$ (Bi2223) [15], $HgBa_2Ca_2Cu_3O_9$ (Hg1223) [14], and $YBa_2Cu_3O_7$ (Y123) [16]. Under pressures, their T_cs all initially increase although at different rates. However, they appear to behave differently at higher pressures. A careful examination shows that certain similarities exist, pointing to the possibility of higher T_c. For instance, the T_c of Bi2223, which possesses a unit cell with three CuO_2 layers, shows a two-step increase with pressure as shown in Fig. 2.7. It increases at a moderate rate from 115 to ~128 K at ~14 GPa and then decreases to ~115 K at 24 GPa but finally increases again up to 136 K at a high rate ~1 K/GPa with **no sign of saturation** up to 36 GPa, the highest pressure applied. The second rise in T_c has been attributed to a possible pressure-induced electronic-structure change in the CuO_2 inner layer, leading to a possible redistribution of charge carriers and a more favorable competition between pairing and phase ordering in different CuO_2 layers in the unit cell. A higher T_c thus appears not just possible but also probable in Bi2223 under higher pressures. Magnetic measurements will tell us if a pressure-induced electronic transition takes place and turns the inner-CuO_2-layer antiferromagnetic to activate a possible antiferromagnetic/metallic interfacial interaction predicted to favor a T_c-enhancement [18]. The T_c-P relation for Hg1223, which has a three CuO_2-layer/cell structure similar to Bi2223 has been extensively

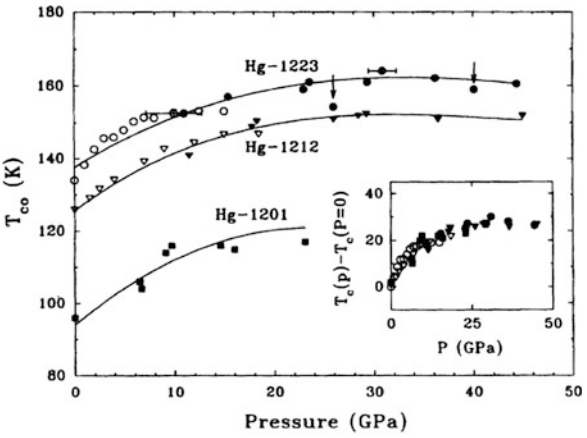

Fig. 2.8 From L. Gao et al., Phys. Rev. B 50, 4260–4263 (R) (1994), Fig. 3

studied [14] and is displayed in Fig. 2.8; its T_c increases with pressure, at a rate higher than those of either Bi2223 or Y123, from 134 to 150 K at ~8 GPa, then peaks at 164 K at ~32 GPa, and finally decreases only slightly to 160 K at 44 GPa, the highest pressure applied. An increased pressure may allow us to observe the second rise of T_c with pressure in Hg1223 by inducing a possible electronic transition in the CuO_2 inner layer, similar to that in Bi2223. In addition, the other two members of the HBCCO family, Hg1201 and -1212, display similar T_c-P behavior also shown in Fig. 2.8, another demonstration of the important similar role of CuO_2 layers in the high T_c of the HBCCO family. The ultrahigh pressure study on all three members of the HBCCO family will provide us an opportunity to test the mechanism proposed for the second T_c-rise in Bi2223 [15]. In other words, one would not expect to see the second T_c-rise in Hg1201 or -1212, which lack the so-called "inner CuO_2", at higher pressures, unless different pressure-induced electronic transitions are induced, as discussed below. The T_c of $YBa_2Cu_3O_7$ (Y123) [16] increases initially with pressure from 91 to ~92 K at ~8 GPa, then deceases to ~60 K at ~23 GPa, but drops precipitously to below 2 K beyond 23 GPa, as shown in Fig. 2.9. This may be attributed to its absence of the inner CuO_2 layer in comparison with Bi2223 and Hg1223. However, the re-emergence of another T_c rise in Y123 at higher pressure is not unlikely in view of the recent report of the re-emergence of superconductivity with a higher T_c in Fe-based chalcogenides at higher pressures after the complete suppression of superconductivity by pressure at ~10 GPa, as displayed in Fig. 2.10 [19]. We therefore are investigating the magnetic, resistive, and optical states of Bi2223, Hg1223, and Y123 up to ~200 GPa to achieve a T_c above 164 K and examining the possible electronic transition associated with the three CuO_2 layers induced by pressure in Bi2223 and Hg1223 and the two CuO_2 layers in YBCO.

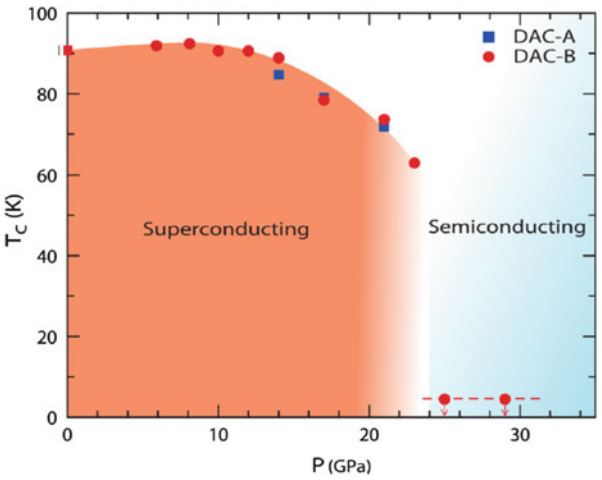

Fig. 2.9 From T. Muramatsu, D. Pham, and C. W. Chu, Appl. Phys. Lett. 99, 052508 (2011), Fig. 3

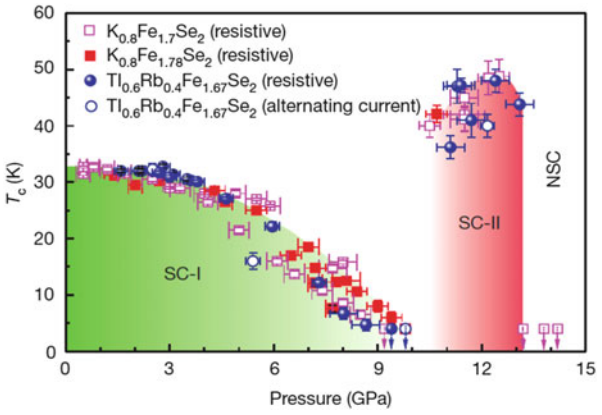

Fig. 2.10 From L. L. Sun et al., Nature 483, 67 (2012), Fig. 4

Hydrogen-Rich Molecular Compounds

The scientific significance of the recent report by Eremets et al. [20] is obvious and multifold: (i) a new T_c record of 203 K at ~200 GPa (vs. the current record of 164 K in HBCCO under 32 GPa set in 1993); (ii) very high T_c in a new class of 3D molecular solid materials (vs. the current 2D-cuprates for the last three decades); and (iii) the possible viability of the so-called "first principle calculations" approach [21] to superconductors with higher T_c through the electron-phonon interaction (vs. the enlightened empirical approach in the strong electron correlation systems [2]). In view of its significance, a careful and preliminary examination of the above claims has been made. We found that crucial questions remain and need to be clarified. In this respect, we are addressing two issues: (1) the existence of the Meissner state in H_nS; and (2) the viability of the current numerical calculations or

"first principle calculations" of T_c using different algorithms and codes. We plan to search for and study the Meissner effect in H_3S under ~200 GPa below its $T_c \sim 200$ K, as well as the high T_c superconductivity predicted in Y-hydrides under pressures below 120 GPa: YH_3 ($T_c \sim 40$ K at 17.7 GPa); YH_4 ($T_c \sim 84$–95 K at 120 GPa); and YH_6 ($T_c \sim 252$–264 K at 100 GPa) [22, 23].

Although there are several excellent ultrahigh pressure labs in the US, China, Japan, and Europe, to date and to the best of our knowledge, there is only one lab (Shimizu's in Japan) that has reproduced the resistive transition in H_3S together with Eremets [24], and none has reported the magnetic transition claimed by Eremets et al. [20], although a ZFC transition by nuclear resonating scattering was later reported by Troyan/Eremets et al. [25] and by an ac susceptibility technique by Huang/Cui [26]. Indeed, the large resistance drop, the negative magnetic field effect, and the isotope effect are consistent with a superconducting transition. However, given the extreme challenges in the resistive and magnetic experiments under ultrahigh pressure, and the fact that similar field and isotope effects can also be observed in some metal-semiconductor transitions of, e.g., transition-metal oxides, a scenario has also been proposed in which the sample undergoes a non-superconducting Keldysh-Kopaev transition at high temperature and is superconducting only below 40 K, after analyzing the resistive data and comparing them with those of HTS cuprates, pnictides, and organic superconductors [27]. We have therefore analyzed in detail all magnetic data published for the Meissner effect, whose existence below 203 K will be a sufficient proof of superconductivity in H_3S under ultrahigh pressures, and have concluded that its existence remains an open question. We therefore are in collaboration with Eremets to search for it by deploying a sensitive magnetic technique as shown in Fig. 2.11 for the search. We will also examine the YH_n, which have been predicted to be

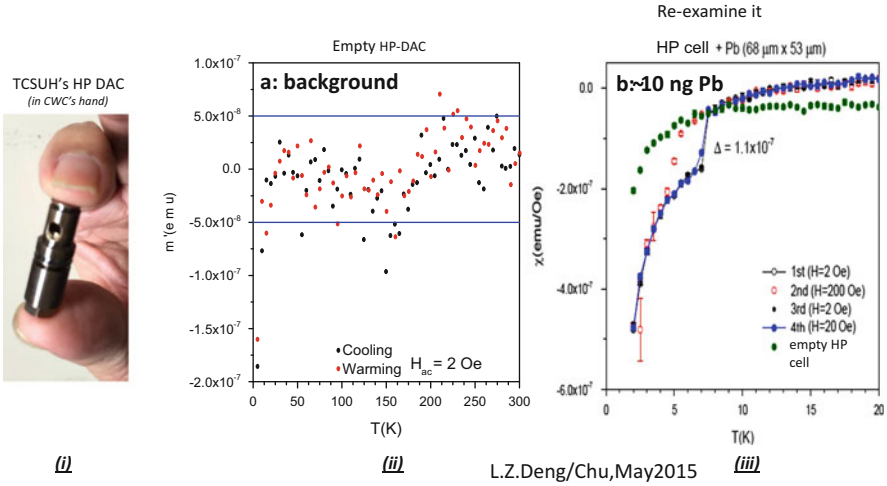

Fig. 2.11 From Deng/Eremets and Chu

superconducting below 150 GPa, to test the predictability of the so-called "first principle calculations".

Optimization of Multi-interaction in Multiferroics

As discussed in [2], known high T_c superconductors exhibit multiple interactions, and magnetic interaction has been considered by many to play an important role. The question arises whether ferroelectric interaction can play a beneficial role for superconductivity as depicted in Fig. 2.12. Given the high ferroelectric or antiferroelectric ordering temperature, a beneficial effect on superconductivity similar to that of magnetism may not be impossible.

Multiferroics exhibit multiple competing interactions and display concurrently various ground states, e.g. the coexistence of magnetism and ferroelectricity. Studies by us and others show that ferroelectricity in multiferroics can be induced by magnetism, pressure, or an external magnetic field. It has also been shown recently that superconductivity can coexist with ferromagnetism and that magnetic field can induce superconductivity. This raises the question whether superconductivity can evolve from ferroelectricity directly or indirectly through magnetism. Since multiferroics belong to the class of highly correlated electron material systems that possess transition temperatures up to above room temperature, it is conjecture that it may not be impossible to achieve superconductivity with a very high T_c by optimizing the various interactions present. The first order of business is to metallize the multiferroics. The chemical doping approach fails because of the high stability of the chemical bonding. We therefore have decided that the most effective way is through high pressure. Unfortunately, no detection of superconductivity has been achieved by us, to date. We have attributed the failure possibly to the Mn element that often

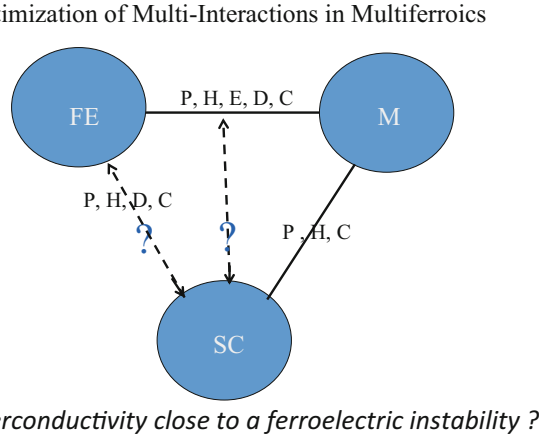

Fig. 2.12 From C. W. Chu, AAPPS Bulletin 18, 9 (2008), Fig. 3

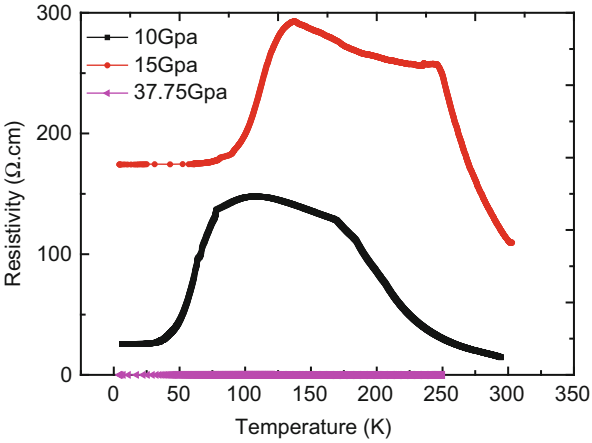

Fig. 2.13 A multiferroic without Mn. From Z. Wu, S. Y. Huyan, L. Z. Deng/ C. W. Chu

appears in the multiferroics, since Mn is a killer of superconductivity (to the best of my knowledge there exist only two low T_c superconducting Mn compounds, including one recently discovered by Cava). We are now looking at multiferroics without Mn. Preliminary results appear encouraging, as demonstrated in Fig. 2.13.

As is evident, this presentation represents only a progress report of the effort to search for higher T_c with great hope at Houston. I understand that vision does not count until real exciting results emerge. We will keep the faith in all of our efforts. With some luck, together we shall reach the 300 K wonderland as an ultimate tribute to Alex.

Acknowledgements I would like to express my gratitude to current and former students and colleagues at TCSUH, B. Lv, Z. Wu, Y.Y. Xue, L.Z. Deng, S.Y. Huyan, H.M. Yuan, B. Lorenz, M. Gooch, F.Y. Wei, Y.Y. Sun, J.K. Meen, K. Zhao, L. Gao, F. Chen, T. Muramatsu, and D. Pham, for technical assistance and discussion. The work in Houston is supported in part by US Air Force Office of Scientific Research Grant FA9550-15-1-0236, the T. L. L. Temple Foundation, the John J. and Rebecca Moores Endowment, and the State of Texas through the Texas Center for Superconductivity at the University of Houston.

References

1. J.G. Bednorz, K.A. Müller, Z. Phys. B **64**, 189 (1986)
2. C.W. Chu, AAPPS Bull. **18**, 9 (2008)
3. R. Kleiner, F. Steinmeyer, G. Kunkel, P. Müller, Phys. Rev. Lett. **68**, 2394 (1992)
4. D. Allender, J. Bray, J. Bardeen, Phys. Rev. B **7**, 1020 (1973)
5. J. Pereiro, A. Petrovic, C. Panagopoulos, I. Bozovic, Phys. Express **1**, 208 (2011)
6. B. Lv et al., Proc. Natl. Acad. Sci. USA **108**, 15705 (2011)
7. S.R. Saha et al., Phys. Rev. B **85**, 024525 (2012)
8. L.Z. Deng et al., Phys. Rev. B **93**, 054513 (2016)
9. H. Xiao et al., Phys. Rev. B **85**, 024530 (2012)
10. S. Ran et al., Phys. Rev. B **83**, 144517 (2011)

11. B. Saparov et al., Sci. Rep. **4**, 4120 (2014)
12. K. Zhao et al., Proc. Natl. Acad. Sci. USA **113**, 12968 (2016)
13. A. Kreyssig et al., Phys. Rev. B **78**, 184517 (2008)
14. L. Gao et al., Phys. Rev. B **50**, 4260(R) (1994.) and references therein
15. X.J. Chen et al., Nature **466**, 950 (2010.) and references therein
16. T. Muramatsu, D. Pham, C.W. Chu, Appl. Phys. Lett. **99**, 052508 (2011)
17. M.R. Presland et al., Phys. C **176**, 95 (1991)
18. D.H. Lee, Chin. Phys. B **24**, 117405 (2015)
19. L.L. Sun et al., Nature **483**, 67 (2012)
20. A.P. Drozdov et al., Nature **525**, 73 (2015)
21. See for example, "Materials by Design: An NSF-Sponsored Workshop at UC Santa Barbara", March 17–19, 2011. http://www.mbd.mrl.ucsb.edu
22. D.Y. Kim, R.H. Scheicher, R. Ahuja, Phys. Rev. Lett. **103**, 077002 (2009)
23. Y.W. Li et al., Sci. Rep. **5**, 9948 (2015)
24. M. Einaga et al., Nat. Phys. 12, 835 (2016)
25. I. Troyan et al., Science **351**, 1303 (2016)
26. X. L. Huang et al., arXiv:1610.02630v1 [cond-mat.supr-con] (2016)
27. L. S. Mazov, arXiv:1510.00123v1 [cond-mat.supr-con] (2015)

Chapter 3
From Granular Superconductivity to High Tc

Guy Deutscher

Tel Aviv, 1978

I first met Alex Muller during his visit at Tel Aviv University, before he went on to his sabbatical year at the IBM Yorktown Heights labs. He had been invited to Tel Aviv by Amnon Aharony with whom he had interacted very fruitfully on the critical behavior of oxide dielectrics near phase transitions.

As one usually does with distinguished visitors, Alex was introduced to several faculty members with whom there was time for in depth discussions. When my turn came I was not too sure whether what I could tell him on my research would be of much interest to him. I was working on superconducting granular Aluminum films, composed of nano-size aluminum grains surrounded by aluminum oxide. By using dark field electron microscopy we had obtained precise measurements of the grain size down to 2 nm (this was nano-science before the word was widely used). We had shown that the smaller the grains, the higher the critical temperature [1, 2]. Alex had not worked previously on superconductivity, and the strange properties of this material was not a matter of broad interest in the solid state community. I feared that my presentation would not retain his attention.

The Tc enhancement phenomenon had been originally discovered by Abeles and his group at the RCA labs in Princeton. After several years of research at Tel Aviv, we had come to the conclusion that the various explanations proposed by several authors to explain this substantial enhancement were not valid. These included a large change in the Aluminum lattice parameter reported by J.J. Hauser at Bell labs, of which my colleague Enrique Grünbaum found no trace in electron diffraction experiments, and a phonon softening that could have enhanced the effective

G. Deutscher (✉)
School of Physics and Astronomy, Tel Aviv University, Ramat Aviv, Tel Aviv 69978, Israel
e-mail: guyde@post.tau.ac.il

A. Bussmann-Holder et al. (eds.), *High-Tc Copper Oxide Superconductors and Related Novel Materials*, Springer Series in Materials Science 255,
DOI 10.1007/978-3-319-52675-1_3

attractive electron interaction according to the theory of McMillan—but this softening did not appear in our tunneling experiments.

Everything was known about superconductivity, or so one thought. But maybe precisely because Alex had had no detailed previous exposure to superconductivity, he was ready to accept the idea that our results raised a question of fundamental importance.

Bardeen, Cooper and Schrieffer had developed the famous BCS theory that explained all the basic experimental features of superconductors. Pierre Gilles de Gennes had declared that everything was understood about superconductivity. His book and that of Tinkham were complete textbooks of all one needed to know about superconductivity. And so, how could it be that there was no explanation for the enhanced critical temperature of granular Aluminum? Maybe our understanding of superconductivity was not complete after all?

Alex Muller Learns and Teaches Superconductivity

This was my feeling, but so far I had been preaching in the desert. As it turned out later I had however convinced Alex that maybe not everything was understood about superconductivity, after all.

Alex asked me whether we could provide him with some granular aluminum samples that he could study during his sabbatical year at Yorktown Heights. And so we did. I asked Dov Abraham, a PhD student whom I was supervising together with Ralph Rosenbaum, to prepare samples for him. The work that came out was the first publication of Alex on superconductivity [3].

Back in Zurich after his sabbatical Alex taught a course on superconductivity at the University.

In 1986 the news broke out that he and Bednorz had discovered high superconductivity in the oxide system Ba–La–Cu–O [4]. Maybe the oxide component of granular aluminum had attracted his attention, as he knew a lot about oxides.

The rest of the story is well known. Following this discovery we all became involved in High Tc, and I forgot about granular aluminum.

Is There Anything Common to Granular Aluminum and the High Tc Oxides?

Yet, the question remained. What was so special about granular aluminum? Maybe its critical temperature is enhanced because of some strange combination of factors, and the connection with the oxides of Bednorz and Muller is purely accidental? Maybe granular aluminum attracted the attention of Alex for the wrong reasons?

Maybe there is no fundamental reason after all behind its enhanced superconductivity?

In other words, is there any connection between granular Aluminum and the high Tc oxides? And if there is, what is it?

The answer to this question lies in the title of the famous book of de Gennes on superconductivity: "Superconductivity in metals and alloys."

It is absolutely true that in the late sixties everything was already known on superconductivity in *metals and alloys*. De Gennes, Anderson and other famous physicists were right. However the high Tc oxides do not fall in this category. They are not metals or alloys in the usual sense. And neither is granular Aluminum. Both are close to an insulating state where spin effects play a fundamental role. This is well known for the cuprates, whose parent compounds are anti-ferromagnets. This is also the case for granular aluminum, which as we have shown recently displays a surprising Kondo effect.

Granular Aluminum Is Not a Metal in the Conventional Sense

The first indication for a Kondo effect in granular aluminum came from a detailed study of the temperature dependence of the resistivity, as shown Fig. 3.1. It is *non-monotonous*, a feature well known in Kondo alloys (and also commonly observed in underdoped cuprates, as seen in the original publication of Bednorz and Muller, see Fig. 3.2).

Although suggestive, a non-monotonous resistance temperature dependence is not sufficient to establish a non-conventional metallic nature, particularly the presence of free spins.

A more direct indication for the presence of such spins came about from a detailed study of the magneto-resistance over a wide range of temperatures. It

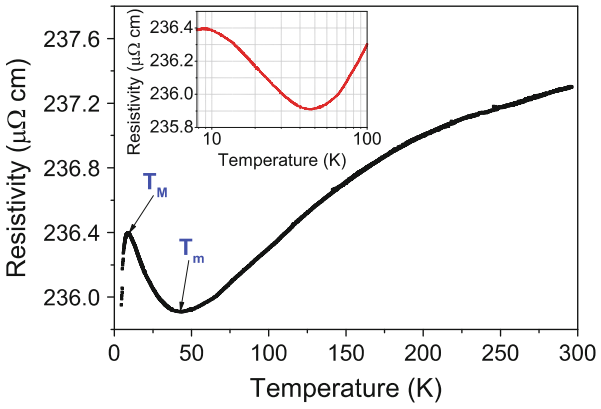

Fig. 3.1 A non monotonous dependence of the resistivity in granular aluminum was the first indication for a possible Kondo effect (after Bachar et al. [5])

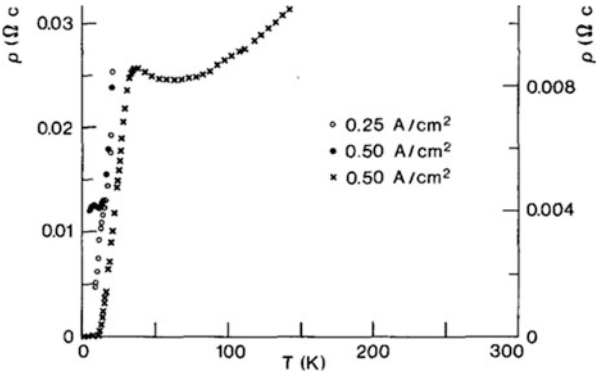

Fig. 3.2 A similar non monotonous resistivity dependence was also reported by Bednorz and Muller in BaLaCuO (after Bednorz and Muller [3])

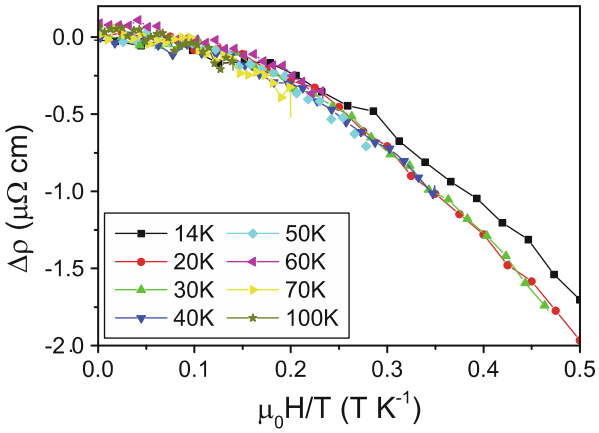

Fig. 3.3 The magneto-resistance of a high resistivity (about 2000 μΩcm) granular aluminum film is negative and scales as $(H/T)^2$ over a broad range of temperatures, a behavior typical of Kondo alloys (after Bachar et al. [6])

turned out that it is negative up to temperatures of the order of 100 K, and that it varies as $(H/T)^2$, as shown Fig. 3.3 [5]. This is a well known property of Kondo alloys far above their Kondo temperature.

Finally a direct proof for the existence of magnetic moments of electronic origin came from musr studies [6]. Figure 3.4 shows both the temperature dependence of the scattering rate and that of the resistance. The scattering rate is temperature dependent at high temperatures, but becomes constant below 10–20 K. This is the temperature range where the resistance ceases to increase logarithmically and approaches its maximum value.

The two sets of data shown Fig. 3.4, obtained on the same sample, demonstrate the Kondo behavior where at low temperatures the spins are locked in. They then cease to interact with conduction electrons. This enables superconductivity to set in. It is in fact the Kondo temperature that limits the superconducting critical temperature. As the metal to insulator transition is approached, both the Kondo temperature and the superconducting critical temperature go down.

According to our current understanding, the origin of spin effects in granular aluminum lies in the very small grain size. The discreteness of the electronic levels

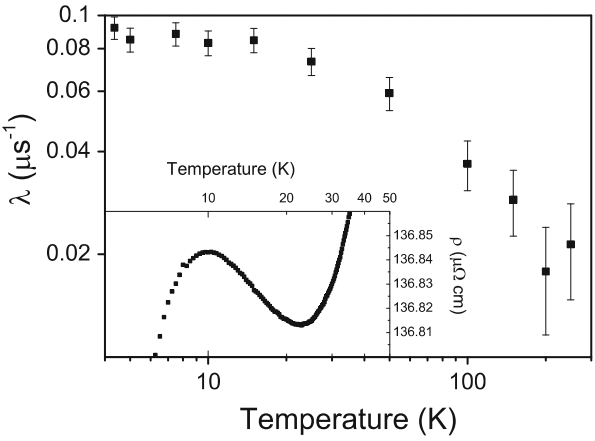

Fig. 3.4 The temperature dependence of the musr scattering rate in a granular aluminum film demonstrates the presence of electronic spins. The scattering rate saturates at low temperatures (after Bachar et al. [6])

then comes into play. When the number of electrons is uneven, a single one sits in the upper occupied level. If the distance between levels is large enough, the spin of that electron becomes relevant. The distance between levels is of the order of 50–100 K, large enough compared to the temperature and to the level broadening due to intergrain coupling in the weak coupling limit.

The interplay between the Coulomb blockade due to the small grain size, and the Kondo effect, has been studied by Florens et al. in the case of quantum dots [7]. They showed that the discreteness of electronic levels combined with the multiplicity of these levels in small grains can substantially raise the value of the Kondo temperature, which can then become accessible. Metallic conduction is then recovered. Assuming that this result can be extended to the case of arrays of quantum dots, this is a favorable factor for the observation of superconductivity. The experimental results that we have briefly summarized here suggest that similar effects indeed can take place in granular aluminum films. The Kondo effect in quantum dots is marked by a strongly modified density of states, with a sharp peak at the Fermi level. It is tempting to conjecture that this peak is at the origin of the enhanced superconducting critical temperature in arrays of nano-size grains.

Conclusion

We do not yet have a full understanding of superconductivity in the high Tc oxides, nor in granular aluminum. What is now clear however is that spin effects play an important role in both materials. Granular aluminum is in fact a simpler system that the high Tc oxides, because chemistry is not at work; the origin of the spins is the discreteness of quantum levels in the small grains. A complete understanding of granular aluminum may help resolve the High Tc problem.

In any case the idea that this material is indeed a case that cannot be explained by the theory of superconductivity in conventional metals, and that other cases might follow as had been anticipated by Alex Muller, has been proven to be right.

References

1. G. Deutscher, H. Fenichel, M. Gershenson, E. Grünbaum, Z. Ovadyahu, Low Temp. Phys. LT **13**(5), 573 (1972)
2. G. Deutscher, H. Fenichel, M. Gershenson, E. Grünbaum, Z. Ovadyahu, J. Low Temp. Phys. **10**, 231 (1973)
3. J.G. Bednorz, K.A. Muller, Z. Phys. B **64**, 189 (1986)
4. K.A. Muller, M. Pomerantz, C.M. Knoedler, D. Abraham, Phys. Rev. Lett. **45**, 832 (1980)
5. N. Bachar, S. Lerer, S. Hacohen-Gourgy, B. Almog, G. Deutscher, Phys. Rev. B **87**, 214512 (2015)
6. N. Bachar, S. Lerer, A. Levy, S. Hacohen-Gourgy, B. Almog, H. Saadaoui, Z. Salman, E. Morenzoni, G. Deutscher, Phys. Rev. B **91**, 041123 (2015)
7. S. Florens, P. San José, F. Guinea, A. Georges, Phys. Rev B **68**, 245311 (2003)

Chapter 4
Alex and the Origin of High-Temperature Superconductivity

Takeshi Egami

Introduction

The discovery of high-temperature superconductivity (HTSC) in the cuprates by Müller and Bednorz [1] was a remarkable event in science which radically and irreversibly changed the course of research in condensed matter physics and materials science. Their chemical complexity gave a shock to physicists who were accustomed to simple solids. Oxides have long been thought to be just insulating, but the demonstration of metallic oxides having exciting properties opened up a whole new field of research on the transport properties of oxides.

This discovery was led by Alex's intuition that HTSC must be found in the system with the strong Jahn-Teller (JT) effect resulting in strong electron-phonon (*e-p*) coupling [2]. The traditional search for the HTSC material followed the path by Matthias [3] and sought after compounds of *d*-band metals with high Fermi density of states as prescribed by the BCS theory [4]. But the JT effect does not occur in metals because of strong dielectric screening. The genius of Alex was to go after the oxides with low electron density where the JT effect survives, even though the low electron density does not favor HTSC in the conventional thinking. Although superconductivity was already observed in $LiTi_2O_4$ [5] and $BaPb_{1-x}Bi_xO_3$ [6], it was a total surprise that high values of T_C were observed in the cuprate compounds.

However, the nature of the parent phase that it is an antiferromagnetic (AFM) Mott insulator [7] led many toward very different paths than those initially conceived by Alex. Actually the history of the HTSC research is teaching us how to do,

T. Egami (✉)
Shull Wollan Center – Joint Institute for Neutron Sciences, University of Tennessee and Oak Ridge National Laboratory, Oak Ridge, TN 37831, USA
e-mail: egami@utk.edu

A. Bussmann-Holder et al. (eds.), *High-Tc Copper Oxide Superconductors and Related Novel Materials*, Springer Series in Materials Science 255,
DOI 10.1007/978-3-319-52675-1_4

or not to do, research on hugely unknown subjects. So many theories were published even before experimental facts were established. For example, the failure of the electronic calculation based on the density functional theory (DFT) to account for the parent compound as a Mott insulator convinced many that strong electron correlation plays a major role in the HTSC mechanism. To formulate the theory the *t-J* Hamiltonian derived from the one-band Hubbard model was used, assuming that doped holes reside on Cu ion [8]. However, it was soon discovered that holes were on oxygen, not on copper [9]. Then the Zhang-Rice model was quickly invented to justify the one-band model [10], even though the three-band model was more realistic [11]. Indeed the validity of the Zhang-Rice model is questionable when carriers are mobile at high levels of doping. Furthermore, the value of U, the on-site Coulomb repulsion, is not extremely large but only comparable to the band-width, W. Because the *t-J* model is derived from the Hubbard model in the limit of $U/t \rightarrow \infty$ [12], this fact casts serious doubt on resorting to the *t-J* model instead of the full Hubbard model. Thus the one-band *t-J* Hamiltonian stands precariously on the two thin layers of fragile assumptions. But the fact that the one-band *t-J* model is a minimalist model which can be solved with reasonable approximations kept it in the mainstream of the theory community for a long time [13].

Even though Alex is not a theoretician, he saw through the unrealistic nature of the theories with the *t-J* model, based upon the experimental facts and his vast experience. He maintained his firm conviction that only the lattice can provide such high transition temperatures, and the only role of the magnetic order is to prevent superconductivity from occurring. In the last three decades a large number of theories, many of which are based upon wild ideas and speculations, were proposed, and were forgotten. In the meantime abundance of new experimental facts became known, discrediting much of these theories. Through the course of events Alex has been the unyielding and unmoving center of force, and guided us all. After more than 30 years of research the true nature of HTSC is finally emerging as discussed here. They are beginning to indicate that Alex may have been right all along, although the battle has not yet been finally won.

Lattice Effects

Soon after I became involved in the HTSC research I found that the local structure of HTSC oxides is significantly distorted from the average lattice structure. This discovery was made by using the method of the atomic pair-density function (PDF) determined by pulsed neutron scattering [14–16]. The PDF,

$$\rho_0 g(r) = \frac{1}{4\pi N r^2} \sum_{i,j} \left\langle \delta\left(r - \left|\mathbf{r}_i - \mathbf{r}_\mathbf{j}\right|\right)\right\rangle, \tag{4.1}$$

where $\boldsymbol{r_i}$ is the position of the ith atom and ρ_0 is the average atomic number density, describes the true distribution of distances between atoms without the assumption of lattice periodicity. The PDF can be determined from the normalized diffraction intensity, the structure function $S(Q)$ where Q is the momentum transfer of scattering, through the Fourier-transformation [17, 18]. This method has been widely used in the structural analysis of liquids and glasses [17], but recently we started to apply it in the study of crystalline materials with defects or with local deviations from the ideal lattice [18]. The key to this new use of the old method was the availability of synchrotron based radiation sources, *i.e.* the synchrotron x-radiation sources and the pulsed neutron sources. For the Fourier-transformation to be accurate $S(Q)$ has to be determined up to high values of Q. The availability of high energy probes from these synchrotron based sources made this method much more accurate than it used to be. The discovery of HTSC in the cuprate was timely for the development of the PDF method. We were able to demonstrate the power of this method through the study of the cuprates.

In particular we discovered that the portion of the PDF corresponding to the distance between the apical oxygen and the in-plane oxygen showed an anomalous temperature dependence as shown in Fig. 4.1 [19]. A possible explanation of this observed change was proposed later [20]. This implies intimate involvement of the lattice dynamics in the HTSC phenomenon of the cuprates. Similar observations of the lattice anomaly at or near T_C were reported also with ion-channeling [21, 22] and EXAFS [23, 24]. Encouraged by the numerous observations of the anomalous lattice behavior, Y. Bar-Yam, J. Mustre de Leon, A. R. Bishop and I organized a conference on the "Lattice Effects in High-T_C Superconductors", in January 1992 at Santa Fe [25]. The meeting was a major success, and helped to establish the lattice effect as one of the major subjects of the HTSC research. This conference prompted various meetings on the lattice effect. The series of meetings on the stripes [26] by

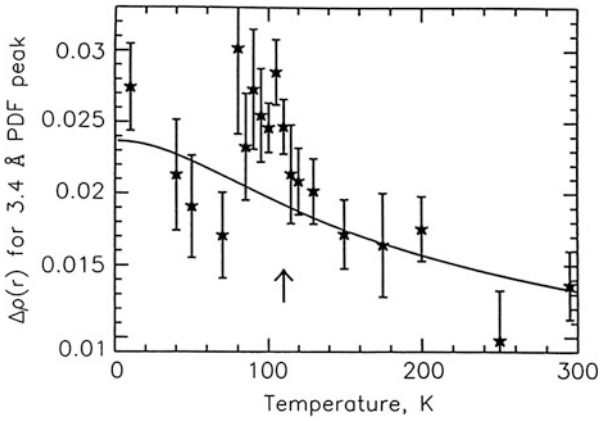

Fig. 4.1 Variation of the PDF peak height of $Tl_2Ba_2CaCu_2O_8$ at 3.4 Å with temperature [19]. The *arrow* indicates T_C (=110 K). The *line* shows the normal behavior

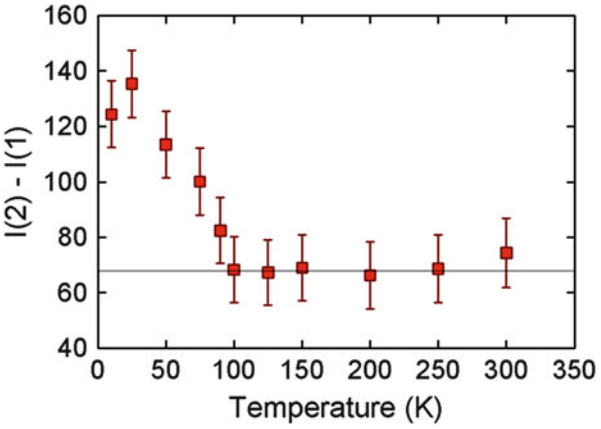

Fig. 4.2 Temperature dependence of the spectral weight of the inelastic neutron scattering intensity at $\boldsymbol{Q} = (3.25, 0, 0)$, I (51–55 meV)–I (56–68 meV) for $YBa_2Cu_3O_{6.95}$ [31]. $T_C = 93$ K for this sample

A. Bianconi are the most visible ones, still being continued today. The stripe conference series focuses not only on the lattice effects but also on the spatial separation of spin and charge, the representative of which is the spin-charge stripe structure [27, 28]. Various anomalous lattice effects in the cuprates observed up to 1995 were reviewed in [29].

Not only the structure, but the lattice dynamics was found to change anomalously across T_C [30] as shown in Fig. 4.2 [31]. Even though the results by themselves do not represent the "smoking gun" of the phonon mechanism, it is clear that the electron-phonon (*e-p*) coupling plays some prominent role in the HTSC phenomena. It is well known that the conventional *e-p* coupling through the charge channel is rather weak in the cuprates, and cannot explain the high T_C [32]. We argued that the strong electron correlation could result in unconventional *e-p* coupling, particularly through the charge transfer induced by the copper-oxygen half-breathing mode [33–35]. Using the vibronic model we showed that T_C exceeding 100 K can be achieved through the overscreened *e-p* coupling [36].

The half-breathing mode modifies the Cu–O *p-d* overlap, and the transfer integral, *t*. This induces charge hopping between Cu ions, which can be spin-dependent. In ferroelectric oxides, such as $PbTiO_3$, such charge transfer induced by lattice distortion produces electronic polarization which adds to the ionic polarization of the lattice to enhance ferroelectricity [37, 38]. However, in the cuprates the electronic polarization is anti-parallel to the ionic polarization, and they cancel each other [35]. Therefore the macroscopic dielectric *e-p* coupling is weak, but the local coupling at the orbital level is very strong. The *e-p* coupling through the orbital excitations potentially is a viable mechanism for promoting HTSC.

The strong *e-p* coupling for the Cu-O half-breathing mode was then confirmed by the angle-resolved photoemission (ARPES) measurement by Lanzara [39, 40]. The observation was made at the nodal point near $(\pi, \pi, 0)$. Even though

the nodal point is not directly relevant to the *d*-wave superconductivity, the unexpected strength of the *e-p* coupling is enough to wipe out doubts on the relevance of the *e-p* coupling. The isotope effects [40] also provides unquestionable evidence of the lattice involvement. The isotope effects are not only large, but also are quite unusual and unconventional. For instance the magnetic screening length shows a larger isotope effects than T_C [41]. A possible explanation of the unconventional nature of superconductivity was provided by Bianconi [42] who argues that the *e-p* coupling is greatly enhanced through the Fano-Feshbach resonance involving the spin-charge stripes which occurs near the Lifshitz transition. The unusual nature of the *e-p* coupling in the cuprates is discussed in the article for the celebration of the 80th birthday of Alex [43].

Iron-Pnictide Superconductors

The discovery of superconductivity in iron pnictides [44, 45] seriously affected the research on the cuprates. Because the highest value of T_C for the pnictides (56 K) is still lower than that of the cuprates by a factor of two, and the cuprate HTSC has the *d*-symmetry [46] whereas the pnictide has the *s*-symmetry [47], many are in the opinion that the cuprates and the pnictides are fundamentally different. However, recent developments are beginning to challenge this view as discussed below. If the cuprates and the Fe pnictides are to share the same origin of HTSC, the observations made for Fe-pnictides squarely challenge the common beliefs regarding the nature of HTSC, primarily deduced from the properties of the cuprates:

Belief #1: Mottness (Strongly Correlated Electron Physics) is Central to HTSC, so the Parent Phase has to be a Mott Insulator
Whereas the parent phases of the Fe-pnictides are again antiferromagnetic [48] just as in the cuprates, they are metallic, and not the Mott insulator. The core level spectroscopy also suggest that electrons are not strongly correlated in the iron pnictides [49].

Belief #2: Doped Carriers Are Responsible for HTSC
In the iron pnictides HTSC is observed over a wide ranges of doping concentration, and T_C is nearly flat within that range [50]. Furthermore HTSC is observed even with isovalent doping, such as P for As [51]. Therefore the role of dopant is not to provide charge carriers, but simply is to suppress the spin ordering. The suppression of spin ordering is not chemical, but physical through the lattice compression, and is described by the Landau theory using the lattice as a variable [52], as shown in Fig. 4.3 [53].

Belief #3: HTSC Occurs in a Spin ½ Systems
If spin fluctuations play an important role in HTSC, spin ½ systems are strongly preferred because of large spin fluctuations. But Fe pnictides are multi-orbital magnets with a spin larger than ½, up to 1 [54].

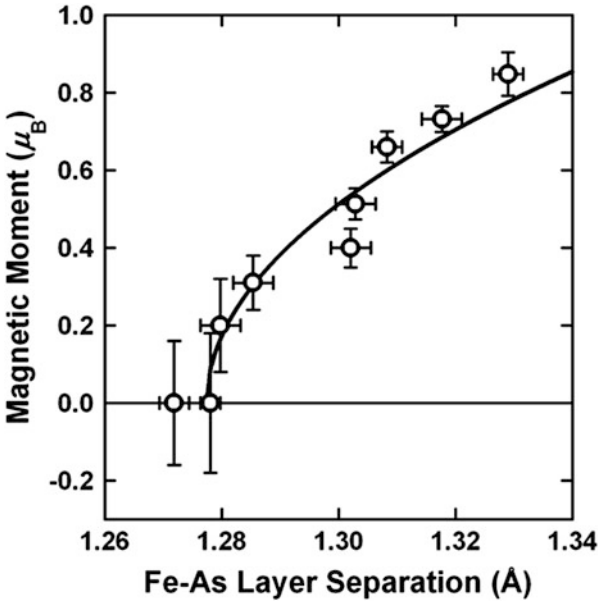

Fig. 4.3 Dependence of the magnetic moment on the Fe-As layer separation for CeFe(As,P)O (*open circles*) [51], and the fit by the Landau theory (*solid curve*) [53]

Belief #4: HTSC Occurs in the Vicinity of the Quantum Critical Point
Near the quantum critical point (QCP) large quantum fluctuations occur, facilitating pairing. Consequently HTSC can occur around the QCP, as illustrated in Fig. 4.4a. Indeed the superconductivity in some heavy fermion systems appears to be strongly linked to quantum fluctuations [55]. However, in Fe pnictides HTSC occurs not in the vicinity of QCP, but over wide ranges of composition, often far from the QCP. In these composition ranges T_C tends to be flat, rather than having a maximum at the QCP, as illustrated in Fig. 4.4b. In this case it is more likely that HTSC occurs independent of the AFM order, and the role of the AFM order is merely to suppress T_C.

P. W. Anderson summarized these beliefs, in particular those related to strong electron correlation, into six "dogmas" regarding the nature of HTSC [13]. However, most of them fail to account for the HTSC of Fe pnictides. Particularly the need of the Mott insulator clearly does not apply to Fe pnictides because they are not strongly correlated electron systems. Unless one insists that the mechanisms of HTSC in the cuprates and the Fe pnictides are totally distinct, we are forced to rethink the theories of HTSC. For instance, although it is most likely that the electron correlations play some prominent role in HTSC, Mottness may not be the only way the electron correlation affects the superconductivity. Being a Mott insulator and being a superconductor are two opposite extremes of the transport behavior. The idea of combining the two apparently diametrical ends to create a new state may be a cool idea, but could be a dangerous one.

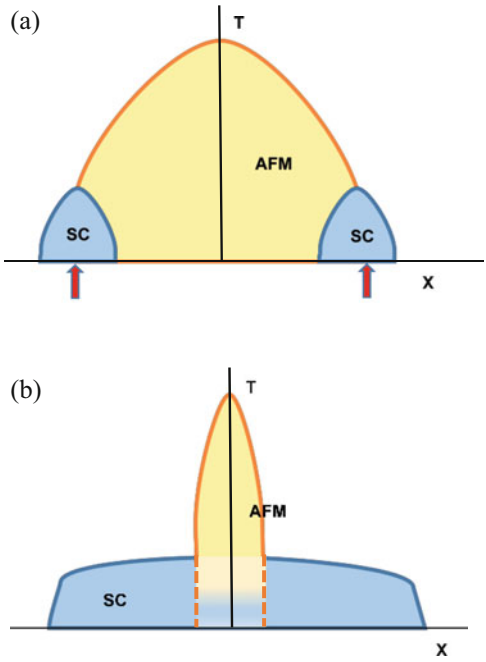

Fig. 4.4 Two scenarios for the phase diagram; x refers to doping, by either hole or electron. (**a**) QCP (*red arrows*) promotes SC, (**b**) AFM suppresses HTSC

Origin of HTSC

Role of the Mottness and AMF Order

In the context of the argument above some of the results on the electron-doped cuprates are quite revealing. In the initial report on the system, $(Nd, Pr)_{2-x}Ce_xCuO_4$, the AFM order extends up to $x = 0.14$, whereas HTSC is observed for a narrow concentration range of $0.14 < x < 0.18$ [56]. However, using a special technique to prevent oxygen from entering the apical site Brinkmann et al. were able to suppress the AFM order and extend the range of HTSC down to $x = 0.04$ [57]. Thus the apparent asymmetry in the phase diagram between the hole-doped and electron-doped HTSC was removed. Furthermore, the recent results on $Pr_{1.3-x}La_{0.7}Ce_xCuO_4$ (PLCCO) by ARPES [58] shows that T_C is almost independent of the doping concentration evaluated from the fermi surface determined by ARPES. Therefore the phase diagram of the cuprates now appears very similar to those of the pnictides as in Fig. 4.4b.

What this means is extremely important. The apparent independence of T_C from the doping concentration means that the concept of doping, which has been widely accepted without any doubt, may not be relevant to HTSC. The concept of doping presumes that the parent undoped phase is the Mott insulator, and doped charge carriers form a small Fermi surface and become superconducting. A corollary is that when the AFM order is suppressed by doping underlying AFM fluctuations

drive HTSC. However, the new data that T_C is almost independent of the doping concentration means that we cannot adopt the small Fermi surface picture which assumes strong AFM fluctuations, and we are forced to come back to the large fermi surface picture where small changes in x have little effects on the fermi density of states. In other words local AFM order is not the determining factor of the electronic behavior. We should then choose the scenario of Fig. 4.4b and conclude that the only role of the AFM phase is to suppress HTSC. If this is true, even the undoped cuprates should exhibit HTSC once AFM order is suppressed, for instance by pressure or isovalent substitution. An attempt to test this bold hypothesis is currently under way.

Another common feature of the HTSC in the cuprates and the pnictides is the magnetic resonance peak observed by inelastic neutron scattering [59–62]. The fact that this was observed for the pnictides means that the resonance peak has nothing to do with the Mottness, and could be explained by the itinerant electron picture [63–65].

Possible Mechanism of HTSC

At this moment we do not have a clear picture on the true origin of HTSC in the cuprates and the Fe pnictides. However, it is possible to speculate on the elements which would constitute the mechanism of HTSC common to both the cuprates and the pnictides.

Spin-Channel *e-p* Coupling

The charge-channel *e-p* coupling is weak, particularly in the cuprates because of the cancellation of the ionic effect and the electronic charge-transfer effect [35]. However, the spin-channel coupling can be strong due to spin-dependent phonon-induced charge transfer [35]. A recent observation of the "forbidden" spin-dependent phonon, the acoustic phonon near the Bragg peak forbidden by symmetry, for the chalcogenides [66, 67] and the cuprates [68] could be a signature of the unconventional spin-channel *e-p* coupling.

Real-Space Polaronic Effect

When the *e-p* coupling is strong the combined *e-p* excitations naturally become polaronic [69, 70]. In particular because the optical phonons responsible for the *e-p* coupling [31, 35, 39] are relatively dispersionless, they can easily be localized and participate in forming polarons. Whereas strongly localized heavy polarons reduce T_C, in the strongly hybridized multi-band model [71] mobility can be restored through hybridization.

Role of the Orbitals

Fe pnictide superconductors are multi-orbital systems with several *d*-orbitals coupled by the Hund coupling [50]. Therefore orbital ordering and excitation can play a role. A recent theory by Kontani [72, 73] proposes that if one goes beyond the conventional adiabatic Migdal-Eliashberg theory and considers the vertex correction, the renormalized Coulomb interaction becomes dependent on spin and orbit. Consequently the orbital excitations can strongly couple to spin, and could contribute to HTSC of Fe pnictides. Because orbitals are intimately coupled to the lattice, this spin-orbital coupling induces spin-channel *e-p* coupling. In the cuprate, on the other hand, only the *p-d* σ-band is involved in the ground state. However, the $d(z^2)$ orbital is close to the fermi level, and is likely to share the doped holes [74]. For this reason possible involvement of the apical oxygen has long been suspected [20, 24, 29, 75]. The $d(z^2)$ orbital occupation is sensitive to the position of the apical oxygen, which has long been known to affect HTSC [76, 77].

Alex and HTSC

The involvement of the $d(z^2)$ orbital and the apical oxygen is precisely the Jahn-Teller effect in an extended sense, which Alex has long been advocating. After 30 years of intense research and many arduous detours, for instance to the Mott state, spin fluctuations and the *t-J* model, we are back to where it all started. Incidentally, Sir Nevil Mott himself did not believe that the Mottness alone will lead to the answer, and believed in the polaron picture [78]. Alex, as well as Nevil Mott, knew that the truth comes out of the minorities, and the majority is always in the wrong.

This field is remarkable not only because of the novelty of the phenomenon and intensity of the competition, but also because of the advances in the experimental techniques it forced on the field. The HTSC phenomenon is so different from anything known so far, and demands much higher precision of measurement to study it. For instance the energy resolution of various methods of spectroscopy, including ARPES and STS, has improved tremendously in order to detect subtle features of the electronic states involved in the HTSC phenomenon. It provided a major drive for the improvement of the precision of the atomic pair-density function (PDF) technique we have been developing. It also prompted many theories to be put forth, although some of them are far-fetched. Furthermore, the discovery of HTSC drove many to study complex oxides and find various exciting properties. It established the research on the correlated electron systems as one of the main foci in condensed matter physics. The overall intellectual impact of the discovery of HTSC is immense, and we have to thank Alex for bringing about such a tremendous gift to us.

Acknowledgment At this happy occasion of congratulating Alex for his 90th birthday, I warmly thank him for leading the field and encouraging us even at the time the majority rushed to opposite extreme directions. Your conviction always inspired us and helped us to come up with more evidence in the right direction. I also thank my collaborators for their passion and endurance which led to valuable contributions, and the colleagues of the same mind in the field, who are too numerous to list here, for making the research so rewarding and enjoyable. This work was supported by the U.S. Department of Energy, Office of Science, Basic Energy Sciences, Materials Science and Engineering Division.

References

1. J.G. Bednorz, K.A. Müller, Z. Phys. B **64**, 189 (1986)
2. J.G. Bednorz, K.A. Müller, Rev. Mod. Phys. **60**, 585 (1988)
3. B.T. Matthias, T.H. Geballe, V.B. Compton, Rev. Mod. Phys. **35**, 1 (1963)
4. J. Bardeen, L.N. Cooper, J.R. Schrieffer, Phys. Rev. **108**, 1175 (1957)
5. D.C. Johnson, H. Prakash, W.H. Zachariasen, R. Viswanathan, Mat. Res. Bull. **8**, 777 (1973)
6. A.W. Sleight, J.L. Gillson, F.E. Biersted, Solid State Commun. **17**, 27 (1975)
7. D. Vaknin, S.K. Sinha, D.E. Moncton, D.C. Johnston, J.M. Newsam, C.R. Safinya, H.E. King, Phys. Rev. Lett. **58**, 2802 (1987)
8. P.W. Anderson, Science **235**, 1196 (1987)
9. A. Bianconi, A. Congiu Castellano, M. De Santis, P. Rudolf, P. Lagarde, A.M. Flank, Solid State Commun. **63**, 1009 (1987)
10. F.C. Zhang, T.M. Rice, Phys. Rev. B **37**, 3759 (1988)
11. V.J. Emery, G. Reiter, Phys. Rev. B **38**, 4547 (1988)
12. A.B. Harris, R.V. Lange, Phys. Rev. **157**, 295 (1967)
13. P.W. Anderson, *The Theory of Superconductivity in the High-T_C Cuprates* (Princeton University Press, Princeton, 1993)
14. T. Egami, W. Dmowski, J.D. Jorgensen, D.G. Hinks, D.W. Capone II, C.U. Segre, K. Zhang, Rev. Solid State Sci. **1**, 247 (1988)
15. W. Dmowski, B.H. Toby, T. Egami, M.A. Subramanian, J. Gopalakrishnan, A.W. Sleight, Phys. Rev. Lett. **61**, 2608 (1988)
16. T. Egami, W. Dmowski, J.D. Jorgensen, D.G. Hinks, D.W. Capone II, C.U. Segre, K. Zhang, in *High-Tc Superconductors III*, ed. by S. M. Bose, S. D. Tyagi. (World Scientific, Singapore, 1988), p. 101
17. B.E. Warren, *X-Ray Diffraction*. (Addison-Wesley, Reading, 1969; Dover, New York, 1990)
18. T. Egami, S.J.L. Billinge, *Underneath the Bragg Peaks: Structural Analysis of Complex Materials*. (Pergamon Press, Elsevier Science, Oxford, 2003, 2012)
19. B.H. Toby, T. Egami, J.D. Jorgensen, M.A. Subrmanian, Phys. Rev. Lett. **64**, 2414 (1990)
20. T. Egami, B.H. Toby, S.J.L. Billinge, C. Janot, J.D. Jorgensen, D.G. Hinks, M.A. Subramanian, M.K. Crawford, W.E. Farneth, E.M. McCarron, in *High-Temperature Superconductivity: Physical Properties, Microscopic Theory and Mechanisms*, ed. by J. Ashkenazi, S. E. Barnes, F. Zuo, G. C. Vezzoli, B. M. Klein. (Plenum Press, New York, 1992), p. 389
21. R.P. Sharma, L.E. Rehn, P.M. Baldo, L.Z. Liu, Phys. Rev. Lett. **62**, 2869 (1989)
22. T. Haga, K. Yamaya, Y. Abe, T. Tajima, Y. Hidaka, Phys. Rev. B **41**, 826 (1990)
23. S.D. Conradson, J.D. Raistrick, Science **243**, 1340 (1989)
24. J. Mustre de Leon, S.D. Conradson, I. Batistic, A.R. Bishop, Phys. Rev. Lett. **65**, 1675 (1990)
25. Y. Bar-Yam, T. Egami, J. Mustre de Leon, A.R. Bishop, *Lattice Effects in High-T_C Superconductors* (World Scientific, Singapore, 1992)
26. http://www.ricmass.eu/superstripes/

27. J.M. Tranquada, B.J. Sternlieb, J.D. Axe, Y. Nakamura, S. Uchida, Nature **375**, 561 (1995)
28. A. Bianconi, N.L. Saini, A. Lanzara, M. Missori, T. Rosetti, H. Oyanagi, H. Yamaguchi, K. Oka, T. Itoh, Phys. Rev. Lett. **76**, 3412 (1996)
29. T. Egami, S.J.L. Billinge, in *Physical Properties of High Temperature Superconductors V*, ed. by D. M. Ginsberg. Lattice Effects in High-T_C Superconductors (World Scientific, Singapore, 1996), p. 265
30. R.J. McQueeney, Y. Petrov, T. Egami, M. Yethiraj, G. Shirane, Y. Endoh, Phys. Rev. Lett. **82**, 628 (1999)
31. J.-H. Chung, T. Egami, R.J. McQueeney, M. Yethiraj, M. Arai, T. Yokoo, Y. Petrov, H.A. Mook, Y. Endoh, S. Tajima, C. Frost, F. Dogan, Phys. Rev. B **67**, 014517 (2003)
32. W.E. Pickett, Rev. Mod. Phys. **61**, 433 (1989)
33. T. Egami, S. Ishihara, M. Tachiki, Science **261**, 1307 (1993)
34. S. Ishihara, T. Egami, M. Tachiki, Phys. Rev. B **55**, 3163 (1997)
35. P. Piekarz, T. Egami, Phys. Rev. B **72**, 054530 (2005)
36. M. Tachiki, M. Machida, T. Egami, Phys. Rev. B **67**, 174506 (2003)
37. R.D. King-Smith, D. Vanderbilt, Phys. Rev. B **47**, R1651 (1993)
38. R. Resta, Rev. Mod. Phys. **66**, 899 (1994)
39. A. Lanzara, P.V. Bogdanov, X.J. Zhou, S.A. Kellar, D.L. Feng, E.D. Lu, T. Yoshida, H. Eisaki, A. Fujimori, K. Kishio, J.-I. Shimoyama, T. Noda, S. Uchida, Z. Hussain, Z.-X. Shen, Nature (London) **412**, 510 (2001)
40. G.-H. Gweon, T. Sasagawa, S.Y. Zhou, J. Graf, H. Takagi, D.H. Lee, A. Lanzara, Nature (London) **430**, 187 (2004)
41. H. Keller, in *Superconductivity in Complex Systems*, ed. by K.A. Müller, A. Bussmann-Holder. Structure and Bonding, vol 114 (Springer, Berlin, 2005), p. 143, and references herein
42. A. Bianconi, Nat. Phys. **9**, 536 (2013)
43. T. Egami, in *High T_C Superconductors and Related Transition Metal Oxides: Special Contributions in Honor of K. Alex Müller and the Occasion of his 80th Birthday*, ed. by A. Bussmann-Holder, H. Keller. (Springer, Berlin, 2007), p. 103
44. Y. Kamihara, T. Watanabe, M. Hirano, H. Hosono, J. Am. Chem. Soc. **130**, 3296 (2008)
45. Z.-A. Ren, W. Lu, J. Yang, W. Yi, X.-L. Shen, Z.-C. Li, G.-C. Che, X.-L. Dong, L.-L. Sun, F. Zhou, Z.-X. Zhao, Chin. Phys. Lett. **25**, 2215 (2008)
46. D.A. Wollman, D.J. Van Harlingen, W.C. Lee, D.M. Ginsberg, A.J. Leggett, Phys. Rev. Lett. **71**, 2134 (1993)
47. K. Nakayama, T. Sato, P. Richard, Y.-M. Xu, Y. Sekiba, S. Souma, G.F. Chen, J.L. Luo, N.L. Wang, H. Ding, T. Takahashi, Europhys. Lett. **85**, 67002 (2009)
48. C. de la Cruz, Q. Huang, J.W. Lynn, J. Li, W. Ratcliff, J.L. Zarestzky, H.A. Mook, G.F. Chen, J.L. Luo, N.L. Wang, P. Dai, Nature **453**, 899 (2008)
49. F. Bondino, E. Magnano, M. Malvestuto, F. Parmigiani, M.A. McGuire, A.S. Sefat, B.C. Sales, R. Jin, D. Mandrus, E.W. Plummer, D.J. Singh, N. Mannella, Phys. Rev. Lett. **101**, 267001 (2008)
50. D.C. Johnston, Adv. Phys. **59**, 803 (2010)
51. C. de la Cruz, W.Z. Hu, S. Li, Q. Huang, J.W. Lynn, M.A. Green, G.F. Chen, N.L. Wang, H.A. Mook, Q. Si, P. Dai, Phys. Rev. Lett. **104**, 017204 (2010)
52. T. Egami, B. Fine, D. Parshall, A. Subedi, D.J. Singh, Adv. Cond. Matter. Phys. **2010**, 164916 (2010)
53. T. Egami, B. Fine, D.J. Singh, D. Parshall, C. de la Cruz, P. Dai, Physica C **470**, S294 (2010)
54. P. Vilmercati, A. Fedorov, F. Bondino, F. Offi, G. Panaccione, P. Lacovig, L. Simonelli, M.A. McGuire, A.S.M. Sefat, D. Mandrus, B.C. Sales, T. Egami, W. Ku, N. Mannella, Phys. Rev. B **85**, 220503(R) (2012)
55. P. Gegenwart, Q. Si, F. Steglich, Nat. Phys. **4**, 186 (2008)
56. H. Takagi, S. Uchida, Y. Tokura, Phys. Rev. Lett. **62**, 1197 (1989)
57. M. Brinkmann, T. Rex, H. Bach, K. Westerholt, Phys. Rev. Lett. **74**, 4927 (1995)

58. M. Horio, T. Adachi, Y. Mori, A. Takahashi, T. Yoshida, H. Suzuki, L.C.C. Ambolode II, K. Okazaki, K. Ono, H. Kumigashira, H. Anzai, M. Arita, H. Namatame, M. Taniguchi, D. Ootsuki, K. Sawada, M. Takahashi, T. Mizokawa, Y. Koike, A. Fujimori, Nat. Commun. **7**, 10567 (2015)
59. J. Rossat-Mignod, L.P. Pegnault, C. Vettier, P. Bourges, P. Burlet, J. Bossy, J.Y. Henry, G. Lapertot, Physica C **185**, 86 (1991)
60. H.A. Mook, M. Yethiraj, G. Aeppli, T.E. Mason, T. Armstrong, Phys Rev. Lett. **70**, 3490 (1993)
61. A.D. Christianson, E.A. Goremychkin, R. Osborn, S. Rosenkranz, M.D. Lumsden, C.D. Malliakas, I.S. Todorov, H. Claus, D.Y. Chung, M.G. Kanatzidis, R.I. Bewley, T. Guidi, Nature **456**, 930 (2008)
62. M.D. Lumsden, A.D. Christianson, D. Parshall, M.B. Stone, S.E. Nagler, H.A. Mook, K. Lokshin, T. Egami, D.L. Abernathy, E.A. Goremychkin, R. Osborn, M.A. McGuire, A.S. Sefat, R. Jin, B.C. Sales, D. Mandrus, Phys. Rev. Lett. **102**, 107005 (2009)
63. I.I. Mazin, V.M. Yankovenko, Phys. Rev. Lett. **75**, 4134 (1995)
64. T.A. Maier, D.J. Scalapino, Phys. Rev. B **78**, 020514(R) (2008)
65. M.M. Korshunov, I. Eremin, Phys. Rev. B **78**, 140509(R) (2008)
66. D.M. Fobes, I.A. Zaliznyak, J.M. Tranquada, Z. Xu, G. Gu, X.-G. He, W. Ku, Y. Zhao, M. Matsuda, V.O. Garlea, B. Winn, Phys. Rev. B **94**, 121103(R) (2016)
67. J. Niedziela, Ph. D. thesis in physics, the University of Tennessee at Knoxville, 2012
68. E.S. Bozin, R. Zhong, K.R. Knox, G. Gu, J.P. Hill, J.M. Tranquada, S.J.L. Billinge, Phys. Rev. B **91**, 054521 (2015)
69. J. Ranninger, in *Polarons in Bulk Materials and Systems with Reduced Dimensionality*, ed. by G. Iadonisi, J. Ranninger, G. De Filippis. (Italian Physical Society, Bologna, 2006), p. 1
70. D. Emin, arXiv: 1611.05813 (2016)
71. A. Bussmann-Holder, K.A. Müller, R. Micnas, H. Büttner, A. Simon, A.R. Bishop, T. Egami, J. Phys. Condens. Matter **13**, L169 (2001)
72. R. Tazai, Y. Yamakawa, M. Tsuchiizu, H. Kontani, Phys. Rev. B **94**, 115155 (2016)
73. Y. Yamakawa, H. Kontani, arXiv: 1611.05375 (2016)
74. C.T. Chen, L.H. Tjeng, J. Kwo, H.L. Kao, P. Rudolf, P. Sette, R.M. Fleming, Phys. Rev. Lett. **68**, 2543 (1992)
75. H. Kamimura, Y. Suwa, J. Phys. Soc. Jpn. **62**, 3368 (1993)
76. Y. Ohta, T. Tohyama, S. Maekawa, Phys. Rev. B **43**, 2968 (1990)
77. E. Pavarini, I. Dasgupta, T. Saha-Dasgupta, O. Jepsen, O.K. Andersen, Phys. Rev. Lett. **87**, 045003 (2001)
78. N.F. Mott, in *Polarons and Bipolarons in High-T_C Superconductors and Related Materials*, ed. by E. K. H. Salje, A. S. Alexandrov, W. Y. Liang. (Cambridge University Press, Cambridge, 1995), p. 1

Chapter 5
Encounters with Alex

Kristian Fossheim

In the 80th anniversary book for Alex Müller I wrote a story of our scientific collaboration, *Shared Fascinations*. This time I will be more personal, about the human side of our collaboration and encounters, while also referring to episodes mentioned in *Shared Fascinations*.

Early Days

Our collaboration started in 1968. I had returned to Oslo from University of Maryland in the fall of 1967 after 2 years there, first on a NATO Fellowship, then as an appointed research associate. I had become totally fascinated by superconductivity, and had in particular been captivated by the sudden change of properties at the transition temperature. I had observed, and described theoretically, the transition of submillikelvin sharpness in metals. Alex and I had never met, but we now agreed, thanks to contact through our common friend Jens Feder, to collaborate in the study of another type of solid state transition, the structural change occurring in $SrTiO_3$.

We collaborated via telephone calls between University of Oslo and the IBM lab in Rüschlikon, near Zurich. Based on results from ultrasonic measurements, we soon agreed to write a paper for PRL on critical attenuation of high frequency acoustic waves near the structural phase transition in $SrTiO_3$ at $T_c = 125$ K, in a collaboration with my old physics mate from student days, Bjørn Berre. I always made sure IBM got the telephone bill since telephone calls abroad were fiercely expensive in those days. One colleague in Oslo almost got his phone confiscated

K. Fossheim (✉)
NTNU, Trondheim, Norway
e-mail: kristian.fossheim@ntnu.no

A. Bussmann-Holder et al. (eds.), *High-Tc Copper Oxide Superconductors and Related Novel Materials*, Springer Series in Materials Science 255,
DOI 10.1007/978-3-319-52675-1_5

because he made so many long international calls. Our paper was sort of a breakthrough since it seemed to show that the behaviour in $SrTiO_3$ was dominated by order parameter fluctuations, hence not classical, or Landau-like, while at the same time Alex had shown classical temperature exponent for the order parameter on approaching T_c. To investigate this further, Bjørn and I did additional measurements of elastic properties by means of sound velocity. Instead of a smooth transition from one level to another across the transition, we found a minimum, thus indicating non-classical, non mean-field like behaviour.

Now it was time, in 1970, to go to a meeting on phase transitions in Varenna, at Lago di Como, from Trondheim, where I had just moved. On the way I flew via Zurich, half-way planning to visit Alex at the Rüschlikon lab. Somehow, I was so much in awe of this man whom I had never met, only spoken with on the phone, that I continued to Varenna without visiting the lab. I am sure he could never suspect this, and I never told him the reason. When we finally met in Varenna, I saw a strong-minded black-haired, slightly moustached sharp-looking guy, confirming my impression that this was a very determined and intelligent man, who deserved my greatest respect. Even though I had just spent 2 years among great physicists at University of Maryland, like Richard Ferrell and Rolf Glover, I thought this was a really tough one. He was only 9 years older than I, but this represented a huge gap in knowledge and experience in my mind, not least because I discovered he spoke both French and Italian fluently, in addition to English, German and Swiss- German dialect, with a rasping r. In addition he was a true champion of EPR, which was outside my experience at the time.

However, in spite of everything, it still turned out I had something important to teach him: The velocity minimum of sound at T_c in $SrTiO_3$, indicating non-classical behaviour, thus contradicting Alex's measurements of the order parameter. He became very interested, and immediately suggested that Bjørn and I should write a PRL. I thought the data were not quite up to PRL standard, and did not follow the advice. But Alex went straight back to Zurich after the meeting, measured much more carefully close to the transition, and found an order parameter exponent of about 0.3 instead of 0.5 very close to T_c. I believe this was the first instance where a non-classical exponent was measured at a structural phase transition. Alex, on the other hand, soon published a PRL on his new data, and the matter was settled.

I guess Alex was pleased with this outcome, and I got the message from another physicist at IBM that I was being considered for a job there. Eventually, instead, I was invited for two summer stays, in 1973 and 1975, when I worked on totally different matters with Ulrich Høchli. During conversations with Alex I understood he was much aware of my experience in superconductivity from Maryland and Oslo, where I had several PRLs, and other papers. Alex told me he never really worked in that field. I got the impression he half way envied me this experience. We all know this would change dramatically later on!

I also discovered that Alex was an automobile *aficionado* and had a Plymouth Valiant, just like me, except I had a newer model, 1967. I understood he was his own mechanic, and shared this interest with his colleague Heini Rohrer who also had a Plymouth Valiant. In addition, as it would later turn out, Alex had several

cars, including a 12 cylinder Rolls Roys, in which I was invited many years later to ride with him and Inge to a concert in Zurich.

Some Differences

During my sabbatical at IBM Thomas J Watson Research Center 1975–1976 one of my main goals was to get involved with the newly developed ultrasonic phase conjugation techniques in the study of solids. I worked there with Norm Shiren, Bob Melcher and Koji Kajimura. Again, Alex's name came up. He made us aware of work at the Ioffe Institute in Leningrad, where even powders showed echo-like phenomena in the spirit of spin echo. The three of us set out to work on it, and it became a major project. Norm Shiren had established the technique in so-called echo single crystal materials which showed this highly nonlinear effect of "time reversal". I came upon the idea to use it as a tool, where the echo material would work like a very advanced time reversal transducer, and could be used to study another material which could be attached. I recruited a PhD student, Rune Holt, in Trondheim, to use this method when studying critical phenomena at phase transitions where any small inhomogeneities would distort the signals. This was a very successful research project, and again the phase transition in perovskite materials was the object.

In this connection a misunderstanding happened, where Alex referred to our method as invented by Shiren. I protested, and there was a somewhat heated exchange between us. I believe I was able to explain the real situation, eventually.

In 1983 I invited Alex to Trondheim to smooth out things for one more reason: One of my PhD students, Sigmund Stokka, a very talented, strongminded fine guy had been doing a nice job to reveal the predicted crossover behavior in perovskites like $SrTiO_3$. By specific heat measurements the phase boundary between cubic and tetragonal structure under pressure was determined, and led to determination of the corresponding crossover exponent of 1.25, for the first time, in $SrTiO_3$, a project Alex had had on his wish list, but not yet accomplished. Sigmund and I had discussed the reference list in the ensuing paper, and there was a reference to Alex's work I wanted to include. Sigmund disagreed, and I said "This will give me trouble with Alex." Sure enough, it did. Alex let me know. Now, Sigmund had left for a job in Stavanger. What could I do? I invited both of them to Trondheim, and the issue was brought up in a meeting between the three of us in my office. Alex was not in a good mood, and Sigmund stubbornly argued his case. There was a stalemate. Then I told Alex: "You have to let young people do some mistakes." Alex immediately softened and agreed. The case was closed right there.

I offered Alex to take my Valiant and look around Mid-Norway with Inge, which they enjoyed. Next, he came along to our cabin on the coast together with my wife, Elsa, and our son Terje, while Inge took the Costal Steamer to Bergen to experience the famous mountain railway to Flåm, and the magnificent Sognefjord. Meanwhile, at the cabin, we experienced a great storm in Taftøysund, and our boat, which was

moored in the harbour, was in trouble. Alex, Terje and I climbed down a very steep rock to the water and saved the boat. An operation Alex enjoyed. The cabin was primitive style where everything had to be carried in and carried out, and Alex took his turn helping Elsa in the kitchen. The cabin was quite new, and Alex was our first guest there. Regrettably, we did not even yet have a guest book for the record of visits, and surely we did not anticipate the fame our first guest would reach. Alex often later referred to the visit and the rescue operation as a nice experience.

Later, Alex continued the crossover experiments in his own lab, and got precisely similar results as we had, but in a different material, $LaAlO_3$. I have to admit I was proud to have been first. Apparently, the PRL referee was not equally impressed, and did not want to follow the story of this new exponent in the saga of critical phenomena, so Physical Review would have to do.

Stockholm

When the news of the discovery of cuprate superconductors came out, I was astonished at the fact that exactly those insulating materials we had collaborated on were at the center of the discovery. It was already late, formally speaking, for nominations for the Nobel prize in physics. But I had regularly received invitations to nominate. I had already nominated Binnig and Rohrer for the 1986-prize, and I surely did not miss the opportunity this time, although I am afraid it was a close call. Very briefly I stated that the discovery was so obviously worthy of the prize, that the world would not understand it if this opportunity was missed. On the day of official announcement I was sitting in my office counting down minutes before the official broadcast from Stockholm. It was full score! Bednorz and Müller got it. My fax to IBM Rüschlikon, congratulating the winners, was sent just minutes later, and apparently it was one of the first they received, maybe the very first.

On approaching December 10, 1987, I received official letter from the Swedish Academy that my wife and I were invited for the event, and hotel reservations were made at Grand Hotel where all the laureates and their families were to stay. So we had been invited on the laureates' quota by Alex. We flew over and moved in, and found a printed program on our hotel bed where, to our surprise, our modest presence was included. Grand Hotel in Stockholm has a dignity and style fit for the occasion.

In the evening, walking out of the hotel door for a minute to draw some fresh Stockholm air, I spotted a tall man standing there looking at the hotel facade. I recognized him, walked up to him and greeted him. It was Heini Rohrer, recipient of the physics prize the year before, shared with Gerd Binnig, also from the IBM lab in Rüschlikon, in itself an unbelievable and unprecedented occurrence. I asked Heini why he was standing there instead of going inside. He said he wanted to recall the experience from the year before and would not enter Grand Hotel again. He wanted to cherish and protect his memory from that time.

Fig. 5.1 In Stockholm at the Nobel banquet in 1992: From the *left*, Alex, Inge, Kristian Fossheim, Elsa Fossheim, Oystein Fischer, Mrs Kitazawa, Hanne Fischer

We were treated practically like family member. During the award ceremony in the Concert Hall Elsa and I were given seats up front with the laureates' families, with Inge. Elsa was of course dressed in the finest outfit she ever wore, and to her great satisfaction, her green dress matched perfectly with that of queen Silvia!

The ensuing banquet in the City Hall was out of this world. A procession came along the balcony and down to the hall, headed by King Carl Gustav and Inge. The food was just exquisite, and had been in preparation for months. I believe Alex gave the after dinner speech, but I am sorry to say I have forgotten the contents. After dinner there was dance in the fabulous room above and aside from the main hall, and we met Alex's father and could see him dance there, very much able. Alex was himself close to 60, so his father must have been well into his 80s. We had the pleasure to join the dance before retreating at midnight. During the night we met several other great friends from the superconductivity science scene. In a very happy photo shot I still have, Fig. 5.1, but this one from my next visit to the Nobel ceremony in 1992, there are Alex and Inge, Øystein and Hanna Fischer from Geneva, and Mrs Kitazawa from Tokyo, my wife and I, the shot having been taken by Koichi Kitazawa. Of these, two great men and friends, Øystein and Koichi both have left us in recent years, to our grief and sorrow.

Trondheim Again

The life of a Nobel laureate is a whirlwind, before as well as after the event. Personally, I had long ago booked Alex for a visit to Trondheim, directly after Stockholm. So he came with Inge. I received them at the airport with the official

Fig. 5.2 Alex and the author on Alex's visit to Trondheim just after receiving the Nobel prize in 1987. Outside the author's office. Both wearing the ties we received at a reception given by physics students at the University of Stockholm

limousine of the university, riding back to Trondheim with our guests, joined also by our rector. Of course, our guests were installed at Trondheim's finest hotel, Britannia. Later, the same evening we took Alex and Inge to our house for dinner where Elsa served a salmon dish, and I had chosen a German *spätlese* to go with it. As soon as we had finished, I offered Alex my new and comfortable armchair, which Elsa had given me for my 50th birthday. Alex quickly fell asleep. Finally, he could relax completely among friends! He needed it badly. Figure 5.2 is a picture from Alex's visit to my institute.

However, next day was another busy day with interviews by several media, and a lecture before a packed audience of 250 or more, meeting with my group, and finally a well prepared banquet at the university's representation building, the Lerchendal Mansion, with leading persons from the university and from IMB Norway who sponsored the event. In my speech during dinner I said that when I was collaborating with Alex in the 1970s I often thought that this physicist was of a caliber which would have earned him the Nobel prize, had he worked in a popular field like superconductivity. But he was not there at the time. Well, eventually he did come to superconductivity, and here he was, having won the prize.

For entertainment I had invited our son Øyvind and his talented music student friend Cecilia. Inge remarked that she could see a future as a really fine violinist in our son, but added that it would be very costly for him to prepare for an international career. Of course, Inge knew the world of music, herself having been an established soprano. At that time I thought wrongly that music would be like physics, just a matter of following the usual university path and work hard. I have

later learned that the area of music is very different, and much tougher. The performance brought back memories from the summer of 1973 when I was at the IBM lab with Alex, and we visited their home in a small village behind the Albis, with our children, Kristin 10, Terje 6 and Øyvind 4. At the barbeque outside their house, Alex was charmed by the small boy Øyvind. He gave him a half dollar coin and commented: "He looks you in your eyes, and you melt!" Well, here at the Lerchendal Mansion was Øyvind again, now an 18 years old, young man. I recalled then, that it was the 16th of December, Beethoven's birthday, and also the date of my thesis defence at University of Oslo many years back. After Øyvind and Cecilia had played, I followed them to the car and waived them off. After that evening they were fiancées. They married some years later, and became parents of two great boys: Andreas, now an ambitious physics student at my university, following in the footsteps of his grandfather it seems, and Yngve, a very talented chess- and football player, dreaming to be a football star. Both Øyvind and Cecilia were soon to become permanent members of the Oslo Philharmonic Orchestra. But as it often happens, have established new families. Alex has since mentioned this particular visit to Trondheim on several occasions, as a nice experience.

Two on the Roof, in Pisa

Of the many episodes and encounters I have had with Alex, perhaps one stands out specially. In the aftermath of the discovery of the high-T_c superconductor YBCO I specially wanted to do two things: (1) Measure the specific heat anomaly at T_c, looking for non-BCS like behavior due to the low concentration of carriers, and (2) measure the elastic behavior for lattice softening related to the high T_c. Alex and George Bednorz immediately provided the samples we needed. At the first European high-T_c meeting in Pisa in the spring of 1987 I could report quite unusual elastic behavior: a strong softening of the lattice on cooling to low temperatures. This was exciting, since it might be related to cooper-pair creation at unusually high temperature. Times were very busy, and on the plane from Copenhagen to Milano I finally wrote a handwritten version of a paper with Alex and George, accompanied by a taste of *Chianti classico*. On arriving in Genova for the meeting, Alex was in a constant whirlwind of people who wanted his attention. How could we have a few moments alone to discuss the paper? We found a stairway leading up to the roof. We got out there and sat down in the sunshine. I handed Alex my handwritten note. He read through, gave it back to me, and said "OK, publish." The paper soon appeared in Solid Sate Communications, and was very regularly cited. It also turned out I had been right about the non-classical specific heat. In my group we measured a broad transition, quite different from the BCS picture which has an extremely sharp onset of the transition coming from above in temperature. In low-T_c classical superconductors I had already at Maryland shown that the transition could be defined with a sharpness of sub—millikelvin, as mentioned. This was indeed different, more like a thousand times broader, absolutely not BCS- like! The problem was, literally nobody else seems to have any clue about the fundamental

difference between this anomaly and that of usual low-T_c. Everybody analyzed the anomaly as BCS-like. It took many, many years before people in the field understood, or accepted, that this was a fundamentally different case, that vortex fluctuations played a major role, as Asle Sudbø and his students in Trondheim calculated convincingly.

Alex in Trondheim Again: Doctor Honoris Causa

In 1992, the board of the University of Trondheim had put me in charge of a new strategic research office, called the Research Academy of the University of Trondheim. Alex was selected that year as the university's only candidate to be conferred the title of Doctor Honoris Causa. It was awarded in a major ceremony in which all new PhDs of the entire university that year were given their diploma. It was, in fact, the first such event, and my responsibility, and I had chosen the great rotunda of the Student Union building for the ceremony. I gave the required ceremonial speech for Alex, as well as the after dinner speech at the banquet in the evening. In that speech in 1992 I talked about future challenges in science, and mentioned three special examples, quote:

1. *Understanding the human brain is a science yet in its infancy. Gaining deeper insights into this marvelous instrument belongs to the greatest challenges in science today. What can we expect the future will bring?*
2. *The genomes of life forms show broad variations which we are just beginning to map out. This is an urgent task, since, as it is said sometimes: "The library of life is on fire." The destruction of life forms must be stopped! And genetic science must be kept on a constructive course.*
3. *Chemistry and physics offer infinite possibilities for new substances and materials, with, as yet, unimagined consequences for science and technology.*

It is tempting to comment on these points today: Regarding point 1 above, the later Nobel laureates May-Britt and Edvard Moser who received the Nobel prize for their brain research at our university in 2015, were at that time, 1992, students in Oslo. Regarding point 2, the human genome was unraveled some 10 years later. And I have myself taken the initiative, and conducted the award process of the first major global prize for sustainability science, in Trondheim, The Gunnerus Sustainability Award, while president of the Royal Norwegian Society of Sciences and Letters, first time in 2012. Regarding point 3, it is especially interesting to point out the later huge developments in nanoscience.

As a kind of amusing *a propos*, between the ceremony and the banquet, I took Alex on foot to the center of the city to inspect an outdoor display of American veteran cars, shown in Fig. 5.3. He made his expert comments and enjoyed the display. The next day, I gathered my PhD students and their families and Alex for a 2 h hike in Bymarka, the wide outdoor area and hills west of Trondheim, Alex wearing my old checkered sweater, as photos from the tour show. I still keep it in my closet, known as it is in the family as the "Müller sweater." Figure 5.4 is from that trip.

Fig. 5.3 Alex and the author visiting an American car display in Trondheim, on the day of the honorary doctor degree ceremony in Trondheim in 1992

Fig. 5.4 Alex and the author on an outing trip near Trondheim the day after he received his honorary doctor degree from University of Trondheim (NTNU) in 1992

Nobel Book and Followup

In 2004 I published a textbook on superconductivity and its applications with my colleague Asle Sudbø. In preparation for this, I traveled along the East Coast of the US, and in Europe, to interview Nobel laureates for a chapter on personalities who have contributed most to the development of the field. Later, these interviews were

Fig. 5.5 Alex in his *Tertianum* office in 2012

printed in full in a book on Springer in 2013: *Discoveries and Discoverers. Ten Nobel Laureates Tell Their Story*. My interview with Alex took place in his office at University of Zurich, and he told vividly about his life, his venture into the field of superconductivity at the age of fifty, like a graduate student he said, during a stay at IBM Thomas J Watson Research Center in New York. And later experiences were covered, of course.

My book was published almost 10 years later. Before that, in the winter of 2012, I visited Alex and Inge who had moved to their *Tertianum*, a Swiss term for retirement homes, where he still enjoyed working in his private office, and where diplomas and reminiscences from all his 22 honorary degrees could be spotted, shown in Fig. 5.5. The whole place was in fact a very nice setting, fitting his status. As a kind of an ironic case, among the inhabitants of the place, Alex pointed out a small, very old man who, he said, had been a German general during World War 2. I was invited to lunch with Inge and Alex in the very nice restaurant of the place. They were both in a good mood, and later Alex and I discussed both history and the contents of the interview. As usual, Alex, at 85, had done his homework, and was as keen on physics as ever, showing his most recent publications.

Since then I learned that my visit had been much appreciated, and our contacts continue. Old friendship has not faded away, and as far as Alex's stamina in physics is concerned: No end in sight!

My encounters with Alex have happened in numerous countries and places all over the Northern Hemisphere. He has been my greatest inspiration in physics, and through this has enriched my life and that of my entire family.

Just as I am writing these lines, the Nobel prizes for physics 2016 are announced. Again, phase transitions of matter are the focus. It reminds me that both Alex and I have had the privilege to participate in, and observe, this progress in one of mankind's great adventures in science. And the search shall continue through new scientific landscapes for the benefit of the whole world.

Chapter 6
The Barocaloric Effect: A Spin-off of the Discovery of High-Temperature Superconductivity

Albert Furrer

Introduction

The magnetocaloric effect, *i.e.*, cooling by adiabatic demagnetization is a well-known technique in condensed matter physics [1]. The effect is a consequence of the variation in the total entropy of a solid by the magnetic field. In a first stage, an external magnetic field is applied isothermally (the system is in contact with a heat sink), thus reducing the magnetic entropy of the system. In a second stage, the magnetic field is removed adiabatically (the system is decoupled from the heat sink). In order to keep the entropy unchanged, the system is forced to reduce the temperature. Magnetic refrigeration has proven to be one of the most efficient cooling techniques in a wide range of temperatures up to room temperature and above [2].

Up to now, all magnetic refrigerators have suffered from the drawback of needing large magnetic fields of a few T in order to achieve cooling effects in the K range. In order to overcome this problem, Alex Müller proposed already in 1984 an alternative, namely to implement adiabatic cooling by the application of pressure. More specifically, he proposed to make use of the pressure-induced structural phase transitions in $PrAlO_3$, which are accompanied by changes of the point symmetry of the Pr^{3+} ions. This results in different splittings of the (2 J + 1)-fold degenerate ground-state multiplet by the crystal field, which governs the thermodynamic properties of the system at low temperatures. Hence the external pressure may well serve to change the magnetic entropy in the very same way as an external magnetic field does in the magnetocaloric effect (MCE). In analogy to the latter,

A. Furrer (✉)
Laboratory for Neutron Scattering, Paul Scherrer Institut, 5232 Villigen PSI, Switzerland

SwissNeutronics AG, Bruehlstrasse 28, 5313 Klingnau, Switzerland
e-mail: albert.furrer@psi.ch

A. Bussmann-Holder et al. (eds.), *High-Tc Copper Oxide Superconductors and Related Novel Materials*, Springer Series in Materials Science 255,
DOI 10.1007/978-3-319-52675-1_6

Alex Müller gave the associated effect the name barocaloric effect (BCE). His idea was patented in several countries [3].

In what follows, I will discuss the developments and the results obtained by barocaloric cooling in co-operation with Alex Müller. The joint research efforts went considerably beyond the originally proposed mechanism based on structural phase transitions and included pressure-induced changes of a variety of phenomena such as magnetic phase transitions, the 4f-conduction-electron hybridization in Kondo systems, valence transitions, and spin fluctuations [4]. Finally, I will briefly summarize some of the key results obtained for high-temperature superconductivity by neutron scattering experiments jointly performed with Alex Müller.

The Barocaloric Effect (BCE)

Basic Principles

Structural phase transition in rare-earth (R) based perovskites usually occur as a function of temperature, but they can also be induced by the application of magnetic fields or pressure. If in one phase the R ions have a non-degenerate ground state and in the other a degenerate one, then cooling can be achieved under adiabatic application (or removal) of pressure (hydrostatic or uniaxial) due to the change of the entropy. The total entropy $S = S_m + S_e + S_p$ has magnetic, electronic, and phononic contributions, respectively. For rare-earth compounds and low temperatures, the magnetic entropy is the dominating contribution, which is determined by the (2 J + 1) split energy levels of the ground-state J-multiplet of the R ions:

$$S_m = -Nk_B \sum\nolimits_i p_i \ln(p_i), \quad p_i = \exp(-E_i/k_B T)/Z, \tag{6.1}$$

where N is the total number of R ions in the system, k_B the Boltzmann constant, p_i the Boltzmann population factor of the energy levels E_i, and Z the partition function. The energy splittings due to the crystal-field interaction can be determined directly by the inelastic neutron scattering (INS) technique as exemplified in Fig. 6.1 for $Pr_{1-x}La_xNiO_3$ with different La concentrations x [5]. For $x = 0.15$ the compound is in the orthorhombic Pbnm phase where the crystal-field interaction completely lifts the ninefold degeneracy of the ground-state multiplet of the Pr^{3+} ions, thus resulting in a singlet ground-state. For the rhombohedral R-3c phase corresponding to $x = 0.70$, some of the crystal-field levels remain degenerate, and the ground state is a doublet. Figure 6.2 shows the corresponding entropy curves calculated from Eq. (6.1) which exhibit a very different behavior over the whole temperature range and only merge together at very low temperatures [6].

Let us assume that the system is in the orthorhombic Pbnm phase at $T = 150$ K, say at the point A marked in Fig. 6.2. We now perform the process of adiabatic pressurization. The system is isolated from its surroundings and an external pressure is

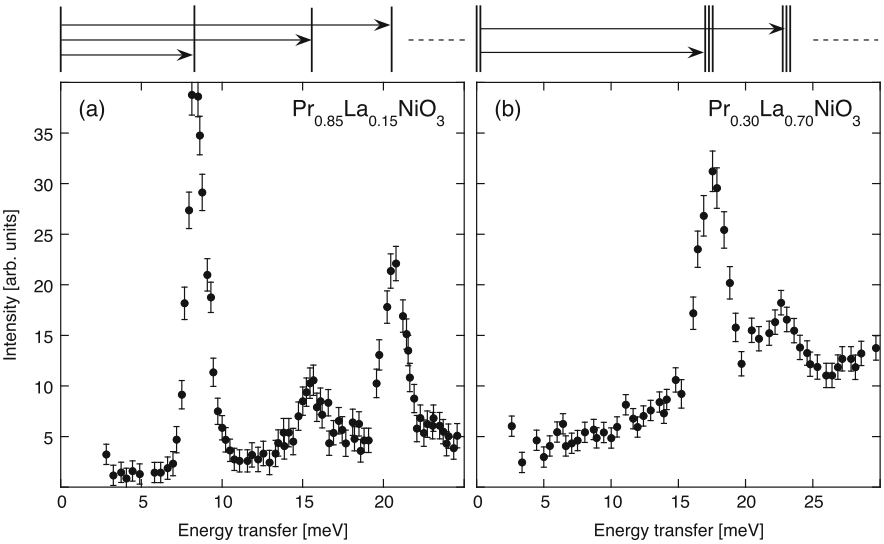

Fig. 6.1 Energy spectra of neutrons scattered from $Pr_{1-x}La_xNiO_3$ taken at T = 10 K and modulus of the scattering vector Q = 2.5 $Å^{-1}$ with x = 0.15 (**a**) and x = 0.70 (**b**) [5]. The *top* displays the crystal-field level sequence derived from the data, and the *arrows* mark the observed transitions. Some of the higher-lying crystal-field levels are not shown

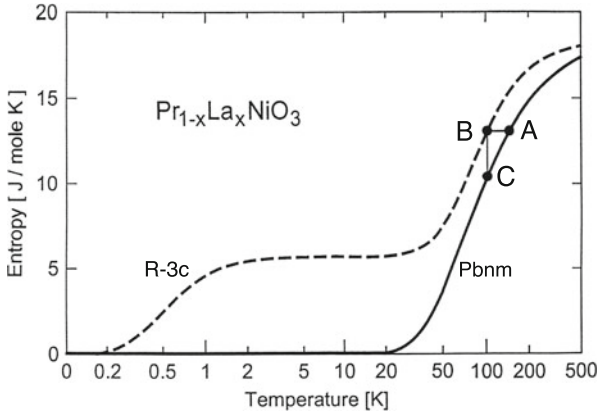

Fig. 6.2 Magnetic entropy calculated for the rhombohedral R-3c (*dashed line*) and orthorhombic Pbmn (*full line*) phases of $Pr_{1-x}La_xNiO_3$

applied such that the system transforms to the rhombohedral phase R-3c, thereby moving horizontally to the point B. The effect of this process is to lower the temperature significantly. For the next step the sample must be allowed to remain in contact with a heat sink, so that the process is isothermal. The sample is depressurized and moves vertically to the point C. In order to cool the system further down, the process of adiabatic pressurization and isothermal depressurization is repeated several times until the lowest possible temperature of about 200 mK is reached (see Fig. 6.2).

Structurally Driven BCE

$PrLaO_3$

The perovskite compound $PrAlO_3$ exhibits a series of structural phase transitions from cubic to rhombohedral to orthorhombic to monoclinic and ultimately to tetragonal symmetry at temperatures of 1320, 205, 151, and 118.5 K, respectively [7–10]. The crystal-field level splittings of the Pr^{3+} ions considerably change across these phase transitions [9]. For instance, in the rhombohedral phase (space group R-3c) the crystal-field ground state is a non-Kramers doublet, whereas in the low-temperature tetragonal phase (space group Pbnm) the crystal-field ground state is a singlet. The phase transitions at 205, 151, and 118.5 K can be suppressed by the application of uniaxial pressure along the (111)-direction, so that the rhombohedral phase can be stabilized at low temperatures. This opens the way for barocaloric cooling as described in the previous paragraph.

INS experiments were planned to investigate the pressure-induced effects on the magnetic excitation spectrum of $PrAlO_3$. For that purpose, Alex Müller and his technician W. Berlinger constructed a uniaxial pressure device for neutron scattering applications as described in [11]. The stress is generated in a hydraulic cylinder and transmitted through a plunger onto the single-crystal sample mounted in a cryostat. The assembly allows the application of a variable force up to 10^4 N at temperatures between 2 and 300 K. Unfortunately, the experiments performed in the year 1985 turned out to be unsuccessful, since the single crystals always broke already at moderate pressures. Nevertheless, Alex Müller generously allowed to use the pressure device for other research projects. This opportunity was an extremely welcome extension of the sample environment for neutron scattering experiments at my laboratory and featured many successful applications such as the determination of (p,T) phase diagrams (see, *e.g.*, the example described in [11]).

$Pr_xLa_{1-x}NiO_3$

The discovery of high-temperature superconductivity temporarily pushed away Alex Müller's research interests from barocaloric cooling, but in the year 1991—at a lunch during a conference in Kanazawa (Japan)—he showed me a preprint of a research work carried out by Jerry B. Torrance (IBM San Jose, USA) [12]. In his letter Jerry Torrance wrote: "Rumor spreads fast, especially when popular personalities are involved! I have heard that you are interested in the insulator-metal phase transitions we have found in rare-earth nickel compounds". Indeed, the $RNiO_3$ compounds turned out to be extremely suitable systems for barocaloric cooling. More specifically, the mixed compound $Pr_{1-x}La_xNiO_3$ undergoes a structural phase transition (SPT) from a high-temperature rhombohedral R-3c to a low-temperature orthorhombic Pbnm phase in the concentration range $0 \leq x \leq 0.7$ [5, 13]. The temperature T_{SPT} is strongly dependent on the La

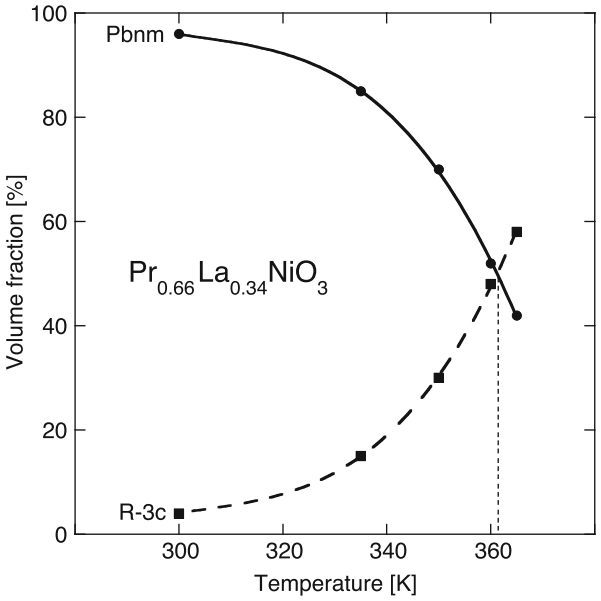

Fig. 6.3 Temperature dependence of the volume fraction of the rhombohedral R-3c phase (*dashed line*) and the orthorhombic Pbnm (*full line*) phases determined for $Pr_{0.66}La_{0.34}NiO_3$ by neutron diffraction [14]

concentration x: For $x = 0$, we have $T_{SPT} \approx 700$ K, and $dT_{SPT}/dx \approx -1000$ K. The SPT exhibits a peculiar temperature behavior as shown for $Pr_{0.66}La_{0.34}NiO_3$ in Fig. 6.3. The region in which the SPT occurs turns out to be very broad, *i.e.*, the two phases coexist in a rather large temperature range, thus $T_{SPT} = 361$ K is defined as the temperature where the R-3c and Pbnm phases have equal weight. The application of hydrostatic pressure was found to shift T_{SPT} to lower temperatures, typically by $dT_{SPT}/dp \approx -5$ K/kbar. This means that external pressure modifies the sample such that the volume fraction of rhombohedral symmetry is enhanced at the expense of the orthorhombic component. As mentioned above, the SPT is accompanied by a change of the degeneracy of the crystal-field ground state, so that barocaloric cooling becomes possible as illustrated in Fig. 6.2. Moreover, by varying the La concentration x, the working point for barocaloric cooling can be chosen at any temperature between 1 and 700 K.

The theoretical predictions of barocaloric cooling were verified in experiments performed for $Pr_{0.66}La_{0.34}NiO_3$ with $T_{SPT} = 361$ K [14]. The setup for the pressure experiments is schematically shown in Fig. 6.4. The sample is enclosed in a cylindrical pressure cell of 5 mm diameter and 6 mm height, which allowed the *in situ* measurement of the sample temperature. The results are summarized in Fig. 6.5. At an initial temperature of 300 K and for hydrostatic pressures up to 15 kbar the compound is predominantly in the orthorhombic state (see Fig. 6.3). Through the application of pressure the compound gains elastic energy, *i.e.*, its entropy is lowered and the sample warms up. A similar situation is encountered at 400 K where the compound is predominantly in the rhombohedral state. At 350 K, however, the application of pressure results in a significant increase of the rhombohedral volume fraction, so that the compound experiences—in addition to the

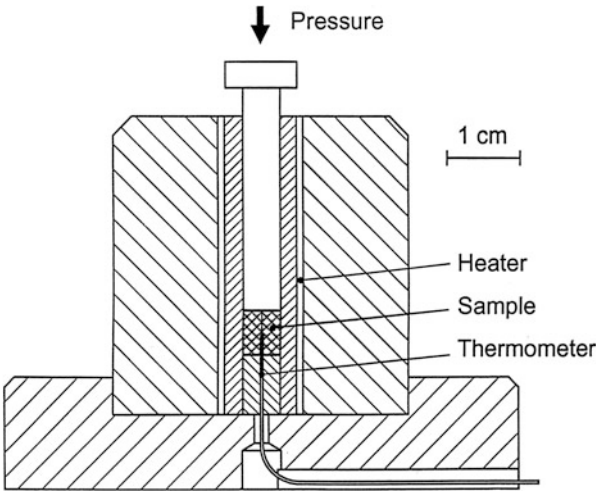

Fig. 6.4 Schematic drawing of the pressure cell

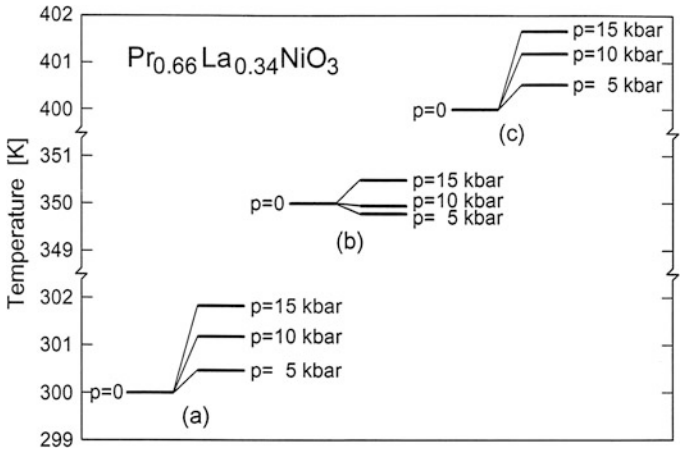

Fig. 6.5 Variation of the temperature of a $Pr_{0.66}La_{0.34}NiO_3$ sample upon applying a hydrostatic pressure up to 15 kbar for initial temperatures of 300 K (**a**), 350 K (**b**), and 400 K (**c**) [14]

elastic heating—the magnetic cooling as described in the previous paragraphs, *i.e.*, we have a situation with two competing effects. As shown in Fig. 6.5b, we observe a slight cooling of the compound for p = 5 kbar, *i.e.*, the magnetic cooling exceeds the elastic heating. For p = 10 kbar we observe an almost perfect counterbalance of the two competing effects. For p = 15 kbar the elastic heating dominates the magnetic cooling.

The undesired effect of elastic heating observed in the above experiments can be drastically reduced by using single crystals and uniaxial pressure. Subsequently we followed this route by studying the BCE in a series of suitable single crystals and

extended the method to include—in addition to the structurally driven BCE demonstrated for $Pr_{0.66}La_{0.34}NiO_3$—other sources of pressure-induced entropy changes. In particular, the magnetically driven BCE due to pressure-induced magnetic phase transitions implies an internal magnetic field resulting in large Zeeman splittings which in many cases are comparatively larger than by externally applied magnetic fields; the magnetically driven BCE may hence be considered the analogue to the MCE. Further, many rare-earth based Kondo systems show a distinct pressure dependence in the degree of 4f conduction electron hybridization and hence allow for a cooling. Finally, cooling can even be realized by the virtual exchange of the type of rare-earth ion via a pressure-induced valence transition, *e.g.*, $Eu^{2+} \rightarrow Eu^{3+}$. All these mechanisms have proven to lead to an effective cooling as summarized below.

Magnetically Driven BCE

The rare-earth monopnictide CeSb orders antiferromagnetically below $T_N \approx 16$ K in various phases [15]. Uniaxial pressure along the [001] axis is known to increase T_N by $dT_N/dp \approx 8$ K/GPa as shown in Fig. 6.6a [16]. In the paramagnetic state the

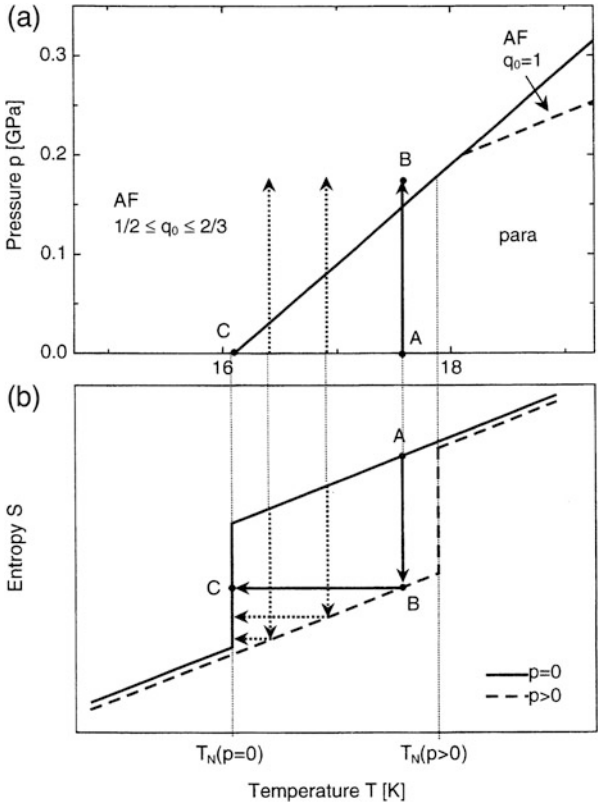

Fig. 6.6 (**a**) p-T phase diagram of CeSb [16]. AF denotes the antiferromagnetic phases defined by the magnetic ordering wavevector $\mathbf{q} = (0,0,q_0)$. Para marks the paramagnetic phase. (**b**) Schematic plot of the associated entropy curves at ambient (*solid line*) and at elevated pressure (*dashed line*)

sixfold degenerate ground-state multiplet of the Ce^{3+} ion is split by the crystal field into a doublet and an excited quartet at 3.2 meV [17]. Below T_N the crystal-field levels are further split by the molecular field due to the Zeeman effect giving rise to a strong decrease of the magnetic entropy as schematically shown in Fig. 6.6b. There is a discontinuity of about $\Delta S \approx 2$ J/mol K when the first-order phase transition occurs. Barocaloric cooling can be implemented as follows: At point A the system is in the paramagnetic state at ambient pressure and an initial temperature $T_A > T_N(p = 0)$. Next we apply pressure while in thermal contact with a heat sink. The system transforms isothermally into the ordered state, *i.e.*, vertically to point B, thereby releasing heat to the heat sink. Finally we isolate the system from the heat sink and release the pressure. The system transforms back into the paramagnetic state along an adiabatic line to point C lowering its temperature by ΔT. Figure 6.7a shows the expected dependence of the cooling rate in function of the initial temperature T_A. The cooling is effective in the temperature range from $T_N(p = 0)$ to $T_N(p > 0)$, giving rise to a characteristic triangular shape of the cooling rate ΔT *versus* T_A. This theoretical prediction was nicely verified in experiments carried out for pressures up to 0.52 GPa. Figure 6.7b exemplifies the

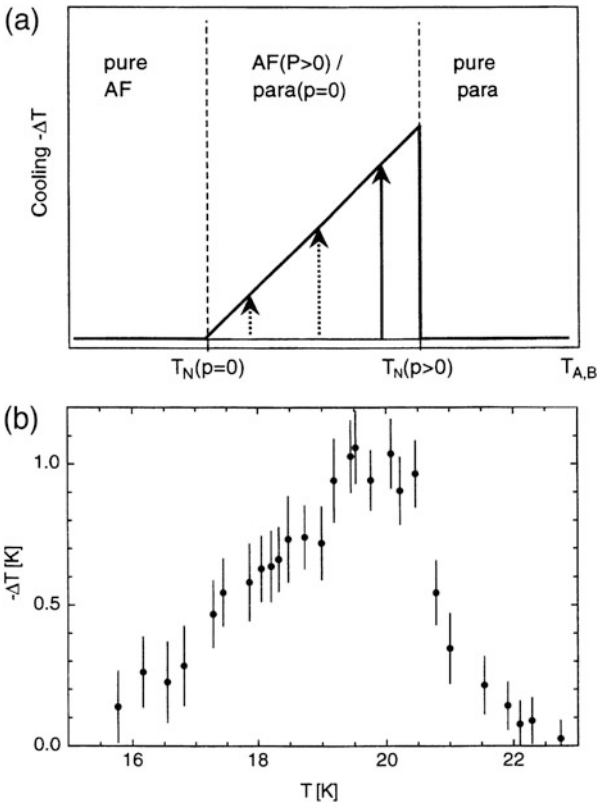

Fig. 6.7 (**a**) Schematic plot of the expected cooling effect in CeSb deduced from the magnetic phase diagram of Fig. 6.6a. (**b**) Measured cooling effect $-\Delta T$ in function of the initial temperature observed in CeSb upon releasing an uniaxial pressure of 0.26 GPa [4, 18, 19]

results upon releasing an uniaxial pressure of 0.26 GPa [4, 18, 19]. Similar experiments were performed for HoAs [4, 20].

BCE in a Kondo System

In rare-earth Kondo compounds it is generally found that the hybridization between the 4f and conduction electrons leads to a reduction of the magnetic entropy. In the metallic Kondo compound $Ce_3Pd_{20}Ge_6$ this reduction is significant, as the crystal-field ground state of the Ce^{3+} ions is a quartet. The application of pressure is expected to influence the magnetic entropy twofold: (i) a reduction of the cell volume is generally found to increase the degree of hybridization; (ii) uniaxial pressure leads to a structural distortion, so that the quartet ground-state is split into two doublets. Both effects will reduce the magnetic entropy and allow barocaloric cooling as verified in [4, 21].

Valence Driven BCE

Eu compounds are especially well suited for a valence driven BCE, since the divalent magnetic Eu^{2+} ion is larger than the trivalent nonmagnetic Eu^{3+} ion, so that pressure can induce a transition $Eu^{2+} \rightarrow Eu^{3+}$ implying drastic changes in the magnetic entropy. More specifically, Eu^{2+} ions with $J = 7/2$ and $S = 0$ have an eightfold degenerate ground state, whereas Eu^{3+} ions with $J = 0$ have a singlet ground state, so that the magnetic entropy difference $\Delta S(Eu^{2+} \rightarrow Eu^{3+}) = R \ln(8)$ is amongst the largest to be realized practically, giving rise to huge temperature changes $\Delta T \approx 10$ K for a single step in the BCE process.

Early in the new millennium, Alex Müller received a message from Frank Steglich that the compound $EuNi_2(Si_{1-x}Ge_x)_2$ under study at the Max-Planck Institute at Dresden might have the right potential for the BCE due to the large pressure dependence of the valence transition T_V with $dT_V/dp = 105$ K/GPa [22]. BCE experiments were performed for a polycrystalline sample with $x = 0.85$ and $T_V = 38$ (48) K for cooling (warming) and hydrostatic pressures up to 0.48 GPa [4, 23]. The observed temperature changes $\Delta T \approx 1$ K per single step in the BCE process turned out to be an order of magnitude smaller than theoretically expected, which is due to the lack in adiabaticity of the experimental setup as well as to the use of a polycrystalline sample (suitable single crystals were not available).

Achievements in High-Temperature Superconductivity

Inhomogeneous Materials Character

Early in the nineties, Alex Müller put my attention to theoretical and experimental work going on at Stuttgart (University and Max-Planck-Institut für Festkörperforschung), which gave evidence for a phase separation in La_2CuO_{4+x} compounds, *i.e.*, the co-existence of domains of essentially stoichiometric insulating La_2CuO_4 and domains of superconducting areas [24, 25]. At the same time, we have been involved in neutron scattering studies of the crystal-field interaction in $RBa_2Cu_3O_x$ (R = rare earth) compounds in order to understand how the antiferromagnetic ordering of the R^{3+} ions can co-exist with the superconducting state. These experiments revealed unusual features which later could be interpreted in terms of phase separation. Since the R^{3+} ions are situated close to the CuO_2 planes where the superconducting carriers are located, the crystal-field interaction at the R site constitutes an ideal probe of the local symmetry and the charge distribution of the superconducting CuO_2 planes and thereby monitors directly changes of the carrier concentration induced by the oxygen nonstoichiometry x. More specifically, the lowest crystal-field excitation observed for $ErBa_2Cu_3O_x$ turned out to be decomposed into three individual transitions A_i whose spectral weights distinctly depend on the oxygen content x [26]. Figure 6.8 shows the fractional proportions p_k of the transitions A_1, A_2, and A_3 which have maximum weight close to $x = 7.0$, $x = 6.5$, and $x = 6.0$, respectively.

It is tempting to identify the transitions A_1, A_2, and A_3 by two local regions of metallic character ($T_c \approx 90$ K, $T_c \approx 60$ K) and a local region of semiconducting character, respectively, thereby providing evidence for the percolation mechanism of superconductivity in cuprates as proposed in [24, 25] as well as for the two-plateau structure of T_c in the compounds $RBa_2Cu_3O_x$. For $x = 6$ the system is a perfect semiconductor. When x increases, oxygen ions are added into the chains, and holes are continuously transferred into the CuO_2 planes. By this mechanism the number of local regions with metallic character (associated with the crystal-field transition A_2) rises, which can partially combine to form larger regions. For a two-dimensional square structure the critical concentration for bond percolation is 50%. According to Fig. 6.8 the critical concentration is $x_2 = 6.40$, where the system undergoes a transition to the conducting state (with $T_c \approx 60$ K). Upon further increasing x, a second (different) type of metallic cluster (associated with the crystal-field transition A_1) is formed; these start to attach to each other, and at the percolation limit $x_1 = 6.84$ a transition into another conducting state (with $T_c \approx 90$ K) is induced.

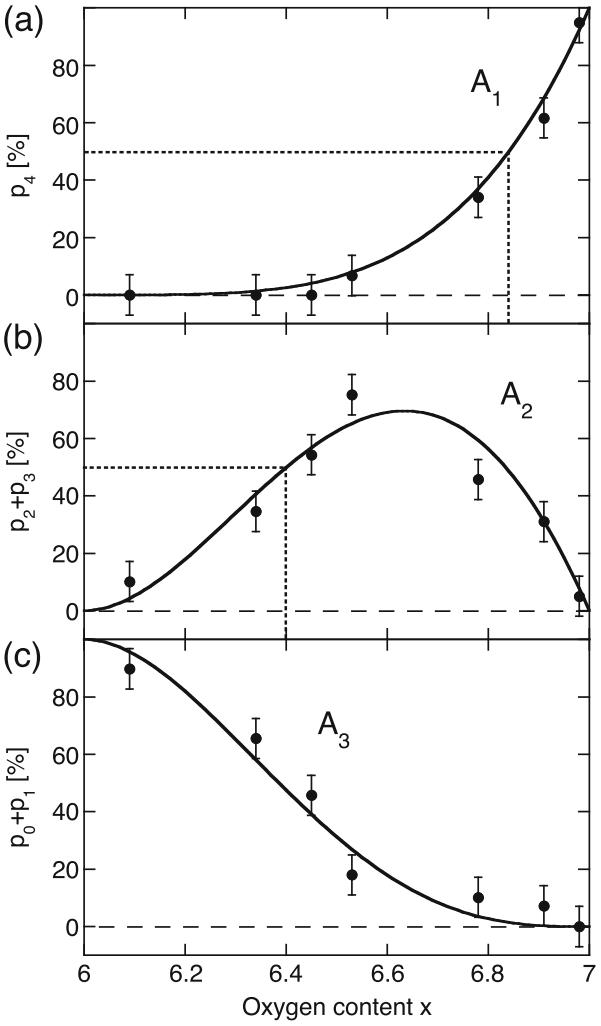

Fig. 6.8 Proportions p_k of the lowest-lying crystal-field transitions A_i of $ErBa_2Cu_3O_x$ as a function of the oxygen content x [26]. The *full lines* correspond to the probabilities p_k to have $0 \leq k \leq 4$ of the four oxygen chain sites nearest to the Er^{3+} ion occupied. The *dotted lines* mark the critical limits for bond percolation

Oxygen and Copper Isotope Effects

The concept which led Alex Müller to the discovery of superconductivity in the cuprates was the vibronic property of the Jahn-Teller effect. Therefore looking for an isotope effect for both oxygen and copper ions was an obvious task, and neutron crystal-field studies provide relevant information through the linewidth of the crystal-field transitions. The interaction with the charge carriers is by far the dominating relaxation mechanism. The corresponding intrinsic linewidth increases almost linearly with temperature according to the well-known Korringa law. In the superconducting state as well as in the pseudogap state, however, the pairing of the charge carriers creates an energy gap Δ, thus crystal-field excitations with energy

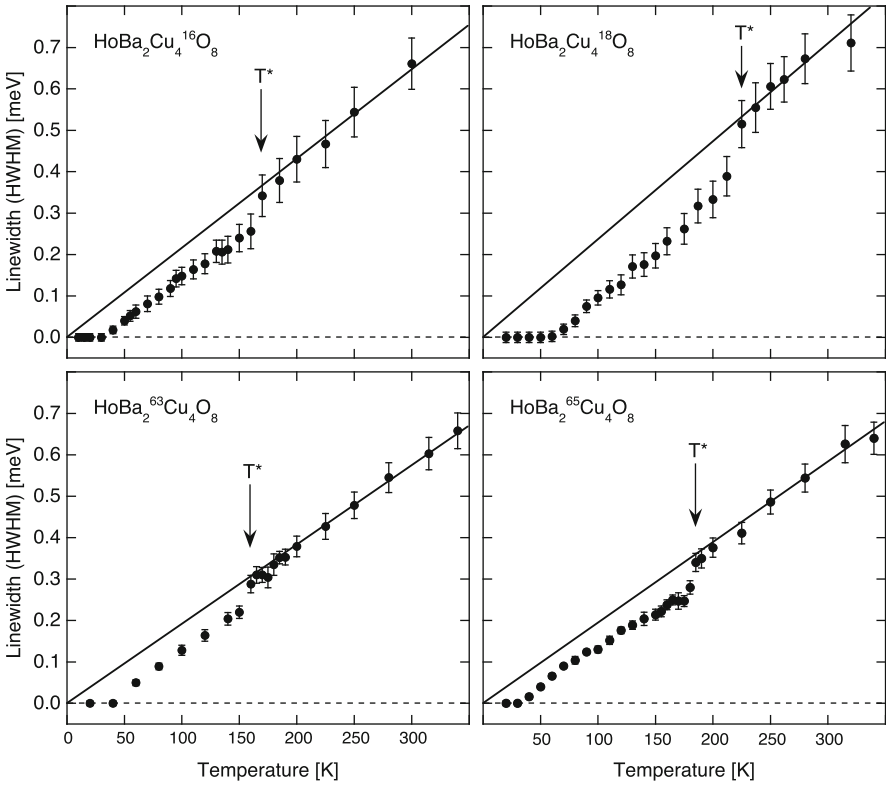

Fig. 6.9 Temperature dependence of the intrinsic linewidth W (HWHM) corresponding to the lowest-lying crystal-field transition in $HoBa_2Cu_4O_8$ for different oxygen and copper isotopes [27, 28]. The *lines* denote the linewidth in the normal state calculated from the Korringa law

$<2\Delta$ do not have enough energy to span the gap, and consequently there is no interaction with the charge carriers.

We applied this method to the compound $HoBa_2Cu_4O_8$ for both oxygen isotope substitution with $T_c(^{16}O) = 79.0(1)$ K and $T_c(^{18}O) = 78.5(1)$ K [27] and copper isotope substitution with $T_c(^{63}Cu) = 79.0$ K and $T_c(^{65}Cu) = 78.6(1)$ K [28]. Figure 6.9 shows the temperature dependence of the intrinsic linewidth (HWHM) corresponding to the lowest-lying crystal-field transition at energy 0.6 meV. The linewidth is zero up to some tens K, then it increases almost linearly up to around 200 K, where a steplike enhancement into the normal state behavior according to the Korringa law occurs. The temperature T* associated with the steplike enhancement is identified as the temperature where the pseudogap opens. Our experiments gave evidence for large isotope shifts $\Delta T^*(O) \approx 50$ K and $\Delta T^*(Cu) \approx 25$ K. The corresponding isotope coefficients α^* defined by the relation $T^* \propto 1/M^{\alpha^*}$ (M is the mass of the O or Cu ion) turn out to be $\alpha^*(O) = -2.2$ and $\alpha^*(Cu) = -4.9$. Giorgio Benedek highlighted the latter coefficient in his lecture presented at an international symposium in Zurich in the year 2006 and suggested to call it the *Alfa Romeo*

number, since Alex Müller is an enthusiastic driver of Alfa Romeo cars such as the model Alfa Romeo Montreal 4.9.

Subsequently this method was applied to the compound $La_{1.96-x}Sr_xHo_{0.04}CuO_4$ [29, 30]. We found oxygen isotope coefficients $\alpha^*(O) = -2.0, -1.3, -0.7$, and -0.3 for $x = 0.11, 0.15, 0.20$, and 0.25, respectively, but the copper isotope coefficient α^*(Cu) turned out to be zero within experimental error. This is in contrast to the case of $HoBa_2Cu_4O_8$, for which the large copper isotope shift was associated with a local copper mode, although the experiment did not provide direct information about the specific type of lattice mode involved. By comparing ΔT^*(Cu) for both $HoBa_2Cu_4O_8$ and $La_{1.96-x}Sr_xHo_{0.04}CuO_4$, it was possible to assign the copper mode to the umbrella-type mode [31], which is present in the former bilayer compound but not in the latter single-layer compound.

Concluding Remarks

Looking back to 30 years of collaboration I realize with pleasure that Alex Müller's impact on my research work was significant. Due to his tremendous experience with perovskite compounds, a novel principle for cooling by the barocaloric effect became possible and could be demonstrated in experiments. I very much appreciated his invaluable contributions and sagacious advice in numerous discussions, often in my office under the inspiring influence of Peter's Flake (this is Alex Müller's favorite pipe tobacco to enjoy the fine art of smoking). I am also grateful to Alex Müller for actively promoting our achievements in neutron scattering studies of copper perovskites (inhomogeneous character of hole-doped cuprates, oxygen and copper isotope effects, nature of the gap function) in various viewpoints published in the literature (see, *e.g.*, [32, 33]).

Acknowledgments The author is indebted to the large number of colleagues for their participation in the experimental work as well as for numerous stimulating discussions.

References

1. C. Kittel, *Introduction to Solid State Physics* (Wiley, New York, 1976)
2. A.M. Tishin, in *Handbook of Magnetic Materials*, vol. 12, ed. by K.H.J. Buschow (Elsevier, Amsterdam, 1999)
3. see, *e.g.*, A. Furrer, K.A. Müller, J. Mesot, Swiss Patent No. 693284 (May 2003); US Patent No. 6,558,434 B1 (May 2003)
4. T. Strässle, A. Furrer, Z. Hossain, C. Geibel, Phys. Rev. B **67**, 054407 (2003)
5. S. Rosenkranz, M. Medarde, F. Fauth, J. Mesot, M. Zolliker, A. Furrer, U. Staub, P. Lacorre, R. Osborn, R.S. Eccleston, V. Trounov, Phys. Rev. B **60**, 14857 (1999)
6. The temperature where the entropy of the R-3c phase vanishes depends on the exchange coupling between the Pr ions. Based on heat capacity data an exchange interaction of the order of 1 K was assumed

7. J.F. Scott, Phys. Rev. **183**, 823 (1969)
8. R.T. Harley, W. Hayes, A.M. Perry, S.R.P. Smith, J. Phys. C **6**, 2382 (1973)
9. R.J. Birgeneau, J.K. Kjems, G. Shirane, L.G. van Uitert, Phys. Rev. B **10**, 2512 (1974)
10. M. D'Iorio, W. Berlinger, J.G. Bednorz, K.A. Müller, J. Phys. C **17**, 2293 (1984)
11. B. Hälg, W. Berlinger, K.A. Müller, Nucl. Instrum. Methods Sect. A **253**, 61 (1986)
12. J.B. Torrance, P. Lacorre, A.I. Nazzal, E.J. Ansaldo, C. Niedermayer, Phys. Rev. B **45**, 8209 (1992)
13. P. Lacorre, J.B. Torrance, J. Pannetier, A.I. Nazzal, P.W. Wang, T.C. Huang, J. Solid State Chem. **91**, 225 (1991)
14. K.A. Müller, F. Fauth, S. Fischer, M. Koch, A. Furrer, P. Lacorre, Appl. Phys. Lett. **73**, 1056 (1998)
15. P. Fischer, B. Lebech, G. Meier, B.D. Rainford, O. Vogt, J. Phys. C **11**, 345 (1978)
16. B. Hälg, A. Furrer, O. Vogt, Phys. Rev. Lett. **57**, 2745 (1986)
17. H. Heer, A. Furrer, W. Hälg, O. Vogt, J. Phys. C **12**, 5207 (1979)
18. T. Strässle, A. Furrer, K.A. Müller, Phys B **276–278**, 944 (2000)
19. T. Strässle, A. Furrer, High Pressure Res. **17**, 325 (2000)
20. T. Strässle, A. Furrer, F. Altorfer, K. Mattenberger, M. Böhm, H. Mutka, J. Alloys Compd. **323–324**, 392 (2001)
21. T. Strässle, A. Furrer, A. Dönni, T. Komatsubara, J. Appl. Phys. **91**, 8543 (2002)
22. H. Wada, A. Nakamura, A. Mitsuda, M. Shiga, T. Tanaka, H. Mitamura, T. Goto, J. Phys. Condens. Matter **9**, 7913 (1997)
23. Z. Hossain, T. Strässle, C. Geibel, A. Furrer, J. Magn. Magn. Mater. **272–276**, 2352 (2004)
24. V. Hizhnyakov, N. Kristoffel, E. Sigmund, Physica C **160**, 119 (1989)
25. R.K. Kremer, E. Sigmund, V. Hizhnyakov, F. Hentsch, A. Simon, K.A. Müller, M. Mehring, Z. Phys. B Condens. Matter **86**, 319 (1992)
26. J. Mesot, P. Allenspach, U. Staub, A. Furrer, H. Mutka, Phys. Rev. Lett. **70**, 865 (1993)
27. D. Rubio Temprano, J. Mesot, S. Janssen, K. Conder, A. Furrer, H. Mutka, K.A. Müller, Phys. Rev. Lett. **84**, 1990 (2000)
28. D. Rubio Temprano, J. Mesot, S. Janssen, K. Conder, A. Furrer, A. Sokolov, V. Trounov, S.M. Kazakov, J. Karpinski, K.A. Müller, Eur. Phys. J. B **19**, 5 (2001)
29. D. Rubio Temprano, K. Conder, A. Furrer, H. Mutka, V. Trounov, K.A. Müller, Phys. Rev. B **66**, 184506 (2002)
30. P.S. Häfliger, A. Podlesnyak, K. Conder, E. Pomjakushina, A. Furrer, Phys. Rev. B **74**, 184520 (2006)
31. J. Röhler, Phys. C **341–348**, 2151 (2000)
32. K.A. Müller, Phil. Mag. Lett. **82**, 279 (2002)
33. K.A. Müller, J. Phys. Condens. Matter **19**, 151002 (2007)

Chapter 7
Personal Reflections on High-T_c Superconductivity

John B. Goodenough

To Alex Mueller on Turning 90

The resistance to electronic conduction in a metal is caused by the scattering of the conducting electrons by phonons as well as by impurities and lattice imperfections. The diamagnetism as well as the absence of resistance of a superconductor below the critical temperature T_c leads to a model of pairs of conducting itinerant electrons of opposite spin captured in a potential well created by cooperative, dynamic atomic displacements. The Bardeen-Cooper-Schrieffer (BCS) model of superconductivity describes opposite-spin Cooper pairs of itinerant electrons captured rather than scattered below T_c by vibrating, cooperative atomic displacements. The concept of capture of pairs of itinerant or molecular-orbital electrons by cooperative atomic displacements led Alex Mueller to explore with Bednorz whether dynamic, cooperative Jahn-Teller deformations might capture mobile electron pairs below a higher T_c than predicted by the BCS model. Static cooperative Jahn-Teller distortions of crystals containing Mn(III) or Cu(II) in octahedral sites had been identified as well as the role of dynamic cooperative Jahn-Teller deformations in the creation of chemical inhomogeneities in the ferrimagnetic oxospinels of the first RAM memory of the digital computer. Since superconductive electron pairs would need to be trapped itinerant electrons, a ceramic containing mixed-valent Cu(III)/Cu(II) cations was a logical choice for Alex Mueller to begin his investigation. The discovery of Bednorz and Mueller of high-temperature superconductivity in a copper oxide in 1986 broke the mindset that the BCS mechanism for capturing superconductive electron pairs was the only mechanism for the superconductive phenomenon.

J.B. Goodenough (✉)
The University of Texas at Austin, Austin, TX, USA
e-mail: jgoodenough@mail.utexas.edu

A. Bussmann-Holder et al. (eds.), *High-Tc Copper Oxide Superconductors and Related Novel Materials*, Springer Series in Materials Science 255,
DOI 10.1007/978-3-319-52675-1_7

In the summer of 1986, I was in transition from the Inorganic Chemistry Laboratory of the University of Oxford, England, to an Engineering Chair at The University of Texas at Austin. I knew that the cooperative Jahn-Teller orbital ordering is normally associated with localized electrons; the Bednorz-Mueller superconductivity, if their initial motivation was correct, should occur with narrow-band electrons on the approach to crossover to localized-electron or molecular-electron behavior. In the 1960s, I had explored transitions from localized to itinerant or molecular-orbital electron behavior in single valent oxides, but it had never occurred to me to look for superconductivity at this transition in mixed-valent oxides. In the single-valent oxides and sulfides I had been studying, the localized-to-itinerant electronic transition was commonly associated with an intermediate charge-density (CDW) phase appearing at a first-order metal-insulator transition.

A congressional mandate in the late 1960s restricted fundamental research at a government-supported laboratory to studies targeted to the mission of the laboratory, and the Lincoln Laboratory was funded by the U.S. Airforce. My investigation of the properties of narrow-band *3d* electrons in oxides with and without the orbital degeneracies required of a cooperative Jahn-Teller orbital ordering was not targeted to enabling an Air Force mission. Since the first energy crisis occurred in about 1970, I turned my attention to materials that could increase energy conservation and reduce the dependence of modern society on fossil fuels, but energy was also not considered an Air Force mission. Therefore, in 1976 I accepted a chemistry professorship in Oxford.

On my return to an Engineering chair in the U.S. in the summer of 1986, I would be free to initiate research of my choosing. The discovery of Bednorz and Mueller that summer resulted in a rapid realization of a superconductive $T_c = 90$ K in a perovskite-related oxide before I could organize a research laboratory; these stunning discoveries drew me back to the study of narrow-3d-band properties in transition-metal oxides with a perovskite-related structure where I had shown years before that the *3d* electrons of this family of oxides can exhibit localized or itinerant *3d*-electron behavior in single-valent perovskites. I had the good fortune to be able to bring with me from Oxford to Texas a post-doctoral solid-state chemist, now Professor Arumugam Manthiram, and to have join me a visiting physics Ph.D. student from Jilin University in China, now Professor Jian-Shi Zhou. Both have remained at The University of Texas at Austin. With these two and my experience with transition-metal oxides, including the interpretation of thermoelectric-power data in oxides with *3d*-electron mixed-valent hopping between co-existing localized and molecular-orbital states, we were able to demonstrate that the high-T_c superconductivity in the copper oxides involves trapping of spin-paired electrons in mixed-valent, linear, positively charged chain segments of four copper cations, 2Cu(II) + 2Cu(III), oriented and moving along the Cu–O–Cu axes of CuO_2 sheets. The electrons of the four- copper, spin-paired centers occupy molecular orbitals in a matrix of localized Cu(II)-cation spins. What I didn't appreciate in 2002 was that the four copper chain segments remain mobile to lowest temperatures, only condensing into a few eight-copper segments rather than into the static, one-dimensional 50:50 Cu(II) + Cu(III) metallic stripes found by Tranquada

et al., is most probably because of a twofold degeneracy at the Cu−O−Cu axes in the CuO_2 sheets of the high-T_c copper-oxide superconductors.

The axial degeneracy scrambles the four-copper chain segments along the two equivalent axes in a given CuO_2 sheet, which made difficult interpretation of the PDF images of Takeshi Egami. Nevertheless, Egami's data aided my deduction that the superconductive pairs of the high-T_c copper-oxide superconductors are trapped in molecular orbitals of a mobile second phase at the crossover from a localized-electron parent phase to an itinerant-electron phase in a mixed-valent 2D CuO_2 sheets containing a mixed Cu(III)/Cu(II) valence. The structure removes the Jahn-Teller localized-orbital degeneracy on an atom, but the crossover CDW condition in a mixed-valent system stabilizes molecular-orbital clusters that are positively charged relative to the localized-electron Cu(II) parent phase; coulomb repulsion between the charged clusters stabilizes the clusters relative to formation of a metallic-stripe second phase. The complexity of mobile chain segments oriented parallel to two degenerate axes in the same CuO_2 sheet complicates experimental imaging of the random and dynamic twofold orientations of the second-phase chain segments that contain two spin-paired delocalized electrons. The twofold degeneracy of the [100] and [010] …Cu-O-… chains allows the positively charged, four-copper centers to change shape and orientation, and their positive charge relative to the Cu(II) matrix provides coulomb repulsions between them that inhibits their coalescence into larger charge segments and makes their motion cooperative as in a traveling CDW or a school of fish. I call attention to the conceptual model of the Bednorz-Mueller superconductive phase as consisting of mobile, four-copper, linear chain-segments in which spin-paired molecular-orbital electrons are trapped by CDW cooperative atomic displacements at the crossover from localized to itinerant electronic behavior in a mixed-valent two-dimensional CuO_2 sheet; I do so in the hope it can provide a starting model for a more rigorous theoretical interpretation of experimental data such as that of Bussmann-Holder and Bishop.

Chapter 8
NMR of Cuprate Superconductors: Recent Developments

Michael Jurkutat, Jonas Kohlrautz, Steven Reichardt, Andreas Erb, Grant V.M. Williams, and Jürgen Haase

Introduction

When Bednorz and Müller discovered cuprate high-temperature superconductivity they speculated about the role of oxygen and the ionic state of copper for reaching the highest critical temperature T_c [1]. Very recently, nuclear magnetic resonance (NMR) showed that the maximum T_c is almost proportional to the planar O hole content of the parent cuprate material [2, 3], while the planar O (n_p) and Cu (n_d) holes for undoped materials add up to the inherent, nominal Cu hole, i.e., $2n_p + n_d = 1$, cf. Fig. 8.1. Optimal doping can unlock the highest possible T_c for a given system. In other words, achieving a higher T_c means transferring O electrons to planar Cu in the CuO_2 plane, already in the parent material, e.g., by inter-planar chemistry.

Much higher T_c with cuprates appear possible given the NMR data. Furthermore, upon doping (x) with holes ($x > 0$) or electrons ($x < 0$) NMR recovers the expected relation, $n_d + 2n_p = 1 + x$, i.e., NMR provides a quantitative measure for local charges in the CuO_2 plane. We thus have, for the first time in cuprate research, material chemistry parameters simply measurable with NMR, which set the maximum achievable T_c (and also the superfluid density below T_c [3]). It was, therefore,

M. Jurkutat • J. Kohlrautz • S. Reichardt • J. Haase (✉)
Faculty of Physics and Earth Sciences, University of Leipzig, Linnéstr. 5, 04103 Leipzig, Germany
e-mail: j.haase@physik.uni-leipzig.de

A. Erb
Walther Meissner Institute for Low Temperature Research, Walther-Meissnerstr. 8, 85748 Garching, Germany

G.V.M. Williams
The MacDiarmid Institute for Advanced Materials and Nanotechnology, SCPS, Victoria University of Wellington, PO Box 600, Wellington 6140, New Zealand

A. Bussmann-Holder et al. (eds.), *High-Tc Copper Oxide Superconductors and Related Novel Materials*, Springer Series in Materials Science 255,
DOI 10.1007/978-3-319-52675-1_8

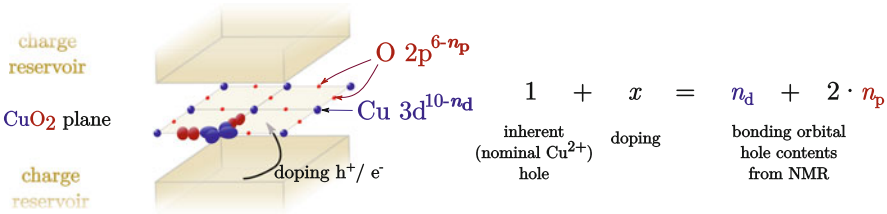

Fig. 8.1 The ubiquitous CuO_2 plane with the bonding orbitals Cu $3d_{x^2-y^2}$ and O $2p_\sigma$. In the undoped parent materials, the nominal Cu^{2+} hole resides in Cu $3d_{x^2-y^2}$ with the corresponding hole content $n_d \lesssim 1$, since the hole is shared with O $2p_\sigma$ ($n_p \gtrsim 0$), but one expects that $2n_p + n_d = 1$. Doping x holes ($x > 0$) or electrons ($x < 0$) into the CuO_2 plane alters the total planar hole count accordingly, i.e., $n_d + 2n_p = 1 + x$. NMR provides a quantitative measure for n_d and n_p, but finds large differences in the sharing of the holes between Cu and O [2, 4]

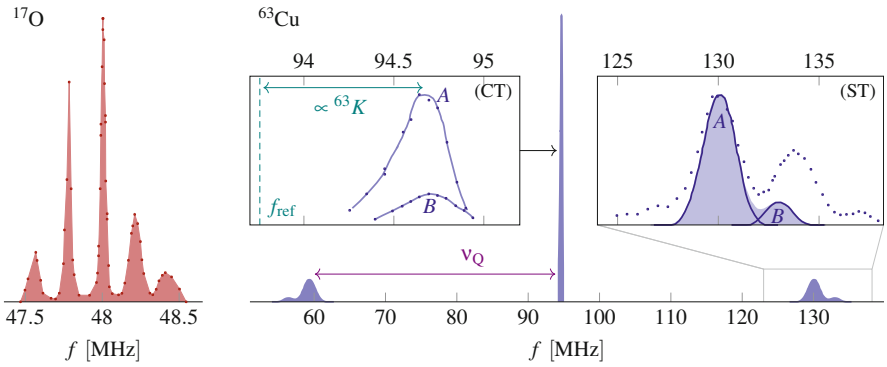

Fig. 8.2 NMR spectra of planar ^{17}O (*left*) and ^{63}Cu (*right*) including all quadrupolar satellite transitions from c-axis-aligned powder of $La_{2-x}Sr_xCuO_4$ near optimal doping ($x = 15\%$) at a field of 8.3 T. ^{17}O data based on [5] and ^{63}Cu data from [6] with signals from two different Cu sites (*A* and *B*). From the spectra, the quadrupole splitting (ν_Q) can be determined (difference between the *lines*), as well as the NMR shift (K) relative to a reference compound at f_{ref}; inset (CT) shows the *central lines* for the *A* and *B* site; (ST) shows signals from the ^{63}Cu satellite transitions from both sites (*shaded*). The overlap with signals from both sites, as well as ^{65}Cu in the raw spectra was separated using double resonance methods, cf. [6]

proposed to use the local holes n_d and n_p as abscissae for the discussion of cuprate properties in a new phase diagram, rather than doping $x = n_d + 2n_p - 1$.

In the past, NMR mostly paid attention to the magnetic susceptibility that determines the magnetic shifts, typically measured at the central transitions of the quadrupolar split Cu and O resonance spectra, cf. Fig. 8.2. For example, benchmark experiments seemed to have proven that a single electronic spin component (as expected from a single electronic fluid) explains NMR shift and relaxation in the cuprates [7, 8]. This is an important issue since a failure of the concept would demand a very different analysis, apart from consequences for theory. Meanwhile, in a set of experiments it was shown that one cannot, in fact, describe the uniform response in a magnetic field by that of a single electronic spin component, also in

experiments on the materials that were deemed to be a cornerstone of the proof [9–12]. Rather, one observes two shift components, one that carries the pseudogap behavior, i.e., it decreases with decreasing temperature already far above T_c, while the other has a Fermi liquid-like susceptibility, i.e., it is temperature independent above T_c and disappears rapidly below. Under pressure, it was shown that the latter component is amplified as pressure closes the pseudogap in $YBa_2Cu_4O_8$ [11]. It is still unclear what the origin of the different components is, but given the recently suggested new phase diagram of the cuprates in terms of n_d and n_p, a multi-component view may even be expected.

Another recent development in terms of NMR concerns the formation of charge density variations. Rather broad and featureless NMR lines (central as well as satellite transitions), cf. Fig. 8.2, had been interpreted as being due to charge and spin density variations early on [13, 14], but it could not be proven whether these linewidths have the suspected interesting physical origin. In fact, since the stoichiometric systems having almost no chemical disorder exhibit very narrow NMR lines, it was argued that the linewidths in the doped materials are due to inhomogeneities from dopants [15]. Very recently, for the underdoped, highly ordered ortho-(II)-phase of $YBa_2Cu_3O_{6+y}$ additional splittings of Cu and O resonances in very high magnetic fields were taken as the first solid evidence for (field induced) charge density variations [16–18]. Meanwhile, it could be shown that even moderate magnetic fields can induce static charge density variations [19], and work in progress reveals that charge density variations are indeed ubiquitous in the cuprates [20] and that inhomogeneities just introduce complexity that is not easily resolved, much as speculated earlier [21].

Alex Müller with his insight into spin resonance techniques never doubted that NMR must hold more clues, as a fundamental bulk probe. In fact, Alex Müller's talk at the 1998 Erice meeting excited J.H. so that he felt that there must be a connection to the strange NMR results he had observed in almost continuous experiments since he began working with Charlie Slichter in Urbana at the end of 1996. J.H. approached Alex Müller after his talk and was delighted to be invited for lunch. The ensuing conversation founded the belief in J.H. that one has to continue investigating these systems. Clearly, it did not foretell how long the road would be and how many turns were still to take. Later encounters, every now and then, kept J.H. on the path. Now, as far as NMR is concerned, we are certain that we entered a new understanding and Alex Müller helped setting it in motion. Actually, Charlie Slichter shared the same conviction and encouraged J.H. to continue irrespective of funding issues.

NMR and Cuprate Superconductors

When the idea was growing in Urbana, Illinois in the 1950ies that classical superconductivity might be related to a gap that develops at the Fermi level, C.P. Slichter realized that accompanying changes in the density of states must

affect nuclear relaxation. And they set out designing experiments to analyze this (the essence of nuclear relaxation in metals was known at least 10 years before NMR was invented, as the 1936 paper by Heitler and Teller shows [22]). Thereby, the first proof of the theory was ready in the same year as BCS published their theory [23, 24]. The Hebel-Slichter peak in nuclear relaxation [25] is a special trait of BCS theory.

In these early experiments, the major problems of NMR in such systems are already evident: the magnetic field and radio frequency penetration in superconductors or even conductors make quantitative NMR very difficult. For example, they used a field cycling method that allowed the measurement of the NMR signal of aluminum metal in a high magnetic field while the nuclei could relax in the superconducting state at almost zero field. Orbital s-wave and spin-singlet pairing in the superconducting state explain the vanishing of nuclear relaxation [25, 26] and vanishing of the Knight shift [27] as the temperature falls below T_c, while the hallmark of a Fermi liquid (above T_c) is its temperature (T) independent spin susceptibility (χ_s) that gives rise to the temperature independent NMR Knight shift. Both, Knight shift (K_s) and nuclear relaxation ($1/T_1$) in metals are determined by the electron density of states, so that $K_s^2 T_1 T = const.$, the well-known Korringa relation [28].

Clearly, with the advent of cuprate superconductivity the search for signatures in the NMR shift and relaxation for changes near and below T_c was most interesting. Different from type-I superconductors, NMR in cuprate superconductors can be performed even at high magnetic fields. However, the inherent shielding in the mixed state still poses problems for precise shift and intensity measurements [29], not to mention effects from fluxoids and their dynamics that enter the scene in these highly anisotropic materials [30, 31].

Cuprate NMR is special yet in other ways. First of all, ^{63,65}Cu and ^{17}O nuclei have nuclear spins of $I = 3/2$ and $I = 5/2$, respectively (for the abundant ^{16}O, $I = 0$, NMR is not possible). Such nuclei with $I > 1/2$ have electric quadrupole moments that interact with local electric field gradients that reflect the charge symmetry at the nucleus (in aluminum metal the field gradient is zero due to lattice symmetry and the quadrupole interaction is absent despite $I = 5/2$ for ^{27}Al). Full shells can only show field gradients from distortions or fields from nearby ions. But partly unfilled (not s-like) shells can have huge effects on the NMR spectrum, i.e., they cause a splitting of the $2I$ nuclear Zeeman transitions.

For NMR of Cu with its hole in the $3d_{x^2-y^2}$ orbital, one expects a large field gradient with its major tensor axis aligned with the crystal's c-axis, and it should have a vanishing asymmetry as the CuO_2 plane is nearly square. This is indeed in agreement with Cu NMR, cf. Fig. 8.2. Planar O is expected to have only a moderate field gradient (nearly full shell configuration) with the largest principal axis along the Cu–O bond (in-plane direction) as it is hybridized with the partly empty Cu orbital. Contrary to Cu, the asymmetry for O is expected to be sizable since there is no axial symmetry about the Cu–O bond direction. For $I = 5/2$ five quadrupolar split

O lines are expected, which is in agreement with experiment [32–34], cf. Fig. 8.2. This atomic picture of the CuO_2 plane is pertinent for the magnetic shifts at planar Cu and O, as well. That is, the partly filled Cu $3d_{x^2-y^2}$ orbital will cause an anisotropic orbital shift, whereas for an almost full $2p_\sigma$ the orbital shift for O is negligible [32, 33, 35]. Essentially, the effect of doping on spin and charge carriers is what one is after with theory and experiments.

Of course, in these layered materials NMR shifts and quadrupole splittings will both show angular dependencies. And if one has to resort to powder samples due to penetration depth issues or since large enough single crystals are not available, angular dependencies can broaden the spectra beyond the detection limit, except for the central resonances that are only slightly affected by the quadrupole interaction (in higher order). Therefore, magnetically aligned powders are often used so that one has at least one preferred axis, i.e., most, but not all crystals will align their c-axis with the external magnetic field, cf. examples in Fig. 8.2.

One must emphasize that even without the sample quality issues, NMR of cuprates is at times very difficult and time-consuming, which explains why complete sets of data are hardly available. For example, the ^{89}Y ($I = 1/2$) nucleus that lacks a quadrupole moment was used in experiments only above T_c to discover the pseudogap [36], but the second spin component was not addressed, for this would require another internal standard [29]. Other early experiments on the most interesting planar (quadrupolar) nuclei had to focus on disentangling the resonances in terms of orbital shift (K_L), Knight shift (K_s), longitudinal or spin-lattice relaxation ($1/T_1$), spin-echo decay ($1/T_2$) and quadrupole splittings (ν_Q) [32–35]. Of course, with all the different resonances from the large unit cell, two Cu isotopes, and the rather large linewidths, the assignment of the resonances was an important aspect, as well. Given the rather large linewidths, in most experiments time-consuming frequency stepped spin echo experiments had to be used, as regular NMR Fourier transform spectra could not be recorded. This led to the discovery of indirect spin coupling (due to exchange coupled electrons) between the nuclei [37].

It appears that most of the data and site assignments are valid as of today, while some interpretations may be subject to change. Two typical plots for ^{17}O and ^{63}Cu NMR of cuprates are shown in Fig. 8.3. At the lowest temperatures, spin shift and relaxation disappear for both nuclei in all superconducting cuprates. It is often not exactly clear from the data where T_c is located since signatures in the shifts can be absent. Above T_c the shifts can be rather temperature independent or show pseudogap behavior, with the tendency that the pseudogap behavior is more prominent in the underdoped materials. Different nuclei can show different behavior. The temperature dependence of the nuclear relaxation can also be different at Cu and O. Nevertheless, for a long time the shifts were considered to be following from a single electronic fluid [7, 8]. However, a temperature independent shift component can easily be missed in these systems (it is very much like a regular orbital contribution above T_c, and the shift is ill-defined below T_c). Differences in relaxation for the two nuclei can be explained by coherence effects, since, e.g., planar O could be shielded from strictly antiferromagnetic fluctuations of Cu spins [38] which is more difficult to reconcile with incommensurate spin fluctuations

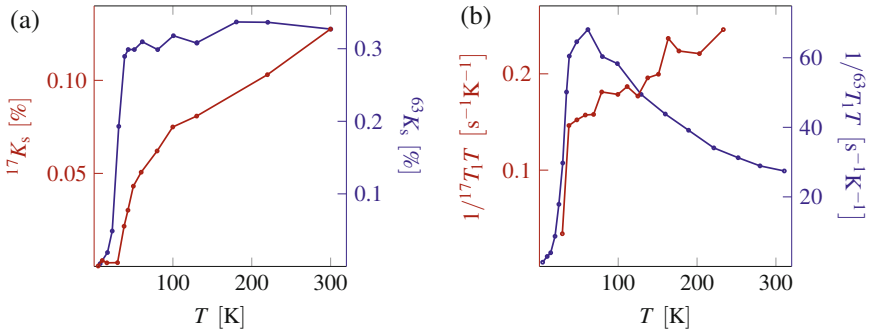

Fig. 8.3 Temperature dependencies of ^{63}Cu (*blue, right ordinate axes*) and ^{17}O (*red, left ordinate axes*) spin shifts K_s (**a**), and $1/T_1T$ (**b**), for optimally doped $La_{2-x}Sr_xCuO_4$. While Cu shows almost Fermi liquid-like shifts, i.e., $^{63}K_s(T) \approx const.$ above T_c, the O shift displays pseudogap-like features, i.e., it decreases with decreasing T above T_c. Neither the O spin-lattice relaxation, $1/^{17}T_1T$, nor that of Cu, $1/^{63}T_1T$ show a Hebel-Slichter peak near T_c, but disappear at the lowest T. Data reproduced from [38–40]

[37, 41, 42]. A more comprehensive overview of cuprate NMR and the corresponding literature can be found elsewhere [43, 44].

Another major factor entering cuprate NMR is the linewidths issue. It turns out that excessive linewidths caused by quadrupolar and magnetic effects are commonplace, an example is given in Fig. 8.2. While it casts doubt on shift measurements when the shifts are of the same size as the corresponding widths (as it is sometimes the case), the signal-to-noise suffers considerably, as well. That is why publications that show complete resonance lines are scarce. NMR linewidths can give information about inter-nuclear interactions, electronic homogeneity or motion, but sample quality can also be an issue. In fact, since the nearly stoichiometric cuprates show comparably rather narrow NMR lines, almost down to the limit of what one expects from indirect nuclear couplings or crystal strain, it was repeatedly argued that the excessive linewidths must be related to structural inhomogeneity and therefore irrelevant for cuprate physics. On the other hand, NMR failed to give clear evidence in terms of certain ordered charge scenarios. We will discuss this issue in a later section.

While NMR experiments in the cuprates are difficult, they contributed significantly to cuprate research with a number of discoveries: (i) There is a spin gap (pseudogap) as the spin shifts above T_c reveal. (ii) Some systems show a sudden change in NMR shifts at or below T_c, and a decrease of shift and relaxation at even lower temperatures favors spin-singlet pairing. (iii) There is no Hebel-Slichter peak, but nuclear relaxation disappears at low temperatures in a way that is consistent with spin singlet pairing, but apparently not orbital s-wave (line nodes lead to a more gradual decrease of the density of states). (iv) There is indirect nuclear coupling and a Gaussian spin-echo decay (in c-direction of the external field), which hints at an enhanced real part of the electronic spin susceptibility at short wavelengths from exchange coupling. (v) The spin shift at Cu and O for two YBaCuO systems led to the inference of a single electronic fluid—a conclusion no longer supported by experimental data. (vi) The NMR signal can suddenly

disappear (much like in spin glasses below the lock-in temperature), which may hint at a motion of larger electronic clusters in some underdoped systems.

Most of this information was inferred from temperature dependent NMR experiments on the central transitions of the $2I$ resonance lines since they are less affected by quadrupole effects. The quadrupole interaction present in the spectra was mainly used for the assignment of the various resonance lines to the crystallographic positions. Nevertheless, on a qualitative level it was even recognized that the maximum T_c had to do with the quadrupole splittings of planar Cu and O [45], cf. also Fig. 8.4, however, given the limited data and a quantitative understanding, it was not clear whether this was significant.

Failure of the Single Fluid Description

For the understanding of NMR data in terms of electron-nucleus interactions, one needs to know whether the magnetic hyperfine interaction ($H_{hf} = \mathbf{I} \cdot \mathbf{A} \cdot \mathbf{S}$) involves only one sort of electronic spin, i.e., the nucleus (**I**) is only coupled (**A**) to one electron spin (**S**). If there is a single spin component, it will be uniformly polarized

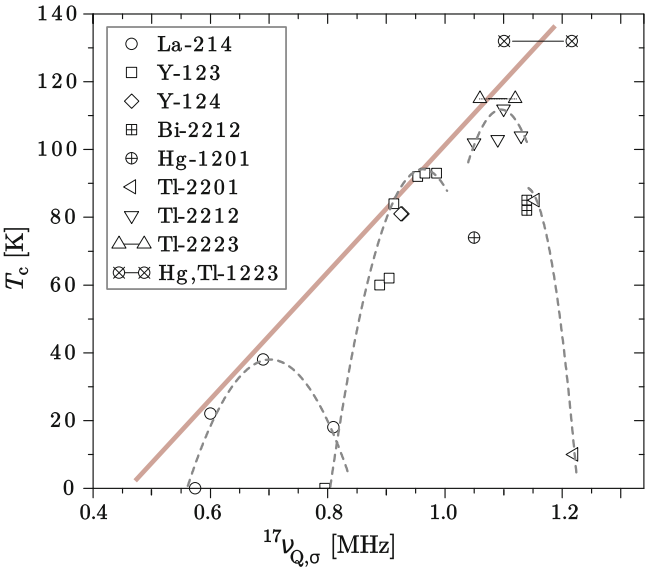

Fig. 8.4 T_c vs. planar O quadrupole splitting for various hole doped cuprates. Superconducting domes (*dashed lines*) are indicated where sufficient data points are available. The *faded red line* serves as guide to the eye indicating an increase of maximum T_c with the O splitting across different families. Note similarities to the Uemura plot [3, 46]

in the large external magnetic field B_0 used for NMR, i.e., $\langle S_z \rangle(T) = \chi_s(T) \cdot B_0/(\gamma_e \hbar)$. As a consequence, a temperature dependent spin shift (relative frequency per field) appears,

$$K_s(T) = \frac{A}{\gamma_e \gamma_n \hbar^2} \cdot \chi_s(T) = a \cdot \chi_s(T), \tag{8.1}$$

where γ_e and γ_n are the gyromagnetic ratios of the electron and nucleus, respectively, and A is the hyperfine coupling constant (a is an effective constant). If there was only one spin component, the changes in the shift ($\Delta K_s \equiv K_s(T_i) - K_s(T_j)$) for different nuclear spins (n and m) must be proportional to each other if taken between any two temperatures, i.e. $\Delta K_{s,n}/\Delta K_{s,m} = const$. For more than one spin component one expects different hyperfine coupling constants to each spin, and the total shifts measured at different nuclei between two temperatures are not proportional to each other anymore, since

$$K_s(T) = \sum a_i \chi_i(T), \tag{8.2}$$

with different effective hyperfine coefficients (a_i). Note that for more than one spin component, any coupling between these components will give rise to another susceptibility term, i.e., for two spin components in (8.2) one has in general to consider three susceptibilities [47].

For relaxation, on the other hand, the local coherence of the fluctuating hyperfine field is important and therefore nuclear relaxation is not a simple probe for deciding on the number of spin components, as noted earlier. However, the uniform response is a very strong criterion, of course, provided the magnetic field at the nucleus itself is not temperature dependent, an effect that could be caused below T_c by shielding in the mixed state. Nonetheless, by measuring another nucleus at the same field as the one of interest (e.g., apical O in addition to planar Cu and planar O), the difference between the two shifts is free from such effects [9, 29].

In a set of very careful experiments, it was proven that a single $\chi_s(T)$ cannot explain the shift data in optimally doped $La_{2-x}Sr_xCuO_4$, and various doping levels in $HgBa_2CuO_{4+\delta}$, but also in $YBa_2Cu_4O_8$, the system with very narrow NMR lines that was the cornerstone of single-fluid behavior [9–12]. The measurements were also performed on different nuclei, outside the CuO_2 plane. In all of these systems one finds that at least two susceptibilities are necessary, $\chi_s(T) = \chi_1(T) + \chi_2(T)$. One of these susceptibilities carries the pseudogap properties, and the other is constant down to about T_c below which it drops to zero. $YBa_2Cu_4O_8$ behaves at ambient pressure almost like a single-component system, that is why the second component was hardly detectable in early experiments [8]. However, as one applies pressure in this system the Fermi liquid-like component is drastically amplified and the same basic two-component scenario appears [11].

For the $HgBa_2CuO_{4+\delta}$ system, more data are available [12], and we show an analysis for this system in Fig. 8.5 together with the bare shifts (only higher order quadrupole contributions are removed). The novelty is the detection of a doping

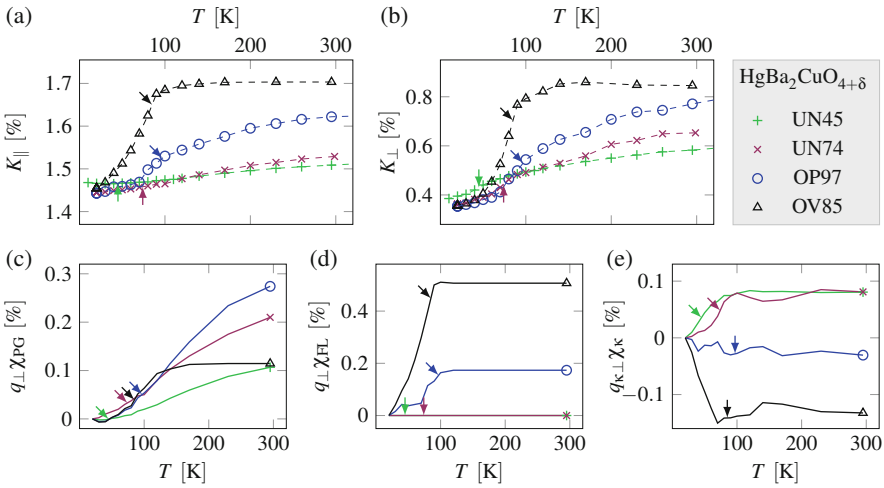

Fig. 8.5 ^{63}Cu shifts in $HgBa_2CuO_{4+\delta}$ single crystals with different dopings (UN45: underdoped, $T_c = 45$ K, $x \approx 6\%$; UN74: underdoped, $T_c = 74$ K, $x \approx 10\%$; OP97: optimally doped, $T_c = 97$ K, $x \approx 16\%$; OV85: overdoped, $T_c = 85$ K, $x \approx 19\%$), as measured in (**a**) $c \parallel B$, and (**b**) $c \perp B$ direction [12]. Based on anisotropy and scaling behaviour at higher temperatures, the shifts are decomposed into (**c**) a pseudogap component χ_{PG}, (**d**) a Fermi liquid-like component χ_{FL}, and (**e**) a third component (χ_{κ}) with a different hyperfine ratio for both orientations. Arrows indicate T_c

dependent third component that is temperature independent above a temperature T_0 that can be above or below T_c, but the component changes sign at optimal doping. More data on the Hg and O nuclei confirm the observation [12, 48]. Whether the third term arises from another spin component, or it originates from a coupling between two spin components remains to be seen.

We will not dare to compare explanations for the multi-component scenario with other methods or theory, however, with the advent of the new phase diagram in terms of two different types of holes, which we discuss below, one may expect that some of this carries over to the shifts.

Average Charge at Cu and O in the CuO_2 Plane

While the electric field gradient at a nucleus is extremely sensitive to the local charge symmetry, its quantitative interpretation is often rather delicate. With varying success, first principle calculations give quantitative results that are at times correct, but often not easily understood in terms of simple models [49–51]. In addition, there have been a number of qualitative attempts to interpret the quadrupole splittings at planar Cu and O in terms of local hole content, for relating it to stripe order, localized holes, or even to T_c [45, 52].

An interesting earlier observation is shown in Fig. 8.4 [46]. It shows that if T_c is plotted as a function of the planar O quadrupole splitting, a dependence is obtained that resembles that of the Uemura plot [53]. Clearly, the electric field gradient (or quadrupole splitting) at planar O must be related to more fundamental quantities. However, an understanding had to wait for a number of years.

In 2004, in search for understanding of Fig. 8.4, some of us learned from collaborators that the local electric field gradient can be calibrated with atomic spectroscopy data measured on ions in various oxidation states in gases. This enables one to relate the quadrupole splittings at planar Cu ($^{63}\nu_Q$) and planar O ($^{17}\nu_Q$) to the charge content of the bonding orbitals [4]:

$$^{63}\nu_Q = 94.3\ \text{MHz} \cdot n_d - 14.2\ \text{MHz} \cdot \beta^2 \cdot \left(8 - 4n_p\right) + {}^{63}C_c \tag{8.3}$$

$$^{17}\nu_Q = 2.45\ \text{MHz} \cdot n_p + {}^{17}C_\sigma \tag{8.4}$$

The respective first terms on the right hand sides of (8.3) and (8.4) reflect the contributions to Cu and O splitting from partial hole content of onsite bonding orbitals $3d_{x^2-y^2}$ (n_d) and $2p_\sigma$ (n_p), respectively. For the Cu splitting ($^{63}\nu_Q$) also the charges in the bonding orbitals $(8 - 4n_p)$ of the four surrounding planar O weighted by the overlap (β^2), i.e., $\langle$Cu 4p| O 2p$\rangle$, with nominally empty Cu 4p are taken into account. The respective last terms in (8.3) and (8.4) capture contributions from charges further away, which are minor ($\propto r^{-3}$) and doping independent. We want to stress that the coefficients in (8.3) and (8.4) are directly derived from atomic spectroscopy data and by no means adjusted to fit experimental data [4].

Indeed, with such an approach one could count the doped planar Cu and O holes in the CuO_2 plane. For example, it reproduces the average hole doping, i.e., $x = \Delta n_d + 2\Delta n_p$ and shows that there is a significant difference between $La_{2-x}Sr_xCuO_4$ and $YBa_2Cu_3O_{6+y}$ in terms of how doping proceeds in these two systems [4]. This was a remarkable advance, but the understanding of what causes the splittings in the parent materials was not clear, and the lack of sufficient data did not make this finding very interesting.

Recent progress is related to the attempt of understanding the electron doped cuprates, where NMR data are sparse. For these materials, rather large inhomogeneous Cu broadening had been proposed [54], but was not quite understood. New experiments confirmed those findings, and revealed that the Cu quadrupole splitting as a function of doping was following the simple equation from above, provided all electrons enter the Cu bonding orbital, a rather trivial result [55]. For a consistency check, some of us also investigated the ^{17}O NMR that had never been reported before (probably due to a significant overlap in resonance lines from inter-planar O). With an extensive investigation of single crystals, it was found that the planar O splitting does not change much as a function of electron doping, again a rather trivial result. However, the residual splitting was found to be very large (bigger than in optimally doped $La_{2-x}Sr_xCuO_4$) [2], indicating a substantial O *hole* content in these *electron* doped systems.

With ensuing NMR experiments on parent materials, it could be shown that (8.3) and (8.4) even capture the large differences in splittings between parent materials. In particular, the constants $^{63}C_c$ and $^{17}C_\sigma$ are, as expected, minor and their material dependence negligible, such that we could set them to 0 and 0.39 MHz, respectively, for all cuprates [2].

Thereby, a unified view of electron and hole doped cuprates in terms of charge was discovered, cf. Fig. 8.6, which revealed a rather simple picture [2],

$$1 + x = n_d + 2\, n_p, \tag{8.5}$$

where the measured charges, n_d and n_p (the factor of two stems from the stoichiometry of the CuO_2 plane), reproduce the expected charges including one inherent hole. Doping x introduces additional holes ($x > 0$) or electrons ($x < 0$).

The quantitative success of this analysis without adjustable parameters, given by the agreement with the simplest expectation from material chemistry expressed by (8.5), is gratifying, but not surprising. Quite unexpected on the other hand is the actual variation of the local charge distribution between different cuprate families, cf. Fig. 8.7. The interpretation of this finding is the following. Parent materials differ in the sharing of the intrinsic Cu hole with O, while the total charge is preserved, i.e., $1 = n_d + 2n_p$ for $x = 0$. It is found that the higher the O hole content, the higher the maximum T_c that can be unlocked by doping with approximately 15% holes or electrons. This explained the findings shown in Fig. 8.4. Doping with electrons is less effective in unlocking the highest T_c. Evidently, the inter-planar chemistry is responsible for setting the hole distribution, that in turn sets the maximum T_c.

We propose, furthermore, that the behavior of the cuprates under pressure that often increases the maximum T_c can be understood in terms of local charges [56]. In particular, we find pressure-induced intraplanar charge redistribution in favor of a higher n_p than chemically achievable at optimal doping [57], and we propose that the very different T_c observed in thin films [58, 59] might also be caused by a change in the actual hole distribution.

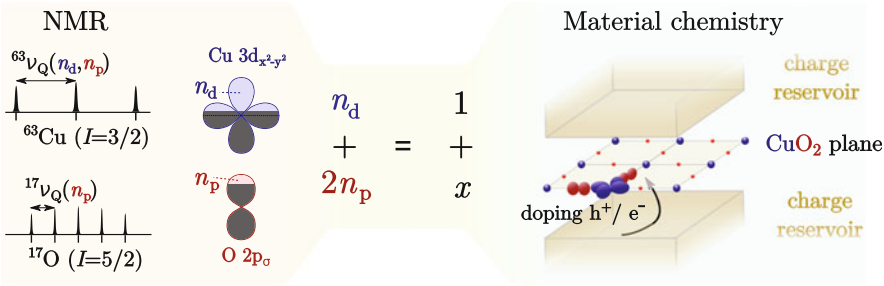

Fig. 8.6 *Left to right*: Cu and O quadrupole splittings are determined by hole contents in bonding orbitals Cu $3d_{x^2-y^2}$ (n_d, in *blue*) and O $2p_\sigma$ (n_p, in *red*). The planar hole content extracted from NMR, $2n_p + n_d$, matches expectation from material chemistry, $1 + x$, given by one inherent (nominal Cu) hole plus doped charges x

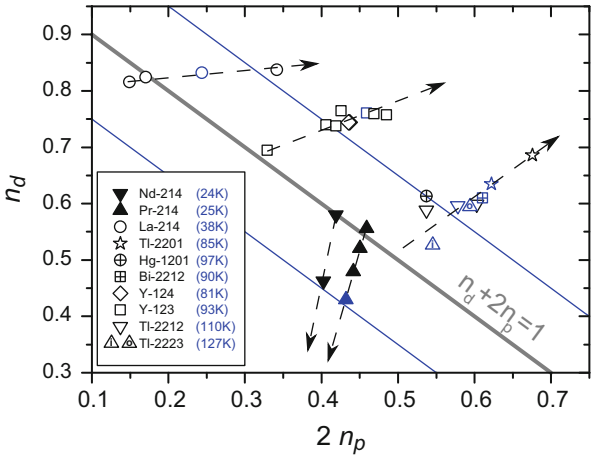

Fig. 8.7 Planar Cu and O hole contents, n_d and $2n_p$, respectively, in various cuprates (maximum T_c indicated in *blue*) determined from NMR quadrupole splittings. Parent line (*thick grey diagonal*) marks zero doping, i.e., $n_d + 2n_p = 1$, parallel *blue lines* correspond to constant doping of $x = \pm 0.15$, close to which data points corresponding to optimal doping (*blue*) can be found. Figure taken from [2]

Now that we have an understanding of the charge distribution in the CuO_2 plane measured by the quadrupole splittings of planar ^{17}O and ^{63}Cu, it is possible to investigate and discuss the charge inhomogeneities that follow from the linewidths of the quadrupole split lines. Before we turn to this subject, we would like to discuss a newly suggested cuprate phase diagram.

Charge-Resolved Cuprate Phase Diagram

In the commonly used electronic cuprate phase diagram one plots T_c as a function of doping x, with distinct differences for electron and hole doping, cf. inset (I) in Fig. 8.8. In such a phase diagram all the physical properties are discussed, whether they concern phases, transitions, cross-overs, or other characteristic properties. We just learned that n_d and n_p that also measure the average doping x (for holes as well as electrons) differ significantly among the cuprates. Therefore, it can only be accidental if a phase diagram that considers only x is the most suitable for understanding the cuprates. Clearly, the cuprate properties should be viewed in a phase diagram that has both hole contents as abscissae, as displayed in Fig. 8.8. This suggestion and a discussion of first resulting insights were presented very recently [3].

Let us shortly summarize the most salient features of Fig. 8.8. Using the planar charge distribution displayed in Fig. 8.7 as two-dimensional abscissae with T_c as ordinate, it is immediately apparent that this representation incorporates electron and hole doped cuprates and orders different cuprate families according to their maximum T_c. While electron doping is less efficient than hole doping in unlocking the maximum T_c, a trend of an increasing maximum T_c with the O hole content (n_p) is observed on both sides of the parent line, i.e., for both types of doped carriers. This can be seen even more clearly in the projection onto T_c vs. $2n_p$ in inset (II) of Fig. 8.8. Here also μSR relaxation rates σ_0 (for $T \to 0$ K) from the famous Uemura

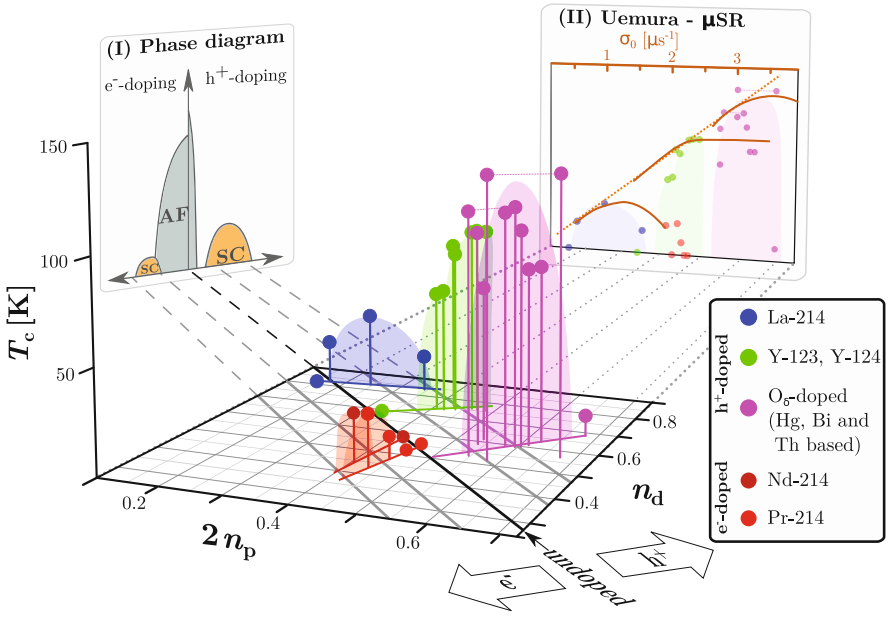

Fig. 8.8 Charge-resolved phase diagram with T_c as a function of the charges at Cu and O $(n_d, 2n_p)$. Projection along constant doping (*black diagonal* for $x = 0$ and *thick gray lines* for $x = \pm 0.1, \pm 0.2$) gives the commonly used phase diagram in inset (I). Projection onto T_c vs. $2n_p$ in inset (II) reveals ordering of cuprates families according to O hole content. The material specific hole contents trace corresponding μSR relaxation rates, that measure superfluid density per effective mass [3]

plot are shown (orange lines, upper abscissa), which trace the corresponding, material-specific O hole content measured by NMR. Although not shown, corresponding data for electron doped cuprates show the same agreement with NMR. This establishes a quite unexpected correlation between a material-chemistry parameter, n_p, (measurable at room temperature and also for non-superconducting doping levels), and superconducting properties, T_c and the superfluid density per effective mass measured by σ_0. We note that while the local charge distribution clearly sets the maximum T_c and superfluid density, we observe no immediate insight into the mechanism of unlocking superconductivity, as optimal doping appears to show no preferential doping distribution between n_d and n_p. However, on the hole doped side, the unlocking of the increasing maximum T_c (n_p) requires increasing number of adjacent CuO_2 planes. While the single, double and triple layer Tl-compounds are quite similar in charge distribution, cf. Fig. 8.7, only the latter achieve the maximum T_c. This may be indicative of the importance of inner layers that are underdoped at optimal doping, and their persisting magnetic correlations. In Fig. 8.8 we only plot T_c as function of n_d and $2n_p$, but we think it may prove beneficial to consider other properties as well.

Some properties, such as the Neél temperature (T_N), which are very sensitive to the charge reservoir composition, are not expected to show clear trends in this charge resolved representation. Properties that are dominated by the CuO_2 planes, on the other hand, should be discussed in the new charge-resolved phase diagram. For instance, the exchange coupling (J) measured by the two-magnon-peak in Raman spectroscopy in cuprate parent materials appears to decrease with increasing $(2n_p/n_d)_{x=0}$. The latter is, in a sense, a measure of covalency of the bond and is expected to increase with decreasing charge transfer gap which is at least qualitatively borne out by first-principle calculations, as discussed in [2]. As expected, the material-specific distribution of doped holes and electrons between O and Cu, reflected by $(2\Delta n_p/\Delta n_d)$, strongly depends on the position on the parent line, i.e. $(2n_p/n_d)_{x=0}$. The quantitative measurement of the widely varying, material-specific charge distribution in the CuO_2 plane clearly promises further insight when considering further aspects of cuprate phenomenology that show strong material dependence. Also, it may prove a useful compass for material chemists and theorists.

In terms of open questions in cuprate NMR, clearly, the multi-component spin description discussed above, and the material-specific Fermi-liquid vs. pseudogap shift phenomenology may be related to the material differences reflected by the local charges n_d and n_p.

Concerning the currently debated charge density waves, the quantitative measurement of local charges with sub-unit cell resolution may provide useful insights. In fact, in their recent analysis of charge order data from various probes on underdoped $YBa_2Cu_3O_{6+y}$, Kharkov and Sushkov [60] used NMR data to determine the amplitude and symmetry of the proposed charge density wave. In a similar spirit, broader but more qualitative and NMR-focused, we now review what is known from cuprate NMR about charge density variations.

Given the rather different NMR linewidth for the different cuprates, a lacking trend in the charge resolved phase diagram suggests that static charge and spin inhomogeneity cannot be vital for the maximum T_c [19]. However, this does not rule out that dynamic inhomogeneity is of fundamental importance [65].

Charge and Spin Density Variations in the CuO_2 Plane

The interest in charge and spin density variations in the CuO_2 plane has increased recently, in particular, due to the discovery of magnetic field induced charge density waves by NMR [16–18], as the magnetic field is, in fact, not expected to induce charge density variations. While other probes also provide evidence for charge density variations, only NMR has thus far been used to measure their amplitude [60].

If the charge density varies spatially, one also expects that the spin density is modulated, details may depend on the model. Many years ago, NMR and in particular NMR double-resonance methods clearly revealed the variation of charge

and spin in the CuO_2 plane for various cuprates [6, 13]. That such modulations are a distinctive feature of the cuprates is most easily seen in the planar ^{17}O spectra, cf. Fig. 8.2 as well as Fig. 8.9. The expected five resonances are there, however, the pronounced asymmetry in the peak intensities and widths is striking. It simply results if there is a correlation between spin and charge variations that have similar size (as is accidentally the case for ^{17}O at typical NMR fields). Then, the broadening effects can cancel for one transition, while they lead to twice the broadening for another transition, since the magnetic shift is the same for all transitions, while the quadrupole related shifts change sign as one goes from high- to low-frequency satellites. Again, such spectra have been reported for many cuprates (also electron doped systems [2]). The correlations also exist for Cu NMR, but here the quadrupole splitting is much larger than the shift, and the correlation is hardly noticeable [13, 61]. One also knows from the ^{17}O spectra that the asymmetry is lost below T_c. This identifies the modulation mechanism to involve the spin shift [13].

If the charge density oscillates, one expects rather special patterns for the NMR satellite lineshape, since the number of nuclei near the wave's extrema is much larger (e.g., see CDW lineshapes in $NbSe_3$ [64]). With the exception of ^{17}O NMR in some cases, where broadened, slightly triangular lineshapes are found, no pronounced patterns are observed in cuprate NMR where Gaussian lineshapes

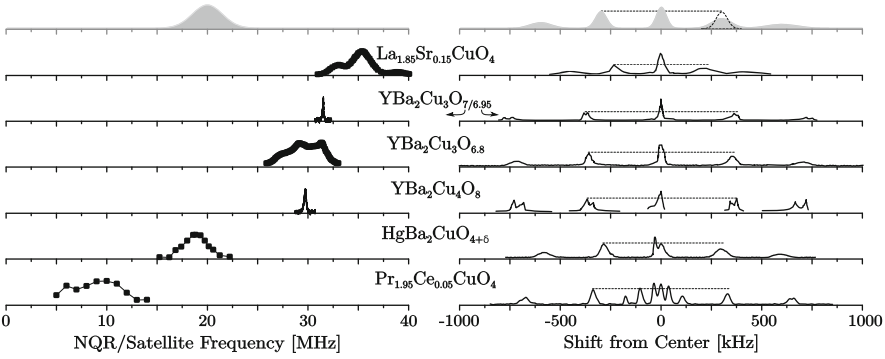

Fig. 8.9 NMR and NQR linewidths reveal charge and spin density variations in the CuO_2 plane for various cuprates. *Left panel*: Planar Cu data; NQR for the La-based, NMR of Y-, Hg-, and Pr-based systems (for NMR data the central transition frequency was subtracted to facilitate comparison with NQR). Note that some lineshapes are influenced by the other isotope or resonances from inequivalent sites. Even so, almost all cuprates, i.e., hole and electron doped systems, including the supposedly very clean Hg-system show linewidths of a few MHz. Exceptions are the stoichiometric compounds, $YBa_2Cu_3O_7$ and $YBa_2Cu_4O_8$, with an order of magnitude smaller widths. *Right panel*: Full spectra of planar O measured by NMR for various cuprates in $c \parallel B_0$ orientation. For better comparison, the shift from the central transition is shown. Magnetic linewidth from spin density variations affects all transitions equally. Broadening of satellite transitions originate from charge density variations. The asymmetry in linewidths and different peak intensities for lower and upper satellite transitions (marked with *gray dashed lines*) show a correlation of charge and spin density variations, such that frequency distributions from charge and spin variations add up for one transition and cancel for another. Literature data from [2, 5, 21, 34, 40, 61–63]

dominate. This may point to the role of disorder [65]. In fact, since in the $YBa_2Cu_3O_{6+y}$ family all planar O satellites are split and since the size of the splitting is not related to the orthorhombicity, it was argued that this family with a higher chemical order may reveal commensurate charge density variations [21], a scenario that work in progress appears to affirm [57].

A summary of ^{17}O and ^{63}Cu lineshapes from the literature is presented in Fig. 8.9. As mentioned before, broad lines are typical except for a few chemically well-ordered systems (the Cu satellite transitions of $YBa_2Cu_3O_7$ can be as narrow as 0.09 MHz while that of $La_{2-x}Sr_xCuO_4$ is typically about 2 MHz). If, in fact, due to charge density variations, the quadrupolar linewidths shown in Fig. 8.9 indicate substantial variations of local charges at Cu ($0.2\,\% \leq \delta n_d \leq 7\%$) and O ($1\,\% \leq \delta n_p \leq 5\%$) [19].

Very interesting examples for the linebroadening in the cuprates are high quality single crystals of $HgBa_2CuO_{4+\delta}$. Such crystals show two rather narrow ^{199}Hg NMR ($I = 1/2$) lines. One line is due to Hg atoms far away from interstitial O that is used as dopant, the other Hg line originates from atoms that have an interstitial O next to them (with the intensity ratio providing a measure of interstitial O content δ in agreement with the hole doping measured by corresponding n_d and n_p in the CuO_2 plane) [61]. This is what one would expect from high quality samples. To the contrary, the planar Cu NMR lines are very broad similar to those in $La_{2-x}Sr_xCuO_4$ [66]. Note that the dopant is far away from the CuO_2 plane, which is often taken as a prerequisite for a homogeneous CuO_2 plane, but the latter is not the case.

It is also known that co-doping the originally stoichiometric materials will result in tremendous linewidths, as well [67]. These facts point to an instability of the cuprates towards charge density variations from dopants, which may remind one of the phase separation taking place in $La_2CuO_{4+\delta}$ [68], or the existence of the so-called *B*-site in $La_{2-x}Sr_xCuO_4$ [39, 69].

Since NMR linewidths measure static properties, it could be possible that dynamic inhomogeneities are omnipresent in the cuprates, and are pinned by impurities or other perturbing interactions. In order to differentiate between a pinning scenario or chemical inhomogeneity, one might expect that the application of pressure will be a helpful tool. In particular NMR of $YBa_2Cu_4O_8$ under pressure should be interesting, which was pursued by some of us. First results showed the closing of the pseudogap and revealed the two-component scenario also for this system [11]. Unfortunately, a sufficiently high ^{17}O exchange of single crystals of $YBa_2Cu_4O_8$ turned out to be problematic in this metastable phase. Preliminary Cu NMR experiments did reveal a substantial line broadening under pressure, and NQR spectra are shown together with those for $YBa_2Cu_3O_{6.9}$ in Fig. 8.10. Indeed, one observes a very significant line broadening under pressure for either material (that is not related to pressure gradients). Obviously, under the given pressures changes of the chemical structure can be excluded and the change in the local field gradient must be from incipient static charge density variations triggered by minute changes of the distances in the lattice. Further details of the new experiments will be published soon [20, 57].

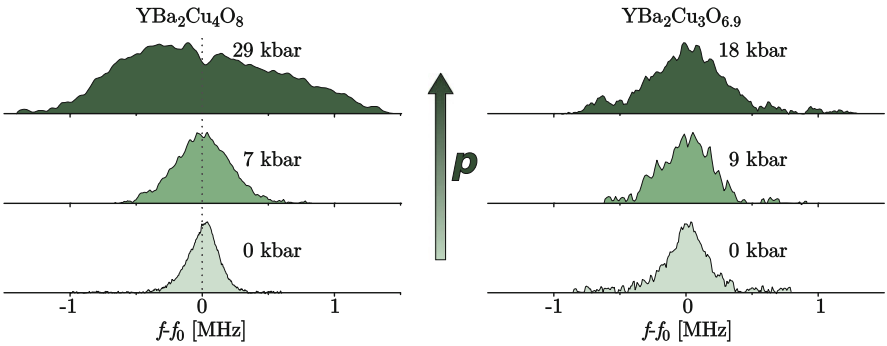

Fig. 8.10 Pressure-induced broadening of the planar ^{63}Cu NQR line in $YBa_2Cu_4O_8$ (*left*) and $YBa_2Cu_3O_{6.9}$ (*right*) at room temperature. f_0 is the center of mass of each line. The full width at half maximum of $YBa_2Cu_4O_8$ ($YBa_2Cu_3O_{6.9}$) increases with a slope of 44 kHz/kbar (10 kHz/kbar). The quadrupolar broadening far exceeds possible effects from pressure inhomogeneity or strain and cannot be caused by chemical effects, thus indicating static charge density variations induced by pressure

In a recent study of $YBa_2Cu_3O_7$ [19], some of us showed that even moderate magnetic fields can reveal significant static charge variations. Comparing quadrupolar linewidths of planar Cu measured with nuclear quadrupole resonance (NQR) and extracted from NMR satellites, at temperatures below 200 K and above T_c, a pronounced quadrupolar broadening by application of a magnetic field was observed. Like the effects observed under increasing pressure, or from doping far from the CuO_2 plane, it is hard to understand that a moderate magnetic field affects the charge in such a manner. A slowing or pinning of an already present, but dynamic charge density variation seems a much likelier scenario.

Finally, one long-standing problem concerns the NMR signal intensity. It was found that underdoped cuprates can show NMR wipe-out, i.e., the NMR signal disappears very rapidly as a function of temperature, while the signal remaining is not very different from that observed before [70, 71]. This is reminiscent of spin-glass behavior when clustered electronic spin-locking percolates the sample rapidly as the temperature is lowered [72]. Clearly, if large parts of the NMR signal are missing, conclusions based on the existing signal may be wrong. Typically, strong signal variation with temperature can be spotted easily, however, absolute intensity measurements with NMR are notoriously difficult. There is evidence that for some systems NMR signal intensities reflect all nuclei [12], while for others there is also evidence that some of the signal is missing [73]. It is well known from Cu NMR in Cu metal that strain can easily wipe out part of the signal for quadrupolar nuclei while the remaining signal carries the important information about the electronic properties. Nevertheless, we feel that absolute intensity measurements should be performed, since incommensurate charge density variations could easily lead to signal loss, which in turn may affect conclusions.

Conclusion and Outlook

NMR is a fundamental local probe that must be in agreement with theory. Early experiments have given important clues about the cuprate properties, but while data are largely undisputed, conclusions drawn from them may have to be revisited. For example, with the failure of the single-component interpretation of the NMR shifts, many conclusions for the description of the cuprates have to be questioned. Another recent breakthrough comes from the understanding of the charge distribution in the CuO_2 plane. Local charges in the CuO_2 plane, quantitatively measurable with NMR, reveal a striking variation between different cuprate families. These differences, set by material chemistry, seem to set superconducting properties, such as T_c and superfluid density, and are reflected in other electronic properties such as the exchange coupling and the charge-transfer gap. It has therefore been proposed to use n_d and n_p as a backdrop for discussing cuprate phenomenology, rather than the total doping x per CuO_2, that misses out on crucial material-specific aspects.

With the new quantitative understanding of the charge distribution, early aspects of spin and charge variations point to ubiquitous charge density variations in the cuprates that are disturbed by chemical inhomogeneity, i.e., it is not chemical inhomogeneity itself that causes such phenomena. Recent experiments, the observation of charge density variations induced by high magnetic fields, the fact that even moderate magnetic fields can lead to the formation of static charge density variations, and the fact that the most homogeneous systems show significant charge variations under pressure, all combined indicate the universality of the phenomenon. Further experiments at high pressure and on single crystals will be very helpful in better characterizing related effects. Nevertheless, it appears that the maximum T_c is set by the charge transfer from oxygen to copper, already in the parent system.

Acknowledgements We acknowledge the financial support from the University of Leipzig, the European Social Fund (ESF), and the Deutsche Forschungsgemeinschaft (DFG, project 23130964). We thank A. Bussmann-Holder for discussions and reading the manuscript.

References

1. J.G. Bednorz, K.A. Müller, Z. Phys. B Condens. Matter **193**, 189 (1986). doi:10.1007/BF01303701
2. M. Jurkutat, D. Rybicki, O.P. Sushkov, G.V.M. Williams, A. Erb, J. Haase, Phys. Rev. B **90**, 140504 (2014). doi:10.1103/PhysRevB.90.140504
3. D. Rybicki, M. Jurkutat, S. Reichardt, C. Kapusta, J. Haase, Nat. Commun. **7**, 1 (2016). doi:10.1038/ncomms11413
4. J. Haase, O.P. Sushkov, P. Horsch, G.V.M. Williams, Phys. Rev. B **69**, 94504 (2004). doi:10.1103/PhysRevB.69.094504
5. J. Haase, C.P. Slichter, C.T. Milling, J. Supercond. **15**, 339 (2002). doi:10.1023/A:1021014028677

6. J. Haase, C.P. Slichter, R. Stern, C.T. Milling, D.G. Hinks, *in* Phase Transitions and Self-Organization in Electronic and Molecular Networks, ed. by M.F. Thorpe, J.C. Phillips (Springer US, Boston, MA, 2001), pp. 413–430. doi:10.1007/0-306-47113-2_27
7. M. Takigawa, A.P. Reyes, P.C. Hammel, J.D. Thompson, R.H. Heffner, Z. Fisk, K.C. Ott, Phys. Rev. B **43**, 247 (1991). doi:10.1103/PhysRevB.43.247
8. M. Bankay, M. Mali, J. Roos, D. Brinkmann, Phys. Rev. B **50**, 6416 (1994). doi:10.1103/PhysRevB.50.6416
9. J. Haase, C.P. Slichter, G.V.M. Williams, J. Phys. Condens. Matter **21**, 455702 (2009). doi:10.1088/0953-8984/21/45/455702
10. J. Haase, D. Rybicki, C.P. Slichter, M. Greven, G. Yu, Y. Li, X. Zhao, Phys. Rev. B **85**, 104517 (2012). doi:10.1103/PhysRevB.85.104517
11. T. Meissner, S.K. Goh, J. Haase, G.V.M. Williams, P.B. Littlewood, Phys. Rev. B **83**, 220517 (2011). doi:10.1103/PhysRevB.83.220517
12. D. Rybicki, J. Kohlrautz, J. Haase, M. Greven, X. Zhao, M.K. Chan, C.J. Dorow, M.J. Veit, Phys. Rev. B **92**, 081115 (2015). doi:10.1103/PhysRevB.92.081115
13. J. Haase, C.P. Slichter, R. Stern, C.T. Milling, D.G. Hinks, J. Supercond. Nov. Magn. **13**, 723 (2000). doi:10.1023/A:1007853912812
14. P.M. Singer, A.W. Hunt, T. Imai, Phys. Rev. Lett. **88**, 047602 (2002). doi:10.1103/PhysRevLett.88.047602
15. W. Chen, G. Khaliullin, O.P. Sushkov, Phys. Rev. B **83**, 064514 (2011). doi:10.1103/PhysRevB.83.064514
16. T. Wu, H. Mayaffre, S. Krämer, M. Horvatić, C. Berthier, W.N. Hardy, R. Liang, D.A. Bonn, M.H. Julien, Nature **477**, 191 (2011). doi:10.1038/nature10345
17. T. Wu, H. Mayaffre, S. Krämer, M. Horvatić, C. Berthier, P.L. Kuhns, A.P. Reyes, R. Liang, W.N. Hardy, D.A. Bonn, M.H. Julien, Nat. Commun. **4**, 2113 (2013). doi:10.1038/ncomms3113
18. T. Wu, H. Mayaffre, S. Krämer, M. Horvatić, C. Berthier, W. Hardy, R. Liang, D.A. Bonn, M.H. Julien, Nat. Commun. **6**, 6438 (2015). doi:10.1038/ncomms7438
19. S. Reichardt, M. Jurkutat, A. Erb, J. Haase, J. Supercond. Nov. Magn. **29**, 3017 (2016). doi:10.1007/s10948-016-3827-1
20. S. Reichardt, M. Jurkutat, A. Erb, J. Haase, To be Published
21. J. Haase, J. Supercond. **16**, 473 (2003). doi:10.1023/A:1023882516857
22. W. Heitler, E. Teller, Proc. R. Soc. A Math. Phys. Eng. Sci. **155**, 629 (1936). doi:10.1098/rspa.1936.0124
23. J. Bardeen, L.N. Cooper, J.R. Schrieffer, Phys. Rev. **106**, 162 (1957). doi:10.1103/PhysRev.106.162
24. J. Bardeen, L.N. Cooper, J.R. Schrieffer, Phys. Rev. **108**, 1175 (1957). doi:10.1103/PhysRev.108.1175
25. L.C. Hebel, C.P. Slichter, Phys. Rev. **113**, 1504 (1959). doi:10.1103/PhysRev.113.1504
26. Y. Masuda, A.G. Redfield, Phys. Rev. **125**, 159 (1962). doi:10.1103/PhysRev.125.159
27. K. Yosida, Phys. Rev. **110**, 769 (1958). doi:10.1103/PhysRev.110.769
28. J. Korringa, Physica **16**, 601 (1950). doi:10.1016/0031-8914(50)90105-4
29. S.E. Barrett, D.J. Durand, C.H. Pennington, C.P. Slichter, T.A. Friedmann, J.P. Rice, D.M. Ginsberg, Phys. Rev. B **41**, 6283 (1990). doi:10.1103/PhysRevB.41.6283
30. E. Helmut Brandt, Phys. C Supercond. **195**, 1 (1992). doi:10.1016/0921-4534(92)90068-N
31. N.J. Curro, C. Milling, J. Haase, C.P. Slichter, Phys. Rev. B **62**, 3473 (2000). doi:10.1103/PhysRevB.62.3473
32. M. Takigawa, P.C. Hammel, R.H. Heffner, Z. Fisk, K.C. Ott, J.D. Thompson, Phys. Rev. Lett. **63**, 1865 (1989). doi:10.1103/PhysRevLett.63.1865
33. C.H. Pennington, D.J. Durand, C.P. Slichter, J.P. Rice, E.D. Bukowski, D.M. Ginsberg, Phys. Rev. B **39**, 2902 (1989). doi:10.1103/PhysRevB.39.2902
34. I. Mangelschots, M. Mali, J. Roos, D. Brinkmann, S. Rusiecki, J. Karpinski, E. Kaldis, Phys. C. Supercond **194**, 277 (1992). doi:10.1016/S0921-4534(05)80005-X

35. M. Takigawa, P.C. Hammel, R.H. Heffner, Z. Fisk, J.L. Smith, R.B. Schwarz, Phys. Rev. B **39**, 300 (1989). doi:10.1103/PhysRevB.39.300
36. H. Alloul, T. Ohno, P. Mendels, Phys. Rev. Lett. **63**, 1700 (1989). doi:10.1103/PhysRevLett.63.1700
37. C.H. Pennington, D.J. Durand, C.P. Slichter, J.P. Rice, E.D. Bukowski, D.M. Ginsberg, Phys. Rev. B **39**, 274 (1989). doi:10.1103/PhysRevB.39.274
38. R.E. Walstedt, B.S. Shastry, S.W. Cheong, Phys. Rev. Lett. **72**, 3610 (1994). doi:10.1103/PhysRevLett.72.3610
39. K. Yoshimura, T. Imai, T. Shimizu, Y. Ueda, K. Kosuge, H. Yasuoka, J. Phys. Soc. Jpn. **58**, 3057 (1989). doi:10.1143/JPSJ.58.3057
40. S. Ohsugi, Y. Kitaoka, K. Ishida, G.Q. Zheng, K. Asayama, J. Phys. Soc. Jpn. **63**, 700 (1994). doi:10.1143/JPSJ.63.700
41. J.M. Tranquada, P.M. Gehring, G. Shirane, S. Shamoto, M. Sato, Phys. Rev. B **46**, 5561 (1992). doi:10.1103/PhysRevB.46.5561
42. J. Haase, D.K. Morr, C.P. Slichter, Phys. Rev. B **59**, 7191 (1999). doi:10.1103/PhysRevB.59.7191
43. C.P. Slichter, in *Handbook of High-Temperature Superconductivity*, ed. by J.R. Schrieffer, J.S. Brooks (Springer, New York, 2007), pp. 215–256. doi:10.1007/978-0-387-68734-6_5
44. R.E. Walstedt, *The NMR Probe of High-T Materials*, 1st edn. (Springer, Berlin, 2007). doi:10.1007/978-3-540-75565-4X
45. G.Q. Zheng, T. Mito, Y. Kitaoka, K. Asayama, Y. Kodama, Phys. C Supercond. **243**, 337 (1995). doi:10.1016/0921-4534(95)00029-1
46. J. Haase, G.V.M. Williams, Private Communication (2000)
47. N.J. Curro, B.L. Young, J. Schmalian, D. Pines, Phys. Rev. B **70**, 235117 (2004). doi:10.1103/PhysRevB.70.235117
48. A.M. Mounce, S. Oh, J.A. Lee, W.P. Halperin, A.P. Reyes, P.L. Kuhns, M.K. Chan, C. Dorow, L. Ji, D. Xia, X. Zhao, M. Greven, Phys. Rev. Lett. **111**, 187003 (2013). doi:10.1103/PhysRevLett.111.187003
49. K. Schwarz, C. Ambrosch-Draxl, P. Blaha, Phys. Rev. B **42**, 2051 (1990). doi:10.1103/PhysRevB.42.2051
50. R.L. Martin, Phys. Rev. Lett. **75**, 744 (1995). doi:10.1103/PhysRevLett.75.744
51. S. Pliberšek, P.F. Meier, EPL **50**, 789 (2000). doi:10.1209/epl/i2000-00550-y
52. P.C. Hammel, B.W. Statt, R.L. Martin, F.C. Chou, D.C. Johnston, S.W. Cheong, Phys. Rev. B **57**, R712 (1998). doi:10.1103/PhysRevB.57.R712
53. Y.J. Uemura, G.M. Luke, B.J. Sternlieb, J.H. Brewer, J.F. Carolan, W.N. Hardy, R. Kadono, J.R. Kempton, R.F. Kiefl, S.R. Kreitzman, P. Mulhern, T.M. Riseman, D.L. Williams, B.X. Yang, S. Uchida, H. Takagi, J. Gopalakrishnan, A.W. Sleight, M.A. Subramanian, C.L. Chien, M.Z. Cieplak, G. Xiao, V.Y. Lee, B.W. Statt, C.E. Stronach, W.J. Kossler, X.H. Yu, Phys. Rev. Lett. **62**, 2317 (1989). doi:10.1103/PhysRevLett.62.2317
54. T. Imai, C.P. Slichter, J.L. Cobb, J.T. Markert, J. Phys. Chem. Solids **56**, 1921 (1995). doi:10.1016/0022-3697(95)00226-X
55. M. Jurkutat, J. Haase, A. Erb, J. Supercond. Nov. Magn. **26**, 2685 (2013). doi:10.1007/s10948-013-2160-1
56. J.S. Schilling, in *Handbook of High-Temperature Superconductivity*, ed. by J.R. Schrieffer (Springer, New York, 2007). doi:10.1007/978-0-387-68734-6_11
57. S. Reichardt, M. Jurkutat, J. Kohlrautz, A. Erb, J. Haase, To be Published (2016)
58. F. Arrouy, J.P. Locquet, E.J. Williams, E. Mächler, R. Berger, C. Gerber, C. Monroux, J.C. Grenier, A. Wattiaux, Phys. Rev. B **54**, 7512 (1996). doi:10.1103/PhysRevB.54.7512
59. I. Bozovic, G. Logvenov, I. Belca, B. Narimbetov, I. Sveklo, Phys. Rev. Lett. **89**, 107001 (2002). doi:10.1103/PhysRevLett.89.107001
60. Y.A. Kharkov, O.P. Sushkov, Sci. Rep. **6**, 34551 (2016). doi:10.1038/srep34551
61. D. Rybicki, J. Haase, M. Lux, M. Jurkutat, M. Greven, G. Yu, Y. Li, X. Zhao, arXiv:1208.4690v1 (2012)

62. J.A. Lee, Y. Xin, W.P. Halperin, A.P.P.L. Reyes, M.K. Chan, C. Dorow, L. Ji, D. Xia, X. Zhao, M. Greven, arXiv:1603.08839 (2016)
63. Y. Yoshinari, H. Yasuoka, Y. Ueda, K. Koga, K. Kosuge, J. Phys. Soc. Jpn. 59, 3698 (1990). doi: 10.1143/JPSJ.59.3698
64. J.H. Ross, Z. Wang, C.P. Slichter, Phys. Rev. Lett. **56**, 663 (1986). doi:10.1103/PhysRevLett.56.663
65. A. Shengelaya, K.A. Müller, EPL **109**, 27001 (2015). doi:10.1209/0295-5075/109/27001
66. D. Rybicki, J. Haase, M. Greven, G. Yu, Y. Li, Y. Cho, X. Zhao, J. Supercond. Nov. Magn. **22**, 179 (2009). doi:10.1007/s10948-008-0376-2
67. G.V.M. Williams, R. Dupree, J.L. Tallon, Phys. Rev. B **60**, 1360 (1999). doi:10.1103/PhysRevB.60.1360
68. P.C. Hammel, A.P. Reyes, S.W. Cheong, Z. Fisk, J.E. Schirber, Phys. Rev. Lett. **71**, 440 (1993). doi:10.1103/PhysRevLett.71.440
69. J. Haase, R. Stern, D.G. Hinks, C.P. Slichter, in *Stripes and Related Phenomena*, ed. by A. Bianconi, N.L. Saini (Kluwer Academic/Plenum, New York, 2000), pp. 303–308. 10.1007/0-306-47100-0_36
70. A.W. Hunt, P.P.M. Singer, A.F. Cederström, T. Imai, Phys. Rev. B **64**, 134525 (2001). doi:10.1103/PhysRevB.64.134525
71. G.V.M. Williams, J. Haase, Phys. Rev. B **75**, 172506 (2007). doi:10.1103/PhysRevB.75.172506
72. M.C. Chen, C.P. Slichter, Phys. Rev. B **27**, 278 (1983). doi:10.1103/PhysRevB.27.278
73. J. Haase, N.J. Curro, M. Jurkutat, Private Communication (2000–2015)

Chapter 9
Towards an Understanding of Hole Superconductivity

J.E. Hirsch

Introduction

The first paper by K. Alex Müller listed in Web of Science, from when he was a youthful 27-year-old, is on an apparatus to measure Hall effect [1]. It shows that from the very beginning of his scientific career, Alex Müller was well aware of the fundamental difference between electrons and holes.

The concept of holes has played a prominent role in semiconductor physics for a long time, as exemplified by the title of Shockley's 1950 book "Electrons and holes in semiconductors". It also of course has played a prominent role in quantum electrodynamics since Dirac discovered holes in 1930. But it had played essentially no role in superconductivity until the discovery of high T_c cuprates.

In his 1987 paper in LT18, 'A Road towards High T_c Superconductivity' [2] Alex spelled it out clearly for the first time: *"Basically, all these materials, are hole superconductors."* Again in his 1987 Science paper 'The Discovery of a Class of High-Temperature Superconductors' [3] Alex remarks *"This new class of materials found at the IBM Zurich Research Laboratory are hole rather than electron superconductors"*. In his 1988 paper in the proceedings of the NEC Symposium on Mechanisms of High Temperature Superconductivity he states [4] *"As the T_c of hole-containing $BaBiO_3$ is more than twice as high as that of the electron-containing compound, one might expect an enhancement of T_c for* ***hole superconductivity*** *over electron superconductivity in the cuprates if the latter are found."* It is clear that Alex was struck by the realization that holes seemed to be favorable for superconductivity, which was not part of his initial theoretical views on high temperature superconductivity (Jahn-Teller polarons) that guided him and Bednorz

J.E. Hirsch (✉)
Department of Physics, University of California, La Jolla, San Diego, CA 92093-0319, USA
e-mail: jhirsch@ucsd.edu

A. Bussmann-Holder et al. (eds.), *High-Tc Copper Oxide Superconductors and Related Novel Materials*, Springer Series in Materials Science 255,
DOI 10.1007/978-3-319-52675-1_9

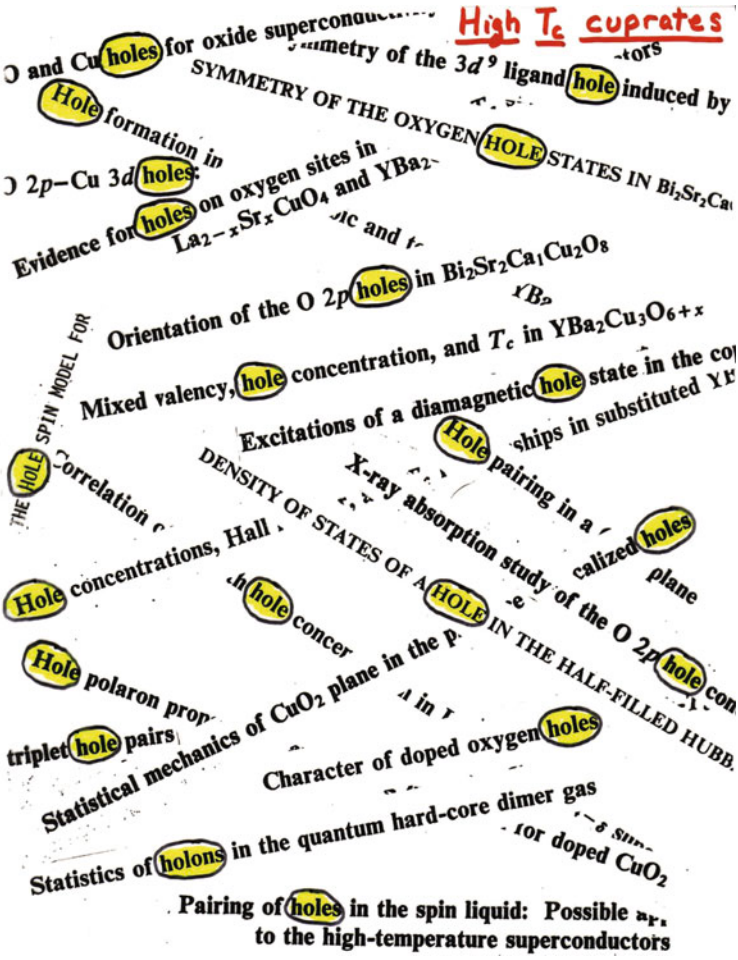

Fig. 9.1 Titles of some papers published in the early days of high T_c research (see text)

in their search and led them to their discovery. Thus, he emphasized the 'hole' aspect in many of his early papers and talks. The era of hole superconductivity had begun.

Soon thereafter, everybody working on cuprates was talking about 'holes'. Figure 9.1 shows a transparency I made in those early days with random titles of papers that I used in talks to emphasize this point.

I met Alex Müller for the first time at the NEC symposium in late 1988 and listened keenly to his talk, one of the first in the program. I still have the handwritten notes I took at the time, 6 pages of them. In the middle of the second page there is the statement "These materials are hole superconductors", with "hole

superconductors" underlined. I still remember vividly the emphasis he put on those words in his presentation, that deeply impressed me at the time.

Later in that meeting, H. Takagi made a comprehensive presentation of transport properties of $(La_{1-x}Sr)_2CuO_4$ [5]. He showed a slide of T_c versus hole concentration (p) and asked "why does superconductivity disappear" at $p = 0.15$?" On the very next slide he showed a graph of Hall coefficient versus hole concentration showing that it changes sign from positive to negative precisely at $p = 0.15$.

Takagi suggested in this presentation that T_c goes to zero in the overdoped regime because of a cross-over from Mott-Hubbard to Fermi liquid regime. He did *not*, to the best of my recollection and according to my notes taken at the time, directly connect the change in sign of the Hall coefficient from positive to negative to the disappearance of superconductivity. I wondered for a long time why he hadn't done that and only much later I learned why [6]. It turns out that at that time, October 1988, he and his coworkers already had discovered the so-called 'electron superconductors'. He did not mention this discovery at that meeting nor did other speakers, those results were announced in January 1989 [7]. But this clearly must have been the reason why he did not think that the type of charge carrier (whether hole or electron) was a determining factor. It took many more years and a lot of experiments to establish that the electron-doped cuprates are in fact also *hole superconductors* [8–10].

In the paragraph above I said the concept of holes had played *essentially* no role in superconductivity. The caveat is because in fact several researchers in the early days of superconductivity did suggest that a positive Hall coefficient was favorable to superconductivity [11–17]. However, the concept fell completely out of favor after the establishment of the BCS theory of superconductivity, within which the character of the carriers, whether electrons or holes, plays no role.

Ever since I heard that fateful talk by Alex Müller in 1988 I have been convinced that hole carriers are essential for superconductivity in all materials [18], not just in high T_c cuprates. Together with Frank Marsiglio and other coworkers we have presented many arguments and calculations in favor of this hypothesis [19]. In this short paper I would like to discuss what I think is the most fundamental reason why holes are indispensable for superconductivity, that I have only understood a few months ago. But first some preliminaries.

Holes in Condensed Matter Physics

The concept of holes in solids was introduced by Werner Heisenberg in 1931 [20]. He writes: *"Die Elektrizitlätsleitung in Metallen mit einer geringen Anzahl von Löchern kann also in jeder Beziehung beschrieben werden wie die Leitung in Metallen mit einer geringen Anzahl von positiven Leitungselektronen. Daraus folgt unmittelbar der anomale Halleffekt fur solche Metalle."* Similarly Peierls in 1932 writes [21] *"Ein Band, in dem sich nur wenige Elektronen befinden, verhalten sich in jeder Beziehung genau so, wie ein Band, in dem nur für wenige Elektronen noch Platz ist, mit dem Unterschied, dass den freien Plätzen eine umgekehrte—also*

TABLE I. Different properties of the carriers at the Fermi energy when the Fermi level is near the bottom (bonding electron) and near the top of the band (antibonding electron).

Bonding electron at the Fermi energy	Antibonding electron at the Fermi energy
Undressed	Dressed
Low kinetic energy	High kinetic energy
Long wavelength	Short wavelength
Small effective mass	Large effective mass
Uniform charge density	Nonuniform charge density
Moves in direction of force	Moves opposite to force
Conducts electricity	Anticonducts electricity
Contributes to Drude weight	Anticontributes to Drude weight
Detached from lattice	Transfers momentum to lattice
Large quasiparticle weight	Small quasiparticle weight
Coherent conduction	Incoherent conduction
Large Drude weight	Small Drude weight
Negative Hall coefficient	Positive Hall coefficient
Good metals	Bad metals
Stable lattices	Unstable lattices
Ions attract each other	Ions repel each other
Carriers repel each other	Carriers attract each other
Normal metals	Superconductors

Fig. 9.2 From a paper the author wrote in 2005 [23]. The most important reason for why holes are necessary for superconductivity is highlighted

positive—Ladung zuzuschreiben ist. Da jedoch die Leitfähigkeit unabhängig vom Vorzeichen der Ladung ist, wird sich dieser Unterschied zunächst in der Leitfähigkeit noch nicht bernerkbar machen." The reason for the 'anomalous' (positive) Hall coefficient in metals with 'hole' carriers was worked out by Peierls upon the suggestion of Heisenberg already in 1929 [22].

Both of the above statements say that *"in jeder Beziehung"*, i.e. *"in every respect"*, holes are just like electrons in solids. This point of view has been pervasive in condensed matter physics ever since. Yet it is incorrect. If it was correct, there would be no superconductivity.

In a paper I wrote in 2005 I listed many reasons why holes are *not* like electrons, as shown in Fig. 9.2. The most relevant one regarding superconductivity is highlighted. I will explain this in a later section.

Electron-Hole Asymmetric Polarons and Dynamic Hubbard Models

Alex Müller has always focused on polarons as being at the root of high temperature superconductivity [24–26]. Somewhat overlapping with his idea, within the theory of hole superconductivity [19] high T_c originates in small *electron-hole asymmetric* polarons [27–29]. In our view the dominant polaronic aspect arises from electron-electron interactions rather than from electron-lattice interactions. Nevertheless, even for electron-phonon polarons electron-hole asymmetry can play a big role and favor hole over electron superconductivity [30], consistent with Alex's expectations.

A very simple, natural and general extension of the conventional Hubbard model leads to 'dynamic Hubbard models' and electron-hole asymmetric electronic polarons. In the conventional Hubbard model, electrons in doubly occupied orbitals pay the Coulomb repulsion price U, but their orbitals are unmodified relative to the singly-occupied orbital. However, in reality a doubly occupied atomic orbital expands relative to the singly-occupied orbital, due to electron-electron repulsion. This 'orbital relaxation' causes a reduction of the bare U and leads to electron-hole asymmetry. Dynamic Hubbard models describe this physics [31]. When a hole propagates, the orbital relaxation causes 'dressing' of the quasiparticle and effective mass enhancement, as in small polarons. Instead, when an electron propagates no such effects exist. The effects are largest when the effective ionic charge is small, so that the modification of the orbital upon double occupancy is large. Figure 9.3 shows a 'cartoon picture' of the physics that is included in dynamic Hubbard models and not in the conventional Hubbard model. The orbital expansion lowers the electronic kinetic energy (as well as the Coulomb repulsion), and causes

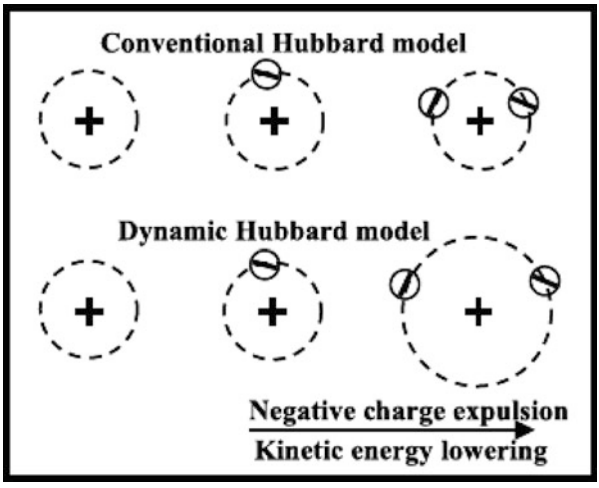

Fig. 9.3 Schematics of the physics described by dynamic Hubbard models

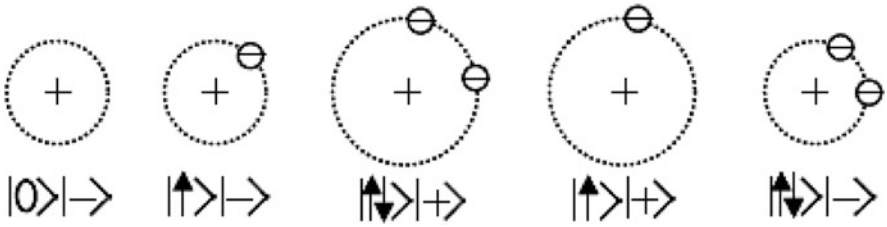

Fig. 9.4 Site states of dynamic Hubbard model with an auxiliary spin degree of freedom with states $|+>, |->$. The *left* three states (as well as $|\downarrow>|->$) are lowest in energy and are the quasiparticle states in the low energy effective Hamiltonian with a correlated hopping term

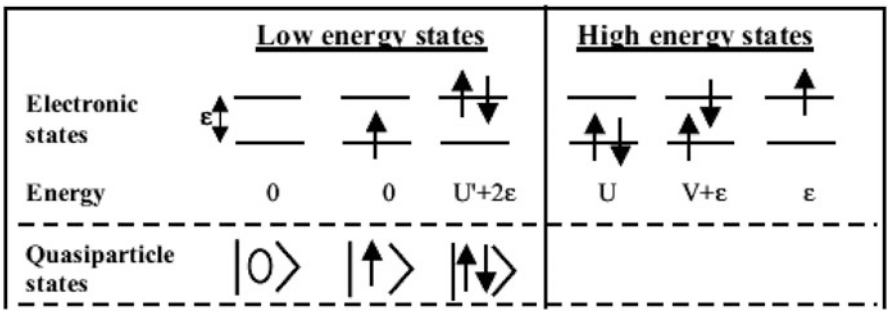

Fig. 9.5 Site states of dynamic Hubbard model with two orbitals per site. The low energy physics is identical to the one described by Fig. 9.4

negative charge to expand outward. Both aspects are relevant to the physics of hole superconductivity [32].

Various versions of dynamic Hubbard models can be constructed to embody this physics, involving auxiliary spin or local vibrational degrees of freedom, or in a purely electronic version a tight binding model with two rather than one orbital per site [33], as shown in Figs. 9.4 and 9.5. The physics of all these models is very similar. Figure 9.6 illustrates the fact that holes have more difficulty propagating than electrons in these models. The low energy effective Hamiltonian that results from these models has a 'correlated hopping' term Δt that gives different hopping amplitudes depending on the occupation of the sites involved in the hopping process and leads to kinetic energy driven pairing and superconductivity when the Fermi level is close to the top of the band, i.e. for hole carriers [34]. The T_c versus hole concentration dependence gives the bell-shaped behavior characteristic of the cuprates as well as the T_c versus e/a (electron/atom) ratio in transition metal alloys [35, 36] (Matthias' rules) [37, 38].

The applicability of these models to high T_c cuprates rests on the assumption that doped holes go into oxygen $p\pi$ orbitals in the plane [27], rather than $p\sigma$ orbitals as generally assumed. This assumption is supported by quantum chemical calculations by Goddard and coworkers [39]. We have recently argued that band structure

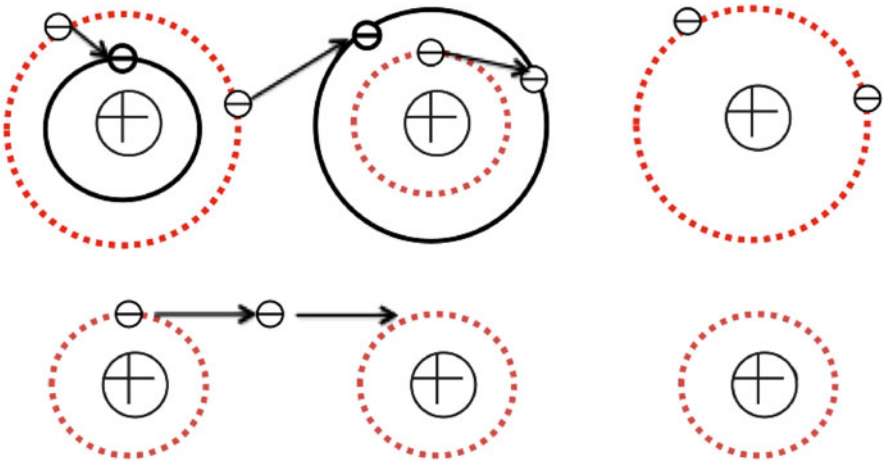

Fig. 9.6 Propagation of holes (*upper pictures*) versus propagation of electrons (*lower pictures*). Holes are highly dressed because they cause a large disruption in their environment as they propagate, electrons are undressed. In the *upper picture* the full (*dotted*) *circles* denote the orbital in the final (initial) state

calculations get this wrong because they do not take into account the energy lowering that results from local orbital relaxation when a hole goes into the doubly occupied O^{--} $p\pi$ orbital [40]. These models also give rise to a strong tendency to charge inhomogeneity and phase separation due to the dominance of kinetic over potential energy [32], which correlates with behavior found in the cuprates [41].

Hole Superconductivity in Materials

The models discussed in the previous section were introduced motivated by the physics of high T_c cuprates. We found that they describe in a very natural way several salient properties of cuprate superconductors [19, 34, 42], in particular their:

1. Dome-like T_c versus hole concentration dependence
2. Positive pressure dependence of T_c
3. Crossover between strong and weak coupling regimes as the hole concentration increases
4. Crossover from incoherent to coherent behavior both as the hole concentration increases and as superconductivity sets in
5. Tunneling asymmetry, with larger current for negatively biased sample
6. Apparent violation of conductivity sum rule, and transfer of optical spectral weight from high frequencies to low frequencies as superconductivity sets in.

In addition, we have argued [43] that these models lead to hole pairing and superconductivity in the following classes [44, 45] of superconducting materials:

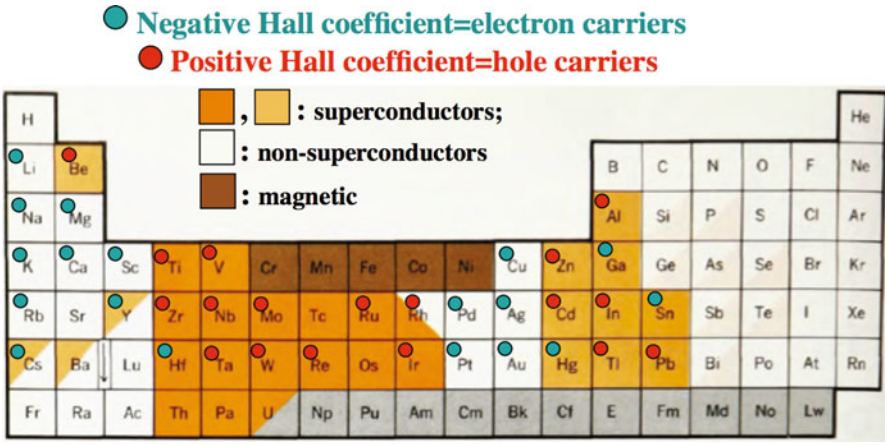

Fig. 9.7 Periodic table, showing the preponderance of superconductors among positive Hall coefficient elements and non-superconductors among negative Hall coefficient elements

1. Hole-doped cuprates [34, 42]
2. Electron-doped cuprates [46]
3. Magnesium diboride [47, 48]
4. Transition metal series alloys [35, 36]
5. Iron pnictides [49]
6. Iron selenides [43]
7. Doped semiconductors [43, 50]
8. Elements under high pressure [51, 52]
9. Sulphur hydride [53]
10. A-15 materials [54–58]
11. All other superconductors [57, 58]

For the simplest materials, the elements, there is an obvious preponderance of positive Hall coefficient for superconducting elements and negative Hall coefficients for nonsuperconducting elements [11–17, 59], as shown in Fig. 9.7. In the following we discuss the most fundamental reason that we believe makes holes indispensable for superconductivity.

The Central Question in Superconductivity

I would like to propose that the central question in the phenomenon of superconductivity is a very basic one that even a child could ask, but scientists have *never* asked, nor answered. That question is the following:

When a superconductor in a magnetic field goes normal, how does the supercurrent stop?

I am assuming an ideal situation where the transition is perfectly reversible. For example, for given applied magnetic field $H < H_c$, the temperature is raised from slightly below $T_c(H)$ to slightly above $T_c(H)$. Alternatively, with the system at temperature $T_c(H)$, the magnetic field is raised from $H - \delta H$ to $H + \delta H$. When the system goes normal, the magnetic field penetrates the body and the supercurrent stops. Upon slightly cooling or slightly reducing the magnetic field, the supercurrent starts flowing again and the magnetic field is expelled.

How the supercurrent stops is a highly non-trivial question. In particular, what happens to its mechanical momentum [60]? The obvious and only possible answer is that the momentum of the supercurrent gets transferred to the body as a whole. For example, if the body is a cylinder hanging from a thread with a magnetic field along the direction of its axis, when the supercurrent stops the body will start to rotate around its axis.

This experiment has never been performed this way. However an equivalent experiment has been performed. If a magnetic field is applied to the superconductor, the current starts flowing in one direction and the body starts rotating in the same direction. The angular momentum of the body reflects the angular momentum of the supercurrent, carried by negative electrons moving in direction opposite to the current flow. In this situation, if the temperature is then raised, both the supercurrent and the rotation of the body will stop.

But *how* is the momentum of the supercurrent transferred to the body as a whole?

The problem is, the process is reversible. The reverse process is the Meissner effect. Any momentum transfer process involving collisions of electrons in the supercurrent with phonons or impurities is an irreversible process, hence not allowed. We argue that the conventional theory of superconductivity *cannot* answer this question. The question has certainly never been posed nor answered in the superconductivity literature.

We have recently posed the question and proposed an answer to it [61]. The key element of the answer is *holes*. We argue that *the only way* that electrons can transfer mechanical momentum to the body as a whole in a reversible way is through the motion of *holes*.

Why Holes Are Not Like Electrons

The velocity of Bloch electrons is given by

$$\vec{v}_k = \frac{1}{\hbar} \frac{\partial \varepsilon_k}{\partial \vec{k}} \tag{9.1}$$

and the acceleration by

$$\frac{d\vec{v}_k}{dt} = \frac{1}{\hbar^2}\frac{\partial^2 \varepsilon_k}{\partial \vec{k}\partial \vec{k}}\frac{\partial}{\partial t}\left(\hbar\vec{k}\right) = \frac{1}{m_k^*}\frac{\partial}{\partial t}\left(\hbar\vec{k}\right). \tag{9.2}$$

The last equality is for the particular case of an isotropic band, with

$$\frac{1}{m_k^*} \equiv \frac{1}{\hbar^2}\frac{\partial^2 \varepsilon_k}{\partial k^2}. \tag{9.3}$$

According to semiclassical transport theory, in the presence of an external force $\vec{F}^k_{ext}$

$$\frac{\partial}{\partial t}\left(\hbar\vec{k}\right) = \vec{F}^k_{ext}. \tag{9.4}$$

The total force exerted on a Bloch electron is

$$m_e\frac{d\vec{v}_k}{dt} \equiv \vec{F}^k_{tot} = \frac{m_e}{m_k^*}\vec{F}^k_{ext} = \vec{F}^k_{ext} + \vec{F}^k_{latt} \tag{9.5}$$

with m_e the bare electron mass, and $\vec{F}^k_{latt}$ the *force exerted by the lattice on the electron* of wave vector k, given by

$$\vec{F}^k_{latt} = \left(\frac{m_e}{m_k^*} - 1\right)\vec{F}^k_{ext} \tag{9.6}$$

Near the bottom of the band m_k^* is positive and $\vec{F}^k_{latt}$ is small. Near the top of the band, m_k^* is negative and $\vec{F}^k_{latt}$ is larger than $\vec{F}^k_{ext}$ and points in opposite direction, causing the electron near the top of the band to accelerate in direction *opposite* to the external force.

The importance of this for superconductivity is that when the lattice exerts a force on the electron, by Newton's third law the electron exerts a force on the lattice, or in other words transfers momentum to the lattice. This indicates that the electrons that are most effective in transferring momentum from the electrons to the body are electrons near the top of the band. In other words, holes. This will answer the central question of how the momentum of the supercurrent is transferred to the body as a whole in a reversible way, without energy dissipation.

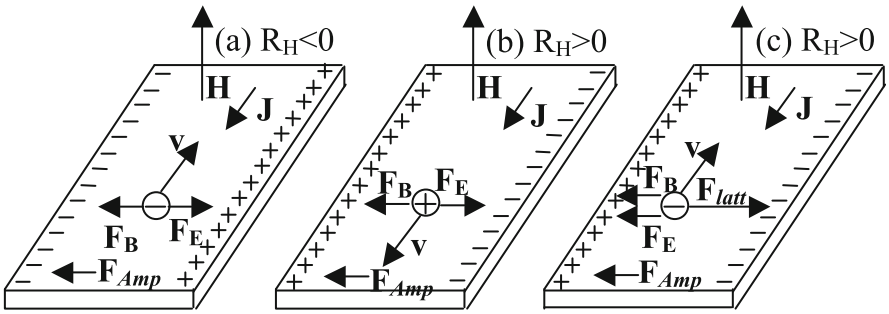

Fig. 9.8 Hall effect for a material with negative Hall coefficient (**a**) and for a material with positive Hall coefficient (**b**, **c**). F_B and F_E are the magnetic and electric Lorentz forces acting on carriers, F_{latt} is the force exerted by the lattice on the electron, $\vec{J}$ is the current density, $\vec{F}_{Amp}$ is the Amperian force on the bar

How Holes Answer the Central Question in Superconductivity

Figure 9.8 shows the balance of forces on carriers in Hall bars with negative and positive Hall coefficients. For $R_H < 0$, (Fig. 9.8a), electric and magnetic forces on electrons are balanced, and for $R_H > 0$, (Fig. 9.8b), electric and magnetic forces on holes are balanced. However, in that case, electric and magnetic forces on electrons are *not* balanced, as shown in Fig. 9.8c). For electrons to propagate along the direction of the current $\vec{J}$, another force is needed to balance electric and magnetic forces when $R_H > 0$. That is the force exerted by the lattice on electrons, F_{latt}.

In the following, the forces under discussion are understood to be in direction perpendicular to the flow of the current $\vec{J}$ in Fig. 9.8. (There is also an electric force in direction parallel to $\vec{J}$ that is of no interest for the issue at hand). It is easy to see that the total force exerted by the lattice on the carriers is zero for a band close to empty with $R_H < 0$ and is not zero for a band close to full and $R_H > 0$: the total force exerted by both the lattice and the external fields on the current carrying carriers has to be zero, hence from Eq. ((9.5))

$$\sum_{occ} \vec{F}^k_{tot} = \sum_{occ} \frac{m_e}{m^*_k} \vec{F}^k_{ext} = 0 \tag{9.7}$$

where the sum is over occupied k states. For the case $R_H < 0$ and the band close to empty we can assume that the effective mass is independent of k, $m^*_k = m^*$. From Eq. ((9.7))

$$\sum_{occ} \frac{m_e}{m_k^*} \vec{F}_{ext}^{\,k} = \frac{m_e}{m^*} \sum_{occ} \vec{F}_{ext}^{\,k} = 0 \tag{9.8}$$

therefore

$$\sum_{occ} \vec{F}_{ext}^{\,k} = 0 \tag{9.9}$$

and Eqs. ((9.6)), ((9.8)), and ((9.9)) imply

$$\sum_{occ} \vec{F}_{latt}^{\,k} = 0 \tag{9.10}$$

so that the total force exerted by the lattice on the carriers in direction perpendicular to the current flow is zero, and so is the total force exerted by the carriers on the lattice.

Instead, for a band that is close to full and $R_H > 0$, we cannot assume that m_k^* is independent of k for the occupied states, instead we assume $m_k^* = -m^*$ for the empty states. Eq. ((9.7)) then implies

$$\sum_{occ} \vec{F}_{tot}^{\,k} = -\sum_{unocc} \frac{m_e}{m_k^*} \vec{F}_{ext}^{\,k} = -\frac{m_e}{m^*} \sum_{unocc} \vec{F}_{ext}^{\,k} = 0 \tag{9.11}$$

and from Eqs. ((9.6)) and ((9.11))

$$\sum_{occ} \vec{F}_{latt}^{\,k} = -\sum_{occ} \vec{F}_{ext}^{\,k} \tag{9.12}$$

$$= -\sum_{all} \vec{F}_{ext}^{\,k} + \sum_{unocc} \vec{F}_{ext}^{\,k} = -2Ne\vec{E} \neq 0$$

where N is the number of $k-$points in the Brillouin zone. To obtain Eq. ((9.12)) we used that the external force is

$$\vec{F}_{ext}^{\,k} = e\vec{E} + \frac{e}{c} \vec{v}_k \times \vec{B} \tag{9.13}$$

with $\vec{E}, \vec{B}$ the electric and magnetic fields.

Equation ((9.12)) shows that when $R_H > 0$ the lattice exerts a force on the conducting carriers that is perpendicular to the current flow. Conversely, the conducting carriers exert a force on the lattice or, in other words, transfer momentum to the lattice in direction perpendicular to the current flow. This force on the lattice, plus the electrostatic force on the positive ions that points in opposite direction (to the right in Fig. 9.8c) gives the Amperian force on the Hall bar, $\vec{F}_{Amp}$. In contrast, if the carriers are electrons with $R_H < 0$, the same $\vec{F}_{Amp}$ results

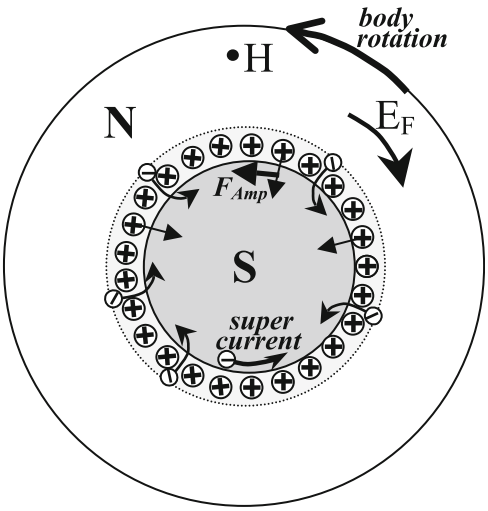

Fig. 9.9 Superconductor to normal transition in a magnetic field H pointing out of the paper. Supercurrent flows clockwise, electrons carrying supercurrent move counterclockwise. The inward motion of the phase boundary is accompanied by inward flow of negative charge, that stops the supercurrent flow, and inward flow of normal hole carriers, that transfers the angular momentum of the supercurrent to the body as a whole that acquires counterclockwise rotation. Details are given in [63]

from the direct force of the electric field on the ions (to the left in Fig. 9.8a) and there is no net force exerted by electrons on the lattice nor by the lattice on electrons in direction perpendicular to the current flow, hence no momentum transfer from the carriers to the lattice.

This is, in essence, why hole carriers are indispensable for superconductivity [62]. Let us next discuss how this explains the process of momentum transfer from the supercurrent to the body when the supercurrent stops.

Figure 9.9 shows schematically how the supercurrent stops when a cylindrical superconductor in a magnetic field pointing out of the paper goes normal. The inward motion of the N/S phase boundary is accompanied by a radial flow and counterflow of charge. In the process of becoming normal, superconducting electrons flow inward and are stopped by the clockwise magnetic Lorentz force resulting from this radial motion. At the same time normal holes flow inward and exert a torque on the body in the counterclockwise direction. The force $\vec{F}_{Amp}$ shown in the figure pointing counterclockwise is the same as the Amperian force in Fig. 9.7c pointing left. In that way, the counterclockwise angular momentum possessed by the supercurrent is transferred to the body as a whole without involving irreversible collisions that would dissipate Joule heat. In the reverse process where a normal cylinder becomes superconducting and expels the magnetic field, the direction of the motions in Fig. 9.9 are simply reversed (except for the direction of the supercurrent). The details of these processes are discussed in [62, 63].

Discussion

Alex Müller's and George Bednorz's breakthrough discovery in 1986 ushered in the era of hole superconductivity. Before their discovery, the term 'hole superconductor' had never been used, after their discovery it became commonplace. The evidence that hole carriers are necessary for superconductivity continues to accumulate. Of course sometimes it is the case that in a multiband situation electron carriers exist and dominate the transport, in which case it may not be obvious that hole carriers also exist and are responsible for superconductivity.

Possibly the one example where it is least obvious that hole carriers exist is for the very low carrier density n-doped semiconductor $SrTiO_3$ [64–66]. It is believed that only electron carriers exist in this material, however according to the physics discussed in this paper superconductivity is impossible without hole carriers. Therefore, we conjecture that there is at least two-band conduction in this material [65] with one of the bands hole-like, the hole carriers would be induced by electron doping just like in the case of the electron-doped cuprates [46]. It is interesting that Alex Müller and coworkers in 1976 reported the finding of trapped holes near dopant impurities [67], which suggests that holes are easily induced in this material.

Thirty years after the discovery of the cuprate superconductors it is becoming increasingly clear that *all superconductors are hole superconductors* [68]. There are many reasons for this, all interconnected [19]. I believe the most fundamental reason is the one discussed in this paper, which can be summarized in the following very simple statements:

- In any superconductor, the mechanical momentum of the supercurrent has to be transferred to the body as a whole when the supercurrent stops.
- The process is reversible under ideal conditions.
- Only *hole carriers* can transfer mechanical momentum from electrons to the body as a whole in a reversible way, electron carriers cannot.

If this is so, it had been glimpsed at in the early days of superconductivity [11–17] but then was well hidden from superconductivity researchers for a long time, buried under the heavy weight of BCS theory, until Alex Müller's and George Bednorz's 1986 discovery of high T_c superconductivity in cuprates started the process of bringing this deep secret of superconductors again into the open.

I am extremely grateful to them for having led me to this understanding. Happy 90th birthday Alex!

References

1. K.A. Müller, J. Wieland, Apparatur zur Messung des Hall-Effektes und der magnetischen Widerstandsänderung mit. Wechselstrom. Helv. Phys. Acta **27**, 690 (1954)
2. J. G. Bednorz, K. A. Müller, Proceedings of 18th International Conference on Low Temperature Physics, Kyoto. Jpn. J. Appl. Phys. **26**(Supplement 26-3), 1781 (1987), http://iopscience.iop.org/article/10.7567/JJAPS.26S3.1781/meta

3. K. A. Müller, J. G. Bednorz, **237**, 1133 (1987)
4. K. A. Müller, in *"Mechanisms of High Temperature Superconductivity", Proceedings of the 2nd NEC Symposium*, Hakone, Japan, 24–27 October 1988, p. 2
5. H. Takagi, Ref. [4], p. 238
6. Private communication
7. Y. Tokura, H. Takagi, S. Uchida, A superconducting copper oxide compound with electrons as the charge carriers. Nature (London) **377**(345) (1989)
8. W. Jiang et al., Anomalous transport properties in superconducting $Nd_{1.85}Ce_{0.15}CuO_{4\pm\delta}$. Phys. Rev. Lett. **73**, 1291 (1994)
9. P. Fournier et al., Thermomagnetic transport properties of $Nd_{1.85}Ce_{0.15}CuO_{4+\delta}$ films: evidence for two types of charge carriers. Phys. Rev. B **56**, 14149 (1997)
10. Y. Dagan, R.L. Greene, 'Hole superconductivity in the electron-doped superconductor $Pr_{2-x}Ce_xCuO'_4$. Phys. Rev. B **76**, 024506 (2007)
11. K. Kikoin, B. Lasarew, Hall effect and superconductivity. Nature **129**, 57 (1932)
12. K. Kikoin, B. Lasarew, Physik. Zeits. d. Sowjetunion **3**, 351 (1933)
13. L. Brillouin, 'Le champ self-consistent, pour des electrons lies; la supraconductibilite', Jour. de Phys. et le Rad. VII, Tome IV, A. Papapetrou, 'Bemerkungen zur Supraleitung', Z. Phys. **92**, 513 (1934)
14. M. Born, K.C. Cheng, Theory of superconductivity. Nature **161**, 968 (1948)
15. R.P. Feynman, Superfluidity and superconductivity. Rev. Mod. Phys. **29**, 205 (1957)
16. I.M. Chapnik, On a possible criterion for superconductivity. Sov. Phys. Dokl. **6**, 988 (1962)
17. I.M. Chapnik, On the empirical correlation between the superconducting T_c and the Hall coefficient. Phys. Lett. A **72**, 255 (1979)
18. J.E. Hirsch, Hole superconductivity. Phys. Lett. A **134**, 451 (1989)
19. References in http://physics.ucsd.edu/~jorge/hole.html
20. W. Heisenberg, Zum Paulischen Ausschlie ungsprinzip. Ann. Phys. **402**, 888 (1931)
21. R. Peierls, Elektronentheorie der Metalle. Ergebnisse der exakten Naturwissenschaften **11**, 284 (1932)
22. R. Peierls, Zur Theorie der galvanomagnetischen Effekte. für Physik **53**, 255 (1929)
23. J.E. Hirsch, Why holes are not like electrons. II. The role of the electron-ion interaction. Phys. Rev. B **71**, 104522 (2005)
24. J.G. Bednorz, K.A. Müller, Possible high T_c superconductivity in the Ba - La- Cu- 0 system. Z. Phys. B **64**, 189 (1986)
25. A. Bussmann-Holder, H. Keller, K.A. Müller, in *Superconductivity in Complex Systems. Evidences for Polaron Formation in Cuprates* (Springer, Berlin, 2005)
26. H. Keller, A. Bussmann-Holder, K.A. Müller, Jahn - Teller physics and high-T_c superconductivity. Mater. Today **11**, 38 (2008)
27. J.E. Hirsch, S. Tang, Hole superconductivity in oxides. Solid State Commun. **69**, 987 (1989)
28. J.E. Hirsch, , in '*Electron-hole Asymmetric Polarons*', ed. by E. K. H. Salje, A. S. Alexandrov and W. Y. Liang. "Polarons and Bipolarons in High-T_c Superconductors and Related Materials" (Cambridge University Press, Cambridge, 1995), p. 234
29. J.E. Hirsch, Physica C **201**, 347 (1992)
30. J.E. Hirsch, Polaronic superconductivity in the absence of electron-hole symmetry. Phys. Rev. B **47**, 5351 (1993)
31. J.E. Hirsch, Dynamic Hubbard model. Phys. Rev. Lett. **87**, 206402 (2001)
32. J.E. Hirsch, Dynamic Hubbard model: kinetic energy driven charge expulsion, charge inhomogeneity, hole superconductivity and Meissner effect. Phys. Scr. **88**, 035704 (2013)
33. J.E. Hirsch, Why holes are not like electrons: a microscopic analysis of the differences between holes and electrons in condensed matter. Phys. Rev. B **65**, 184502 (2002)
34. J.E. Hirsch, F. Marsiglio, Superconducting state in an oxygen hole metal. Phys. Rev. B **39**, 11515 (1989)
35. J.E. Hirsch, F. Marsiglio, On the dependence of superconducting T_c on carrier concentration. Phys. Lett. A **140**, 122 (1989)

36. X.Q. Hong, J.E. Hirsch, Superconductivity in the transition-metal series. Phys. Rev. B **46**(14), 702 (1992)
37. B.T. Matthias, Transition temperatures of superconductors. Phys. Rev. **92**, 874 (1953)
38. B.T. Matthias, Empirical relation between superconductivity and the number of valence electrons per atom. Phys. Rev. **97**, 74 (1955)
39. Y. Guo, J.M. Langlois, W.A. Goddard III, Electronic structure and valence-bond band structure of cuprate superconducting materials. Science **239**, 896 (1988)
40. J.E. Hirsch, Effect of orbital relaxation on the band structure of cuprate superconductors and implications for the superconductivity mechanism. Phys. Rev. B **90**, 184515 (2014)
41. A. Shengelaya, K.A. Müller, The intrinsic heterogeneity of superconductivity in the cuprates. EPL **109**, 27001 (2015)
42. F. Marsiglio, J.E. Hirsch, Hole superconductivity and the high-T_c oxides. Phys. Rev. B **41**, 6435 (1990)
43. J.E. Hirsch, 'Materials and mechanisms of hole superconductivity', Physica C **472**, 78 (2012) and references therein
44. J.E. Hirsch, M.B. Maple, F. Marsiglio, Superconducting materials: conventional, unconventional and undetermined. Physica C **514**(Special Issue), 1–444 (2015)
45. J.E. Hirsch, M.B. Maple, F. Marsiglio, Superconducting materials classes: Introduction and overview. Physica C **514**, 1 (2015)
46. J.E. Hirsch, Role of reduction process in the transport properties of electron-doped oxide superconductors. Physica C **243**, 319 (1995)
47. J.E. Hirsch, Hole superconductivity in MgB_2: a high T_c cuprate without Cu. Phys. Lett. A **282**, 392 (2001)
48. J.E. Hirsch, F. Marsiglio, Electron-phonon or hole superconductivity in MgB_2? Phys. Rev. B **64**, 144523 (2001)
49. F. Marsiglio, J.E. Hirsch, Hole superconductivity in arsenic—iron compounds. Physica C **468**, 1047 (2008)
50. E. Bustarret, Superconductivity in doped semiconductors. Physica C **514**, 36 (2015)
51. J.E. Hirsch, J.J. Hamlin, Why non-superconducting metallic elements become superconducting under high pressure. Physica C **470**, S937 (2010)
52. Jing Guo et al, 'The vital role of hole-carriers for superconductivity in pressurized black phosphorus', arXiv:1611.03330 (2016)
53. J.E. Hirsch, F. Marsiglio, Hole superconductivity in H_2S and other sulfides under high pressure. Physica C **511**, 45 (2015)
54. A.A. Manuel et al., Contribution to the determination of the Fermi surface of V_3Si by positron annihilation. Solid State Commun. **31**, 955 (1979)
55. S. Berko, M. Weger, Investigation of the Fermi surface of V_3Si by means of positron annihilation. Phys. Rev. Lett. **24**, 55 (1970)
56. L. Hoffmann, A.K. Singh, H. Takei, N. Toyota, Fermi surfaces in Nb_3Sn through positron annihilation. J. Phys. F **18**, 2605 (1988)
57. J.E. Hirsch, Bond-charge repulsion and hole superconductivity. Physica C **158**, 326 (1989)
58. J.E. Hirsch, Coulomb attraction between Bloch electrons. Phys. Lett. A **138**, 83 (1989)
59. J.E. Hirsch, Correlations between normal-state properties and superconductivity. Phys. Rev. B **55**, 9007 (1997)
60. J.E. Hirsch, The missing angular momentum of superconductors. J. Phys. Condens. Matter **20**, 235233 (2008)
61. J.E. Hirsch, On the reversibitity of the Meissner effect and the angular momentum puzzle. Ann. Phys. (New York) **373**, 230 (2016)
62. J.E. Hirsch, Momentum of superconducting electrons and the explanation of the Meissner effect. Phys. Rev. B **95**, 014503 (2017)
63. J.E. Hirsch, The disappearing momentum of the supercurrent in the superconductor to normal phase transformation. Europhys. Lett. **114**, 57001 (2016)
64. J.F. Schooley et al., Phys. Rev. Lett. **14**, 305 (1965)

65. A. Bussmann-Holder, A.R. Bishop, A. Simon, $SrTiO_3$: from quantum paraelectric to superconducting. Ferroelectrics **400**, 19 (2010)
66. X. Lin, Z. Zhu, B. Fauque, K. Behnia, Fermi surface of the most dilute superconductor. Phys. Rev. X **3**, 021002 (2013)
67. O.F. Schirmer, W. Berlinger, K.A. Müller, Holes trapped near Mg^{2+} and Al^{3+} impurities in $SrTiO_3$. Solid State Commun. **18**, 1505 (1976)
68. J. E. Hirsch, in '*Electron-hole Asymmetry: The Key to Superconductivity*', ed. by J. Ashkenazi et al. "High Temperature Superconductivity: Physical Properties, Microscopic Theory, and Mechanisms" (Springer, New York, 1991), p. 295

Chapter 10
Short Scale Phase Separation of Polarons

Victor V. Kabanov

Introduction

It is well known that the ground state in many of oxides is not homogeneous [1, 2]. In cuprates, for example it was suggested that the phase segregation takes place in the form of stripes or short segments of stripes [3, 4]. Up to now it is not clear whether this phase segregation is associated with magnetic interactions or it is governed by the lattice degrees of freedom. On the other hand it is also generally accepted that the charge density in cuprates is not homogeneous.

Very soon after the discovery of high-T_c superconductors it was suggested that superconductivity is strongly related with the phase separation (see for example [5–9]). In charged systems the phase separation is often accompanied by the charge segregation. Breaking of the charge neutrality leads to the appearance of the electric field and substantial contribution of the electrostatic energy to the thermodynamic potential [10, 11]. On the other hand it is well established that polaronic effects in cuprates are strong [12]. On the basis of that it was suggested that interplay of the short range lattice attraction and the long-range Coulomb repulsion between polarons could lead to the formation of short metallic [13–16] or insulating [15–17] stripes of polarons. In the case of isotropic attraction between polarons the charged bubbles have a spherical shape. Kugel and Khomskii [18, 19] proposed that the anisotropic attraction forces between Jahn-Teller centers could lead to the formation of stripes. The long-range anisotropic attraction forces appear as the solution of the full set of elasticity equations (see [20]). Alternative approach to take into account elasticity potentials was proposed in [21, 22] and is based on the proper consideration of compatibility constraint caused by absence of a dislocation

V.V. Kabanov (✉)
J. Stefan Institute, Jamova 39, 1001, Ljubljana, Slovenia
e-mail: viktor.kabanov@ijs.si

A. Bussmann-Holder et al. (eds.), *High-Tc Copper Oxide Superconductors and Related Novel Materials*, Springer Series in Materials Science 255,
DOI 10.1007/978-3-319-52675-1_10

in the solid. Note that the idea of phase separation is consistent with the so called two component paradigm [23, 24]. Phenomenological aspects of the phase separation were discussed recently in the model of Coulomb frustrated phase transition [25–27].

In this article we consider a different type of ordering of *charged* polarons. The formation of polaronic droplets in this case is due to competition of two types of interactions: the long range Coulomb repulsion and attraction generated by the deformation field. Electron–phonon interaction may be short range and long range, depending on the type of phonons involved. Here we consider phonons of the molecular type, leading to short range forces.

Single Polaron in the Adiabatic Approximation

Adiabatic theory of polarons was formulated many years ago [28–31] and we briefly formulate here the main principles of adiabatic theory for the particular case of interaction with molecular vibrations (Holstein model). The central equation in the adiabatic theory is the Schrödinger equation for the electron in the external potential of the deformation field. In the discrete version it has the following form [32]:

$$-\sum_{m\neq 0} t(m)\left[\psi_n^k - \psi_{n+m}^k\right] + \sqrt{2}g\omega_0\phi_n\psi_n^k = E_k\psi_n^k \tag{10.1}$$

Here t(m) is hopping integral, ψ_{n} is electronic wave function on the site n, φ_{n} is the deformation at the site n, g is electron phonon coupling constant and ω_0 is phonon frequency, k describes quantum numbers of the problem. Important assumption of the adiabatic approximation is that deformation field is very slow and we assume that φ_{n} is time independent $\partial\varphi/\partial t = 0$ when we substitute it to the Schrödinger equation for electron. Therefore, $\omega_0 \to 0$ and $g^2 \to \infty$ but the product $g^2\omega_0 = E_p$ is finite and called polaron shift. The equation for φ_{n} has the form [32]:

$$\phi_n = -\sqrt{2}g\left|\psi_n^0\right|^2 \tag{10.2}$$

Here $\psi_{\mathrm{n}}{}^0$ corresponds to the ground state solution of Eq. (10.1). After substitution of Eq. (10.2) to Eq. (10.1) we obtain:

$$\sum_{m\neq 0} t(m)\left[\psi_n^k - \psi_{n+m}^k\right] - 2E_p\left|\psi_n^0\right|^2\psi_n^k = E_k\psi_n^k \tag{10.3}$$

As a result nonlinear Schrödinger equation [Eq. (10.3)] describes the ground state of the polaron. All excited states are the eigenvalues and eigenfunctions of the *linear* Schrödinger equation in the presence of the external field determined by the

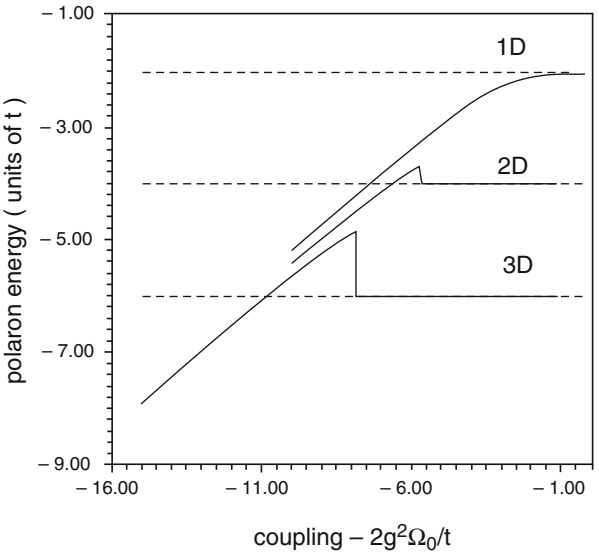

Fig. 10.1 Polaron energy as a function of coupling constant in 1D, 2D and 3D cases. *Dashed lines* represent the energy of delocalized solution in 1D, 2D and 3D respectively

deformation field Eq. (10.2). Polaron energy is the sum of two contributions. The first is the energy of electron in the self-consistent potential well determined by Eq. (10.3), and the second is the energy of the strain field φ itself

$E_{pol}=E_{0+}\omega_0\sum_n \varphi_n^2/2$. The polaron energy is presented in Fig. 10.1 as a function of the dimensionless coupling constant $2g^2\omega_0/t$ in 1D, 2D and 3D cases.

There is very important difference between 1D and 2,3D cases. Polaron energy for 1D case is always less than the energy of the delocalized state (dashed line). Polaron is always stable in 1D. In 2D and 3D cases there is critical value of the coupling constant where first localized solution of Eq. (10.3) appears. It is interesting that the energy of the solution is higher than energy of the delocalized state. Therefore in 2D and 3D cases there is range of coupling constant where polaron is metastable. Delocalized solution is always stable in 3D case. Therefore, the barrier, which separates localized and delocalized states exists in the whole region of the coupling constants, where self-trapped solution exists. In 2D case the delocalized state is unstable at large value of the coupling constant. The barrier separating localized and delocalized states forms only in the restricted region of the coupling constant [32]. To demonstrate that we have plotted polaron energy as a function of its radius in 2D in Fig. 10.2. As it is clearly seen from this figure, the barrier has disappeared at $g > g_{c3} = (2\pi t/\omega_0)^{1/2}$ [32].

There are two types of non-adiabatic corrections to adiabatic polaron. The first is related to renormalization of local phonon modes. Fast motion of the electron within polaronic potential well leads to the shift of the local vibrational frequency:

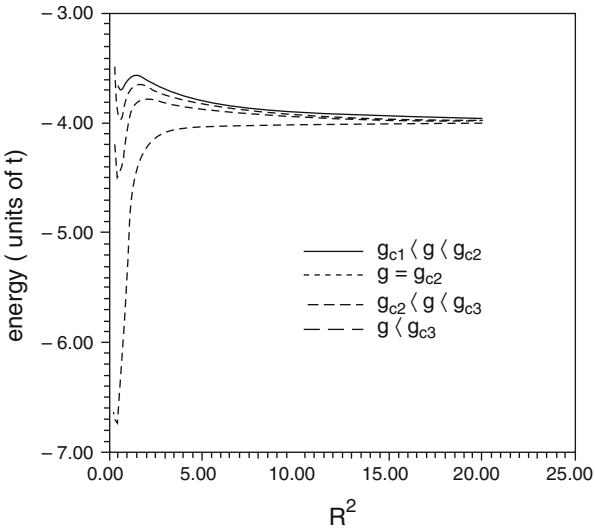

Fig. 10.2 Polaron energy as a function of radius in 2D. For $g > g_{c3}$ $\partial E_{pol}/\partial R < 0$ $g_{c1} = 1.69(t/\omega_0)^{1/2}$ and $g_{c2} = 1.87(t/\omega_0)^{1/2}$

$$\omega = \omega_0 \left[1 - zt^2/2\left(g^2\omega_0\right)^2\right]^{1/2} \tag{10.4}$$

here z is the number of nearest neighbors. This formula is valid in the strong coupling limit $g^2\omega_0 \gg t$ and when tunneling frequency of the polaron is much smaller then phonon frequency.

Another type of correction is related to the restoration of translational symmetry and describes polaron tunnelling and formation of the polaron band. This correction was calculated in the original paper of Holstein [28, 29]. Slightly improved formula was derived in [33]. In the adiabatic limit polaron tunnelling is exponentially suppressed $t_{eff} \approx (E_p\,\omega_0)^{1/2} exp(-g^2)$ (see Eq. (10.9) of [33]) and should be smaller than phonon frequency ω_0.

In the following we will neglect all nonadiabatic corrections. We will consider polaron as pure localized state, and all corrections which contain phonon frequency itself and tunnelling amplitude for polaron are neglected.

Ordering of Charged Polarons: Lattice Gas Model

In this section we consider macroscopic system of polarons in the thermodynamic limit. To underline nontrivial geometry of the phase separation we consider two-fold degenerate electronic states which interact with nonsymmetric deformation field. In our derivation we follow particular model for high-T_c superconductors. Nevertheless the results are general enough and are applicable to many Jahn-Teller systems.

Let us start with the construction of a real-space Hamiltonian which couples 2-fold degenerate electronic states (or near-degenerate states) with optical phonons. Two-fold degeneracy is essential because in that case formation of the polaronic complexes leads to reduction not only of translational symmetry but also reduction of the point group symmetry. Since the Hamiltonian needs to describe a 2-fold degenerate system, the 2-fold degenerate states—for example the two E_u states corresponding to the planar hybridized Cu $d_{x^2-y^2}$, O p_x and p_y orbitals, or the E_u and E_g states of the apical O—are written in the form of Pauli matrices σ_i. Taking into account symmetry arguments we can construct *effective* electron-spin-lattice interaction Hamiltonian given in [34, 35]. Here we consider a simplified version of the JT model Hamiltonian [34, 35], taking only the deformation of the B_{1g} symmetry:

$$H_{JT} = g \sum_{n,l} \sigma_{3,l} f(n) \left(b^{+}_{l+n} + b_{l+n} \right) \tag{10.5}$$

here the Pauli matrix $\sigma_{3,l}$ describes two components of the electronic doublet, and f (n) = $(n^2_x - n^2_y) f_0(n)$ where $f_0(n)$ is a symmetric function describing the range of the interaction. For simplicity we omit the spin index in the sum. The model could be easily reduced to a lattice gas model [27]. We use a pseudospin operator $S = 1$ to describe the occupancies of the two electronic levels n_1 and n_2. Here $S^z = 1$ corresponds to the state with $n_1 = 1, n_2 = 0, S_i^z = -1$ to $n_1 = 0, n_2 = 1$ and $S_i^z = 0$ to $n_1 = n_2 = 0$. Simultaneous occupancy of both levels is excluded due to a high on-site Coulomb repulsion energy. The Hamiltonian in terms of the pseudospin operator is given by [27]

$$H_{LG} = \sum_{i,j} \left(- V_l(i-j) S_i^z S_j^z + V_c(i-j) Q_i Q_j \right. \tag{10.6}$$

where $Q_i = (S_i^z)^2$. V_c(n) = $e^2/\epsilon_0 a (n^2_x + n^2_y)^{1/2}$ is the Coulomb potential, e is the charge of electron, ϵ_0 is the static dielectric constant and a is the effective unit cell period. The anisotropic short range attraction potential is given by $V_l(n) = g^2/\omega \sum_m f(m) f(n+m)$. The attraction in this model is generated by the interaction of electrons with optical phonons. The radius of the attraction force is determined by the radius of the electron-phonon interaction and the dispersion of optical phonons [15, 16].

A similar model can be formulated in the limit of continuous media [27]. Irrespective of whether the resulting interaction between polarons is generated by acoustic or optical phonons the main physical picture remains the same. In both cases there is an anisotropic attraction between polarons on short distances. The interaction could be either ferromagnetic or antiferromagnetic in terms of the pseudospin operators depending on mutual orientation of the orbitals. Without loosing generality we assume that V (n) is nonzero only for the nearest neighbors.

Our aim is to study the model [Eq. (10.6)] at constant average density,

$$n = \frac{1}{N} \sum_i Q_i \tag{10.7}$$

where N is the total number of sites. To investigate the ffects of the long range-forces, we performed Monte Carlo simulations on the system (10.6) [27]. The simulations were performed on a square lattice with dimensions up to $L \times L$ sites with $10 \leq L \leq 100$ using a standard Metropolis algorithm [36] in combination with simulated annealing [37]. For $L > 20$ we observe virtually no dependence of the results on the system size.

We use open boundary conditions to avoid complications due to the long range Coulomb forces and ensure overall electroneutrality by adding a uniformly charged background electrostatic potential (jellium) to Eq. (10.6). The short range potential $v_l(\mathrm{i}) = V_l(\mathrm{i})\epsilon_0 a/e^2$ was taken to be nonzero only for $|\mathrm{i}| < 2$ and is therefore specified only for nearest, and next-nearest neighbours as $v_l(1, 0)$ and $v_l(1, 1)$ respectively.

Model Eq. (10.6) leads to broad variety of textures that are governed by the anisotropy of the potential, concentration of electrons and the temperature. The resulting clustering and ordering of clusters at $t = k_B T\, \epsilon_0 a/e^2 = 0.04$ is shown in Fig. 10.3. As expected, a more symmetric attraction potential leads to the formation of more symmetric clusters. On the other hand, for $v_l(1, 1) = 1$, the "antiferrodistortive" interaction along diagonals prevails, resulting in diagonal stripes. Importantly the reduction of the temperature leads to the increase of the size of clusters (Fig. 10.3b). Note that while locally there is no four-fold symmetry the overall correlation function still retains 4-fold symmetry.

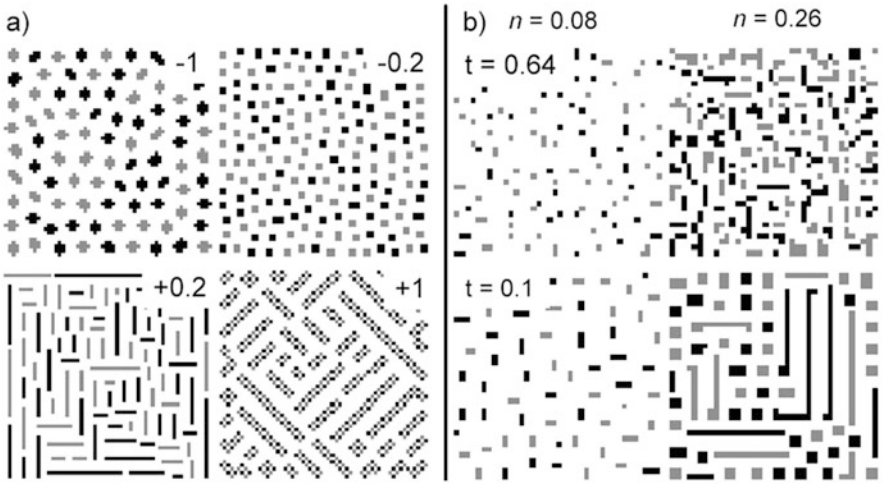

Fig. 10.3 (**a**) Snapshots of clusters ordering at $t = k_B\, T\, \epsilon_0 a/e^2 = 0.04$, $n = 0.2$ and $v_l(1,0) = -1$ for different diagonal $v_l(1,1)$ (given in each figure). *Grey* and *black dots* represent particles in clusters in state $S_l^z = 1$and states $S_l^z = -1$ respectively. The preference for even-particle-number clusters in certain cases is clearly observed, for example for $v_l(1, 1) = 0.2$. (**b**) Snapshots of the particle distribution for two densities at two different temperatures $t = 0.64$ and $t = 0.1$ respectively

In the temperature region where clusters partially order the heat capacity ($c_L = \partial E_L/\partial T$ where E is the total energy) displays the peak at t_{co}. The peak displays no scaling with L indicating that no long range ordering of clusters appears. Inspection of the particle distribution snapshots at low temperatures (Fig. 10.3a) reveals that finite size domains form. Within domains the clusters are perfectly ordered. The domain wall dynamics seems to be much slower than our Monte Carlo simulation timescale preventing domains to grow. The effective L is therefore limited by the domain size. This explains the absence of the scaling and clear evidence for a phase transition near t_{co}.

To get further insight in the cluster formation we measured the cluster-size distribution [27]. In Fig. 10.4 we present the temperature and density dependence of the cluster-size distribution function $x_L(j) = N_p(j)_L/(nL^2)$, where $N_p(j)$ is the total number of particles within clusters of size j. At the highest temperature $x_L(j)$ is close to the distribution expected for the random ordering. As the temperature is decreased, the number of larger clusters starts to increase at the expense of single particles. Remarkably, as the temperature is further reduced, clusters of certain size start to prevail. This is clearly seen at higher densities. Depending on the density, the prevailing clusters are pairs up to $n \approx 0.2$, quadruples for $0.1 < n < 0.3$ etc. We note that for a large range of $v_l(1,\ 0)$, the system prefers clusters with an even number of particles. Odd particle-number clusters can also form, but have a much narrower parameter range of stability. The preference to certain cluster sizes

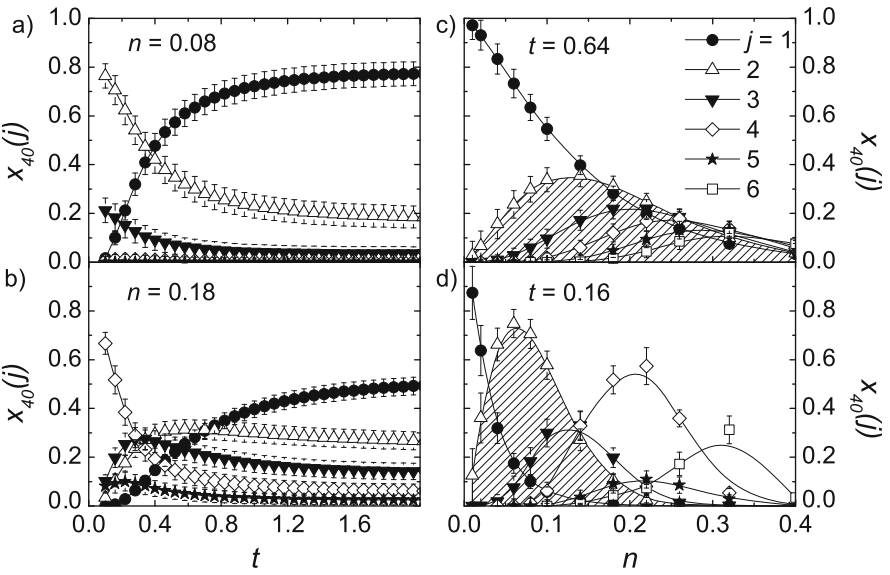

Fig. 10.4 The temperature dependence of the cluster-size distribution function $x_L(j)$ (for the smallest cluster sizes) as a function of temperature at two different average densities $n = 0.08$ (**a**) and $n = 0.18$ (**b**). $x_L(j)$ as a function of n at the temperature between t_0 and t_{cl} (**c**), and near t_{co} (**d**). The ranges of the density where pairs prevail are very clearly seen in (**d**). *Error bars* represent the standard deviation

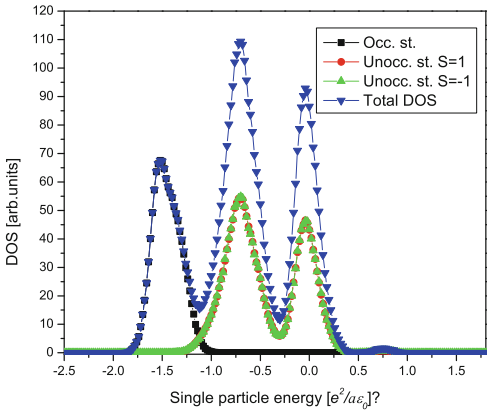

Fig. 10.5 Energy dependent DOS for n = 0.25 and t = 0.07. The gap is always centered near Fermi energy

becomes clearly apparent only at temperatures lower then t_{cl}, and the transition is not abrupt but gradual with the decreasing temperature. Similarly, with increasing density changes in textures also indicate a series of crossovers.

It is interesting to note that this model allows to understand the origin of the pseudogap in cuprates [38]. Calculated DOS is presented in Fig. 10.5. As it is clearly seen from this figure the occupied states and unoccupied states are always separated by the Coulomb gap. This effect does not depend on doping and the gap is always present near Fermi level.

We conclude that a model with only anisotropic JT strain and a long-range Coulomb interaction indeed is unstable with respect to the short scale phase separation and gives rise to a remarkably rich phase diagram including pairs, stripes and charge- and orbital- ordered phases, of clear relevance to oxides. The energy scale of the phenomena is defined by the parameters used in H_{LG} (10.6). For example, using the measured value $\epsilon_0 \simeq 40$ [39] for La_2CuO_4, we estimate $V_c(1, 0) = 0.1$ eV, which is also the typical energy scale of the "pseudogap" in the cuprates. The robust prevalence of the paired state in a wide region of parameters (Fig. 10.4c, d) is particularly interesting from the point of view of superconductivity, where the onset of superconductivity occurs as a result of phase percolation [40]. A similar situation occurs in manganites and other oxides with the onset of a conductive state at the threshold of percolation, but different textures are expected to arise due to different magnitude (and anisotropy) of V_l(n), and static dielectric constant ϵ_0 in the different materials [41, 42].

Coulomb Frustrated First Order Phase Transition

As it is stated in the previous section uncharged JT polarons have the tendency to ordering. The ordering transition is a phase transition of the first order. At the fixed density of polarons the system is unstable with respect to the global phase

separation. The global phase separation is frustrated by charging effects leading to short-scale phase separation. Therefore the results of the Monte-Carlo simulation of the model (10.6) allow general model independent interpretation. Let us consider the classical free energy density corresponding to the first order phase transition:

$$F_1 = \left[(t-1) + \left(\eta^2 - 1\right)^2\right]\eta^2 \tag{10.8}$$

Here $t = (T - T_c)/(T_0 - T_c)$ is dimensionless temperature. At $t = 4/3$ ($T = T_0 + (T_0 - T_c)/3$) the nontrivial minimum in the free energy appears. At $t = 1$ ($T = T_0$) the first order phase transition occurs, but the trivial solution $\eta = 0$ corresponds to the metastable phase. At $t = 0$ ($T = T_c$) trivial solution becomes unstable. In order to study the case of Coulomb frustrated phase transition we have to add coupling of the order parameter η to local charge density. Our order parameter describes sublattice magnetization and therefore only square of the order parameter may be coupled to the local charge density ρ:

$$F_{coupl} = -\alpha\eta^2\rho \tag{10.9}$$

The total free energy density should contain the gradient term and the electrostatic energy:

$$F_{grad} + F_{el} = C(\nabla\eta)^2 + \frac{K}{2}[\rho(r) - \overline{\rho}]\int dr'\left[\rho\left(r'\right) - \overline{\rho}\right]/|r - r'| \tag{10.10}$$

Here we write $\overline{\rho}$ explicitly to take into account global electroneutrality. Total free energy Eqs. (10.8–10.10) should be minimized at fixed t and $\overline{\rho}$.

Let us demonstrate that Coulomb term leads to the phase separation in the 2D case. Minimization of F with respect to the charge density ρ(r) leads to the following equation:

$$-\alpha\nabla_{3D}^2\eta^2 = 4\pi K[\rho(r) - \overline{\rho}]d\delta(z) \tag{10.11}$$

here we write explicitly that density ρ(r) depends only on 2D vector r and introduce layer thickness d, to preserve correct dimensionality. Solving this equation by applying the Furrier transform and substituting the solution back to the free energy density we obtain:

$$F = F_1 - \alpha\eta^2\overline{\rho} + C(\nabla\eta)^2 - \frac{\alpha^2}{8\pi Kd}\int dr'\frac{\nabla\left(\eta(r)^2\right)\nabla\left(\eta\left(r'\right)^2\right)}{|r - r'|} \tag{10.12}$$

As a results the free energy functional is similar to the case of the first order phase transition with shifted critical temperature due to the presence of the term $\alpha\eta^2\overline{\rho}$ and nonlocal gradient term of higher order.

To demonstrate that uniform solution has higher energy then nonhomogeneous solution we make Fourier transform of the gradient term:

$$F_{grad} \propto Ck^2|\eta_k|^2 - \frac{\alpha^2 k\left|(\eta^2)_k\right|^2}{4\pi Kd} \tag{10.13}$$

here η_k and $(\eta^2)_k$ are Fourier components of the order parameter and square of the order parameter respectively. If we assume that the solution is uniform i.e. $\eta_0 \neq 0$ and $(\eta^2)_0 \neq 0$ small nonuniform corrections to the solution reduces the free energy at small k, where second term dominates. Indeed direct numerical minimization of Eq. (10.12) leads to variety of textures depending on temperature and the coupling strength [43]. At low temperatures the stripe phase dominates the phase diagram. With increase of temperature the crossover to the bubble phase takes place [43].

Proposed free energy functional is similar to that proposed in [26]. The important difference is that in our case the charge is coupled to the square of the order parameter and it plays the role of local temperature, while in the case of [26] there is linear coupling of the charge to the order parameter. Charge in that case plays the role of the external field. Moreover, contrary to the case of [26] where charge is accumulated near *domain walls*, in our case charge is accumulated near *interphase boundaries*.

Conclusion

We have shown that competition of the anisotropic interaction between Jahn-Teller polarons generated by optical and/or acoustical phonons and of the long range Coulomb repulsion leads to the short range charge segregation. Topology of this phase separation ranges from charged bubbles to oriented charged stripes depending on the anisotropy of the polaron-polaron interaction. More generally the inhomogeneous phase appears due to the tendency of polarons to the global phase separation. On the other hand the global phase separation becomes unstable because of the long-range Coulomb forces. We derived the standard Landau functional with nonlocal long-range gradient term which describes the short range phase segregation.

References

1. T. Egami et al., J supercond **13**, 709 (2000)
2. J. Tranquada et al., Nature **375**, 561 (1995)
3. A. Bianconi et al., Phys. Rev. Lett. **76**, 3412 (1996)
4. H.A. Mook, F. Dogan, Nature **401**, 145 (1999)

5. K. A. Muller, G. Benedek (eds.), *Phase Separation in Cuprate Superconductors* (World Scientific, 1993)
6. E. Sigmund, K. A. Muller (eds.), *Phase Separation in Cuprate Superconduc-tors* (Springer-Verlag, 1994)
7. J. Zaanen, O. Gunnarsson, Phys. Rev. B **40**, 7391 (1989)
8. V.J. Emery, S. Kivelson, O. Zachar, Phys. Rev. B **56**, 6120 (1997) and references therein.
9. L.P. Gorkov, A.V. Sokol, Pisma ZhETF **46**, 333 (1987)
10. L.P. Gorkov, J. Supercond. **14**, 365 (2001)
11. U. Low, V.J. Emery, K. Fabricious, S. Kivelson, Phys. Rev. Lett. **72**, 1918 (1994)
12. K.A. Muller, J. Supercond. **12**, 3 (1999)
13. F.V. Kusmartsev, Phys. Rev. Lett. **84**, 530 (2000)
14. F.V. Kusmartsev, Phys. Rev. Lett. **84**, 5026 (2000)
15. A.S. Alexandrov, V.V. Kabanov, Pisma ZhETF **72**, 825 (2000)
16. A.S. Alexandrov, V.V. Kabanov, JETP Letters **72**, 569 (2000)
17. F.V. Kusmartsev, J. Phys. IV **9**, 321 (1999)
18. D.I. Khomskii, K.I. Kugel, Europhys. Lett. **55**, 208 (2001)
19. D.I. Khomskii, K.I. Kugel, Phys. Rev. B **67**, 134401 (2003)
20. M.B. Eremin, A.Y. Zavidonov, B.I. Kochelaev, ZhETF **90**, 537 (1986)
21. S.R. Shenoy, T. Lookman, A. Saxena, A.R. Bishop, Phys. Rev. B **60**, R12537 (1999)
22. T. Lookman, S.R. Shenoy, K.O. Rasmussen, A. Saxena, A.R. Bishop, Phys. Rev. B **67**, 024114 (2003)
23. D. Mihailovic, K.A. Muller, High-Tc Superconductivity 1996: Ten Yars After the Discovery, Ed. by E. Kaldis et al. (Kluwer Academic Publishers, 1997), p. 243-256.
24. D. Mihailovic, T. Mertelj, K.A. Muller, Phys. Rev. B **57**, 6116 (1998)
25. C. Ortix, J. Lorenzana, C. Di Castro, Phys. Rev. B, **73**, 245117 (2006) and referece therein.
26. R. Jamei, S. Kivelson, B. Spivak, Phys. Rev. Lett. **94**, 056805 (2005)
27. T. Mertelj, V.V. Kabanov, D. Mihailovic, Phys. Rev. Lett. **94**, 147003 (2005)
28. T. Holstein, Ann. Phys.(N.Y.) **8**, 325 (1959)
29. T. Holstein, Ann. Phys.(N.Y.) **8**, 343 (1959)
30. E.I. Rashba, Opt. Spektrosk. **2**, 78 (1957)
31. E.I. Rashba, Opt. Spektrosk. **2**, 88 (1957)
32. V.V. Kabanov, O.Y. Mashtakov, Phys. Rev. B **47**, 6060 (1993)
33. A.S. Alexandrov, V.V. Kabanov, D.K. Ray, Phys. Rev. B **49**, 9915 (1994)
34. D. Mihailovic, V.V. Kabanov, Phys. Rev., B **63**, 054505 (2001)
35. V.V. Kabanov, D. Mihailovic, Phys. Rev. B **65**, 212508 (2002)
36. N. Metropolis, A.W. Rosenbluth, M.N. Rosenbluth, A.H. Teller, E. Teller, J. Chem. Phys. **21**, 1087 (1953)
37. S. Kirkpatrick, C.D. Gelatt, M.P. Vecchi, Science **220**, 671–680 (1983)
38. J. Miranda, T. Mertelj, V.V. Kabanov, D. Mihailovic, J Supercond. Nov. Magn. **20**, 587 (2007)
39. D. Reagor et al., Phys. Rev. Lett. **62**, 2048 (1989)
40. D. Mihailovic, V.V. Kabanov, K.A. Muller, Europhys. Lett. **57**, 254 (2002)
41. E. Dagotto, T. Hotta, A. Moreo, Phys. Rep. **344**, 1 (2001)
42. A.S. Alexandrov, A.M. Bratkovsky, V.V. Kabanov, Phys. Rev. Lett. **96**, 117003 (2006)
43. J. Miranda, V.V. Kabanov, Physica C **468**, 358 (2008)

Chapter 11
Jahn-Teller-Effect Induced Superconductivity in Copper Oxides: Theoretical Developments

Hiroshi Kamimura, Osamu Sugino, Jaw-Shen Tsai, and Hideki Ushio

Introduction by Hiroshi Kamimura

It is a great pleasure to honor Alex on the occasion of his 90th birthday. I first met him in 1987, almost 30 years ago, when I attended the Adriatico Research Conference on high temperature superconductors which was held in International Centre for Theoretical Physics in Trieste, Italy. There we immediately found common interests in the Jahn-Teller (JT) effect involved mechanism in copper oxide superconductors. In October of 1988, I organized the NEC Symposium entitled "Mechanism of High Temperature Superconductivity in Hakone, Japan to invite him as a plenary speaker, and he kindly attended it. Since then, our scientific interaction developed through the exchange of mails and conferences held in Kyoto (Director, Toshiba International School of superconductivity, 1991), Rome (Stripes, Lattice Instabilities and HTS, 1996), Giens in South France (Superconductivity, CMR and Related Materials, 2002), Tsukuba Cuprate superconductors, 2005) and Zurich (20th anniversary of HTST discovery, 2006). This paper is dedicated to Alex, and, in the close relationship to his motivation of JT-effect induced high

H. Kamimura (✉)
Tokyo University of Science, 1-3 Kagurazaka, Shinjuku-ku, Tokyo, 162-8601, Japan
e-mail: kamimura@rs.kagu.tus.ac.jp

O. Sugino
University of Tokyo, Institute of Solid State Physics, 5-1-5 Kashiwanoha, Kashiwa, Chiba, 277-8581, Japan

J.-S. Tsai
Tokyo University of Science, 1-3 Kagurazaka, Shinjuku-ku, Tokyo, 162-8601, Japan

RIKEN Center for Emergent Matter Science (CEMS), Wako, Saitama, 351-0198, Japan

H. Ushio
Tokyo National College of Technology, Hachioji, 193-0097, Japan

A. Bussmann-Holder et al. (eds.), *High-Tc Copper Oxide Superconductors and Related Novel Materials*, Springer Series in Materials Science 255,
DOI 10.1007/978-3-319-52675-1_11

temperature superconductivity, I think that the present theory is the most suitable tribute to him.

General Introduction

Copper oxide (cuprate) superconductors exhibit a number of mysterious electronic properties [1], and extensive experimental and theoretical researches have been made on these properties [2, 3]. Among those, central issues were the clarification of Fermi surface structures, in particular pseudogap and the mechanism of d-wave superconductivity.

Regarding the Fermi surface, there were two views. One view was based on the single-component theory of the t–J model [4], which predicts that a metallic state has a large Fermi surface (FS). Since angle-resolved photoemission spectroscopy (ARPES) experiments did not show the evidence of a large FS, the phenomenological idea of a pseudogap to conceal the part of a large FS was introduced [5]. An alternative view was based on the two-component theory originated from the orbital near-degeneracy, and it was shown that the coexistence of a metallic state and local AF order results in small Fermi pockets constructed by doped holes [6]. This two-component theory is called K–S model [7].

Non-rigid Energy Band Theory for Copper Oxide Superconductors

Cuprate superconductors are different from ordinarysuperconductors in the production process of carriers. That is, the carriers in cuprates are produced from doping chemical elements or making oxygen deficiencies. Thus, the cuprate superconductors are disordered materials. In the present paper, by paying attention to this key feature, we improve the K–S model allowing the band to change non-rigidly when doping holes. We show that the thus-calculated band structure for LSCO is no longer rigid, but changes drastically upon doping holes. The new band structure leads to the Fermi surface structure consisting of the Fermi pocket and Fermi arcs, and it clarifies the origins of pseudogap and d-wave superconductivity.

The K–S model takes account of the two key factors: (i) The undoped cuprate La_2CuO_4 is an antiferromagnetic (AF) Mott insulator, thus, electron correlation plays an important role [8]. (ii) Cuprates consist of JT active Cu ions [1], so that when holes are doped, the JT distorted octahedrons or pyramids in cuprates transform their shapes so as to recover the undistorted shape, to gain the attractive electrostatic energy. Since this transformation occurs in the opposite direction to the JT deformation, it is called the anti-JT effect [9]. Accordingly, the energy separation between the two types of orbital states (Fig. 11.1a), the a_{1g} antibonding

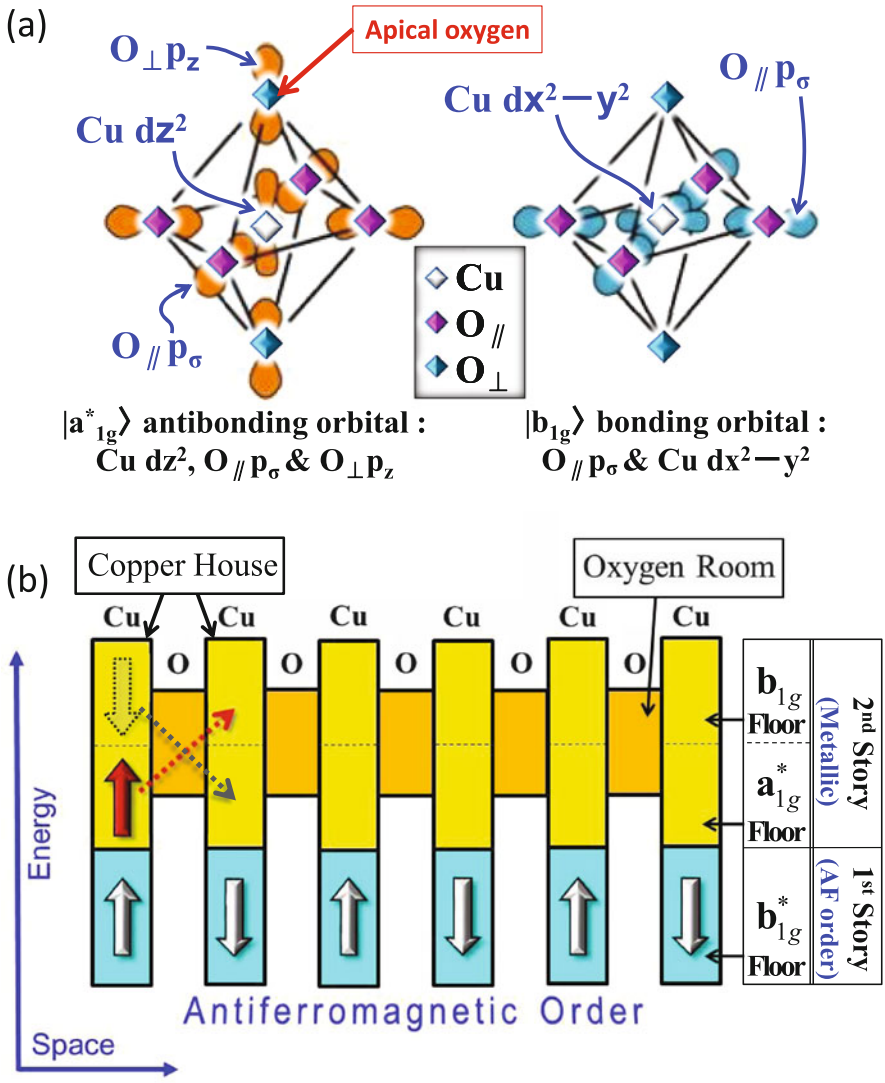

Fig. 11.1 Relevant electronic orbitals and a heuristic explanation of K–S model. (**a**) Relevant electronic orbitals for a doped hole in LSCO: a_{1g} antibonding orbital $|a^*_{1g}>$ and b_{1g} bonding orbital$|\ b_{1g}>$. Here O|| and O⊥ mean the in-plane oxygen in a CuO_2 plane and the apical oxygen in a CuO_6 octahedron, respectively. In addition to the $|a^*_{1g}>$ and $|\ b_{1g}>$ orbitals, b_{1g} antibonding orbital $|b^*_{1g}>$ accommodates the localized holes. Both $|b_{1g}>$ and$|\ b^*_{1g}>$ extend along a CuO_2 plane while $|a^*_{1g}>$ orbital extends over a three-dimensional space. (**b**) Heuristic explanation of the K–S model using an extended two-story-house model. The extended two-story-house model consists of an array of CuO_6 octahedrons called Cu houses. The first story of a Cu house is occupied by Cu localized spins, which form the AF order in the spin-correlated region by the superexchange interaction. The second story in the Cu house consists of two floors due to the anti-JT effect; the lower a^*_{1g} floor and the upper b_{1g} floor. The second stories of neighboring Cu houses are connected by oxygen rooms, reflecting the transfer interaction due to the hybridization of

Table 11.1 The values of parameters in the K–S Hamiltonian (in unit of eV)[6] [6, 15]

1. Transfer integrals (3 kinds)
$t_{a^*1g,a^*1g} = 0.2, t_{b1g,b1g} = 0.4, t_{a^*1g,b1g} = \sqrt{t_{a^*1g,a^*1g} t_{b1g,b1g}} = 0.28$
2. Exchange Constants within the same CuO_6 octahedron $K_{a^*1g} = -2.0, K_{b1g} = 4.0$
3. Superexchange constant $J = 0.1$
4. The one-electron energy of the a^*_{1g} and b_{1g} orbital states (See the Method Section)

orbital state $|a^*_{1g}>$ and the b_{1g} bonding orbital state $|b_{1g}>$ which were originally split by the JT effect, becomes smaller upon doping holes. This feature of the electronic structure is called the "orbital near-degeneracy". The feature of the orbital near-degeneracy in copper oxides was supported experimentally [10–12] and by the band calculations including the electron-correlation effect [13].

In Fig. 11.1b, the key features of the K–S model are explained for LSCO in a heuristic manner using an extended two-story-house model [14]. The characteristic feature of the K–S model is that the doped holes with up spin or with down spin in the underdoped regime of LSCO form a metallic state by alternately taking Hund's coupling spin-triplet and spin-singlet states without destroying the AF order. A particle which has the feature of the K–S model is called the KS particle and its state is called the KS state.

In the K–S Hamiltonian [6] to describe the K–S model (see the Method Section at the end of the text), a unique feature lies in its fourth term $H_{ex}H_{ex}$; the exchange interactions between the spin of a doped hole and that of a localized hole in the b_{1g} antibonding orbitals within the same CuO_6 octahedron, given by

$$H_{ex} = \Sigma_{i,m} K_m s_{im} \cdot \ S_i. \tag{11.1}$$

Here K_m (m = a^*_{1g} or b_{1g}) is the exchange integral between the spin of a doped hole $\boldsymbol{s}_{im}$ and the spin of a localized hole $\boldsymbol{S}_i$ in the ith CuO_6 octahedron. There are two exchange constants, K_{a^*1g} and K_{b1g}, for the Hund's coupling spin-triplet and spin-singlet (SS) states, respectively, and their numerical values for LSCO are $K_{a^*1g} = -2.0$ eV and $K_{b1g} = 4.0$ eV [15] (see Table 11.1 of the Method Section).

Using the K–S Hamiltonian, the energy bands in underdoped LSCO was calculated by treating H_{ex} in Eq. (11.1) in the mean-field approximation [16], which replaces the localized spins $\boldsymbol{S}_i$ with their average value $<\boldsymbol{S}>$, given by

$$H_{ex} = \Sigma_i \left(K_{a^*1g} s_{i,a^*1g} \cdot < S > + K_{b1g} s_{i,b1g} \cdot < S > \right). \tag{11.2}$$

Cu d and O p orbitals. The characteristic feature of the K–S model is that the doped holes with up spin (*red arrow* in the figure) or with down spin (*dotted arrow* in the figure) in the underdoped regime of LSCO form a metallic state by alternately taking Hund's coupling spin-triplet and spin-singlet states without destroying the AF order. A particle which has the feature of the K–S model is called the KS particle and its state is called the KS state

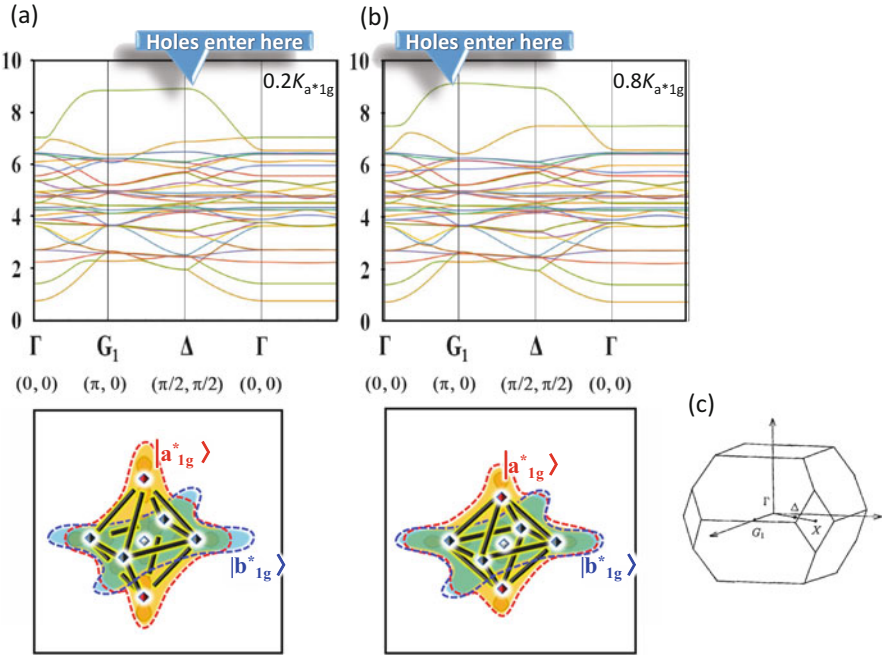

Fig. 11.2 Doping-induced alterations in the energy bands of LSCO. (**a**) Energy band structure of LSCO for x = 0.03 in the spin-disordered insulating phase. The lower figure shows schematically a small overlap between $|a^*_{1g}>$ antibonding orbital (*orange* color) for a hole carrier and $|b^*_{1g}>$ antibonding orbital for a localized hole (*green*) due to the anti-JT-effect, leading to a small value of $0.2|Ka^*_{1g}(0)|$ for $|Ka^*_{1g}|$, where $K_a{}^*_{1g}(0) = -2.0$ eV. The bonding b_{1g} orbital $|b_{1g}>$ (*green* color) is not shown. (**b**) Energy band structure of LSCO for a metallic state with x = 0.12 in the underdoped regime. The lower figure shows a large overlap between $|a^*_{1g}>$ antibonding orbital (*orange* color) for a hole carrier, and $|b^*_{1g}>$ antibonding orbital for a localized hole (*green*) due to the anti-JT-effect, leading to a large value of $0.8|Ka^*_{1g}(0)|$ for $|K_a{}^*_{1g}|$, where $Ka^*_{1g}(0) = -2.0$ eV. (c) Ordinary Brillouin zone of LSCO. The Γ point (0, 0, 0), △ point (π/2a, π/2a, 0), G_1 point (π/a, 0, 0), and X point (π/a, π/a, 0) are the symmetry points in the kx – ky plane, where a is the length of the Cu–O–Cu distance. In the undoped case, these energy bands are fully occupied by electrons, resulting in the AF insulator, consistent with experimental result

In the previous calculations [16], the Hund's coupling exchange $\left|K_{a^*1g}\right|$ and the SS exchange K_{b1g} in Eq. (11.2) were treated as constant. However, in this paper, we notice that $\left|K_{a^*1g}\right|$ and K_{b1g} in Eq. (11.2) are proportional, respectively, to the overlap between the $|a^*_{1g}>$ and $|b^*_{1g}>$ orbitals, and that between the b_{1g} bonding and antibonding orbitals, $|b_{1g}>$ and $|b^*_{1g}>$. When holes are doped into the AF insulator, the apical-oxygen -Cu distance in CuO_6 octahedrons decreases by the anti-JT effect. Thus, the overlap between $|a^*_{1g}>$ and $|b^*_{1g}>$ orbitals increases, leading to the increase of $\left|K_{a^*1g}\right|$ while K_{b1g} does not change.

In this context, a new method of improving the previous band calculations [16] is proposed in the present paper, where a value of K_{a^*1g} in Eq. (11.2) changes with the hole concentration. Figure 11.2a shows the thus-calculated energy band structure for

the hole concentration $x = 0.03$ in the insulating phase just below the metal-insulator transition $x_o = 0.05$. Doped holes enter the #1 band, the highest band, from its highest state, the Δ point ($\pi/2a$, $\pi/2a$, 0) in the ordinary Brillouin zone (Fig. 11.2c), where a is the length of the Cu–O–Cu distance. When x increases from the insulating phase to a metallic phase above $x_o = 0.05$, the energy band changes drastically. As an example, Fig. 11.2b shows the energy band structure for $x = 0.12$ in a metallic phase in the underdoped regime between $x_o = 0.05$ and optimum doping $x_{opm} = 0.15$. Doped holes in this case enter the #1 band from the G_1 point (π/a, 0, 0) in the Brillouin zone, at which the saddle-point singularity exists. In these two figures, the ordinate shows the electron energy but not the hole energy.

Emergence of Spin-Singlet Quasiparticles and the Origin of Fermi Arcs

By investigating the wavefunction of a hole at the Δ point in the #1 band in Fig. 11.2a, we notice that a doped hole at the Δ point has the character of an $O_{\|}p_{\sigma}$ orbital. This means that an electron is extracted from O^{2-} ion in CuO_2 planes. As a result, the O^{2-} ion changes to an O^{1-} ion upon doping holes, and thus, the superexchange interactions among the localized spins via a closed shell of the O^{2-} ions in CuO_2 planes are partly destroyed, causing the inhomogeneous distribution of non-AF regions at the border of the AF region in real space.

Thus, in the insulating phase below $x_o = 0.05$, the spins of localized holes in the b^*_{1g} orbital become free with regard to their directions in the non-AF region. Then, a subsequently doped hole in an upper b_{1g} orbital at the Δ point (the b_{1g} floor in the second story in Fig. 11.1b) forms an SS state with a localized b^*_{1g} hole by the strong SS exchange interaction with K_{b1g} (= 4 eV) [15] within a CuO_6 octahedron.

This causes the emergence of a new particle called an SS quasiparticle. The twisted lines between a b_{1g} doped hole and a b^*_{1g} localized hole in the right hand of Fig. 11.3a represent an entangled coupling produced by SS exchange. Then, the wave function of an SS quasiparticle at the A site, $\Psi_{ss,A}(\boldsymbol{r}_1\sigma_1, \boldsymbol{r}_2\sigma_2)$, has a functional form, given by

$$\begin{aligned}\Psi_{SS,A}(r_1\sigma_1, r_2\sigma_2) = \quad & 1/\sqrt{2}\{\phi(r_1 - R_A)\chi(r_2 - R_A) + \phi(r_2 - R_A)\chi(r_1 - R_A)\} \\ & \times 1/\sqrt{2}\{\alpha(1)\beta(2) - \beta(1)\alpha(2)\},\end{aligned} \tag{11.3}$$

where $\varphi(\boldsymbol{r})$ and $\chi(\boldsymbol{r})$ represent the wavefunctions of the upper b_{1g} doped hole and lower b^*_{1g} localized orbitals, respectively. The resonance valence bond (RVB) model [8] and the t–J model [4] used a similar type of functional form in their theoretical developments.

A transfer interaction H_{tr} (see the K–S Hamiltonian in the Method Section) between neighboring A and B sites ($\equiv <\Psi_{ss,A}|H_{tr}|\Psi_{ss,B}>$) takes positive and

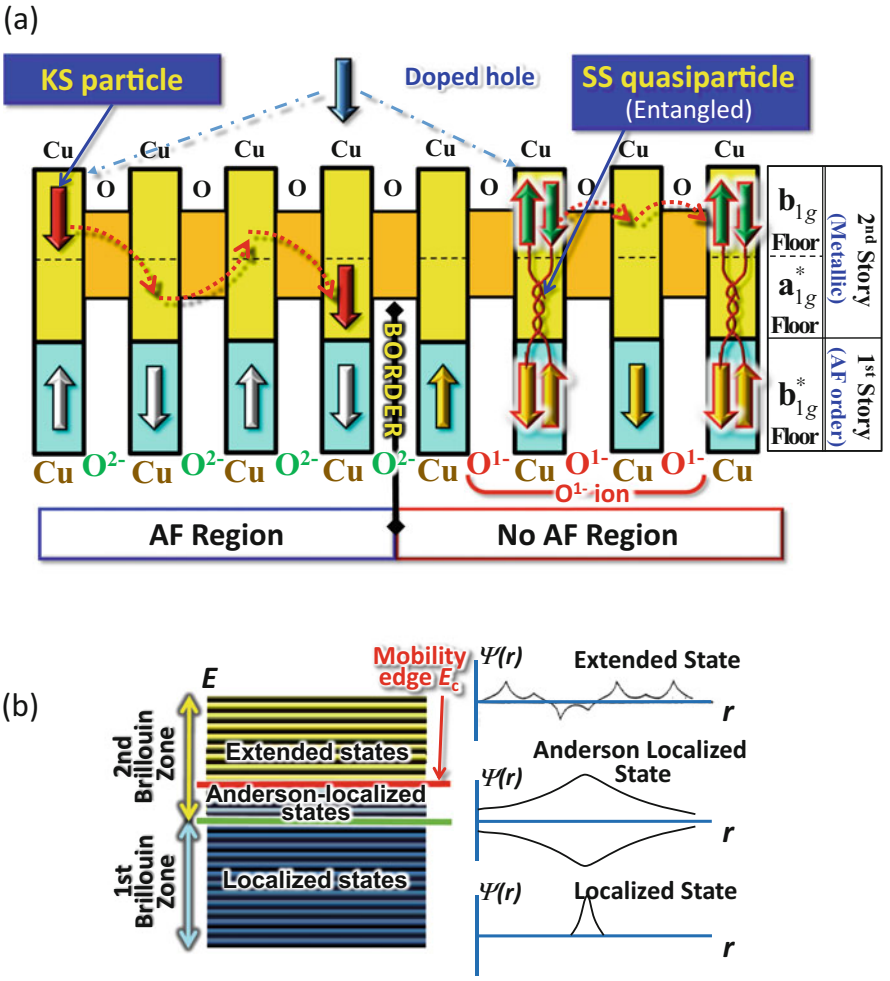

Fig. 11.3 The emergence of an SS quasiparticle with character of an Anderson-localized state and the emergence of a KS particle with character of metallic and superconducting properties. (**a**) Right side of this figure shows the emergence of an SS quasiparticle and the mechanism of its hopping process by the interplay between the transfer interaction and the entanglement character of the SS quasiparticle in the non-AF region. A doped hole in upper b_{1g} floor in the SS quasiparticle can hop to a neighboring site, regardless of the spin direction of a localized b^*_{1g} hole at a neighboring site, up or down, by the transfer interaction. The left side of this figure shows the emergence of a KS particle in the AF region. The KS particle forms a metallic state in the AF region by alternately taking Hund's coupling spin-triplet and spin-singlet states without destroying the AF order and contributes to the occurrence of d-wave superconductivity below T*c*. (**b**) Character of SS quasiparticles in the first and second Brillouin zone. Since the b^*_{1g} localized holes fully occupy the states in the first Brillouin zone (a region of *dark blue* color in the figure), doped holes to form SS quasiparticles occupy the second Brillouin zone from the lowest energy state. Thus, states in the low-energy region in the second Brillouin zone exhibit an Anderson-localized state while those in the higher energy region have an extended nature. The mobility edge (*red* line) exists between Anderson-localized states and extended states

negative values in a random manner, corresponding to a random spin direction of localized holes in the non-AF region. Thus, an energy level structure of an SS quasiparticle in the non-AF region has a feature of a disordered lattice. When an SS quasiparticle moves in a non-AF region (the right side of Fig. 11.3a), the spins of the b^{*}_{1g} localized holes (in the first story) tend to order in a certain sub-region so as to lower the kinetic energy of an SS quasiparticle [17, 18] in two ways. In one case the localized spins in a certain sub-region order in a ferromagnetic (FM) manner, so that SS quasiparticles can propagate with the transfer interaction $<\Psi_{ss,A}|H_t|\Psi_{ss,B}>$ $(= +t)$ towards the $+x$ direction in the FM sub-region, In the other case, the localized spins in another sub-region order in AF manner, so that SS quasiparticles can propagate with the transfer interaction $<\Psi_{ss,A}|H_t|\Psi_{ss,B}>$ $(= -t)$ towards the—x direction in the AF sub-region. Since these two waves (SS quasiparticles) propagate towards opposite directions, they are scattered by a spin-disordered sub-region between the FM and AF sub-regions.

Following the theories of Anderson [19] and Mott [20], these two scattered waves interfere with each other in the spin-disordered sub-region, resulting in Anderson-localized states, as shown in Fig. 11.3b. Each Anderson localized state has the degeneracy representing the number of their localized centers in real space. Because of this degeneracy, each Anderson-localized state has a density of states (DOS). When the Fermi energy in a system of SS quasiparticles, $E_F(SS)$, increases from the lowest energy in the second Brillouin zone, a particular energy level E_c appears. This energy level separates the Anderson-localized states and the extended states in momentum space, and is called a mobility edge, as shown in the left side of Fig. 11.3b, where the states on the mobility edge have a metallic nature. The hole-concentration regime in which $E_F(SS)$ is below the mobility edge consists of Anderson-localized states only. We call this concentration regime a spin-disordered insulating phase.

When $E_F(SS)$ reaches the mobility edge, the b_{1g} doped holes (SS quasiparticles) begin to occupy metallic states from the Δ points on the mobility edge. We refer to these occupied states on the mobility edge as a Fermi arc, which has a metallic nature. In this context, the origin of the Fermi arcs we clarified is different from those based on the t–J model [4, 21, 22].

Emergence of the KS Particles at the Metal-Insulator Transition and the Occurrence of Fermi Pockets

The hole concentration at which $E_F(SS) = E_c$ corresponds to $x_o = 0.05$, Thus, both energies of the highest states in the # 1 bands at the Δ point in Fig. 11.2a and at the G_1 point in Fig. 11.2b become equal, and the metal-insulator transition occurs. Since the wavefunction at the G_1 point has the KS character, KS particles emerge in the AF region, as shown in the left side of Fig. 11.3a. These KS particles can itinerate in a wider space than the whole AF region, by the spin fluctuation effect in the 2D Heisenberg AF spin system in a CuO_2 plane.

Fermi Surface Structure of LSCO, and the Doping and Temperature Dependences of the Electronic Entropy of LSCO

A. Construction of the Fermi Surface (FS) of LSCO from the Energy Bands Having the Feature of Doping-Induced Alteration

In this paper, we can treat the KS particles as carriers in a periodic AF potential, as shown in the left side of Fig. 11.3a. Thus, the KS particles form Fermi pockets (closed Fermi surfaces) around the G_1 points (antinodal regions) in a square AF Brillouin zone, which is obtained by folding the ordinary Brillouin zone in Fig. 11.2c. These Fermi pockets are stabilized owing to the van Hove singularity located at the G_1 points.

From the calculated results of Figs. 11.2a, b and 11.3a, b, we notice that when the hole concentration reaches $x = 0.05$ from the insulating phase, Fermi arcs start occupying metallic states from the nodal region (Δ points) on the mobility edge and the Fermi pockets of 4-pointed petal shape appear in the antinodal region (G_1 points) simultaneously. Thus, we conclude that a FS structure of LSCO in a metallic state consists of the Fermi pockets in the antinodal region and Fermi arcs in the nodal region, as shown in Fig. 11.4a, where the FS for $x = 0.10$ is shown. Now we want to discuss the hole-concentration and temperature dependences of the FS structure of LSCO. For this purpose, we use the calculated results of doping and temperature dependences of the electronic entropy for LSCO [7], which will be summarized in the next section, Then, we will discuss the doping and temperature dependences of the FS structure in Section "Notable doping and temperature revolutions of FS structure of LSCO".

B. The Doping and Temperature Dependences of the Electronic Entropy of LSCO (Theory and Experimental Results)

In order to discuss the doping and temperature dependences of the FS structure of LSCO, we use the results of electronic entropies calculated for LSCO [7]. In particular, the density of states (DOS) calculated from the K–S Hamiltonian for LSCO, $\rho_{KS}(\varepsilon)$, shown in Fig. 11.5a plays an important role. Since the K–S Hamiltonian describes the K–S model, one may consider that $\rho_{KS}(\varepsilon)$ reflects the characteristic feature of the K–S model.

The thus-calculated electronic entropies for the mixed phase consisting of KS particles and SS quasiparticles in LSCO are shown in Fig. 11.5b. In this figure, the electronic entropies at $T = 100$ K and 200 K are respectively denoted as $S_{mix}(100, x)$ and $S_{mix}(200, x)$, which are shown by solid red curves. The measured electronic

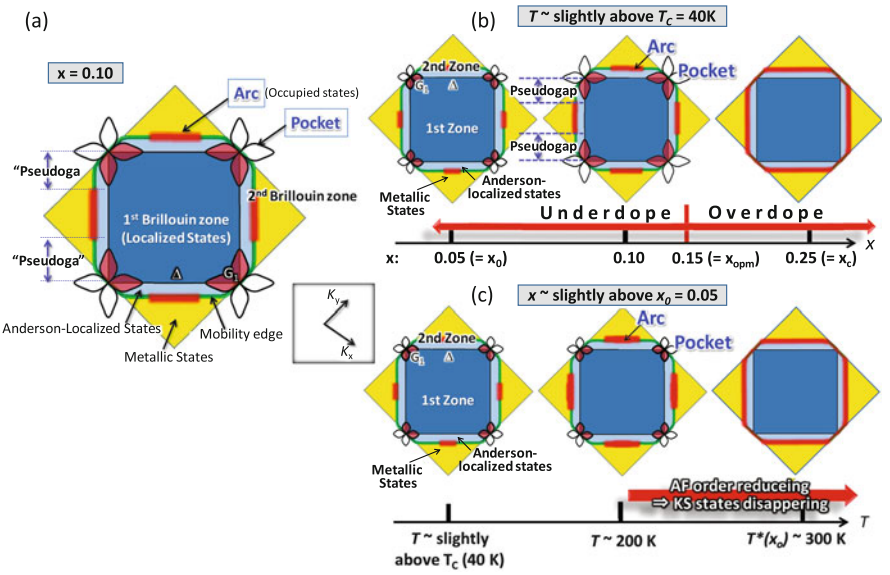

Fig. 11.4 Fermi surface structure and its notable doping and temperature dependences. (**a**) Fermi surface structure of underdoped LSCO with x = 0.10, where the mobility edge, Fermi arcs and Fermi pockets are shown, respectively, by green color lines, *red lines* and 4-pointed petal shapes, respectively. (**b**) Doping dependence of the Fermi surface structure of LSCO in the metallic regime from $x_o = 0.05$ to the overdoped regime. Here, the three hole concentrations are chosen; $x_o = 0.05$, x ~ 0.1 (the underdoped regime), and xc = 0.25 (the overdoped regime). When the concentration of doped holes with the character of an O//pσ orbital increases from the underdoped to overdoped regime, the superexchange interactions are destroyed partially in the AF region so that the KS character gradually diminishes while the SS character increases. Reflecting this feature, the area of Fermi pockets decreases gradually while the length of Fermi arcs (red line regions) increases with increasing the hole concentration. The line width of a Fermi arc represents DOS of Anderson-localized states. (**c**) Temperature evolution of the Fermi surface structure of LSCO. The Fermi surface structure changes gradually with increasing temperature above Tc while the hole concentration is fixed at xo = 0.05, just above the meal-insulator transition. In this figure, the temperature evolution of the Fermi surface structure is shown for the three temperatures: Immediately above Tc (~40 K), the medium temperature such as 200 K, and T^* (x = 0.05) ~ 300 K

entropy [23] is also shown by solid squares for compa rison. There is an excellent agreement between the theoretical and experimental results without introducing adjustable parameters. A thin solid curve denoted by $S_{\mathrm{LDA}}(100, x)$ in this figure represents the electronic entropy at $T = 100$ K calculated for a doped hole in the LDA (Local Density Approximation) band, assuming that a doped hole in LSCO is described by the LDA energy band. We find that $S_{\mathrm{LDA}}(100, x)$ are too small not only in the underdoped regime but also in the overdoped regime. Thus, we conclude that the electronic structure based on the LDA band may not be appropriate not only for KS particles in the underdoped regime but also for SS quasiparticles in the overdoped regime of LSCO. From this conclusion, we find that the effective mass

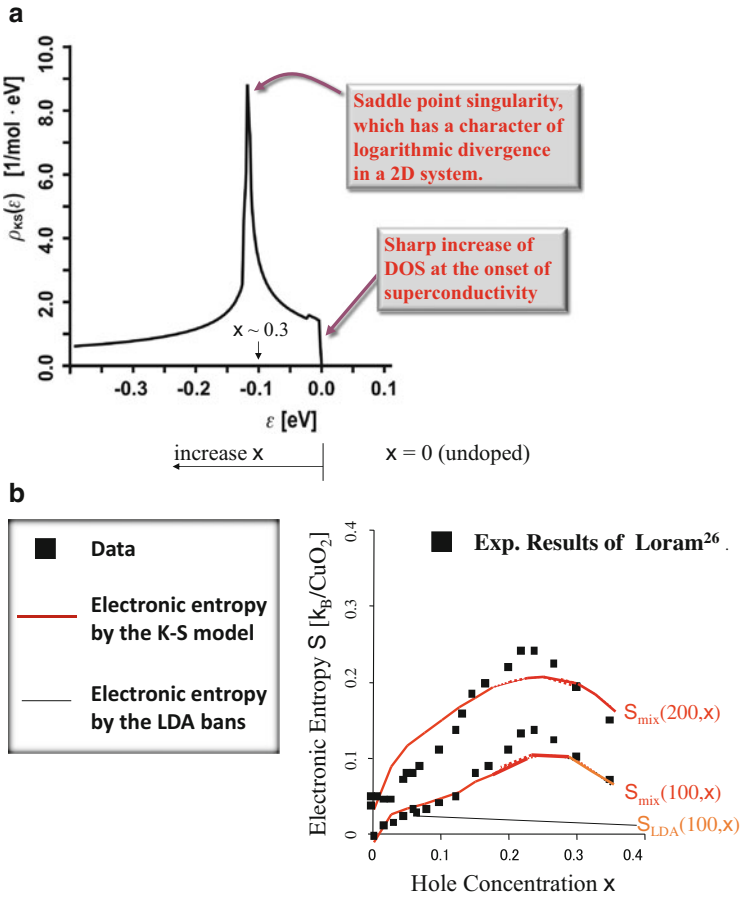

Fig. 11.5 Calculated density of states and electronic entropy of LSCO. (**a**) Calculated density of states for $La_{2-x}Sr_xCuO_4$ from the K–S model [16]. (**b**) Calculated electronic entropy (*red curves*) for the mixed phase S_{mix}, pure SS phase S_{ss}, and for a hole carrier in the LDA band, S_{LDA} [7]. The electronic entropy measured by Loram et al. [23] is shown by *solid squares*

of a hole carrier is about six times heavier than the free electron mass, and thus that one may call the hole carriers in cuprates "Jahn-Teller polarons".

Reflecting the appearance of a saddle point singularity in $\rho_{KS}(\epsilon)$ at $x = 0.25$ in Fig. 11.5a, the calculated results of $S_{mix}(100, x)$ and $S_{mix}(200, x)$ in Fig. 11.5b show broad peaks in the doping dependence. This suggests that the character of the KS state changes from the mixed phase to a pure phase consisting of SS quasiparticles only around $x = 0.25$. This change is due to the gradual destruction of local AF order upon doping holes.

Next we discuss the temperature dependence of the FS structure of LSCO in the case of $x = 0.05$, just above the metal-insulator transition. When the temperature

increases, the local AF order is gradually destroyed by thermal agitation. As a result, the KS state is also disturbed and the character of the SS state becomes dominant. Therefore, the FS structure changes from the feature having coexisting Fermi pockets and Fermi arcs at low temperatures slightly above Tc (40 K) to that only having a Fermi arc near $T^*(x)$. Finally, the Fermi arc is extended to the edge of AF Brillouin zone when temperature reaches $T^*(x = 0.05)$. Here we assume $T^*(x = 0.05) = 300$ K. In this way, we clarified the mechanism of the temperature evolution of the FS structure in LSCO in the underdoped regime.

Notable Doping and Temperature Revolutions of FS Structure of LSCO

Figure 11.4b and c show, respectively, the thus-obtained hole-concentration and temperature dependences of the FS structure of LSCO. From the temperature evolution of the Fermi surface structure in Fig. 11.4c, one may understand that the coexistence of Fermi pockets and Fermi arcs is kept below 200 K. Since the local AF order is gradually destroyed by thermal agitation when temperature increases, the character of the SS state increases together with the expansion of the non-AF region. Thus, with increasing temperature, Fermi-pocket regions decrease while Fermi-arc regions increase. In the overdoped region, only Fermi-arc regions remain. The calculated FS structure captures characteristics of the spectral weight maps at the Fermi energy observed for $x = 0.07$–0.25 [24].

Summarizing the features shown in Fig. 11.4b, c, we conclude that with increase of the hole concentration, the character of the KS state changes from a mixed phase consisting of KS particles and SS quasiparticles to a pure SS phase consisting of only SS particles at $x = 0.25$ in the overdoped region, together with the expansion of the non-AF region. Thus, we define $x = 0.25$ as the quantum critical point x_c, at which a phase change occurs from the mixed phase to the pure SS phase. Experimentally, the two-gap scenario on the nodal and antinodal regions in momentum space, deduced from the angle-resolved photoemission (ARPES) experiments [25, 26] seems support the present FS structure.

The Origin of Pseudogap

From the FS structure of LSCO in Fig. 11.4a, it is clear that the pseudogap in momentum space, previously postulated by Norman et al. [5] has a close relationship to the existence of Fermi pockets. Furthermore, the remarkable temperature and doping evolutions of the Fermi surface structure in LSCO predicted in Fig. 11.4b, c can explain successfully the unusual behavior of the Fermi surface that has been ascribed to the pseudogap [5, 27].

New Phase Diagram for LSCO,

In order to construct a new phase diagram for LSCO, based on the results in Fig. 11.4a, b, c, we introduce the free energy of the mixed phase, $F_{\mathrm{mix}}(T, x)$, and that of the pure SS phase, $F_{\mathrm{SS}}(T, x)$. Then, the difference between the free energies of the two phases, $\Delta F(T, x)$, is calculated:

$$\begin{aligned}\Delta F(T,x) &\equiv F_{\mathrm{mix}}(T,x) - F_{\mathrm{SS}}(T,x) \\ &= (E_{\mathrm{mix}}(T,x) - E_{\mathrm{SS}}(T,x)\ ) - T(S_{\mathrm{mix}}(T,x) - S_{\mathrm{SS}}(T,x)),\end{aligned} \tag{11.4}$$

where $E\,(T, x)$ is the internal energy and $S\,(T, x)$ is the electronic entropy calculated for LSCO [7], which was discussed in the subsection B "The doping and temperature dependences of the electronic entropy of LSCO (theory and experimental results)".

Furthermore, we define $T^*(x)$ by the following equation:

$$\Delta F(T,x) = 0. \tag{11.5}$$

A thus-established phase diagram is shown in Fig. 11.6. Here, $T^*(x)$ represents the phase change between the mixed phase with the local AF order and the pure SS phase without the local AF order. Thus, at the quantum critical point x_{c}, $T^*(x_{\mathrm{c}}) = 0$. The order parameter in the mixed phase below T^*(x) is the spin-correlation length. Since KS particles on the Fermi pockets are responsible for the occurrence of d-wave superconductivity in the phonon mechanism [28], d-wave superconductivity also disappears at $x = x_{\mathrm{c}}$, that is $Tc\ (x_{\mathrm{c}}) = 0$. The present new phase diagram seems consistent with experimental results by Takagi, et al. [29] on $Tc\ (x)$, Yang et al. [30] on the opening of a symmetry gap only in the anti-nodal region, McEtroy et al. [31] on the antinodal quasiparticles, and Vishik, et al. [32] on the phase diagram for $Bi_2Sr_2CaCu_2O_{8+\delta}$.

Phonon-Mechanism in d-Wave Superconductivity

In this section we discuss the mechanism of superconductivity due to KS particles on the Fermi pockets in the mixed phase [28]. Figure 11.1b shows that the wavefunctions of a doped hole with up and down spins, $\Psi_{k,\uparrow}(\boldsymbol{r})$ and $\Psi_{k,\downarrow}(\boldsymbol{r})$, have the unique phase relation

$$\Psi_{k,\downarrow}(\boldsymbol{r}) = \exp(\mathrm{i}\,\boldsymbol{k}\cdot\,\boldsymbol{a})\Psi_{k,\uparrow}(\boldsymbol{r}), \tag{11.6}$$

where $\boldsymbol{a}$ is a vector representing the Cu–O–Cu distance. From this phase relation, it can be shown that the Fermi pockets in Fig. 11.4a contribute to the d-wave superconductivity in the phonon mechanism [28]. Occurrence of the d-wave superconductivity was previously discussed assuming the Fermi pockets to exist at the nodal region $(\pi/2a, \pi/2a, 0)$ [28]. Although the present calculation shows that the Fermi pockets are located at the antinodal region $(\pi/a, 0, 0)$, the difference in the location of

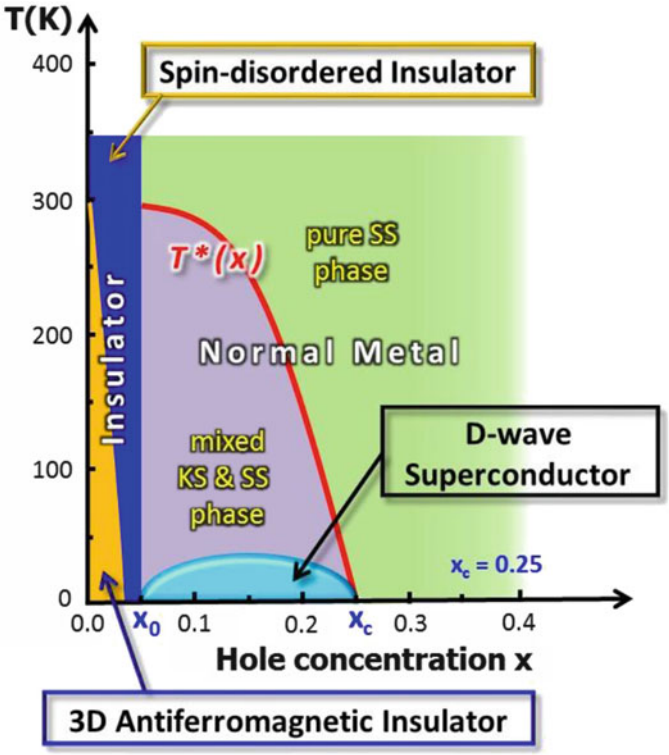

Fig. 11.6 New phase diagram, T vs x for LSCO. The undoped La_2CuO_4 is a three-dimensional (3D) AF insulator. Then, upon doping holes, the 3D AF order changes to the 2D AF order with the Heisenberg AF spin system in CuO_2 plane. A phase below the metal-insulator transition at x_o is the spin-disordered insulating phase constructed by SS quasiparticles. The phase transition occurs at T*(x), below which the mixed phase consisting of SS and KS particles exists. At $T^*(x)$, the KS character disappears, although the SS character crosses over from the low temperature side to the pure SS phase on the high-temperature side. Thus, the origin of the pseudogap phase corresponds to the Fermi pockets in the mixed phase. This phase diagram clearly shows that both $T^*(x)$ and $T_c(x)$ vanish at $x = x_c$, where xc is the quantum critical point (QPC), at which the phase change occurs from the mixed phase with the local AF order to the pure SS phase without the AF order

Fermi pockets is not relevant because the Fermi pockets in both cases have the four-fold symmetry, which is an essential key to the d-wave superconductivity.

According to [28], the matrix elements of electron–phonon interactions from state $\boldsymbol{k}$ to state $\boldsymbol{k'}$ of a KS particle with up spin in the AF Brillouin zone, scattered by a phonon with wave vector $\boldsymbol{q}$, $V_\uparrow(\boldsymbol{k}, \boldsymbol{k'}, \boldsymbol{q})$, have the following spin-dependent property,

$$V_\uparrow(\boldsymbol{k}, \boldsymbol{k'}, \boldsymbol{q}) = \exp(\mathrm{i}\, \boldsymbol{K} \cdot \boldsymbol{a}) V_\downarrow(\boldsymbol{k}, \boldsymbol{k'}, \boldsymbol{q}), \tag{11.7}$$

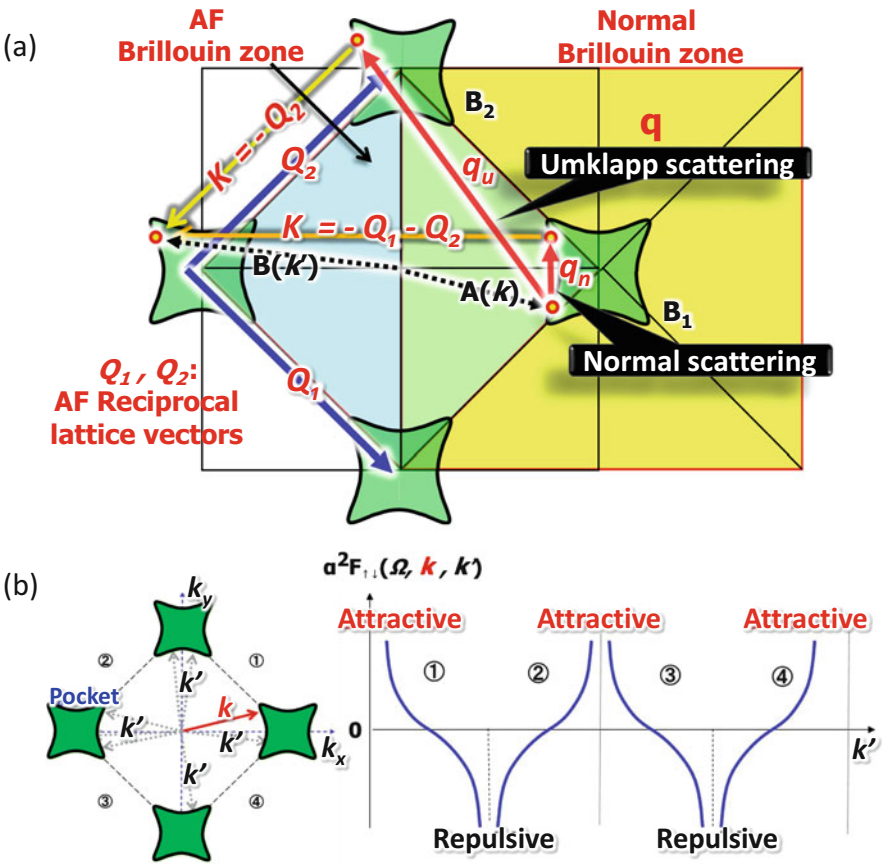

Fig. 11.7 Verification of d-wave superconductivity. (**a**) Illustration of two scattering processes by phonons: Normal and Umklapp. This figure shows that there are two kinds of scattering processes from states $\boldsymbol{k}$ (at **A** point) to $\boldsymbol{k'}$ (at **B** point) of a KS particle with up spin by a phonon with wave vector q in the AF Brillouin zone. A scattering which satisfies $\boldsymbol{K} = \boldsymbol{k} - \boldsymbol{k'} + \boldsymbol{q}_n = \boldsymbol{Q}_1 - \boldsymbol{Q}_2$ is a normal scattering, while a scattering which satisfies $\boldsymbol{K} = \boldsymbol{k} - \boldsymbol{k'} + \boldsymbol{q}_U = -\boldsymbol{Q}_2$ is an Umklapp scattering. (**b**) Heuristic explanation of d-wave superconductivity. The calculated momentum-dependent spectral function $\alpha^2F\uparrow\downarrow(\Omega, k, k')$ varies with the signs taken in sections ① to ④ in the 2D square AF Brillouin zone, when $\boldsymbol{k'}$ changes from section ① of the Fermi pocket to section ④, while $\boldsymbol{k}$ (*red arrow*) is fixed in the square AF Brillouin zone ($kx - ky$ plane)

where $\boldsymbol{K} = \boldsymbol{k} - \boldsymbol{k'} + \boldsymbol{q}$ is a reciprocal lattice vector in the AF Brillouin zone. Since $\boldsymbol{K} = (n\pi/a, m\pi/a, 0)$ with n + m = even in a 2D square AF Brillouin zone in the k_x–k_y plane, the electron–phonon interaction in Eq. (11.7) may have a different sign depending on the value of $\boldsymbol{K}$. That is, $\exp(i\boldsymbol{K}\bullet\boldsymbol{a}) = +1$ for n = even (normal scattering) while $\exp(i\boldsymbol{K}\bullet\boldsymbol{a}) = -1$ for n = odd (Umklapp scattering), where $\boldsymbol{a}$ is taken as $(a, 0, 0)$.

Thus, from Fig. 11.7a, we obtain the following relations;

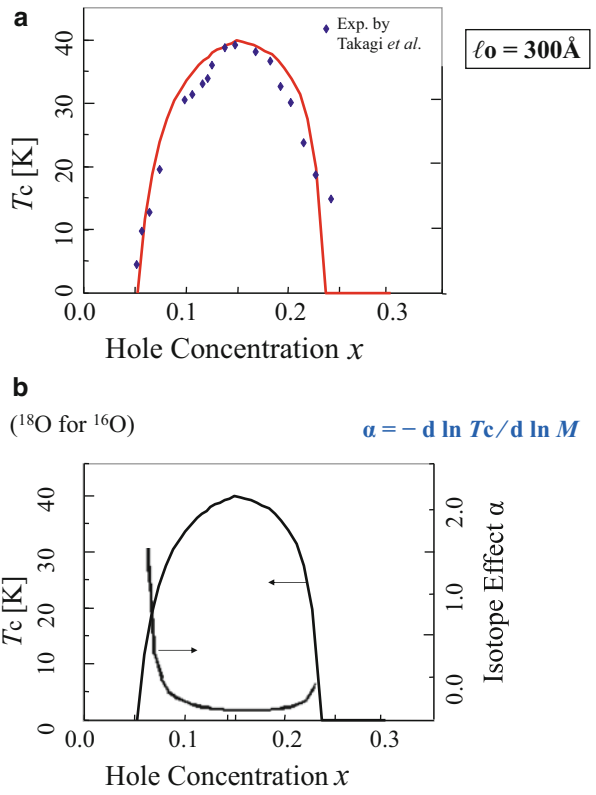

Fig. 11.8 Calculated hole concentration dependence of Tc (x) and the isotope effect for LSCO. (**a**) This theoretical result of the hole concentration dependence of Tc (*x*) (*red curve*) [32] is compared with the experimental results by Takagi et al. [29] (solid lozenge). By fitting the calculated value of Tc (x) at the optimum concentration (x = 0.15) to the experimental value of 40 K, the mean-free-path of hole carriers, ℓo, which is an adjustable parameter, is determined to be 300 Å (= 30 nm). (**b**) The calculated isotope constant α shown on the ordinate at the right side is remarkably large near the onset concentration of superconductivity while it is small around the optimum concentration. This theoretical result is consistent with experimental results by Bishop and coworkers [34]

$$V_{\uparrow}(\boldsymbol{k},\boldsymbol{k}',\boldsymbol{q}) = +V_{\uparrow}(\boldsymbol{k},\boldsymbol{k}',\boldsymbol{q}), \quad \text{for normal scatterings,} \tag{11.8a}$$

$$V_{\uparrow}(\boldsymbol{k},\boldsymbol{k}',\boldsymbol{q}) = -V_{\uparrow}(\boldsymbol{k},\boldsymbol{k}',\boldsymbol{q}), \quad \text{for Umklapp scatterings.} \tag{11.8b}$$

In this context, the total effective interaction between states $\boldsymbol{k}$ and $\boldsymbol{k}'$ of the KS particles for the formation of a Cooper pair is expressed by the sum of normal and Umklapp scatterings as follows:

$$\left[V_{\uparrow}(\mathbf{k},\mathbf{k}') \cdot V_{\downarrow}(-\mathbf{k},-\mathbf{k}')\right]_{\text{sum}} = V_{\uparrow}(\mathbf{k},\mathbf{k}',\mathbf{q})_{\text{normal}} \cdot V_{\downarrow}(-\mathbf{k},-\mathbf{k}',\mathbf{q})_{\text{normal}} + V_{\uparrow}(\mathbf{k},\mathbf{k}',\mathbf{q})_{\text{umklapp}} \cdot V_{\downarrow}(-\mathbf{k},-\mathbf{k}',\mathbf{q})_{\text{umklapp}}. \tag{11.9}$$

In this context, from Eqs. (11.8a), (11.8b) and (11.9), we conclude that the effective interaction for normal scattering results in attractive interaction, while Umklapp scattering results in repulsive interaction in LSCO.

We applied the above results to the FS structure for LSCO shown in Fig. 11.4a, and calculated the electron–phonon spectral function $\alpha^2 F^{(2)}{}_{\uparrow\downarrow}(\Omega)$ for LSCO as a

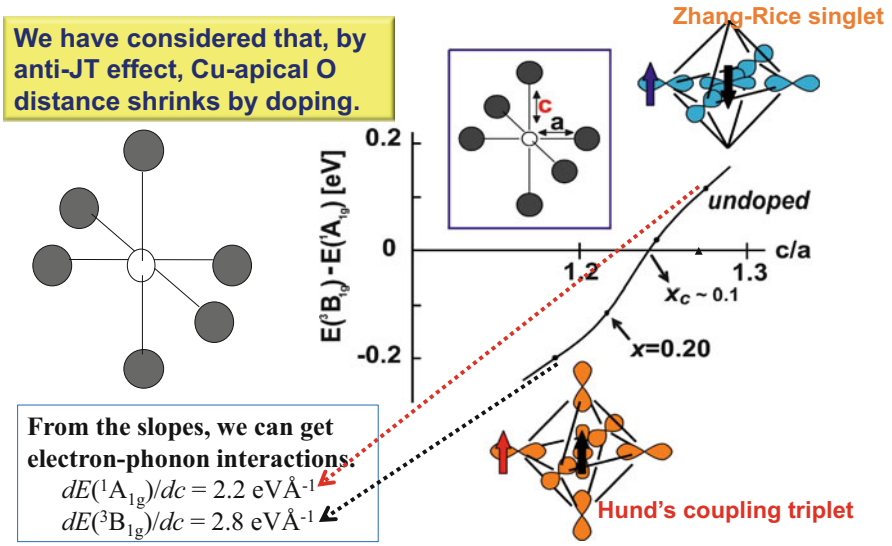

Fig. 11.9 Explanation of why the electron-phonon interactions in copper oxides superconductors are very strong

function of phonon frequency Ω, where $F_{\uparrow\downarrow}(\Omega, k, k')$ is the density of phonon states with phonon energy Ω, and α^2 is the square of the electron–phonon coupling constant.

The calculated momentum-dependent spectral function, $\alpha^2 F^{(2)}{}_{\uparrow\downarrow}(\Omega)$ for LSCO is shown in Fig. 11.7b. This variation clearly shows the d-wave behavior of dx^2–y^2. In this calculation, Fermi arcs are not considered because they are formed by the SS quasiparticles in the non-AF region, and thus do not contribute to superconductivity.

The Doping Dependence of the Critical Temperature and the Isotope Effect

The hole concentration dependences of the critical temperature T_c and the isotope effect α for LSCO were calculated, assuming that the Fermi pockets in the normal phase appear at the Δ point ($\pi/2a$, $\pi/2a$, 0) and three other equivalent points in the 2D square AF Brillouin zone [33]. Figure 11.8a shows the calculated and experimental results for the concentration dependence of Tc. In this calculation, one adjustable parameter, the mean-free-path of a hole carrier in a metallic state, ℓ_o, was introduced. A value of ℓ_o was determined so as to reproduce the highest value of T_c (40 K) at the optimum doping ($x_{opm} = 0.15$) in LSCO. The thus-determined mean-free-path ℓ_o was 30 nm, which is approximately six times longer than the spin-correlation length at the optimum doping. A good agreement was obtained

between the theoretical result and the experimental data of Takagi et al. [29]. In particular, the hole concentration at which T_c vanishes coincides with the quantum critical point x_c (= 0.25) in the new phase diagram of LSCO, as shown in Fig. 11.6. Figure 11.8b shows the calculated isotope effect on Tc in LSCO [33]. Their result shows that the isotope effect is extremely large near the onset concentration of superconductivity. This is consistent with the experimental result reported by Bishop et al. [34]

Why Are the Electron–Phonon Interactions in Cuprates Strong?

Here we remark on the value of the dimensionless electron–phonon coupling constant λ_d for LSCO. The value of λ_d in the case where Fermi pockets are located at the Δ points was calculated to be 1.96 for optimum doping (x_{opm} = 0.15) [28]. This result suggests that LSCO is a strong superconductor.

According to [28], there are two contributions to λ_d. (1) One contribution is the change of transfer interactions due to atomic displacements. This is a common echanism. A value of the derivative of transfer integral between neighboring Cu sites in a CuO_2 plane [28] is

$$dt/dR = 2.6\ eV\mathring{A}^{-1}. \tag{11.10a}$$

(2) The other contribution is due to the change of the on-site energies due to atomic displacements. This is obtained by calculating the change of the lowest state energies of Hund's coupling spin-triplet multiplet $^3B_{1g}$ and of the spin-singlet multiplet $^1A_{1g}$ with respect to variation in the Cu—apical O distance. These values are given in Fig. 11.9: The appearance of these multiplets are due to Eq. (11.2) (the anti-JT effect). Figure 11.9 clearly shows that both the lowest state energies (on-site energies) of Hund's coupling spin-triplet $^3B_{1g}$ and spin-singlet $^1A_{1g}$ in LSCO change with the displacement of the apical oxygens in a CuO_6 octahedron along the c-axis, c, which is parallel to the direction of the Cu—apical oxygen [28]. From the slopes of the curves showing the change of the on-site energy of Hund's coupling spin triplet $^3B_{1g}$, $E(^3B_{1g})$, and that of SS $^1A_{1g}$, E ($^1A_{1g}$), with respect to the Cu—apical O distance, c, we obtained the variations of the lowest state energies of $^3B_{1g}$ and $^1A_{1g}$ with the change in c as follows [28]:

$$dE\left(^1A_{1g}\right)/dc = 2.2\ eV\mathring{A}^{-1} \tag{11.10b}$$

$$dE\left(^3B_{1g}\right)/dc = 2.8\ eV\mathring{A}^{-1}. \tag{11.10c}$$

Thus, we conclude that the contribution from the variation of the on-site energies of $^3B_{1g}$ and $^1A_{1g}$ is twice that of the transfer interactions. Because of this outstanding

feature of the electron–phonon interactions, the electron–phonon interactions are unexpectedly strong in LSCO.

In summary, taking account of the strong interaction with the JT distortion and anti-JT transformation, the non-rigid band theory was developed for the cuprate superconductors. By this theory, the following important results were clarified: (1) The coexistence of Fermi pockets in the antinodal region and Fermi arcs in the nodal region is the FS of LSCO; (2) the origin of the pseudogap is the existence of Fermi pockets; and (3) only the KS particles on the Fermi pockets contribute to the phonon mechanism in d-wave superconductivity.

The present paper is based on our recent paper uploaded in Ref. [35].

Method Section

The K–S Hamiltonian

The following effective Hamiltonian is introduced to describe the K–S model[6]. It consists of four parts: the one-electron Hamiltonian H_{orbital} for the a^*_{1g} and b_{1g} orbital states, the transfer interactions between neighboring CuO_6 octahedrons H_{tr}, the superexchange interaction between the Cu dx^2–y^2 localized spins in b^*_{1g} orbitals H_{AF}, and the exchange interactions between the spins of doped holes and of dx^2–y^2 localized holes in the same CuO_6 octahedron H_{ex}. Thus, we have

$$\begin{aligned} H &= H_{orbital} + H_{tr} + H_{AF} + H_{ex} \\ &= \sum_{im\sigma} \varepsilon_m c^+_{im\sigma} c_{im\sigma} + \sum_{(i,j)mn\sigma} t_{mn}\left(c^+_{im\sigma} c_{jn\sigma} + h.c.\right) + J\sum_{(i,j)} S_i \bullet S_j \\ &\quad + \sum_{im} K_m s_{im} \bullet S_i \quad , \end{aligned}$$

where ε_{m} ($\text{m} = a_{1g}{}^*$, or b_{1g}) represents the one-electron energy of the a^*_{1g} and b_{1g} orbital states, $C^{\dagger}_{\text{im}\sigma}$ and $C_{\text{im}\sigma}$ are the creation and annihilation operators of a dopant hole with soin σ in the ith CuO_6 octahedron, respectively, t_{mn} is the transfer integral of a doped hole between the m- and n- type orbitals of neighboring CuO_6 octahedrons, J ($J > 0$) is the superexchange interaction between localized spins $\boldsymbol{S}_{\text{i}}$ and $\boldsymbol{S}_{\text{j}}$, and K_{m} is the exchange integral for the exchange interaction between the spin of a doped hole $\boldsymbol{s}_{\text{im}}$ and the spin of a dx^2–y^2 localized hole $\boldsymbol{S}_{\text{i}}$ in the ith CuO_6 octahedron. There are two exchange constants, K_{a^*1g} and K_{b1g}, for the Hund's coupling spin-triplet and spin-singlet (SS) states, respectively, where $K_{a^*1g} < 0$ and $K_{b1g}, > 0$.

This effective Hamiltonian is called the K–S Hamiltonian [6].

The energy difference between a^*_{1g} and b_{1g} orbital states, ε_{a^*1g}–ε_{b1g}, is determined so as to reproduce the energy difference between $^3B_{1g}$ and $^1A_{1g}$ multiplets in the first principles cluster calculations for a CuO_6 octahedron in LSCO [14]. It is −2.6 eV for $x_{\text{opm}}(= 0.15)$ in LSCO.

Acknowledgments Two of the authors (Hiroshi Kamimura and Hideki Ushio) are very grateful to Professor Alex Müller for stimulating discussion on the subject of this paper for the long time. We would like to acknowledge the collaboration of Shunich Matsuno, Kunio Ishida, and Mikio Eto. Finally we would like also to thank Profs. Atsushi Fujimori and Kazuyoshi Yamada for their valuable discussion on experimental results. This work was supported by Tokyo University of Science and the Japanese Cabinet-Office-Projects: FIRST and ImPACT.

References

1. J.G. Bednorz, K.A. Müller, Possible high Tc superconductivity in the Ba-La-Cu-O system. Z. Phys. B **64**, 189–193 (1986)
2. C.C. Tsuei, J.R. Kirtley, Pairing symmetry in cuprate superconductors. Rev. Mod. Phys. **72**, 969 (2000)
3. B. Keimer, S.A. Kivelson, M.R. Norman, S. Uchida, J. Zaanen, From quantum matter to high-temperature superconductivity in copper oxides. *Nature* **518**, 179–186 (2015)
4. F.C. Zhang, T.M. Rice, Effective Hamiltonian for the superconducting Cu oxides. Phys. Rev. B **37**, 3759–3761 (1988)
5. M.R. Norman, H. Ding, M. Randeriat, J.C. Campuzano, T. Yokoya, T. Takeuchi, T. Takahashi, T. Mochiku, K. Kadowaki, P. Guptasarma, D.G. Hinks, Destruction of the Fermi surface in underdoped high-T_c superconductors. Nature **392**, 157–160 (1998)
6. H. Kamimura, Y. Suwa, New theoretical view for high temperature superconductivity. J. Physical Soc. Japan **62**, 3368–3371 (1993)
7. H. Kamimura, T. Hamada, H. Ushio, Theoretical exploration of electronic structure in cuprates from electronic entropy. Phys. Rev. B **66**, 054504 (2002)
8. P.W. Anderson, Resonating valence bond state in La_2CuO_4 and superconductivity. Science **235**, 1196–1198 (1987)
9. H. Kamimura, S. Matsuno, T. Mizokawa, K. Sasaoka, K. Shiraishi, H. Ushio On the important role of the anti-Jahn-Teller effect in underdoped cuprate superconductors. J. Phys. Conf. Ser. **428**, 012043 (2013) and related references therein
10. See, for example, R.J. Cava, B. Batlogg, S.A. Sunshine, T. Siegrist, H.M. Fleming, K. Rabe, F. Scheemeyer, D.W. Murphy, R.B. van Dover, P.K. Gallagher, S.H. Clarum, S. Nakayama, R.C. Farrow, J.J. Krajewski, S.R. Zahurak, J.V. Waszak, J.H. Marshall, P. Marsh, L.W. Rupp Jr., W.F. Peck, E.A. Rietman, Studies of oxygen-deficient $Ba_2YCu_3O_{7-\delta}$ and superconductivity Bi(Pb)-Sr-Ca-Cu-O. Physica C **153-155**, 560-565 (1988).
11. C.T. Chen, L.H. Tjeng, H. Kwo, L. Kao, P. Rudolf, P. Sette, R.M. Fleming, Out-of-plane orbital characteristics of intrinsic and doped holes in $La_{2-x}Sr_xCuO_4$. Phys. Rev. Lett. **68**, 2543–2546 (1992)
12. E. Pellegrin, N. Nücker, J. Fink, S.L. Molodtsov, A. Gutierre, E. Navas, O. Sterebel, Z. Hu, M. Domke, G. Kaindl, S. Uchida, Y. Nakamura, J. Marki, M. Klaude, G. Saemann-Ischenko, A. Krol, J.L. Peng, Z.Y. Li, R.L. Greene, Orbital character of states at the Fermi level in $La_{2-x}Sr_xCuO_4$ and $R_{2-x}Ce_xCuO_4$ (R = Nd_2Sm). Phys. Rev. B **47**, 3354–3367 (1993)
13. V.L. Anisimov, S.Y. Ezhov, T.H. Rice, Singlet and triplet hole-doped and configuration in $La_2Cu_{0.5}Li_{0.5}O_4$. Phys. Rev. B **55**, 12829–12832 (1997)
14. See H. Ushio, S. Matsuno, H. Kamimura On the interplay of Jahn-Teller physics and Mott physics in the mechanism of high T_c superconductivity, in *Vibronic Interactions and the Jahn-Teller Effect*. Eds. M. Atanasov, C. Dual and P.L.W. Tregenna-Pigott (Springer, Heidelberg 2012), pp. 397-417.
15. M. Eto, H. Kamimura: First principles investigation of the electronic structures of copper oxide superconductors by the MCSCF cluster method, J. Physical Soc. Japan **60**, 2311-2323 (1991) and related references therein

16. H. Ushio, H. Kamimura, Electronic structure and renormalized Fermi surface of $La_{2-x}Sr_xCuO_4$. J. Physical Soc. Japan **64**, 2585–2593 (1995)
17. T. Hamada, K. Ishida, H. Kamimura, Y. Suwa, Computational study on the ground state of a dopant hole in a two-dimensional quantum spin system. J. Physical Soc. Japan **70**, 2033–2037 (2001)
18. K. Yamada, C.H. Lee, K. Kurahashi, J. Wada, S. Wakimoto, S. Ueki, H. Kimura, Y. Endoh, Doping dependence of the spatially modulated dynamical spin correlations and the superconducting transition temperature in $La_{2-x}Sr_xCuO_4$. Phys. Rev. B **57**, 6165–6172 (1998)
19. P.W. Anderson, Absence of diffusion in certain random lattices. Phys. Rev. **109**, 35 (1958)
20. N.F. Mott, *Conduction in Non-Crystalline Materials* (Oxford University Press, New York, 1987) and related references therein
21. K.-Y. Yang, T.Y. Rice, F.-C. Zhang: Phenomenological theory of the pseudogap. Phys. Rev. B **73**, 174501 (2006) and related references therein
22. T.J. Reber, N.C. Plumb, Z. Sun, Y. Gao, Q. Wang, K. McElroy, H. Iwasawa, M. Arita, J.S. Wen, Z.J. Xu, G. Gu, Y. Yoshida, H. Eisaki., Y. Aiura, D.S. Dessau: The origin and non-quasiparticle nature of Fermi arcs in $Bi_2Sr_2CaCu_2O_{8+\delta}$. Nat. Phys. **8**, 606-610 (2012) and related references therein
23. J.W. Loram, K.A. Mirza, J.R. Cooper, J.L. Tallon, Specific heat evidence on the normal state pseudogap. J. Phys. Chem. Solid **59**, 2091–2094 (1998)
24. T. Yoshida, X.J. Zhou, K. Tanaka, W.L. Yang, Z. Hussain, Z.-X. Shen, A. Fujimori, S. Sahrakorpi, M. Lindroos, R.S. Markiewicz, A. Bansi, S. Komiya, Y. Ando, H. Eisaki, T. Kakeshita, S. Uchida, Systematic doping evolution of the underlying Fermi surface of $La_{2-x}Sr_xCuO_4$. Phys. Rev. B **74**, 224510 (2006)
25. K. Tanaka, W.S. Lee, D.H. Lu, A. Fujimori, T. Fujii, I. Risdiana, D. Terasaki, J. Scalapino, T.P. Devereaux, Z. Hussain, Z.-X. Shen, Distinct Fermi-Momentum-Dependent Energy Gaps in Deeply Underdoped Bi2212. Science **314**, 1910–1913 (2006)
26. W.S. Lee, M. Vishik, K. Tanaka, D.H. Lu, N. Sasagawa, T.P. Devereaux, Z.-X. Shen, Abrupt onset of a second energy gap at the superconducting transition of underdoped Bi2212. Nature **450**, 81–84 (2007)
27. A. Kanigel, M.R. Norman, M. Randeria, U. Chatterjee, S. Souma, A. Kaminski, H.M. Fretwell, D. Hinks, L. Ozyuzer, J.C. Camuzano, Evolution of the pseudogap from Fermi arcs to the nodal liquid. Nat. Phys. **2**, 447–451 (2006)
28. H. Kamimura, S. Matsuno, Y. Suwa, H. Ushio, Occurrence of d-wave pairing in the phonon-mediated mechanism of high temperature superconductivity in cuprates. Phys. Rev. Lett. **77**, 723–726 (1996)
29. H. Takagi, T. Ido, S. Ishibashi, M. Uota, S. Uchida, Y. Tokura, Superconductor-to-nonsuperconductor transition in $(La_{1-x}Sr_x)CuO4$ as investigated by transport and magnetic measurements. Phys. Rev. B **40**, 2254–2261 (1989)
30. H.-B. Yang, J.D. Rameau, P.D. Johnson, T. Valla, A. Tsvellk, G.D. Gu, Emergence of preformed copper pairs from the doped Mott insulating state in $Bi_2Sr_2CaCu_2O_{8+\delta}$. Nature **456**, 77–80 (2008)
31. K. McElroy, R.W. Simmonds, J.R. Hoffman, D.-H. Lee, J. Orenstein, H. Eisaki, S. Uchida, J.C. Davis, Relating atomic-scale electronic phenomena to wave-like quasiparticle states in superconducting $Bi_2Sr_2CaCu_2O_{8+\delta}$. Nature **422**, 592–596 (2003)
32. I.M. Vishik, M. Hashimoto, R.-H. He, W.-S. Lee, F. Schmitt, D. Lu, B.G. Moore, C. Zhang, W. Meevasana, T. Sasagawa, S. Uchida, K. Fujita, S. Ishida, M. Ishikado, Y. Yoshida, H. Eisaki, Z. Hussain, P. Thomas, T.P. Devereaux, Z.-X. Shen, Phase competition in trisected superconducting dome. Proc. Natl. Acad. Sci. U. S. A. **109**, 18332–18337 (2012)
33. H. Kamimura, H. Hamada, S. Matsuno, H. Ushio, A Novel Approach to the polaronic metallic state of cuprate superconductors and the d-wave pairing mechanism. J. Supercond. **15**, 379–385 (2002)

34. A.R. Bishop, A. Bussmann-Holder, M. Cardona, O.V. Dolgov, A. Furrer, H. Kamimura, H. Keller, R. Khasanov, R.K. Kremer, D. Manske, K.A. Müller, A. Simon, Real and marginal isotope effects in cuprate superconductors. J. Supercond. Novel Magn. **20**, 393–400 (2007)
35. The present paper is based on our recent paper by H. Kamimura, J.S. Tsai, O. Sugino, K. Ishida, H. Ushio, arXiv: 1608.08338

Chapter 12
Isotope Effect on the Transition Temperature T_c in Fe-Based Superconductors: The Current Status

Rustem Khasanov

Introduction

Historically, the isotope effect plays an important role in elucidating the origin of the pairing interaction leading to the occurrence of superconductivity. The discovery of the isotope effect on the superconducting transition temperature T_c in metallic Hg [1, 2] in the year 1950 provided the key experimental evidence for phonon-mediated pairing and leads to the subsequent formulation of the BCS theory.

An involvement of the lattice degrees of freedom into the supercarrier formation is generally considered by measuring the isotope effect exponent on T_c:

$$\alpha = -\frac{\Delta T_c/T_c}{\Delta M/M}, \tag{12.1}$$

(M is the isotope mass and ΔM is the mass difference) and by further comparing it with the universal value $\alpha_{\mathrm{BCS}} \equiv 0.5$ as is predicted within the framework of BCS theory of electron–phonon mediated superconductivity.

In conventional phonon-mediated superconductors like simple metals, alloys, *etc*. α, typically, ranges from 0.2 to 0.5, (see [3] and references therein). The only exceptions are Ru and Zr exhibiting zero isotope effect and PdH(D) with $\alpha_{\mathrm{H(D)}} = -0.25$ [4, 5]. The negative isotope effect of PdH(D) is explained, however, by the presence of strong lattice anharmonicty caused by the double-well potential in the proton (deuteron) bond distribution [6]. A similar finding exists in

R. Khasanov (✉)
Laboratory for Muon Spin Spectroscopy, Paul Scherrer Institute, 5232 Villigen PSI, Switzerland
e-mail: rustem.khasanov@psi.ch

A. Bussmann-Holder et al. (eds.), *High-Tc Copper Oxide Superconductors and Related Novel Materials*, Springer Series in Materials Science 255,
DOI 10.1007/978-3-319-52675-1_12

organic superconductors where the H(D) isotope effect changes sign as compared, *e.g.*, to ^{34}S, ^{13}C, and ^{15}N isotope replacements, (see [7] and references therein). Again, an unusually strong anharmonic lattice dynamics are attributed to this observation [7, 8]. Recently the sine changed isotope effect was reported by Stucky et al. [9] for $n-$doped $SrTiO_3$ which supposed to be purely phonon-mediated superconductor. It was observed that the substitution of the natural ^{16}O atoms by the heavier isotope ^{18}O causes a giant (of the order of 50%) enhancement of T_c. Also the magnetic critical field H_{c2} is increased by a factor $\sim$2. Such a strong impact on T_c and H_{c2}, with a sign opposite to conventional superconductors was assumed to be caused by strong coupling to the ferroelectric soft modes of $SrTiO_3$.

The cuprate high-temperature superconductors (HTS) are characterized by a vanishingly small but positive isotope effect exponent in optimally doped compounds which increases in a monotonic way upon decreasing doping [10–24]. For the optimally doped cuprate HTS the smallest value of the oxygen-isotope exponent $\alpha_O \simeq 0.02$ was obtained for $YBa_2Cu_3O_{7-\delta}$ and $Bi_2Sr_2Ca_2Cu_3O_{10+\delta}$, while it reaches $\alpha_O \simeq 0.25$ for $Bi_2Sr_{1.6}La_{0.4}CuO_{6+\delta}$ [10–13, 23, 24]. In addition, it was demonstrated that in underdoped materials α_O exceeds substantially the BCS limit $\alpha_{BCS} \equiv 0.5$ [11, 12, 14, 24].

It is worth to emphasize here that the values of both, the oxygen and the copper isotope exponents in cuprate HTS are *always* positive. Similar tendencies, with the only few above mentioned exceptions, are also realized in a case of conventional phonon-mediated superconductors.

Since the discovery of high-temperature superconductivity in Fe-based compounds few experiments to study the isotope effect on T_c in this new class of materials were performed. The current statement of isotope effect studies on Fe-based HTS remains, however, rather contradicting [25–30]. Liu et al. [25] and Khasanov et al. [28] have found a *positive* Fe isotope effect (Fe–IE) exponent α_{Fe} for $Ba_{0.6}K_{0.4}Fe_2As_2$ ($T_c \simeq 38$ K), $SmFeAsO_{0.85}F_{0.15}$ ($T_c \simeq 41$ K), and $FeSe_{1-x}$ ($T_c \simeq 8$ K) with the corresponding values $\alpha_{Fe} = 0.34(3)$, 0.37(3), and 0.81(15), respectively. Note that $\alpha_{Fe} = 0.81(15)$ for $FeSe_{1-x}$ exceeds substantially the universal BCS value $\alpha_{BCS} \equiv 0.5$. In the other studies Shirage et al. [26, 27] have reported a *negative* $\alpha_{Fe} = -0.18(3)$ and $\alpha_{Fe} = -0.024(15)$ for $Ba_{0.6}K_{0.4}Fe_2As_2$ ($T_c \simeq 38$ K) and $SmFeAsO_{1-y}$ ($T_c \simeq 54$ K), respectively. The negative Fe–IE exponents were also reported recently by Tsuge and co-workers for $FeSe_{0.35}Te_{0.65}$ ($T_c \simeq 15$ K, $\alpha_{Fe} = -0.54$) and $Ca_{0.4}Na_{0.6}Fe_2As_2$ ($T_c \simeq 34$ K, $\alpha_{Fe} = -0.19$) [29, 30]. Note that the sine changed isotope effect is unlikely to stem from different pairing mechanisms going to be realized in different Fe-based superconductors. Especially, in the case of $Ba_{0.6}K_{0.4}Fe_2As_2$, when nominally *identical* samples exhibit once a positive [25] and next a negative isotope exponent [26].

The main purpose of the present study is to show that the very controversial results for Fe–IE on T_c are caused by small structural changes occurring simultaneously with the Fe isotope exchange. We demonstrate that the Fe–IE exponent on T_c needs to be decomposed into the one related to the structural changes (α_{Fe}^{str}) and the genuine (intrinsic one, α_{Fe}^{int}) to result in:

$$\alpha_{\mathrm{Fe}} = \alpha_{\mathrm{Fe}}^{\mathrm{int}} + \alpha_{\mathrm{Fe}}^{\mathrm{str}}. \tag{12.2}$$

The validity of such decomposition is further confirmed by the fact that $\alpha_{\mathrm{Fe}}^{\mathrm{int}}$ coincides with the Fe–IE exponent on the characteristic phonon frequency ω_{ph} as is observed in EXAFS and Raman experiments [31, 32]. The value of $\alpha_{\mathrm{Fe}}^{\mathrm{int}}$ was found to be the same for representatives of various families of Fe-based superconductors and it stays in the range of $\alpha_{\mathrm{Fe}}^{\mathrm{int}} \sim 0.3 - 0.4$ in good agreement with the theory prediction of Bussmann-Holder et al. [33].

The paper is organized as follows. In section "Fe isotope effect on T_c and the crystal structure of $FeSe_{1-x}$" we demonstrate the influence of the Fe isotope exchange on the crystal structure. As an example, $FeSe_{1-x}$ Fe-based HTS with $T_c \simeq 8$ K is considered. It is shown that the substitution of natural Fe (containing $\simeq$92% of ^{56}Fe) by its lighter ^{54}Fe isotope leads not only to a shift of T_c, but affects also the structural parameters such as the lattice parameters a, b, and c, the lattice volume V, the distance between the Se atom and Fe plane, and the Se height h_{Se}. Results presented in this section are adapted from [28]. In section "Genuine (intrinsic) and structural isotope effects in Fe-based HTS" the currently available Fe isotope effect data on the superconducting transition temperature T_c for various Fe-based HTS were reanalyzed by separating the measured Fe–IE exponent α_{Fe} into a structural and an intrinsic (unrelated to the structural changes) components. By taking structural corrections into account we infer that the value of the genuine Fe–IE exponent is close to $\alpha_{\mathrm{Fe}}^{\mathrm{int}} \sim 0.3 - 0.4$. The results presented section "Genuine (intrinsic) and structural isotope effects in Fe-based HTS" are partially adapted from [34]. The conclusions follow in section "Conclusions".

Fe Isotope Effect on T_c and the Crystal Structure of $FeSe_{1-x}$

In this section the ^{56}Fe/^{54}Fe isotope effects on the superconducting transition temperature and the crystal structure of the iron–chalcogenide superconductor $FeSe_{1-x}$ are described.

The preparation procedure for ^{56}Fe/^{54}Fe isotope submitted $FeSe_{1-x}$ powder samples is given in [28]. The Fe–IE on the structural properties and the transition temperature T_c were studied in neutron powder diffraction (NPD) and magnetization experiments, respectively.

Fe Isotope Effect on the Crystal Structure of $FeSe_{1-x}$

The refined structural parameters at $T = 250$ K and 5 K obtained in neutron powder diffraction experiments are summarized in Table 12.1. The results of NPD measurements imply that the substitution of ^{56}Fe by ^{54}Fe leads to a small, but detectable

Table 12.1 Structural parameters of $^{54}FeSe_{1-x}$ and $^{56}FeSe_{1-x}$ at $T = 250$ and 5 K as obtained from the refitment of neutron powder diffraction (NPD) data (after [28])

	$T = 250$ K		$T = 5$ K	
	$^{54}FeSe_{1-x}$	$^{56}FeSe_{1-x}$	$^{54}FeSe_{1-x}$	$^{56}FeSe_{1-x}$
Space group	*P4/nmm*		*Cmma*	
Se content	0.975(5)	0.975(4)	Fixed to 0.975	
a(Å)	3.77036(3)	3.76988(5)	5.33523(10)	5.33426(10)
b(Å)			5.30984(10)	5.30933(10)
c(Å)	5.51619(9)	5.51637(9)	5.48683(9)	5.48787(9)
Volume (Å^3)	156.883(3)	156.797(3)	155.438(5)	155.424(5)
z−Se	0.2319(2)	0.2326(0.3)	0.2321(2)	0.2322(3)

enhancement of the lattice along the crystallographic a and b directions and a *compression* of it along the c-axis, resulting in a change of the shape of the Fe_4Se pyramid (see Fig. 12.1a). As is shown in Fig. 12.1b, for temperatures below 100 K the Se atom is located closer to the Fe plane in $^{54}FeSe_{1-x}$ than in $^{56}FeSe_{1-x}$.

It is important to note that the observed Fe–IE's on the lattice parameters are intrinsic and not just a consequence of slightly different samples. As shown in [35], various samples of $^{56}FeSe_{1-x}$ with $1 - x \simeq 0.98$ and $T_c \simeq 8.2$ K indeed exhibit the same lattice parameters within the experimental error.

Fe Isotope Effect on T_c of $FeSe_{1-x}$

The Fe–IE on the transition temperature T_c was studied by means of magnetization experiments. In order to avoid artifacts and systematic errors in the determination of the isotope shift of T_c a *statistical* study were performed: *i.e.* the series of $^{54}FeSe_{1-x}$/$^{56}FeSe_{1-x}$ samples synthesized exactly at the same way (the same thermal history, the same amount of Se in the initial composition) were investigated.

The magnetization experiments were conducted for six $^{54}FeSe_{1-x}$ and seven $^{56}FeSe_{1-x}$ samples, respectively. Figure 12.2 shows an example of zero-field cooled (ZFC) magnetization curves for a pair of $^{54}FeSe_{1-x}$/$^{56}FeSe_{1-x}$ samples (M_{norm} was obtained after subtracting the small paramagnetic offset M_{magn} measured at $T > T_c$ and further normalization of the obtained curve to the value at $T = 2$ K, see Fig. 1 in [35] for details). The magnetization curve for $^{54}FeSe_{1-x}$ is shifted almost parallel to higher temperature, implying that T_c of $^{54}FeSe_{1-x}$ is higher than that of $^{56}FeSe_{1-x}$. The resulting transition temperatures determined from the intercept of the linearly extrapolated $M_{norm}(T)$ curves with the $M = 0$ line for all samples investigated are summarized in the inset of Fig. 12.2. The T_c's for both sets of $^{54}FeSe_{1-x}$/$^{56}FeSe_{1-x}$ samples fall into two distinct regions: $8.39 \leq {}^{54}T_c \leq 8.48$ K and $8.15 \leq {}^{56}T_c \leq 8.31$ K, respectively. The corresponding mean values are: $^{54}\bar{T}_c = 8.43(3)$ K and $^{56}\bar{T}_c = 8.21(4)$ K. Note, that one out of the seven $^{56}FeSe_{1-x}$ samples had $T_c \simeq 8.44$ K which is by more than 5 standard deviations above the average calculated for the rest

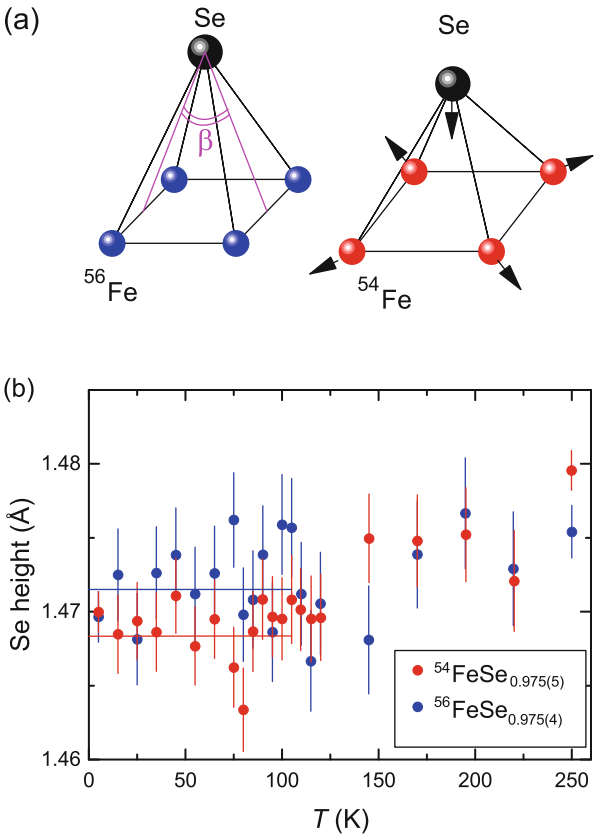

Fig. 12.1 (**a**) The transformation of the Fe_4Se pyramid caused by $^{56}Fe/^{54}Fe$ isotope substitution in $FeSe_{1-x}$. The *arrows* show the direction of atom displacements. (**b**) The temperature dependence of the distance between the Se atom and Fe plane h_{Se}. The *straight lines* correspond to averaging the data below 100 K. After [28]

of the six samples. We have no explanation for this discrepancy, but decided to show this point for completeness of the data collected.

The value of the Fe–IE exponent α_{Fe} determined from the data presented in Fig. 12.2 by means of Eq. (12.1) leads to $\alpha_{Fe} = 0.81(15)$.

The Structural and the Intrinsic Contributions to the Fe–IE in $FeSe_{1-x}$

The Fe–IE exponent $\alpha_{Fe} = 0.81(15)$ obtained for $FeSe_{1-x}$ iron–chalcogenide superconductor is larger than the BCS value $\alpha_{BCS} \equiv 0.5$ as well as more than twice as large as $\alpha_{Fe} \simeq 0.35$ reported for $SmFeAsO_{0.85}F_{0.15}$ and $Ba_{0.6}K_{0.4}Fe_2As_2$ [25]. We want to emphasize, however, that our structural refined NPD data suggest that part of the large Fe–IE exponent $\alpha_{Fe} = 0.81(15)$ may result from the tiny structural changes occurring due to $^{54}Fe/^{56}Fe$ substitution.

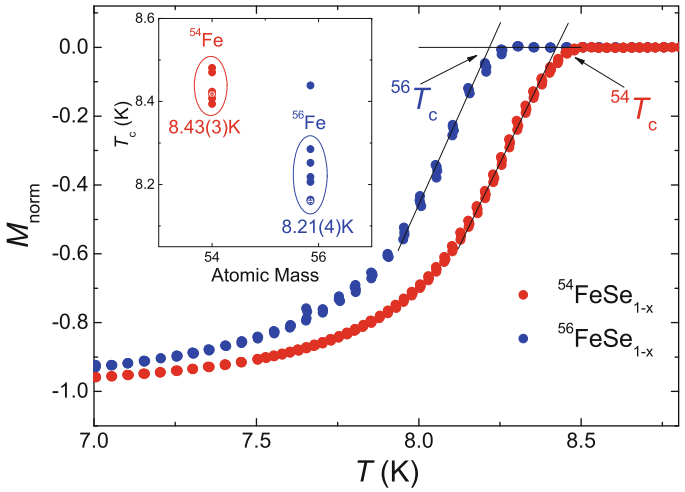

Fig. 12.2 The normalized zero-field cooling magnetization curves $M_{norm}(T)$ for one pair of $^{54}FeSe_{1-x}$ and $^{56}FeSe_{1-x}$ samples. The transition temperature T_c is determined as the intersection of the linearly extrapolated $M_{nomr}(T)$ curve in the vicinity of T_c with the $M=0$ line. The *inset* shows the superconducting transition temperature T_c as a function of Fe atomic mass for $^{54}FeSe_{1-x}/^{56}FeSe_{1-x}$ samples studied in the present work. The open symbols correspond to the samples studied by NPD experiments. The T_c's fall into the regions marked by the colored ovals with the corresponding mean values $^{54}\bar{T}_c = 8.43(3)$ K and $^{56}\bar{T}_c = 8.21(4)$ K. After [28]

An estimate of the structural contribution to the Fe–IE exponent in $FeSe_{1-x}$ can be made based on the observed proportionality between T_c and the crystal lattice constant a for the 11 family $FeSe_{1-y}Te_y$ [36, 37]. Assuming the relation T_c vs. a also holds for $FeSe_{1-x}$ one obtains from the data presented in [37] for $y \leq 0.5$ the relation $\Delta T_c^a/(\Delta a/a) \approx 6$ K/%. With $(\Delta a + \Delta b)/(a+b) = 0.0195(14)\%$ (see Table 12.1 and [28]) this results in a *structural* shift of T_c of $\Delta T_c^{str} \approx 0.1$ K. Taking this correction into account yields a rough estimate of the structural and the intrinsic Fe–IE exponents of $\alpha_{Fe}^{str} \simeq \alpha_{Fe}^{int} \simeq 0.4$. Note that the value of $\alpha_{Fe}^{int} \simeq 0.4$ is comparable with $\alpha_{Fe} \simeq 0.35$ reported for $SmFeAsO_{0.85}F_{0.15}$ and $Ba_{0.6}K_{0.4}Fe_2As_2$ [25].

We want to stress, that the "structural" contribution into the Fe–IE exponent in $FeSe_{1-x}$ consists of both: a positive and negative parts. Indeed, in $FeSe_{1-x}$ a decrease of the Se height caused by compression of the Fe_4Se pyramid (see Fig. 12.1b) leads to an increase of T_c by $\Delta T_c^{h_{Se}}/(\Delta h_{Se}/h_{Se}) \simeq 3.4$ K/% [38, 39]. In contrast, an increase of the Se(Te)-Fe-Se(Te) angle in the $FeSe_{1-y}Te_y$ family (angle β in our notation, see Fig. 12.1a) results for $y \leq 0.5$ in a decrease of T_c by $\Delta T_c^{\beta}/(\Delta\beta/\beta) \simeq 2.9$ K/% [36]. Based on the structural data presented in Fig. 12.1 and Table 12.1 one obtains $\Delta h_{Se}/h_{Se} = 0.22(8)\%$ and $\Delta\beta/\beta = -0.13(4)\%$, leading to $\Delta T_c^{h_{Se}} = 0.7(3)$ K and $\Delta T_c^{\beta} = -0.4(2)$ K (in this estimate the values of h_{Se} were averaged over the temperature regions denoted as solid lines in Fig. 12.1b). Bearing in mind that all Fe-based HTS are similarly sensitive to structural changes as $FeSe_{1-x}$ (see, *e.g.*, Refs. [36–38, 40]) we conclude that depending on the particular

structural changes caused by the Fe isotope substitution, the shift of the transition temperature T_c could be either *positive*, *negative* or may stay at *zero*. Which particular case is going to be realized would require precise studies of the structural properties for each individual isotope experiment.

Genuine (Intrinsic) and Structural Isotope Effects in Fe-based HTS

The observation of tiny but not negligible isotope effect on the crystal structure observed in $FeSe_{1-x}$ Fe-based HTS reported in the previous section requires to separate the Fe–IE exponent on T_c into the genuine (intrinsic) and the structural components (see Eq. (12.2)). In fact, the superconductivity in all Fe-based HTS is intimately related to small structural changes as reported in various works. As an example the strong nonlinear dependence of the superconducting transition temperature on the anion atom height (h_{An}, An = As, P, or Se) with a sharp maximum of T_c at $h_{An} \simeq 1.38$ Å, was reported by Mizuguchi et al. [38] (see Fig. 12.3).

Summary of Fe–IE Measurements on the Transition Temperature T_c

The results of Fe–IE measurements of T_c for various Fe-based HTS's obtained up to date are summarized in Table 12.2 and Fig. 12.4a. In order to account for the structural changes caused by the Fe isotope exchange we have also included in Table 12.2 the c-axis lattice constants as they measured for the pairs of Fe isotope substituted samples. The choice of the c-axis lattice constant as the relevant quantity in deriving the structural isotope effect might appear to be rather arbitrary since T_c is influenced by all structural details, namely tetrahedral angle, a-axis lattice constant, internal bond lengths, *etc*. However, the c-axis lattice constant provides a very sensitive probe since its compression(expansion) is directly accompanied by the corresponding variation of the distance from the Fe-planes to the above(below) lying anions which, in turn, is a well characterized property for many Fe-based compounds [38]. A survey of the literature shows that the proportionality between the anion atom height and the c-axis lattice constant indeed holds for various families of Fe-based HTS considered in the present study [39, 41, 42].

From Table 12.2 it follows that in $Ba_{0.6}K_{0.4}Fe_2As_2$ and $SmFeAsO_{0.85}F_{0.15}$ studied in [25] the c-axis constants are the same within the experimental error for both isotopically substituted sets of the samples. In $FeSe_{1-x}$ [28] the c-axis constant is larger, while in $Ba_{0.6}K_{0.4}Fe_2As_2$ [26] it is smaller for the sample with the heavier Fe isotope. In $SmFeAsO_{1-y}$, studied by Shirage et al., [27] both c-axis lattice constants seem to coincide within the experimental resolution. However,

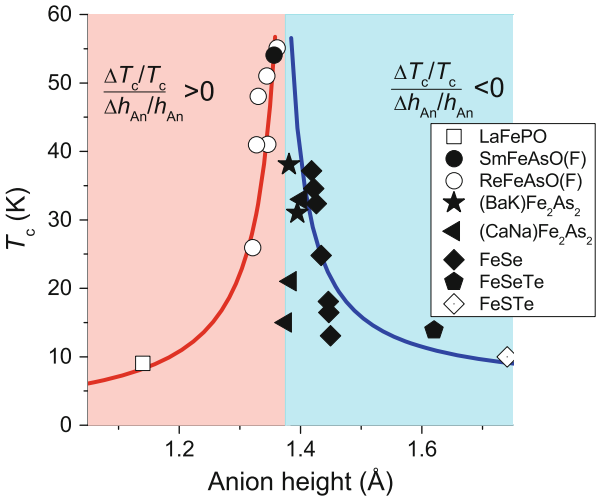

Fig. 12.3 Dependence of the superconducting transition temperature T_c on the height of the anion atom (h_{An}, An = As, Se, P) for varios families of Fe-based HTS, after Mizuguchi et al. [38] The closed symbols represent the samples which are relevant for the present study. The *lines* are guided for the eye. The *red*(*blue*) area represents part of T_c vs. h_{An} diagram where T_c increases(decreases) with increasing h_{An}

since the difference between them is 1.5 times larger than one standard deviation, it is conceivable to attribute an increase in the *c*-axis lattice constant in $SmFeAsO_{1-y}$ with the heavier Fe isotope. It should also be noted here that the accuracy in lattice constants determination for $Ca_{0.4}Na_{0.6}Fe_2As_2$ from [30] is from one to two orders of magnitude worse than it is reported for other isotope substituted samples, and no structural data were reported for $FeSe_{0.35}Te_{0.65}$ in [29, 30].

The use of the empirical T_c vs. h_{An} relation from [38] combined with the intrinsic relation of the proportionality between the *c*-axis constant and the anion atom height ($\Delta c \propto \Delta h_{An}$, see [39, 41, 42]) enables us to determine the sign of the structurally related shift of T_c induced by isotopic exchange. By following Mizuguchi et al. [38] (see also Fig. 12.3) the sign of $(\Delta T_c/T_c)/(\Delta h_{An}/h_{An})$ is positive for SmFeAsO(F) as well as for various Fe-based HTS belonging to ReFeAsO (F) family (Re = Nd, Ce, La) and negative for $(BaK)Fe_2As_2$, $(CaNa)Fe_2As_2$, Fe (SeTe), and $FeSe_{1-x}$. Consequently the change of the *c*-axis constant caused by Fe isotope substitution as presented in Table 12.2 results in an additional structurally related shift of T_c being positive for $FeSe_{1-x}$, [28] negative for $Ba_{0.6}K_{0.4}Fe_2As_2$ and $SmFeAsO_{1-y}$, [26, 27] and close to 0 for $Ba_{0.6}K_{0.4}Fe_2As_2$ and $SmFeAsO_{0.85}F_{0.15}$ [25]. Note that for the lack of pure(absent) structural data, such estimate is not possible to be made for $Ca_{0.4}Na_{0.6}Fe_2As_2$ and $FeSe_{0.35}Te_{0.65}$ from [29, 30].

We want to emphasize that the above mentioned discussion allows only to determine the sign of the structurally related isotope effect but not its absolute value. The reasons are the following. (i) The relative change of the *c*-axis constant is proportional, but not identical to the one of h_{An}. As an example, ^{56}Fe to ^{54}Fe isotope substitution in $FeSe_{1-x}$ leads to an increase of the *c*-axis constant by approximately 0.02%, while the change of the Se height amounts to ten times higher value $\simeq$0.22% (see Table 12.1, Fig. 12.1b, and [28]). (ii) The height of the

Table 12.2 Summary of Fe isotope effect studies for $SmFeAsO_{0.85}F_{0.15}$ and $Ba_{0.6}K_{0.4}Fe_2As_2$ [25], $Ba_{0.6}K_{0.4}Fe_2As_2$ [26], $SmFeAsO_{1-x}$ [27], $FeSe_{1-x}$ [28], $FeSe_{0.35}Te_{0.65}$ [29] and $Ca_{0.4}Na_{0.6}Fe_2As_2$ [30]

Sample	Reference	$T_c(^{nat}Fe)$, (K)	α_{Fe}	c-axis($^{light}Fe$), (Å)	c-axis($^{heavy}Fe$), (Å)	$\Delta c/c$	α_{Fe}^{str}	α_{Fe}^{int}
$Ba_{0.6}K_{0.4}Fe_2As_2$	[25]	37.30(2)	0.37(3)	13.289(7)	13.288(7)	~ 0	~ 0	~ 0.35
$Ba_{0.6}K_{0.4}Fe_2As_2$	[26]	37.78(2)	−0.18(3)	13.313(1)	13.310(1)	< 0	~ -0.5	–
$SmFeAsO_{0.85}F_{0.15}$	[25]	41.40(2)	0.34(3)	8.490(2)	8.491(2)	~ 0	~ 0	~ 0.35
$SmFeAsO_{1-y}$	[27]	54.02(13)	−0.024(15)	8.4428(8)	8.4440(8)	$\gtrsim 0$	~ -0.35	–
$FeSe_{1-x}$	[28]	8.21(4)	0.81(15)	5.48683(9)	5.48787(9)	> 0	$\simeq 0.4$	$\simeq 0.4$
$FeSe_{0.35}Te_{0.65}$	[29]	13.10(5)	−0.54	–	–	–	–	–
$Ca_{0.4}Na_{0.6}Fe_2As_2$	[30]	34.3(2)	−0.19	12.19	12.19	–	–	–

The parameters are: T_c—superconducting transition temperature for the sample with the natural Fe isotope (^{nat}Fe); α_{Fe}—Fe isotope effect exponent; c—the c-axis lattice constant for the sample with the lighter ($^{light}Fe$) and the heavier ($^{heavy}Fe$) Fe isotope; $\Delta c/c$—the relative shift of the c-axis constant caused by the Fe isotope substitution; α_{Fe}^{str} and α_{Fe}^{int}—the structural and the intrinsic contributions to α_{Fe}

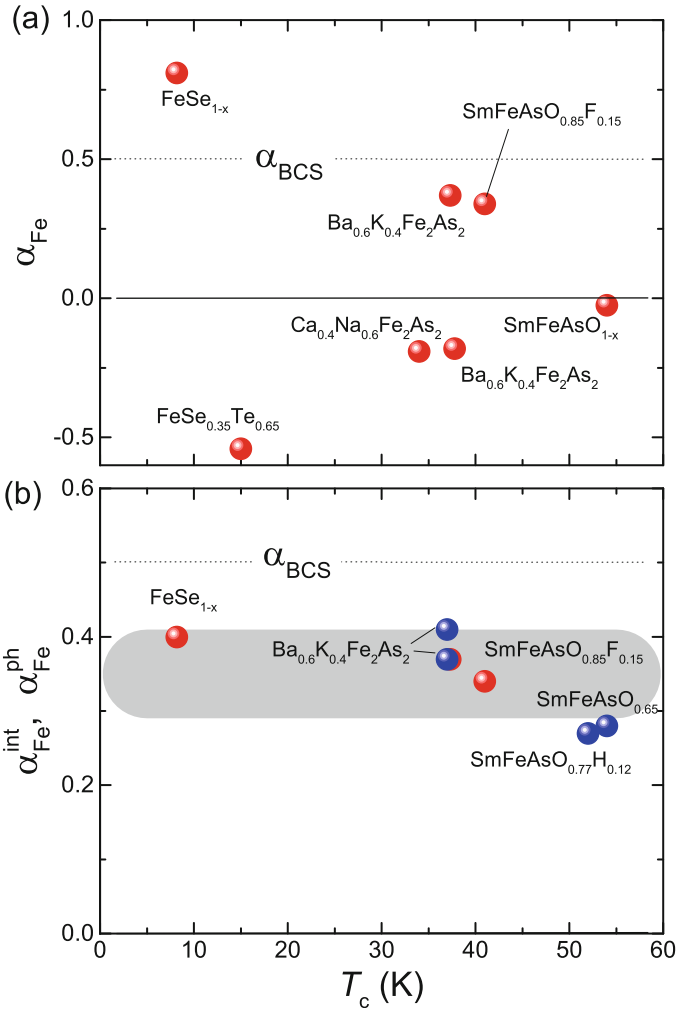

Fig. 12.4 (**a**) Fe isotope effect exponent α_{Fe} as a function of the superconducting transition temperature T_c for the samples considered in the present study: $Ba_{0.6}K_{0.4}Fe_2As_2$ and $SmFeAsO_{0.85}F_{0.15}$ [25], $Ba_{0.6}K_{0.4}Fe_2As_2$ [26], $SmFeAsO_{1-x}$ [27], $FeSe_{1-x}$ [28], $FeSe_{0.35}$ $Te_{0.65}$ [29] and $Ca_{0.4}Na_{0.6}Fe_2As_2$ [30]. $\alpha_{BCS} \equiv 0.5$ denotes the BCS value for electron–phonon mediated superconductivity. (**b**) The "intrinsic" α_{Fe}^{int} (*red circles*) and the phonon α_{Fe}^{ph} (*blue circles*) Fe isotope effect exponents as they obtained in the present study and the EXAFS [31] and Raman [32] experiments, respectively. The *grey* area denotes the region of $0.3 \leq \alpha \leq 0.4$. See text for details

anion atom is clearly not the only parameter which is crucial for T_c of Fe-based HTS as already mentioned above.

The analysis of the structural data together with the dependence of T_c on the *a*-axis lattice constant in $FeSe_{1-x}$, as is presented in section "Fe isotope effect on T_c and the crystal structure of $FeSe_{1-x}$", was allowing to extract the "structural" Fe

isotope effect exponent $\alpha_{\mathrm{Fe}}^{\mathrm{str}} \simeq 0.4$ for ^{56}Fe to ^{54}Fe substituted $FeSe_{1-x}$ samples. The absence of precise structural data for the samples studied in [25–27, 29, 30] complicates their analysis. However, a zero, within the experimental accuracy, Fe isotope shift of the c-axis lattice constant for $Ba_{0.6}K_{0.4}Fe_2As_2$ as reported by Liu et al. [25] is a clear indication that no structural effect is present for this particular set of the samples. Consequently, the negative isotope effect exponent $\alpha_{Fe} \simeq -0.18$ obtained for nominally identically doped $Ba_{0.6}K_{0.4}Fe_2As_2$ by Shirage et al. [26] stems from summing both effects, *i.e.*, $-0.18(\alpha_{\mathrm{Fe}}) = 0.35\left(\alpha_{\mathrm{Fe}}^{\mathrm{int}}\right) - 0.52\left(\alpha_{\mathrm{Fe}}^{\mathrm{str}}\right)$, see Eq. (12.2). The similar analysis by comparing SmFeAsO(F) Fe–IE exponents from [25, 27] results in $\alpha_{\mathrm{Fe}}^{\mathrm{str}} \simeq -0.35$ for $SmFeAsO_{1-y}$ from [27]. It is worth to note, however, that the SmFeAsO(F) samples studied in [25, 27] have different doping levels (different T_c's, see Table 12.2 and Fig. 12.4a).

The Genuine Fe–IE Exponent via Phonon Frequency Measurements

The BCS expression for the superconducting transition temperature T_c relates it to the characteristic phonon frequency ω_{ph} and the coupling constant λ via [43]:

$$T_c \propto \omega_{\mathrm{ph}} \exp(-1/\lambda). \tag{12.3}$$

The consequences of this equation are two fold. First of all, since the coupling constant λ is independent of the ion mass M (see *e.g.* [44]) and the characteristic phonon frequency ω_{ph} is proportional to $1/\sqrt{M}$, as a frequency of any harmonic oscillator, α_{BCS} becomes equal exactly to 0.5. Note that the Coulomb repulsion and the anharmonicity of phonons, which are not considered in Eq. (12.3), would lead to smaller α values [44]. Second, due to direct proportionality between T_c and ω_{ph} the isotope exponents on both these quantities are equal to the each other:

$$\alpha = -\frac{\Delta T_c/T_c}{\Delta M/M} \equiv -\frac{\Delta \omega_{\mathrm{ph}}/\omega_{\mathrm{ph}}}{\Delta M/M}. \tag{12.4}$$

Currently we are aware of two experimental works where the Fe–IE on ω_{ph} was studied by means of EXAFS and Raman techniques on $(BaK)Fe_2As_2$, $SmFeAsO_{0.65}$, and $SmFeAs_{0.77}H_{0.12}$ Fe-based HTS.[31, 32] The corresponding $\alpha_{\mathrm{Fe}}^{\mathrm{ph}}$'s are shown in Fig. 12.4b together with presently obtained $\alpha_{\mathrm{Fe}}^{\mathrm{int}}$'s (see section "Summary of Fe–IE measurements on the transition temperature T_c" and Table 12.2). Remarkably enough both sets of Fe–IE exponents stay quite close to the each other with $\alpha_{\mathrm{Fe}}^{\mathrm{int}} \simeq \alpha_{\mathrm{Fe}}^{\mathrm{ph}} \simeq 0.35 \pm 0.07$.

Isotope Effect Within the Multiple Gap Scenario of Fe-Based HTS

Bussmann-Holder et al.[33] investigated a multiple gap scenario of superconductivity in Fe-based HTS with the aim to search for possible sources of the isotope effect on T_c. Typical phonon-mediated scenarios were contrasted to polaronic effects and found to have very different impacts on the isotope effect. While phonon-mediated superconductivity slightly suppresses the isotope effect as compared to the BCS value $\alpha_{\mathrm{BCS}} \equiv 0.5$, polaronic effects can largely enhance it. The scenario of electron–phonon mediated superconductivity within the dominant gap channel predicts a T_c independent isotope effect with the α value being slightly smaller than 0.5. This agrees rather well with that observed for $FeSe_{1-x}$, [28] $(BaK)Fe_2As_2$, [25, 26, 31] $SmFeAsO_{0.85}F_{0.15}$, [25] $SmFeAsO_{0.65}$, [32] and $SmFeAs_{0.77}H_{0.12}$ [32]. Indeed, for these particular samples, which are belong to 3 different families of Fe-based HTS and have T_c's ranging from 8 to 54 K, the "intrinsic" Fe isotope exponent is almost constant with $\alpha_{\mathrm{Fe}}^{\mathrm{int}} \sim 0.3 - 0.4$, see Table 12.2 and Fig. 12.4b.

Conclusions

The purpose of the present study was two-fold. First, by presenting results obtained on $FeSe_{1-x}$ iron–chalcogenide superconductor it was demonstrated that the tiny changes of the structural parameters caused by Fe isotope substitution are clearly contributing to the resulting Fe–IE exponent on the transition temperature T_c. Depending on the particular changes caused by the Fe isotope substitution, the "structurally" related shift of the transition temperature T_c could be either positive, negative or stays at zero. Such effects may help to clarify or even be the origin of the previously reported controversial results [25–30].

Second, the currently available Fe isotope effect data on the superconducting transition temperature T_c for various Fe-based HTS were analyzed by separating the measured Fe–IE exponent α_{Fe} into a structural ($\alpha_{\mathrm{Fe}}^{\mathrm{str}}$) and an intrinsic (unrelated to the structural changes, $\alpha_{\mathrm{Fe}}^{\mathrm{int}}$) components. The validity of decomposition the Fe–IE exponent α_{Fe} was further confirmed by the fact that $\alpha_{\mathrm{Fe}}^{\mathrm{int}}$ almost coincides with the Fe–IE exponent on the characteristic phonon frequencies as observed in recent EXAFS and Raman experiments [31, 32]. We infer that the value of the genuine Fe–IE exponent is close to $\alpha_{\mathrm{Fe}}^{\mathrm{int}} \sim 0.3 - 0.4$ for compounds having T_c ranging from 8 to 54 K and belonging to at least three different families of Fe-based HTS.

Acknowledgments The author acknowledges the broad and successful collaboration with people without whom this work could not be performed: Markus Bendele, Hugo Keller, Annette Bussmann-Holder, Kazimierz Conder, Ekaterina Pomjakushina, and Volodya Pomjakushin. The

special thank goes to Karl Alex Müller and Hugo Keller who were initiated my interest to the isotope effect studies.

References

1. E. Maxwell, Phys. Rev. **78**, 477 (1950)
2. C.A. Reynolds, B. Serin, W.H. Wright, L.B. Nesbitt, Phys. Rev. **78**, 487 (1950)
3. C.P. Poole, *Handbook of Superconductitivy* (Academic Press, Oval Road, London, 2000), pp. 24–28
4. W. Buckel, B. Strizker, Phys. Letters A **43**, 403 (1973)
5. J.E. Schriber, C.J.M. Northrup Jr., Phys. Rev. B **10**, 3818 (1974)
6. M. Yussouff, B.K. Rao, P. Jena, Solid State Commun. **94**, 549 (1995)
7. J.A. Schlueter, A.M. Kini, B.H. Ward, U. Geiser, H.H. Wang, J. Mohtasham, R.W. Winter, G.L. Gard, Physica C **351**, 261 (2001)
8. M.H. Whangbo, J.M. Willimas, A.J. Schultz, T.J. Emge, M.A. Beno, J. Am. Chem. Soc. **109**, 90 (1997)
9. A. Stucky, G. Scheerer, Z. Ren, D. Jaccard, J.-M. Poumirol, C. Barreteau, E. Giannini, D. van der Marel, Sci. Rep. **6**, 37582 (2016)
10. B. Batlogg, G. Kourouklis, W. Weber, R.J. Cava, A. Jayaraman, A.E. White, K.T. Short, L.W. Rupp, E.A. Rietman, Phys. Rev. Lett. **59**, 912 (1987)
11. J.P. Franck, J. Jung, M.A.-K. Mohamed, S. Gygax, G.I. Sproule, Phys. Rev. B **44**, 5318 (1991)
12. J.P. Franck, in *Physical Properties of High Temperature Superconductors IV*, edited by D. M. Ginsberg (World Scientific, Singapore, 1994), pp. 189–293
13. D. Zech, H. Keller, K. Conder, E. Kaldis, E. Liarokapis, N. Poulakis, K.A. Müller, Nature (London) **371**, 681 (1994)
14. G.-M. Zhao, H. Keller, K. Conder, J. Phys. Condens. Matter **13**, R569 (2001)
15. R. Khasanov, A. Shengelaya, K. Conder, E. Morenzoni, I.M. Savić, H. Keller, J. Phys. Condens. Matter **15**, L17 (2003)
16. R. Khasanov, A. Shengelaya, E. Morenzoni, M. Angst, K. Conder, I.M. Savić, D. Lampakis, E. Liarokapis, A. Tatsi, H. Keller, Phys. Rev. B **68**, 220506(R) (2003b)
17. R. Khasanov, A. Shengelaya, E. Morenzoni, K. Conder, I.M. Savić, H. Keller, J. Phys. Condens. Matter **16**, S4439 (2004)
18. R. Khasanov, D.G. Eshchenko, H. Luetkens, E. Morenzoni, T. Prokscha, A. Suter, N. Garifianov, M. Mali, J. Roos, K. Conder, H. Keller, Phys. Rev. Lett. **92**, 057602 (2004)
19. R. Khasanov, A. Shengelaya, K. Conder, E. Morenzoni, I.M. Savić, J. Karpinski, H. Keller, Phys. Rev. B **74**, 064504 (2006)
20. R. Khasanov, A. Shengelaya, D. Di Castro, D.G. Eshchenko, I.M. Savić, K. Conder, E. Pomjakushina, J. Karpinski, S. Kazakov, H. Keller, Phys. Rev. B **75**, 060505(R) (2007)
21. R. Khasanov, S. Strässle, K. Conder, E. Pomjakushina, A. Bussmann-Holder, H. Keller, Phys. Rev. B **77**, 104530 (2008)
22. J.L. Tallon, R.S. Islam, J. Storey, G.V.M. Williams, J.R. Cooper, Phys. Rev. Lett. **94**, 237002 (2005)
23. X.-J. Chen, B. Liang, C. Ulrich, C.-T. Lin, V.V. Struzhkin, Z. Wu, R.J. Hemley, H.-k. Mao, H.-Q. Lin, Phys. Rev. B **76**, 140502 (2007)
24. R. Khasanov, A. Shengelaya, D. Di Castro, E. Morenzoni, A. Maisuradze, I.M. Savić, K. Conder, E. Pomjakushina, A. Bussmann-Holder, H. Keller, Phys. Rev. Lett. **101**, 077001 (2008)
25. R.H. Liu, T. Wu, G. Wu, H. Chen, X.F. Wang, Y.L. Xie, J.J. Yin, Y.J. Yan, Q.J. Li, B.C. Shi, W.S. Chu, Z.Y. Wu, X.H. Chen, Nature **459**, 64 (2009)

26. P.M. Shirage, K. Kihou, K. Miyazawa, C.-H. Lee, H. Kito, H. Eisaki, T. Yanagisawa, Y. Tanaka, A. Iyo, Phys. Rev. Lett **103**, 257003 (2009)
27. P.M. Shirage, K. Miyazawa, K. Kihou, H. Kito, Y. Yoshida, Y. Tanaka, H. Eisaki, A. Iyo, Phys. Rev. Lett. **105**, 037004 (2010)
28. R. Khasanov, M. Bendele, K. Conder, H. Keller, E. Pomjakushina, V. Pomjakushin, New J. Phys. **12**, 073024 (2010)
29. Y. Tsuge, A. Iyo, Y. Tanaka, H. Eisaki, T. Nishio, Physics Procedia **36**, 731 (2012)
30. Y. Tsuge, T. Nishio, A. Iyo, Y. Tanaka, H. Eisaki, J. Phys.: Conf. Ser. **507**, 012037 (2014)
31. W. Chu, J. Cheng, S. Chu, T. Hu, A. Marcelli, X. Chen, Z. Wu, Sci. Rep. **3**, 1750 (2013)
32. B. Singh, P.M. Shirage, A. Iyo, P. Kumar, AIP Adv. **6**, 105310 (2016)
33. A. Bussmann-Holder, A. Simon, H. Keller, A.R. Bishop, J. Supercond. Nov. Magn. **24**, 1099 (2011)
34. R. Khasanov, M. Bendele, A. Bussmann-Holder, H. Keller, Phys. Rev. B **82**, 212505 (2010)
35. E. Pomjakushina, K. Conder, V. Pomjakushin, M. Bendele, R. Khasanov, Phys. Rev. B **80**, 024517 (2009)
36. K. Horigane, H. Hiraka, K. Ohoyama, J. Phys. Soc. Jpn. **78**, 074718 (2009)
37. Y. Mizuguchi, F. Tomioka, S. Tsuda, T. Yamaguchi, Y. Takano, J. Phys. Soc. Jpn. **78**, 074712 (2009)
38. Y. Mizuguchi, Y. Hara, K. Deguchi, S. Tsuda, T. Yamaguchi, K. Takeda, H. Kotegawa, H. Tou, Y. Takano, Supercond. Sci. Technol. **23**, 054013 (2010)
39. S. Margadonna, Y. Takabayashi, M.T. McDonald, M. Brunelli, G. Wu, R.H. Liu, X.H. Chen, K. Prassides, Phys. Rev. B **79**, 014503 (2009)
40. J. Zhao, Q. Huang, C. de la Cruz, S. Li, J.W. Lynn, Y. Chen, M.A. Green, G.F. Chen, G. Li, Z. Li, J.L. Luo, N.L. Wang, P. Dai, Nat. Mater. **7**, 953 (2008)
41. M. Rotter, M. Pangerl, M. Tegel, D. Johrendt, Angew. Chem. Int. Ed. **47**, 7949 (2008)
42. T.M. McQueen, Q. Huang, V. Ksenofontov, C. Felser, Q. Xu, H.W. Zandbergen, Y.S. Hor, J. Allred, A.J. Williams, D. Qu, J. Checkelsky, N.P. Ong, R.J. Cava, Phys. Rev. B **79**, 014522 (2009)
43. M. Tinkham, *Introduction to Superconductivity* (Krieger Publishing Company, Malabar, Florida, 1975)
44. A.S. Alexandrov, *Theory of Superconductivity: From Weak to Strong Coupling* (Institute of Physics Publishing, Bristol, 2003)

Chapter 13
Electron Paramagnetic Resonance in Superconducting Cuprates

Boris I. Kochelaev

Introduction

The way to a discovery of the high temperature superconductivity (HTSC) was started by Alex Müller with his study of partially covalent character of transition elements in oxides having perovskites structure by the electron paramagnetic resonance (EPR) method. It was actually the beginning of his scientific carrier: the first results were obtained in his thesis "Paramagnetische Resonanz von Fe^{3+} in $SrTiO_3$ Einkristall" [1]. It is appropriate to remind that the discovered many years later superconducting cuprates have just the perovskites structure. Between the first step and this discovery were obtained a long chain of important results concerning the Jahn–Teller effect, structural phase transitions, photochromism, ferroelectricity, itinerant polarons and other properties of perovskites using the EPR and other methods. The relevant original works (concluded by the HTSC discovery) are collected in a volume "Properties of Perovskites and Other Oxides", containing 562 pages [2]. It seems that these milestones on the way to a discovery were not occasional ones. From one hand a deep insight into condensed matter physics from the very beginning became possible due to a very good background: in his student time Alex Müller had a course of lectures in theoretical physics given by Wolfgang Pauli during four semesters. On the other hand there were some stimuli, which supported the following investigations of the perovskites properties. One of them was quite unusual: a lofty dream which had Alex about that time. A description of this dream can be found in the KAM's article "Annäherungen ans Feuer" ("Approaching to a fire"), which was published in a volume dedicated to a

B.I. Kochelaev (✉)
Institute of Physics, Kazan Federal University, Kremlevskaya 18, Kazan 42008, Russian Federation
e-mail: bkochelaev@gmail.com

A. Bussmann-Holder et al. (eds.), *High-Tc Copper Oxide Superconductors and Related Novel Materials*, Springer Series in Materials Science 255,
DOI 10.1007/978-3-319-52675-1_13

psychiatrist C.G. Jung and a writer E. Jünger [3]. Below is given my attempt to translate it from German (page 39):

> In a dream I saw Wolfgang Pauli sitting similar to Buddha in a deep meditation (1.5 years before his death), having in his right hand a high-symmetric crystal of $SrTiO_3$ with a cubic symmetry of the lattice. A coming white beam of light was decomposed by it into the colored spectra. This dream, looking back now, was for me during four decades decisive, namely for my scientific research and its success, and for my health too.

Few pages later (page 44) there is a remark:

> . . .in the lofty dream of the 1957 year the escaped from the perovskite-lattice lightspectrum possibly could include also an aspect of a superconductivity.

In his following research after the thesis Alex Müller was using mainly also the EPR method. At the Colloque Ampere of the 1966 year in Yugoslavia Alex Müller gave a talk "Jahn–Teller effect in magnetic resonance" [4]. I had there my first contact with Alex, which developed later into a scientific collaboration and friendship. In 1969 year Alex Müller visited Kazan to participate in the conference, dedicated to 25th year of the EPR discovery by E. K. Zavoysky at the Kazan University. Many well-known experts in the field of magnetic resonance and spin relaxation, in spite of the cold war at the soviet time, attended the conference: A. Abragam, K. Gorter, A. Kastler, M. V. Strandberg, B. R. Judd, K. D. Jeffries, A. Lösche, C.P. Hartman and others from 16 countries.

In June of 1986 year Alex Müller visited Kazan University to give a talk at the seminar. Later we had an excursion on a small motorboat along the Volga River. In a middle of the river Alex told me about a discovery of the high temperature superconductivity. On my question about a substance he answered: "some ceramics". It was a great surprise for me, since I was naively sure that any ceramic should be one of the best isolator. The paper of George Bednorz and Alex Müller containing this discovery was published very soon after that, already in September [5].

After the HTSC discovery Alex Müller was very interested in the EPR study of superconducting cuprates. At the International Conference in Kazan, dedicated to the 60th year of the EPR discovery he gave a plenary lecture "EPR and high temperature superconductivity". Some results of the EPR investigations, related to the superconducting cuprates, were described by Alex Müller in the paper "The Impact of ESR (EPR) on the Understanding of the Cuprates and their Superconductivity" [6]. The results before the 2005 year were discussed in details in the review "Nanoscale Properties of Superconducting Cuprates Probed by the Electron Paramagnetic Resonance" [7], and some later results in a short review [8]. In the following sections of this paper some aspects of experimental and theoretical results of the EPR study of cuprates, in which the author and Alex Müller were involved, will be described.

The EPR Silence and the Cuprum Spin Excitations Bottleneck

The discovery of the high temperature superconductivity created a great interest to study doped layered cuprates and their parent compounds by different methods, including nuclear magnetic resonance (NMR) and the EPR. The main reason for the EPR measurements was a widely accepted opinion that the basic superconducting events occur in CuO planes. The ion Cu^{2+} in this plane of the parent compounds has an electronic configuration d^9 with a singlet orbital $d(x^2 - y^2)$ as a ground state. This type of ion was used as a probe in many dielectric crystals and was giving a very good EPR signal [9, 10]. Moreover, the search for high-T_c superconductivity by Bednorz and Müller was guided by the Jahn-Teller polaron model, associated with the Cu^{2+} ion in the oxygen octahedron and very strong interactions of d-electrons with the octahedron vibrational modes. At the same time an absence of the isotope effect of the critical temperature T_c in the cuprates with an optimal doping and other experiments, related to the symmetry of the order parameter, created a widespread belief that the Cooper pairing mechanism in cuprates is not related to the electron-phonon interaction contrary to the conventional superconductors. In particular, a great attention was paid to the role of the antiferromagnetic spin fluctuation in the CuO_2 planes caused by the huge isotropic exchange interactions between the Cu ions. It was quite natural to study the spin dynamics in these planes by the EPR method. However, any attempt to observe the bulk EPR response of the Cu spin-system was giving a negative result. The nature of the EPR silence of superconducting cuprates and their parent compounds was a subject of intensive theoretical and experimental investigations (see the review [11]). In particular, Chakravarty and Orbach proposed that the EPR line in the undoped La_2CuO_4, is severely broadened below room temperature by the anisotropic Dzyaloshinskii-Moriya (DM) interactions [12]. They argued that the EPR could be observed at elevated temperatures, since the linewidth should be greatly narrowed by the fast spin fluctuations. Simon et al. have extended the search of the EPR signal in $La_2CuO_{4+\delta}$ ($0 \leq \delta \leq 0.12$) up to 1150 K and no EPR signal had been observed [13]. We do not discuss other more exotic reasons for the EPR silence mentioned in [11].

Because of the problem stated above, it was natural to use paramagnetic impurities as the EPR probes to find a way to solve this problem. In the work [14] the Mn^{2+} ion was chosen for the following reasons. An electron configuration of this ion is $3d^5$ with a ground state having a zero orbital moment $L = 0$ and the spin $S = 5/2$. In this case a modulation of the spin-orbit interaction by the lattice vibrations is frozen, resulting in a slow spin-lattice relaxation rate. At the same time, since the Mn^{2+} ion substitutes the Cu^{2+} ion in the CuO_2 planes, an exchange coupling between the Mn and Cu ions is of the same nature as for the Cu–Cu coupling and expected to be not too much smaller. In this situation one could expect that the spin relaxation of the Mn ions should consist of two steps: at first will be established a quasi-equilibrium state between the spin systems of the Mn and Cu

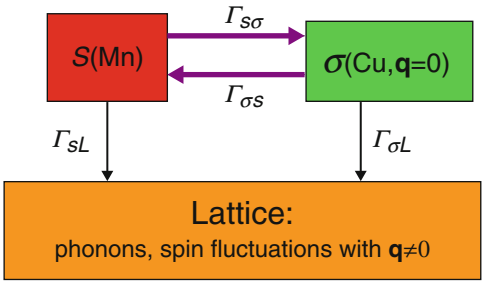

Fig. 13.1 A block-scheme of the relaxation rates between the magnetic moments of the Mn (S) and Cu ions (σ) and the lattice

ions and then will take place their collective relaxation to other degree of freedom—"lattice". By measurements of the latter relaxation rate we can obtain some information on the Cu ions spin kinetics. A similar situation happens often in metals with paramagnetic impurities interacting by exchange coupling with conduction electrons (the electron bottleneck regime, see the review of Barnes [15]). In our system this regime happens, if the spin relaxation rates of the Mn and Cu ions to the lattice Γ_{sL} and $\Gamma_{\sigma L}$ are much less than the spin relaxation between them $\Gamma_{s\sigma}$ and $\Gamma_{\sigma s}$ (see Fig. 13.1) as well as the difference of their Larmor frequencies ω_s and ω_σ:

$$\Gamma_{sL} + \Gamma_{\sigma L} \ll |\Gamma_{s\sigma} + \Gamma_{\sigma s} + i(\omega_s - \omega_\sigma)|. \tag{13.1}$$

In this case an effective spin relaxation of the coupled spin systems is given by the following expression

$$\Gamma_{eff} = \frac{\chi_s^0 \Gamma_{sL} + \chi_\sigma^0 \Gamma_{\sigma L}}{\chi_s + \chi_\sigma} + \frac{\left\langle (\Delta\omega_s)^2 \right\rangle}{\Gamma_{s\sigma}}. \tag{13.2}$$

Here χ_s^0, χ_σ^0 are bar magnetic susceptibilities of the Mn and Cu spin systems, while χ_s, χ_σ are the renormalized by the interactions ones. It is remarkable that the first main term does not contain the relaxation rate between the two spin systems. It is a consequence of the commutation of the total spin and isotropic exchange interactions operators. The second term in (2) takes into account a partial opening of the bottleneck, $\langle(\Delta\omega_s)^2\rangle$ is the mean square of the local fields distribution at the impurity sites. We remind that for the usual sample sizes and frequencies of the alternating magnetic field the EPR response is homogeneous (a wave vector $\mathbf{q} = 0$). In the case of anisotropic exchange coupling between the Mn and Cu ions one has to take into account additional corrections (see [16]). An intensity of the collective response I_{eff} is proportional to the total magnetic susceptibility. Since the cuprates are antiferromagnetic, the temperature dependence of the EPR intensity in this case is expected to be roughly (neglecting all renormalizations):

$$I_{eff} \propto \chi_s + \chi_\sigma \approx N_s S(S+1)\frac{(g_s\mu_B)^2}{3k_BT} + N_\sigma \frac{(g_\sigma\mu_B)^2}{4k_B(T+T_N)}. \tag{13.3}$$

Here N_s and N_σ are the concentrations of the Mn and Cu ions in the CuO_2 planes, T_N is the Neel temperature. An existence of the spin excitations bottleneck regime in cuprates was proven by the experimental group of Bruno Elschner in Darmstadt by the series of experiments with the system $La_{1.8}Sr_{0.2}Cu_{1-y}Mn_yO_{4+\delta}$ and with the Mn impurities concentrations $y = 0.01, 0.02, 0.03, 0.06$ [14]. Measurements of the static magnetic susceptibility have revealed that it was dominated by the Mn impurities for all used concentrations [see the first term in Eq. (13.3)]. Figure 13.2 shows the temperature dependence of the inverse total susceptibility. This result was expected because of large values of the Mn ion's spin $S = 5/2$ and the Neel temperature $T_N > T$.

Having in mind that the relaxation rate Γ_{sL} is very small and can be neglected, the effective spin relaxation in the case $\chi_s \gg \chi_\sigma$ is expected to be

$$\Gamma_{eff} \approx \frac{\chi_\sigma^0}{\chi_s}\Gamma_{\sigma L} + \frac{\left\langle (\Delta\omega_s)^2 \right\rangle}{\Gamma_{s\sigma}}. \tag{13.4}$$

It means that the main contribution coming from the relaxation of the Cu spin–system is greatly reduced by the factor χ_σ^0/χ_s and possibly can be measured. An important feature of Eq. (13.4) is the inverse dependence of the first term on the Mn ions concentration due to the Mn susceptibility in the denominator. Figure 13.3 shows results for Γ_{eff} as a function of temperature obtained by the EPR

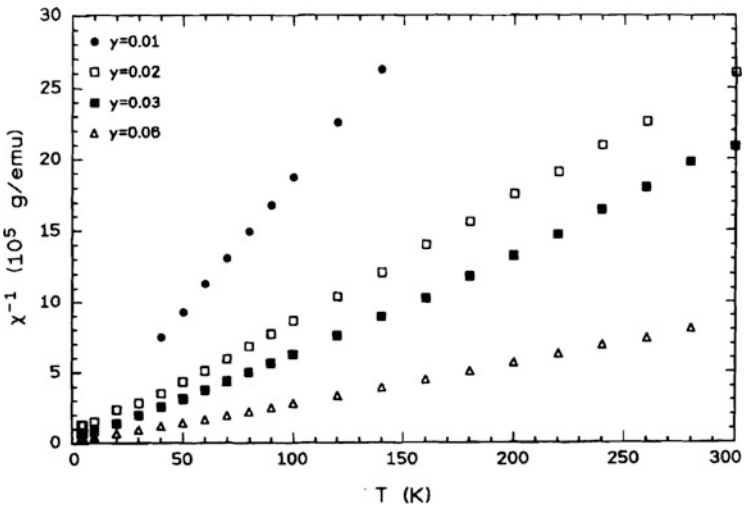

Fig. 13.2 Temperature dependence of the total reciprocal magnetic susceptibility for $La_{1.8}Sr_{0.2}Cu_{1-y}Mn_yO_{4+\delta}$

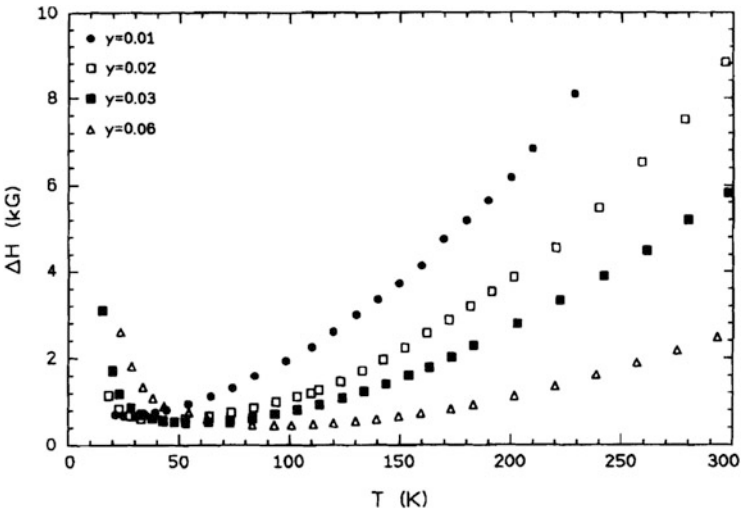

Fig. 13.3 Temperature dependence the EPR linewidth of the Mn^{2+} ion in $La_{1.8}Sr_{0.2}Cu_{1-y}Mn_yO_{4+\delta}$ with y = 0.01, 0.02, 0.03, 0.06

measurements. One can see that at the temperatures $T > 50$ K the dependence of the effective relaxation rate on the Mn ions concentration and the temperature is consistent with the first term in Eq. (13.4). At low temperatures $T < 50$ the situation is vice versa because of the second term in Eq. (13.4), which was related to the spin-spin interactions of Mn ions.

The key experiments, which threw light on the nature of the electron spin-lattice relaxation in the CuO_2 plane, were performed by the group of Alex Müller at the Zürich University using the method of the spin excitations bottleneck regime described above [17]. The EPR signal was studied in $La_{2-x}Sr_xCu_{0.98}Mn_{0.02}O_4$ with oxygen isotopes ^{16}O and ^{18}O to look for a possible isotope effect of the Cu spin dynamics. A large effect on the EPR linewidth in the underdoped samples was observed, see Fig. 13.4.

The isotope effect decreases with Sr doping and practically disappears in the overdoped region and at high temperatures. The temperature dependence of the linewidth for the both isotopes displayed in Fig. 13.5 is very similar to the observed one earlier; compare Fig. 13.3.

The isotope effect indicates an important role of the lattice motion in the relaxation of the Cu magnetization.

The spin-lattice relaxation of the Cu^{2+} ion in dielectric crystals happens due to the modulation of the crystal electric field by the lattice vibrations and the spin-orbit coupling of the Cu ions. This mechanism gives usually a rather slow spin-lattice relaxation, since the Kramers doublet is not sensitive to the electric field because of its time reversal symmetry properties. Nonvanishing matrix elements of the spin-lattice coupling usually appear due to the external magnetic field H, which gives a very small factor $(g\mu_B H/\triangle)$, where $g\mu_B H$ is the Zeeman energy and $\triangle$ is the crystal field splitting between the ground and the excited orbital states. However, in the

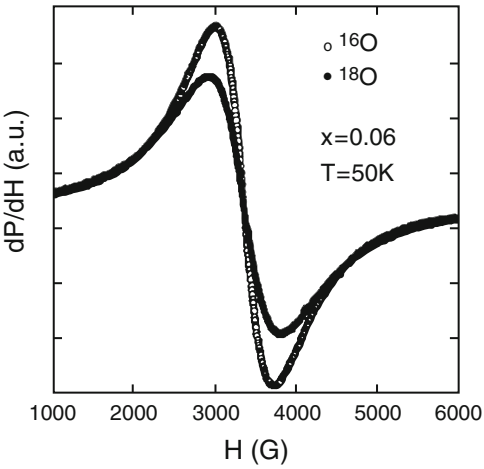

Fig. 13.4 EPR signal of ^{16}O and ^{18}O samples of $La_{1.94}Sr_{0.06}Cu_{0.98}Mn_{0.02}O_4$ at $T = 50$ K under identical experimental conditions

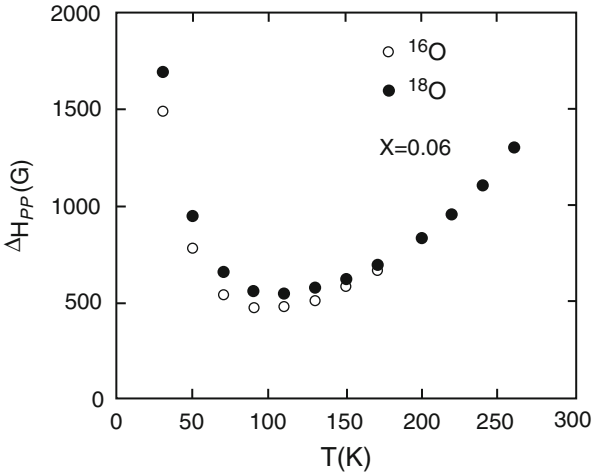

Fig. 13.5 Temperature dependence of the peak-to-peak EPR line-width $\triangle H_{pp}$ for ^{16}O and ^{18}O samples of $La_{1.94}Sr_{0.06}Cu_{0.98}Mn_{0.02}O_4$

case of the CuO_2 plane the eigenstates of the Cu spin-system are defined mainly by the very large isotropic Cu–Cu exchange interactions instead of the Zeeman interaction. Roughly speaking, the role of the magnetic field splitting will play the Cu–Cu exchange coupling $J_{\sigma\sigma} \sim 1500$ K. It should greatly enhance the spin-lattice relaxation rate [18]. Moreover, there is an additional reason for such enhancement related to a strong anharmonicity of the involved normal modes of the oxygen octahedron. It turns out that the spin-lattice interaction in the Cu orbital ground state $d(x^2–y^2)$ involves only the Q_4 and Q_5, modes related to the tilts of the octahedron z- axis and pure rotations of the octahedra. These modes are strongly anharmonic, being responsible for a structural phase transition from a high-temperature tetragonal (HTT) to a low-temperature orthorhombic and tetragonal (LTO, LTT) phase. As a result, besides vibrations near the minima of a potential

energy, there is quantum tunneling between the minima. The latter leads to a more sufficient modulation of the crystal field at the Cu ion causing a more effective spin-lattice relaxation. Since the tunneling frequency between the minima depends exponentially on the oxygen mass, it gives a large isotope effect of the Cu electron spin-lattice relaxation rate $\Gamma_{\sigma L}$. For typical values of parameters this mechanism gave estimation $\Gamma_{\sigma L} \sim 10^{11} s^{-1}$ at $T \sim 100\,\mathrm{K}$ [17]. This value is too large for observing the EPR signal from Cu ions without Mn probes at the usual frequencies. This can explain the EPR silence in the superconducting cuprates and their parent compounds. The described model is in a good agreement with experimental results on the temperature dependence of the EPR linewidth and the isotope effect.

Spin Dynamics and A Phase Separation in Superconducting Cuprates Near the Phase Transition

The phenomenon of a transformation of antiferromagnetic quasi-two-dimensional copper oxides into high-temperature superconductors by doping of their CuO_2 planes with electronic holes still remains a subject of intensive investigations. Detailed inelastic neutron scattering experiments in the bilayer compound $YBa_2Cu_3O_{6+y}$ reveal the long range antiferromagnetic (AF) order at $y < 0.15$ with the Neel temperature $T_N = 415\,\mathrm{K}$ [19–21]. The oxygen electronic p-holes appear in the CuO_2 planes at $y > 0.15$ producing the local distortions of the AF order, and its full destruction happens at $y = 0.4$. There were suggested many scenarios of this process, in particular due to creating of polarons, domain walls, vortices, skyrmions, and some others objects [22–25]. Although enormous number of experiments using neutron scattering, angle-resolved photoemission, and other methods seem to reveal some of these scenarios, there is no common agreement which of them are the most actual. It was evident that additional experiments are desirable for understanding of next steps of an evolution of these oxides on the way to become metals and then superconductors.

The EPR method is a powerful technique for probing both the local magnetic properties and studying the spin kinetics using as the EPR-probes ions having local d- or f-electrons. We have described above that the Mn^{2+} impurities in the CuO_2 plane allowed revealing a very fast spin relaxation rate of the Cu-ions due to their spin-phonon interaction, which prevents the observation of the EPR signal directly from them. A choice of the Yb^{3+} ion as the EPR probe to study the spin kinetics in $YBa_2Cu_3O_{6+y}$ ($y = 0.5, 0.6, 0.98$) in a metal and superconducting state was found also effective [26]. This EPR probe was also very useful for investigations of the AF state evolution in $YBa_2Cu_3O_{6+y}$ with $y = 0.1, 0.2, 0.3, 0.4$.

The Yb^{3+} ion as the EPR probe in cuprates is very different from the Mn^{2+} ion. In the samples of $YBa_2Cu_3O_{6+y}$ it substitutes the isovalent ion Y^{3+}, what results in a rather week coupling with the Cu^{2+} ions in the CuO_2 planes. A ground-state multiplet $^2F_{7/2}$ of the Yb^{3+} ion is split by the crystal electric field of tetragonal symmetry into four Kramers doublets. Inelastic neutron-scattering measurements

showed that in $YbBa_2Cu_3O_7$ the first-excited doublet lies 1000 K above the ground state doublet [27]. The latter can be described by the effective spin $S = 1/2$. An expected broadening of the Yb^{3+} ion EPR signal could be related to the magnetic dipole-dipole interactions between the Yb^{3+} ions, their spin-phonon interactions, and interactions with the antiferromagnetic spin waves in the CuO_2 planes.

As a first step it was necessary to study the EPR parameters of the Yb^{3+} ions in the samples having long-range AF order ($y < 0.15$). This analysis was necessary in order to reveal new features of the EPR signal appearing due to additional doping. The next steps were related to investigations of the destruction of the long-range AF order by the oxygen doping ($y = 0.2, 0.3, 0.4$) and a phase separation revealed by the changing of the EPR signal [28, 29].

The measurements in the sample with the long-range AF order $Y_{0.98}Yb_{0.02}Ba_2Cu_3O_{6.1}$ reveal a very strong anisotropy of the EPR linewidth (see Fig. 13.6). It was easy to check that the magnetic dipole-dipole interactions cannot give such a strong anisotropy of the EPR signal. A detailed analysis had shown that this phenomenon is related to the symmetry properties of the spin-spin interactions between the Yb3+ ions via antiferromagnetic spin waves in the CuO2 planes (Suhl-Nakamura interactions) [28].

In the samples with doping levels $y = 0.2, 0.3, 0.4$ the Yb^{3+} EPR signal can be described by the sum of two lorentzians with sufficiently different linewidths. Figure 13.7 shows the temperature dependence of the narrow and the broad lines

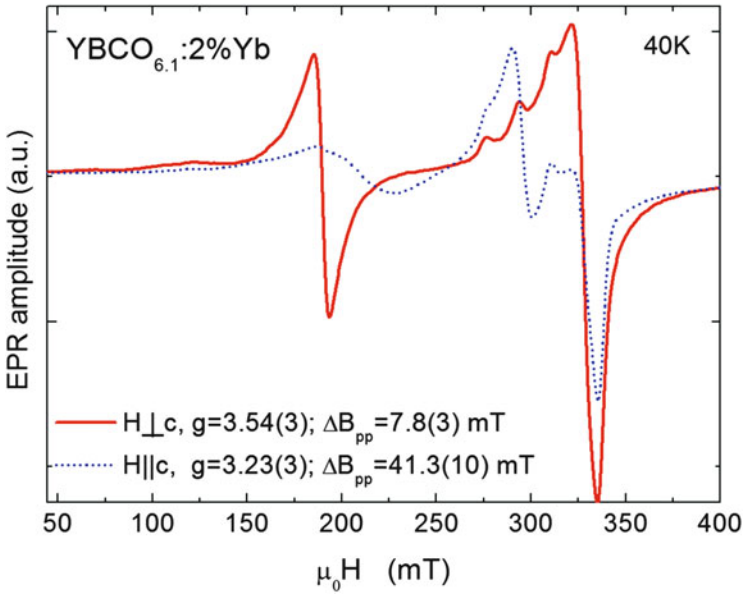

Fig. 13.6 EPR spectra of Yb^{3+} in $Y_{0.98}Yb_{0.02}Ba_2Cu_3O_{6.1}$ at $T = 40$ K (the *left* signal; the *right* signal is related to defects, see [30]). The *solid line* corresponds to the external magnetic field perpendicular to the crystal *c*-axis, while the *dotted line* corresponds to the field along the *c*-axis

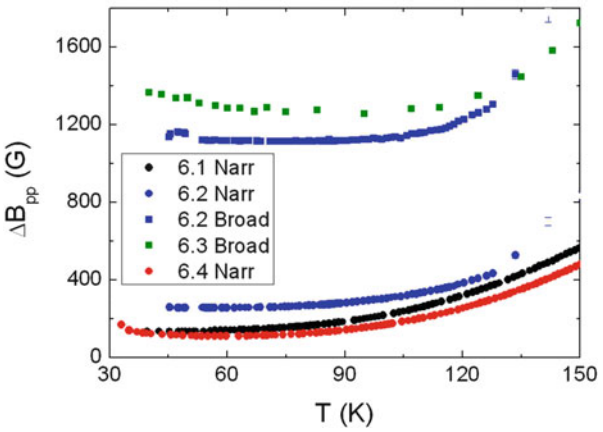

Fig. 13.7 Temperature dependence of the EPR linewidths for the *broad* and *narrow lines* fitted with *Lorentzian line* shape

for different levels of oxygen doping [29]. The intensity of the broad line increases with doping and disappears at $y = 0.4$. In the case $y = 0.3$ almost only the broad line is seen.

We have assumed that this EPR signal behavior could be explained by the electronic phase separation into the rich and poor in holes regions in the CuO_2 planes. The separation can be related naturally to creation of charged domain walls (stripes). The local distortions of the antiferromagnetic order in the domain walls should give an additional inhomogeneous broadening to the Yb^{3+} EPR signal due to exchange coupling between the ytterbium and copper ions. One could expect an existence of collinear and coplanar anti-phase domain walls, which were created by the *p*-holes localized in the CuO_2 planes on the oxygen ions around the Cu^{2+} ions.

The detailed investigation of the collinear charged domains was performed by Giamarchi and Lhuillier based on the standard two-dimensional Hubbard model with U as the on-site Hubbard repulsion, and t as the hopping parameter [31]. The numerical solutions were investigated by the Monte Carlo variational technique using the Hartree-Fock trial function. For the strong enough Hubbard repulsion ($U/t \geq 4$) the stable collinear domain-wall solutions were found, where the doped *p*-holes are localized within a stripe around the each Cu^{2+} site. This stripe separates two AF ordered regions with opposite signs in the AF order parameter (see Fig. 13.8).

The magnetizations of both AF sublattices are changed only in absolute value but not in direction. In the presence of the external magnetic field directed along the stripe appears a component of the order parameter along the magnetic field; the corresponding angle is defined by the values of the external magnetic field and the exchange coupling between the Yb and Cu ions $\alpha \sim g\mu_B H/J$. These components of the AF sublattices give a contribution to the Yb^{3+} ions Zeeman energy due to their exchange coupling with the neighboring Cu^{2+} ions. This interaction is the source of the additional inhomogeneous EPR signal broadening due to the Yb^{3+} ions located in the domain walls. The estimated value of the contribution to the EPR linewidth $\left(\Delta H_{\text{broad}}^{\text{theor}} \sim 100\,\text{G}\right)$ was much less than the experimental value of the broad EPR

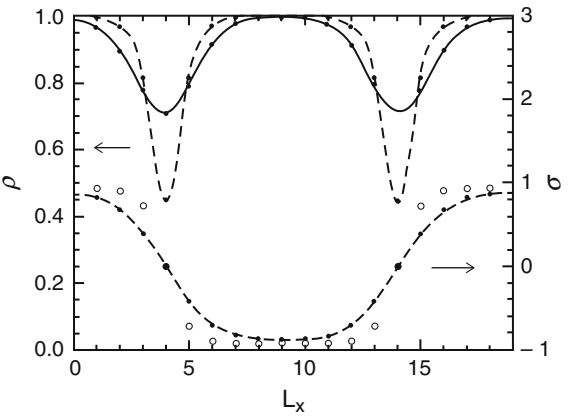

Fig. 13.8 Charge density ρ and magnetization σ change between two collinear domain walls [31]

signal $\Delta H_{\text{broad}}^{\text{exp}} \approx 1200$ G because of a very small value of the angle α. This result stimulated investigations of a possible role of the coplanar domain walls.

An existence of the coplanar domain walls in the AF order of the CuO_2 planes was predicted by Zachar, Kivelson, and Emery on the basis of the Landau theory of phase transitions [32]. Particular spin and charge textures for elliptical domain walls were calculated by Seibold within the two-dimensional Hubbard model [33]. It was shown that for the completely filled domain wall (i.e. one hole per site along the stripe) only the collinear solutions exist whereas the coplanar structures become stable for half-filled walls for small hole concentrations. Figure 13.9a shows the spin texture for the case when two holes occupy alternatively the neighboring sites along the charged stripe. In this case the spin texture is similar to the coupled vortex-antivortex structure. We suggested the following phenomenological model to reproduce the calculated spin texture [29].

(a) The hole is present in the stripe:

$$S_n^{ya} = S_0 \sin\alpha \frac{\tanh(x_n/\xi)}{\cosh(x_n/\xi)}, \quad S_n^{yb} = -S_0 \sin\alpha \frac{\tanh(x_n/\xi)}{\cosh(x_n/\xi)}. \tag{13.5}$$

(b) The hole is absent in the stripe:

$$S_n^{ya} = S_0 \sin\alpha \frac{1}{\cosh(x_n/\xi)}, \quad S_n^{yb} = -S_0 \sin\alpha \frac{1}{\cosh(x_n/\xi)}. \tag{13.6}$$

Here $\sin\alpha$ defines the eccentricity of the elliptical domain wall; the case $\alpha = \pi/4$ describes an ideal spiral solution, whereas $\alpha = 0$ reduces the spin structure to a collinear domain wall.

The experimental value for the broad EPR linewidth was achieved with a rather small eccentricity of the elliptical domain wall: $\sin\alpha = 2.9 \cdot 10^{-2}$. One could expect that at the level of oxygen doping approaching $y = 0.4$ the AF order will be

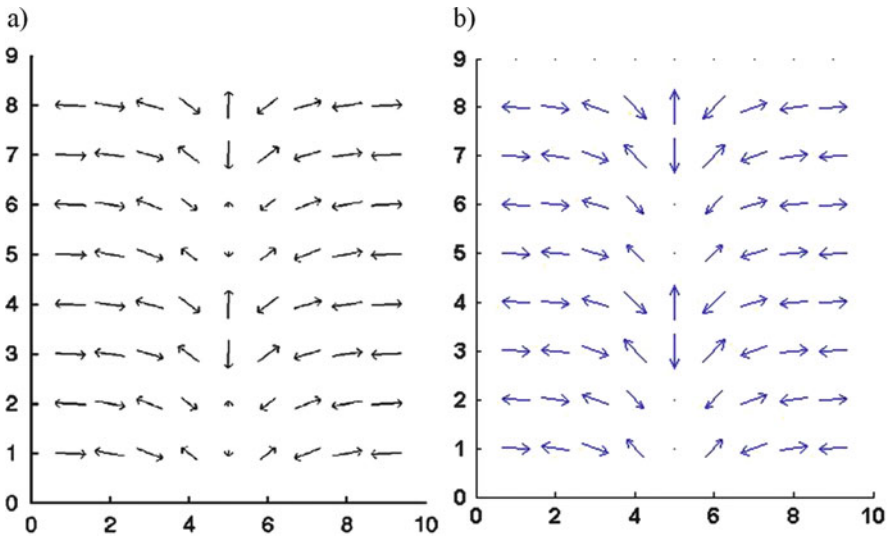

Fig. 13.9 Spin structures for the elliptical domain wall: the pattern (**a**) was calculated numerically by Seibold [33]; the pattern (**b**) shows our phenomenological model, calculated using formulas (13.5) and (13.6)

destroyed, the holes in the CuO_2 planes delocalized creating metal regions, and the inhomogeneous broadening of the Yb^{3+} EPR line will vanish. Such a behavior was actually observed in these experiments. The microscopic electronic phase separation into metallic and dielectric regions in the CuO_2 planes was observed previously by the EPR method in lightly doped $La_{2-x}Sr_xCuO_4$ also in a metallic state [34]. It was proposed then that the starting point for the creation of metallic regions is a formation of a bipolaron by two three-spin-polarons with an assistance of phonons [35]. It is remarkable that a subsequent transition of the metal cuprates into a superconducting state is accompanied by a strong isotope effect on the critical temperature T_c by substituting the naturally present ^{16}O by the ^{18}O isotope. As mentioned above this effect is decreasing from underdoped region to almost negligible at optimal doping. It can indicate that the isotope effect is a carrier concentration dependent (see Weyeneth and Müller [36]). Recently there was suggested that this phenomenon is related to a dependence of the metal regions formation on the electron phonon interactions in the CuO_2 planes [37]. In this respect it would be reasonable to repeat experiments, which have been revealed the three-spin-polarons [38], using the samples with substituted ^{16}O by the ^{18}O isotopes. The corresponding additional theoretical analysis is quit desirable.

Concluding Remarks

Instead of a traditional conclusion I will quote a couple remarks of Alex Müller concerning the EPR investigations of the high temperature superconductivity. Some results he estimated very high (maybe overestimated due to his favorable attitude to this method). The concluding remark in his short review [6] is the following:

"One might as well compare the advance of these but two experiments with the very large number of NMR results published, which were for a long time interpreted in terms of single band theories, and even more so regarding the expensive work in photoemission. In the latter dispersions of energies versus wavelength are measured. This is valuable in presence of large correlation lengths present as in classical superconductors. However in the doped cuprates with the bipolarons as quasi precursors of the Cooper pairs present, the coherence lengths are on the order of a lattice and a description in terms of local deformations and time is more appropriate, as is usually used in EPR".

The plenary lecture at the International Conference in Kazan, dedicated to the 60th year of the EPR discovery Alex Müller concluded by words:

> 60 years after the discovery of EPR in Kazan the method is able to contribute at the forefront in condensed matter physics, such as high temperature superconductivity. This is especially so if properly employed, and the results theoretically interpreted in a scholar way, as well as relate them to other important experiments. Because the EPR spectrometers used are standard, and low cost as are the samples, the research budgets are low; this puts the scientist in a serene mood without stress.

Acknowledgments I am very grateful to a fortune for a chance to know Karl Alex Müller with his dedication to science, high moral standards, good sense of humor, and for his continuous encouragement and a longtime friendship. This work was partially funded by the subsidy allocated to Kazan Federal University for the project part of the state assignment in the sphere of scientific activities.

References

1. K.A. Müller, Helv. Phys. Acta **31**, 24 (1958)
2. K. Alex Müller, T. W. Kool (eds.), *Properties of Perovskites and Other Oxides* (World Scientific, 2010)
3. K. Alex Müller, in a volume "Jung und Jünger. Gemeinsamkeiten und Gegensätzliches in den Werken von Carl Gustav Jung und Ernst Jünger", editors Thomas Arzt, K. Alex Müller und Maria Hippius-Gräfin Dürckhim (Sonderdruck, Königshausen & Neumann, 2001), pp. 37–50
4. K. A. Müller, in Proceedings of the International Conference on Magnetic Resonance and Relaxation. XIY Colloque Ampere, Ljubljana, ed. R. Blinc (North-Holland) (1967), pp. 192–208
5. J.G. Bednorz, K.A. Müller, Z. Phys. B **64**, 188 (1986)
6. K.A. Müller, EPR Newslett. **22**, 5 (2012)

7. B.I. Kochelaev, G.B. Teitel'baum, a chapter in the book "Superconductivity in Complex Systems". Editors K.A. Müller and A. Bussmann-Holder (Springer-Verlag, Berlin Heidelberg, 2005), pp. 203–266
8. B.I. Kochelaev, J. Low Temp. Phys. **183** (2016). doi:10.1007/s10909-016-1602-0
9. S.A. Al'tshuler, B.M. Kozyrev, *Electron paramagnetic resonance of transition elements compounds*, 2nd edn. (Nauka, Moscow, 1972)
10. A. Abragam, B. Bleaney, *Electron paramagnetic resonance of transition ions* (Clarendon Press, Oxford, 1970)
11. A. Punnoose, R.J. Singh, Int. J. Mod. Phys. B **10**, 1123 (1995)
12. S. Chakravarty, R. Orbach, Phys. Rev. Lett. **64**, 224 (1991)
13. P. Simon, J.M. Bassat, S.B. Oseroff, Z. Fisk, S.W. Cheong, A. Wattiaux, S. Schulz, Phys. Rev. B **48**, 4216 (1993)
14. B.I. Kochelaev, L. Kan, B. Elschner, S. Elschner, Phys. Rev. B **49**, 13106 (1994)
15. S.E. Barnes, Adv. Phys. **30**, 801 (1981)
16. B.I. Kochelaev, A.M. Safina, Phys. Solid State **46**, 226 (2004)
17. A. Shengelaya, H. Keller, K.A. Müller, B.I. Kochelaev, K. Conder, Phys. Rev. B **63**, 144513 (2001)
18. B.I. Kochelaev, J. Supercond. **12**, 53 (1999)
19. C. Vettier, P. Burlet, J.Y. Henry, M.J. Jurgens, G. Lapertot, L.R. Regnault, J. Rossat-Mignod, Phys. Scr. T **29**, 110 (1989)
20. S. Shamoto, M. Sato, J.M. Tranquada, B.J. Sternlieb, G. Shirane, Phys. Rev. B **48**, 13817 (1993)
21. J. Rossat-Mignod, L.P. Regnault, C. Vettier, P. Burlet, J.Y. Henry, G. Lapertot, Physica B **169**, 58 (1991)
22. W.P. Su, X.Y. Chen, Phys. Rev. B **38**, 8879 (1988)
23. D. Poilblanc, T.M. Rice, Phys. Rev. B **39**, 9749 (1989)
24. J.A. Verges, E. Louis, P.S. Lomdahl, F. Guinea, A.R. Bishop, Phys. Rev. B **43**, 6099 (1991)
25. B.I. Shraiman, E.D. Siggia, Phys. Rev. Lett. **61**, 467 (1988)
26. A. Maisuradze, A. Shengelaya, B.I. Kochelaev, E. Pomjakushina, K. Conder, H. Keller, K.A. Müller, Phys. Rev. B **79**, 054519 (2009)
27. M. Guillaume, P. Allenspach, J. Mesot, U. Staub, A. Furrer, R. Osborn, A.D. Tailor, F. Stucki, P. Unternaher, Solid State Commun. **81**, 999 (1992)
28. A.A. Vishina, A. Maisuradze, A. Shengelaya, B.I. Kochelaev, H. Keller, J. Phys.: Conf. Ser. **394**, 012014 (2012)
29. A.A. Vishina, A. Maisuradze, A. Shengelaya, B.I. Kochelaev, H. Keller, Magn. Reson. Solids **14**, 12102 (2012)
30. J. Sichelschmidt, B. Elschner, A. Loidl, B.I. Kochelaev, Phys. Rev. B **51**, 9199 (1995)
31. T. Giamarchi, C. Lhuillier, Phys. Rev. B **42**, 10641 (1990)
32. O. Zachar, S.A. Kivelson, V.J. Emery, Phys. Rev. B **57**, 1422 (1998)
33. G. Seibold, Phys. Rev. B **58**, 15520 (1998)
34. A. Shengelaya, M. Bruun, B.I. Kochelaev, A. Safina, K. Conder, K.A. Müller, Phys. Rev. Lett. **93**, 017001 (2004)
35. B.I. Kochelaev, A.M. Safina, A. Shengelaya, H. Keller, K.A. Müller, K. Conder, Mod. Phys. Lett. B **17**, 415 (2003)
36. S. Weyeneth, K.A. Müller, J. Supercond. Nov. Magn. **24**, 1235 (2011)
37. B.I. Kochelaev, K.A. Müller, A. Shengelaya, J. Mod. Phys. **5**, 473 (2014)
38. B. Kochelaev, J. Sichelschmidt, B. Elschner, B. Lemor, A. Loidl, Phys. Rev. Lett. **79**, 4274 (1997)

Chapter 14
Electron-Lattice Interaction and High T_c Superconductivity

Vladimir Kresin

Introduction

The dream about room temperature superconductivity was born shortly after the initial discovery in 1911. It had been clear even in the earlier days that superconductivity can create entirely different technology, so that the London's equation will be more important than the Ohm's law.

That's why scientists have been always trying to find the material with higher value of the critical temperature. Figure 14.1 shows an increase in the maximum value of T_c with time. One can see that during first 75 years since the discovery the increase was rather modest (from $T_c = 4.1$ K for mercury up to $T_c = 22.3$ K for Nb_3Ge).

The discovery of high T_c oxides [1] was a real milestone in the field. The importance of this breakthrough is a twofold. First of all, a study of superconductivity has moved to different scale. It is not occasional that the Journal of Low Temperature Physics almost stopped publishing papers on superconductivity stating that this is not low temperature physics anymore. Because of this new scale, the search for room temperature superconductivity becomes perfectly realistic.

But, in addition, there is another important aspect of the discovery. It can be seen from Fig. 14.1 that niobium was playing a special role. There used to be an empirical rule that future materials with higher T_c should contain Nb as a key component. And it was shocking for the scientists involved in the search that the new superconductor discovered by Bednorz and Mueller did not contain Nb. This was a lesson, stressing the importance of search in different direction. This lesson initially was not very well taken. During next 10–15 years people were focusing on

V. Kresin (✉)
Lawrence Berkeley Laboratory, University of California, Berkeley, CA 94720, USA
e-mail: vzkresin@lbl.gov

A. Bussmann-Holder et al. (eds.), *High-Tc Copper Oxide Superconductors and Related Novel Materials*, Springer Series in Materials Science 255,
DOI 10.1007/978-3-319-52675-1_14

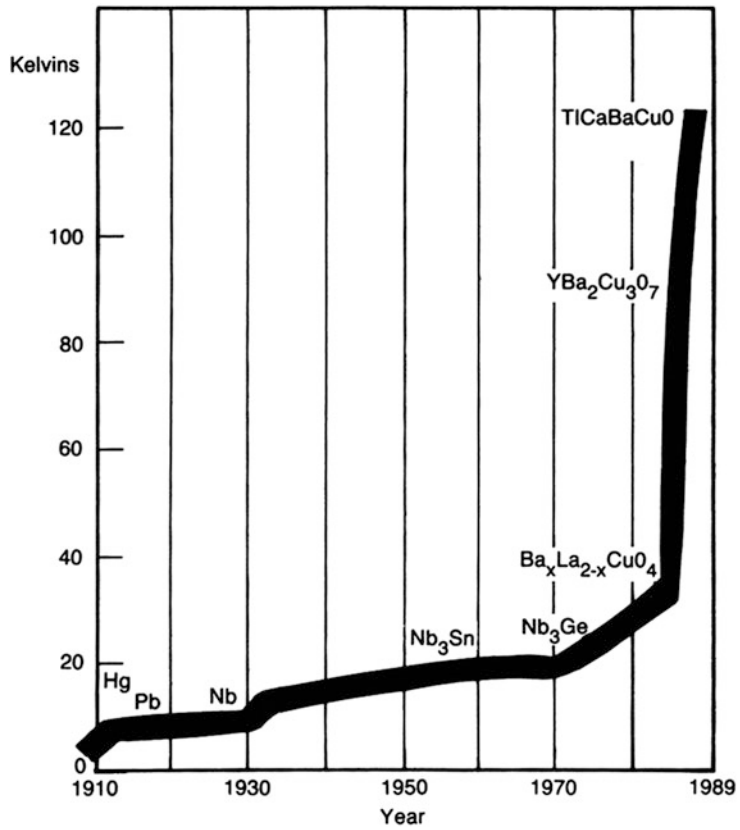

Fig. 14.1 Increase in the maximum value of T_c with time

the new oxides only. But at present the situation is entirely different. There was not a time when so many different materials have been simultaneously studied. In addition to the cuprates, organics, heavy fermions, the many new systems were discovered: MgB_2, fullerides, princides, hydrides, etc.

It is not surprising, that shortly after the discovery of the high T_c cuprates scientists created many different explanations of the novel superconductivity. It was a "paradise" for theoreticians, because at the beginning almost nothing was known about properties of these materials. As a whole, this was a very fruitful period for development of the theory of superconductivity.

Unfortunately, a number of theoreticians did not bother to study the physics of the phenomenon and existing microscopic theory. I remember that I was sitting in my office in Berkeley and one man came rushing into the room; he was so excited that did not even bother to knock at the door. It turns out that he was an expert in the plasma physics. He runs into my room, because he wanted to let me know that he derived the London equation. He was very upset to learn that this equation was

derived 30 years ago and it was described in the original BCS paper as well as in many books.

A number of interesting models were developed. Sadly, it also resulted in formation of separate groups without any discussions and communication between them. I recall a joke, which, nevertheless, describes the spirit of that time: "Two scientists committed crimes and were sentenced to be executed. On the day of execution both of them were approached and asked about their last wishes. One of them told that he developed a new theory of high T_c superconductivity and wanted to present it. It was granted. And then the second scientist told that he wanted to be executed before the neighbor presents his talk".

"Legend" and Its End

Shortly after the discovery of the high T_c superconductivity the "legend" was born that the phonon mechanism is unable to provide the critical temperatures, which exceed the value $T_c \approx 30$ K. Unfortunately, this "legend" persists even today among some scientists. Here I should confess that many times during last 30 years I confronted people who made such a statement during their presentations at different conferences or seminars and asked to explain me why such a limitation exists. The response was the same: "It is known", and nothing else. It is not surprising, since it is impossible to explain the statement, which is incorrect. Indeed, the modern microscopic theory of superconductivity, does not contain any upper limit for T_c.

Probably, for some scientists the argumentation is based on the well-known McMillan expression for T_c: [2]:

$$T_c = \left(\widetilde{\Omega}/1.2\right)\exp\left[-\frac{1.04(1+\lambda)}{\lambda_{\cdot} - \mu*(1+0.62\lambda)}\right] \tag{14.1}$$

Here $\widetilde{\Omega} = \left\langle \Omega^2 \right\rangle^{1/2}$, Ω is the phonon frequency. Using this equation, one can obtain the maximum value of the critical temperature. Indeed, neglecting μ^* for simplicity and calculating $\partial T_c/\partial\Omega$, one can easily find the maximum value of T_c, but this value corresponds to $\lambda \approx 2$. However, the McMillan equation is valid only for $\lambda \lesssim 1.5$. Therefore, the value $\lambda = 2$ is outside the range of its applicability. The absence of the upper limit can be seen from the expressions for larger values of λ [3], or the expression valid for any λ [4], see the review [5]:

$$\begin{aligned} T_C &= \frac{0.25\widetilde{\Omega}}{\left[e^{2/\lambda_{eff}} - 1\right]^{1/2}} \\ \lambda_{eff} &= (\lambda - \mu^*)[1 + 2\mu^* + \lambda\mu^* t(\lambda)] \\ t(x) &= 1.5\exp(-0.28x) \end{aligned} \tag{14.2}$$

Another faulty restriction was related not to the dependence of T_c on λ (see above), but to the limiting value of the coupling constant λ. This question was intensively discussed shortly after the creation of the BCS theory. Based on the so-called Froehlich Hamiltonian: $\widehat{H} = \widehat{H}_{\text{el.}} + \widehat{H}_{\text{ph.}} + \widehat{H}_{\text{int.}}$ which contains the phonon term with experimentally measured phonon frequency, one can obtain the expression: $\Omega = \Omega_0(1 - 2\lambda)^{1/2}$ One can conclude that the value of the coupling constant λ cannot exceed $\lambda_{\max} = 0.5$, and therefore the value $T_c \lesssim 0.1\ \widetilde{\Omega}\left(\widetilde{\Omega} \approx \Omega_D\right)$ is the upper limit of T_c. However, there are many superconductors with $\lambda > 0.5$ (e.g., Sn, Pb, Hg). The analysis, based on rigorous adiabatic theory [6, 7] has demonstrated that the mentioned limitation on the coupling constant is absent. There are number of superconductors with large values of the coupling constant (e.g., $\lambda \approx 1.5$ for Pb, $\lambda \approx 1.6$ for Hg). The same is true for some compounds, for example, $\lambda \approx 2.6$ for Am-$Pb_{0.45}Bi_{0.55}$ (see [8]). Such materials form a family of the so-called superconductors with strong coupling and their properties are described by the Migdal-Eliashberg theory [9, 10], which is the generalization of the BCS method [11] for the strong coupling case. The combination of high characteristic phonon frequency and large coupling constant can provide the superconducting state at high temperature.

Critical Experiments

Critical experiments allow us to support or rule out various theoretical concepts. For example, the observation of the Josephson current is a real prove of existence of the pairing, as well as measurements of heat capacity at low temperature display the presence of the energy gap.

At the same time to probe the nature of the pairing force is a very serious challenge. For example, the special method based on tunneling spectroscopy developed by MacMillan and Rowell [12] is the most rigorous prove that the pairing in conventional superconductors is provided by the phonons exchange. As we know, the Eliashberg equation has been formulated specifically for the phonon mechanism. The authors [12] have developed the special method of inversion of this equation. The inversion allows one to reconstruct the function $\alpha^2(\Omega)F(\Omega)$; here $\alpha^2(\Omega)$ describes the electron-phonon interaction, and $F(\Omega)$ is the phonon density of states. The coupling constant λ is equal to $\lambda = \int d\Omega \alpha^2(\Omega)F(\Omega)/\Omega$. Usually the function $\alpha^2(\Omega)F(\Omega)$ contains peaks, which corresponds to the peaks in $F(\Omega)$.

The phonon density of states can be measured also with totally independent technique, namely with use of neutron scattering. This technique has nothing to do with superconductivity and is a direct measure of the phonon spectrum. The coincidence of the peak structure obtained by these two methods is a direct evidence that pairing, indeed, is due to the phonons exchange.

Note also that the observation of the isotope effect, especially if the value of the isotope coefficient is large is the evidence of the phonon mechanism. Indeed, its

existence means that the lattice is involved in the pairing. The importance of studying the isotope effect was stressed by Alex Mueller in many articles (see, e.g., [13–15]). It follows from his interest in polaronic effects. In fact, the formation of the Jahn-Teller polaronic state was a main motivation to search for high T_c superconductivity in oxides [1]. Note that the presence of the polaronic state does not allow to present the total wave function as a product of the electronic and lattice terms. Therefore, it is impossible to separate the electronic and ionic motions. This inseparability strongly supports the notion that the electron-lattice interaction provides the high T_c state.

The isotope effect was observed in the cuprates (see, e.g., the review [16]). A special method allowing one to study a selective isotope effect has been developed [17]. The peculiar dependence of the isotope coefficient on doping was observed in [18] and described theoretically in [19].

As a whole, a number of critical experiments and studies (see, e.g., the review [5]) lead to conclusion that the electron-lattice interaction provides the high T_c superconducting state in the cuprates.

Let us discuss several recent experimental developments related to manifestations of various mechanisms.

Pressure and High T_c Superconductivity in Hydrides

Recent discovery [20, 21] (see review [22]) of a new superconducting compound (sulfur hydride) with record value of the critical temperature ($T_c \approx 203$ K(!)) under high pressure ($P \approx 150$ GPa) has attracted a lot of interest (see, e.g., [23–30]). It is generally accepted that this phenomenon is caused by the presence of high frequency optical phonon modes, which describe the motion of light hydrogen ions. This conclusion is supported by the observation of the large isotope effect ($\alpha \approx 3.5$). More specifically, we are dealing with strong electron-phonon interaction with high frequency phonons, and one can use the Migdal–Eliashberg theory (ME) [9, 10] for the analysis.

The presence of hydrogen ions is the necessary, but not sufficient condition for reaching such a high T_c. Indeed, sulfur hydride has $T_c \approx 90$ K at the pressure $P \approx 90$ GPa. Only subsequent increase in pressure leads to a large increase in the value of the critical temperature up to $T_c \approx 200$ K. At the same time the sample at $P \lesssim 90$ GPa contains already the hydrogen and, therefore, has high frequency modes. The value $T_c \approx 90$ K is rather high and would be sensational 30 years ago, but it is much below the value $T_c \approx 200$K achieved under higher pressure. Therefore, there are some additional factors, created by further increase in pressure. It turns out that the key factor is a change in the crystal structure of the material (structural phase transitions), and the new structure appears to be stable in the presence of higher pressure.

The phase with the highest value of $T_c \approx 200$ K has a cubic structure and contains H_3S units, which are different from H_2S units for the initial phase. This cubic structure (so called Im-3m system) is characterized by equal S-H distances. A decrease in pressure leads to the transition to the phase (so called R3m structure) with different symmetry and lower value of $T_c \approx (100–120)$ K. One can raise the question: how to explain such a large difference between these two neighboring phases? To answer this question, one should take into account that the phonon spectrum is broad and contains two well-separated groups: acoustic and optical phonons. Based on the approach [30], which is a generalization of the usual ME treatment, one can introduce two coupling constants $\lambda_{opt.}$ and $\lambda_{ac.}$, and two characteristic frequencies. Then one can demonstrate that the transition into higher T_c state is accompanied by redistribution of the interaction with its shift to the high frequency part ("re-distribution" concept). This shift corresponds to a noticeable increase in a number of hydrogen ligands near the S-site (it becomes equal to six) and it leads to a large raise in T_c.

The transformation $H_2S- \rightarrow H_3S$ is related to the mixed valence state of sulfur. This feature is similar to that in the high T_c cuprates [1], there we are dealing with mixed valence state of Cu. Note that a number of novel systems such as the cuprates, manganites, sulfur hydrides are characterized by mixed valence, which is their key property.

It is interesting that there is a difference in the value of the isotope coefficient for $H \rightarrow D$ substitution between the high T_c phase and the R3m structure with lower T_c. This difference is caused by different contributions of high frequency optical modes into the pairing [30].

Nanoclusters: High T_c State Some selected metallic clusters, for example, the Al_{66} (it contains 66 atoms and, correspondingly, 198 delocalized electrons, since each Al atom has 3 valence electrons) also characterized by strong electron-vibrational coupling and it leads to high value of $T_c \approx 120$ K [31]; this value exceeds that for the bulk Al for more than two orders of magnitude (!).

Electronic states in some clusters form the energy shells similar to those in atoms and nuclei (s,p,d,. . . shells; see, e.g., the reviews [5, 32]). For small nanoclusters we are dealing with pairing of electrons with opposite values of the projection of orbital momenta. The clusters with filled upper shell have a spherical shape and their states are classified by orbital momenta with the degeneracy $g = 2(2L + 1)$, L is the orbital momentum. For example, for $L = 7$ the degeneracy $g = 30$ (!). This value greatly exceeds that ($g = 2$) for usual quantization. Large degeneracy means that there are many electrons on the same energy level (in this case on the Fermi level, E_F). Qualitatively it means a large density of states and, correspondingly, a large value of the electron-vibrational coupling constant. As a result, one can observe the high T_c superconducting state.

The Al clusters are not magnetic systems and this rules out the magnetic mechanism. One can conclude that the phonon mechanism provides this high T_c state in nanoclusters.

How to observe the phenomenon in an isolated cluster? Of course, it is senseless to talk about the resistance of such a nanoparticle. What is observable is the impact

of the pairing on the electronic spectrum. One can observe a strong temperature dependence of the spectrum. Below T_c the excitation energy is strongly modified by the gap parameter and noticeably exceeds the energy spacing in the region above T_c.

Such change in the spectrum has been observed in [31]. In principle, it is possible to build a cluster-based tunneling network, which would allow to transmit a high-temperature macroscopic superconducting current. The charge transfer is due to the Josephson coupling between clusters.

As was described above, the phonon mechanism can provide the high T_c state in metallic nanoclusters.

Experimental Observation of the Electronic Mechanism A very interesting experimental paper was published recently [33]. As we know, W. Little published in 1964 the milestone paper [34], where he introduced the electronic mechanism of superconductivity. The model is based on the presence of two group of electrons. The pairing in one group (this group must contain delocalized electrons) is provided by the Coulomb interaction with the second group and corresponding virtual electronic transitions. The large scale, namely, the electronic energy, which is much higher relative to Ω_D, can lead to high value of T_c. W. Little also predicted the possibility of the superconducting state in organic materials, and this prediction was verified later [35].

The paper [33] describes the first experimental observation of the electronic mechanism. The system used in this experiment contains a set of two carbon nanotubes. Amazingly precise nano-technology method (special quantum dots system) was developed and used in [33]. The fundamental block is the two-site system and the "polarizer", which mediates the pairing. Unique tunability allows one to control the distance between the paired electrons and the "polarizer". It has been demonstrated that the pairing energy (repulsive $\rightarrow$ attractive transition) increases with decreasing the device dimensions. This pioneering experiment achieved about 8 K scale for the pairing energy. However, the size of the quantum dot was relatively large (400 nm).Future use of nanoscales is promising for reaching high T_c values up to room temperature.

Spin Liquid Magnetic Mechanism The spin-liquid system was studied in [36] (the resonance valance bond model, RVB). The corresponding doping leads to metallization and then to superconductivity at high temperatures. This model was considered as relevant to the phenomenon observed in cuprates.

The authors of recent experimental study [37] model the system by making initially the so-called herbertsmithite $ZnLi_x(OH)_6Cl_2$, which represent 2D lattice realization of the spin liquid.

The material was doped. The doping occurs by substitution of Cu^{3+} for zinc, that is, by formation of the electron-doped $ZnCu_3(OH)_6Cl_2$. According to the theory, the doping should lead to rich phase diagram which includes the transition into metallic state and then to high T_c superconductivity. However the experimental measurements did not display any metallicity; despite of large number of electrons, introduced into the sample, it continuous to be insulating down to low temperatures. The precise heat capacity measurements have not determined any sign of the transition into superconducting state.

One can add also that the pairing can be provided by another magnetic mechanism, namely, by spin fluctuations; this is. However, It is hard to expect the high value of T_c, caused by this mechanism.

Discussion We describe above several key experimental studies performed recently. They demonstrated that high T_c superconducting state can be caused by the electron-ion interaction or by interaction between two different electronic subsystems. In other words, only Coulomb force which is relatively strong, can provide the phenomenon of strong pairing and, correspondingly, high T_c. Despite being a theoretician, I am focusing here on experimental data, since this is the only way to confirm or rule out the proposed mechanisms.

Personal Remarks

I am delighted to write this contribution to the Special Festschrift, celebrating Alex Mueller's birthday. I met Alex for the first time at the famous 1987 March Meeting ("Woodstook" in physics). Later I met him at numerous conferences and seminars and eventually my wife, Lilia, and I become good friends with Alex and his charming family: Inge, Sylvia, Eddy and bright young Micha. Even in 2015 I was unable to communicate with Micha, but last summer, just 1 year later, he was totally fluent in English, so that we had a nice conversation about his future life in physics.

Alex likes travelling; the same is true about his whole family. He enjoys driving while traveling. In addition, he has been active member of the Swiss "Jaguar Society". I remember also when Alex, while being guest in Berkeley, visited unique California Automobile Museum and was happy seeing many different old and new car models. Speaking of this hobby, one should mention that he is able to take apart his Jaguar in hundred small pieces and then bring all of them back, so that his car is always in an excellent state (Fig. 14.2).

To be so famous as Alex Mueller is not an easy task. I remember the March Meeting in 2011 in Dallas, where Alex was giving an invited talk. The auditorium was overcrowded; many people came specially in order to see such a celebrity. But Alex has not been affected by his fame (Fig. 14.3). Everybody who met him is impressed by his charm, intelligence, soft-spoken style and his sense of humor. Speaking of sense of humor, I recall a remarkable International Conference in 2000 (Kloster, Switzerland), which had a very "modest" title "Superconductivity in Next Millennium". At the end of the Conference Alex presented a summary talk describing state of the art in the area of superconductivity. He noticed in the beginning of his talk that there is a key question:" Where are we in our field?". And he was continuing with a story about the recital given by famous Fritz Kreisler in Carnegie Hall. He and his accompanist were playing some sonata. All of the sudden Kreisler understood that he completely lost communication with his partner and they were playing simultaneously different parts of the sonata. While playing, he did approach slowly the accompanist and asked him in a low voice "where are we?". And he

Fig. 14.2 Alex Mueller and his favorite car (Jaguar) are inseparable

Fig. 14.3 On the lake. Pictured: Alex Mueller, Inge Mueller, Lilia Kresin

received the answer: "In the Carneque Hall". Then Alex noted: Speaking of the question: "where are we?" one can answer "in Kloster".

Alex is a renaissance man with very broad range of interests. He is interested in other areas of physics, which are not related to his immediate activity, and also in other fields of science. His erudition in history is very impressive. Recently he

finished writing his recollections and thoughts, and the insights are non-trivial and very interesting.

Alex Mueller is in excellent shape and one can expect from him many more remarkable ideas and results.

References

1. G. Bednorz, K. Mueller, Z. Phys. **B64**, 189 (1986)
2. W. McMillan, Phys. Rev. **B167**, **331** (1968)
3. P. Allen, R. Dynes, Phys. Rev. B **12**, 905 (1975)
4. V. Kresin, Phys. Lett. A **122**, 434 (1987)
5. V. Kresin, H. Morawitz, S. Wolf, *Superconducting state, Mechanisms and Properties* (Oxford Press, NY, 2014)
6. Y. Browman, Y. Kagan, JETP **25**, 365 (1967)
7. B. Geilikman, J. Low Temp. Phys. **4**, 189 (1971)
8. E. Wolf, *Principles of Electron Tunneling Spectroscopy* (Oxford University Press, Oxford, 2012)
9. A. Migdal, JETP **7**, 996 (1958)
10. G. Eliashberg, JETP **11**, 696 (1960)
11. J. Bardeen, L. Cooper, J. Schrieffer, Phys.Rev. **108**, 1175 (1957)
12. W. McMillan, J. Rowell, in *Superconductivity*, ed. by R. Parks, vol 1 (Marcel Dekker, New York, 1969), pp. 561–614
13. K. Mueller, Z. Phys. **B80**, 193 (1990)
14. K. Mueller, Nature **337**, 130 (1995)
15. K. Mueller, J. Supercond. Novel Magn. **25**, 2101 (2012)
16. H. Keller, in *Structure and Bonding*, ed. by K. Mueller, A. Bussmann-Holder. (Springer, Heidelberg, 2005)
17. D. Zech, H. Keller, K. Mueller, et al., Nature **371**, 681 (1994)
18. S. Weyeneth, K. Mueller, J. Supercond. Novel Magn. **24**, 1205 (2011)
19. V. Kresin, S. Wolf, Phys. Rev. B. **49**, 3652 (1994)
20. A. Drozdov, M. Eremets, et al., Nature **525**, 73 (2015)
21. M. Einaga, K. Shimisi, M. Eremets, et al., Nat. Phys. **12**, 835 (2016)
22. M. Eremets, A. Drozdov, Uspechi **186**, 1257 (2016)
23. Y. Li et al., J. Chem Phys. **140**, 174712 (2014)
24. D. Duan et al., Sci. Rep. **4**, 6968 (2014)
25. A. Bianconi, T. Jarlborg, Novel. Super. Mater. **1**, 15 (2015)
26. I. Errea et al., Nature **532**, 81 (2016)
27. D. Papaconstantopoulos et al., Phys. Rev. B. **91**, 184511 (2015)
28. E. Gordon et al., Angew. Chem. Int. Ed. Engl. **55**, 1 (2016)
29. W. Sano et al., Phys. Rev. B **93**, 094525 (2016)
30. L. Gor'kov, V. Kresin, Sci. Rep. **6**, 25608 (2016)
31. A. Halder, V.V. Kresin, Phys. Rev. B. **92**, 214506 (2015)
32. W. de Heer, Rev. Mod. Phys. **65**, 611 (1993)
33. A. Hamo et al., Nature **535**, 395 (2016)
34. W. Little, Phys. Rev. **134**, A416 (1964)
35. D. Jerome et al., J. Phys. Lett. (Paris) **41**, L95 (1980)
36. P. Anderson, Science **235**, 1196 (1987)
37. Z. Kelly et al., Phys. Rev. X **6**, 041007 (2016)

Chapter 15
Raman Study of the Anharmonicity in $YBa_2Cu_3O_x$

Efthymios Liarokapis

Introduction

It is now 30 years since Georg Bednorz and K. Alex Müller surprised the scientific community with their discovery of a superconductor with a transition temperature (T_c) above 30 K [1], opening the way for the discovery of other compounds with T_c above the liquid nitrogen temperature [2]. At that time it was generally believed that 30 K was strictly an absolute upper limit for T_c, and the majority of the scientists had abandoned the search for high temperature superconductors (HTSC). It was the discovery of the new layered superconductor that revived the interest on this field. Right after the discovery it was found that the new family of superconductors (the cuprates) had unusual properties quite different from the conventional superconductors. The existence of magnetism and a Mott transition at low doping [3], the d-wave symmetry of the energy gap [4], the very small isotopic shift of T_c at optimal doping [5, 6], the existence of a pseudogap (PG) [7, 8], etc, have shown that this new class of compounds had exotic properties, quite different from the conventional superconductors. The great majority of the scientists being certain that electron-phonon interaction, that was the basic mechanism for superconductivity in the BCS theory, could not explain such T_c values found in the cuprates, have assumed that other alternative coupling mechanisms must be present, and the lattice should not play a role in the process. But, it was found that the isotopic shift of the transition temperature was strongly dependent on the amount of doping [9]. Besides, isotope effects were discovered on the magnetic penetration depth [10], the pseudogap temperature (T*) [11], etc, showing a substantial involvement of the lattice in the processes and pointing to a polaronic approach to superconductivity.

E. Liarokapis (✉)
Physics Department, National Technical University, Athens 157 80, Greece
e-mail: eliaro@central.ntua.gr

A. Bussmann-Holder et al. (eds.), *High-Tc Copper Oxide Superconductors and Related Novel Materials*, Springer Series in Materials Science 255,
DOI 10.1007/978-3-319-52675-1_15

An explanation of the small oxygen isotope effect of T_c observed in the ceramic superconductors, within the frame of the phonon mediated pair coupling mechanism, was based on the enhancement of the electron-phonon coupling strength through the anharmonic motion of the oxygen atoms [12–14] in a double-well potential [15]. Among the different oxygen sites of $YBa_2Cu_3O_x$, the apex oxygen (O_{ap}) has been observed to move in a double well potential [16, 17], and the relative A_g-symmetry mode was detected anharmonic [18]. A detailed investigation of the effect of the oxygen isotopic substitution on the phonon modes of $YBa_2Cu_3O_x$ over the whole range of doping (x = 6–7) revealed that, among the modes that involve motion along the c-axis of the oxygen atoms, the B_{1g} symmetry out-of-phase vibrations of the plane oxygen atoms (O_{pl}) follow well the harmonic approximation, while the in-phase vibrations of O_{pl} and the apical phonon present doping dependent deviation from the harmonic approximation [19, 20]. Recent investigations in $YBa_2Cu_3O_{6.5}$ have found strong indications for the double-well potential of the apical oxygen in the ortho-II phase [21] in complete agreement with the Raman data. On the other hand, the anharmonicity observed by Raman spectroscopy seems to diminish close to optimal doping (increasing towards the ortho-II phase) and it is stronger for the in-phase vibrations of A_{1g}-symmetry of the plane oxygen atoms, than for the apical one [19, 20]. This appears to contradict and question the double-well potential picture observed at optimal oxygen concentration [16, 17].

In this work the results of the Raman measurements on the $YBa_2Cu_3{}^{16,18}O_x$ compounds in the full range of oxygen doping will be reviewed and compared with measurements that strongly indicate the motion of the apical oxygen in a double-well potential. The idea of these measurements was entirely due to Prof. Dr. K.-A. Müller interested to obtain information about the amount of anharmonicity in the cuprates in the whole range of oxygen concentration. This required samples of excellent quality that have been provided by the group in ETH of Prof. Dr. E. Kaldis.

Experiment

Two series of samples of $YBa_2Cu_3O_x$ (x = 6–7) have been examined, with the isotopic substitution of ^{16}O by ^{18}O around 90–94%. The samples were prepared under similar conditions with those described before [18]. The amount of oxygen in the YBCO samples has been measured with a volumetric method [22] with an extremely high accuracy ($\Delta x = \pm 0.001$). No other phases have been detected by X-ray powder diffraction and Raman measurements. Raman spectra were obtained with a T64000 Jobin-Yvon triple spectrometer equipped with a liquid nitrogen cooled charge coupled device (CCD) and a microscope (magnification $\times 100$). The 514.5 and 488.0 nm and the 647.1 nm line of an Ar^+ and a Kr^+ lasers respectively were used for excitation at a power level of ~0.15 mW on the sample, while the laser spot diameter was of the order of 1–2 μm. Local sample heating due to the laser beam was estimated to be <10 K. The spectra were obtained from individual

micro-crystallites in the approximate $y(zz)\bar{y}$ (or $x(zz)\bar{x}$) and $y(xx)\bar{y}$ (or $x(yy)\bar{x}$) scattering configurations as the x and y axis could not be discriminated in the twinned samples. Accumulation times were of the order of 1–3 h and several micro-crystallites have been examined for each oxygen concentration. The proper orientation of the microcrystallites was selected from their shapes and from the scattering selection rules.

Results and Discussion

The strong modes of $YBa_2Cu_3O_x$ are those of $4A_g$ and $1B_{1g}$-like symmetry and involve vibrations along the c-axis of the Ba atom, the Cu of the CuO_2 planes (Cu_{pl}), the apical oxygen, and the two vibrations, in-phase (A_g) and out-of-phase (B_{1g}) of the plane oxygen atoms. Characteristic spectra for selected concentrations and the two isotopes have been presented elsewhere [19, 20]. Apart from a frequency shift of the oxygen modes due to the isotopic substitution, the two sets of spectra looked the same. No frequency difference is observed between the two isotope compounds regarding the Ba and the Cu_{pl} phonons due to the negligible amount of coupling between the motion of the oxygen atoms and the vibrations of the Ba, Cu_{pl} atoms [19, 20]. Figure 15.1a–c show the frequencies of the three oxygen modes (B_{1g}, in-phase, and apex) for the whole range of oxygen doping for ^{16}O and for ^{18}O, corrected according to the square root of the mass ratio, for two ^{18}O contents, i.e., 90% and 94%. The amount of the ^{18}O substitution for ^{16}O was estimated to be equally distributed to all oxygen sites [23], that will induce a frequency shift of 5.5% (for 90% or 5.7% for 94%) according to the average mass ratio of the two isotopes, or slightly smaller (5.3% for 90%) with lattice dynamic calculations [24]. Theoretical calculations have shown that the oxygen isotope correction factor may slightly depend on the phonon modes [24] or on the oxygen concentration [25], but the changes expected are small. Since the error in the frequency shift from the uncertainty in the exact amount of oxygen substitution (90–94%) is larger than the difference between the simple mass ratio law and the lattice dynamic calculations, we have used the former simple equation in correcting the frequencies for the ^{18}O data (Fig. 15.1a–c).

One can induce from the data that the out-of-phase B_{1g}-symmetry oxygen mode (observed in xx-polarization) for both correction factors (5.5% or 5.7%) agree within statistical error (mean square deviation of frequency values obtained from many microcrystallites), in most of the oxygen doping range, except for a small deviation ($<2\ cm^{-1}$) close to tetragonal to orthorhombic structural phase transition ($x \sim 6.35$) and possibly in the overdoped region (Fig. 15.1a). These results agree also with those from IR measurements [18]. The deviation varies with the amount of isotopic mass correction and it could be due to the correction factor that may vary with doping [25]. For both isotopes, there seems to be a small non-linear dependence of the B_{1g} frequency on the oxygen doping level (Fig. 15.1a). Since the frequency of the B_{1g} mode does not vary appreciably with the amount of oxygen,

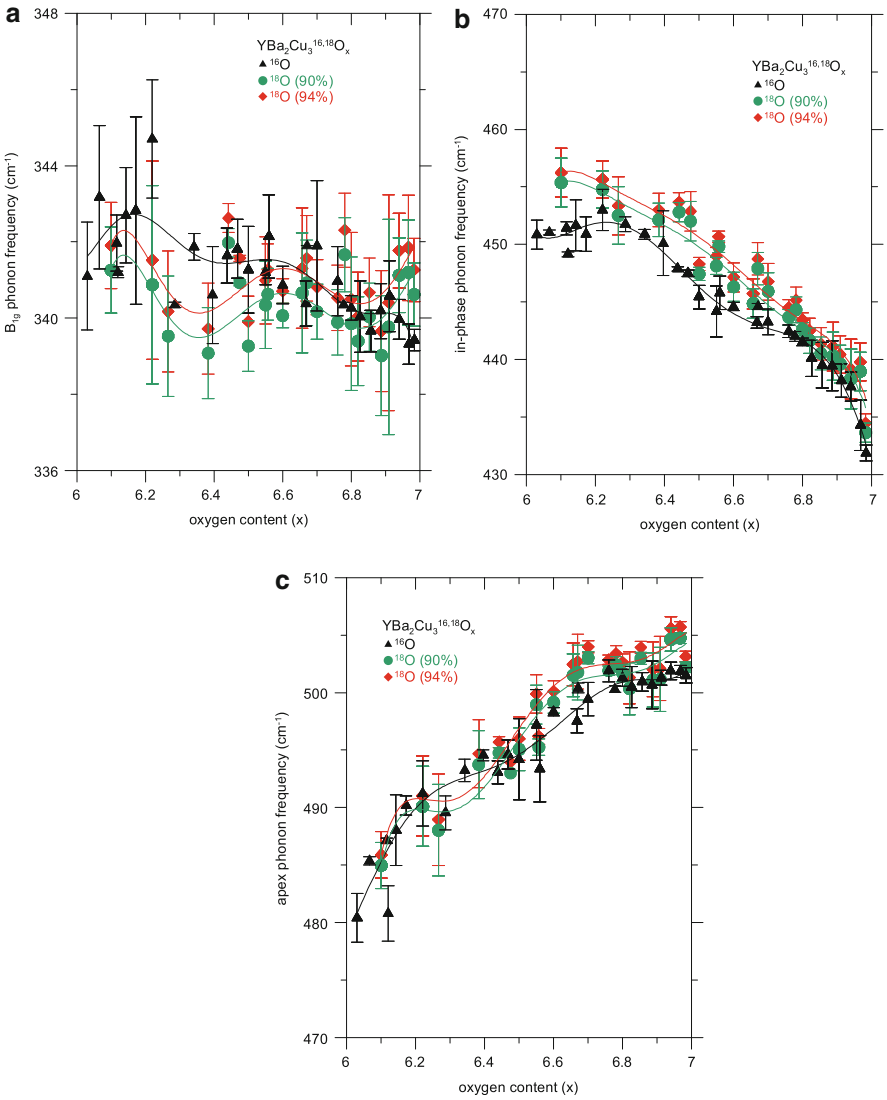

Fig. 15.1 The variation of the frequency of the B_{1g}-like (**a**), in-phase (**b**), and apical (**c**) oxygen phonons with the amount of doping x for the ^{16}O and the ^{18}O. The data for ^{18}O have been normalized according to the two isotopes average mass ratio (for 90% and 94% substitution). The continuous lines are guides to eye

one could use the average values of the two frequencies for ^{16}O and ^{18}O in order to estimate the average correction factor, which turns out to be very close to the amount of ^{18}O substitution measured by other means (≈90%).

For the in-phase mode of the same O_{pl} atoms (of A_{1g}-symmetry) the deviation is much stronger (up to 5 cm^{-1}) and depends on the amount of oxygen concentration.

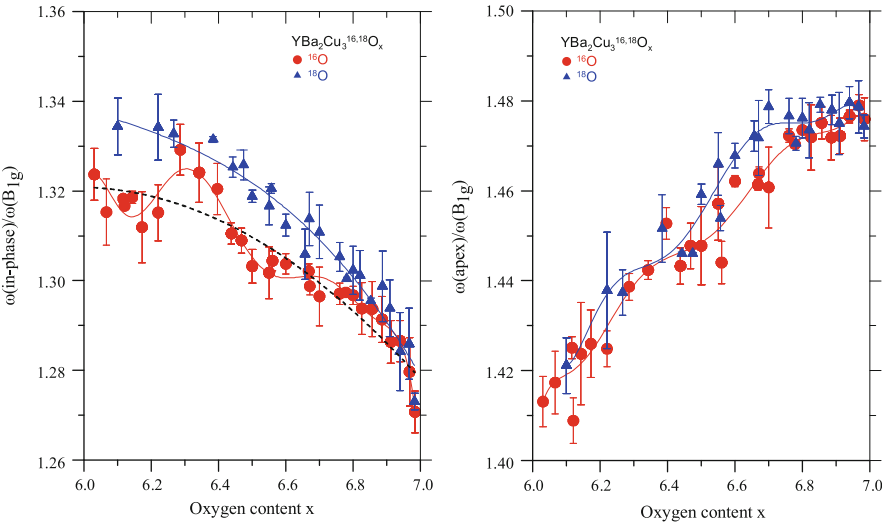

Fig. 15.2 The variation of the relative frequency of the in-phase (**a**) and the apical (**b**) to B_{1g}-like phonon for all oxygen concentration x and the two isotopes. The continuous lines are guides to eye. The broken line in Fig. 15.2a indicates an average (2nd order polynomial curve) of the data

Again, depending on the chosen isotopic correction, the data from the two isotopes agree quite well close to optimal doping. Even the softening of the in-phase mode, discovered in the overdoped region [26] has the same behavior (sudden drop around optimal doping) for both isotopes (Fig. 15.1b). The maximum amount of anharmonicity seems to appear around the ortho-II phase ($x = 6.5$) and for the tetragonal one ($x < 6.2$). Due to the uncertainty of the exact amount of substitution and the possible dependence of the correction factor on oxygen doping, it is difficult to obtain exact information on the amount of anharmonicity.

Figure 15.1c presents the data for apical oxygen (A_{1g} symmetry). The difference between the two isotopes is smaller than for the in-phase mode and depends again on oxygen doping and the correction factor. One can generally induce that there is some amount of anharmonicity that disappears in the tetragonal phase ($x < 6.2$). In the optimally doped region, depending on the correction factor, there might be anharmonicity. From the data it becomes obvious that since we are dealing with small anharmonicity, we should find a way to bypass the uncertainty in the evaluation of the amount of ^{18}O substitution for ^{16}O and the correction factor. Assuming that there is an equal amount of ^{18}O substitution in the planes and the chains, we can take the ratio of the frequencies for both isotopes and avoid this uncertainty. For the in-phase mode, the assumption of equal amounts of site substitution is not needed, but it remains a possible uncertainty about the correction factor for the two phonons from the same atoms but of different symmetry.

Figure 15.2a presents for the two isotopes the ratio of the in-phase and B_{1g} phonon frequencies that involve vibrations of the plane oxygen atoms. Since the frequency ratio does not depend on the exact amount of ^{18}O substitution and the

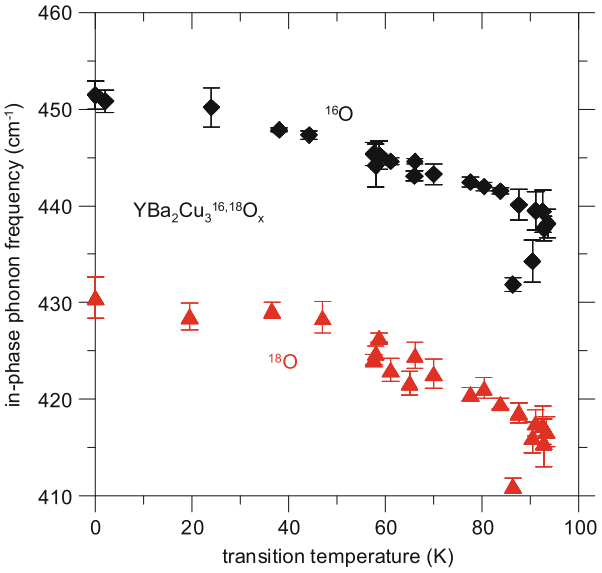

Fig. 15.3 The dependence of the in-phase phonon frequency on T_c for the two oxygen isotopes

correction factor, the statistical variation of the data has been reduced and more accurate conclusions can be drawn. Although the ratio of the ^{18}O data varies smoothly with doping, there is a remarkable deviation for the ^{16}O compounds (Fig. 15.2a). The average variation of the ratio is presented with the dashed line. It is clear that the deviation from the harmonic potential is almost zero towards optimal doping and increases with the reduction of the amount of oxygen. Besides, there is a strong fluctuation in the amount of anharmonicity, which becomes very small or zero at $x \approx 6.3$ and for $x \geq 6.85$. Its maximum value occurs for $x \approx 6.5$ (apparently at the ortho-II phase) and for $x \approx 6.15$ (a tetragonal phase). The anharmonicity seems to disappear close and above the optimal doping. In the overdoped region ($x \geq 6.94$), where the in-phase mode was found to soften suddenly [26], the anharmonicity in the compound remains very small or even zero. The similarity of the in-phase mode in the two isotopes can be clearly observed in Fig. 15.3, where the frequency is plotted vs the transition temperature. Since the softening of the phonon was correlated with a change in the CuO_2 buckling, it is induced that this deviation from flatness of the CuO_2 is not related with an increased anharmonicity.

The corresponding ratio of the apical phonon mode frequency to the B_{1g} is presented in Fig. 15.2b. As discussed before, in this case there is an uncertainty on the relative amount of site selective oxygen substitution, although the controllable methodology followed in sample preparation points to an equal amount of substitution at the plane and apical oxygen sites [23]. A similar trend of anharmonicity is observed as in the case of the in-phase mode of Fig. 15.2a. Close to the ortho-II and the tetragonal phases the amount of anharmonicity appears to become maximum and it reduces towards optimal doping, although in this case there is a small amount

of anharmonicity for $x > 6.85$. In the case of apex phonon, the data for the two sets of isotopes coincide at $x \approx 6.35$, i.e., close to the tetragonal to orthorhombic (T-O) structural phase transition (Fig. 15.2b). Considering the statistical errors, we can safely assume that for both phonons (apex and in-phase) the anharmonicity vanishes at the T-O transition. The small downshift in frequency at the overdoped region appears to be the same for both isotopes, as was the case for the in-phase mode.

The above results disagree with those of [18] concerning the apex oxygen (in that work the in-phase mode could not be studied). This difference could be attributed to the different excitation wavelength used in [18]. It has been shown [26] that mainly three phases coexist and contribute to a different amount to the apex mode (Fig. 15.4), and a resonance behavior for the phases of the apex mode has been also established [27]. If we therefore assume, as our data indicate, that the degree of anharmonicity varies considerably among the phases (maximum for ortho-II and tetragonal, minimum for the ortho-I), and take into consideration the resonance of the other phases with increasing laser wavelength excitation [27], the deviation between our data and those of [18] can be explained. The excitation with IR will enhance the anharmonicity as we approach optimal doping, because of the increased contribution of the anharmonic phases to the Raman signal. It is possible that the small anharmonicity observed in our data in the apex mode (Fig. 15.2b) express small contribution of the other anharmonic phases.

In the ortho-II and other phases there will be a folding of the unit cell and, therefore, more phonons will be Raman active [28]. One could expect the new extra phonons at the Γ-point of the ortho-II phase to either induce new modes at the side of the existing phonons of ortho-I phase or, being very close in frequency, modify their width and intensity. New modes appear mainly for the Ba mode [19, 20], but not close in frequency to the apex phonon, which retains almost the same width with the ortho-I phase (Fig. 15.5). These results agree with the theoretical investigations [28], which predict weak modes not far in frequency for the apical phonon. Since the width of the apical phonon in ortho-II (and the tetragonal) is as narrow as for the ortho-I phase, it is unlikely that the phonon frequency modifications with isotopic substitution to be related with new modes that appear at the Γ-point, although it cannot be excluded.

As described, our data do not seem to support any strong anharmonicity of the apex oxygen close to optimal doping, disagreeing with the conclusions of [16, 17] that the apical oxygen moves in a double well potential, occupying two distinct sites quite apart (0.12 Å distance). Since their measurements had been carried out at low temperatures, we have tested the anharmonicity at near optimal doping 77 K. The results are shown in Fig. 15.6 and it is clear that the two isotopes follow the same trend, being independent of temperature. Therefore, even these preliminary data at low temperature show that there is no appreciable change in the amount of anharmonicity for the region 77–300 K and, therefore, the different temperature of our measurements with those of [16, 17] cannot be the reason of the discrepancy. The motion of the apical oxygen in two potential wells does not agree also with the

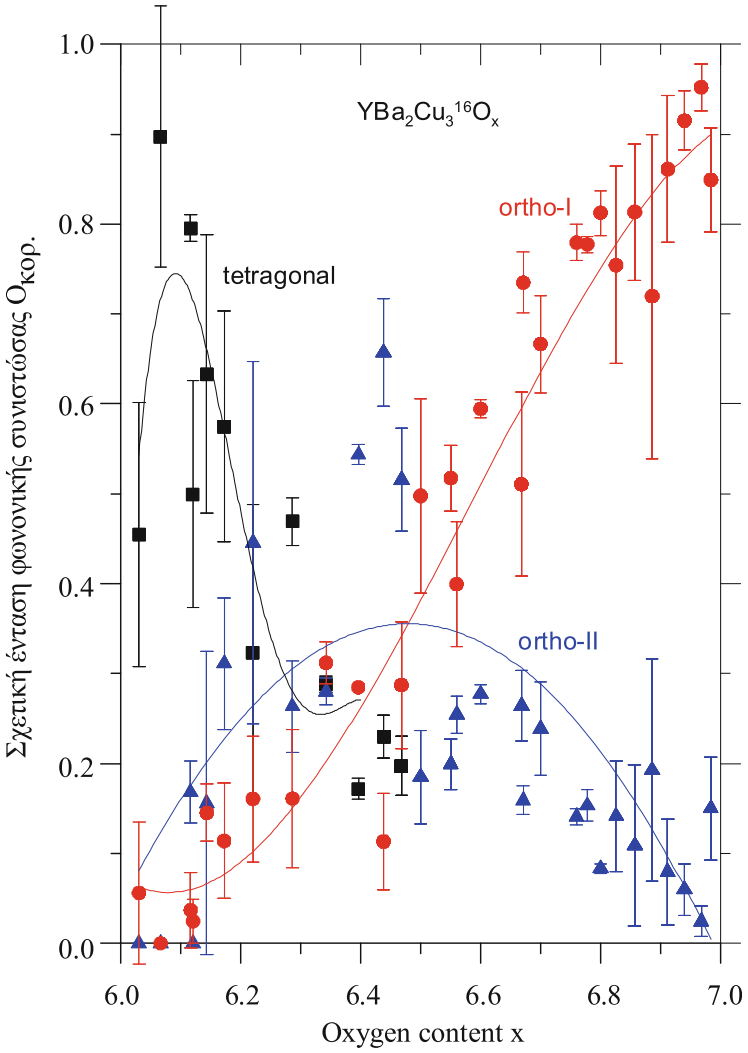

Fig. 15.4 The relative amount of the three phases (ortho-I, ortho-II, and tetragonal) for the ^{16}O isotope, as induced by deconvolution of the apical phonon. A similar curve is obtained for ^{18}O

phonon width, which remains smaller in the ortho-I, the ortho-II and the tetragonal phases (Fig. 15.5), increases substantially in the intermediate doping levels where many phases coexist (Fig. 15.4) and decreases, as expected, at low temperatures. Furthermore, the distance of 0.12 Å between the two sites of the apical oxygen should correspond to a substantial shift of the apical oxygen phonon. Based on the data of the apical phonon frequency along the c-axis A_{1g}-symmetry for the whole range of doping and the measured variation of the apical oxygen position [19, 20] one would expect a shift of ~20 cm^{-1} between the phonon frequencies from the two

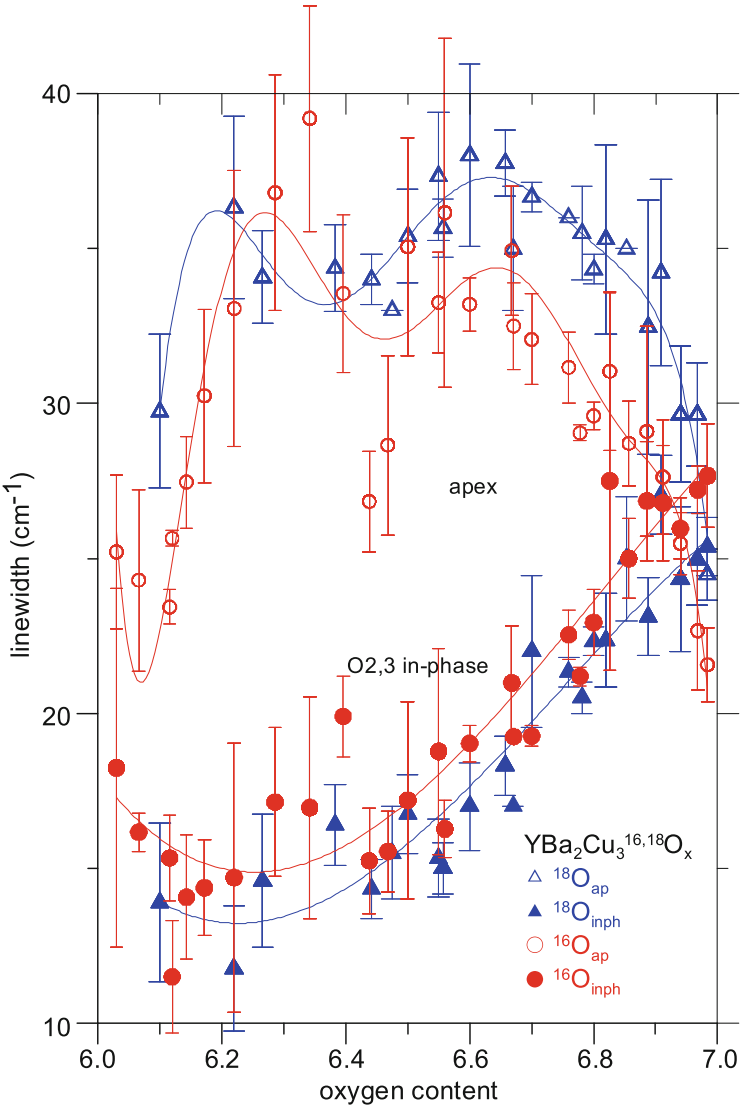

Fig. 15.5 The doping dependence of the apex and in-phase phonon width for the two isotopes

wells. This is comparable with the total width of the phonon mode at optimal doping (Fig. 15.5), which decreases with temperature. Therefore, the discrepancy between the Raman measurements and those which find a double well potential in the ortho-I phase remains.

For the ortho-II phase it is clear from our data that there is anharmonicity, which appears stronger for the in-phase mode, it is smaller for the apical oxygen atom and almost absent for the B_{1g} phonon. It is likely that the in-phase vibrations of the

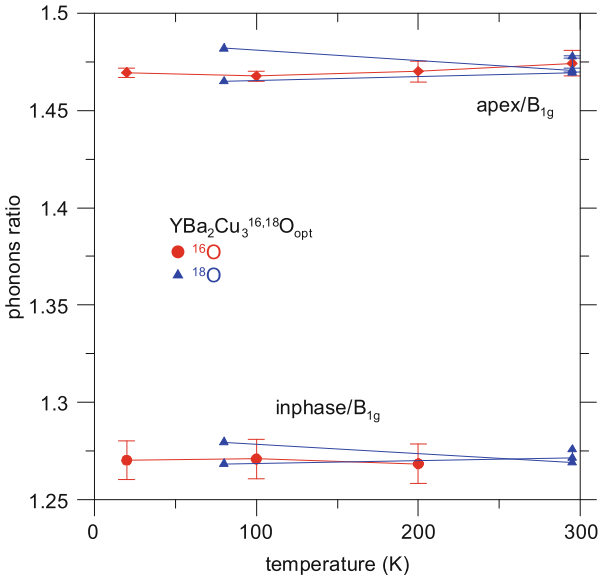

Fig. 15.6 The variation of the relative frequency with temperature of the in-phase and the apical to B_{1g}-like phonon for optimally doped compound for both oxygen isotopes

CuO_2 planes are affected more than the out-of-phase ones (B_{1g} mode) from the apical motion that modify the amount of charge transfer. In any case our data agree with other measurements that have found strong anharmonicity for the ortho-II phase [21]. In our data we have found equally strong anharmonicity for a tetragonal phase, which must correspond to a low oxygen concentration and should be checked by other techniques as well. It should be also marked the absence of ahnarmonicity at the tetragonal to orthorhombic structural phase transition (Fig. 15.2). Since the softening of the modes relaxes at this T-O transition, the anharmonicity could be related with parallel to the plane modifications, as other measurements indicate [29].

Concerning the discrepancy between the Raman data and other measurements for the optimally doped samples, one possible explanation can be based on the assumption that Raman active phonons at the Γ-point cannot detect the lattice distortion as the long wavelength phonons will feel only the average position of the oxygen atoms. Then, we have to accept the view that the anharmonicity observed in the ortho-II and the tetragonal phase is due to the contribution of the folded phonons from the edge of the Brillouin zone back to its center or that the effect is dynamic and at low doping level evolves towards a static disorder.

Summary

In conclusion the presenter Raman data indicate that there is anharmonicity for the in-phase vibrations of the O_{pl} oxygen that depends strongly on the amount of oxygen, being maximum in the ortho-II phase and another one in the tetragonal structure of the compound. At optimal doping the amount of anharmonicity diminishes, and the softening of the mode in the overdoped region seems to scale according with the mass law. For the apical oxygen the problem is more complicated due to existence of many contributing phases, which appear to have a different amount of anharmonicity, with the ortho-I phase being almost harmonic and the ortho-II phase the most anharmonic. The Raman data do not agree with a static double well potential for the apical oxygen at least in the optimally doped region. It is possible that phonons at the Γ-point cannot detect this lattice distortion, which can only be observed from edge phonons of the Brillouin zone.

Acknowledgments I would like to thank Prof. Dr. K.A. Müller who had proposed this experimental Raman study, Prof. Dr. E. Kaldis and Dr. K. Conder who provided the excellent quality samples, and Dr. N. Poulakis and Dr. D. Palles who had carried out the time consuming Raman measurements.

References

1. J.G. Bednorz, K.A. Müller, Z. Phys. B **64**, 189 (1986)
2. M.K. Wu, M.K. Wu, J.R. Ashburn, C.J. Torng, P.H. Hor, R.L. Meng, L. Gao, Z.J. Huang, Y.Q. Wang, C.W. Chu, et al., Phys. Rev. Lett. **58**, 908 (1987)
3. S.E. Sebastian, N.H. Harrison, G.G. Lonzarich, Rep. Prog. Phys. **75**, 102501 (2012)
4. C.C. Tsuei, J.R. Kirtley, Rev. Mod. Phys. **72**, 969 (2000)
5. B. Batlogg et al., Phys. Rev. Lett. **58**, 2333 (1987)
6. L.C. Bourne et al., Phys. Rev. Lett. **58**, 2337 (1987)
7. D.S. Marshall et al., Phys. Rev. Lett. **76**, 4841 (1996)
8. H. Ding et al., Nature **382**, 51 (1996)
9. D.J. Pringle, G.V.M. Williams, J.L. Tallon, Phys. Rev. B **62**, 12527 (2000), and references therein
10. H. Keller, A. Bussmann-Holder, K.A. Müller, Mat. Today **11**, 9 (2008), and references therein
11. M. Bendele et al., arxiv.1606.04251
12. N.M. Plakida, V.L. Aksenov, S.L. Drechsler, Europhys. Lett. **4**, 1309 (1987)
13. R.E. Cohen, W.E. Pickett, H. Krakauer, Phys. Rev. Lett. **64**, 2575 (1990)
14. K.A. Müller, Z. Phys. B Condens. Matter **80**, 193 (1990)
15. V.H. Crespi, M.L. Cohen, Phys. Rev. B **48**, 398 (1993)
16. J. Mustre de Leon, S.D. Conradson, I. Batistic, A.R. Bishop, Phys. Rev. Lett. **65**, 1675 (1990)
17. S.D. Conradson, I.D. Raistrick, A.R. Bishop, Science **248**, 1394 (1990)
18. G. Ruani, C. Taliani, M. Muccini, K. Conder, E. Kaldis, H. Keller, D. Zech, K.A. Müller, Physica C **226**, 101 (1994)
19. D. Palles, N. Poulakis, E. Liarokapis, K. Conder, E. Kaldis, K.A. Müller, Phys. Rev. B **54**, 6721 (1996)
20. E. Liarokapis, D. Palles, K. Conder, E. Kaldis, J. Raman Spectrosc. **32**, 821 (2001)
21. R. Mankowsky et al., Nature **516**, 71 (2014)

22. K. Conder, S. Rusiecki, E. Kaldis, Mater. Res. Bull **24**, 581 (1989)
23. K. Conder, E. Kaldis, M. Maciejewski, K.A. Müller, E.F. Steigmeier, Physica C **210**, 282 (1993)
24. M. Cardona, R. Liu, C. Thomsen, W. Kress, E. Schonherr, M. Bauer, L. Gentzel, W. Konig, Solid State Commun. **67**, 789 (1988)
25. E. Altendorf, J. Chrzanowski, J.C. Irwin, J.P. Franck, Phys. Rev. B **43**, 2771 (1991)
26. N. Poulakis, D. Palles, E. Liarokapis, K. Conder, E. Kaldis, K.A. Müller, Phys. Rev. B **53**, 534 R (1996)
27. M. Iliev, C. Thomsen, V. Hadjiev, M. Cardona, Phys. Rev. B **47**, 12341 (1993)
28. V.G. Tyuterev, P. Manca, G. Mula, Physica C **297**, 32 (1998)
29. W. Reichardt et al., J. Supercon. **7**, 399 (1994)

Chapter 16
Inter-site Pair Superconductivity: Origins and Recent Validation Experiments

Dragan Mihailovic

Introduction

The challenge of understanding high-temperature superconductivity has led to a plethora of ideas, but 30 years after its discovery in cuprates, very few have achieved convincing experimental validation. While Hubbard and t-J models were given a lot of attention, a number of recent experiments appear to give decisive support to the model of real-space inter-site pairing [1–3] and percolative superconductivity [4] in cuprates. Systematic measurements of the doping dependence of the superfluid density ρ_s show a linear dependence on T_c—rather than doping—over the entire phase diagram [5], in accordance with the model's predictions. The doping-dependence of the anomalous lattice dynamics of in-plane Cu-O mode vibrations observed by inelastic neutron scattering [6], gives remarkable reciprocal space signature of the inter-site pairing interaction [1] whose doping dependence closely follows the predicted pair density. Symmetry-specific time-domain spectroscopy shows carrier localization, polaron formation, pairing and superconductivity to be distinct processes occurring on distinct timescales throughout the entire superconducting phase diagram. The three diverse experimental results confirm non-trivial predictions made more than a decade ago by the inter-site pairing model

D. Mihailovic (✉)
Jozef Stefan International Postgraduate School and CENN Nanocenter, Jozef Stefan Institute, Jamova 39, Ljubljana 1000, Slovenia
e-mail: dragan.mihailovic@ijs.si

A. Bussmann-Holder et al. (eds.), *High-Tc Copper Oxide Superconductors and Related Novel Materials*, Springer Series in Materials Science 255,
DOI 10.1007/978-3-319-52675-1_16

in the cuprates, remarkably also confirming some of the fundamental notions mentioned in the seminal paper on the discovery of high-temperature superconductivity in cuprates [7].

The possible relevance of polaron physics was mentioned in the 1986 paper on the discovery of HTS by Bednorz and Müller [7]. Reference was made to a paper by Hock, Nickisch and Thomas [8] who discussed itinerant small Jahn-Teller (JT) polarons. The idea of small superlight (but non-JT) bipolarons was later pursued also by Sasha Alexandrov, where the doping dependence was attributed to a crossover from Bose-Einstein condensation to BCS superconductivity in the metallic overdoped state [9–11]. As an alternative model, paying detailed attention to experimental observations, we proposed the existence of inter-site bipolarons. Some relevant experimental facts in this direction were apparent already by 1990: (i) the presence of doped holes on in-plane oxygens, which suggests dynamical symmetry-breaking around O sites [12], (ii) the anomalous mid-zone phonon dispersion along the $(\xi, 0, 0)$ direction in the Brillouin zone reported originally by Reichardt and Pintschovius at the APS March meeting in 1990, and later explored in more detail by McQueeney et al. [13] and Reznik et al. [14], and (iii) the evidence for broken inversion symmetry from pyroelectricity [15], (iv) a polaronic signature in the mid-infrared [16] accompanied by symmetry-breaking local modes [17] and (v) the possible presence of broken-symmetry pairs above T_c from early A_{1g}-symmetry Raman experiments on $YBa_2Cu_3O_{6.9}$ [18]. (This A_{1g} scattering was later confirmed as anomalous and unexplained within standard superconductivity theories [19]). These essential data on carrier localization and symmetry breaking led to the proposal of a new paradigm for the presence of localized polarons co-existing with itinerant fermions [20–22]. Mihailovic and Müller [23] in their review explicitly highlighted the simultaneous presence of (bosonic) bipolarons and itinerant fermions in stripes, as well as the essential role of a long-range Coulomb interaction. Remarkably, the possible coexistence of localized (polarons) and itinerant states in cuprates was discussed on theoretical grounds in the early paper on by Gork'ov and Sokol [24]. Important data in the development of the inter-site model came from ESR [25, 26], X-ray absorption fine structure [27] and magnetic susceptibility measurements as often discussed by Alex Müller [28]. A specific proposal of symmetry-based inter-site interaction soon followed thereafter [1, 2].

The formal formulation of the inter-site polaron model is based specifically on the observed symmetry-breaking in-plane Cu–O phonon anomalies observed in inelastic neutron scattering experiments which I proposed at the time to be a direct consequence of pair formation [1]. Later Monte-Carlo simulations of the inter-site pairing model [3, 29] predicted inter-site pair density which follows T_c, rather than being proportional to doping. The model calculation also made the prediction that with increasing doping the metallicity systematically increases with the formation of ever larger itinerant clusters. These predictions have now been apparently confirmed by two decisive experiments which we discuss below.

The importance of percolation appeared in the original "discovery" paper by Bednorz and Müller perhaps in the context of enhanced T_cs in granular aluminium,

which was of interest at the time. Modifying the percolation idea to one of phase coherence percolation (PCP) between inter-site pairs [4], leads to a simple quantitative prediction of the upper limit of T_c for superconductivity, with the pairing energy and pair size as the only parameters, which we will show below in the context of inter-site pairing.

This research direction was very much outside the box (or "tent") of the mainstream of electronic mechanisms which were probably motivated by the report of the absence of an isotope effect in optimally doped $YBa_2Cu_3O_7$ and $EuBa_2Cu_3O_7$ by Battlogg early in 1987 [30]. Later, with extensive and careful isotope effect measurements this result at optimum doping was found to be correct [31], but anomalous. Moreover, it was shown to be consistent with the polaron picture [31].

In this paper, I first summarize the model's main predictions, highlight new and remarkable experimental confirmations of inter-site pairing and then discuss predictions of carrier localization, pair-formation and superconductivity from the viewpoint of recent time-domain experiments.

The Predictions of the JT-C Model

The JT-like interaction responsible for the formation of inter-site pairs was formulated by Kabanov and Mihailovic in 2000 [1, 32, 33], which described the pairing interaction of a single polaron on the CuO_2 plane, taking into account that stretching along one direction necessarily means contraction along the other (Fig. 16.1). This

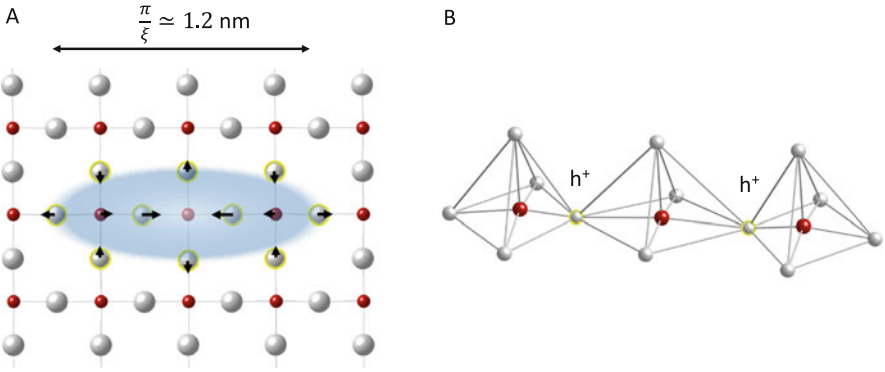

Fig. 16.1 The inter-site (bi)polaron on a CuO_2 plane. (**a**) Its size is defined by the wavevector of the inelastic neutron scattering anomaly $(\xi, 0, 0)$, where $\frac{\pi}{\xi} \simeq 1.2$ nm as shown. The corresponding displacements of the Cu–O mode have different magnitude and phase on different lattice sites, as indicated schematically by arrows. Their intersite pair symmetry must conform to compatibility conditions [29], which means that while the inter-site pair breaks fourfold rotational symmetry of the tetragonal lattice leading to a Jahn-Teller-like symmetry breaking, the lattice must also experience smaller displacements of other surrounding ions as shown exaggerated in (**b**) for the $YBa_2Cu_3O_7$ structure.

is formally expressed in terms of St. Venan's strain compatibility equations [1, 3, 29, 34]. These considerations give an interaction with a Jahn-Teller-like term, in the sense that two (degenerate) configurations are possible in the ground state along x and y axes respectively. Extending the model to multiple polarons, and thus including an essential long range Coulomb repulsion term, the JT-C Hamiltonian is given by [3, 29, 35]:

$$H_{JT-C} = \sum_{i,j} -V_{JT}(i-j)S_i^z S_j^z + \sum_{i,j} V_C(i-j)Q_i Q_j$$

where V_{JT} is the strain coupling with the lattice and $V_C = \frac{e^2}{\epsilon_0 am}$ is the long-range Coulomb interaction in which ϵ is the static electric constant, e is the elementary charge, a is the lattice constant. $S^z = \pm 1,\ 0$ are the pseudospin operators, and $Q_i = (S_i^z)^2$. The application of compatibility conditions ensures that other surrounding bonds must also deform slightly. Although the Cu–O in-plane bond stretch is the dominant displacement, other bonds also change, as indicated schematically in Fig. 16.1b). Thus fourfold symmetry breaking is dominant, but the accompanying displacements mean that the local symmetry is much lower, perhaps as low as C_1, in which case all excitations associated with pair formation are reduced to the totally symmetric representation. Experimentally this means that A symmetry excitations are dominant, accompanied with "nematicity" (i.e. loss of fourfold symmetry), while B_{1g} and B_{2g}-like excitations appear as remnants of the underlying tetragonal symmetry. An additional effect is the loss of inversion symmetry, which has been observed experimentally [15].

Quantitative predictions of the polaron ordering were made with a Monte-Carlo simulation of the JT-C Hamiltonian by performed by Mertelj et al. [3, 29] (see also contribution by Kabanov in this volume). The main results of the model are summarized in Fig. 16.2. The model predicts polaron aggregation into pairs and stripes driven by the interplay of attractive strain and repulsive Coulomb interaction. Remarkably, pairs are seen to be present over a range of doping which coincides with the superconducting region of the cuprate phase diagram. Single polarons appear quite distinct localized states at low doping, and are dominant in the "pseudogap" state, persisting into the non-superconducting part of the phase diagram. Their localization is observed in time-resolved optical experiments. Stripes and larger aggregates appear at higher doping levels and dominate on the overdoped side of the phase diagram, naturally explaining the origin of the two components observed experimentally. The fermions within stripes give rise to band-like behavior, increasing metallic conductivity, the development of a Fermi surface and the appearance of quantum oscillations at low temperature.

It is worth pointing out that in the JT-C model, the lattice strain plays a major role in determining the pair phase diagram shown in Fig. 16.2. The pairing energy scale V_{JT} depends on the local deformation potential for the Cu–O bond. A systematic measurement of the electron-lattice strain coupling relaxation rate of many superconductors with ultrafast spectroscopy shows a direct linear relation

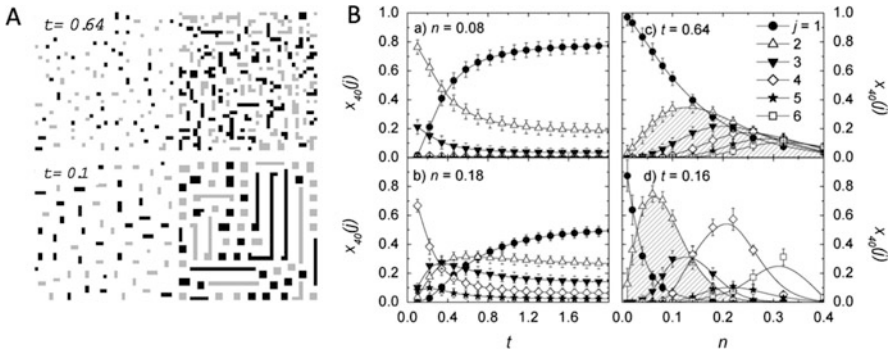

Fig. 16.2 (**a**) Aggregation of localized polarons into bipolarons and stripes from [29] calculated using a Monte-Carlo simulation for two densities (underdoped, n = 0.08 and overdoped with n = 0.26) at two different temperatures (t = 0.64 and t = 0.1 in units of V_{JT}). The interaction parameters are given in [3]. Each square corresponds to a polaron. The *light square* and *dark squares* correspond to symmetry breaking along x or y axes respectively. The similarity with scanning tunnelling microscopy real-space images [49] is striking. (**b**) the particle count *x(j)* as a function of temperature *t* and doping level *n* of single polarons ($j = 1$), pairs ($j = 2$), three-polaron clusters ($j = 3$) etc. from the JT-C model using the same parameters shown in panel A. The pair density is shown shaded. Note that single polarons are dominant in the underdoped region. Remarkably, the pair density shows a dome-like dependence on doping (The lines are a guide to the eye)

between strain and electron-phonon coupling [36] λ_{ep}. However, the maximum T_c achievable in different compounds depends non-monotonically on the strain or λ_{ep}. The empirical fact is that there is an optimum Cu–O bond length which maximizes the pairing susceptibility near $a_{opt.} \simeq 1.92$ Å, showing that λ_{ep} alone cannot control T_c. It is inherent in the JT-C model that the competition between the local strain caused by the carriers' presence and inter-site Coulomb repulsion between inter-site carriers which governs the phase diagram, pair density and T_c. Decreasing the Cu–O distance increases λ_{ep}, but also increases Coulomb repulsion, leading to a non-monotonic dependence of T_c on the Cu–O bond length [37]. This phenomenon has escaped understanding till now.

With real space bosonic singlet inter-site pairs, we proposed that superconductivity arises through phase coherence percolation between them [4]. According to the phase diagram in Fig. 16.2, on the underdoped side the percolation threshold at T_c corresponds to superconductor-insulator-superconductor (SIS) tunneling, while on the overdoped side, the threshold corresponds to SNS tunneling through metallic regions. In Fig. 16.3 we show the calculated T_c as a function of doping, based on the Monte-Carlo calculation results such as shown in Fig. 16.2. To obtain the data in the plot, I used the Monte-Carlo simulations performed by Mertelj for different temperatures at different doping levels (see Fig. 7 in [29]), and then counted the number of pairs in each point on the phase diagram. Figure 16.3 shows the number of pairs (in colour scale) as a function of temperature and doping. The T_c line (indicated in Fig. 16.3) corresponds to the calculated threshold reached at the volume fraction

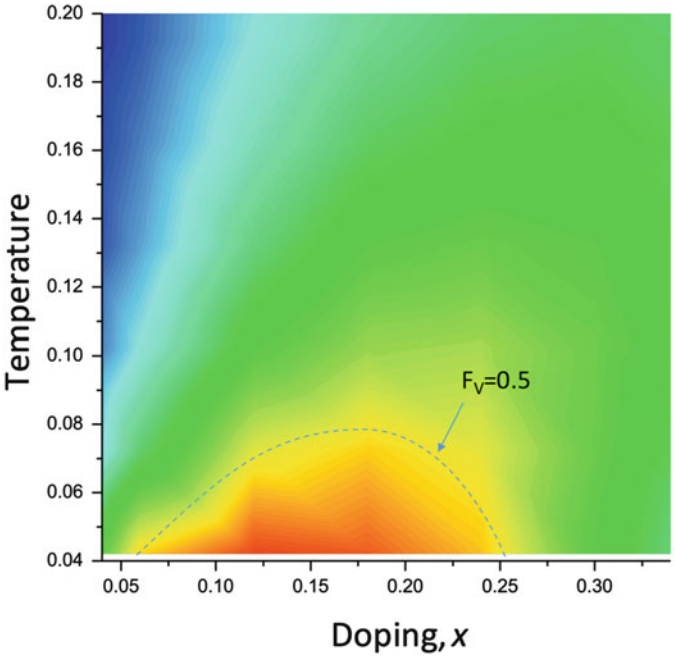

Fig. 16.3 Pair density n_{pairs} as a function of temperature and the critical temperature based on phase coherence percolation calculated from the Monte-Carlo calculation of n_{pairs}. The dashed line represents the T_c when phase coherence percolation threshold is reached in two dimensions, i.e. the volume fraction of pairs $F_v = 0.5$

appropriate for 2D pair percolation [4] showing the ubiquitous dome-like T_c curve as a function of doping.

New Experimental Evidence

The Doping Dependence of Superfluid Density A very important new systematic experimental result by Bozovic et al. [5] building on the original Uemura plot [38] substantially changed the perception of theory in the HTS field [39]. A measurement of penetration depth as a function of doping in a very large number of $La_{2-x}Sr_xCuO_4$ samples establishes that T_c scales linearly with the phase stiffness ρ_{s0} in the limit $T \to 0$ limit, which is proportional to the superfluid density n_s via $\rho_{s0} = \frac{\hbar^2}{4k_B}\left(\frac{n_s}{m^*}\right)$, as shown in Fig. 16.4. This means that the pair density (which we equate with n_s) is proportional to T_c throughout the entire phase diagram. This result is incompatible with the prediction of the majority of models of HTS so far, including BCS, as noted by Zaanen [39]. On the other hand, the observed dependence of T_c on pair density naturally arises within the JT-C model as illustrated in

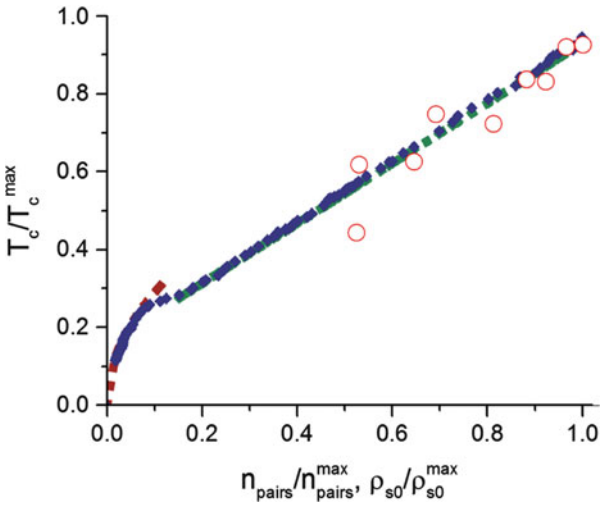

Fig. 16.4 The experimental relation between T_c and superfluid density ρ_{s0} from penetration depth measurements [5] (*black* and *green symbols*), and the predicted relation of T_c versus the number of pairs n_{pairs} calculated on the basis of a model of percolation [4] between inter-site bipolarons [29] (*open circles*) from the data in Fig. 16.3

Figs. 16.2 and 16.3. Comparing the calculated T_c on the basis of the JT-C model (Fig. 16.3) as a function of doping with the experimental data on the superfluid density, one obtains remarkable agreement. The JT-C model thus naturally explains why ρ_s decreases on the overdoped side, while the normal state conductivity (metallicity) keeps increasing with increasing doping.

Thus, combining this result of Bozovic et al. [5] with the large body of literature discussing the Fermi-liquid like properties from systematics of the transport in the normal state, and convincing data on low-temperature quantum oscillations on both sides of optimum doping [40, 41], one arrives at the conclusion that the carriers which exhibit the Fermi liquid behaviour are not the ones that give rise to superconductivity. Instead, as the JT-C model predicts that they are continuously exchanged with the carriers in pairs through fluctuations. The importance of these fluctuations in the critical region at the onset of superconductivity was recently discussed from a time-dynamics point of view by Madan et al. [42].

The Doping Dependence of the Neutron Anomaly New data by Reznik and co-workers [6] lend further support to the idea that the neutron anomaly (i.e. the anomalous phonon linewidths along $(\xi, 0, 0)$ and $(0, \xi, 0)$) is related to pairing. They report that the width of the anomalous in-plane "half-breathing mode" follows T_c and shows a similar dependence on doping as n_{pairs} and ρ_{s0}, as shown in Fig. 16.5. The position of the anomaly at $\xi = 0.25 \sim 0.3$ reciprocal lattice units (r.l.u.) in the Brillouin zone along the bond axes is proposed to be associated with the ionic displacements resulting from pairing of two holes on opposite sides of a Cu ion (Fig. 16.1). The JT-C model predicts that the linewidth will follow n_{pairs} and the

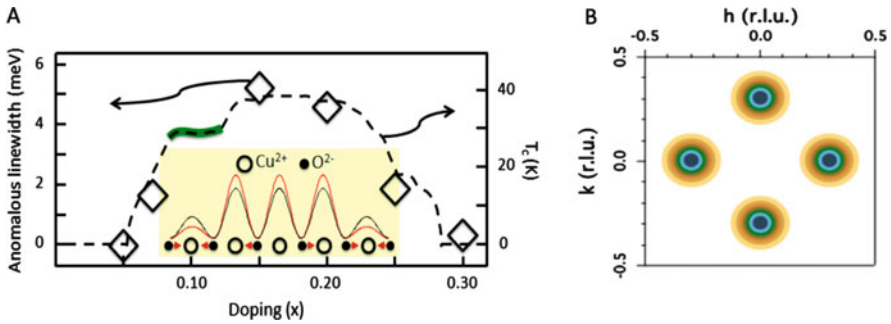

Fig. 16.5 (**a**) The doping dependence of the anomalous Cu–O vibration linewidth [6]. (**b**) The position in the Brillouin zone where the anomaly is observed corresponds to the JT-C model. $(\xi, 0, 0)$ and $(0, \xi, 0)$ with $\xi \sim 1/4$ in r.l.u.

anomaly will vanish if there are no pairs present. While first principles modelling of the lattice dynamics associated with the inter-site pairing fluctuations, single polarons and clusters (stripes) is computationally challenging, and has yet to be performed, we can make some qualitative statements on the basis of the existing model. The lattice distortion of single polarons will not show this particular anomaly at $\xi \simeq 1/4$ r.l.u., which will disappear at low doping. On the overdoped side, bigger fermionic aggregates (stripes or clusters) will change the q-vector of the Cu–O mode and introduce other modes with other displacements, washing out the signature of pairing. The presence of the Cu–O anomaly at this particular $q-$vector is thus specific to pair formation. The authors [6] discuss in detail other possible explanations and note that other existing theories of HTS do not give any satisfactory explanation for the observed anomaly, and particularly its doping and q-dependence.

Evidence for Distinct Single Polaron Localization and Pseudogap Formation A time-domain investigation of the relaxation timescales of the different excitations (polarons, pseudogap excitations, superconducting quasiparticles) shows that they can be distinguished on the basis of symmetry, and temperature dependence in optical pump probe experiments. Recent experiments show rotational symmetry breaking associated with the pseudogap and superconducting gap are both dominantly A_{1g} symmetry, but contain admixtures of B_{1g} and B_{2g} components respectively [43], which help in identifying them by symmetry. The observed symmetry breaking associated with pairing [43, 44] is in full agreement with the JT-C model's predictions mentioned earlier. Experiments using multiple pulses which were specially designed to reveal the relaxation timescales of different excitations show a rather unexpected result that single carrier localization (single polarons) in BiSCO takes place in $\tau_{polaron} \sim 250\ fs$, while the PG state recovery time (suggested to be associated with pairing) is nearly 3 times longer, $\tau_{pseudogap} \sim 600\ fs$ [44]. Such distinct behavior can be attributed to single particle localization, pairing and aggregation dynamics respectively and may

also be seen in the JT-C model predictions [3, 29], as discussed above and summarized in Fig. 16.2. In contrast, the superconductivity (with an accompanying B_{2g} symmetry signature) is established with a timescale of $\tau_{sc} = 3 \sim 5\ ps$ [45]. The superconductivity appears from fluctuations on the same timescale as the quasiparticle recombination lifetime τ_{QP}, which implies that the recovery is governed by Rothwarf-Taylor bottleneck dynamics [46]. The temperature dependence of the single particle excitations and pairs by time-resolved spectroscopy is also important [42]. Experiments show that the latter, associated with superconducting fluctuations are present at temperatures up to $\sim 1.3\ T_c$.

An important fundamental issue in time-domain is to consider whether the pairs live for long enough for phase coherence to be established. Comparing the measured lifetimes for the pairing ($\tau_{PG} \sim 600\ fs$) with the Josephson time ($\tau_J \sim 300 fs$), which characterizes the phase coherence timescale, we see that this condition clearly is fulfilled in $Bi_2Sr_2CaCu_2O_8$ [42].

Discussion

The JT-C model extends the basic ideas of Mott physics with the addition of a long-range Coulomb repulsion, and explicit consideration of the symmetry breaking effect of localized bipolarons indicated experimentally by various observations. This important difference leads to specific symmetry-breaking phenomena and the simultaneous presence of localized carriers (single polarons and bipolarons) and itinerant fermions. Within this model, the spin degrees of freedom are of secondary importance, as the AF order is destroyed by doping very quickly, and only fluctuations remain. The experimental fact that singlet pairing is observed means that the inter-site pairs have $S = 0$, in agreement with ESR experiments [25]. The strain effectively has d-wave symmetry, just as the more commonly considered B_{1g} zone-boundary e-p interaction. But there is a crucial difference, the JT-C interaction is centered mid-zone near $q = (1/4, 0, 0)$ r.l.u., not at the zone boundary.

The two-component paradigm of coexisting itinerant and localized states has recently been applied also to other systems [47], theoretically discussing the coexistence of excited polarons and metastable itinerant states in photoexcited metals. Under conditions when the characteristic phonon mode frequency is smaller than the electron hopping, a semiclassical argument predicts an energy barrier between delocalized and localized states [48]. The 2-component paradigm experimentally expounded and theoretically developed for the cuprates thus appears to be of wider interest. The mechanism may also be relevant in pnictide superconductors, where a similar non-monotonic variation of T_c on bond angle implies an interplay of lattice strain and inter-site Coulomb repulsion leading to an optimum inter-particle distance for pairing. In principle, it should be expected to be relevant for any superconductor whose coherence length is comparable to the unit cell size, the Sulphur hydrides being an obvious case. As superconducting T_cs gradually approach room temperature, and coherence lengths become ever shorter, the

physics introduced by the JT-C model may serve as a guide to understanding pairing in such materials.

A final remark is in order, regarding the overwhelming importance of the Coulomb interaction, as emphasized by P.W. Anderson. In some sense pairing and stripe formation within the JT-C model is indeed driven by Coulomb repulsion. Without it, polarons would phase separate, preventing pairing. However, it is clear that the simple Hubbard model with only on-site Coulomb repulsion does not capture the essential physics.

Concluding Remarks

Ultimately, a useful superconductivity theory is one which demonstrates predictive power, not only regarding T_c, but makes unexpected and non-trivial predictions in advance of experiments. The linear relation between pair density and T_c, and anomalous behavior of the inelastic neutron scattering finite wavevector phonon anomaly were such predictions by the JT-Coulomb model and were not generally expected on the basis of more common models at the time, particularly the Hubbard model or the $t-J$ model. While the majority of the popular opinion is that *somehow* the Hubbard model should describe the physics of HTS, these new observations are clearly outside its scope. Specifically, as pointed out by Zaanen [39], the dependence of T_c on superfluid density is outside the Hubbard model's predictions as well as other currently popular models, with the exception of inter-site pairing.

At a very memorable private dinner in Geneva at the occasion of the M2S meeting in 2015, Alex Müller remarked that in his opinion HTS was essentially solved with intersite polarons. To my complaint some time ago that the JT-C model did not have very wide acceptance, he commented that a good theory is like a deposit in the bank: experimental proof would come at some time in the future, sooner or later. The persistent development of the inter-site model against significant opposition by the mainstream HTS community and journal editors would not have been possible without numerous discussions and persistent encouragement by K. Alex Müller.

Acknowledgments The original work reviewed here was performed in close collaboration with Viktor V. Kabanov, and in the case of MC simulations, with Tomaž Mertelj and Joaquin Miranda-Mena.

References

1. D. Mihailovic, V.V. Kabanov, Finite wave vector Jahn-Teller pairing and superconductivity in the cuprates. Phys. Rev. B **63**, 054505 (2001)
2. V.V. Kabanov, D. Mihailovic, Manifestations of mesoscopic Jahn-Teller real-space pairing and clustering in $YBa_2Cu_3O_{7-delta}$. Phys. Rev. B **65**, 212508 (2002)

3. T. Mertelj, V. Kabanov, D. Mihailovic, Charged particles on a two-dimensional lattice subject to anisotropic Jahn-Teller interactions. Phys. Rev. Lett. **94**, 147003 (2005)
4. D. Mihailovic, V. Kabanov, K. Muller, The attainable superconducting T-c in a model of phase coherence by percolating. Europhys. Lett. **57**, 254–259 (2002)
5. I. Bozovic, X. He, J. Wu, A.T. Bollinger, Dependence of the critical temperature in overdoped copper oxides on superfluid density. Nature **536**, 309–311 (2016)
6. S.R. Park et al., Evidence for a charge collective mode associated with superconductivity in copper oxides from neutron and x-ray scattering measurements of $La_{2-x}Sr_xCuO_4$. PRB **89**, 020506 (2014)
7. J.G. Bednorz, K.A. Müller, Possible high Tc superconductivity in the Ba−La−Cu−O system. Z. Phys. B Condens. Matter **64**, 189–193 (1986)
8. K.H. Hock, H. Nickisch, H. Thomas, Jahn Teller effect in itinerant electron systems – The Jahn-Teller polaron. Helv. Phys. Acta. **56**, 237–243 (1983)
9. A.S. Alexandrov, Bose–Einstein condensation of strongly correlated electrons and phonons in cuprate superconductors. J. Phys. Condens. Matter **19**, 125216 (2007)
10. A.S. Alexandrov, N.F. Mott, Bipolarons. Rep. Prog. Phys. **57**, 1197–1288 (1994)
11. A. Alexandrov, New theory of strong-coupling superconductors and high-temperature superconductivity of metallic oxides. Phys. Rev. B **38**, 925–927 (1988)
12. N. Nücker, J. Fink, J. Fuggle, P. Durham, W. Temmerman, Evidence for holes on oxygen sites in the high-Tc superconductors $La_{2-x}Sr_xCuO_4$ and $YBa_2Cu_3O_{7-y}$. Phys. Rev. B **37**, 5158–5163 (1988)
13. R.J. McQueeney et al., Anomalous dispersion of LO phonons in $La_{1.85}Sr_{0.15}CuO_4$ at low temperatures. PRL **82**, 628–631 (1999)
14. D. Reznik et al., Electron–phonon coupling reflecting dynamic charge inhomogeneity in copper oxide superconductors. Nature **440**, 1170–1173 (2006)
15. D. Mihailovic, A. Heeger, Pyroelectric and piezoelectric effects in single crystal of $YBa_2Cu_3O_{7-\delta}$. Solid State Commun. **75**, 319–323 (1990)
16. D. Mihailovic et al., Application of the polaron-transport theory to sigma (omega) in $Tl_2Ba_2Ca_{1-x}Gd_xCu_2O_8$, $YBa_2Cu_3O_{7-d}$, and $La_{2-x}Sr_xCuO_4$. Phys. Rev. B **42**, 7989–7993 (1990)
17. D. Mihailovic, C. Foster, K. VOSS, T. Mertelj, Anomalous shifts of oxygen-mode frequencies in $La_{2-x}Sr_xCuO_4$, $YBa_2Cu_3O_{7-\delta}$ and $Tl_2Ba_2Ca_{1-x}Gd_xCu_2O_8$ studied by photoinduced infrared absorption and Raman spectroscopy. Phys. Rev. B **44**, 237–241 (1991)
18. D. Mihailovic, M. Zgonik, M. Copic, M. Hrovat, Quasiparticle excitations in the superconducting state observed in light scattering. Phys. Rev. B **36**, 3997 (1987)
19. T.P. Devereaux, R. Hackl, Inelastic light scattering from correlated electrons. Rev. Mod. Phys. **79**, 175 (2007)
20. D. Mihailovic, C. Stevens, B. Podobnik, J. Demsar, Evidence for two-component superconductivity in the femtosecond optical and transient photoconducting …. Physica C **282–287**, 186–189 (1997)
21. C. Stevens, D. Smith, C. Chen, J. Ryan, B. Podobnik, Evidence for two-component high-temperature superconductivity in the femtosecond optical response of …. Phys. Rev. Lett. **78**, 2212 (1997)
22. T. Mertelj, J. Demsar, B. Podobnik, I. Poberaj, D. Mihailovic, Photoexcited carrier relaxation in YBaCuO by picosecond resonant Raman spectroscopy. Phys. Rev. B **55**, 6061–6069 (1997)
23. D. Mihailovic, K.A. Müller, *High-Tc Superconductivity 1996: Ten Years After the Discovery* (Springer, Netherlands, 1997), pp. 243–256. doi:10.1007/978-94-011-5554-0_10
24. L. Gorkov, A. Sokol, Phase stratification of an electron liquid in the new superconductors. JETP Lett. **46**, 420–423 (1987)
25. K. Müller, A. The, Impact of ESR (EPR) on the understanding of the cuprates and their superconductivity. EPR Newsl. **22**, 5–6 (2012)
26. B. Kochelaev, J. Sichelschmidt, B. Elschner, W. Lemor, Intrinsic EPR in $La_{2-x}Sr_xCuO_4$: manifestation of three-spin polarons. Phys. Rev. Lett. **79**, 4274 (1997)

27. A. Bianconi, N.L. Saini, A. Lanzara, M. Missori, Determination of the local lattice distortions in the CuO_2 plane of $La_{1.85}Sr_{0.15}CuO_4$. Phys. Rev. Lett. **76**, 3412–3415 (1996)
28. K.A. Müller, G.-M. Zhao, K. Conder, H. Keller, The ratio of small polarons to free carriers in $La_{2-x}Sr_xCuO_4$ derived from susceptibility measurements. J. Phys. Condens. Matter **10**, L291–L296 (1998)
29. T. Mertelj, V.V. Kabanov, J.M. Mena, D. Mihailovic, Self-organization of charged particles on a two-dimensional lattice subject to anisotropic Jahn-Teller-type interaction and three-dimensional Coulomb repulsion. Phys. Rev. B **76**, 9 (2007)
30. B. Batlogg et al., Isotope effect in the high-Tc superconductors $Ba_2YCu_3O_7$ and $Ba_2EuCu_3O_7$. PRL **58**, 2333–2336 (1987)
31. A. Bussmann-Holder, H. Keller, Unconventional isotope effects, multi-component superconductivity and polaron formation in high temperature cuprate superconductors. J. Phys. Conf. Ser. **108**, 012019 (2008)
32. A.V. Boris et al., Josephson plasma resonance and phonon anomalies in trilayer $Bi_2Sr_2Ca_2Cu_3O_{10}$. PRL **89**, 277001 (2002)
33. V.V. Kabanov, D. Mihailovic, Finite-wave-vector phonon coupling to degenerate electronic states in $La_{2-x}Sr_xCuO_4$. J. Supercond. **13**, 959–962 (2000)
34. T. Lookman, S.R. Shenoy, K.Ø. Rasmussen, A. Saxena, A.R. Bishop, Ferroelastic dynamics and strain compatibility. Phys. Rev. B **67**, 024114 (2003)
35. V.V. Kabanov, T. Mertelj, D. Mihailovic, Mesoscopic phase separation in the model with competing Jahn-Teller and Coulomb interaction. J. Supercond. Nov. Magn. **19**, 67–71 (2006)
36. C. Gadermaier et al., Strain-induced enhancement of the electron energy relaxation in strongly correlated superconductors. Phys. Rev. X **4**, 011056 (2014)
37. C.N.R. Rao, A.K. Ganguli, Structure–property relationship in superconducting cuprates. Chem. Soc. Rev. **24**, 1–7 (1995)
38. Y. Uemura et al., Universal correlations between Tc and ns/m (carrier density over effective mass) in high-Tc cuprate superconductors. Phys. Rev. Lett. **62**, 2317–2320 (1989)
39. J. Zaanen, Condensed-matter physics: Superconducting electrons go missing. Nature **536**, 282–283 (2016)
40. S. Nakamae et al., Electronic ground state of heavily overdoped nonsuperconducting $La_{2-x}Sr_xCuO_4$. Phys. Rev. B **68**, 4 (2003)
41. S. Badoux et al., Universal quantum oscillations in the underdoped cuprate superconductors. Nat. Phys. **9**, 761–764 (2013)
42. I. Madan et al., Separating pairing from quantum phase coherence dynamics above the superconducting transition by femtosecond spectroscopy. Sci. Rep. **4**, 5656 (2014)
43. Y. Toda et al., Rotational symmetry breaking in Bi2212 probed by polarized femtosecond spectroscopy. Phys. Rev. B **90**, 094513 (2014)
44. I. Madan et al., Evidence for carrier localization in the pseudogap state of cuprate superconductors from coherent quench experiments. Nat. Commun. **6**, 6958 (2015)
45. I. Madan et al., Real-time measurement of the emergence of superconducting order in a high-temperature superconductor. Phys. Rev. B **93**, 224520–224528 (2016)
46. V.V. Kabanov, D. Mihailovic, Kinetics of a superconductor excited with a femtosecond optical pulse. PRL **95**, 147002 (2005)
47. S. Sayyad, M. Eckstein, Coexistence of excited polarons and metastable delocalized states in photoinduced metals. PRB **91**, 104301 (2015)
48. V.V. Kabanov, O.Y. Mashtakov, Electron localization with and without barrier formation. Phys. Rev. B **47**, 6060–6064 (1993)
49. J.E. Hoffman et al., Imaging quasiparticle interference in Bi2Sr2CaCu2O8+d. Science **297**, 1148–1151 (2002)

Chapter 17
Dynamical Lattice Distortions in High-Tc Cuprate Superconductors

Jose Mustre de León

Introduction

The discovery of high temperature superconductivity by G. Bednorz and K.A. Müller in 1986, guided by the Jahn-Teller polaron model as a means to increase Tc [1], initiated a new era in the study of materials in which the electronic degrees of freedom and the lattice are strongly correlated. Besides the breakthrough in achieving high temperature superconductivity, this discovery lead to a change in paradigms of both experimental techniques and theoretical frameworks as these materials exhibit intrinsic inhomogeneity at the nanoscale level, dynamical local lattice distortions, non-conventional electronic ground states and excitation spectra. It has been necessary to understand experimental signatures of intrinsically dynamically inhomogeneous systems, and also to develop theoretical tools which go beyond the description of homogeneous ordered systems. Here, we address the experimental signatures of local structural distortions that appear in the inhomogeneous systems. We will not discuss other relevant aspects, related to the polaronic origin of these distortions, as the anomalous isotopic coefficients of their excitation spectrum or their role in the pairing mechanism, as they have been discussed by other authors (see *e.g.*, [2, 3], two component models [4–7]). However, an overview of the evidence for the ubiquitous presence of these distortions in high-Tc superconductor cuprates and understanding of the proper way to probe their dynamical nature is important.

J. Mustre de León (✉)
Departamento de Física Aplicada, Cinvestav-Mérida, Carretera Antigua a Progreso Km. 6.5, A.P. 73, 97310 Merida, Yucatan, Mexico

Cinvestav-Zacatenco, Av. IPN 2508, 07000 Cd. De México, Mexico
e-mail: jmustre@me.com

A. Bussmann-Holder et al. (eds.), *High-Tc Copper Oxide Superconductors and Related Novel Materials*, Springer Series in Materials Science 255,
DOI 10.1007/978-3-319-52675-1_17

The parent compounds of cuprate superconductors form ordered crystalline structures and exhibit antiferromagnetic order at low temperatures. However, in compounds like $La_{1.85}Sr_{0.15}CuO_4$ and $La_2CuO_{4.1}$, the dopant atoms necessary to achieve a superconducting compound are not placed at the crystal symmetry allowed sites yielding to intrinsically structurally inhomogeneous systems [8]. While in other cases, like $YBCO_{6+\delta}$, extra dopant atoms reside in crystal symmetric positions but the departure from stoichiometry yields compositional disorder [9, 10] with the same consequence. In these systems the crystalline translational symmetry is broken. Consequently theoretical models which assume a perfect crystalline order are at least not formally valid. Although from this structural inhomogeneity does not necessarily follow an inhomogeneous electronic ground state, for some regions of the phase diagram, depending on the dopant concentration, such state is realized. This region of phase space has been identified as the pseudogap phase [11–13]. An important consideration is that, although the dopant atoms are at fixed positions, the structural inhomogeneity has a dynamical character [14, 15] and it is present even in compounds with perfect crystallographic symmetry like $HoBa_2Cu_4O_8$ [16]. In addition to the breaking of the crystalline translational symmetry the pseudogap phase exhibits other broken symmetries. Time-reversal symmetry breaking was found using angular resolved photoemission spectroscopy with circularly polarized photons in $Bi_2Sr_2CaCu\$\_2O_{8+\delta}$ [17]. It has also been found, by x-ray absorption spectroscopy, that the crystalline group symmetry is locally broken in $La_{1.85}Sr_{0.15}CuO_4$, with alternating regions of tetragonal and orthorhombic symmetry [7]. A perspective of the observation of broken symmetries in high-Tc superconductors, emphasizing that some of these broken symmetries are hidden from common observational techniques, has been discussed in [18]. The clues provided by these broken symmetries yield a precise understanding of the ground state in this pseudogap phase, its elementary excitations and the appearance of superconductivity at temperatures below the onset of the pseudogap phase. Here, we concentrate on the observation of local lattice distortions, which yield the dynamical structural inhomogeneity, resulting in the broken crystal translational symmetry, and its interpretation in terms of bipolaronic excitations in the pseudogap phase.

Dynamical Local Lattice Distortions

Early determinations of the crystal structure of cuprates by diffraction methods did not show significant distortions associated with either in-plane oxygen atoms or apical oxygen atoms [19, 20]. Moreover, the determination of average bond lengths in diffraction has a precision of about 0.001 Å [21], significantly higher than the precision in bond length determination that local probes, like extended x-ray absorption fine structure spectroscopy (EXAFS) can achieve [22]. For this reason,

early reports of local lattice distortions related to the oxygen atoms were not accepted by the diffraction community (see e.g. [23, 24]).

One of the first observations of a local lattice distortion in cuprates was the report of a two-site distribution for the Cu(1)-apical oxygen in $YBa_2Cu_3O_7$ appearing at temperatures above the superconducting transition temperature, Tc, using Cu K-edge EXAFS [25, 26]. This distribution showed two sites separated by approximately 0.11 Å that changed into a single site distribution in the vicinity of the superconducting transition temperature. These measurements were carried out using polarized x-rays on magnetically oriented powders, an improvement in the technique which allowed to isolate the Cu(1)-axial oxygen [O(4)] (see Fig. 17.1) signal with an increased sensitivity not achievable for the Cu-O EXAFS signal in other cuprates (see below). This result was received with skepticism, based on earlier diffraction results [19, 20, 27] and optical spectroscopy [28]. However, it was later confirmed by EXAFS measurements in other oriented samples [29, 30], single crystals [31], and also found in $YBa_2Cu_3O_{6.7}$, $YBa_2Cu_3O_{6.5}$ and Co doped $YBa_2Cu_3O_7$ [32]. The explanation of the discrepancies between these results with diffraction and optical spectroscopical results lead us to propose the origin of this Cu(1)–O(4) distribution as a dynamical distortion of polaronic origin [33]. Hence, we concluded that given the dynamical character of the distortion it could not be directly observed with elastic scattering techniques, such as diffraction [34].

Similar two site distributions obtained from EXAFS spectra were also found for the Cu(2)–O(4) distribution in $Bi_2Sr_2CaCu_2O_8$ [35] and in $TlBa_2Ca_3Cu_4O_{11}$ [36] starting at temperatures above Tc. It is important to remark that in these compounds (and other cuprates) the average Cu(2)–O(4) bond length lies between 2.49 and 2.73 Å, which is much longer than the Cu(1)–O(4) bond length in $YBa_2Cu_3O_7$ (1.87 Å). This fact makes more difficult the identification of details of the O (4) distribution due to the stronger mixing of the Cu(2)–O(4) EXAFS signal with those of other atoms and the increased zero point motion of the O(4) atom due to weaker Cu(2)–O(4) bond compared with the Cu(1)–O(4) bond. For this reason in most EXAFS studies addressing the O(4) motion a Gaussian *single site* broadened distribution has been used, reporting only changes in the width of the distribution as a function of temperature [37–39].

In plane Cu(2)–O local lattice distortions were identified in $La_{1.85}Sr_{0.15}CuO_4$ appearing below 100 K, [15, 38], in $TlBa_2CuO_6$ below 120 K [40] and in $La_2CuO_{4.1}$ below 150 K [41, 42]. In this case the observation of such distortions in $YBa_2Cu_3O_7$ and related compounds becomes more difficult due the similarity in Cu–O bond lengths in the Cu planes and Cu chains, whose contributions are mixed in the EXAFS signal [32, 40]. For this reason, it has been difficult to fully characterize the full local structure of polaronic objects, including both in and out of plane Cu–O bonds.

Up to now only in $La_{1.85}Sr_{0.15}CuO_4$ has been possible to identify local lattice distortions involving both in plane oxygen and apical oxygen atoms [15]. We also stress that from all these EXAFS experiments it is only possible to probe with enough detail the nearest neighbor environment around the Cu atoms, thus the

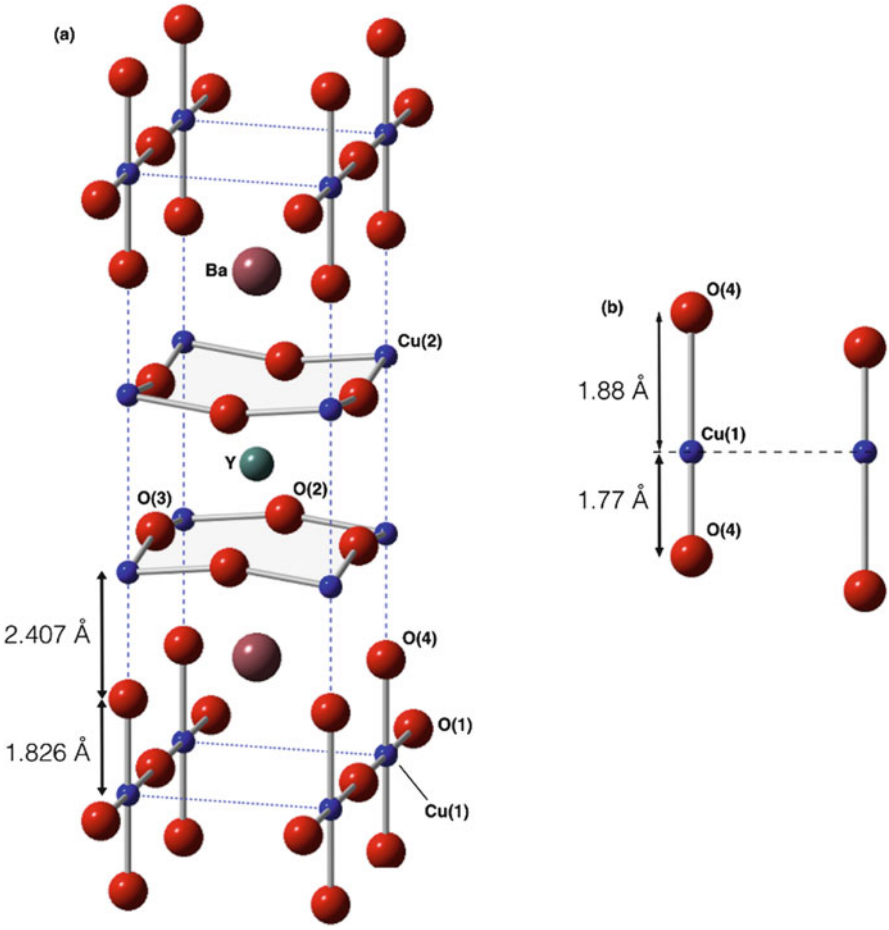

Fig. 17.1 (**a**) Crystal structure of $YBa_2Cu_3O_7$. The *dashed line* denotes de unit cell. (**b**) The two possible configurations in the O(4)–Cu(1)–O(4) cluster due to the split O–Cu bond distances (not to scale)

spatial extension of the distortions cannot be determined solely from these measurements. Additional structural information [43] is needed to formulate models about the extension of the distortions as discussed in [15]. However, it is expected that the full extension of the distortion varies between two and four lattice sites.

Pair distribution function (PDF) analysis of diffraction, x-ray and neutron inelastic scattering can provide additional information about the intermediate range (up to 10–15 Å) atomic structure, complementary to the information obtained from EXAFS [44]. PDF results in $La_{1-x}Sr_xCuO_4$ [45, 46] indicate that the atomic structure in this material is a combination of nanoscale regions with different local Cu–O environments, in agreement with the model proposed in [15]. A homogeneous structure only appears when dopant concentrations are above $x = 0.25$. In this

region the electronic behavior can be described in terms of free fermion quasiparticles, with electronic properties simpler that those found in the pseudogap phase.

To conclude, it is important to address the time scale of different probes, which allows the detection of dynamical distortions. The time scale of the EXAFS is such that dynamical distortions can be detected, which depending on the size of the distortion cannot be detected using elastic techniques like neutron diffraction [34]. This explains the differences between diffraction and EXAFS results. Indeed it has been shown that the two-site O (4) distribution in $Tl_2Ba_2CaCu_2O_8$ could be only detected in a pair distribution function obtained from neutron *inelastic* scattering but not with that obtained from neutron diffraction [47]. Consequently, it is important to take into account both the spatial resolution and time resolution of the techniques used to study the actual atomic structure of these materials [14]. Typical observation times of different spectroscopical techniques, used to probe local structure are for X-ray absorption spectroscopy: 10^{-15} sec, neutron scattering: 10^{-13} sec, nuclear quadrupole resonance (NQR) and Mössbauer spectroscopy: 10^{-9} sec, muon spin resonance (μSR): 10^{-6} sec. These differences in observation times explain why some of the results regarding the characterization of the distortions in cuprates, using different techniques are at variance.

Conclusions

We have presented an overview of the evidence for the existence of a dynamically lattice distortions, which imply an inhomogeneous ground state in the pseudogap region. In this state there are bipolaronic objects which form at a characteristic temperature T*. The manifestations of these objects in the lattice appear as dynamical local lattice distortions in regions in which the charge and lattice motions become correlated. The excitations of these bipolaronic objects exhibit different isotopic shifts depending on the nature of the excitation ranging from large negative to quasi-harmonic shifts [48]. These peculiar shifts are consistent with experimental observations and can explain discrepancies in values determined by different techniques, as they probe different excitations depending on the time and spatial resolution of the specific technique [48, 49]. The role in the pairing of free fermions of these bipolaronic excitations, and enhancement of Tc is not yet known. Some models have considered the interaction between fermionic *pairs* and bipolaronic bosonic objects [4–7] explaining several properties of the normal state in this pseudogap region and possible mechanisms of Tc enhancement due to exchange between bipolaronic objects and quasi-free fermions.

Acknowledgements I would like to thank A. Bishop for the introduction to the study of polaronic systems and the continuous collaboration in this subject for over two decades. I acknowledge the financial support of CONACYT-Mexico.

References

1. K.A. Müller, Nobel lecture: Perovskite-type oxides the new approach to high-Tc superconductivity. Nobelprize.org. Nobel Media AB (2014)
2. A.R. Bishop, A. Bussmann-Holder, O.V. Dolgov, A. Furrer, H. Kamimura, H. Keller, R. Khasanov, R.K. Kremer, D. Manske, K.A. Müller, A. Simon, Real and marginal isotope effects in cuprate superconductors. J. Supercond. Nov. Magn. **20**(5), 393–396 (2007). doi:10.1007/s10948-007-0235-6
3. A. Garcıa Saravia Ortız de Montellano, J. Mustre de Leon, Characterization of an electronic excitation on a PeierlsHubbard Hamiltonian for a small cluster, J. Supercond. Nov. Magn. **27** (4), 991–994 (2013). doi:10.1007/s10948-013-2424-9
4. Y. Bar-Yam, Two-component superconductivity. I. Introduction and phenomenology. Phys. Rev. B **43**(1), 359–377 (1991). doi:10.1103/PhysRevB.43.359
5. A. Bussmann-Holder, H. Keller, Polaron formation as origin of unconventional isotope effects in cuprate superconductors. Eur. Phys. J. B **44**(4), 487–490 (2005). doi:10.1140/epjb/e2005-00148-9
6. D. Mihailovic, V. Kabanov, Finite wave vector Jahn-Teller pairing and superconductivity in the cuprates. Phys. Rev. B **63**(5), 054505 (2001). doi:10.1103/PhysRevB.63.054505
7. A. Bianconi, N.L. Saini, S. Agrestini, D. Di Castro, G. Bianconi, The strain quantum critical point for superstripes in the phase diagram of all cuprate perovskites, Int. J. Mod. Phys. B **14** (29n31), 3342–3355 (2000). doi:10.1142/S0217979200003812
8. N. Poccia, M. Fratini, A. Ricci, G. Campi, L. Barba, A. Vittorini-Orgeas, G. Bianconi, G. Aeppli, A. Bianconi, Evolution and control of oxygen order in a cuprate superconductor. Nat. Mater. **10**(10), 733–736 (2011). doi:10.1038/nmat3088
9. C. Chen, D. Werder, L. Schneemeyer, P. Gallagher, J. Waszczak, Observation of oxygen-vacancy-ordered domains in oxygen-deficient single-crystal $YBa_2Cu_3O_{6.7}$, Phys. Rev. B **38**(4), 2888–2891 (1988). doi:10.1103/PhysRevB.38.2888
10. N. Andersen, B. Lebech, H. Poulsen, The structural phase diagram and oxygen equilibrium partial pressure of $YBa_2Cu_3O_{6+x}$ studied by neutron powder diffraction and gas volumetry. Phys. C Supercond. **172**(1–2), 31–42 (1990). doi:10.1016/0921-4534(90)90639-V
11. V. Kresin, S. Wolf, Colloquium: Electron-lattice interaction and its impact on high Tc superconductivity. Rev. Mod. Phys. **81**(2), 481–501 (2009). doi:10.1103/RevModPhys.81.481
12. K.A. Müller, On the superconductivity in hole doped cuprates. J. Phys. Condens. Matter **19** (25), 251002 (2007). doi:10.1088/0953-8984/19/25/251002
13. T. Timusk, B. Statt, The pseudogap in high-temperature superconductors: An experimental survey. Rep. Prog. Phys. **62**(1), 61–122 (1999). doi:10.1088/0034-4885/62/1/002
14. D. Mihailovic, Optical experimental evidence for a universal length scale for the dynamic charge inhomogeneity of cuprate superconductors. Phys. Rev. Lett. **94**(20), 207001 (2005). doi:10.1103/PhysRevLett.94.207001
15. A. Bianconi, N. Saini, A. Lanzara, M. Missori, T. Rossetti, H. Oyanagi, H. Yamaguchi, K. Oka, T. Ito, Determination of the local lattice distortions in the CuO_2 plane of $La_{1.85}Sr_{0.15}CuO_4$. Phys. Rev. Lett. **76**(18), 3412–3415 (1996). doi:10.1103/PhysRevLett.76.3412
16. D. Rubio Temprano, J. Mesot, S. Janssen, K. Conder, A. Furrer, H. Mutka, K. Müller, Large isotope effect on the pseudogap in the high-temperature superconductor $HoBa_2Cu_4O_8$. Phys. Rev. Lett. **84**(9), 1990–1993 (2000). doi:10.1103/PhysRevLett.84.1990
17. A. Kaminski, S. Rosenkranz, H. M. Fretwell, J. C. Campuzano, Z. Li, H. Raffy, W. G. Cullen, H. You, C. G. Olson, C. M. Varma, H. Höchst, Spontaneous breaking of time-reversal symmetry in the pseudogap state of a high-Tc superconductor, Nature 416 (6881) (2002) 610–61613. doi:10.1038/416610a.
18. S. Chakravarty, Quantum oscillations and key theoretical issues in high temperature superconductors from the perspective of density waves. Rep. Prog. Phys. **74**(2), 022501 (2011). doi:10.1088/0034-4885/74/2/022501

19. J.J. Capponi, C. Chaillout, A.W. Hewat, P. Lejay, M. Marezio, N. Nguyen, B. Raveau, J.L. Soubeyroux, J.L. Tholence, R. Tournier, Structure of the 100 K superconductor $Ba_2YCu_3O_7$ between (5÷300) K by neutron powder diffraction. Europhys Lett **3**(12), 1301–1307 (1987). doi:10.1209/0295-5075/3/12/009
20. W. Schäfer, E. Jansen, G. Will, J. Faber, B. Veal, Structural anomalies of $YBa_2Cu_3O_{6.9}$ at the superconducting transition temperature. Mater. Res. Bull. **23**(10), 1439–1445 (1988). doi:10.1016/0025-5408(88)90269-3
21. P. Miceli, J. Tarascon, L. Greene, P. Barboux, F. Rotella, J. Jorgensen, Role of bond lengths in the 90-K superconductor: a neutron powder-diffraction study of $YBa_2Cu_{3-x}Co_xO_{7-y}$. Phys. Rev. B **37**(10), 5932–5935 (1988). doi:10.1103/PhysRevB.37.5932
22. J.J. Rehr, Theoretical approaches to x-ray absorption fine structure. Rev. Mod. Phys. **72**(3), 621–654 (2000). doi:10.1103/RevModPhys.72.621
23. H. Takagi, R. Cava, M. Marezzio, B. Battlog, W. Krajewski, J.J. Peck Jr., P. Bordet, D. Cox, Re-examination of the phase diagram in heavily-doped $La_{2-x}Sr_xCuO_4$, in *Lattice Effects in High-Tc Superconductors*, ed. by Y. Bar-Yam, T. Egami, J. M. de Leon, A. R. Bishop, Proceedings of the Conference: Santa Fe, New Mexico, World Scientific, 13–15 January 1992, pp. 548–557
24. G.H. Kwei, A.C. Larson, W. Hults, J.L. Smith, Temperature dependence of the structure of $YBa_2Cu_3O_7$. Phys. C Supercon. **169**(3–4), 217–226 (1990). doi:10.1016/0921-4534(90)90178-H
25. J. Mustre de Leon, S. Conradson, I. Batistic, A. Bishop, Evidence for an axial oxygen-centered lattice fluctuation associated with the superconducting transition in $YBa_2Cu_3O_7$. Phys. Rev. Lett. **65**(13), 1675–1678 (1990). doi:10.1103/PhysRevLett.65.1675
26. S.D. Conradson, I.D. Raistrick, A.R. Bishop, Axial oxygen-centered lattice instabilities and high-temperature superconductivity. Science **248**(4961), 1394–1398 (1990). doi:10.1126/science.248.4961.1394
27. R. Sharma, F. Rotella, J. Jorgensen, L. Rehn, Neutron diffraction and ion-channeling investigations of atomic displacements in $YBa_2Cu_3O_{7-\delta}$ between 10 and 300 K. Phys. C Supercon. **174**(4–6), 409–422 (1991). doi:10.1016/0921-4534(91)91577-Q
28. C. Thomsen, M. Cardona, Comment on axial oxygen-centered lattice instabilities in $YBa_2Cu_3O_7$: An application of the analysis of extended x-ray-absorption fine structure in anharmonic systems. Phys. Rev. B **47**(18), 12320–12321 (1993). doi:10.1103/PhysRevB.47.12320
29. E. Stern, Y. Yacobi, M. Qian, Cu–O bonds in $YBa_2Cu_3O_{7-\delta}$, in *Lattice Effects in High-Tc Superconductors*, ed. by Y. Bar-Yam, T. Egami, J. M. de Leon, A. R. Bishop, Proceedings of the Conference: Santa Fe, New Mexico, World Scientific, 13–15 January 1992, pp. 101–104.
30. E. Stern, M. Qian, Y. Yacoby, S. Heald, H. Maeda, Apical Cu–O bond in $YBa_2Cu_3O_{7-\delta}$ superconductors by XAFS. Phys. C Supercond. **209**(1–3), 331–334 (1993). doi:10.1016/0921-4534(93)90935-J
31. C. Booth, F. Bridges, J. Boyce, T. Claeson, B. Lairson, R. Liang, D. Bonn, Comparison of local structure measurements from c-axis polarized XAFS between a film and a single crystal of $YBa_2Cu_3O_{7-\delta}$ as a function of temperature. Phys. Rev. B **54**(13), 9542–9554 (1996). doi:10.1103/PhysRevB.54.9542
32. J. Mustre de Leon, S. Conradson, I. Batistic, A. Bishop, Correlation between axial-oxygen anharmonicity and Tc in $YBa_2Cu_3O_7$ and related compounds. Phys. Rev. B **44**, 2422–2425 (1991). doi:10.1103/PhysRevB.44.2422
33. J. Mustre de Leon, I. Batistic, A. Bishop, S. Conradson, S. Trugman, Polaron origin for anharmonicity of the axial oxygen in $YBa_2Cu_3O_7$. Phys. Rev. Lett. **68**, 3236–3239 (1992). doi:10.1103/PhysRevLett.68.3236
34. M. Salkola, A. Bishop, J. Mustre de Leon, S. Trugman, Dynamic polaron tunneling in $YBa_2Cu_3O_7$: Optical response and inelastic neutron scattering. Phys. Rev. B **49**, 3671–3674 (1994). doi:10.1103/PhysRevB.49.3671

35. A. Bianconni, S. Della Longa, M. Missori, I. Pettiti, M. Pompa, Non homogeneous Cu site structure configurations and Cu apical oxygen vibrations at the normal to superconducting transition, in *Lattice Effects in High-Tc Superconductors*, ed. by Y. Bar-Yam, T. Egami, J. M. de Leon, A. R. Bishop, Proceedings of the Conference: Santa Fe, New Mexico, January 13–15, World Scientific, 1992, pp. 65–83
36. P. Allen, J. Mustre de Leon, S. Conradson, A. Bishop, Characterization of a split axial-oxygen site in $TlBa_2Ca_3Cu_4O_{11}$ by extended x-ray-absorption fine-structure spectroscopy. Phys. Rev. B **44**(17), 9480–9485 (1991). doi:10.1103/PhysRevB.44.9480
37. C. Booth, F. Bridges, E. Bauer, G. Li, J. Boyce, T. Claeson, C. Chu, Q. Xiong, XAFS measurements of negatively correlated atomic displacements in $HgBa_2CuO_{4+\delta}$. Phys. Rev. B **52**(22), R15745–R15748 (1995). doi:10.1103/PhysRevB.52.R15745
38. H. Oyanagi, A. Tsukada, M. Naito, N. Saini, Local structure of superconducting $(La,Sr)_2CuO_4$ under strain: Microscopic mechanism of strain-induced Tc variation. Phys. Rev. B **75**(2), 024511 (2007). doi:10.1103/PhysRevB.75.024511
39. C. Zhang, H. Oyanagi, Local lattice instability and superconductivity in $La_{1.85}Sr_{0.15}Cu_{1-x}M_xO_4$ (M=Mn, Ni, and Co). Phys. Rev. B **79**(6), 064521 (2009). doi:10.1103/PhysRevB.79.064521
40. S.D. Conradson, J.M. Leon, A.R. Bishop, Local phase separation in Tl-based oxide superconductors. J. Supercond. 10(4), 329–332 (1997). doi:10.1007/BF02765713
41. A. Lanzara, N. L. Saini, A. Bianconi, J. L. Hazemann, Y. Soldo, F. C. Chou, D. C. Johnston, Temperature-dependent modulation amplitude of the CuO2 superconducting lattice in La2CuO4.1, Phys. Rev. B 55(14), 9120–9124 (1997). doi:10.1103/PhysRevB.55.9120
42. J. Mustre de Leon, M. Acosta-Alejandro, S.D. Conradson, A.R. Bishop, Local structure fluctuations as a signature of an inhomogeneous ground state in high-Tc superconductors. J. Synchrotron Radiat. 12(Pt 2), 193–196 (2005). doi:10.1107/S0909049505000063
43. A. Bianconi, M. Lusignoli, N. Saini, P. Bordet, A. Kvick, P. Radaelli, Stripe structure of the CuO_2 plane in $Bi_2Sr_2CaCu_2O_{8+y}$ by anomalous x-ray diffraction. Phys. Rev. B **54**(6), 4310–4314 (1996). doi:10.1103/PhysRevB.54.4310
44. T. Egami, S. Billinge, *Underneath the Bragg Peaks Structural Analysis of Complex Materials* (Pergamon, Kiddington, Oxford, Boston, 2003)
45. E. Bozin, S. Billinge, G. Kwei, H. Takagi, Charge-stripe ordering from local octahedral tilts: Underdoped and superconducting $La_{2-x}Sr_xCuO_4$ ($0 \leq x \leq 0.30$), Phys. Rev. B **59**(6), 4445–4454 (1999). doi:10.1103/PhysRevB.59.4445
46. E. Bozin, G. Kwei, H. Takagi, S. Billinge, Neutron diffraction evidence of microscopic charge inhomogeneities in the CuO_2 plane of superconducting $La_{2-x}Sr_xCuO_4$ ($0 \leq x \leq 0.30$). Phys. Rev. Lett. **84**(25), 5856–5859 (2000). doi:10.1103/PhysRevLett.84.5856
47. T. Egami, B. Toby, S. Billinge, H. Rosenfeld, J. Jorgensen, D. Hinks, B. Dabrowski, M. Subramanian, M. Crawford, W. Farneth, E. Mc-Carron, Local structural anomaly near Tc observed by pulsed neutron scattering. Phys. C Supercon. **185–189**, 867–868 (1991). doi:10.1016/0921-4534(91)91657-P
48. J. Mustre de Leon, R. de Coss, A. Bishop, S. Trugman, Isotopic substitution in a model polaronic system. Phys. Rev. B **59**(13), 8359–8362 (1999). doi:10.1103/PhysRevB.59.8359
49. G.-M. Zhao, M.B. Hunt, H. Keller, K.A. Müller, Evidence for polaronic supercarriers in the copper oxide superconductors $La_{2-x}Sr_xCuO_4$. Nature **385**, 238 (1997)

Chapter 18
Exciting Times in Condensed-Matter Physics

Hans Rudolf Ott

My first personal encounter with Alex Müller dates back to the second half of the seventies of the last century. On the occasion of a meeting of MECO (Middle European Cooperation Organisation) in Switzerland, I presented a poster on the induced Jahn-Teller effect in $PrCu_2$ [1]. Induced-moment magnetic ordering, i.e., magnetic order in a number of rare-earth (RE) compounds where the ground state of the localized 4f electrons on the RE ions is a singlet state, had occasionally been observed [2]. Not yet reported then was the structural counterpart, i.e., spontaneous lattice distortions due to a cooperative Jahn-Teller effect and $PrCu_2$ was shown to be the first such case [3]. As we now know, the Jahn-Teller effect later became a rather important aspect in the scientific activities of Alex but at that time, he didn't seem to be particularly impressed by my explanations.

Next, a few years later, we met at the IBM research laboratories at Yorktown Heights where Alex spent some sort of sabbatical leave from the Rüschlikon labs near Zurich. He mentioned that he was now interested in superconductivity of granular Aluminium, which used to be prepared by evaporation of the pure metal in a suitable atmosphere of Oxygen [4]. It had been found that the critical temperature T_c of that material was up to a factor three higher than that of very pure Al but by most, this was not considered as a major breakthrough because T_c was still of the order of only 3–4 K. By experiment it was shown that the granular structure of the material led to the appearance of low-frequency phonon modes [5] and therefore, a softening of the lattice and hence, according to MacMillan [6], an enhancement of the electron-phonon interaction and thus to the observed increase of T_c.

Probably unknown to the world outside the Rüschlikon lab, Alex seems to have continued with his search for new superconductors exhibiting higher T_cs by enhancing the electron-phonon interaction of potentially promising materials.

H.R. Ott (✉)
Laboratorium für Festkörperphysik, ETH Zürich, 8093 Zürich, Switzerland
e-mail: ott@solid.phys.ethz.ch

A. Bussmann-Holder et al. (eds.), *High-Tc Copper Oxide Superconductors and Related Novel Materials*, Springer Series in Materials Science 255,
DOI 10.1007/978-3-319-52675-1_18

Among the highest T_cs for superconductivity found at the time were for compounds featuring the cubic A-15 structure, of which V_3Si, V_3Ga and Nb_3Sn were particularly prominent examples. It had been observed that these materials underwent martensitic phase transformations due to a structural instability [7] a few K above the superconducting transition. Because of the particular electronic band structure, this instability was interpreted as being driven by a band Jahn-Teller distortion involving the redistribution of electrons between the d-sub-bands of different symmetries [8]. In an collaboration between the ETH in Zürich and the University of Geneva, invoking dilatometric measurements on V_3Si, it was shown that the cubic to tetragonal distortion was abruptly terminated by the onset of superconductivity and therefore it was concluded that not the structural effect per se but rather the strong electron-phonon coupling was favouring the occurrence of superconductivity in this case [9, 10]. At about the same time, theoretical work aiming at investigating the similarities between localized pairs of electrons termed bipolarons, caused by a deformation-induced attraction and itinerant Cooper pairs in a superconductor showed that both pairings are a consequence of the general Hamiltonian capturing the electron-phonon interaction [11]. The caveat here is, however, that if the coupling strength exceeds a certain value, the result is a bipolaronic insulator. This new point of view naturally suggested the possible formation of Jahn-Teller polarons [12] and, according to later-told stories it was this approach which guided Alex in his efforts to find suitable materials.

Meanwhile I had followed up another puzzling development in superconductivity, namely the occurrence of superconductivity in a strongly paramagnetic background which was first reported for $CeCu_2Si_2$ [13]. Because this observation was really unexpected and not in line with the then current understanding of superconductivity, it was confronted with strong doubts by many of the community. In a collaboration between my group at ETH Zürich and friends at Los Alamos National Laboratory, we succeeded to confirm this feature of pairing of electrons with extremely large effective masses, i.e., heavy or rather slow itinerant electrons in metals, to also be exhibited by the actinide compound UBe_{13} [14]. The data also indicated some unconventional type of superconductivity, in some way analogous to the previously reported superfluid states of ^3He. The discussion of the data started what later turned into the hunt for power laws in the temperature dependencies of relevant physical quantities, such as the specific heat, below T_c [15]. Such power laws are expected to replace the conventional exponential reduction of electronic excitations in the superconducting state with no gap nodes. At the time, the existence of superconductors exhibiting nodes in the gap, was not very popular but many new experimental data pointed in that direction and induced corresponding work in the theoretical sector. The observation [16] of two subsequent transitions between two superconducting states in $U_{1-x}Th_xBe_{13}$, depending on x, added another strong argument for the unconventional character of this superconductivity, in the sense that in this case it is not the electron-phonon interaction that causes the instability of the ensemble of itinerant electrons. On the occasion of a talk describing these developments in the realm of the Physikalische Gesellschaft Zürich, Alex asked whether this type of

superconductivity might also be favourable for high critical temperatures. Since large effective electron masses imply a low value of the Fermi energy E_F, the characteristic energy of the itinerant-electron subsystem, my answer was, of course: rather unlikely. In retrospect it is clear that Alex already had some hints on the onset of superconductivity in the cuprates that he was investigating with Georg Bednorz.

As far as I remember, I had already heard that something was brewing before the public announcement in the form of an article that appeared in Zeitschrift für Physik in October 1986 [17]. As expected, the reported discovery of La-based cuprates being superconductors with a T_c exceeding 30 K was so unexpected that it first met with a lot of skepticism. It didn't take long, however, until the first confirmations appeared in preprints and Conference talks [18–20] and it was clear that the discovery was real and meant serious business. The chapter of high-T_c superconductivity had been opened. This also became clear at a Conference on *Valence Fluctuations and Heavy Fermions* at Bangalore in early January 1987. It was there where Phil Anderson addressed the stunned audience by proposing a novel mechanism as the cause for high-T_c superconductivity in doped La_2CuO_4 [21].

At this point I should like to add some remarks on how a discovery is made. To many the fact, once established, may seem to be a lucky punch which everybody might have landed. But this is almost never the case. In our perspective it is interesting to note, that the same class of cuprate materials had been synthesized and studied by a Russian group of chemists in 1979 [22]. They noted that some of them exhibited metallic conductivity, i.e., $\partial\rho/\partial T > 0$ at room temperature, in particular compounds of the type $La_{2-x}MO_4$ with M = Ba or Sr. They had correctly identified the crystal structure as being of tetragonal K_2NiF_4-type but were mainly interested in the temperature dependence of the resistivity as a function of the varying c/a ratio upon replacing La by Sr or Ba. Everything for a great discovery was in their hands but it didn't happen. It may well be that they did not dispose of cryogenic equipment for cooling the samples to low temperatures. What is more decisive, however, is that they did not have the vision for exploring the possibility of superconductivity in materials of this type as Bednorz and Müller did 6 years later. In other words, in most cases experimental discoveries are either made because you are looking for it or, you recognize it when unusual results are looking at you. Nevertheless, I always felt that it was somewhat unfair that these Russian authors were never cited for their work in the flood of papers on $La_{2-x}M_xCuO_4$ that appeared in the literature after the beginning of 1987.

Meanwhile in December 1986, Gerd Binnig and Heini Rohrer, both also members of the IBM research lab in Rüschlikon, were awarded with the Nobel Prize for inventing and pioneering the scanning tunneling microscopy (STM). During a celebration of their achievement in a leading hotel in Zürich in January 1987, rumours were spread that one would meet again for the same reason at the same location in early 1988. For the few present that were in the game, it was clear what was meant and, as is well known now, it did happen. Two consecutive Nobel prizes exclusively awarded to scientists of a relatively small research laboratory of a private company, a really amazing fact.

The new field of high-T_c superconductivity got an immediate boost in early 1987 via the announcement of the observation of the onset of superconductivity in a not yet identified material containing Y, Ba, Cu and O at 93 K, i.e., distinctly above the boiling point of liquid nitrogen [23]. Again, it didn't take long, barely a few weeks, for numerous confirmations and the identification of the actual compound, $YBa_2Cu_3O_7$, to appear in the literature. At ETH, in spring 1987, Fritz Hulliger and myself embarked on a study of this type of cuprates with a series of compounds where Y was replaced by rare-earth (RE) elements [24]. Contrary to conventional superconductors, the presence of large magnetic moments due to the RE ions had virtually no influence on the value of T_c, especially true for the heavy RE elements beyond Gd where all T_c values exceed 90 K. Neutron diffraction experiments revealed that some of these compounds exhibit magnetic order at temperatures below 1 K without losing superconductivity, i.e., the coexistence of the two long-range order phenomena [25]. These early observations were, of course, no convincing evidence for unconventional superconductivity in these cuprates, but at least among the first hints in this direction.

In early summer 1987, the Swiss community involved in research on superconductivity reached the conclusion that the already planned *Conference on Superconductivity in d- and f-band metals*, to be held in Switzerland in 1988, should be restructured to include the materials class of copper oxides. The new Conference title *Materials and Mechanisms of Superconductivity, M^2S-HTSC* was quickly adopted and a committee with Alex and myself as co-chairs, supported by colleagues from the Swiss community, set to work. As many still remember, the result was the memorable Interlaken meeting from February 29 to March 4, 1988. The conference attracted more than 1100 participants from 39 countries, an extraordinary large number for this type of meetings, and got the then still unusual attention of all types of media. The audience also included more than 30 delegates from the Soviet Union, again a before unheard number of colleagues from that part of the world together in a single event in the West. Most memorable were the late night sessions where everybody could register to present new data which daily came in through the at the time very new channel of telefax. These sessions often ended between 2 and 3 a.m. and morning sessions started again at 08:30 or 9 a.m. It was a tough week for everybody and, although we had to cope with ample snowfall, we even managed to order some sunshine for the excursion up to Eiger, Mönch and Jungfrau.

During 1987, yet another class of cuprate superconductors made the headlines. Based on indications for superconductivity of $Bi_2Ba_2CuO_6$ around 20 K [26], it was soon realized that by inserting a plane of Ca atoms into the original structure, resulting in the compound $Bi_2Ba_2CaCu_2O_8$, T_c could be raised to above 80 K [27]. The trick with inserting Ca planes and, in addition, enhance the number of the notoriously essential Cu–O planes in cuprate structures, turned out to be a key element for raising T_c. For the Bi-based cuprates, adding even one more Ca and Cu–O plane, respectively, T_c values exceeding 100 K were reached. Early in 1988 and even during the Interlaken meeting, results from studies of yet another class of cuprates starting with $Tl_2Ba_2CuO_6$ and, applying the Ca/Cu–O trick with now five

components Tl, Ba, Ca, Cu and O, were reported and a T_c of 125 K was finally reached [28, 29].

It took a few years until a renewed excitement with respect to raising T_c even further emerged. Based on results of a new compound, $HgBa_2CuO_{4+\delta}$, exhibiting an onset for superconductivity at 94 K, by far the highest T_c for a cuprate compound with only one Cu–O plane per structural unit [30]. In that work it was mentioned that the above mentioned Ca-trick doesn't work. Since we had done a few excursions into sample preparation and had some experience in synthesizing cuprate materials [31], we thought we would try it anyway. The courage paid off and we could announce a new record-high critical temperature of 133.5 K [32] for $HgBa_2Ca_2Cu_3O_{8+\delta}$. Later work revealed that under the application of external pressure, T_c could be enhanced substantially, however, the results obviously depended a lot on the chosen samples and their composition [33, 34].

In the mean time, most worldwide research efforts, both in theory and experiment, had been devoted to characterize the normal and the superconducting state of these cuprate compounds and to identify possible pairing mechanisms for the onset of superconductivity at these, from the traditional point of view, extraordinary high temperatures. Starting already in 1986, the first theory-based claims for a superconducting state with intrinsic gap nodes appeared in the literature [35]. The first reliable experimental indications appeared a few years later, mostly in the form of the above mentioned power laws in the temperature dependencies of relevant parameters below T_c, such as the NMR Knight shift and the penetration depth of external magnetic fields [36]. A more rigorous experimental verification of the suggested d-wave, i.e., to be precise, the $d_{x^2-y^2}$ symmetry of the gap was suggested by Sigrist and Rice [37], based on an idea of Geshkenbein and Larkin for the case of heavy-electron superconductors [38], to probe the relative phase of the gap at different points of the Fermi surface. Results of the first successful experimental attempt were reported by Wollman et al. [39] and not much later, our group at ETH presented data obtained with a somewhat different experimental set-up, which confirmed the claimed gap-node configuration [40]. At about the same time, a very elegant but technologically more demanding experiment by Tsuei and Kirtley [41] led again to the same conclusion. Shortly after these developments, Alex Müller reacted and argued that in order to capture the overall 3-D features of the order parameter, a scenario considering a mix of d- and s-wave symmetry would have to be taken into account [42]. With respect to mechanisms, Alex, mainly based on experimental evidence of isotope effects on T_c of $La_{2-x}Sr_xCuO_4$ [43], never got tired to remind the community that the influence of the lattice, resulting in the formation of Jahn-Teller polarons, should not be neglected.

The discovery of high-T_c superconductivity in copper-oxide materials not only initiated experimental and theoretical research to unravel the secrets of this type of conductors and their superconductivity. A special feature of these cuprate compounds were and are their low-dimensional (low-D) structural subunits in the form of Cu–O planes and chains as, e.g., in $YBa_2Cu_3O_7$. This led to a very intense activity of synthesizing similar materials in the form of transition-metal oxides.

Many of them were not superconductors but they served as a testbed for experimental studies of the behaviour of low-D systems, particularly with respect to their magnetic properties. For example, the mentioned subunits can be regarded as chains, ladders or planes of spin arrays. Of particular interest are compounds that can be regarded as containing individual spin chains or coupled chains to form 2-leg ladders, for instance. Aspects of physical properties of such quasi 1-D cuprate materials were first discussed by Dagotto and Rice [44]. Depending on the choice of the transition-metal element the individual spins adopt a half-integer or integer value. Although in real materials these low-D subunits are components of a three-dimensional crystal structure, in many cases, the anisotropy of the relevant interactions is large enough to hope that some of the typical low-D features that had extensively been studied theoretically since many years, would survive to show up in experimental data of appropriate physical properties of these materials.

For our purposes, outlined below, various Cu-oxide compounds are of particular interest. Examples are Sr_2CuO_3, $SrCuO_2$ and $Sr_{14}Cu_{24}O_{41}$. Structurally they contain linear spin-½ chains, ribbons and 2-leg spin ladders, running along a given crystallographic axis, depending on the material [45]. Therefore they represent physical realizations of specific low-D spin array models whose physical properties can be tested and compared with theoretical predictions. Very early theoretical work [46] had claimed that the spin diffusion constant for spin chains with Heisenberg-type antiferromagnetic (HAFM) coupling diverges for $S = ½$, implying that in this case the transport of energy is not diffusive but ballistic. More recent work invoking other approaches to investigate the flow of energy in such systems concluded that the thermal conductivity κ_s based on itinerant spin excitations, not exposed to extrinsic perturbations, is infinite [47]. The only excitations and thus carriers of energy in a HAFM spin-½ chain are spinons and the corresponding excitation spectrum is gapless. In a real material, for example an insulator, their motion is certainly hampered by lattice defects and possibly lattice excitations (phonons). From our measurements of the thermal conductivity of all the above-mentioned compounds below room temperature, it turned out that at intermediate temperatures, the thermal conduction via spinons along the chain or ladder directions is a significant component and corresponding analyses indicated very long mean free paths for these magnetic excitations, limited by spinon interactions with lattice defects [45].

In [46] it is also claimed that the diffusion constant for spin excitations does not diverge for $S > ½$ and therefore the energy transport is diffusive. We tested this prediction with measurements of $\kappa_s(T)$ on $AgVP_2S_6$, where the V-ions a form a linear array along the **a** axis of the monoclinic crystal structure, and thus can be regarded as spin chain compound with $S = 1$ [48]. In this case, the excitation spectrum is gapped. From our results we concluded that the mean free path of the magnon excitations is much shorter and the corresponding diffusion constant does not diverge but is rather rapidly reduced with decreasing temperature. This direct comparison confirms the characteristically different features of the energy transport of spin arrays with either $S = ½$ or $S = 1$.

After the year 2000, the number of experimental and theoretical studies probing, explaining and predicting the magnetic properties of spin-chain and -ladder compounds as those mentioned above has grown enormously. Theoretical studies mainly concentrated on aspects of quantum criticality and many-body effects. Experiments served to test predictions of model calculations or to explore new and unexpected features of these systems [49]. Particular attention was devoted to spin-1/2 antiferromagnets with a singlet ground state and boson-like $S = 1$ triplet excitations termed triplons, where the application of external magnetic fields is expected to lead to quantum phase transitions (QPT). For example, by closing the gap between the singlet and the triplet states, the triplons can undergo a Bose-Einstein-type condensation (BEC) at low temperatures and the BEC is reflected by a magnetic order of the spin component orthogonal to the applied-field direction. Other aspects worth studying are the influences of frustration and disorder on the ground state of the system.

Our group at ETH embarked on experimental investigations of Cu-containing compounds ($S = ½$) whose structures feature either chain- ($BaCu_2Si_2O_7$) or ladder-type ($BiCu_2PO_6$) subunits in the sense outlined above. The experiments employed methods of nuclear magnetic resonance (NMR) probing either ^{29}Si or ^{31}P nuclei, depending on the compound under investigation. With the introduction of maximum disorder without changing the overall structure by randomly replacing Si by Ge to obtain the random Heisenberg chain (RHC) system $BaCu_2SiGeO_7$, we succeeded to identify the theoretically predicted random-singlet (RS) state [50]. NMR is well suited to explore the low-energy dynamics of an RHC system, not accessible by standard neutron-scattering techniques. Experimental data revealing the details of the NMR spin-lattice relaxation allowed to extract the distribution of relaxation functions in a random Heisenberg-type spin chain directly. Taking into account additional information from magnetization measurements and quantum Monte-Carlo (QMC) calculations finally justified the experimentally-based conclusion that the RS state is indeed the ground state of such systems [51].

As regards $BiCu_2PO_6$, we first explored the possibility to directly observe impurity-induced magnetic features in $BiCu_{2-x}Zn_xPO_6$. Again probing static and dynamic features of the NMR response (line positions and -shapes, and relaxation data) obtained from measurements on single crystals, as well as invoking QMC calculations, the set goal was reached [52]. With essentially the same experimental approach we also attempted to map the [H,T] phase diagram of the pristine compound. In a first approach, the range of external magnetic fields up to 32 T could be mapped, including the field-induced quantum phase transition FI-QPT at approximately 21 T at zero temperature, at about the same time confirmed by other authors employing different experimental techniques [53]. The description of the structure of the magnetic order above this critical field demanded a lot of analysis and calculations employing the density matrix renormalisation group (DMRG) method. Finally we claimed that our data suggest that the magnetization process involves the formation of a soliton lattice [54]. Current efforts aim at unraveling the development of the magnetization pattern upon increasing the magnetic field up to above 40 T.

Dear Alex, I hope that this brief essay doesn't bore you. It is intended to illustrate that your discovery, together with Georg, of superconductivity in copper-oxides gave a big boost to the field of superconductivity in general and in details, but not exclusively. I believe that it also had a very beneficial impact on materials-driven solid-state physics in general. People were encouraged to try to synthesize new materials, often with 5 or 6 chemical elements as constituents and in unexplored compositions. For instance, the discovery of superconductivity in so-called Iron-pnictide compounds [55], currently at temperatures up to 55 K, initiated a similar gold-rush excitement as did your findings in 1986. For other materials it turned out that a number of them have the potential to serve as model materials for studying different aspects of condensed-matter physics. Thus the availability of new materials is certainly one of the reasons why this sector of physics that is briefly outlined above, flourished so much in the last 30 years.

Finally I wish you all the best concerning health, spirit and fun in your life beyond 90.

References

1. H.R. Ott, K. Andres, P.S. Wang, Y.H. Wong, B. Lüthi, *Crystal Field Effects in Metals and Alloys* (Plenum, New York, 1977), p. 84
2. see, e.g., K. Andres, E. Bucher, S. Darack, J.P. Maita, Phys. Rev. B **6,** 2716 (1972)
3. J. Kjems, H.R. Ott, S.M. Shapiro, K. Andres, J. Phys. **39**, C61010 (1978)
4. R.W. Cohen, B. Abeles, Phys. Rev. **167**, 444 (1968)
5. J. Klein, A. Léger, Phys. Lett. **28A**, 134 (1968)
6. W.L. McMillan, Phys. Rev. **167**, 331 (1968)
7. B.W. Batterman, C.S. Barrett, Phys. Rev. Lett. **13**, 390 (1964)
8. J. Labbé, J. Friedel, J. Phys. **27**, 303 (1966)
9. B.S. Chandrasekhar, H.R. Ott, B. Seeber, Solid State Commun. **39**, 1265 (1981)
10. H.R. Ott, B.S. Chandrasekhar, B. Seeber, Phys. Rev. B **31**, 2700 (1985)
11. B.K. Chakraverty, J. Phys. **42**, 1351 (1981)
12. K.-H. Hoeck, H. Nickisch, H. Thomas, Helv. Physica Acta **56**, 237 (1983)
13. F. Steglich, J. Aarts, C.D. Bredl, W. Lieke, D. Meschede, W. Franz, H. Schäfer, Phys. Rev. Lett. **43**, 1892 (1979)
14. H.R. Ott, H. Rudigier, Z. Fisk, J.L. Smith, Phys. Rev. Lett. **50**, 1595 (1983)
15. H.R. Ott, H. Rudigier, T.M. Rice, K. Ueda, Z. Fisk, J.L. Smith, Phys. Rev. Lett. **52**, 1915 (1984)
16. H.R. Ott, H. Rudigier, Z. Fisk, J.L. Smith, Phys. Rev. B **31**, 1651 (1985)
17. J.G. Bednorz, K.A. Müller, Z. Phys. B **64**, 189 (1986)
18. H. Takagi, S. Uchida, K. Kitazawa, S. Tanaka, Jpn. J. Appl. Phys. **26**, L123 (1987)
19. C.W. Chu, P.H. Hor, R.L. Meng, L. Gao, Z.J. Huang, Y.Q. Wang, Phys. Rev. Lett. **58**, 405 (1987)
20. R.J. Cava, R.B. van Dover, B. Batlogg, E.A. Rietman, Phys. Rev. Lett. **58**, 408 (1987)
21. P.W. Anderson, in *Theoretical and Experimental Aspects of Valence Fluctuations and Heavy Fermions*, ed. by L.C. Gupta, S.K. Malik (Plenum Press, New York, 1987) p. 9
22. I.S. Shaplygin, B.G. Kakhan, V.B. Lazarev, Zh. Neorg. Khim. **24**, 1478 (1979)
23. M.K. Wu, J.R. Ashburn, C.J. Torng, P.H. Hor, R.L. Meng, L. Gao, Z.J. Huang, Y.Q. Wang, C.W. Chu, Phys. Rev. Lett. **58**, 908 (1987)
24. F. Hulliger, H.R. Ott, Z. Phys. B **67**, 291 (1987)

25. see, e.g., P. Fischer, K. Kakurai, M. Steiner, K.N. Clausen, B. Lebech, F. Hulliger, H.R. Ott, P. Brüesch, P. Unternährer, Phys. C **152**, 145 (1988)
26. C. Michel, M. Hervieu, M.M. Borel, A. Grandin, F. Deslandes, J. Provost, B. Raveau, Z. Phys. B **68**, 421 (1987)
27. H. Maeda, Y. Tanaka, M. Fukutomi, T. Asano, Jpn. J. Appl. Phys. Lett. **27**, L209 (1987)
28. Z.Z. Sheng, A.M. Hermann, Nature (London) **332**, 55 (1988)
29. S.S.P. Parkin, V.Y. Lee, E.M. Engler, A.I. Nazzal, T.C. Huang, G. Gorman, R. Savoy, R. Beyers, Phys. Rev. Lett. **60**, 2539 (1988)
30. S.N. Putilin, E.V. Antipov, O. Chmaissem, M. Marezio, Nature **362**, 226 (1993)
31. A. Schilling, H.R. Ott, F. Hulliger, Phys. C **157**, 144 (1989)
32. A. Schilling, M. Cantoni, J.D. Guo, H.R. Ott, Nature **363**, 56 (1993)
33. L. Gao, Z.J. Huang, R.L. Meng, J.G. Lin, F. Chen, L. Beauvais, Y.Y. Sun, Y.Y. Xue, C.W. Chu, Phys. C **213**, 261 (1993)
34. D. Tristan Jover, R.J. Wijngarden, H. Wilhelm, R. Griessen, S.M. Loureiro, J.J. Capponi, A. Schilling, H.R. Ott, Phys. Rev. B **54**, 4265 (1996)
35. see, e.g., P.A. Lee, N. Read, Phys. Rev. Lett. **58**, 2691 (1987)
36. see, e.g., D.J. Scalapino, Phys. Rep. **250**, 329 (1995)
37. M. Sigrist, T.M. Rice, J. Phys. Soc. Jpn. **61**, 4283 (1992)
38. V.B. Geshkenbein, A.I. Larkin, JETP Lett. **43**, 395 (1986)
39. D.A. Wollman, D.J. Van Harlingen, W.C. Lee, D.M. Ginsberg, A.J. Leggett, Phys. Rev. Lett. **71**, 2134 (1993)
40. D.A. Brawner, H.R. Ott, Phys. Rev. B **50**, 6530 (1994)
41. C.C. Tsuei, J.R. Kirtley, C.C. Chi, L.S. Yu-Yahnes, A. Gupta, T. Shaw, J.Z. Sun, M.B. Ketchen, Phys. Rev. Lett. **73**, 593 (1994)
42. K.A. Müller, Nature (London) **377**, 133 (1995)
43. Guo-meng Zhang, M.B. Hunt, H. Keller, K.A. Müller, Nature (London) 385, 236 (1997)
44. E. Dagotto, T.M. Rice, Science **271**, 618 (1996)
45. see, e.g., A.V. Sologubenko, H.R. Ott, in *Strong Interactions in Low Dimensions*, ed. by D. Baeriswyl, L. Degiorgi (Kluwer Academics, Dordrecht, 2004) p. 383
46. D.L. Huber, J.S. Semura, C.G. Windsor, Phys. Rev. **186**, 534 (1969)
47. see, e.g., X. Zotos and P. Prelovsek, ref. 45, p.347
48. A.V. Sologubenko, S.M. Kazakov, H.R. Ott, T. Asano, and Y. Ajiro, Phys. Rev. B **68**, 094432 (2003)
49. see, e.g., T. Giamarchi, Ch. Rüegg, O. Tschernyshyov, Nat. Phys. **4**, 198 (2008)
50. see, e.g., D.S. Fisher, Phys, Rev, B **50**, 3799 (1994)
51. T. Shiroka, F. Casola, A. Zheludev, K. Prša, H.R. Ott, J. Mesot, Phys. Rev. Lett. **106**, 137202 (2011)
52. F. Casola, T. Shiroka, S. Wang, K. Conder, E. Pomjakushina, J. Mesot, H.R. Ott, Phys. Rev. Lett. **105**, 067203 (2010)
53. Y. Kohama, S. Wang, A. Uchida, K. Prsa, S. Zvyagin, Y. Skourski, R.D. McDonald, L. Balicas, H.M. Ronnow, Ch. Rüegg, M. Jaime, Phys. Rev. Lett. **109**, 167204 (2012)
54. F. Casola, T. Shiroka, A. Feiguin, S. Wang, M.S. Grbić, M. Horvatić, S. Krämer, S. Mukhopadhyay, K. Conder, C. Berthier, H.R. Ott, H.M. Rønnow, C. Rüegg, J. Mesot, Phys. Rev. Lett. **110**, 187201 (2013)
55. Y. Kamihara, T. Watanabe, M. Hirano, H. Hosono, J. Am. Chem. Soc. **130**, 3296 (2008)

Chapter 19
Intimacy Between Local Lattice and High Temperature Superconductivity: Perspective View on Undeniable Facts

Hiroyuki Oyanagi

Background

Almost 30 years after the discovery of high temperature superconductivity (HTSC) [1], the mechanisms of pairing for doped cuprates, doped Fe pnictides [2], recently reported pressure-induced HTSC [3] and laser-induced HTSC [4] are not described systematically nor seamlessly connected to the conventional phonon mechanism. Indeed, a conventional phonon mechanism has been considered "unlikely" by many researchers, as the DFT calculations indicated a weak electron-phonon coupling. Yet, the purely electronic mechanism [5] is also "less likely" than the case of cuprates [6] as the Hubbard U is not large ($U \sim 5$ eV) [7]. On the other hand, it is also true that the familiar phonon mechanism needs to further evolve to be able to describe a broader range of HTSC phenomena (defined as nonconventional superconductivity). For example, muon spin rotation experiments suggested possibility of multigap BCS-type superconductivity in $Ba_{0.6}K_{0.4}Fe_2As_2$ [8].

Some of the iron pnictides (doped with holes) have local lattice anomaly [9] similar to cuprates [10, 11] which is strongly dependent on the band filling, indicating a strong intimacy between local lattice and the doping-induced unconventional electronic structure, i.e., a pseudogap. It became therefore necessary to investigate the local lattice of a high-quality model cuprate with a state-of-the-art synchrotron instrumentation. We therefore revisited LSCO controlling superconductivity through magnetic-impurity doping.

A polaron is formed when an electron is strongly coupled to the atoms in a crystal [12]. Polarons in highly correlated electron systems relate to a variety of physical properties including colossal magnetoresistance (CMR). In manganites,

H. Oyanagi (✉)
High Energy Research Organization, 1-1 Oho, Tsukuba, Ibaraki, Japan
e-mail: oyanagi@post.kek.jp

A. Bussmann-Holder et al. (eds.), *High-Tc Copper Oxide Superconductors and Related Novel Materials*, Springer Series in Materials Science 255,
DOI 10.1007/978-3-319-52675-1_19

coherent polaron condensation is believed to be the driving mechanism of CMR phenomena [13]. Strong coupling between electrons and lattice in HTSC cuprates has been demonstrated by angle-resolved photoemission spectroscopy (ARPES) [14] and later works. Considering these facts, renewed interests in a possible role of polarons in HTSC seems natural but have been neglected in most of modern theoretical approaches because of difficulty to seriously take into account within the Hubbard framework.

Following previous studies by means of polarized extended x-ray absorption fine structure (EXAFS) interpreted as a nanometer-scale self-organization (stripe) [15], in a more recent work briefly summarized here, we showed that the lattice effect at T_d^{max} is more catastrophic, resulting in a bond alternation, *i.e.*, splitting into a equal number of elongated and shortened Cu-O(1) bonds. The unusual local lattice deviation from a normal phonon behavior is interpreted in terms of polarons [15–20]. Our high-quality XAS data owes due to the special instrumentation efforts realized by combining a state-of-the-art pixel Ge x-ray detector [21] and an MPW beamline at the Photon Factory [22]. Here we describe deepened knowledge on local lattice distortion by studying LSCO with magnetic impurity doping [10].

Local Lattice Matters: Carrier-Induced Local Distortion in LSCO

LSCO is a typical HTSC cuprate with a K_2NiF_4-type structure [1], where copper atoms are coordinated by four in-plane oxygen atoms O(1) and two out-of-plane (apical) oxygen atoms O(2). The CuO_6 octahedron is elongated along the c-axis with two long (2.40 Å) and four short (1.89 Å) bonds as a result of Jahn-Teller (JT) distortion as illustrated in Fig. 19.1a [10, 11]. The Cu K-EXAFS oscillations in Fig. 19.2b originate from the interference of photoelectrons provide polarized radial distribution of atoms around a specific (excited) atom.

The displacement of local lattice can be therefore evaluated by the mean-square relative displacement $\sigma^2_{Cu\text{-}O}$ plotted in Fig. 19.3 where open circles denote temperature dependence of the *in-plane* Cu-O in optimally doped LSCO. Difference between the superconducting and non-superconducting samples needed minimizing the effect of chemical doping. Therefore, we compared the data with those for non-superconducting specimen prepared by substituting copper atom with 5% magnetic impurity (Ni), completely suppressing superconductivity by magnetic pair breaking [23]. Reflecting a fast time scale of the probe (10^{-12} s), the experiment can see an instantaneous relative displacement of dynamic and static nature. It is obvious that only superconducting LSCO samples show this unusual temperature dependence. Although a general behavior is similar to early works, a striking difference here is that the magnitude of anomaly became much more significant. They are described by the following features:

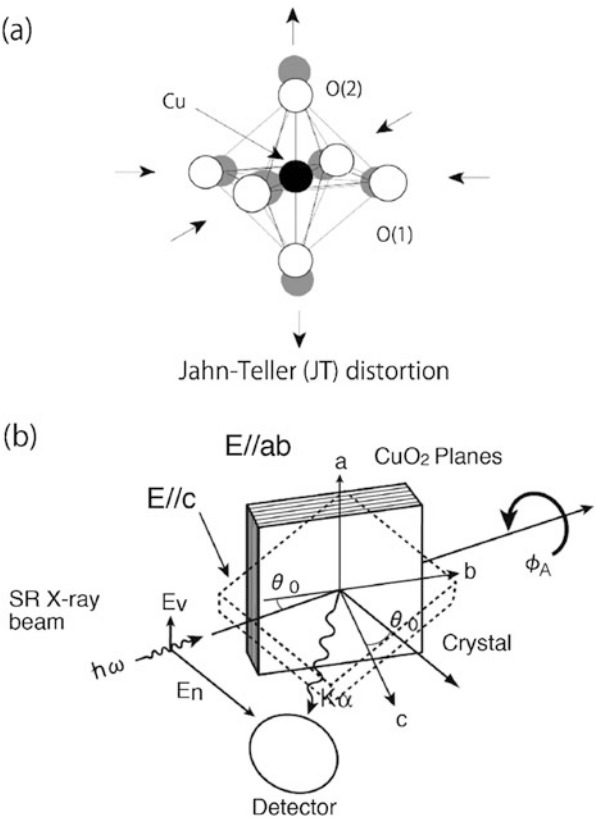

Fig. 19.1 Jahn-Teller distortion of CuO_6 octahedral unit (**a**) and geometry of experimental setup (**b**). Taken from the literature [10]

1. an upturn of $\sigma^2_{\text{Cu-O}}$ beginning at T^* (70–80 K) ~$2T_c$ maximizes at $T_d^{\max} \sim T_c^{\text{onset}}$ (37 K)
2. a sharp drop upon superconductivity
3. the upturn of $\sigma^2_{\text{Cu-O}}$ below T_c

These anomalies are in contrast to the smooth background temperature dependence caused by normal phonons essentially described by a non-correlated Debye model. In fact in a normal state, such a normal phononic behavior is commonly observed without the presence of structural phase transformation such as Jahn-Teller distortions. A deviation from this normal background *i.e.*, a negative temperature dependence (upturn) indicates the presence of a broadened radial distribution function (RDF) either due to disorder or a split of bond distance of static or dynamic nature. Because of the presence of a beat arising from an interference of the two closely separated atom positions, we can exclude broadening of the RDF without ambiguity. In Fig. 19.4a, a beat feature appears around $k = 12$ Å^{-1} which is consistent with a distortion model with a bond length split by $\Delta R \sim 0.12$ Å. This indicates that at $T_d^{\max}$, the local lattice is described by a bond alternation

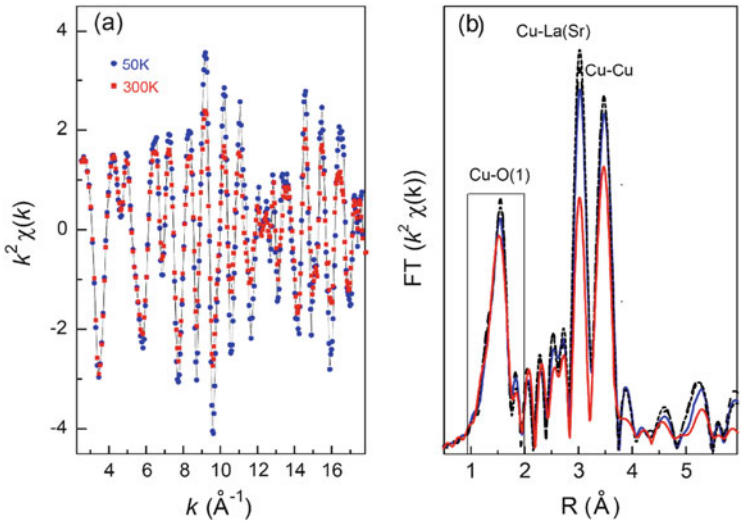

Fig. 19.2 The normalized Cu-K EXAFS oscillations for $La_{1.85}Sr_{0.15}CuO_4$ single crystal multiplied by k^2 (**a**) and the Fourier transform magnitude (**b**). Taken from the literature [10]

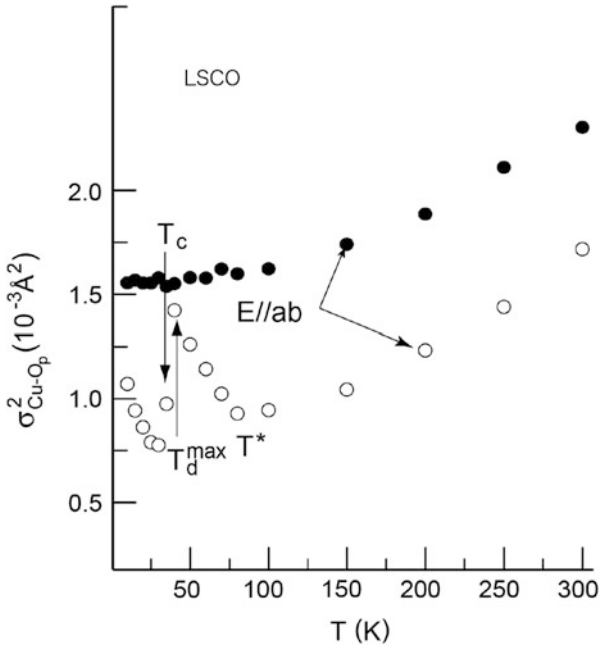

Fig. 19.3 *E//ab* mean-square relative displacement for the Cu-O(1) bond in $La_{2-x}Sr_xCuO_4$ (x = 0.15) *Open* and *closed* circles indicate the values for superconducting and non-superconducting samples of LSCO single crystals, respectively. The latter sample was prepared by substituting Cu with 5% Ni. Taken from the literature [10]

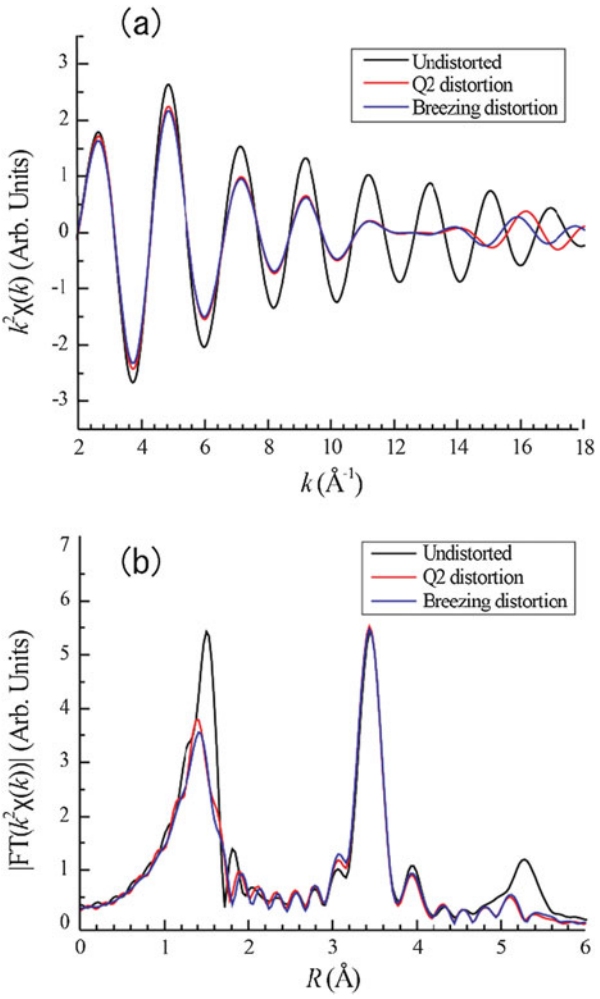

Fig. 19.4 The first-shell *E*// *ab* Cu KEXAS oscillations for $La_{2-x}Sr_xCuO_4$ multiplied by k^2 (**a**) and the Fourier transform magnitudes (**b**). Experimental results are compared with those of the simulation for distorted models. Taken from the literature [10]

(alternation of single and double bonds) like a one-dimensional doped organic molecule such as polyacetylene.

One can also find that the maximum distortion at T_d^{max} exactly coincides with the onset of superconductivity at T_c^{onset}, as illustrated in Fig. 19.3a [10, 11]. We note that our analysis of the *out-of-plane* Cu-O bond showed essentially no anomaly, in contrast to the early work which related the anomaly to a low temperature tetragonal (LTT) deformation which causes stripe inhomogeneity [15]. The effect of anti Jahn-Teller (AJT) static displacement of apical oxygen results in the electron transport without destroying the anti ferromagnetic order [24]. One of the possible cases is the dynamical *in-plane* lattice distortion with an AJT-type displacement consistent with polaron or bipolaron formation.

Undeniable Facts: Local Lattice Dancing in LSCO

Magnetic impurities substituting copper sites in the conducting layer of superconducting cuprates are expected to strongly affect the superconducting properties because of magnetic pair breaking described by the Abrikosov theory [24]. The *E*//*ab* polarized EXAFS confirmed that all dopants (Mn, Ni, Co) are incorporated in a K_2NiF_4-type structure with a chemical formula of $La_{1.85}Sr_{0.15}Cu_{1-x}M_xO_4$. Fig. 19.5a–c summarize temperature dependence of the in-plane $\sigma^2_{Cu\text{-}O}$ and susceptibility which shows a significant element-dependence

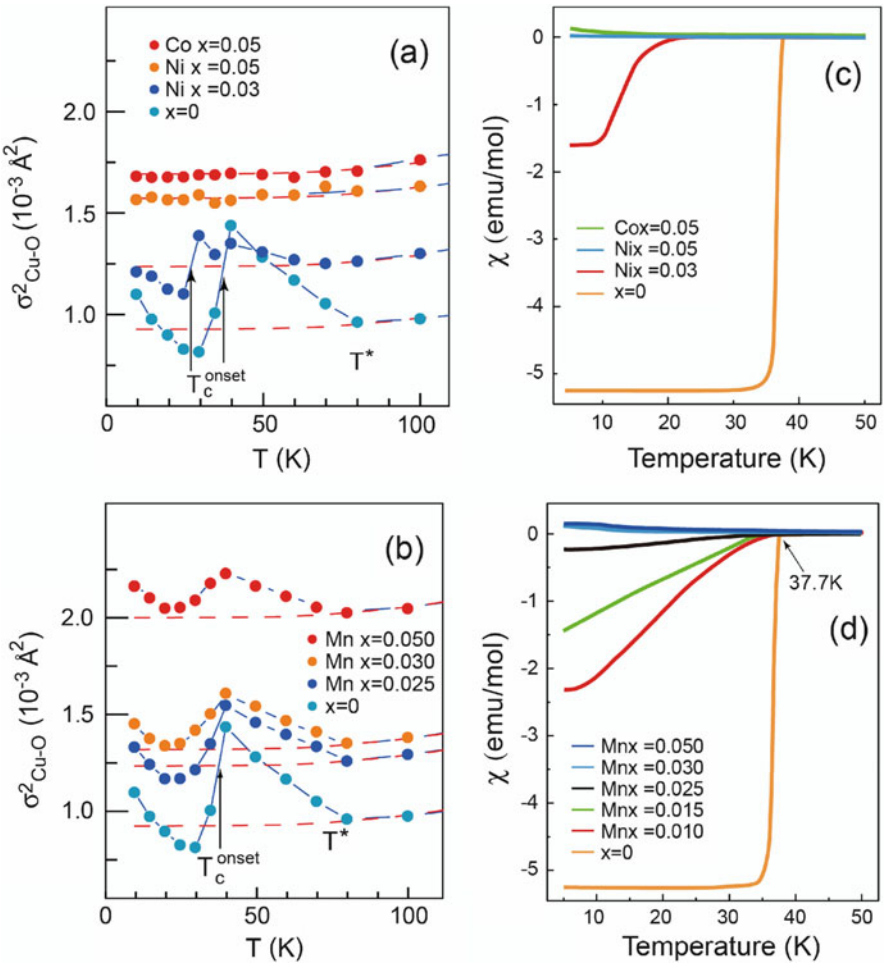

Fig. 19.5 Temperature dependence of the mean square relative displacement of the in-plane Cu-O bond $\sigma^2_{Cu\text{-}O}$ for LSCO single crystals with Ni, Co substitution (**a**) and Mn substitution (**b**) derived from the EXAFS data. Temperature dependence of the magnetic susceptibility of LSCO single crystals with Ni, Co substitution (**c**) and Mn substitution (**d**). Taken from the literature [10]

of impurity doping, *i.e.*, introducing a small amount of Ni and Co impurities at the Cu site quickly suppresses both the local lattice anomaly and susceptibility change. With a 5% Ni or Co substitution, the lattice anomaly completely disappears associated with a collapse of superconductivity, which is not surprising since $T_d^{max} = T_c^{onset}$. In contrast, the substitution of Mn weakens the magnetic pair breaking associated with a less perturbed lattice distortion, i.e., superconductivity persists as long as the lattice anomaly exists for $x < 0.03$.

Magnetic impurities have been believed to be detrimental to superconductivity based on the pair breaking theory. Although a magnetic scattering (pair breaking) has no indication of polaron (bipolaron), at least the magnetic effect is weakened while the polaron (bipolaron) is mobile as detected by temperature-dependent local distortion during which $T_d^{max} = T_c^{onset} = \text{const.}$

This situation is realized only in the case of Mn doping. In Ni- and Co-doped LSCO samples, in contrast, both T_d^{max} and T_c^{onset} sharply drop as x increases, indicating a superconducting phase coherence (superfluid density) is sensitive to impurity doping. Mn doping, however, lowers the slope of susceptibility curve and the $x = 0.05$ sample hardly shows superconductivity while the local lattice anomaly is still present. The apparent discrepancy indicates that the Mn doping causes inhomogeneous superconductivity because of the loss of coherence between the local pairs but within such a domain, lattice distortion could survive.

It is remarkable that Mn doping maintains the onset of superconductivity with the presence of apparently AJT-type distortion, unlike Ni and Co doping that immediately destroys superconductivity and distortion. Since the uniqueness of Mn doping is associated with the dynamical AJT distortion of the host lattice, it is likely that the AJT polaron (bipolaron) is a prerequisite to superconductivity. In this context, let us now examine the local structure of non-superconducting M:LSCO samples. AJT is expected to be of static nature for the case of Mn doping. The *in-plane* M-O(1) distance (1.92 Å) is significantly longer than that of LSCO (~1.88 Å) while the Mn-O(2) distance is shorter, the impurity site in the CuO_2 plane is strongly AJT-distorted. In summary, a close correlation between the polaron (bipolaron) and onset of superconductivity is demonstrated.

What Is a Realistic Model?: Bond Alternation as a Criterion

Our early studies [16] indicate that the magnitude of the $\sigma^2_{Cu\text{-}O}$ drop due to the magnitude of distortion and superconducting correlation) is roughly proportional to the superfluid density. The magnitude of $\sigma^2_{Cu\text{-}O}$ drop is a measure of superconducting fraction and the disappearance of inhomogeneity upon superconductivity or homogeneous electron states. The observed coincidence of the onset of superconductivity with the maximum lattice distortion or fraction of distorted domain (T_d^{max}) relates to a superconducting phase coherence, for which a critical length may exist between the Josephson Junction (JJ)-coupled "metallic" domains and undistorted "insulating" domain. If a distance between metallic domain and

insulating domain exceeds this critical limit, "macroscopic" superconductivity and lattice (distortion) may loose consistence as illustrated in the case of Mn substitution. In such a case, lattice distortion can exist even when superconductivity is not observed.

As doping proceeds, reduced Coulomb repulsion (U) would promote integration into extended domains with a larger size. The average distance between extended domains L decreases allowing tunneling over insulating domains [25]. When L becomes greater than a critical value (z), quantum tunneling is prohibited. For instance, suppressed tunneling under a tensile strain decreases superfluid density, and hence the critical temperature. Near the Mn dopants in Mn:LSCO ($x = 0.05$), non-superconducting regions are formed and superconducting domains are limited to small domains. As a distance between the superconducting domains becomes large, quantum tunneling [25] or percolation [26] is prohibited and the superconductivity eventually disappears although the onset temperature remains unaffected.

Several different models have been proposed to describe the AJT-like distortion below the pseudogap temperature. Here we focus on the existence of "beat" in k-space at 12 $Å^{-1}$ which indicates the presence of two different bond lengths with almost equal fraction, often called "bond alternation". If we apply the bond alternation observed at T_d^{max} as a criterion to differentiate the possible models, only two models remain. Possible structural models in Fig. 19.6a, b satisfy the criterion

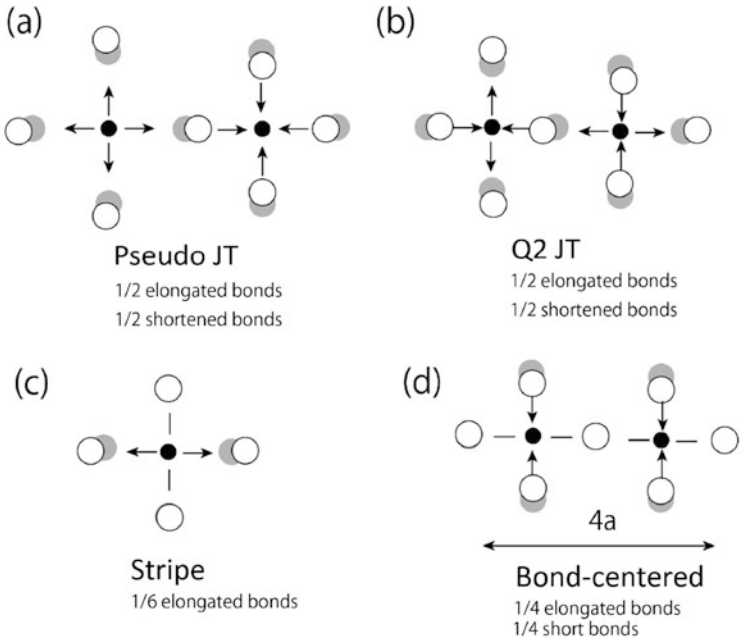

Fig. 19.6 Schematic representation of possible distortion models; pseudo JT (breathing-like distortion) [20] (**a**), Q_2 JT (**b**) [19, 31], stripe with LTT tilting of the CuO_6 unit [15]. (**c**), and stripe with Cu-O stretching (half breathing-like distortion) [27] (**d**). Taken from the literature [10]

[19, 20] in the limit of inhomogeneity (distortion extending all over the basal plane) while two models in Fig. 19.6c, d [15, 27] are excluded by the criterion. The completion of phase coherence requires the extended AJT distortion over the crystal. Interestingly, in two possible candidates, the two adjacent CuO_6 units are linked each other so that the elastic energy is minimized by the complimentary distortions. This coupled CuO_6 units are familiar to a bipolaron concept. The well-known disadvantage of a JT polaron, *i.e.*, a heavy mass [28] that leads to immobility is compensated by a bipolaron [29] which does not perturb the antiferromagnetic order [30]. As the coupling of the two units is driven by elastic forces [31], the findings that both AJT models fit to the observed bond alternation seem to be reasonable. Polarons may perturb spin configurations (antiferromagnetic order) and lead to spin vortices around that grow into spin loop current [20] or their one dimensional hopping may enhance strong coupling among spin, charge and lattice [19].

Other distortion models failed to satisfy the criterion [15, 27] are based on the stripes of distorted domains sandwiched by undistorted ones whose overall statistics is diluted by the spacing of undistorted domains. Because of this inhomogeneity, stripe models can not meet the criterion. The real space image of a Cu-O-Cu bond-centered electronic glass with disperse $4a_0$-wide domains of displaced oxygen atoms is observed by tunneling asymmetry imaging for $Bi_2Sr_2CaCu_2O_{8+d}$ (Bi2212) [32]. As the spatial variations in tunneling asymmetry occurs at the *in-plane* oxygen sites and the observed 2D texture pattern dispersed throughout the crystal may partially reflect the original dynamical distortion without long-range order, such patterns are taken as a frozen disorder because of a slow time scale of STM. In the model in Fig. 19.6d, the observed sharp contrast between a central ladder consisting of a column of oxygen atoms and the two neighboring Cu–O–Cu columns form a charge stripe [32]. Recent photoemission study on Bi2212 reported the growth of pseudogap component attributed to the preformed pair is associated with the planar modulation of electronic states observed by the STM. In this context, the polaronic lattice distortion may explain the local structural origin of pseudogap. Recent model calculations [33] indeed showed bipolarons form a charge-inhomogeneous texture pattern. The observed *in-plane* bond alternation may describe coherence of preformed pairs. More recently, the Q_2-type AJT distortion model originally based on the three-centered spin (ESR) [34] was interpreted in terms of bipolaron [35, 36] which could stay one of the most likely models.

Perspective View: Never Stop Quest for the Unified Mechanism

In our findings, the split of the Cu-O(1) bond in LSCO and its strong correlation with the onset of superconductivity is a key issue. The distortion is essentially in an *in-plane* local lattice which suggests the existence of polaron (bipolaron) as a player in the mechanism of pairing. The observed local distortion maximizes its

magnitude at $T_d^{max} \sim T_c^{onset}$ and appears upon the opening of a pseudogap (*ca.* 80 K ~ $2T_c$) where an unconventional electronic state begins to grow. Mn doping uniquely sustains the onset of superconductivity in LSCO, in sharp contrast with Ni and Co which quickly destroy the superconductivity. The effect of magnetic impurity doping further evidences an intimate relation between superconductivity onset (phase coherence) and the dynamic AJT-type distortion of host lattice. The current Hubbard framework lacks the proper treatment of lattice although modern theoretical developments are impressive [37].

The authors anticipate that continuing efforts and further developments would take into account undeniable facts that local lattice matters and find the way out to a unified theoretical model that seamlessly cover conventional and unconventional superconductivity. Unfortunately, we are still not allowed to enter in "a promised land of HTSC" which, in a wilderness waiting for our future entry since 1986. However, it would not be difficult to imagine we will be allowed to enter a promised land in the near future if we view the phenomena with unbiased eyes recognizing undeniable facts-intimacy with local lattice with HTSC. After all, a promised land is open for anybody who dares to take such efforts.

Acknowledgments Without the encouragement and inspiration to the author by K. Alex Müller, it would have been totally impossible to keep focusing on this work for over two decades. During this period, the author has engaged in experimental instrumentation including the development of a synchrotron beamline with an insertion device and a highly efficient x-ray detector. He expresses his greatest thanks to Changjing Zhang who contributed to the later collaborative studies, especially crystal growth and synchrotron experiments. The authors also would like to thank Annette Bussmann-Holder and Hugo Keller for encouragements and fruitful discussions which played as an engine of our work. In early days, the international collaboration between Italy and Japan has played an important role in kicking off the local lattice studies. The author expresses thanks to Antonio Bianconi who proposed a timely topic for a joint research based on the bilateral program. The author would like to express a special thanks to the Italian Embassy in Japan for the financial support. Finally the author expresses his thanks to a long term collaborator Naurang Saini.

References

1. J.G. Bednorz, K.A. Müller, Z. Phys. B **64**, 189 (1983)
2. Y. Kamihara, T. Watanabe, M. Hirano, H. Hosono, J. Am. Chem. Soc. **130**, 3296 (2008)
3. A.P. Drozdov, M.I. Eremets, I.A. Troyan, V. Ksenofontov, S.I. Shylin, Nature **525**, 73 (2015)
4. S. Kaiser, C.R. Hunt, D. Nicoletti, W. Hu, I. Gierz, H.Y. Liu, M. Le Tacon, T. Lowe, D. Haug, B. Keimer, A. Cavalleri, Phys. Rev. B **89**, 184516 (2014)
5. C. Fang, H. Yao, W.-F. Tsai, J.P. Hu, S. Kievelson, Phys. Rev. B 77, 224509 (2008).
6. P.W. Anderson, *The Theory of Superconductivity in the Cuprates* (Princeton University Press, Princeton, M.A., 1997)
7. W. Malaeb, T. Yoshida, T. Kataoka, A. Fujimori, M. Kubota, K. Ono, H. Usui, K. Kuroki, R. Arita, H. Aoki, Y. Kamihara, M. Hirano, H. Hosono, J. Physical Soc. Japan **77**, 093714 (2008)
8. M. Hiraishi, R. Kadono, S. Takeshita, M. Miyazaki, A. Koda, H. Okabe, J. Akimitsu, J. Physical Soc. Japan **78**, 023710 (2009)
9. C.J. Zhang, H. Oyanagi, Z.H. Sun, Y. Kamihara, H. Hosono, Phys. Rev. B **78**, 214513 (2008)
10. C.J. Zhang, H. Oyanagi, Phys. Rev. B **79**, 064521 (2009)
11. H. Oyanagi, C.J. Zhang, J. Phys.: Conf. Ser. **428**, 012042 (2013)

12. A.S. Alexandrov, J. Supercond. Nov. Magn. **22**, 95 (2008)
13. N. Mannela, W.L. Yang, K. Tanaka, X.J. Zhou, H. Zheng, J.F. Mitchell, J. Zaanen, T.P. Devereaux, N. Nagaosa, Z. Hussain, Z.–.X. Shen, Phys. Rev. B **76**, 233102 (2007)
14. A. Lanzara et al., Nature **412**, 510 (2001)
15. A. Bianconi, N.L. Saini, A. Lanzara, M. Missori, T. Rossetti, H. Oyanagi, H. Yamaguchi, K. Oka, T. Ito, Phys. Rev. Lett. **76**, 3412 (1996)
16. N.L. Saini, A. Lanzara, H. Oyanagi, H. Yamaguchi, K. Oka, T. Ito, A. Bianconi, Phys. Rev. B **55**, 12759 (1997)
17. J. Mustre de Leon, S.D. Conradson, I. Batistic, A.R. Bishop, Phys. Rev. Lett. **65**, 1675 (1990)
18. D. Mihailovic, Phys. Rev. Lett. **94**, 207001-1 (2005)
19. A. Bussmann-Holder, H. Keller, Eur. Phys. J. B. **44**, 487 (2005)
20. H. Koizumi, J. Physical Soc. Japan **77**, 034712 (2008)
21. H. Oyanagi, C. Fonne, D. Gutknecht, P. Dressler, R. Henck, M.–.O. Lampert, S. Ogawa, K. Kasai, Nucl. Inst. Methods A **513**, 340 (2002)
22. H. Oyanagi, A. Tsukada, M. Naito, N.L. Saini, Phys. Rev. B **75**, 024511 (2007)
23. A.A. Abrikosov, L.P. Gork'ov, Sov. Phys. -JETP **12**, 1243 (1961)
24. H. Kamimura, H. Ushio, S. Matsuno, T. Hamada, *Theory of Copper Oxide Superconductors* (Springer, Berlin, 2005)
25. D. Mihailovic, V.V. Kabanov, K.A. Müller, Europhys. Lett. **57**, 254 (2001)
26. J.C. Phillips, Phys. Rev. B **75**, 214503 (2007)
27. G. Deutcher, P.G. de Gennes, C.R. Phys. **8**, 937 (2007)
28. K.H. Höck, H. Nickisch, H. Thomas, Helv. Phys. Acta. **56**, 237 (1983)
29. A.M. Stoneham, L.W. Smith, J. Phys. Condens. Matter **3**, 225 (1990)
30. J.E. Hirsch, Phys. Rev. B **47**, 5351 (1993)
31. B. Kochelaev, A.M. Safina, A.S. Shengelaya, K.A. Müller, K. Conder, Mod. Phys. Lett. B **17**, 415 (2003)
32. Y. Kohsaka, C. Taylor, K. Fujita, A. Schmidt, C. Lupien, T. Hanaguri, M. Azuma, M. Takano, H. Eisaki, H. Takagi, S. Uchida, J.C. Davis, Science **315**, 1380 (2007)
33. D. Mihailovic, V.V. Kabanov, Phys. Rev. B **63**, 054505 (2001)
34. B.J. Kochelaev, J. Sichelschmidt, B. Elschner, W. Lemor, A. Loidl, Phys. Rev. Lett. **79**, 4274 (1997)
35. A.S. Alexandrov, V.V. Kabanov, N.F. Mott, Phys. Rev. Lett. **77**, 4796 (1996)
36. K.A. Müller, J. Phys. Condens. Matter **19**, 251002 (2007)
37. S. Onari, H. Kontani, Phys. Rec. Lett. **109**, 137001 (2012)

Chapter 20
Chemical Aspects of the Phase Separation in Alkali Metal Intercalated Iron Selenide Superconductors

Ekaterina Pomjakushina and Kazimierz Conder

Introduction

It is already 31 years since Alex Müller together with Georg Bednorz invited us to a journey through the fascinating world of the HT_c superconductivity. The starting point of this journey was their discovery of superconductivity in lanthanum barium cuprate with following many mile-stones within the cuprate mainland before new continents (MgB_2, iron superconductors) were discovered. As MgB_2 is a conventional (phonon-mediated) superconductor, the second real family of unconventional high temperature superconductors consists of Fe-based pnictides and chalcogenides. Their discovery in 2008 by Kamihara et al. [1] was very surprising as generally no superconductivity was expected in compounds containing magnetic ions. Within the big family of iron superconductors, iron selenide FeSe (so called 11 phase) has the simplest layered structure, with Fe cations tetrahedrally coordinated by Se within the layers. In more complex iron pnictides, discovered as a first, similar layers contain arsenic instead of selenium. Thus, iron selenides can be considered as prototypes of the whole Fe-superconductor family and a good model system to study the origin of superconductivity. The superconducting transition temperature T_c of only 8 K for FeSe [2] was increased to over 30 K applying a high pressure [3] or introducing (intercalating) alkali metals between the FeSe layers [4]. The last mentioned group of iron selenides with a general formula $A_xFe_{2-y}Se_2$ (where A = K, Rb, Cs, Tl/K, and Tl/Rb), discovered in 2010, is especially interesting as the materials possess several unique properties. The compounds (so called 122 phases) crystallize in a relatively simple structure consisting

E. Pomjakushina • K. Conder (✉)
Laboratory for Scientific Developments and Novel Materials, Paul Scherrer Institute, 5232, Villigen PSI, Switzerland
e-mail: kazimierz.conder@psi.ch

A. Bussmann-Holder et al. (eds.), *High-Tc Copper Oxide Superconductors and Related Novel Materials*, Springer Series in Materials Science 255,
DOI 10.1007/978-3-319-52675-1_20

of FeSe layers intercalated (sandwiched) with alkali metal cations. As the compounds are typically Fe-deficient and the existing Fe-vacancies order below ~550 K, the structure is, however, more complicated. Moreover, an antiferromagnetic (AFM) ordering with Néel temperature fairly above room temperature and a phase separation at lower temperatures (~480 K) are observed. From two separated phases one stays magnetic down to the lowest temperatures and the second becomes superconducting below ~30 K. Thus, in the alkali metal intercalated iron selenides complex relationships between the structure, magnetism and superconductivity are observed.

Synthesis and Crystal Growth

$K_{0.8}Fe_2Se_2$ was synthetized as a first member from the $A_xFe_{2-y}Se_2$ superconductor family [4]. Shortly after that, crystallization of the next 122-superconductor intercalated with caesium, namely $Cs_{0.8}(FeSe_{0.98})_2$ with $T_c \approx 27$ K was reported [5]. Following that, ternary superconductors with rubidium: $Rb_{0.8}Fe_2Se_2$ ($T_c \sim 31$ K) [6], $Rb_{0.78}Fe_2Se_{1.78}$ ($T_c \sim 32$ K) [7], and quaternary compounds containing thallium: $K_{0.3}Tl_{0.4}Fe_{2-y}Se_2$ ($T_c \sim 28$ K) [8], $Rb_{0.4}Tl_{0.4}Fe_{2-y}Se_2$ ($T_c \sim 31.8$ K) [6], $Rb_{0.42}Tl_{0.58}Fe_{1.72}Se_2$ ($T_c \sim 32$ K) [9] and $Cs_{0.26}Tl_{0.59}Fe_{1.9}Se_2$ ($T_c \sim 28$ K) [10] were obtained. Polycrystalline samples are usually synthesized via a two-step route involving in the first step a preparation of the FeSe precursor, which is then annealed in alkali metal vapors in the second step. For the second step an appropriate amount of the iron chalcogenide precursor and the alkali metal (packed into additional quartz tube) are sealed in a quartz ampoule. Reagents are heated to 700–750 °C for over 24–48 h and then cooled to ambient temperature. The intercalated compounds are extremely moisture and oxygen sensitive so that protective atmosphere is indispensable for all operations.

Single crystals of $A_xFe_{2-y}Se_2$ are usually obtained by the Bridgman method. For this, different starting materials, such as ceramic FeSe-precursors and alkali metals or mixtures of elements were already used. Typically, a piece of FeSe-precursor or a pellet pressed out of a mixture of high purity elements is loaded into a quartz ampoule. After that a suitable amount of the alkali metal is added and the ampoule is sealed under vacuum. The quantity of the alkali metal added depends on the desired stoichiometry of the compound. However, as the alkali metal reacts with quartz, usually 5% alkali metal excess is applied. A principle of the crystal growth by the Bridgman method and pictures of the ampoule before and after the syntheses are shown in Fig. 20.1.

Superconducting properties of the 122 materials are related to their compositions. These usually deviate from the ideal stoichiometry and show significant iron and alkali metal deficiency. It looks that the iron oxidation state achieved is decisive for a subtle balance between the magnetic and superconducting properties. Our recent review [11] gives an overall insight into this topic.

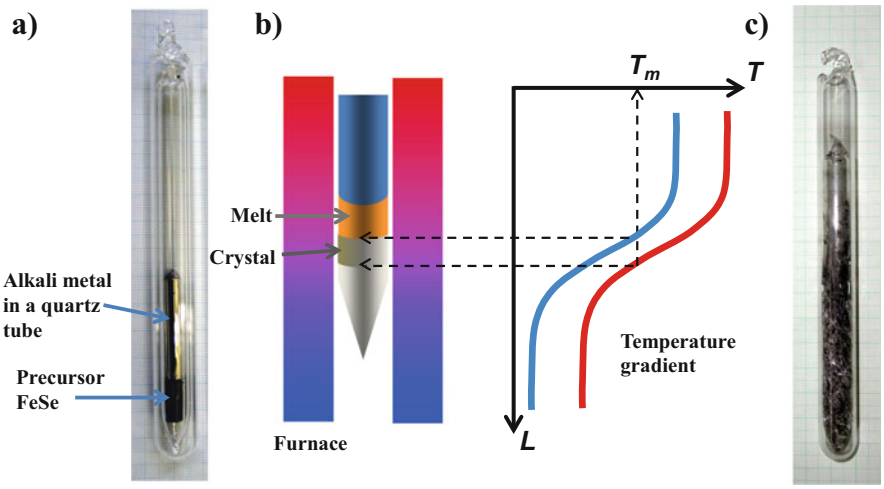

Fig. 20.1 A double-wall quartz ampoule before (**a**) and after (**c**) synthesis is shown- please note that as the solid material after crystallization has larger volume than the liquid, the inside ampoule is always broken. (**b**) Principle of the Bridgman crystal growth method (temperature gradient freezing technique). Slow cooling of the furnace causes upward moving of the melt-crystal interface

Structural Properties. Iron Vacancy Ordering. Phase Separation

Structure of the $A_xFe_{2-y}Se_2$ alkali metal intercalated iron selenides can be derived from the $ThCr_2Si_2$ structure type (space group *I4/mmm*) discovered more than 50 years ago [12]. There are more than 600 known compounds crystallizing in the $ThCr_2Si_2$ structure type. Figure 20.2a is showing an idealized unit cell of the $A_xFe_{2-y}Se_2$ superconductors with x = 1 and y = 0. In compounds which are superconducting, both A and Fe sites are deficient with the typical occupancies of around 0.8 and 1.6, respectively. At ambient temperatures the Fe vacancies are ordered resulting in a larger $\sqrt{5} \times \sqrt{5} \times 1$ (a ~ 9, c ~ 15 Å) unit cell (Fig. 20.2b) and a lower symmetry with the space group *I4/m*.

The vacancy order-disorder transition observed at about 535 K is of a first order and can be detected by Differential Scanning Calorimetry (DSC) measurements as shown in Fig. 20.3. At even lower temperatures two other transitions are visible by the DSC measurements. This at 520 K corresponds to the AFM ordering. The magnetic structure observed below this temperature consists of blocks of four ferromagnetically ordered Fe cations with the spins aligned along tetragonal c-axis, with antiferromagnetic alignment between these blocks (see Fig. 20.3). Further on cooling a phase separation is observed and two phases are created. The main phase, which occupies about 90% of the volume of the sample, exhibits the Fe-vacancy ordered larger $\sqrt{5} \times \sqrt{5}$ supercell and stays antiferromagnetic down

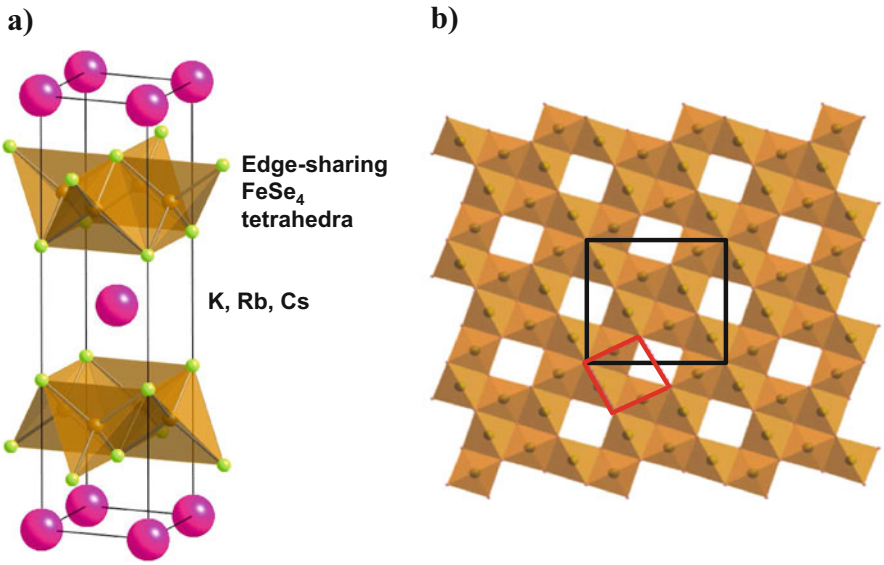

Fig. 20.2 (**a**) Structure model of the $A_xFe_{2-y}Se_2$ unit cell (space group *I4*/*mmm*). (**b**) Fe-vacancy ordering in $A_xFe_{2-y}Se_2$ (*I*4/*m*). *Red* and *black lines* show the original *I*4/*mmm* and the new *I*4/*m* $\sqrt{5} \times \sqrt{5} \times 1$ unit cells, respectively

to the lowest temperatures. The second minority phase has compressed lattice parameters in the tetragonal *a*-*b* plane and expanded along the *c* direction, with completely filled iron sites. It is not magnetic and becomes superconducting below $T_c \sim 30$ K. The minority phase can be approximately described by the *I4*/*mmm* Fe-vacancy free structure with stoichiometry $A_{0.60}Fe_2Se_2$. The minority phase fills about 10–15% of the crystal volume and is uniformly distributed within the volume of the crystal as shown in Fig. 20.4.

The observed phase separation process looks to be a typical eutectoid reaction when on cooling a solid phase transforms into two other solid phases, both with compositions which differ from the original one. Usually in one of these phases (majority phase) the crystal structure is preserved and only the chemical composition slightly changes. Accordingly, the second minority phase is commonly quite different. A typical example of such reaction is decomposition of austenite i.e. iron-carbon solid solution containing 0.76 wt.% of carbon. Upon cooling below 727 °C austenite decomposes into ferrite (containing almost no carbon) and cementite Fe_3C (containing 25 wt.% of carbon). The cementite phase is distributed in the ferrite matrix creating a lamellar microstructure very similar to that observed in our system. The microstructure detected in our crystals is common to so known cellular (discontinuous) precipitation transformations. In this process the second minority phase nucleates at grain boundaries of a polycrystalline material or at structural imperfections, e.g. dislocations, in a case of single crystals. The crystallization fronts of the nucleus move during the transformation process in a certain direction

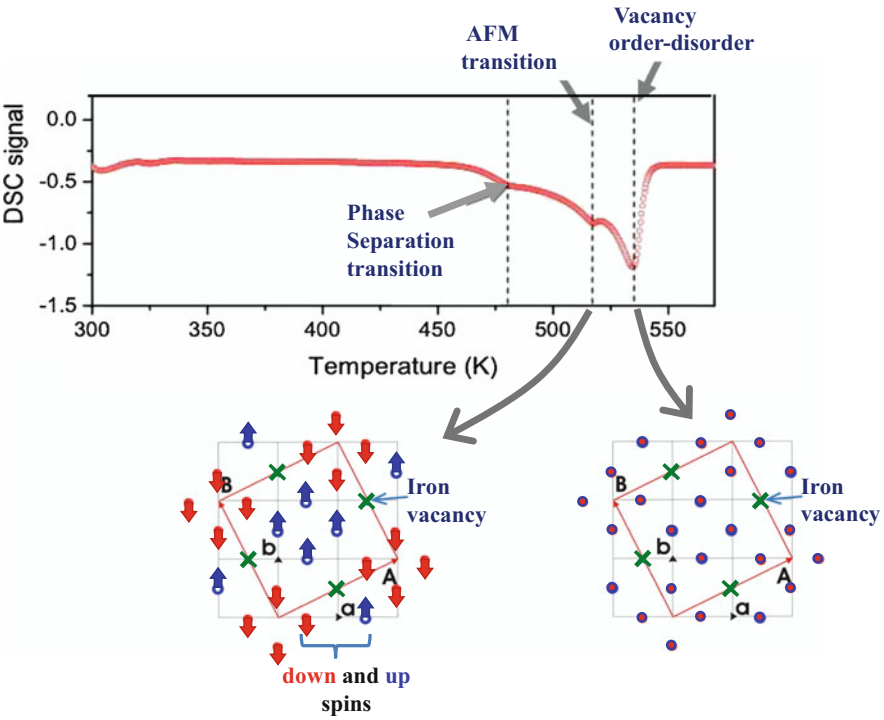

Fig. 20.3 Differential Scanning Calorimetry (DSC) measurements of $Rb_xFe_{2-x}Se_2$ performed on heating indicate three phase transitions. The largest peak at 535 K corresponds to the I4/m–I/4mmm order–disorder transition (ordering of the iron vacancies). The transitions at 520 K and 480 K correspond to the AFM ordering and phase separation, respectively

resulting in lamellar, fibrous or rod like microstructure of the growing phase. This is because the secondary phase grows in the direction of a high concentration of an active component (Fe in our case). The material remaining between the lamellas is becoming poor in the active component and the phase cannot grow in this direction. Figure 20.5 is schematically showing the mechanism of formation of cellural precipitates.

It looks to be impossible to increase significantly the fraction of the minority phase in $A_xFe_{2-y}Se_2$ and it is also not possible to synthesize it as a single phase. This probably results from the certain kind of the chemical phase diagram for this system. Figure 20.6 shows how such a hypothetical diagram would look like. As schematically depicted, the crystals can be grown from a melt at temperatures around 1340 K. Iron nonstoichiometric crystals grown at high temperatures are disordered, with statistically distributed iron vacancies. These are becoming ordered below Ts ~ 535 K. Further, at lower temperature (~480 K) the single phase with ordered vacancies is not thermodynamically stable and splits into two phases. The relative amount of the phases after separation is determined by the

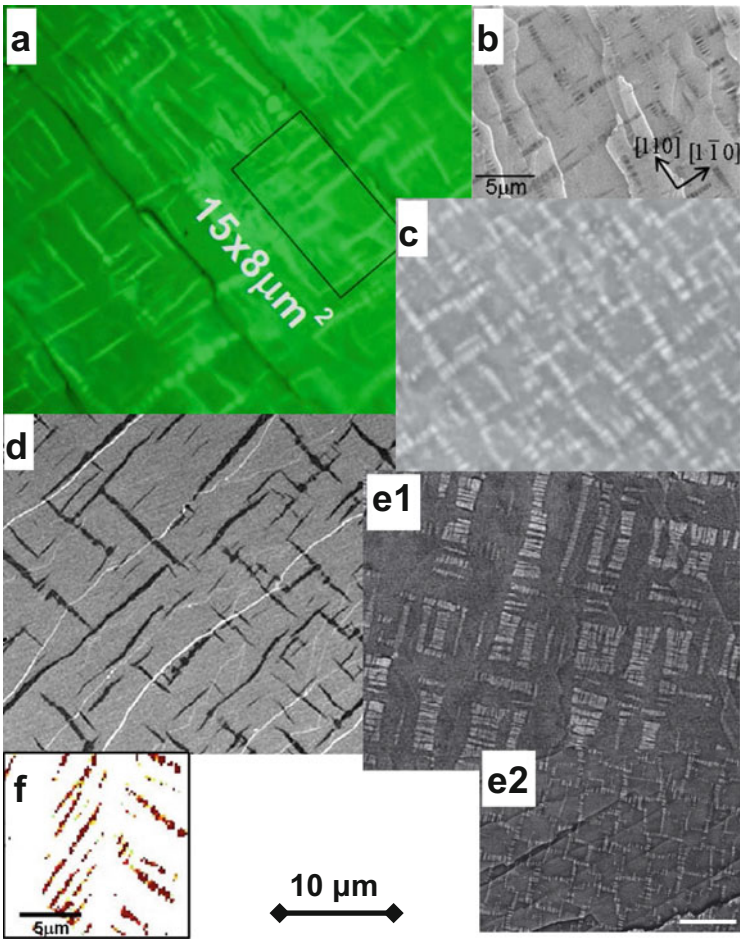

Fig. 20.4 Phase separation observed for crystals cleaved perpendicular to the *c*-axis. (**a**) Polarizing microscope picture of $Rb_2Fe_4Se_5$ crystal [13]. The stripes of the minority phase appear at about 45° to the *a*-axes of the majority phase. (**b**) Scanning Electron Microscope (SEM) picture of $Cs_{0.72}Fe_{1.57}Se_2$ crystal [14]. (**c**) SEM picture of $K_{0.80}Fe_{1.76}Se_{2.00}$ crystal. [15] (**d**) SEM picture of $K_{0.80}Fe_{1.75}Se_{2.00}$ [16]. (**e1**), (**e2**) SEM pictures, brighter domains: $K_{0.68}Fe_{1.78}Se_2$ background $K_{0.8}Fe_{1.63}Se_2$. Sample quenched from 250 °C (**e1**) or 350 °C (**e2**) down to liquid nitrogen [17]. (**f**) High-resolution Electron Backscatter Diffraction (HR-EBSD) pattern mapping lattice parameters c/a ratio. The regions with c/a > 3.9 (minority phase) are shown [14]

lever rule. Please note that creation of a pure minority $A_xFe_2Se_2$ phase will demand synthesis at temperatures below 480 K at which the kinetics of chemical reaction is becoming extremely sluggish.

The phase separation transition looks to be reversible as our diffraction studies have shown. Temperature-dependent behavior of the Bragg and diffuse scattering of phase-separated $Rb_{0.8}Fe_{1.6}Se_2$ single crystal was studied in details at the SNBL BM01A beamline at ESRF (Grenoble, France) using PILATUS 2M detector with

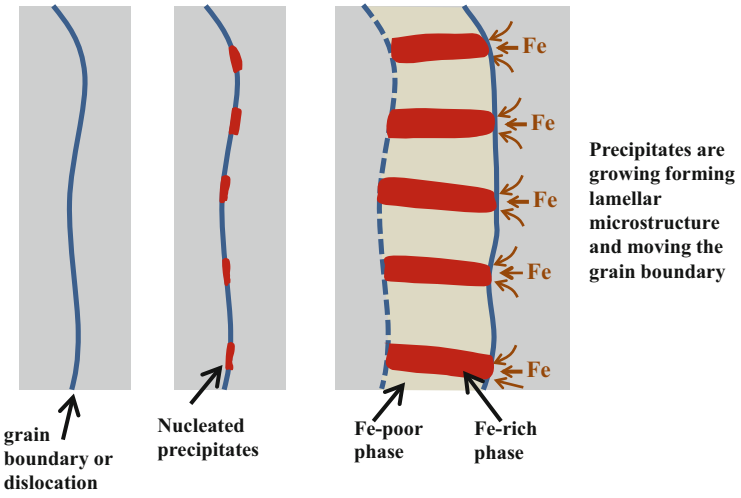

Fig. 20.5 Mechanism of the formation of cellular precipitates. Precipitates of the second phase are formed on the grain boundary or lattice imperfections. The precipitates grow in a preferred direction determined by the diffusion of iron ions into the crystallization front

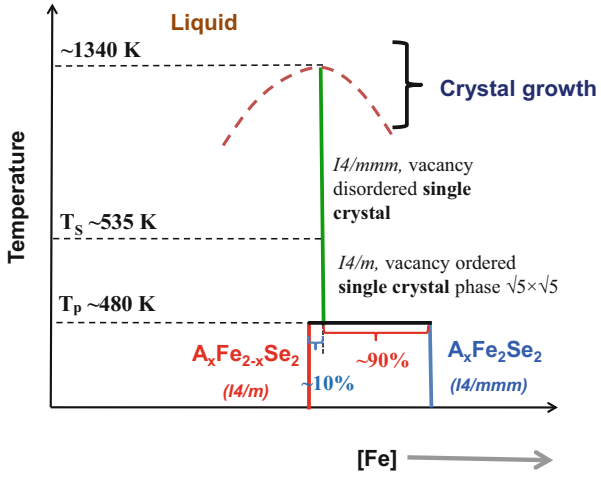

Fig. 20.6 Schematic chemical phase diagram for $A_xFe_{2-y}Se_2$. The lever rule determines the relative amounts of the separated phases—about 10% of $A_xFe_2Se_2$ and 90% of $A_xFe_{2-x}Se_2$

a 0.6997 Å wavelength [18]. At least three phases were experimentally observed as a function of temperature, which is illustrated by the temperature evolution of the (4 -2 0) Bragg peak (Fig. 20.7). At 300 K (upper panel) there are only two Bragg peaks observed, corresponding to the main AFM phase (left peak) and the minor phase (right peak). The third phase appears during annealing at 500 K and is kinetically inhibited. By annealing the sample at 500 K the first and the second

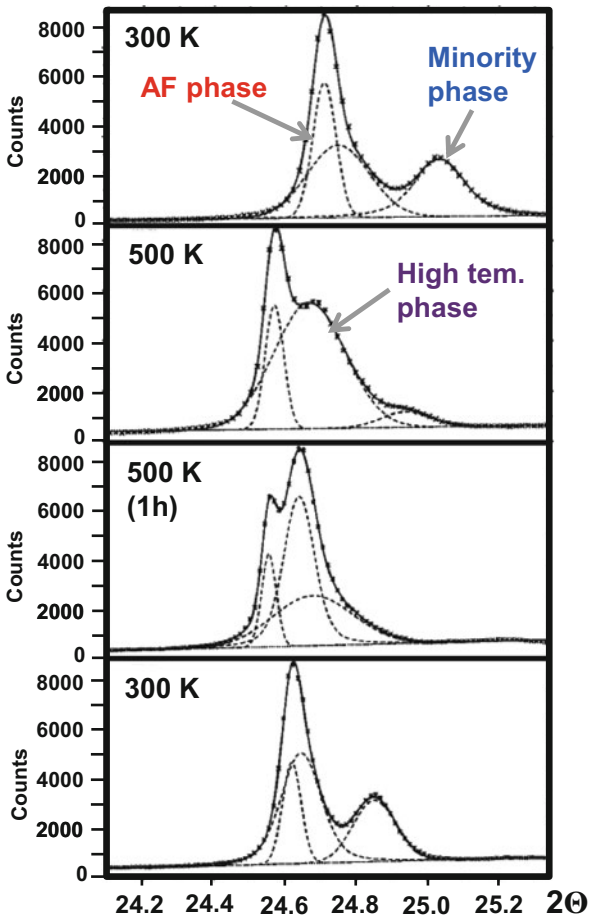

Fig. 20.7 Temperature evolution of the (4 -2 0) Bragg peak of $Rb_{1-y}Fe_{2-x}Se_2$ single crystal

phase merge into the third one with longer *a*-*b* unit cell parameters in comparison to the minor phase and very close to the main AFM one, resulting in growing of the corresponding middle Bragg peak. Finally, the first two phases completely transform into the third average high temperature 122-phase. Upon cooling down to room temperature the first and the second phase reemerge. Please note that the refurbished peaks are shifted to lower 2Θ values, e.g. the peak position of the main phase moves from 24.7° to 24.65°, which corresponds to an increase of the unit cell in *ab*-plane. This effect can be possibly explained by a reconstruction of the alkali metal sublattice triggered by a high mobility of alkali ions. It is also possible that the distribution of iron concentration is becoming less homogeneous after the phase separation and "unification" cycle. Both effects can consequently influence the unit cell parameters and cause irrevocable changes after thermal cycling of the crystal.

Structural investigations of the intrinsic phase separation in $A_xFe_{2-y}Se_2$ by x-ray and neutron diffraction as well as many complimentary methods are presented in

[11] reviewing over 50 papers published during 2011–2015 concerning phase separation in alkali metal intercalated iron chalcogenides.

Summary

In alkali metal intercalated iron chalcogenides both magnetism and superconductivity can coexist, as a phase separation occurs in apparently single crystals. The majority phase is insulating, magnetic and shows ordered pattern of Fe vacancies in the structure. The second, minority phase of the composition $A_{0.6}Fe_2Se_2$ (122) is conducting/semiconducting and becomes superconducting below $T_c \sim 30$ K. The phase separation is the intrinsic property of the system. The phase separation is observed at about 480 K, when the vacancy ordered single crystal $\sqrt{5} \times \sqrt{5}$ phase becomes thermodynamically not stable and undergoes solid–solid eutectoid reaction resembling those known from the Fe-C system, where austenite decomposes into ferrite and cementite Fe_3C. Such a process is controlled by the diffusion of one of the component—in our case iron, composition of which becomes firmly different in both phases. It is amazing that the iron diffusion in iron chalcogenides is fast enough to ensure a pronounced progress of the phase separation reaction at temperatures as low as 480 K.

Prof. Alex Müller at International Seminar on HTSC, Dubna, USSR (1989). Electronic photo archive of Joint Institute for Nuclear Research, Dubna, Russia (http://photo.jinr.ru/)

References

1. Y. Kamihara, T. Watanabe, M. Hirano, H. Hosono, J. Am. Chem. Soc. **130**, 3296 (2008)
2. F.C. Hsu, J.Y. Luo, K.W. Yeh, T.K. Chen, T.W. Huang, P.M. Wu, Y.C. Lee, Y.L. Huang, Y.Y. Chu, D.C. Yan, M.K. Wu, Proc. Natl. Acad. Sci. U. S. A. **105**, 14262 (2008)
3. Y. Mizuguchi, F. Tomioka, S. Tsuda, T. Yamaguchi, Y. Takano, Appl. Phys. Lett. **93**, 152505 (2008)
4. J. Guo, S. Jin, G. Wang, S. Wang, K. Zhu, T. Zhou, M. He, X. Chen, Phys. Rev. B **82**, 180520 (R) (2010)
5. A. Krzton-Maziopa, Z. Shermadini, E. Pomjakushina, V. Pomjakushin, M. Bendele, A. Amato, R. Khasanov, H. Luetkens, K. Conder, J. Phys. Condens. Matter **23**, 052203 (2011)
6. C.H. Li, B. Shen, F. Hang, X. Zhu, H.H. Wen, Phys. Rev. B **83**, 184521 (2011)
7. A.F. Wang, J.J. Ying, Y.J. Yan, R.H. Liu, X.G. Luo, Z.Y. Li, X.F. Wang, A. Zhang, G.J. Ye, P. Cheng, Z.J. Xiang, X.H. Chen, Phys. Rev. B **83**, 060512 (2011)
8. R.H. Liu, X.G. Luo, M. Zhang, A.F. Wang, J.J. Ying, X.F. Wang, Y.J. Yan, Z.J. Xiang, P. Cheng, G.J. Ye, Z.Y. Li, X.H. Chen, Europhys. Lett. **94**, 27008 (2011)
9. H. Wang, C. Dong, Z. Li, S. Zhu, Q. Mao, C. Feng, H.Q. Yuan, M. Fang, Europhys. Lett. **93**, 47004 (2011)
10. K.J. Syu, H.H. Sung, W.H. Lee, Physica C **471**, 591 (2011)
11. A. Krzton-Maziopa, V. Svitlyk, E. Pomjakushina, R. Puzniak, K. Conder, J. Phys. Condens. Matter **28**, 293002 (2016)
12. Z. Ban, M. Sikirica, Acta Crystallogr. **18**, 594 (1965)
13. A. Charnukha, A. Cvitkovic, T. Prokscha, D. Pröpper, N. Ocelic, A. Suter, Z. Salman, E. Morenzoni, J. Deisenhofer, V. Tsurkan, A. Loidl, B. Keimer, A.V. Boris, Phys. Rev. Lett. **109**, 017003 (2012)
14. S.C. Speller, T.B. Britton, G.M. Hughes, A. Krzton-Maziopa, E. Pomjakushina, K. Conder, A.T. Boothroyd, C.R.M. Grovenor, Supercond. Sci. Technol. **25**, 084023 (2012)
15. D.H. Ryan, W.N. Rowan-Weetaluktuk, M. Cadogan, R. Hu, W.E. Straszheim, S.L. Bud'ko, P.C. Canfield, Phys. Rev. B **83**, 104526 (2011)
16. Z.-W. Wang, Z. Wang, Y.-J. Song, C. Ma, Y. Cai, Z. Chen, H.-F. Tian, H.-X. Yang, G.-F. Chen, J.-Q. Li, J. Phys. Chem. C **116**, 17847 (2012)
17. X. Ding, D. Fang, Z. Wang, H. Yang, J. Liu, Q. Deng, G. Ma, C. Meng, Y. Hu, H.-H. Wen, Nat. Commun. **4**, 1897 (2013)
18. Ekaterina Pomjakushina, Volodymyr Svitlyk, Alexei Bossak, Vladimir Pomjakushin and Dmitry Chernyshov, ESRF experimental report 01-02-1003 (2012)

Chapter 21
Essential Role of Barium for Reaching the Highest Tc's in Superconducting Cuprates

Bernard Raveau

Dedicated to Professor K.A. Müller on the Occasion of his 90th Birthday.

The remarkable discovery of superconductivity at 35 K by Bednorz and Müller in 1986 [1] in the system Ba-La-Cu-O has opened an avenue to the exploration of strongly correlated electron systems based on transition metal oxides. The clever idea for exploring superconductivity in this system was clearly expressed by the authors in their article: "*This system exhibits a number of oxygen deficient phases with mixed-valent constituents* [2], i.e. *with itinerant electronic states between the non-J.T.* Cu^{3+} *and the J.T.* Cu^{2+} *ions, and thus was expected to have considerable electron-phonon coupling and metallic conductivity*". Several phases of this system had been shown as soon as 1984 to exhibit metallic conductivity above 90 K, as for instance, the oxides $La_{2-x}Ba_xCuO_4$ [2] and $BaLa_4Cu_5O_{13+\delta}$ [3], but no attempt to investigate superconductivity below this temperature had been made before. Then, it was rapidly found that the mixed valence of copper was not sufficient to induce high Tc superconductivity, but that a 2D character of the structure forming $[CuO_2]$ planes was absolutely necessary for the appearance of this exceptional phenomenon. This feature was emphasized very early in 1988 by the Van Hove scenario proposed by Labbé and Bok [4], which requires a critical hole doping concentration in the copper layers. This explains that in the La-Ba-Cu-O system, the oxide $La_{2-x}Ba_xCuO_4$ is the 35 K superconductor due to the bi-dimensional character of its K_2NiF_4-type structure (Fig. 21.1a) [2], whereas $BaLa_4Cu_5O_{13+\delta}$ [3] does not superconduct due to the fact that, in its structure (Fig. 21.1b) the CuO_6 octahedra and CuO_5 pyramids are 3D-linked. The appearance of superconductivity in this structure is not specific to barium since isostructural oxides $La_{2-x}A_xCuO_4$, with A=Sr, Ca were also found to exhibit superconductivity with the same Tc [5]. In other words, the origin of superconductivity in the $La_{2-x}A_xCuO_4$ oxides with A=

B. Raveau (✉)
Laboratoire CRISMAT, UMR 6508, ENSICAEN-CNRS, University of Caen, 6 boulevard du Maréchal Juin, 14032, Caen cedex, France
e-mail: bernard.raveau@ensicaen.fr

A. Bussmann-Holder et al. (eds.), *High-Tc Copper Oxide Superconductors and Related Novel Materials*, Springer Series in Materials Science 255,
DOI 10.1007/978-3-319-52675-1_21

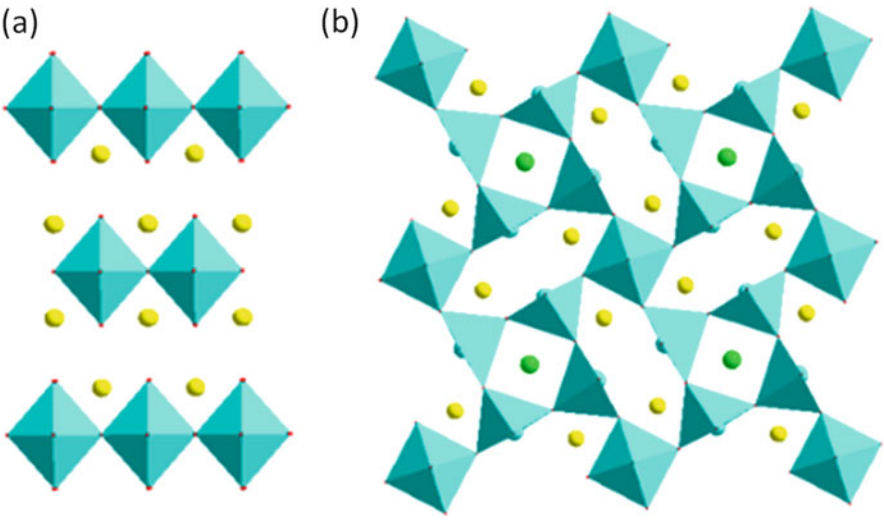

Fig. 21.1 (**a**) Layered structure of $La_{2-x}Ba_xCuO_4$, La and Ba (*yellow*) are distributed at random and (**b**) 3D-structure of $La_4BaCu_5O_{13}$, La (*yellow*) and Ba (*green*) are ordered

Ca,Sr,Ba is independent on the nature of the alcaline earth and depends on two separate effects: (i) the ability of lanthanum to form rock salt layers adaptable to single copper perovskite layers (Fig. 21.1a), generating in this way the 2D character and (ii) the affinity of divalent alkaline earth cations for oxygen, which keeps the oxygen "O_4" stoichiometry, realizing in this way the mixed valence Cu^{2+}/Cu^{3+}, i.e. hole doping.

Thirty years after the discovery of high Tc superconductivity in cuprates the role of the different components upon the appearance of this property and especially upon Tc is not completely understood. An important issue deals with the fact that among the numerous superconductive cuprates that were synthesized during the 1990s, the barium cuprates are ranked as the highest Tc superconductors. We discuss herein the role of barium in the properties of the high Tc cuprates.

Within the Ln-A-Cu-O systems with A=Ca, Sr, Ba and Ln=Y, La, Nd to Yb, it is observed that the oxides with A=Ba exhibit the highest Tc of 92 K [5]. The layered structure of the prototype of this series (Fig. 21.2a), the ordered oxygen deficient triple $YBa_2Cu_3O_7$ [6] clearly shows that barium is the driving force for the appearance of superconductivity in this oxide. Due its larger size compared to lanthanides it generates a 2:1 ordering of the Ba/Y layers and consequently is at the origin of the 2D character of the structure, which is built up of rows of square planar CuO_4 groups sandwiched between layers of CuO_5 pyramids. This bi-dimensional character cannot be stabilized in the case of strontium, in agreement with the fact that the layered oxide "$YSr_2Cu_3O_7$" cannot be synthesized due to the too small size difference between strontium and lanthanides. Then, in this framework, barium favors the partial oxidation of Cu^{2+} into Cu^{3+} keeping the oxygen content to "O_7", rather similar to the doping in $La_{2-x}Ba_xCuO_4$, but at a larger scale due to the much

higher Ba content. In this way an optimum hole content can be reached in the CuO_2 layers, with a Tc of 92 K. Indeed, the presence of barium allows a large proportion of copper (i.e. 1/3) to be oxidized into the trivalent state. The partial substitution of Sr for Ba which decreases Tc [7, 8], supports the crucial role of barium for reaching the highest Tc in this system. Thus, barium has a double role, as promotor of the layered structure and as "strong catalyst" for copper oxidation. Based on this observation, we tried to realize in 1987, the double oxygen deficient perovskite built up of double layers of CuO_5 pyramids, according to the hypothetical formula "$YBaCu_2O_5$" and would imply a 1:1 ordering of the Ba/Y layers (Fig. 21.2b). The synthesis of this compound failed, showing that the presence of barium cannot induce a so high Cu^{3+} content (50% of the total Cu amount). Nevertheless, the possibility to replace trivalent copper by Fe^{3+} allowed the first "112" structure to be discovered for the oxide $YBaCuFeO_5$ [9] (Fig. 21.2b), opening the route to numerous studies on magnetic and multiferroic materials.

The crucial role of barium for reaching the highest Tc's in cuprates, up to 125 K, is shown by the Tl-Ba-Cu-O and Tl-Ba-Ca-Cu-O systems [10, 11]. Considering the two series of superconductors, $TlBa_2Ca_{n-1}Cu_nO_{2n+3}$, $Tl_2Ba_2Ca_{n-1}Cu_nO_{2n+4}$ (Fig. 21.3), it clearly appears that the presence of barium is a key parameter for the generation of such layered structures with very high Tc's. The greater ability of barium to form layered structures with the highest Tc is shown by the $Tl_2Ba_2Ca_{n-1}Cu_nO_{2n+4}$ series, with double $[TlO]_2$ layers sandwiched by BaO layers: all the members with n = 1,2,3,4,5 could be synthesized by numerous authors (see for more details [12, 13]) and exhibit an optimum Tc ranging from 92 to 125 K. This behavior of barium is exceptional compared to strontium: numerous attempts to realize the $Tl_2Sr_2Ca_{n-1}Cu_nO_{2n+4}$ series allowed only one superconductive member $Tl_2Sr_2CaCu_2O_8$ (n = 2) to be synthesized with a Tc of ~44 K [14], i.e. much smaller than that of the homologous barium phase $Tl_2Ba_2CaCu_2O_8$ (Tc ~ 108 K) [15, 16]. In the same way, the whole series of superconductive cuprates $TlBa_2Ca_{n-1}Cu_nO_{2n+3}$, with single TlO layers could be synthesized from n = 2 to n = 5 [12, 13]. Quite remarkably, all these members exhibit the highest Tc, from 110 to 120 K, rather close to that of the homologous oxides of the $Tl_2Ba_2Ca_{n-1}Cu_nO_{2n+4}$ series. Here again, the preeminent role of barium compared to strontium for inducing superconductivity is confirmed by the fact that only one superconductor, $TlSr_2CaCu_2O_7$ [17] could be obtained for the hypothetical series $TlSr_2Ca_{n-1}Cu_nO_{2n+3}$. Moreover, this oxide could not be observed as a pure phase and its Tc of ~50 K is much smaller than that of the homologous phase $TlBa_2CaCu_2O_7$ which Tc was shown to reach 112 K [18, 19]. This behavior is explained by the double role played by barium: as promotor of the layered structure, it stabilizes this member, but as "catalyst" for oxidation of Cu^{2+} into Cu^{3+} it allows the quasi absence of anionic vacancies in the CuO_2 plane to be realized. Note that the n = 1-member, $TlBa_2CuO_{5-\delta}$ was also synthesized but is not superconductive due to the fact that the ideal formula $TlBa_2CuO_5$ would require the complete oxidation of Cu^{2+} into Cu^{3+}.

Thus, besides its size effect for creating bi-dimensionality, barium appears as an extremely efficient ingredient for tuning the oxygen content and consequently the hole carrier density for an optimum value of the Tc. This feature can be illustrated

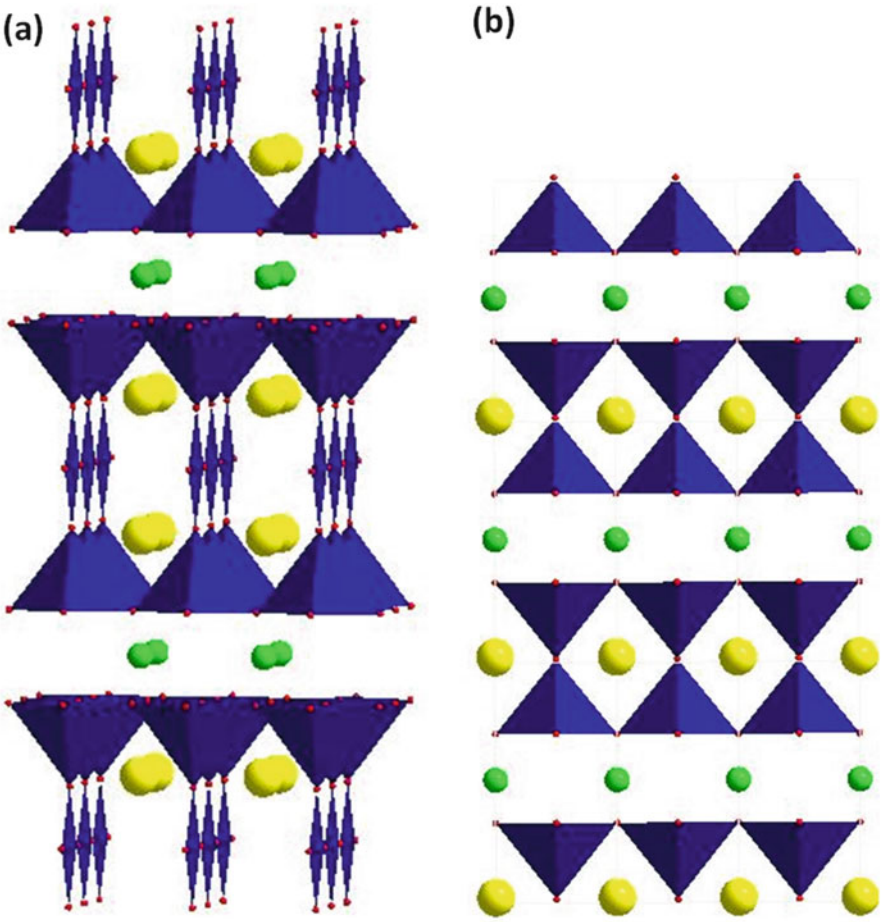

Fig. 21.2 Layered structures of (**a**) the "123" $YBa_2Cu_3O_7$ cuprate and (**b**) hypothetical "$YBaCu_2O_5$", obtained for $YBaFeCuO_5$. Ba (*yellow*) and Y (*green*) layers show a 2:1 and 1:1 ordering respectively

by the history of $Tl_2Ba_2CuO_6$, n = 1-member of the $Tl_2Ba_2Ca_{n-1}Cu_nO_{2n+4}$ series. In 1988, this cuprate was found by Parkin et al. [18] to be a superconductor with a rather low Tc of ~20 K, whereas Torardy et al. [20] observed for this phase a Tc of 55 K for monophasic sample prepared at 850 °C in air and of about 85 K for partially melted polyphasic sample of this nominal composition heated in air at 900 °C. The fact that the Tc of this cuprate is strongly affected by the oxygen content was then demonstrated in 1989 by Shimakawa et al. [21]. These authors showed that starting from non-superconducting samples with nominal composition $Tl_2Ba_2CuO_x$ superconductivity could be induced either by quenching or by Ar-annealing up to about 70 K due to decrease of oxygen content. The possibility to increase Tc up to ~84 K by varying the thermal treatments during the synthesis

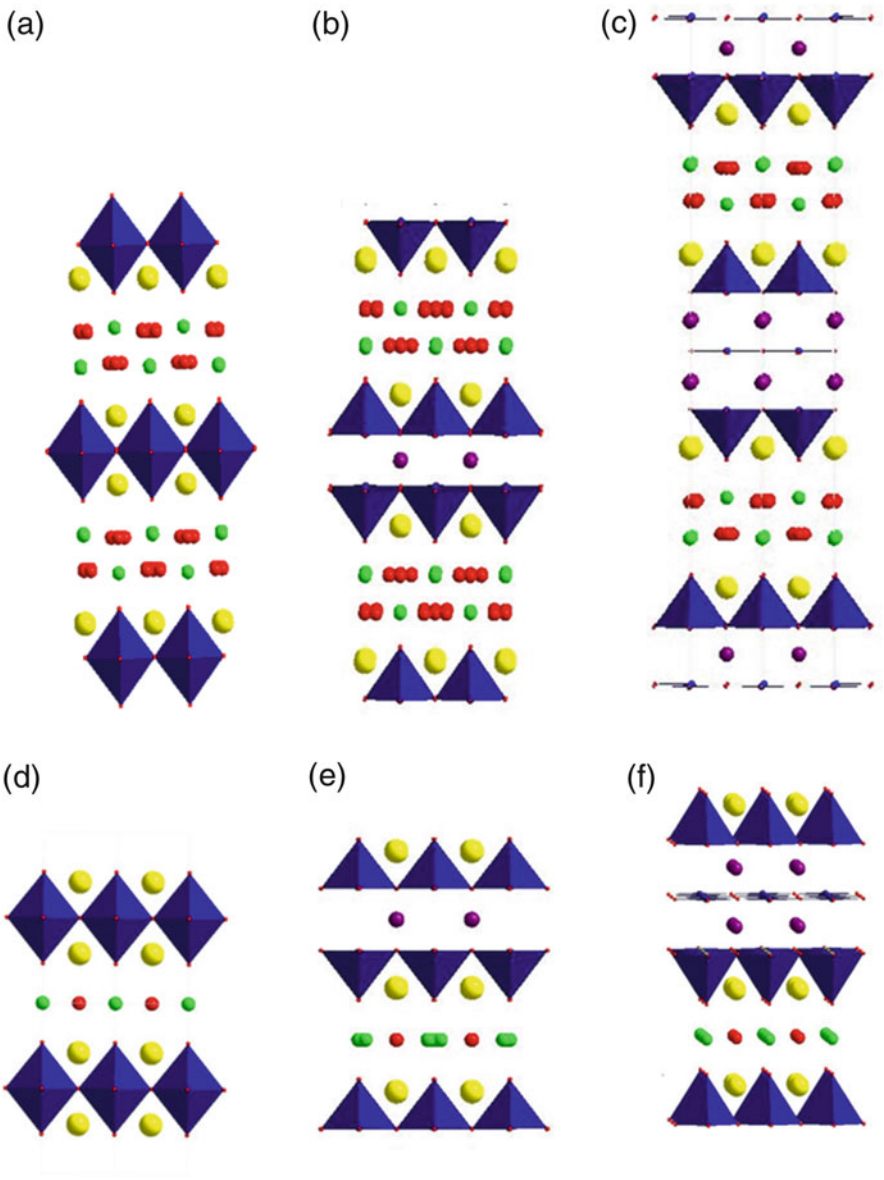

Fig. 21.3 Layered structures of thallium cuprates: (**a**) $Tl_2Ba_2CuO_6$, (**b**) $Tl_2Ba_2CaCu_2O_8$, (**c**) $Tl_2Ba_2Ca_2Cu_3O_{10}$, (**d**) $TlBa_2CuO_{5-\delta}$, (**e**) $TlBa_2CaCu_2O_7$, (**f**) $TlBa_2Ca_2Cu_3O_9$

was shown later on by Ramanujachary and Greenblatt [22]. The possibility to control the Tc in $Tl_2Ba_2CuO_{6\pm\delta}$ by tuning the oxygen content was shown by the CRISMAT group [23]. Mixtures of Tl_2O_3/CuO/BaO_2/Cu_2O (or Cu) with nominal compositions "$Tl_2Ba_2CuO_7$" or "$Tl_2Ba_2CuO_8$" were heated in sealed ampoules at ~880 °C,

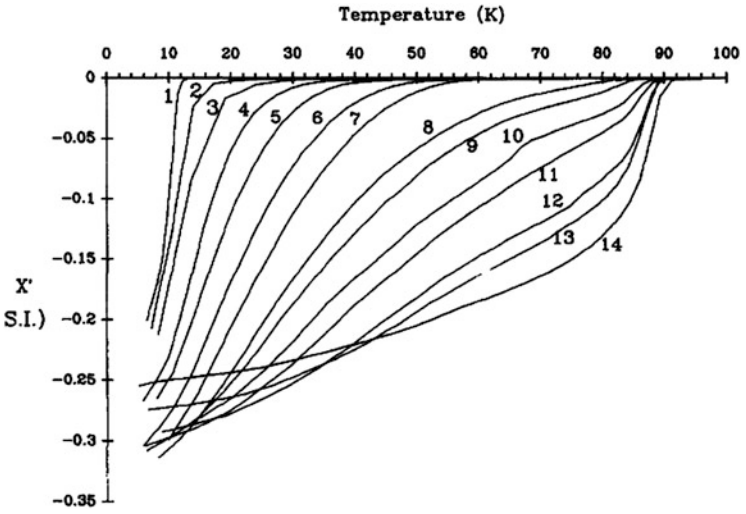

Fig. 21.4 Magnetic AC susceptibility of "$Tl_2Ba_2CuO_8$" samples (nominal composition): as-synthesized (1) and after successive and variable H_2/Ar annealing times, (2) 2 min, (3) 6 min, (4) 14 min, (5) 26 min, (6) 50 min, (7) 74 min, (8) 122 min, (9) 146 min, (10) 196 min, (11) 242 min, (12) 338 min, (13) 430 min, (14) 480 min

corresponding to oxygen pressures of about 3–6 bars during the synthesis, due to partial decomposition of BaO_2. In this way, pure phases $Tl_2Ba_2CuO_{6\pm\delta}$ were synthesized, either non-superconductive or with Tc ranging from 10 to 15 K, depending on the cooling method. Such samples were considered as over-doped due to the high oxygen pressure used for the synthesis. Then, for the optimization of the Tc, the samples were annealed in an H_2/Ar flow in order to decrease the oxygen content, but working at low temperature (290 °C) in order to avoid any thallium loss. The magnetic AC susceptibility curves registered on one sample annealed at this temperature for different times (Fig. 21.4) show that the Tc increases continuously with the annealing time from 12 K for the as-synthesized sample ($\tau = 0$ min) to the maximum Tc of 92 K after an annealing time τ of 480 min.

From the numerous studies performed on barium-thallium cuprates, we still do not understand the role of thallium in superconductivity. However, we can emphasize the primordial role of barium for the stabilization of a perfect layer stacking, for its ability to provide higher oxygen content compared to strontium, and for the creation of charge transfer between Ba/Tl/O layers playing the role of hole reservoirs and the CuO_2 layers which superconduct.

The specific role of barium in the superconductivity of copper based oxides is finally shown by the mercury cuprates [24, 25] $HgBa_2Ca_{n-1}\ Cu_nO_{2n+2}$, which Tc's ranges from 98 K up to 135 K. The structure of these phases (Fig. 21.5) is very similar to that of the first family of Tl-based cuprates. The layered character of the structure originates from the large size of barium compared to mercury and calcium, combined with the ability of mercury to adopt a linear two-fold

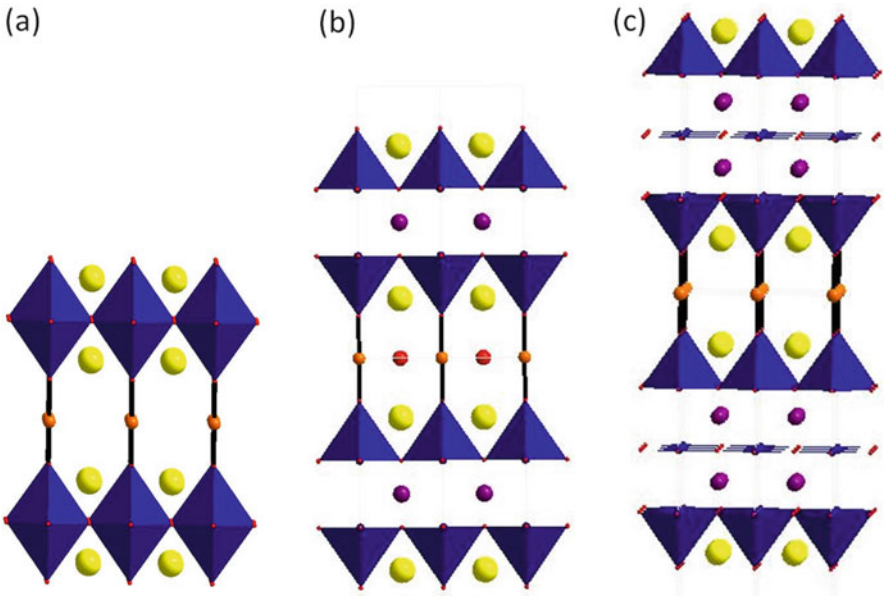

Fig. 21.5 Structure of the mercury cuprates (**a**) $HgBa_2CuO_4$, (**b**) $HgBa_2\ CaCu_2O_6$, (**c**) $HgBa_2Ca_2Cu_3O_8$

coordination. As a consequence, the ideal structure consists of an ordered stacking of [BaO] layers with [Hg] layers. In fact, here again barium acts as an "oxidation catalyst", so that additional oxygen can be incorporated at the level of mercury, leading to strongly oxygen deficient [HgO_δ] layers instead of single [TlO] layers. It is the tuning of this oxygen excess which plays a crucial role for the optimization of the Tc's in these cuprates. The impossibility to synthesize the strontium-mercury compounds confirms also the important role of barium for the stabilization of such layered structures.

The comparison of these barium cuprates with all other high Tc cuprates shows also the great potential of barium for reaching the highest Tc's. Indeed, the consideration of the homologous bismuth cuprates $Bi_2Sr_2Ca_{n-1}Cu_nO_{2n+4}$ clearly shows that for a same number of copper planes (n) the latter exhibit a significantly lower Tc, i.e. 22 K for the n = 1-Bi member [26] instead of 92 K for the Tl/Ba phase and 88 K for the n = 2-Bi member [27] instead of 108 K for the Tl/Ba-phase. The n = 3-Bi member exhibits also a smaller Tc of 110 K [28] compared to homologous Tl/Ba (125 K). Moreover, it is difficult to prepare and can be stabilized by the introduction of lead on the bismuth site [29]. In fact in the bismuth series two ingredients are playing a role separately for the appearance of superconductivity: the Bi^{3+} cation, due to its $6s^2$ electronic lone pair effect generates Bi_2O_2 layers necessary to the appearance of the layered structure, whereas Sr^{2+} plays the role of "oxygenation catalyst" for the introduction of hole carriers in the CuO_2 layers. In those cuprates, barium cannot be introduced due to its "higher oxidation power"

compared to strontium, which would oxidize Bi^{3+} into Bi^{5+} and consequently would hinder the formation of the layered structure. In fact, among all the cuprates that have been synthesized to date only one exhibits a Tc as high as that of its barium homologous: a Tc of 120 K was indeed observed for both $Tl_{0.5}Pb_{0.5}Sr_2Ca_2Cu_3O_9$ [30] and $TlBa_2Ca_2Cu_3O_9$ (see [12, 13] for a review).This particular behavior is explained by the ability of Pb^{2+} to be oxidized into Pb^{4+} in the presence of strontium, providing in this way an additional oxygen content, which contributes to the tuning of the oxygen stoichiometry for the optimization of the Tc's.

In conclusion, from the considerable number of studies carried out on cuprates, it appears that barium, due to its large size and to its "oxygenation power" plays an essential role in the appearance and optimization of superconductivity in these materials. This fascinating behavior for generating and controlling the mixed valence of copper and governing the dimensionality of the structure opens the route to the investigation of its role in the study of other strongly correlated systems, namely mixed valent transition metal oxides with promising magnetic and multiferroic properties.

References

1. J.G. Bednorz, K.A. Müller, Z. Phys. B-Condens. Matter **64**, 189–193 (1986)
2. C. Michel, B. Raveau, Rev. Chim. Miner. **21**, 407 (1984). Cited by JG B and KA M in their article as ref 16
3. C. Michel, L. Er-Rakho, B. Raveau, Mater. Res. Bull. **20**, 667 (1985)
4. J. Labbé, J. Bok, Europhys. Lett. **3**, 1225 (1988)
5. P. Hor, R.I. Meng, I. Gao, Z.J. Huang, Y.Q. Wang, C.W. Chu, Phys. Rev. Lett. **58**, 908 (1987)
6. J. Capponi, C. Chaillout, A.W. Hewat, P. Lejay, M. Marezio, N. Nguyen, B. Raveau, J.L. Soubeyroux, J.L. Tholence, R. Tournier, Europhys. Lett. **12**, 1301–1307 (1987)
7. B.M. Veal, W.K. Kvok, A. Umezawa, G.W. Crabtree, J.D. Jorgensen, J.W. Downey, L.J. Nowicki, A.W. Mitchell, A.P. Paulikas, C.H. Sowers, Appl. Phys. Lett. **51**, 279 (1987)
8. H.M. Sung, J.H. Kung, J.M. Liang, R.S. Liu, Y.C. Chen, P.J. Wu, L.J. Chen, Physica C **153**, 868 (1988)
9. L. Er-Rakho, C. Michel, P. Lacorre, B. Raveau, J. Solid State Chem. **73**, 531–535 (1988)
10. Z.Z. Sheng, A. Hermann, Nature **332**, 55–58 (1988)
11. Z.Z. Sheng, A. Hermann, Nature **332**, 138–139 (1988)
12. B. Raveau, C. Michel, M. Hervieu, D. Groult, *Crystal Chemistry of High-Tc Superconducting Oxides* (Springer-Verlag, Berlin, 1991)
13. B. Raveau, *Comprehensive Inorganic Chemistry (II)*, vol 2, (Elsevier B.V., 2013) pp. 63–102
14. E.A. Hayri, M. Greenblatt, Physica C **156**, 775 (1988)
15. M.A. Subramanian, J.C. Calabrese, C.C. Torardi, J. Gopalakrishnan, T.R. Askew, R.B. Flippen, K.J. Morissey, U. Chowdry, A.W. Sleight, Nature **332**, 420 (1988)
16. A. Maignan, C. Michel, M. Hervieu, C. Martin, D. Groult, B. Raveau, Mod. Phys. Lett. B **2**, 681 (1988)
17. C. Martin, J. Provost, D. Bourgault, B. Domengès, C. Michel, M. Hervieu, B. Raveau, Physica C **157**, 460 (1989)
18. S. Parkin, V.Y. Lee, A.I. Nazzal, R. Savoy, T.C. Huang, G. Gurman, R. Beyers, Phys. Rev. B **38**, 6531 (1988)

19. M. Morosin, R.J. Banghman, D.S. Ginley, J.E. Schireband, E.L. Venturini, Physica C **161**, 115 (1990)
20. C.C. Torardi, M.A. Subramanian, J.C. Calabrese, J. Gopalakrishnan, E.M. McCarron, K.J. Morissey, T.R. Askew, R.B. Flippen, U. Chowdry, A.W. Sleight, Phys. Rev. B **38**, 225 (1988)
21. Y. Shimakawa, Y. Kubo, T. Manako, T. Sato, S. Ijima, T. Ichihashi, H. Igarashi, Physica C **157**, 279 (1989)
22. K.V. Ramanujachary, M. Greenblatt, Physica C **165**, 377 (1990)
23. A. Maignan, C. Martin, M. Huvé, J. Provost, M. Hervieu, C. Michel, B. Raveau, Physica C **170**, 350 (1990)
24. S.N. Putilin, E.V. Antipov, O. Chmaissen, M. Marezio, Nature **362**, 226–228 (1993)
25. A. Schilling, M. Cantoni, J.D. Guo, H.R. Ott, Nature **363**, 56–58 (1993)
26. C. Michel, M. Hervieu, M.M. Borel, A. Grandin, F. Deslandes, J. Provost, B. Raveau, Z. Phys. B **68**, 421 (1987)
27. H. Maeda, J. Tanaka, M. Fuktumi, T. Asano, Jpn. J. Appl. Phys. **27**(L209), L548 (1988)
28. J.M. Tarascon, W.R. McKinnon, P. Barboux, D.M. Hwang, B.G. Bagley, L.H. Greene, G. Hull, Y. Lepage, N. Stoffel, M. Giroud, Phys. Rev. B **38**, 8885 (1988)
29. N. Mizumo, H. Endo, J. Tshuchiya, N. Kijima, A. Sumiyama, Y. Oguri, Jpn. J. Appl. Phys. **27**, L1225 (1988)
30. M.A. Subramanian, T.R. Askew, R.B. Flippen, A.W. Sleight, Science **242**, 249 (1988)

Chapter 22
Scientific Remembrances and Some Comments

Attilio Rigamonti

First Meeting and the Ferroelectric Transition

The first meeting and the acquaintance with Alex Muller goes back to the year 1968, at the AMPERE Meeting in Grenoble. I had published a letter dealing with an effect of the critical slowing-down dynamics at the ferroelectric transition: a peak around the transition temperature in the NMR-NQR relaxation rate W driven by the fluctuations of the electric field gradients (EFG) at the nuclear site [1]. Alex (already internationally known for his EPR studies) approached me, having in his hand the PRL issue open at the page of my paper. Gently, in half an hour he explained what I had not deeply understood. My interpretation of the effect was along the line pointed out by Cochran for the behavior of the dielectric constant: when to the elastic energy (that in the quasi-harmonic approximation is written $(a + bT)x^2$) the long-range potential energy due to the electric interactions was added, then the peak in the dielectric constant at the ferroelectric transition was justified. I thought that an analogous approach could be suited for the relaxation rate W, in terms of the slowing down of an optical vibrational mode (the "soft mode") yielding the critical EFG fluctuations.

In the conversation Alex pointed out how in an uni-axis crystal, of order-disorder type ($NaNO_2$), the root of the experimental observation for W had better to be searched in the dynamics of a *pseudo-spin in transverse field*. In collaboration with R. Brout and Harry Thomas, he had already published, for order-disorder ferroelectrics, a significant work [2] along that line, based on the Hamiltonian

A. Rigamonti (✉)
Emeritus of "Structure of Matter" at the University of Pavia, Pavia, Italy

Department of Physics "A. Volta", University of Pavia, Pavia, Italy

Istituto Lombardo, Academy of Science and Letters, Milano, Italy
e-mail: attilio.rigamonti@unipv.it

A. Bussmann-Holder et al. (eds.), *High-Tc Copper Oxide Superconductors and Related Novel Materials*, Springer Series in Materials Science 255,
DOI 10.1007/978-3-319-52675-1_22

$$H = -\Gamma\hbar \sum_i S_x^{(i)} - (1/2) \sum_{i,j} I_{ij} S_z^{(i)} S_z^{(j)}.$$

Nowadays this Hamiltonian is well established, furthermore being the starting point for the description of many phenomena in crystals and in magnetic systems.

The Debye-Waller Factor at Structural Transitions

After a few months Alex came to Pavia, visited our laboratories providing stimulating remarks. Besides the connection of the measurements we were carry on by NMR-NQR and the ones he was doing in Zurich by EPR (that we shall address later on) another common scientific interest was found. I was trying to detect, at the structural phase transitions, an effect on the Mossbauer γ- Ray recoiless fraction f, related to the Debye- Waller factor : $f = \exp[-4\pi^2 \langle x^2 \rangle / \lambda^2]$. Alex said that the same he was doing in Zurich, in collaboration with Multani. I was using an elementary equipment, moving the source at constant velocity, collecting the γ photons by a single channel detector, changing the velocity step by step, with painstaking measurements. Instead in Zurich they were sweeping the velocity and collecting the events with a multichannel detector. I had the feeling that any competition was hopeless. However, fairly Alex commented that my method was more appropriated for the purpose, that in Zurich they had little success and encouraged me to go on, in spite of a certain scientific competition. Indeed, a year later the observation of a dip in the Mossbauer fraction around the structural transition in $Ge_x\ Sn_{1-x}\ Te$ was successfully detected [3, 4]. Alex, fair and fore sighting!

Structural Phase Transitions

During the first visit by Alex we had fruitful discussions. In a way, a kind of road map for the study of structural transitions in perovskite crystals was designed, particularly of the ones driven by the critical zone-boundary modes, assimilatory to the rotations of the oxygen octahedral and leading to antiferrodistortive phase. In Pavia we were planning to use NMR and NQR spectroscopies, while at the IBM in Zurich the leading technique was EPR, with the direction by Alex and the valuable technical assistance by W. Berlinger. The theoretical framework was provided by Harry Thomas.

A group of researches was successfully carried out, involving the studies of the non-classical temperature dependence of the order parameter and an exhaustive analysis of the symmetry and the anisotropies of the critical fluctuations, in

$NaNbO_3$, $SrTiO_3$, $LaAlO_3$ and $KNbO_3$. A very valuable collaboration in Pavia was provided by Ferdinando Borsa.

A joint book [5], published some years later (most because of the Alex involvement in the search of novel superconductivity) presents the main results of the studies carries out in about 5 years.

By means of radiofrequency and microwave spectroscopies and by anelastic neutron scattering, by optical and dielectric methods, a significant body of interesting experiments had been achieved. Meantime the theories on phase transitions and critical phenomena had seen a great deal of progress and the field was acquiring strong interest. So Alex and myself decided to apply to the Italian Physical Society for the assignment of a Fermi International School in Varenna.

The Fermi School on Local Properties at Phase Transitions

The major aim of the School was to emphasize the insights of *local character* (somewhat corresponding to a full branch of wavevectors **q** of the collective excitations) in comparison to light and neutron scattering or dielectric techniques, (where only one or a limited range of **q'**s was explored). The aim was not limited to the ferroelectric and structural transitions, but also included the magnetic systems (where a variety of effects had been detected) and the transitions in liquid crystals. Furthermore, we had in mind to benefit of a suited theoretical framework by the leading scientists in the field of phase transitions and critical phenomena.

A book by the title "*Local Properties at Phase Transitions*", published in 1976 by North Holland [6] collects the large part of the lectures and seminars presented at the School. Even nowadays it seems to be useful, especially for researchers entering in the field.

Essentially, for the timeliness and the quality of the contributions addressed by the participants, one can say that the School has been successful. Alex deserves the large part of the merit. To his credit it goes the group of scientists and researchers he had been able to gather, due to his high reputation.

Again Structural Transitions and the "Central Peak"

The comparison of the results obtained by means of the different experimental approaches and the discussions dealing with the theoretical aspects, were usually addressed by referring to the Dynamical Structure Factor (DSF) S (**q,** ω), namely the Fourier transform of the time correlation function $<v_{\mathbf{q}}$ (t) $v_{\mathbf{q}}$ (0)$>$ of the collective critical variable whose anomalous temperature dependence was driving

the transition. In general the displacive transitions were displaying a DSF characterized by *resonant peaks*, with the central frequencies moving towards zero on cooling towards the transition (possibly turning to *diffusive peaks* very close to the critical temperature), for wavevectors **q** around the critical $\mathbf{q_c}$ (corresponding to the spatial modulation of the cooperatively displaced low temperature phase). At variance, the order-disorder transitions were expected to exhibit in the DSF *diffusive peaks*, centered at zero frequency and progressively narrowing for $T \rightarrow T_c^+$.

Soon it appeared that things were more complicated, that a further "central peak" around zero frequency was present in the DSF. Correspondently, the local potential (expected quasi-harmonic for displacive transitions and of double-wells character for order-disorder ones) could experiment significant modifications in the temperature range around the transition.

The problem was a tricky one, for the concurrence of a variety of factors: the character of the critical dynamics (often a mixture of displacive and order-disorder), the interplay of the thermal energy $k_B T$ with respect to the height $\Delta E = a^2/4b$ in the anharmonic local potential

$$V(x) = a x^2 + b x^4, \quad \text{with } a < 0 \text{ and } b > 0,$$

the role of defects, impurities or disorder. Furthermore the different experimental techniques (low frequency or high frequency spectroscopies, neutron scattering, optical methods) were detecting different regions in the **q** or in the ω ranges of the DSF, some mainly at the surface while others in the bulk of the sample.

A passionate scientific debate arose. Through meetings, papers, seminars in various circumstances Alex provided lucid insights and paved the way to a proper setting of the matter [7–9], in particular by stimulating *ad-hoc* experiments.

In Pavia we could enlighten in a satisfactory way at least the case when the matrix ideally is a perfect one, as in the strongly paraelectric crystal ($KTaO_3$) that enhances the interactions. The disorder in the interactions was introduced by Na for Ta substitutions.

The Na ions sit in an anharmonic local potential and the correspondent dynamics is characterized by a wide distribution of correlation times and of local barriers, furthermore with metastability and resonant tunneling (at very low temperature). The features of the DSF could be analyzed by considering the motion of interacting particles, each in a strongly anharmonic local potential (i.e. $kT << \Delta E$). The ^{23}Na spin-lattice relaxation rate driven by the quadrupolar interaction, as a function of temperature and in different ranges of frequencies, pointed out significant insights and the transformation from resonant to diffusive dynamics. Clarifying remarks could be drawn [5 (Chap. 2), 10, 11].

In summary, it could be concluded that there were *extrinsic* and *intrinsic* mechanisms yielding to the appearance of the central peak. The extrinsic mechanism was attributed to the presence of impurities, surface effects, locally breaking

the symmetry and ideally absent in a pure, infinitely large and translational invariant single crystal. The intrinsic mechanism was though as the direct consequence of a dynamics arising from non-linear terms in the Hamiltonian, thus being present in principle also in an ideal crystal. Furthermore, three intrinsic mechanisms were indicated: one due to the non-linear excitations occurring in the vicinity of a second order phase transition, because of the large fluctuations; the second by hetero phase fluctuations of precursor character that may occur also in the absence of impurities (expected most at first order phase transitions and often difficult to detect) and implying the appearance of pre-transitional clusters with long-range order. Finally because of the presence of impurities, defects or strains capable to affect directly the intrinsic cooperative dynamics.

Most colleagues seemed to agree on such a picture about the origin of the central peak, others were not so convinced. Meantime a dramatic event (the high-temperature superconductivity) turned the interests of the family of solid-state physicists somewhere else.

Possibly the tireless and valiant effort pursued by Alex for the deep understanding of the antiferrodistortive phase transitions in perovskite crystals (under pressure, electric field, with atomic substitutions etc.) and to which in Pavia we had the chance to contribute, has been a kind of training school for leading Alex to the inspiring goal of the superconductivity in cuprates.

Laurea H.C. in Pavia

In the spring of the year 1987, before the announcement of the reward of the Nobel price, in consequence of the scientific connections and of the Alex's reputation, the Faculty of Sciences of the University of Pavia unanimously voted for the assignment to Alex Muller of the Laurea in Physics *Honoris Causa*. The bureaucratic procedures took some time (the Ministers in Rome had to give the final approval) and the ceremony, with the *Lectio Magistralis*, could be fixed only a few weeks before his trip to Stockholm. In spite of the obviously hectic period, Alex did accept to come to Pavia.

During the trip with him from Lugano to Pavia, sitting in the rear of the car, although somewhat intimidated I found the courage to ask clarifications about the following astonishing effects, as they were appearing to me.

Since the ratio of the critical fields (H_{c2}/H_{c1}) was estimated very high, by resorting to a reasonable London penetration length λ_L in the relation

$(H_{c2}/H_{c1}) \approx \lambda_L(0)^2/\xi(0)^2$, the *coherence length* ξ had be very short, a few A°!

Second, how to explain a continue superconductive transition in a two-dimensional (2D) system (the process of Josephson-like tunneling of the

Cooper pairs between layers was not in my mind). Furthermore the Hubbard Hamiltonian was claimed do not allow superconductivity in 2D. Alex had the patience to clarify those aspects, in terms of polarons and bi-polarons.

The *Lectio Magistralis* by him was very appealing and the graduate students he personally met after that (some nowadays distinguished Physicists) still have vivid remembrance of that "beautiful day for the science".

The HT_cSC, Astonishing Consequences and "Collateral" Effects

Any solid state Physicist does not need my recall about the world-wide scientific atmosphere in the spring of the year 1987. Many questions were daily debated in research laboratories. The astonishing consequences from the unexpected superconductivity in oxides and in the presence of magnetic ions have already been mentioned. It is only added the remarkable fact that, in spite of the very short coherence length, the Ginzburg-Landau theory, with minor amends for the anisotropy and particularly in the ingenious and extensive application carried out by Abrikosov, it works quite well in HT_cSC. It remains the most workable way to describe proximity effects, interfaces and boundary conditions, flux flow and dissipation.

In the following, three significant "collateral effects" of the phenomenon discovered by Bednorz and Muller will be addressed in some detail. Before that, I mention that in 1999 Alex was co-optated, with the totality of the votes, as foreign Member of the "Istituto Lombardo" the Academy of Science and Letters in Milano, founded by Napoleon as counterpart of the *Institut de France*. In the October of the year 1996 the Academy organized a meeting on HT_cSC by the title "After ten years: certainties and perspectives". In spite of a number of invitations from everywhere, Alex did attend the meeting and offered a nice talk devoted to the historical development of the superconductivity in the oxides, recalling some yet unknown aspects or events.

Collateral Effect 1: The Parent of HT_cSC as 2DQHAF

In the light of the discovery by Bednorz and Muller the parent of HT_cSC's was inferred to be La_2CuO_4, basically a planar array of $S = 1/2$ Cu^{2+} magnetic ions onto a square lattice. It was soon realized that this crystal was the experimental realization of the model two-dimensional (2D), quantum ($S = 1/2$), Heisenberg antiferromagnet (AF). Thus a great deal of interest was triggered towards low dimensional quantum magnetism. A number of experimental and theoretical physicists had the chance to benefit of this aspect of the discovery of HT_cSC (for a review on the

subject see [12]). On the desk of many solid state physicists in the world, for months one could see the complex phase diagram of 2DQHAF as a function of hole doping and/or disorder and temperature, with various regimes, the normalized classical regime, the quantum critical, the quantum disordered and the superconducting one.

In Pavia, most by NQR and μSR techniques, we studied the pure, the spin and charge doped La_2CuO_4, along several years. Among other groups, I should recall the excellent work independently carried out by the same experimental approaches in Zurich, by Detlef Brinkmann, M. Mali and J. Roos, I think with the involvement of Hugo Keller and Alex himself.

Attention was devoted to the in-plane magnetic correlation length ξ_{2D} involved in the equal-time spin correlation function $<S_i\ (0)\ S_j\ (0)>$; to the critical dynamics driving the system towards the long-range ordered state; to the validity of the dynamical scaling; to the modifications induced by spin dilution (Zinc for Copper substitution) and by charge doping (through hetero-valent substitutions), both in the lightly doped La_2CuO_4 as well as in the vicinity of the percolation threshold (where the AF order is about to be hampered at any finite temperature). For collection of data, see Refs. [13–15]. For some illustrative results see the Figures below.

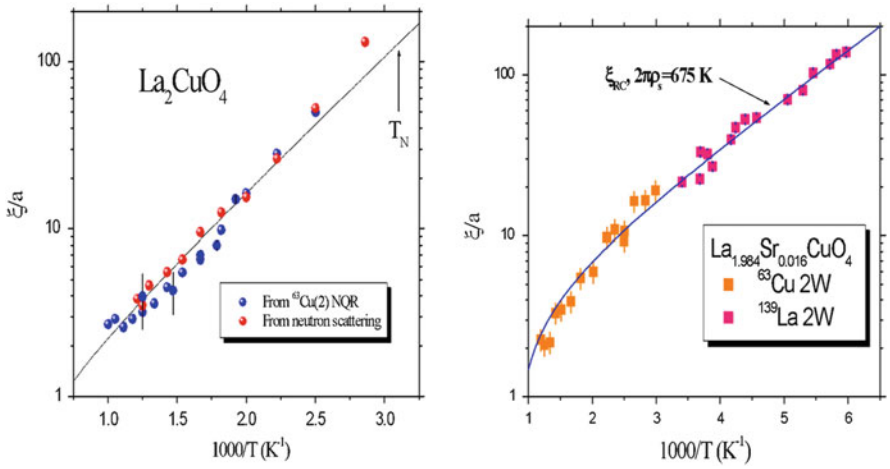

In-plane magnetic correlation length ξ_{2D} as a function of temperature in pure and in charge doped La_2CuO_4

The drop of the antiferromagnetic transition temperature T_N upon charge and spin doping

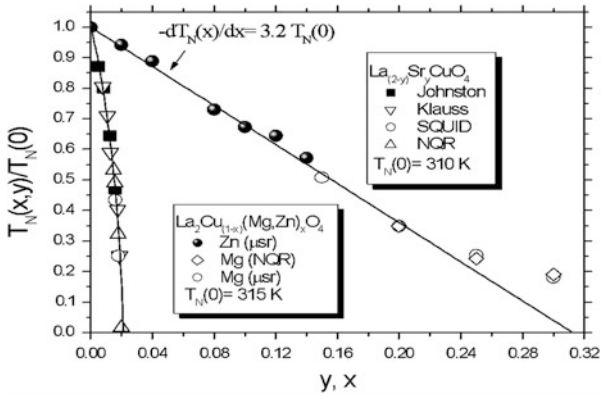

The spin stiffness and the staggered magnetic moment upon spin dilution.

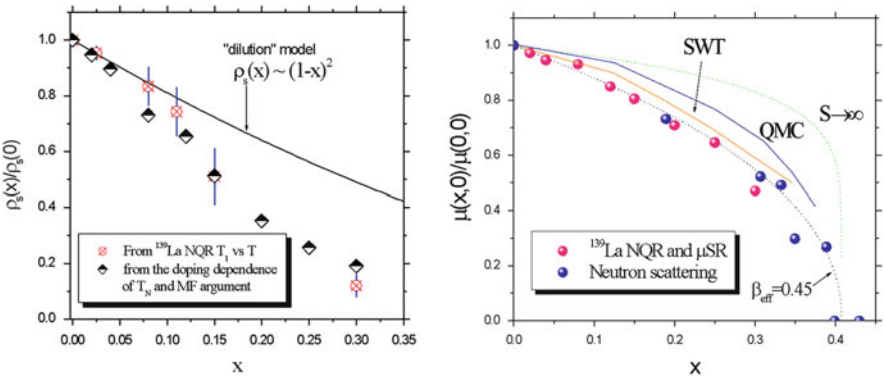

Rarely in the development of the science a side-effect of a discovery has been so prolific of research works, debates and perspectives.

Comparable consequences in this aspect also had another side-effect.

Collateral Effect 2: The Thermal Excitation of the Abrikosov Vortices

As it is known, in HT_cSC, strongly of type 2, an external magnetic field larger than the critical field H_{c1} penetrates in the bulk in form of Abrikosov vortices (or flux lines, FL). At variance with the classical BCS superconductors, the high temperature range, the layered structure and the anisotropy of HT_cSC permit the thermal excitation of the vortices. Thus the FL, when no locked by pinning, exhibit a novel dynamics, with vibrational, diffusion-like and fluctuations properties. The paper by Muller, Takashige and Bednorz [16], of extraordinary importance, was the first one

to point out the existence of a temperature range of FL motion, thus implying irreversibility effects, with difference in the field-cooled or zero-field-cooled diamagnetic susceptibility. In a few years after that, a number of experimental and theoretical studies pointed out how as a function of the external field and temperature, a rich B–T phase diagram of the FL occurs, including the crossing of the "thermal melting" line and of the decoupling temperature line.

Many researches were carried out involving this aspect of the main discovery. I would like to address only a nice piece of work that could be performed in Pavia by measurements of ^{89}Y NMR spin-lattice relaxation rate W_{FL} in YBCO124, as a function of temperature and magnetic field. The merit of this work [17] is that it indicates the basic insights that can be achieved by NMR experiments in regards of the thermally excited diffusion-like motions of the vortices. It should be remarked that the displacement of a flux line implies the motion of the field profile in the bulk of the material. This local modulation of the field provides the relaxation mechanisms for the nuclei.

It was found that for a given external field H_{ext} a maximum in the relaxation rate $W_{FL}{}^{max}$ occurred at a given temperature T_m when an effective sliding frequency $\omega_{eff} = D/l_e{}^2$ becomes of the order of the measuring frequency $\omega_m = H_{ext}\,\gamma$ (γ nuclear gyromagnetic ratio). In the above D is a diffusion-like two dimensional constant for the vortex "pancake", while l_e is the inter-vortices distance. The strength of maximum can be written

$$W_{FL}^{max} \approx \gamma^2 h_e^2/\omega_m,$$

h_e being the r.m.s. amplitude of the profile of the local magnetic field from vortex to vortex (to give an idea, at $T \approx T_m$, h_e is of the order of 1 mTesla for H_{ext} in the range 5–15 Tesla). On decreasing H_{ext} the irreversibility temperature and then the frequency triggering the FL dynamics, are increased towards $T_c{}^-$. For a reduced H_{ext}, also ω_m is decreased and according to Equation above the maximum $W_{FL}{}^{max}$ should increased, while occurring at higher temperature.

Indeed, by decreasing the field from 14.9 Tesla to 9.4 Tesla, $W_{FL}{}^{max}$ was noticed to increase. However a further decrease of the field from 9.4 to 5.9 Tesla caused a *decrease* of $W_{FL}{}^{max}$. This somewhat unexpected effect is related to the strong decrease of the field profile when the transition temperature is approached on warming.

The interplay between "profile-of-the internal field"—"frequency of the 2D sliding motion of the vortex pancake", let one to imagine the richness of the insights that can be achieved by resorting to the experimental procedure outlined above. For instance, again in YBCO124, from the analysis of the data for $1/T_1 \equiv W_{FL}\,(H_{ext}, T)$ the barrier U for the internal depinning could be inferred, proving that U is inversely proportional to H_{ext} [17]. For illustration see the Figures below.

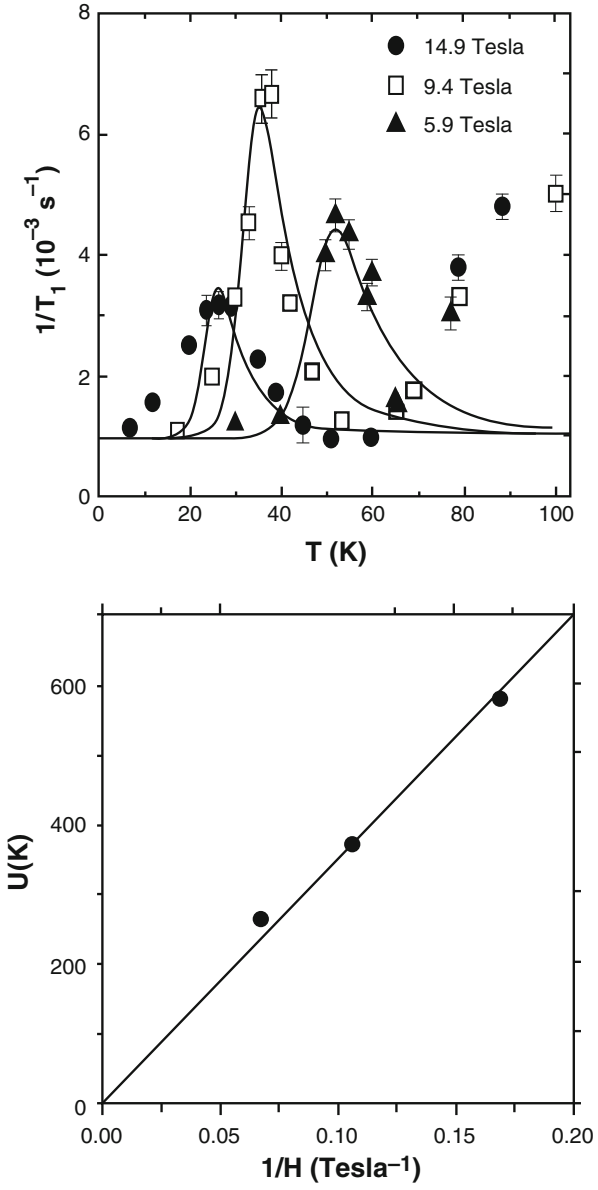

For several other effects, studied by means of NMR-NQR relaxation, line width and echo dephasing, see [18].

Collateral Effect 3: The Superconducting Fluctuations and the Diamagnetism Above T_c

As for any second-order phase transitions, enhancement of the order parameter fluctuations is expected on approaching T_c^+. Superconducting fluctuations (SF) imply that the mean square amplitude of the of the order parameter is different from zero also above T_c. One can think that SF's are locally generating non-equilibrium Cooper pairs, lacking long-range spatial coherence, that are not stable while their life-time critically increases on approaching T_c. The effects of SF were hardly evidenced in conventional BCS superconductors and because of the enlarged temperature range in which they occur, they had been studied most in films.

The discovery by Bednorz and Muller changed dramatically the scenario of the SF's. Because of the reduced coherence volume ξ^3, the low dimensionality of the carrier spectrum and of the density, and the high value of the transition temperature, the SF's became an appealing field for experimental analysis over a relatively large temperature range. Furthermore in HT_cSC the hierarchy of the various contributions to SF is modified and they manifest themselves in unusual form [19, 20].

A variety of intriguing and long-debated phenomena have involved the SF's.

Under the driving force of Andrey Varlamov, in Pavia we first carried out an experiment to evidence the SF through the spin susceptibility $\chi''(\mathbf{k}, \omega)$ involved in the relaxation process [21]. The idea was to compare the relaxation rate around T_c obtained in the NQR regime with the one in the NMR regime, at the aim to wipe out with the magnetic field the positive Maki-Thompson contribution and to evidence the negative density of states (DOS) contribution. The research (as analogous ones carried out by other authors) was only partially successful, mainly because the DOS contribution also was more or less affected by the field (for a critical discussion and reference to other authors, see [20], p. 266).

On the contrary, by looking at the diamagnetic susceptibility χ_{dia} by means of isothermal SQUID magnetization curves M_{dia} vs. H for $T \rightarrow T_c^+$, unexpected aspects of the fluctuating diamagnetism were found and widely studied in Pavia [22].

In extreme synthesis, M_{dia} vs. H in *underdoped cuprates* was found to exhibits an *upturn* in the field dependence, with a field H_{up} orders of magnitude smaller than the field expected to affect the Cooper pairs according to the Ginzburg-Landau theory. A detailed explanation of the phenomenon should not be given here. It is just pointed out that the major novelty was the first discovery of the occurrence of *phase fluctuations* between the precursor superconducting "islands" at non-zero local order parameter, still lacking of long-range coherence. Thus the decrease of the thermodynamic transition temperature in underdoped superconductors with respect to the optimally doped samples, is justified. Furthermore it was possible to prove that the phenomenon of phase fluctuations was quite different from the case of diffuse transition with a local $T_c(r)$, in principle possible in underdoped HT_cSC [23]. In fact, the upturn field (see Figure below) *increases on increasing temperature*, at variance of what must occur for the case of diffuse transition related to in-homogeneities.

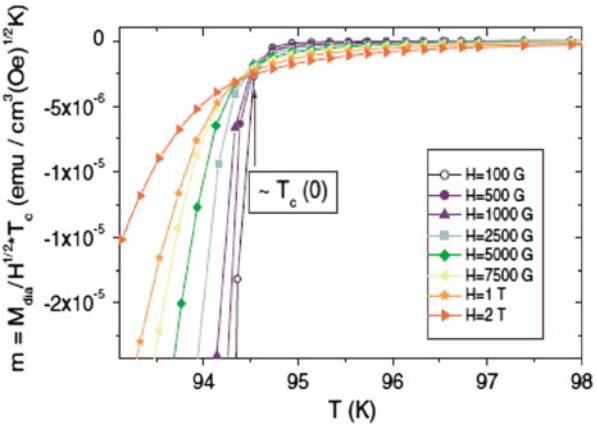

Optimally doped SC ($SmBa_2Cu_3O_7$). The crossing of the scaled magnetizations at $T_c(0)$ respects the scaling laws; the magnetizations curves are in agreement with the classical Ginzburg-Landau precursor diamagnetism.

At variance, in underdoped compound $SmBa_2Cu_{2.85}$ $Al_{0,15}$ O_7 at $T_c(0)$ about 56 K the isothermal magnetization curves reported below are quite different, an upturn field occurring at the value orders of magnitude smaller than the classical Ginzburg-Landau one in optimally doped SC, expected around 100 Tesla. For details see [22].

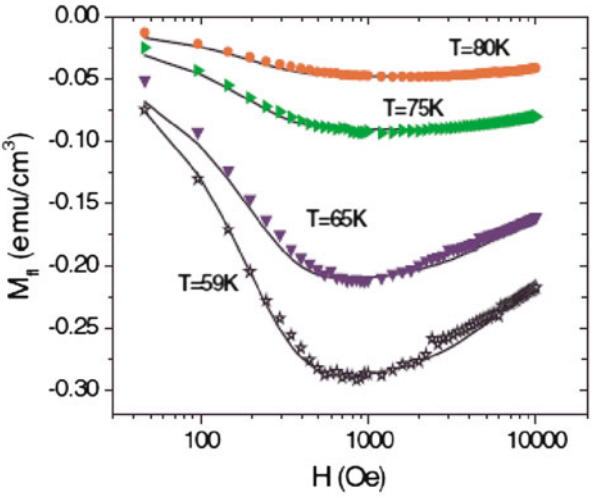

A Further Remark

Some comments have been formulated along the recall of the scientific remembrances. The role of Alex Muller in the history of Physics is obviously definitely set. In regards of the HT_cSC, the purpose of this report was most to emphasize the wealth of novel effects, studies, elaborations, discussions and passionate debates that the discovery has generated in a wide area of solid state physics.

I would like to conclude with a particular comment taken *verbatim* from a book (coauthors Andrey Varlamov and Jacques Villain) published by Belin [24].

Une découverte aux particularités remarquables

La découverte de cette supraconductivité à haute température a des particularités rares dans la physique moderne. D'abord elle est due à seulement deux chercheurs travaillant seuls et munis de fonds modestes. D'autre part, les matériaux étudiés ne contenaient que des éléments facilement accessibles (pas d'isotopes rares, par exemple). Ces supraconducteurs pouvaient être obtenus en un jour dans n'importe quel laboratoire universitaire. Quel contraste avec, par exemple, la physique des hautes énergies, qui requiert des équipes énormes, des équipements de quelques milliards d'Euros, et où la liste des auteurs d'un article tient une page entière ! Müller et Bednorz nous ont rappelé l'importance de l'initiative individuelle, même si leur succès est largement dû au fait qu'ils étaient très informés de l'actualité scientifique et en constante discussion avec de nombreux spécialistes. De nombreux supraconducteurs à haute température aient été déjà préparés avant Müller et Bednorz par différents chercheurs mais que ceux-ci n'aient pas eu l'idée de mesurer leur résistance électrique (ou la possibilité de le faire facilement).

Une autre particularité de la découverte de Müller et Bednorz est qu'elle fut annoncée par un article dans un journal allemand, Zeitschrift fur Physik. Une découverte européenne annoncée dans un journal européen, quoi de plus normal? Eh bien non, c'est un évènement unique dans les dernières décennies. Les physiciens européens ont l'habitude de publier leurs découvertes importantes dans la presse américaine. En 2005 un chercheur américain eut l'idée de dresser une liste des articles de physique les plus cités. Müller et Bednorz n'apparaissaient pas. Surprenant! En fait, la liste, publiée par la revue Physics Today en 2005, se limitait aux articles publiés par l'American Physical Society et aux citations dans des revues americaines. Or l'article de Bednorz et Müller était paru dans la Zeitschrift für Physik et, s'il avait été mentionné, il serait apparu en deuxième position, comme le montrent les statistiques publiées par Thomson-Reuters (ISI).

L'anecdote est révélatrice des habitudes actuelles parmi les physiciens: la quasi-totalité de ceux-ci cherchent à publier de préférence dans la presse américaine, à tel point qu'on peut se permettre de faire une statistique en ignorant la presse européenne. Cette anecdote montre aussi que les articles publiés dans la presse

européenne, s'ils sont très bons, sont tout aussi lus et cités que ceux qui paraissent dans la presse américaine.

References

1. A. Rigamonti, Phys. Rev. Lett. **19**, 436 (1967)
2. R. Brout, K.A. Muller, H. Thomas, Solid State Commun. **4**, 507 (1966)
3. A. Rigamonti, G. Petrini, Phys. Status Solidi **41**, 591 (1970)
4. F. Borsa, A. Rigamonti, Phys. Lett. **40A**, 399 (1972)
5. K.A. Muller, J.C. Fayet, F. Borsa, A. Rigamonti, *Structural Phase Transitions II* (Springer, Berlin, 1991)
6. *Local Properties at Phase Transitions*, ed. by K.A. Muller, A. Rigamonti (North Holland, Amsterdam, 1976)
7. K.A. Muller, in *Structural Phase Transition I*, ed. by K. A. Muller, H. Thomas. (Springer, Berlin, 1981)
8. K.A. Muller, in *Dynamical Critical Phenomena and Related Topics*, ed. by C.P. Enz. Lecture Notes in Physics, vol 104 (Springer, Berlin, 1979), p. 210
9. K.A. Muller, J.C. Fayet, *Structural Phase Transitions Studied by Electron Paramagnetic resonance*, (Springer, Berlin), Chapter 1 in Ref. 4
10. A. Rigamonti, S. Torre, Phys. Rev. B **33**, 2024 (1986)
11. S. Torre, A. Rigamonti, Phys. Rev. B **36**, 8274 (1987)
12. D.C. Johnston, in *Handbook of Magnetic Materials,* vol. 10, ed. by K.H.J. Buschoww (Elsevier, Amsterdam), Chapter 1
13. P. Carretta, A. Rigamonti, R. Sala, Phys. Rev. B **55**, 3734 (1997)
14. A. Rigamonti, P. Carretta, N. Papinutto, in *Novel NMR and EPR Techniques*, *Lectures Notes in Physics*, ed. by J. Dolinsek, M. Vilfan, S. Zumer. *Correlated Spin Dynamics at Phase Transitions in Pure and in Disordered 2D S= ½ Antiferromagnets* (Springer, Berlin, 2006)
15. A. Rigamonti and F. Tedoldi, in *NMR-MRI, μSR and Mossbauer Spectroscopies in Molecular Magnets*, ed. by P. Carretta, A. Lascialfari (Springer, Milan, 2007)
16. K.A. Muller, M. Takashige, J.G. Bednorz, Phys. Rev. Lett. **58**, 1143 (1987)
17. M. Corti et al., Phys. Rev. B **54**, 9469 (1996)
18. A. Rigamonti, F. Borsa, P. Carretta, Rep. Prog. Phys. **61**, 1367 (1998)
19. A. Varlamov et al., Adv. Phys. **48**, 655 (1999)
20. A. Larkin, A. Varlamov, *Theory of Fluctuations in Superconductors* (Oxford Scientific Publications, Oxford, 2005)
21. P. Carretta, D. Livanov, A. Rigamonti, A.A. Varlamov, Phys. Rev. B **54**, R 9682 (1996)
22. E. Bernardi, A. Lascialfari, A. Rigamonti, L. Romanò, M. Scavini, C. Oliva, Phys. Rev. B **81**, 064502 (2010) and references therein
23. A. Rigamonti, A. Lascialfari, L. Romanò, A. Varlamov, I. Zucca, *Superconducting Fluctuating Diamagnetism versus Precursor Diamagnetism in Heterogeneous Superconductors*. J. Supercond. **18**, 763–767 (2005). doi:10.1007/s 10948-005-0077-z
24. A. Rigamonti, A.A. Varlamov, J. Villain, *Le kaleidoscope de la physique* (Belin, Paris, 2014)

Chapter 23
Method for Accurate Determination of the Electron Contribution: Specific Heat of $Ba_{0.59}K_{0.41}Fe_2As_2$

Costel R. Rotundu, Thomas R. Forrest, Norman E. Phillips, and Robert J. Birgeneau

Introduction

The 1986 discovery of superconductivity in $La_{1.85}Ba_{0.15}CuO_4$ (LBCO) at a critical temperature T_c of 35 K by Bednorz and Müller [1] was a milestone in the search for superconductivity in materials with higher T_c, and an important contribution to the

Costel R. Rotundu and Thomas R. Forrest contributed equally to this work.

C.R. Rotundu
Materials Sciences Division, Lawrence Berkeley National Laboratory, Berkeley, CA, 94720, USA

Stanford Institute for Materials and Energy Sciences, SLAC National Accelerator Laboratory, 2575 Sand Hill Road, Menlo Park, CA, 94025, USA

T.R. Forrest
Department of Physics, University of California, Berkeley, CA, 94720, USA

Diamond Light Source, Harwell Science and Innovation Campus, Didcot, Oxfordshire, OX11 0DE, UK

N.E. Phillips (✉)
Materials Sciences Division, Lawrence Berkeley National Laboratory, Berkeley, CA, 94720, USA

Department of Chemistry, University of California, Berkeley, CA, 94720, USA
e-mail: nephill@berkeley.edu

R.J. Birgeneau
Materials Sciences Division, Lawrence Berkeley National Laboratory, Berkeley, CA, 94720, USA

Department of Physics, University of California, Berkeley, CA, 94720, USA

Department of Materials Science and Engineering, University of California, Berkeley, CA, 94720, USA

A. Bussmann-Holder et al. (eds.), *High-Tc Copper Oxide Superconductors and Related Novel Materials*, Springer Series in Materials Science 255,
DOI 10.1007/978-3-319-52675-1_23

incentive for further research in this area. Soon after the discovery of LBCO, cuprates with much higher T_c's were found. Other classes of superconductors, some of which are remarkable include MgB_2 [2] with its highest T_c among BCS superconductors and the iron pnictide high temperature superconductors [3]; they were discovered in 2001 and 2008, respectively.

These high-T_c superconductors make an important contribution to the understanding of superconductivity, but they pose a new challenge to the determination of the conduction-electron contribution to the specific heat, a useful source of the values of important parameters and other information relevant to the nature of the superconductivity. In the conventional analyses of specific-heat data the electron contribution (C_e), (C_{es}) in the superconducting state and (C_{en}) in the normal state, is obtained by subtracting the contribution of the lattice vibrations (C_{lat}) from the total measured specific heat (C), and therein lies the problem: High values of T_c ensure high values of the upper critical field (H_{c2}) effectively eliminating the normal-state specific-heat measurements that give C_{lat} by analyzing the normal-state C as the sum of C_{lat} and $C_{en} = \gamma_n T$. As a consequence, C_{lat} has to be obtained by some kind of approximation, and the requirements are stringent: Meaningful analysis and interpretation of the resulting C_{es} requires that the approximation for C_{lat} be valid over a wide range of temperature for $T \leq T_c$. The fact that many different approximations have been used attests the general recognition of the difficulty of the problem. The approximations used include fitting normal-state data above T_c to obtain C_{lat} and extrapolating the result to low T, and using C_{lat} for a structurally similar non-superconducting material. The problem is compounded by the fact that for these materials C_{es} is a small fraction of C_{lat} at the temperatures of interest for determining the order parameter in the superconducting state, and the errors in C_{lat} are greatly magnified in C_{es}. The analysis of the C data should give the conduction-electron density of states (DOS) and the values of the energy gaps in the superconducting state, but the conventional analyses gives a variety of results for these parameters in similar materials that reflect the errors in the approximations for C_{lat}. Recently we recognized that the α model, which gives a good representation of C_{es}, offers a way out of this dilemma: We showed that C_{es} for $Ba_{0.59}K_{0.41}Fe_2As_2$ could be extracted directly from the total C data by using α-model expressions for C_{es}, bypassing the need for an independent determination of C_{lat} [4]. That paper included discussions of C_{lat}, its proper mathematical representations in different temperature regions, the approximations used in the conventional analyses, and a comparison of our results for $Ba_{0.59}K_{0.41}Fe_2As_2$ with those obtained by conventional analyses of specific-heat data on similar materials as well as with results obtained by ARPES. Here we offer a reorganized and somewhat simplified description of the basic analytical procedures, without the supporting material.

Contributions to the Specific Heat; The Determination of the Lattice Contribution

The normal-state electron contribution to C is usually taken to be

$$C_{en} \equiv \gamma_n T, \tag{23.1}$$

where γ_n is a temperature-independent constant (but see below) that is proportional to the DOS. If there are two bands γ_n represents the sum of the two contributions. (When it is convenient to distinguish the specific-heat contributions or other properties of two bands, additional subscripts, 1 and 2, are used, e.g., $\gamma_n = \gamma_{n1} + \gamma_{n2}$, $C_{es} = C_{es1} + C_{es2}$, α_1 and α_2, etc.)

The superconducting-state electron contribution given by the BCS theory in the weak-coupling limit, has been tabulated by Mühlschlegel [5] in the form $C_{es}/\gamma_n T_c$ as a function of the reduced temperature, $t \equiv T/T_c$. Experimental results for strong-coupling materials are inconsistent with this result, and they are also inconsistent with general limitations on the effects of strong coupling in the BCS theory [6]. This led to the formulation of the α model [6], a phenomenological extension of the BCS theory to include strong-coupling effects. In the α model the temperature dependence of the energy gap is taken to be that calculated [5] for the BCS theory in the weak-coupling limit, but the amplitude of the gap at $T = 0$, $\Delta(0)$, is an adjustable parameter represented by $\alpha \equiv \Delta(0)/k_B T_c$ that provides an empirical measure of the strength of the coupling. In the weak-coupling limit of the BCS theory $\alpha = 1.764 \equiv \alpha_{BCS}$. Early applications were focused on superconductors that showed other evidence of strong coupling, which gave values of α greater than α_{BCS}, but for some superconductors the thermodynamic properties were represented by values of α less than α_{BCS}, and recently this has been interpreted in terms of weak coupling. For MgB_2 at the lowest temperatures C_{es} shows a large excess over that given by the BCS theory. It was recognized [7] that this could be represented by the α model with α *much* less than α_{BCS}, but this would not be consistent with C_{es} near T_c (see Fig. 2 of [7]). This suggested the extension of the α model to a two-band, two-gap superconductor in which C_e is taken to be the sum of two independent additive contributions, even though the equality of T_c in the two bands requires some interband coupling [7]. The α-model fits represent C_{es} for MgB_2 to within the experimental accuracy [7] giving α values of 2.2 and 0.6, which are consistent with detailed theoretical calculations [8] that show both strong and weak coupling. Currently, essentially all specific heat measurements on high-T_c Fe pnictide superconductors are compared with a model of this kind.

The vortex-state electron contribution of a superconductor with an isotropic gap includes two terms:

$$C_{ev}(H) = C_{evs}(H) + \gamma_v(H)T. \tag{23.2}$$

The first term, $C_{evs}(H)$, which is associated with the residual superconducting condensate, is the in-field counterpart of C_{es} in zero field. It decreases in magnitude

with increasing H but the details of its H and T dependences are not theoretically established. The other term, $\gamma_v(H)T$, is associated with localized quasiparticle states in the vortex cores [9]. Its coefficient varies from $\gamma_v(0) = 0$ to $\gamma_v(H_{c2}) = \gamma_n$, with a variation that is, at least for a single-band superconductor, linear in H. (Non-linear variations associated with structure in the energy gaps are considered in section "Discussion".) In most samples of superconducting materials there is a "residual" DOS that produces a normal-state-like contribution to C even in zero field. This appears as a non-zero value of $\gamma_v(0)$, $\gamma_r \equiv \gamma_v(0) \neq 0$, and is generally attributed to non-superconducting regions of the same material.

It is generally accepted that in the low-T limit the lattice contribution can be represented by

$$C_{lat} = \mathrm{B}_3 T^3 + \mathrm{B}_5 T^5 + \mathrm{B}_7 T^7 + \quad , \tag{23.3}$$

with

$$\mathrm{B}_3 = (12/5)\pi^4 \mathrm{R}/{\theta_\mathrm{D}}^3, \tag{23.4}$$

where θ_D is the Debye temperature. The higher-order terms represent the effects of phonon dispersion, and they may also serve as an approximation for the low-T contributions of low-frequency optical modes if the lattice has a basis with more than one atom in the primitive unit cell. However, Eq. (23.3) is often used in an interval of temperature at higher temperatures, in which case it is just a convenient fitting expression with no physical meaning. In particular, coefficients obtained in the high-T fits cannot be expected to give a valid expression for C_{lat} at lower temperatures. Combinations of Debye and Einstein functions are also used to represent C_{lat} at higher temperatures, where they are physically more reasonable fitting expressions, but the fits are relatively insensitive to the values of the fitting parameters, and the parameters derived, like those derived from high-T fits with Eq. (23.3), should not be expected to give C_{lat} accurately at lower temperatures.

For the high-T_c Fe pnictides two methods for obtaining an approximation for C_{lat} for $T \leq T_c$ have been used. In one, the first step is to obtain C_{lat} for $T \leq T_c$ for a comparison material for which the normal-state specific heat is known. The comparison materials that have been used include the undoped non-superconducting parent compound, an overdoped non-superconducting sample, and a material with a different dopant that suppresses both the superconductivity and the high-T structural/magnetic transition. In some cases adjustments to C_{lat} of the comparison material for the differences in stoichiometry or structure are made, but they are necessarily rough approximations. Furthermore, the effect on C_{lat} of the substantial differences in the DOS are quite generally ignored. The other method is to obtain C_{lat} for the sample itself by fitting the normal-state data for $T \geq T_c$ with $C = \gamma_n T + C_{lat}$, and extrapolating the resulting C_{lat} to $T < T_c$. In addition to the fact that an expression obtained for C_{lat} in a high-T interval cannot be expected to be accurate at low temperatures, there are other reasons for doubting the validity of the derived C_{lat} (and also γ_n, if it is derived in the fit): Since C is measured at

constant pressure it includes a contribution to C_{lat} associated with the anharmonicity of the lattice vibrations that can also be approximately T proportional [10]. For samples of $Ba_{1-x}K_xFe_2As_2$ this contribution has been estimated [11] to increase rapidly from zero at $T = 0$ to ~600 mJ K^{-1} mol^{-1} at 100 K, to increase less rapidly at higher temperatures, and to become more nearly T proportional above 150 K, with a coefficient ~ 12 mJ K^{-2} mol^{-1}. Furthermore, the phonon enhancement that contributes to γ_n, and therefore γ_n itself, is expected to be T dependent (see, e.g., [12, 13]). The complicated temperature dependence of C_{lat}, including the anharmonic contribution, prevents the identification of this effect in specific-heat measurements, but there is compelling evidence for its reality in cyclotron resonance experiments [14]. There is no basis for estimating its magnitude in the Fe pnictides, but it could be substantial. The difficulties associated with obtaining an independent approximation for C_{lat}, ensure substantial uncertainty in any C_{es} obtained in the conventional analyses.

The determination of C_{lat} is the major obstacle to obtaining C_e from experimental data, but in most samples there are paramagnetic centers that also make a significant contribution to C, which is best represented by an H-dependent approximation to a Schottky function, $C_{\mathrm{Sch}}(H)$. With this contribution, the total specific heat in a field H is

$$C(H) = C_{lat} + C_e(H) + \mathrm{m}C_{\mathrm{Sch}}(H), \tag{23.5}$$

where m is the molar concentration of paramagnetic centers. For $0 \leq H < H_{c1}$, where H_{c1} is the lower critical field (and omitting the possible $\gamma_r T$ contribution) $C_e(H) = C_{es}$; for $H_{c1} \leq H < H_{c2}$, $C_e(H) = C_{evs}(H) + \gamma_v(H)T$; for $H \geq H_{c2}$, $C_e(H) = \gamma_n T$.

The requirement of entropy conservation, the equality of the conduction-electron entropies in the normal and superconducting states at T_c, is frequently invoked, either as a constraint in a fitting procedure used to obtain C_{lat} or as a test of the validity of a derived C_{lat}. In zero field it takes the form

$$\int (C_{es}/T)dT = \gamma_n T_c, \tag{23.6}$$

where $C_{es} = C - C_{lat}, -\mathrm{m}C_{\mathrm{Sch}}$ and the integration extends from $T = 0$ to $T = T_c$. In the special case of a C_{lat} that is determined in a high-temperature fit to normal-state data and then extrapolated to low temperatures, imposition of the entropy-conservation constraint can reduce gross errors in the derived C_{lat} (a detailed analysis is presented in Sect. 6 of [4]). More generally however, its effect is limited by the small fraction of the entropy at T_c that is electron entropy, e.g., ~13% in the results reported here. At best, even if an accurate value of γ_n is known independently, satisfaction of Eq. (23.6) shows only that C_{es} gives the correct *entropy* at T_c, i.e., that it is only a T^{-1}-weighted *average* of C_{es} that is correct. This leaves room for T-dependent errors that are comparable in magnitude to small contributions to C_{es} that have been attributed to small-gap bands in temperature intervals near or

below $T_c/2$. An incorrect value of γ_n will tend to produce values of C_{es} that are, on the average, either too high or too low. Furthermore, in many cases the validity of the value of γ_n used in Eq. (23.6) is not obvious, and in some cases its origin is not specified.

Samples and Measurements

Nearly optimally doped $Ba_{0.59}K_{0.41}Fe_2As_2$ single crystals were grown by a self-flux method [15]. The potassium doping value reported is as determined by inductively coupled plasma and its homogeneity is confirmed by electron microprobe wavelength-dispersive X-ray spectroscopy. The superconducting transition with an onset of 36.9 K has a width of ~1 K, as measured by magnetization. It is well known that magnetization measurement cannot provide a reliable value of the volume fraction of superconductivity. Instead, the residual DOS in the superconducting state, which is measured by the value of γ_r, is the best measure of the volume fraction of superconductivity. For our sample $\gamma_r = 0$ (see section "Specific-Heat Results and Analysis") suggesting 100% superconductivity. This is in agreement with the absence of a heat capacity signature near 70 K that would indicate the presence of FeAs, a common impurity reported in the series (see, e.g., [2, 11]). The sharp step-like magnetization at T_c, the absence of a residual DOS in the superconducting state, the absence of a detectable level of FeAs, the low concentration of paramagnetic centers (see section "Specific-Heat Results and Analysis"), and the discontinuities in C_e and its temperature derivative at T_c (see section "Specific-Heat Results and Analysis") attest the high quality of the sample. The specific heat of a 10.3-mg, plate-like single crystal was measured in the PPMS from 2 to 300 K in zero field. Below 50 K, measurements were also made in nine fields applied perpendicular to the *ab* plane, to a maximum $\mu_0 H = 14$ T. A different set of measurements on the same sample was reported in an earlier paper [16]. To exploit the PPMS' sensitivity to its maximum the specific heat of the addenda and the sample were measured at the same temperatures, and the platform thermometer was calibrated in each of the fields in which the specific heat was measured.

Specific-Heat Results and Analysis

The specific heat results for $H = 0$ at lower temperatures in shown in Fig. 23.1 (and shown in Fig. 1 of [4] for 2–300 K temperature range). The discontinuity in C at 36.9 K marks the transition to the superconducting state. The solid sloping lines in inset Fig. 23.1, which represent the ideally sharp mean-field transition in zero field, are the results of somewhat arbitrary, but typical, straight-line fits to the data just outside the regions of curvature associated with the broadening of the transition by sample inhomogeneity and fluctuation effects. Their extrapolations to T_c, together

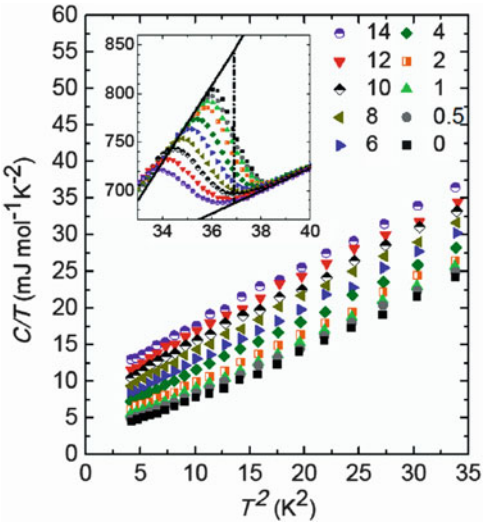

Fig. 23.1 The specific heat as C/T vs T^2 to 6 K, in 10 fields, $0 \leq \mu_0 H \leq 14$ T. The deviations from linearity suggest the presence of a low concentration of paramagnetic centers. *The inset*: The same specific heat data in the vicinity of T_c, as C/T *vs* T. The *solid sloping lines* are the results of fits to the data just outside the transition region (see text). The *dashed*, *vertical line* is an entropy-conserving construction that determines T_c as 36.9 K. The extrapolations of the solid lines to T_c represent the mean-field transition in zero field

with the entropy-conserving dash-dot vertical line, determine T_c as 36.9 K. Since $C_{lat,}$ is continuous at T_c, the solid lines give the discontinuity in C_e, $\Delta C_e(T_c)/T_c = 157.5$ mJ K^{-2} mol^{-1}. With some mathematical manipulation, $dC/dT = Td(C/T)/dT + C/T$, they also give the discontinuity in dC_e/dT, $\Delta(dC_e/dT)|_{Tc} = 1183$ mJ K^{-2} mol^{-1}. In comparison with other measurements on similar materials the transition is relatively sharp and the discontinuities are relatively large, e.g., although $\Delta C_e(T_c)/T_c$ seems to be similar to that found in one of the five measurements on similar materials (described in Sect. 6 of [4]) it is clearly larger than those in the other four.

The first step in the analysis is to obtain approximate, provisional values of γ_n and α from the data in the vicinity of T_c using α-model expressions for a single gap. The α model gives the discontinuities in C_e and dC_e/dT in terms of the parameters γ_n and α. Conversely, it can be used to obtain γ_n and α from the experimental values of the two discontinuities. For any value of α it gives C_{es} as a function of the reduced temperature, $t \equiv T/T_c$,

$$C_{es}(t)/\gamma_n T_c \equiv f_\alpha(t). \tag{23.7}$$

Since $C_{en} = \gamma_n T$, $C_{en}(T_c)/T_c = \gamma_n$, and the discontinuity in C_e at T_c is

$$\Delta C_e(T_c)/T_c = C_{es}(T_c)/T_c - C_{en}(T_c)/T_c = \gamma_n[\mathrm{f}_\alpha(1) - 1]. \tag{23.8}$$

Since $(\mathrm{d}C_{es}/\mathrm{d}t)/\gamma_n T_c = \mathrm{d}f_\alpha(t)/\mathrm{d}t \equiv \mathrm{f}_\alpha'(t) = (\mathrm{d}C_{es}/\mathrm{d}T)/\gamma_n$, and $(\mathrm{d}C_{en}/\mathrm{d}T)|_{Tc} = \gamma_n$, the discontinuity in $\mathrm{d}C_e/\mathrm{d}T$ *is*

$$\Delta(dC_e/dT)|_{Tc} = (dC_{es}/dT)|_{Tc} - (dC_{en}/dT)\big|_{Tc} = \gamma_n[\mathrm{f}_\alpha'(1) - 1]. \tag{23.9}$$

If γ_n is known independently, either Eqs. (23.8) or (23.9) would give the value of α, and each of these equations has been used in that way. However, taken together, they can be used to obtain the values of both α and γ_n: e.g., the ratios of the left- and right-hand sides of Eqs. (23.8) and (23.9) give

$$T_c\Delta(dC_e/dT)\big|_{Tc}/\Delta C_e(T_c) = [\mathrm{f}_\alpha'(1) - 1]/[\mathrm{f}_\alpha(1) - 1], \tag{23.10}$$

which determines the value of α as that for which the function of α on the right-hand side agrees with the experimental quantity on the left. With the value of α determined by Eq. (23.10), Eq. (23.8) or Eq. (23.9) can be used to obtain γ_n. The results are $\gamma_n = 32.2$ mJ K^{-2} mol^{-1}, and $\alpha = 3.27$. These would be the correct values if there were only a single band, but if there is also a small-gap band the discontinuities would have to be corrected for its contributions and the parameters of the large-gap band recalculated.

The test for the existence of a small-gap band and the determination of the characteristic parameters were based on a "global" fit with Eq. (23.5) to the data for all H and $T \leq 12$ K. It is desirable to fit the data for all H together because the H dependence of the vortex-core contribution gives important information about the energy gap (see section "Discussion") and it is best determined in a fit that takes the other contributions into account. In addition, the ratio of data points in the fit to fitting parameters is increased, reducing the uncertainties in the derived parameters (see below). The details of the final fitting expression were based on the results of trials of a number of different fitting expressions and different temperature intervals for the fits. The results of some of these preliminary fits are described, together with other evidence of the validity of the fit, in the last two paragraphs of this section. The final fitting expression made allowance for four contributions to $C(H)$: the lattice contribution, represented by three terms of Eq. (23.3); the vortex-core contribution, $\gamma_v(H)T$; the superconducting-condensate contribution, C_{es} for $H = 0$, and C_{evs} for $H \neq 0$; the paramagnetic-center contribution, represented by a two-level Schottky function (see below) with an H-dependent characteristic temperature, $\theta_{\mathrm{Sch}}(H) = \theta_{\mathrm{Sch}}(0)(1 + \beta H^2)^{1/2}$. Inclusion of the paramagnetic-center contribution was suggested by the deviations from linearity in the plot of C/T vs T^2 (see Fig. 23.1) which are typical indications of the presence of a low concentration of paramagnetic centers.

For $T \leq 12$ K the component of C_{es} associated with a large-gap band with $\alpha \sim 3$ and $\gamma_n \sim 30$ mJ K^{-2} mol^{-1} would be negligible, and it is only the component associated with a small-gap band that needs to be considered. As given by Eq. (23.7), that component would be $C_{es2}(T) = \gamma_{n2}T_c\mathrm{f}_\alpha(T)$. For this interval of

temperature and the values of α that turn out to be of interest (~1) it can be represented by the exponential of a three-term polynomial in T^{-1}, $-X_\alpha(T)$, giving

$$C_{es2}(T) = \gamma_{n2}T_c f_\alpha(T) = \gamma_{n2}T_c \exp[-X_\alpha(T)], \tag{23.11}$$

with the three coefficients in $X_\alpha(T)$ determined by the value of α. (The polynomial in T^{-1} was suggested by the T dependence of C_{es} given by the BCS theory, and it was found that sums of a constant term, a term in T^{-1}, and term in $T^{-1/2}$ gave good fits to the α-model expressions.) Generalizing that expression to extend its validity to the in-field data, i.e., to represent $C_{evs2}(H)$ for $H \neq 0$, requires allowing for its H dependence in the vortex state. There is little theoretical guidance for such a generalization, but experimental results on other superconductors suggest two changes: the replacement of the pre-exponential coefficient, $\gamma_{n2}T_c$, with an H-dependent coefficient, $a(H)$, to allow for the reduction in the magnitude of the residual superconducting condensate contribution that is complementary to the increase in the vortex core contribution, and the inclusion of an H-dependent factor, $b(H)$, in the exponent to allow for the effective reduction of the gap by the pair-breaking effect of the field. With these changes, the component of $C_{evs}(H)$ and C_{es} associated with the small-gap band is $a(H)\exp[-b(H)X_\alpha(T)]$ and the fitting expression becomes

$$C(H) = C_{lat}(T) + \gamma_v(H)T + a(H)\exp[-b(H)X_\alpha(T)] + mC_{Sch}(H,T). \tag{23.12}$$

Fitting the data for $H \neq 0$ simultaneously with the $H = 0$ data more than doubles the ratio of number of points in the fit to number of adjustable parameters, and gives more reliable values of the parameters. (However, with more precise data, which might be obtained in other apparatus, it might be possible to obtain comparably reliable values of the $H = 0$ parameters without invoking the empirical generalization of Eq. (23.11) to include the $H \neq 0$ data.)

A fit has to be made for a particular value of α, which determines the values of the three fixed parameters in $X_\alpha(T)$ that are needed to make the fit. The derived values of the adjustable parameters depend on the value of α for which the fit was made, and the correct value of α is identified by comparison of the results of fits made with different values: The third term in Eq. (23.12), with the adjustable parameters $a(H)$ and $b(H)$, represents the contribution of the superconducting condensate of the small-gap band for all H, but for $H = 0$ its T dependence is correct for the value of α for which the fit was made *only* if the derived $b(0) = 1$. This provides the criterion for recognizing the correct value of α, i.e., that for which the fit gives $b(0) = 1$. For the same reason, that fit gives γ_{n2}, as $\gamma_{n2} = a(0)/T_c$. The derived values of $b(0)$ have a strong dependence on α—e.g., $b(0) = 1.109$, 0.946, and 0.822 for $\alpha = 0.8$, 0.9, and 1.0—ensuring a precise determination of α. The result $b(0) = 1$ was obtained for $\alpha = 0.86$, and for that fit $a(0) = 337 \pm 17$ mJ K^{-1} mol^{-1}. These results show the existence of a small-gap band characterized by the parameters $\alpha_2 = 0.86$ and $\gamma_{n2} = (337 \pm 17)/36.9 = 9.1 \pm 0.5$ mJ K^{-2} mol^{-1}. Because of the small value of γ_{n2}, and particularly the small value of α_2, this

band makes only small contributions to the discontinuities at T_c: $\Delta C_{e2}(T_c)/T_c = 3.1$ mJ K^{-2} mol^{-1}; $\Delta[(dC_{e2}/dT)|_{Tc}] = 3.5$ mJ K^{-2} mol^{-1}. Correcting the measured discontinuities for these contributions gives $\Delta C_{e1}(T_c)/T_c = 154.4$ mJ K^{-2} mol^{-1} and $\Delta[(dC_{e1}/dT)|_{Tc}] = 1180$ mJ K^{-2} mol^{-1}, which in turn give $\alpha_1 = 3.30$, $\gamma_{n1} = 31.0$ mJ K^{-2} mol^{-1}, and a total $\gamma_n = 40.1$ mJ K^{-2} mol^{-1}. The characteristic parameters of the two bands are listed in Table 23.1. In Table 23.2 they are compared with the values obtained from measurements on five other near-optimally hole-doped 122 Fe-pnictide superconductors (see Sect. 6 of [4]) and the comparison suggests some consideration of the uncertainties: A quantitative measure of the uncertainty in our value of γ_{n2} is given directly by the fit, $\gamma_{n2} = 9.1 \pm 0.5$ mJ K^{-2} mol^{-1}. It is a measure of the validity of the mathematical expression for C_{es} in representing the data. The provisional value of γ_n, 32.2 mJ K^{-2} mol^{-1}, was determined from the straight-line construction in Fig. 23.1, which, in the absence of mathematical expressions for the effects of fluctuations and sample inhomogeneity on the transition, represents a qualitative estimate of those effects. The real uncertainty in γ_n arises from the way the lines were drawn. Only a qualitative estimate is possible, and, on the basis of the shape of the transition in Fig. 23.1 and comparisons with other measurements, 5% would seem to be reasonable for the uncertainty in the provisional value of γ_n and, therefore, in γ_{n1} and in the final value of γ_n, 40.1 mJ K^{-2} mol^{-1}. The more complicated analyses that led to the parameters derived from the other measurements in Table 23.2 make identification of the

Table 23.1 Characteristic parameters of the two electron bands

Electron band	α	$\Delta(0)$ (meV)	γ (mJ K^{-2} mol^{-1})
1	3.30	10.49	31.0
2	0.86	2.73	9.1

Table 23.2 Characteristic parameters of the electron bands for five other near-optimally hole-doped Fe-pnictide superconductors in the 122 series, compared with the values reported here

Composition/Reference	γ_n	α	γ_{n1}	γ_{n2}	α_1	α_2
$Ba_{0.59}K_{0.41}Fe_2As_2$/This work [4]	40.1		31.0	9.1	3.30	0.86
$Ba_{0.6}K_{0.4}Fe_2As_2$/[17, 18]	71.0	1.9				
$Ba_{0.6}K_{0.4}Fe_2As_2$/[19, 20]	9.0	2.07	9.2	39.8	3.7	1.9
$Ba_{0.68}K_{0.32}Fe_2As_2$/[21]	50.0		25.0	25.0	3.3	1.1
$Ba_{0.65}Na_{0.35}Fe_2As_2$/[22]	57.5		29.9	27.6	2.08	1.06
$Ba_{0.55}K_{0.45}Fe_{1.95}\ Co_{0.05}As_2$/[23]	40.5	2.57	34.8	5.7	3.9	0.86

The values in the top row, this work, were derived by comparing α-model expressions for the electron contribution directly with the total measured specific heat. The other values were derived in conventional analyses in which the α-model expressions were compared with a superconducting-state electron specific heat that had been obtained by subtracting an independently determined approximation for the lattice contribution from the total specific heat. The values of γ_n are the totals for two bands, however they were derived; the values of α are the results of single-band fits, if they were made; the values in the 4th–7th columns are the results of two-band fits. For the two-band fit in 19 α_1 and α_2 were fixed at values obtained from ARPES measurements. The units of γ_n, γ_{n1}, and γ_{n2} are mJ K^{-2} mol^{-1}

origins of the uncertainties and estimates of their magnitudes much more difficult, and the uncertainties are not discussed in the publications.

The other contributions to $C(H)$ obtained in the fit are plausible and consistent with the behavior shown by other superconductors, e.g., the evolution with increasing H of the different contributions in Eq. (23.12) and the derived parameters characteristic of the small-gap band, which fall within the *ranges* suggested by other measurements (see Table 23.2). The H-independent parameters obtained in the fit are: $m = 1.29 \pm 0.15 \times 10^{-3}$ mol mol^{-1}; $\theta_{Sch}(0) = 7.32 \pm 0.41$ K; $\beta = 3.30 \pm 1.17 \times 10^{-2}$ T$^{-1/2}$; $B_3 = 0.602 \pm 0.022$ mJ K^{-4} mol^{-1}; $B_5 = 7.23 \pm 2.1 \times 10^{-4}$ mJ K^{-6} mol^{-1}; $B_7 = -6.1 \pm 7.0 \times 10^{-7}$ mJ K^{-8} mol^{-1}. While the H-dependent parameters are given in a table in [4], $\gamma_v(H)$ is displayed graphically in Fig. 23.2. The evolution with increasing H of each of the three H-dependent contributions to $C(H)$ is illustrated in Fig. 23.3 for $\mu_0 H = 0$, 6, and 14 T, with the H-independent C_{lat} included for comparison. The H dependences of the coefficient of the contribution of the superconducting condensate and the energy gap that were introduced empirically, the factors $a(H)$ and $b(H)$, give a satisfactory representation of the experimental data. Furthermore, and as expected, the results of the fit are consistent with the behavior seen in measurements on other superconductors: The contribution of the superconducting condensate decreases with increasing H, as shown by the values of $a(H)$ and by the plots of C_{es2} and C_{evs2} in Fig. 23.3. The T and H dependences of C_{es2} and C_{evs2} are plausible, and the exponential downturns at low temperatures occur at temperatures consistent with

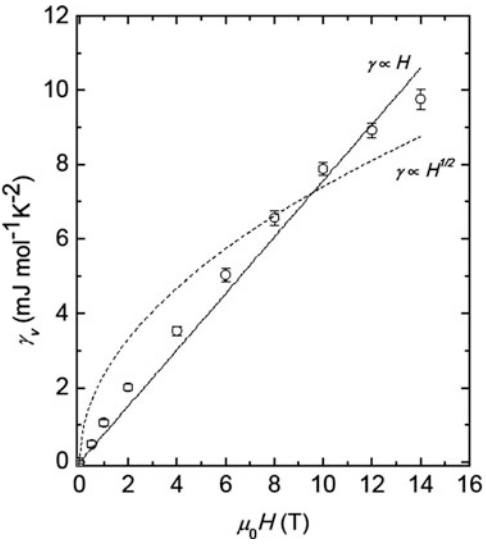

Fig. 23.2 The H dependence of $\gamma_v(H)$ as obtained in a "global" fit to the data for $2 \leq T \leq 12$ K in 10 fields, $0 \leq \mu_0 H \leq 14$ T. The *solid* and *dashed lines* represent least-squares fits to H and $H^{1/2}$ dependences. The *error bars* correspond to the uncertainties determined in the fit

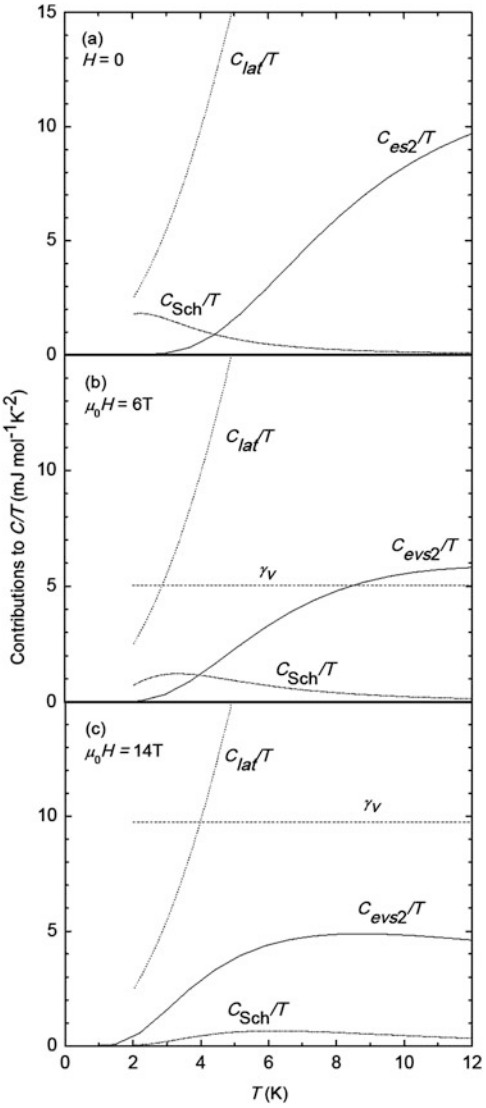

Fig. 23.3 Lattice, paramagnetic-center, and electron contributions to C/*T*, for $\mu_0 H = 0$, 6, and 14 T in (**a**), (**b**), and (**c**), as obtained in a "global" fit to the data for $2 \leq T \leq 12$ K in 10 fields, $0 \leq \mu_0 H \leq 14$ T. In (**a**) C_{es2}/T is the contribution of the small-gap band to C_{es}/T, i.e., in the superconducting state. In (**b**) and (**c**) C_{evs2}/T is the corresponding contribution of the small-gap band to C_{ev}/T, i.e., in the vortex state. In this temperature interval and on this scale the analogous contributions of the large-gap band are negligible. In (**b**) and (**c**) γ_v is the total contribution of the vortex cores

the values of $b(H)$ in showing the expected decrease in the effective gap with increasing H.

The identification of a band with a small energy gap requires the accurate determination of C_{es} at the low temperatures at which it would make a significant contribution to $C(0)$, typically $T \leq 15$ K for the small gaps that have been reported in these materials. The problem, *for any analysis*, is to identify the small C_{es2}—a maximum of only 12% of $C(0)$, near 9 K in our results—and separate it from the much greater C_{lat}. In the conventional analyses an error of only a few percent in the independently determined C_{lat} that is subtracted from $C(0)$ would have a substantial effect on any evidence for a small gap that might be obtained from the derived C_{es}. Our analysis, unlike the conventional analyses, does not require an independent, quantitative determination of C_{lat} that is subtracted from $C(0)$ before the fit is made. It does require making an *allowance* for C_{lat} in the fitting expression, and this takes the form of the sum of the $T,^3$ $T,^5$ and T^7 terms in Eq. (23.3), which is generally accepted as representing the T dependence of C_{lat} in this low-T interval. The coefficients of these three terms are an incidental byproduct of the fit, and they do determine C_{lat} in this limited T interval. However, since they were determined in the low-T fit they do not prejudice the outcome of the determination of C_{es} in the way that independently determined coefficients would. The choice of the three-term expression for C_{lat} was based on a number of preliminary fits with Eq. (23.12), eight of which, with or without the T^7 term, to either 10 or 12 K, and for α either 0.8 or 0.9, gave the same value of $a(0)$ to within $\pm 5\%$, and to within $\pm 2.5\%$ for each group of four for which α was the same. These fits suggested that the T^7 term would make only a marginal contribution, but it was included to give maximum flexibility in the determination of the other contributions. It did make only a small contribution in the final fit, and the large uncertainty in the coefficient shows that the results of the fit would have been essentially the same without it, except that a small compensating change in B_5 would be expected. The paramagnetic-center contribution presented the major problem with the fitting expression. The two-level Schottky anomaly in the final fitting expression is clearly too narrow in temperature, but broader anomalies that were tried—two-level Schottky anomalies with different degeneracies of the levels or with Gaussian or Lorentzian broadening, and a three-level Schottky anomaly—made no significant improvement in the fit and did not suggest an alternative. However, the Schottky contribution is relatively small, and significant only at the lowest temperatures and in low fields (see Fig. 23.3). Its small size accounts for the relatively large uncertainties in the parameters m, $\theta_{Sch}(0)$ and β, but it is only the sharp drop off on the high-T side, which is not sensitive to the details of the fitting expression, that is relevant to the separation of the four contributions to $C(H)$. For that reason, and because the Schottky contribution is not of any interest in itself, the inadequacy of this term in the fitting expression is not important.

In the final fitting expression, Eq. (23.12), there are 36 adjustable parameters, six of which are independent of H and represent the magnitudes and T dependences of the lattice and Schottky contributions to $C(H)$. Of the 30 H-dependent parameters, 10 represent the relatively simple H dependence expected for $\gamma_v(H)$ and 20 model

the comparably simple H dependences of the superconducting-condensate contribution, as suggested by results for other superconductors. There are 320 data points in the fit, an adequate excess over the number of parameters, especially considering the limited roles of the H-dependent parameters. The fit was made using a non-linear least-squares procedure using Matlab, and carried to the smallest convergence tolerance allowed. To ensure that the fitting process converged to the best possible result (an absolute minimum of the reduced χ^2) a number of fits were made with different initial values of the parameters and different iteration step sizes. The T dependences of the four contributions to $C(H)$ are all well defined and substantially different, which is of considerable importance in connection with the validity of their separation. While the fractional deviations in the final fit are up to $\pm 3\%$ at 2 K, where the Schottky contribution to $C(H)$ is significant, they decrease to ± 1 and $\pm 0.25\%$ at 5 and 12 K, the temperatures that define the interval that is most important for determining $C_{es2.}$ The results of the fit are generally plausible and consistent with the behavior of other superconductors. The validity of the fit is also supported by the uncertainties in the parameters, which are relatively small for the most important parameters, in particular $a(0) = 337. \pm 17.$ mJ K^{-1} mol^{-1} and $b(0) = 1.00 \pm 0.04$, which define C_{es2}. The result for C_{es2} is also supported indirectly by the strong dependence of $b(0)$ on α (see above), which is clear evidence of the existence of a term in $C(0)$ with a T dependence corresponding to the contribution of a small-gap band with a value of α within the range of the fits. The difficulties in determining C_{es2} notwithstanding, the evidence for a small-gap band characterized by $\alpha_2 = 0.86$ and $\gamma_{n2} = 9.1 \pm 0.5$ mJ K^{-2} mol^{-1} is persuasive.

Discussion

The major result of the analysis is the identification of two electron bands that contribute to the DOS, and have substantially different energy gaps in the superconducting state. [As noted in the Introduction, *some* of the measurements on other near-optimally hole-doped 122 Fe-pnictide superconductors (described in more detail in Sect. 6 of [4]) showed evidence of two gaps, and the details and references are given in Table 23.2.] The total DOS, as measured by the coefficient of the electron contribution to the specific heat, corresponds to $\gamma_n = 40.1$ mJ K^{-2} mol^{-1}, and it is comprised of a contribution, $\gamma_{n1} = 31.0$ mJ K^{-2} mol^{-1}, from the band with the larger gap, $\Delta_1(0) = 10.49$ meV, and a contribution, $\gamma_{n2} = 9.1$ mJ K^{-2} mol^{-1}, from the band with the smaller gap, $\Delta_2(0) = 2.73$ meV. The results for C_{es} and its two components are shown graphically in Fig. 23.4, with the result of the BCS theory in the weak coupling limit and for the same γ_n, included for comparison. Although circumvention of the need for an independent determination of C_{lat} is an important feature of our analysis, C_{lat}, and its relation to $C(0)$, is of some interest for comparison with the results of other measurements. The 2–12 K fit with Eq. (23.12) gives C_{lat} for that temperature interval. At higher temperatures the apparent C_{lat} can be obtained by subtracting C_{es} or C_{en} from $C(0)$, and for that

purpose the actual $C(0)$ data in the immediate vicinity of T_c were replaced by the straight lines in Fig. 23.1 that represent the idealized sharp transition. The results for C_{lat} to 40 K, the limit of the straight-line construction in Fig. 23.1, are represented by the solid lines in Fig. 23.5. The small difference between $C(0)$ and C_{lat} for $T \leq 20$ K emphasizes the sensitivity to errors in C_{lat} of a C_{es2} derived from that difference.

Several other techniques give values of the energy gaps that can be compared with those derived from the specific-heat data. Quite generally, the results obtained by these techniques suggest that there are two gaps with substantially different magnitudes in the Fe–pnictide superconductors (see, e.g., [24]). Here we focus on those obtained from angle-resolved photoemission spectroscopy (ARPES) measurements on $Ba_{1-x}K_xFe_2As_2$, which are the most extensive and detailed of the other measurements. The comparison is best made on the basis of the values of $\Delta_1(0)$ and $\Delta_2(0)$, which are given directly by the ARPES results, and are independent of T_c. In the following. $\Delta_1(0)$ and $\Delta_2(0)$ are used for the larger and smaller gaps, respectively, regardless of the notation used in the other publications. As derived from the specific-heat data, these quantities are averages in the sense that small differences between different sheets of the Fermi surface and anisotropies on a single sheet are not resolved. ARPES measurements give more detailed information but the results are often summarized by two averages over narrow ranges of gap magnitude. For a sample with $T_c = 32$ K, Evtushinsky et al. [25] report $\Delta_1(0) = 9.2 \pm 1$ meV for an inner hole-like barrel at the Γ point, and smaller gaps on all other elements of the Fermi surface. However, the feature that showed the opening of the larger gap was not observed for the smaller gaps, and they

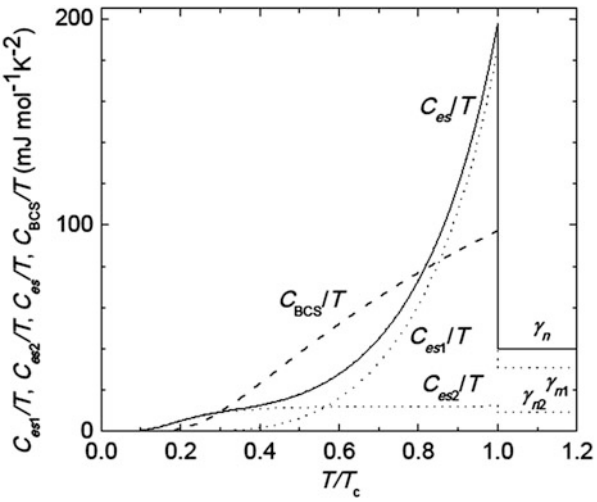

Fig. 23.4 The total electron contribution to C/T, the *solid line*, and its two components, the *two dotted lines*, as functions of T/T_c, in the superconducting state for $T/T_c \leq 1$, and in the normal state for $T/T_c \geq 1$. The large-gap component is identified by the labels C_{es1}/T and γ_{n1}, the small-gap component by the labels C_{es2}/T and γ_{n2}, and the total by the labels C_{es}/T and γ_n. The *dashed line*, C_{BCS}/T, represents the result of the BCS theory in the weak-coupling limit for the same γ_n

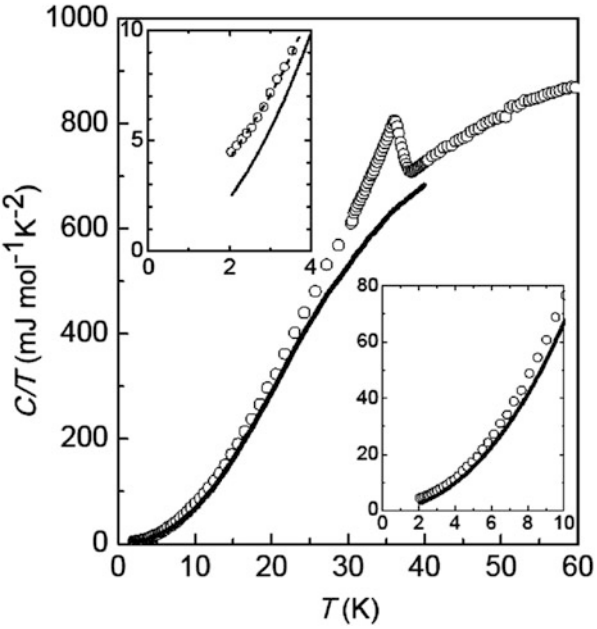

Fig. 23.5 The specific heat in zero field, as C/T *vs* T, for 2–50 K in the main panel, and for intervals at lower temperatures in the insets. The superconducting transition is marked by the sharp drop in C/T in the vicinity of $T_c = 36.9$ K. The *solid curves* represent the apparent C_{lat}, obtained by different methods, as described in the text. The *dashed curve* in the *upper inset* represents $C_{lat} + C_{\mathrm{Sch}}$ in zero field, as determined in a "global" fit to the data for $2 \leq T \leq 12$ K in 10 fields, $0 \leq \mu_0 H \leq 14$ T

conclude only that $\Delta_2(0) < 4$ meV. For a sample with $T_c = 37$ K and x = 0.4, Ding et al. [26] report $\Delta_1(0) \sim 12.5$ meV for the inner Γ barrel and $\Delta_2(0) \sim 5.5$ meV for the outer Γ barrel, but the unusual temperature dependence of the gaps leaves some doubt about the extrapolation to 0 K. For a sample with $T_c = 35$ K and x = 0.4, Zhao et al. [20] report anisotropic gaps, $\Delta_1(0) = 10$–12 ± 1.5 meV for the inner Γ barrel, and $\Delta_2(0) = 7$–8 ± 1.5 meV for the outer Γ barrel. The two Fermi surface spots near the M point are gapped below T_c but the gaps persist above T_c. For a sample with x = 0.45, but unspecified T_c, Liu et al. [27] report measurements on samples that "display bulk superconductivity" but the superconducting gaps are not detected in measurements at 12 K. Our value of $\Delta_1(0)$ falls well within the range of those obtained from ARPES results, but, while the value of $\Delta_2(0)$ is consistent with that obtained by Evtushinsky et al. [25] it is substantially lower than the other two ARPES values. Although our value was obtained from a small feature in the low-temperature specific heat, the sensitivity of the fits to the value of α_2, which determines $\Delta_2(0)$, argues against such an error in $\Delta_2(0)$. Comparably small values of $\Delta_2(0)$, as measured by α_2, have been reported in electron-doped $BaFe_2As_2$ – α_2 = 0.95 in [28] and $\alpha_2 = 0.957$ in [29]—but, given the differences between the

electron- and hole-doped compounds, the implications of this similarity in the values of α_2 are not clear.

The H dependence of $\gamma_v(H)$ gives information about the symmetry of the order parameter, most directly on the existence of nodes. For "conventional" s-wave superconductors with an isotropic gap, $\gamma_v(H)$ varies linearly with H. For a d-wave superconductor Volovik predicted an $H^{1/2}$ dependence associated with extended quasiparticle states near line nodes [30]. This effect was first observed by Moler et al. [31] in a cuprate superconductor. It has been suggested that this $H^{1/2}$ dependence is modified to $H\ln H$ at low fields in a dirty superconductor [32]. Modifications of the H-proportional dependence in the case of an isotropic gap, negative curvature in high fields, have also been suggested [33]. The H dependence of $\gamma_v(H)$ is compared with H and $H^{1/2}$ dependences in Fig. 23.2. Overall, $\gamma_v(H)$ is better represented by the solid straight line, which has a slope 0.75 mJ K^{-2} mol^{-1} T^{-1}, than the dashed curve for $H^{1/2}$. (The $H\ln H$ dependence suggested for a dirty d-wave superconductor [32] would not give a better fit.) For this reason, and particularly because the low-field data suggest a finite limiting slope, these results are more consistent with an isotropic gap than with the low-energy excitations associated with nodes. Two other measurements of $\gamma_v(H)$, to 9 T, on K-doped $BaFe_2As_2$ have been interpreted in the same way: For $Ba_{0.6}K_{0.4}Fe_2As_2$ an approximately H-proportional dependence [17] with a slope 0.63 mJ K^{-2} mol^{-1} T^{-1}, and for $Ba_{0.55}K_{x0.45}Fe_2As_2$ a more precisely determined H-proportional dependence [23] with a slope 0.60 mJ K^{-2} mol^{-1} T^{-1} have been reported. There is no obvious explanation for the curvature in $\gamma_v(H)$ in Fig. 23.2. The curvature predicted for an isotropic gap [33] seems to be significant only at higher fields. For MgB_2 there is a relatively sharp bend in $\gamma_v(H)$ vs H that is associated with different values of H_{c2} for the two bands [34], and perhaps an effect of that kind, but with a smaller difference in the values of H_{c2}, could be at work here. It is also interesting that a calculation of the "Volovik" effect for a two-band superconductor with different isotropic gaps and impurity scattering [35] gives a transition from the generic H-proportional dependence of $\gamma_v(H)$ at low H to something approaching $H^{1/2}$ at higher H. The resulting negative curvature of $\gamma_v(H)$ depends on the ratio of the gap sizes and is particularly strong for ratios of the order of 3.3 to 5. However, the calculations give substantial non-zero values of $\gamma_v(0)$, precluding quantitative comparison with our results.

Band-structure calculations [36] for $Ba_{1-x}K_xFe_2As_2$ using the local-density approximation (LDA), the virtual-crystal model, and allowing the positions of the As atoms to relax according to the LDA energy minimization criterion, show a very weak dependence of the DOS on doping. For the undoped $BaFe_2As_2$ the "bare" band-structure DOS is $N(E_F) = 3.06$ states eV^{-1} $f.u.^{-1}$; for the $x = 0.4$ hole-doped material $N(E_F) \sim 3.12$ states eV^{-1} $f.u.^{-1}$. However, the rigid-band calculation [36] which gave essentially the same result for $x = 0$, gave $N(E_F) \sim 4.38$ states eV^{-1} $f.u.^{-1}$ for $x = 0.4$ [36]. Another calculation [37] gave $N(E_F) = 4.553$ states eV^{-1} $f.u.^{-1}$ for $BaFe_2As_2$, and, using a supercell model, $N(E_F) = 5.526$ states eV^{-1} $f.u.^{-1}$ for $x = 0.5$. The increase in $N(E_F)$ for $x = 0.5$ in that calculation was ascribed to the use of the fixed experimental As position for the undoped compound [36]. For

comparison with experimental quantities, we take, somewhat arbitrarily, the value $N(E_F) = 3.12$ states eV^{-1} f.u.$^{-1}$ from [36]. The corresponding electron contribution to the specific heat, represented as the coefficient of a T-proportional term, is $\gamma_0 = 7.35$ mJ K^{-2} mol^{-1}. The experimental value of γ_n, 40.1 mJ K^{-2} mol^{-1}, then suggests an effective mass renormalization that would be unusually strong for a simple metal, for which the mass renormalization is produced by the electron-phonon interaction represented by the electron-phonon coupling parameter (λ) and $\gamma_n = (1 + \lambda)\gamma_0$. The value of λ would be 4.5, a factor 10 or so higher than the values commonly attributed to the electron-phonon interaction in "simple" metals. The theoretical value of $N(E_F)$ chosen for the comparison was among the lowest, but the experimental value of γ_n was also among the lowest (see Sect. 6 of [4]), and any of the possible comparisons would still give an extraordinarily high value of λ. Although the mass renormalization for F-doped LaOFeAs, in the 1111 series of Fe pnictide superconductors is not as strong as that found here for a member of the 122 series, it is strong enough to have attracted attention and it has motivated several calculations of the electron-phonon interaction. In one calculation [38], the electron-phonon λ was found to be ~0.2, and in another [39] 0.21. In both cases it was concluded that these numbers are too small to explain the apparent mass renormalization, and that the electron-phonon interaction is also too weak to account for the observed T_c. There are differences between the 1111 and 122 series, but, since the superconductivity occurs in the FeAs layers in both, it is reasonable to assume that these conclusions, with some allowance for differences in the numbers, would apply to $Ba_{1-x}K_xFe_2As_2$. It therefore seems likely that calculation of the electron-phonon interaction for $Ba_{0.59}K_{0.41}Fe_2As_2$ would not account for the observed mass enhancement.

The electron-phonon interaction accounts for both the normal-state mass renormalization and the superconducting-state electron pairing in "conventional" superconductors. The fact that it doesn't account for either in the Fe pnictides raises the question as to whether there is another interaction that contributes to both. Interaction with spin fluctuations, which can support spin-singlet superconductivity only if there is a sign-changing order parameter, has been suggested as the mechanism for the electron pairing [38]. It was also suggested that the pairing would be "extended" s wave, designated $s_{\pm}$, in which isotropic order parameters on different sheets of the Fermi surface have opposite signs [38]. The approximate linearity of $\gamma_v(H)$ in H (see Fig. 23.2) supports the argument in [38] that the $s_{\pm}$ pairing is more likely than d-wave, which could also satisfy the requirement of a sign-changing order parameter, but which would have nodes in the energy gaps. With respect to the mass renormalization, it is suggested in [40], which includes a general comparison of the superconductivity in the 1111 and 122 series, that while spin fluctuations might produce the strong mass enhancement in the 1111 series they might not produce the stronger effect in the 122 series. However, there seem to be no quantitative calculations. The specific-heat results emphasize the importance of theoretical consideration of magnetically mediated electron-electron interactions and their role in both mass enhancement and the occurrence of superconductivity. In connection with other theoretical predictions, we note that, in common with most

other experimental work, the relations between energy gaps and the DOS that we report seem to be inconsistent with a theory of the superconductivity [40] based solely on interband interactions.

Summary

The specific heat of a high-quality single crystal of $Ba_{0.59}K_{0.41}Fe_2As_2$, a near-optimally hole-doped superconductor in the 122 series of Fe pnictides, was measured from 2 to 300 K, and below 50 K in fields to $\mu_0 H = 14$ T.

A novel method of analysis of the data, based on *direct* comparisons of α-model expressions for the *electron contribution* with the *measured total specific heat*, was used to obtain the parameters characteristic of the electron bands. It bypasses the independent determination of the lattice contribution, an essential step in the conventional analyses, in which the lattice contribution is subtracted from the total to obtain the electron contribution, and it eliminates the substantial uncertainties in the electron contribution associated with the approximations inherent in the determination of the lattice contribution. The derived parameters characteristic of the electron contribution are significantly different from those obtained by conventional analyses for a group of five other near-optimally hole-doped $BaFe_2As_2$ superconductors, which also show significant differences within the group. We suggest that the approximations used in obtaining the lattice contribution in the conventional analyses make an important contribution to these differences.

For $Ba_{0.59}K_{0.41}Fe_2As_2$ the total DOS, as measured by the value of γ_n, 40.1 mJ K^{-2} mol^{-1}, is the sum of two contributions, $\gamma_{n1} = 31.0$ mJ K^{-2} mol^{-1} and $\gamma_{n2} = 9.1$ mJ K^{-2} mol^{-1}, from bands with superconducting-state energy gaps that are, respectively, larger and smaller than the weak-coupling BCS value. As measured by the gap-proportional parameter α, which is $1.764 \equiv \alpha_{BCS}$ in the weak-coupling limit of the BCS theory, the gaps correspond to $\alpha_1 = 3.30$ and $\alpha_2 = 0.86$. The energy gaps derived from the specific-heat data are within the ranges of values obtained in ARPES measurements, but there are some significant differences. The H dependence of the T-proportional term in the vortex-state specific heat suggests a nodeless order parameter and is consistent with extended s-wave pairing. The relations between the DOS and energy gaps for the two bands are not consistent with theoretical predictions [41] for a model in which superconductivity is produced by interband interactions alone. Comparison of the total DOS, as deduced from the value of γ_n, with band-structure calculations shows a strong effective mass renormalization that is without precedent in simple metals and is not theoretically explained.

Acknowledgements This work was supported by the Director, Office of Science, Office of Basic Energy Sciences, U.S. Department of Energy, under Contract No. DE-AC02-05CH11231 and Office of Basic Energy Sciences U.S. DOE under Grant No. DE-AC03-76SF008. We are grateful

to J. E. Gordon for help with the α-model calculations and helpful discussions about the method of analyzing the data.

References

1. J. G. Bednorz, K. A. Müller, Z. Physik B Condens. Matt. **64**, 189 (1996)
2. J. Nagamatsu, N. Nakagawa, T. Muranaka, Y. Zenitani, J. Akimitsu, Nature **410**, 63 (2001)
3. Y. Kamihara, T. Watanabe, M. Hirano, H. Hosono, J. Am. Chem. Soc. **130**, 3296 (2008)
4. C.R. Rotundu, T.R. Forrest, N.E. Phillips, R.J. Birgeneau, JPSJ **84**, 114701 (2015)
5. B. Mühlschlegel, Z. Phys. **155**, 313 (1959)
6. H. Padamsee, J.E. Neighbor, C.A. Shiffman, J. Low Temp. Phys. **12**, 387 (1973)
7. F. Bouquet, Y. Wang, R.A. Fisher, D.G. Hinks, J.D. Jorgensen, A. Junod, N.E. Phillips, Europhys. Lett. **56**, 856 (2001)
8. H.J. Choi, D. Roundy, H. Sun, M.L. Cohen, S.G. Louie, Nature (London) **418**, 758 (2002)
9. C. Caroli, P.G. de Gennes, J. Matricon, Phys. Lett. **9**, 307 (1964)
10. N.W. Ashcroft, N.D. Mermin, *Solid State Physics* (Saunders College, Philadelphia, 1976)
11. J.G. Storey, J.W. Loram, J.R. Cooper, Z. Bukowski, J. Karpinski, arXiv:1001.0474v1
12. G. Grimvall, J. Phys. Chem. Solids **29**, 1221 (1968)
13. P.B. Allen, M.L. Cohen, Phys. Rev. B **1**, 1329 (1970)
14. J.J. Sabo Jr., Phys. Rev. B **1**, 1325 (1970)
15. H. Luo, Z. Wang, H. Yang, P. Cheng, X. Zhu, H.-H. Wen, Supercond. Sci. Technol. **21**, 125014 (2008)
16. C.R. Rotundu, B. Freelon, S.D. Wilson, G. Pinuellas, A. Kim, E. Bourret-Courchesne, N.E. Phillips, R.J. Birgeneau, J. Phys. Conf. Ser. **273**, 012103 (2011)
17. U. Welp, G. Mu, R. Xie, A.E. Koshelev, W.K. Kwok, H.Q. Luo, Z.S. Wang, P. Cheng, L. Fang, C. Ren, H.-H. Wen, Phys. C **469**, 575 (2009)
18. G. Mu, H. Luo, Z. Wang, L. Shan, C. Ren, H.-H. Wen, Phys. Rev. B **79**, 174501 (2009)
19. C. Kant, J. Deisenhofer, A. Günther, F. Schrettle, A. Loidl, M. Rotter, D. Johrendt, Phys. Rev. B **81**, 014529 (2010)
20. L. Zhao, H.-Y. Liu, W.-T. Zhang, J.-Q. Meng, X.-W. Jia, G.-D. Liu, X.-L. Dong, G.-F. Chen, J.-L. Luo, N.-L. Wang, W. Lu, G.-L. Wang, Y. Zhou, Y. Zhu, X.-Y. Wang, Z.-Y. Xu, C.-T. Chen, X.-J. Zhou, Chin. Phys. Lett. **25**, 4402 (2008)
21. P. Popovich, A.V. Boris, O.V. Dolgov, A.A. Golubov, D.L. Sun, C.T. Lin, R.K. Kremer, B. Keimer, Phys. Rev. Lett. **105**, 027003 (2010)
22. A.K. Pramanik, M. Abdel-Hafiez, S. Aswartham, A.U.B. Wolter, S. Wurmehl, V. Kataev, B. Büchner, arXiv:1106.5471v1
23. K. Gofryk, J.C. Lashley, F. Ronning, D.J. Safarik, F. Weickert, J.L. Smith, A. Leithe-Jasper, W. Schnelle, M. Nicklas, H. Rosner, Phys. Rev. B **85**, 224504 (2012)
24. D.V. Evtushinsky, D.S. Inosov, V.B. Zabolotnyy, M.S. Viazovska, R. Khasanoc, A. Amato, H.-H. Klauss, H. Luetkens, C. Niedermayer, G.L. Sun, V. Hinkov, C.T. Lin, A. Varykhalov, A. Koitzsch, M. Knupfer, B. Büchner, A.A. Kordyuk, S.V. Borisenko, New J. Phys. **11**, 055069 (2009)
25. D.V. Evtushinsky, D.S. Inosov, V.B. Zabolotnyy, A. Koitzsch, M. Knupfer, B. Büchner, M.S. Viazovska, G.L. Sun, V. Hinkov, A.V. Boris, C.T. Lin, B. Keimer, A. Varykhalov, A.A. Kordyuk, S.V. Borisenko, Phys. Rev. B **79**, 054517 (2009)
26. H. Ding, P. Richard, K. Nakayama, K. Sugawara, T. Arakane, Y. Sekiba, A. Takayama, S. Souma, T. Sato, T. Takahashi, Z. Wang, X. Dai, Z. Fang, G.F. Chen, J.L. Luo, N.L. Wang, Europhys. Lett. **83**, 47001 (2008)

27. C. Liu, G.D. Samolyuk, Y. Lee, N. Ni, T. Kondo, A.F. Santander-Syro, S.L. Bud'ko, J.L. McChesney, E. Rotenberg, T. Valla, A.V. Fedorov, P.C. Canfield, B.N. Harmon, A. Kaminski, Phys. Rev. Lett. **101**, 177005 (2008)
28. F. Hardy, T. Wolf, R.A. Fisher, R. Eder, P. Schweiss, P. Adelmann, H.V. Löhneysen, and C. Meingast, Phys. Rev. B **81**, 060501(R) (2010)
29. K. Gofryk, A.S. Sefat, E.D. Bauer, M.A. McGuire, B.C. Sales, D. Mandrus, J.D. Thompson, F. Ronning, New J. Phys. **12**, 023006 (2010)
30. G.E. Volovik, JETP Lett. **58**, 469 (1993)
31. K.A. Moler, D.J. Baar, J.S. Urbach, R. Liang, W.N. Hardy, A. Kapitulnik, Phys. Rev. Lett. **73**, 2744 (1994)
32. C. Kübert, P.J. Hirschfeld, Solid State Commun. **105**, 459 (1998)
33. N. Nakai, P. Miranovic, M. Ichioka, K. Machida, Phys. Rev. B **70**, 100503 (2004)
34. F. Bouquet, Y. Wang, I. Sheikin, T. Plackowski, A. Junod, S. Lee, S. Tajima, Phys. Rev. Lett. **89**, 257001–257001 (2002)
35. Y. Bang, Phys. Rev. Lett. **104**, 217001–217001 (2010)
36. D.J. Singh, Phys. Rev. B **78**, 094511 (2008)
37. I. R. Shein and A. L. Ivanovskii, arXiv: 0806.0750 (unpublished)
38. I.I. Mazin, D.J. Singh, M.D. Johannes, M.H. Du, Phys. Rev. Lett. **101**, 057003 (2008)
39. L. Boeri, O.V. Dolgov, A.A. Golubov, Phys. C **469**, 628 (2009)
40. O. V. Dolgov, I. I. Mazin, D. Parker, and A. A. Golubov, Phys. Rev. B **79**, 060502(R) (2009).
41. I.I. Mazin, J. Schmalian, Phys. C **469**, 614 (2009)

Chapter 24
Thermal and Quantum Critical Properties of Overdoped $La_{2-x}Sr_xCuO_4$

Toni Schneider

Considering thin films and adopting the phase transition point of view the thermal (TSP) and quantum (QSM) superconductor to metal transitions are expected to fall onto the respective two dimensional (2D) xy-universality class. Accordingly the TSP transition should exhibit the characteristic Kosterlitz-Thouless-Berezinski (KTB) behavior [1, 2] including a discontinuous drop in the superfluid stiffness $\rho_s(T) \propto d/\lambda^2(T)$ from [3],

$$\frac{d}{\lambda^2\left(T_c^-\right)} = \frac{32\pi^2}{\Phi_0^2} k_B T_c \simeq 1.017 T_c, \tag{24.1}$$

to zero, with $d/\lambda^2\left(T_c^-\right)$ in cm^{-1} and T_c in K. $\Phi_0 = hc/2e \simeq 2.07 \times 10^{-7} \mathrm{erg}^{1/2}\mathrm{cm}^{1/2}$. d denotes the film thickness. In a homogenous film this relationship applies if $d/\lambda^2(T)$ is measured at zero frequency and $\lambda^2(T)/d$ is large compared to the lateral extent of the film. Otherwise there is a rounded BKT-transition. In particular, if the lateral extent of the homogeneous regions L is finite the correlation length cannot grow beyond L. Similarly, there is no phase transition at finite frequency because the frequency scales as $1/\omega \propto \xi^{z_{cl}} \propto L^{z_{cl}}$ and so gives rise to a smeared Nelson-Kosterlitz jump [4]. Noting that $d/\lambda^2(T)$ and $\rho_s(T)$ are related by

$$\frac{d}{\lambda^2(T)} = \frac{4\pi\alpha k_B}{\hbar c} \rho_s(T), \tag{24.2}$$

where k_B is Boltzmann's, $\hbar$ Planck's, α the fine structure constant, and c speed of light. From Eqs. (24.1) and (24.2) we obtain for the BKT line the relation

T. Schneider (✉)
Physik-Institut der Universität Zürich, Winterthurerstrasse 190, 8057 Zürich, Switzerland
e-mail: tnschndr@gmail.com

A. Bussmann-Holder et al. (eds.), *High-Tc Copper Oxide Superconductors and Related Novel Materials*, Springer Series in Materials Science 255,
DOI 10.1007/978-3-319-52675-1_24

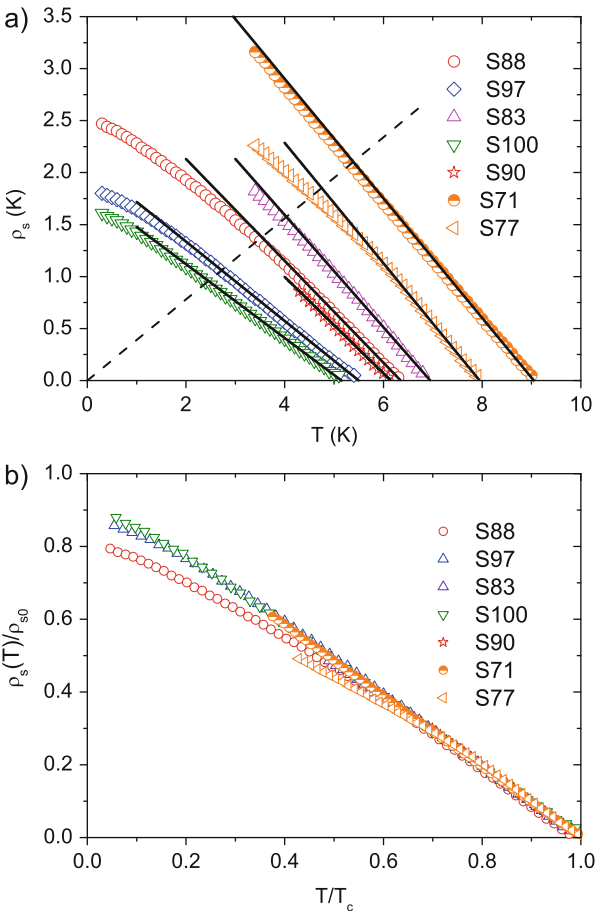

Fig. 24.1 (**a**) Superfluid stiffness $\rho_s(T)$ for a selection of overdoped thin films taken from Božović et al. [5]. S denotes the selected samples. The *dashed line* marks the KTB transition temperature where the universal jump in the superfluid stiffness should occur (Eq. 24.3). The *solid lines* are fits to Eq. (24.4) yielding for ρ_{s0} and T_c the estimates collected in Fig. 24.2. (**b**) Scaling plot $\rho_s(T)/\rho_{s0}$ vs. T/T_c.

$$T_c = \frac{\Phi_0^2 \alpha}{8\pi\hbar c}\rho_s(T) \simeq 0.39\rho_s(T), \tag{24.3}$$

with T_c and ρ_s in K. Figure 24.1a shows data taken from Božović et al. [5] of the superfluid stiffness $\rho_s(T)$ for a selection of overdoped thin $La_{2-x}Sr_xCuO_4$. S denotes the selected samples. The dashed line is the KTB transition temperature where at the intersection with $\rho_s(T)$ the universal jump should occur. Obviously there are no signs for the universal jump at the respective KTB transition temperatures. In fact, the rather sharp TSM transitions occur considerably above the respective KTB transition temperatures and reveal remarkable consistency with the mean-field temperature dependence

$$\rho_s(T) = \rho_{s0}(T_c)t = \frac{4\pi\alpha k_B}{\hbar c}\frac{d}{\lambda^2(T)}$$
$$= \frac{4\pi\alpha k_B}{\hbar c}\frac{d}{\lambda_0^2(T_c)}t = \frac{4\pi\alpha k_B}{\hbar c}\frac{d}{\lambda_0^2(T_c)}t, \tag{24.4}$$

where $t = (1 - T/T_c)$. Note that such an extended linear t dependence is a characteristic of feature of d-wave BCS superconductors where thermal phase fluctuations, driving the BKT transition, are fully neglected [6]. The solid lines in Fig. 24.1a are fits to Eq. (24.4). The resulting fit parameters, ρ_{s0} and T_c, are collected in Fig. 24.2 and yield the scaling plot shown in Fig. 24.1b. Obviously, when the QSM transition is reached, the data fall onto a straight line and thus confirm the BCS d-wave scenario very impressively. Given the evidence for the irrelevance of phase fluctuations, another unexpected empirical fact emerges from Fig. 24.2, depicting $T_c\left(\rho_{s0}^{1/2}\right)$. The dashed line $T_c = f\rho_{s0}^{1/2}$, describing the approach to the QSM transition rather well, agrees with the zero temperature counterpart $T_c \propto \rho(0)^{1/2}$, verified by Božović et al. [5]. In fact, this relationship contradicts the general belief that the measured penetration depth corresponds to the London penetration depth, whereupon

$$\rho_s(0) \propto 1/\lambda(0)^2 \propto n, \tag{24.5}$$

applies, where n is fully determined by the shape of the Fermi surface [7]. For circular or spherical Fermi surfaces it corresponds to the electron density in the normal state. As shown by angle-resolved photoemission experiments, this is not the case in overdoped $La_{2-x}Sr_xCuO_4$ [8]. However, the result is determined by the shape of the Fermi surface and independent of T_c. Therefore even the more general

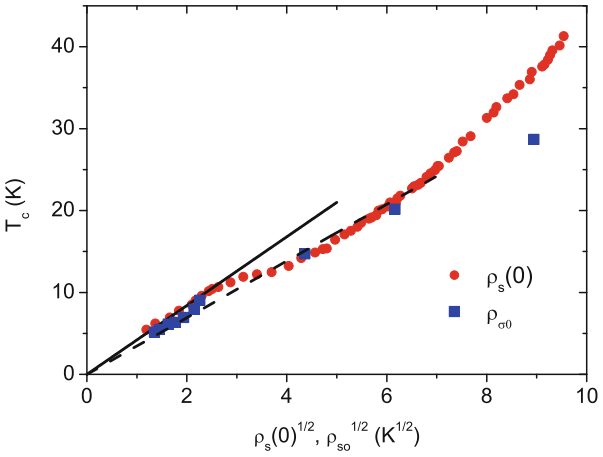

Fig. 24.2 Estimates for the critical amplitude $\rho_{s0}(T_c)$, shown as T_c versus $\rho_{s0}^{1/2} \propto 1/\lambda_o^{1/2}$, derived from the fits shown in Fig. 24.1a. The *dashed line* is $T_c = f\rho_{s0}^{1/2}$ with $f = 3.46$ K$^{1/2}$. For comparison we included T_c versus $\rho_s(0)^{1/2}$ of Božović et al. [5] $\rho_s(0) \propto 1/\lambda(0)^2$ is the zero temperature superfluid stiffness and the solid line is $T_c = g\rho_s(0)^{1/2}$ with $g = 4.2$ K$^{1/2}$

treatment of the zero temperature penetration depth is incompatible with the empirical relation

$$T_c \propto \rho_s(0)^{1/2} \propto \rho_{s0}^{1/2} \propto 1/\lambda(0) \propto 1/\lambda_0, \tag{24.6}$$

emerging from Fig. 24.2. $T_c \propto \rho_s(0)^{1/2}$ was verified by Božović et al. [5] and $T_c \propto \rho_{s0}^{1/2}$ follows from our analysis shown in Fig. 24.1, yielding $\rho_{s0}(T_c)$ depicted in Fig. 24.2. Note that the observation of a diminishing $\rho_s(0)$ in the overdoped regime is confirmed by earlier measurements [9–13]. In addition there is the hyperscaling prediction [4, 14]

$$T_c \propto \rho_s(0)^{z/(D+z-2)}, \tag{24.7}$$

where z denotes the dynamic critical exponent of the quantum transition. It is applicable whenever a phase transition line $T_c(x)$ exhibits a critical endpoint at $x = x_c$ of the tuning parameter x. Here the transition temperature vanishes and a quantum phase transition occurs. In thin films ($D = 2$) it yields $T_c \propto \rho_s(0)$, irrespective of the value of the dynamic critical exponent z, and with that it contradicts the empirical relation (24.5). Given the unexpected empirical relation (24.5), the evidence for d-wave BCS behavior in the temperature dependence of $\rho_s(T)$, and the resulting irrelevance of phase fluctuations, it is suggestive to explore the BCS scenario further. Considering the observable $O(T)$ with critical amplitude O_0 and $O(T = 0) = O(0)$, including the gap Δ, the correlation length ξ and the upper critical field H_{c2}, the critical amplitudes should scale as [4, 15]

$$T_c \propto \Delta_0 \propto \xi_0^{-1} \propto H_{c20}^{-1/2} \propto \Delta(0) \propto \xi(0)^{-1} \propto H_{c2}(0)^{-1/2}, \tag{24.8}$$

Here, $\lambda(T) = \lambda_0 t^{-1/2}$, $\Delta(T) = \Delta_0 t^{1/2}$, $\xi(T) = \xi_0 t^{-1/2}$, $H_{c2} = H_{c20} t \propto 1/\xi^2$, where $t = 1 - T/T_c$. These scaling relations follow from $\Delta(T) \propto 1/\xi(T) \propto H_{c2}(T)^{-1/2}$, and $\Delta(0) \propto \Delta_0 \propto T_c$.

In order to clarify their consistency with experimental facts, we need the T_c dependence of H_{c2} and the gap Δ. In Fig. 24.3a we depicted T_c versus $H_{c2}(0)$ taken from Y. Wang and H.-H. Wen derived from specific heat measurements on single crystals [16]. Although the data are rather sparse the flow to the QSM transition is revealed, and consistency with the BCS scaling law (24.8) can be anticipated. Consistency also emerges from Fig. 24.3b, depicting the magnetoresistance measurements of Rourke et al. [18] on single crystals. Quantitative agreement with BCS theory for a d-wave superconductivity in overdoped cuprates stems from heat transport measurements in $Tl_2Ba_2CuO_{6+\vartheta}$ [19].

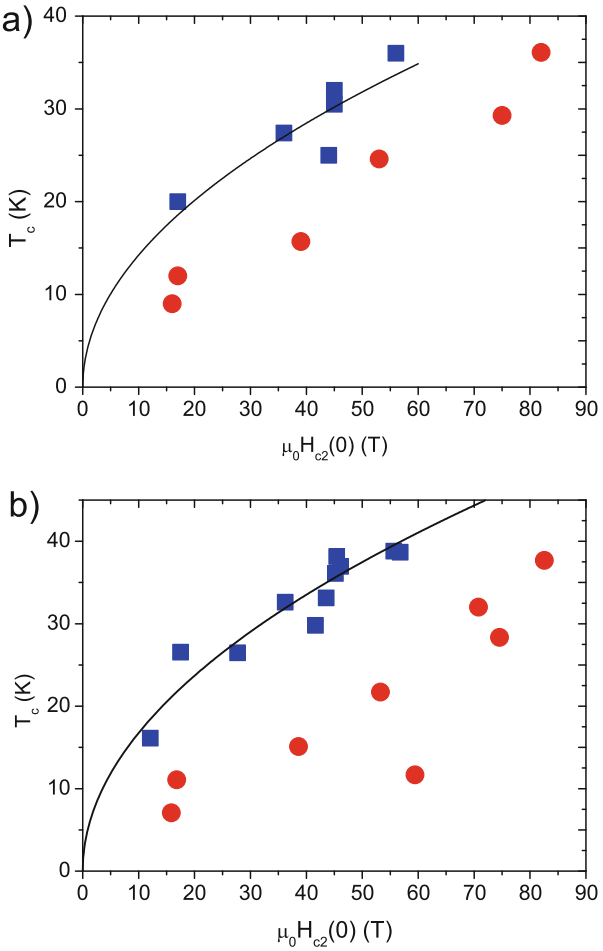

Fig. 24.3 T_c versus $H_{c2}(0)$. (**a**) Taken from Y. Wang and H.-H. Wen as derived from specific heat measurements on $La_{2-x}Sr_xCuO_4$ single crystals [18] (*filled squares* overdoped regime, *filled circles* underdoped regime). The line is $T_c = aH_{c2}(0)^{1/2}$ with $a = 4.5KT^{-1/2}$. (**b**) Taken from Rourke et al. as derived from magnetoresistance measurements $La_{2-x}Sr_xCuO_4$ single crystals [19] (*filled squares* overdoped regime; *filled circles* underdoped regime). The line is $T_c = aH_{c2}(0)^{1/2}$ with $a = 5.3KT^{-1/2}$

Fig. 24.4 shows the doping dependence of the gap in terms of $\Delta(0)/k_BT_c$ versus x for $La_{2-x}Sr_xCuO_4$ taken from Wang et al. [17], derived from low temperature specific heat measurements on single crystals. The *dotted line* marks the d-wave BCS value $\Delta(0)/k_BT_c \simeq 2.14$. Note that for $x \gtrsim 0.19$ the data are consistent with the scaling form (24.8) and in addition with d-wave BCS (weak coupling) superconductivity. More compelling evidence for this scenario stems from heat transport measurements in $Tl_2Ba_2CuO_{6+\vartheta}$ [19]. Potential candidates appear to be the nonlocal effects on the penetration depth of clean d-wave superconductors explored by Kosztin and Legget [20]. Taking the nonlocal effects into account they obtained for a specular boundary the relation

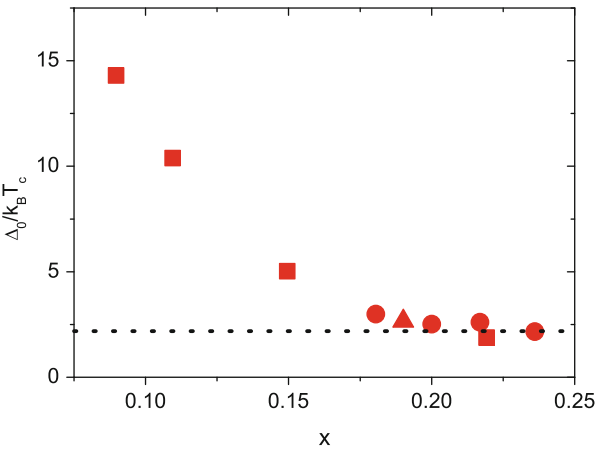

Fig. 24.4 Gap $\Delta(0)/k_BT_c$ versus x for $La_{2-x}Sr_xCuO_4$ taken from Wang et al. [17]. The *dotted line* marks the limiting d-wave BCS value $\Delta(0)/k_BT_c = 2.14$. Note that for $x \gtrsim 0.19$ the data are consistent with the scaling form (24.8)

$$\frac{\lambda_{spec}(0)}{\lambda_L(0)} = 1 + \frac{\pi\sqrt{2}}{16}\frac{\xi(0)}{\lambda_L(0)}, \tag{24.9}$$

where $\lambda_L(0)$ is the zero temperature London penetration depth. Considering the limit $\xi(0)/\lambda_L(0) >> 1$ they expected no significant corrections at zero temperature. This differs from the present case where the QSM transition is approached, $\xi(0) \propto 1/T_c$ tends to diverge and the limit $\xi(0)/\lambda_L(0) >> 1$ is attained. In this case the nonlocal corrections dominate and Eq. (24.9) reduces, in accordance with the empirical relation (24.6), to $\lambda_{spec}(0) \propto \xi(0) \propto 1/T_c$. To estimate the T_c regime where this limit is reached we calculate the T_c dependence of $\xi(0)$. With $\xi(0)^2 = \Phi_0/(2\pi H_{c2}(0))$ and $T_c = aH_{c2}(0)^{1/2}$ with $a = 5\ \mathrm{KT}^{-1/2}$ (see Fig. 24.3) we obtain $\xi(0) \simeq 900/T_c$ A with T_c in K. Consequently $\xi(0)/\lambda_L(0) >> 1$ is fulfilled if $\lambda_L(0) << 900/T_c$ A, where $\lambda_L(0)$ is fully determined by the properties of the Fermi surface. In summary, we analyzed the temperature dependence of the superfluid stiffness of selected overdoped $La_{2-x}Sr_xCuO_4$ thin films, using the data of Božović et al. [5]. The temperature dependence did not exhibit any sign of the expected KTB transition. We observed remarkable consistency with a linear temperature dependence, pointing to d-wave BCS behavior. On the other hand, we have shown that the critical amplitude ρ_{s0} and the zero temperature counterpart $\rho_s(0)$ adopt essentially the same T_c power law dependence. This contradicts the standard result, whereupon $\rho_s(0)$ remains finite and is determined by Fermi surface properties. Exceptions include dirty limit superconductors, where $\rho_s(0) \propto T_c$. Moreover we have shown that the T_c of $\Delta(0)$ and $H_{c2}(0)$ are consistent with the expected BCS behavior, as it should be, because both are proportional to some power of the correlation length $\xi(0)$. Noting that the correlation length is the essential length scale the measurements of Božović et al. [5] imply that $\rho_s(0) \propto \rho_{s0} \propto \xi(0)^{-2} \propto \xi_0^{-2}$ holds by approaching the TSM and QSM transitions down to 5 K. We observed that potential candidates appear to be the nonlocal effects on the penetration depth of clean d-wave superconductors explored by Kosztin and Legget [20]. It should be

kept in mind, that closer the QSM transition ($T_c = T = 0$) quantum fluctuations are expected to modify the outlined scaling behavior and uncover the difference between bulk and thin film samples.

Acknowledgements Karl Alex Müller I am grateful for our friendship dating back to discussions on high temperature superconductivity in metallic hydrogen in 1970.

References

1. J.M. Kosterlitz, D.J. Thouless, J. Phys. C **6**, 1181 (1973)
2. V. L. Berezinskii, Zh. Eksp. Teor. Fiz. **61**, 1144 (1971) [Sov. Phys. JETP **34**, 610 (1972)]
3. D.R. Nelson, J.M. Kosterlitz, Phys. Rev. Lett. **39**, 1201 (1977)
4. T. Schneider, J.M. Singer, *Phase Transition Approach to High Temperature Superconductivity* (Imperial College Press, London, 2000)
5. I. Božović, X. He, J. Wu, A.T. Bollinger, Nature **536**, 309 (2016)
6. R. Prozorov, Supercond. Sci. Technol. **21**, 082003 (2008)
7. B.S. Chandrasekhar, D. Einzel, Ann. Phys. (Leipzig) **2**, 535 (1993)
8. R. Razzoli et al., New J. Phys. **12**, 125003 (2010)
9. C. Niedermayer et al., Phys. Rev. Lett. **71**, 1764 (1993)
10. C. Bernhard et al., Phys. Rev. B **52**, 10488 (1995)
11. J.P. Locquet et al., Phys. Rev. B **54**, 7481 (1996)
12. C. Panagopoulos et al., Phys. Rev. B **67**, 220502 (2003)
13. T.R. Lemberger et al., Phys. Rev. B **83**, 140507 (2011)
14. K. Kim, P.B. Weichman, Phys. Rev. B **43**, 13583 (1991)
15. A.L. Fetter, J.D. Walecha, *Quantum Theory of Many-Particle Systems* (McGraw-Hill, New York, 1971)
16. Y. Wang, H.-H. Wen, EPL **81**, 5700 (2008)
17. Y. Wang, J. Yan, L. Shan, H.-H. Wen, Phys. Rev. B **76**, 064512 (2007)
18. M.C. Patrick, Rourke et al. Nat. Phys. **7**(455) (2011)
19. C. Proust et al., Phys. Rev. Lett. **89**, 147003 (2002)
20. I. Kosztin, A.J. Leggett, Phys. Rev. Lett. **79**, 135 (1997)

Chapter 25
Scientific Collaboration with Warm Relations

A. Shengelaya

Introduction: Hydrogen Effects in Cuprate High-T_c Superconductors

It was in 1987 when I first time heard about the discovery of high-T_c superconductivity in cuprates. At that time I was a physics student at Kazan State University in Russia. I remember well a special session in a big auditorium of physics where I was listening with great interest to our physics professors enthusiastically describing different aspects of this discovery. At that time I knew very little about superconductivity, but looking how fascinated were our professors, it became clear to me that something extraordinary important has happened. This motivated me to choose high-T_c superconductivity as a subject for my diploma work. So I can say I was lucky that this important discovery was announced just before the start of my diploma thesis.

My supervisor for diploma work was Dr. Nail Suleimanov at the Kazan Physical-Technical Institute. We decided to study hydrogen doping effects in $La_{2-x}Sr_xCuO_4$ (LSCO). Hydrogen is a very interesting dopant. It has a simple electronic structure and a small mass, but is capable to substantially modify the charge carrier concentration in various materials with a relatively small distortion of the lattice. As a result of our work we were able to determine optimal temperature conditions for hydrogen doping in LSCO. It was found that hydrogen atoms enter interstitial sites in LSCO lattice and electrons transferred from hydrogen neutralize holes. Therefore, hydrogen doping allows to decrease the hole concentration in cuprates. Based on obtained results we published paper which was my first scientific publication [1]. I continued to work on this subject also during my

A. Shengelaya (✉)
Department of Physics, Tbilisi State University, Chavchavadze 3, 0128 Tbilisi, Georgia
e-mail: alexander.shengelaya@tsu.ge

A. Bussmann-Holder et al. (eds.), *High-Tc Copper Oxide Superconductors and Related Novel Materials*, Springer Series in Materials Science 255,
DOI 10.1007/978-3-319-52675-1_25

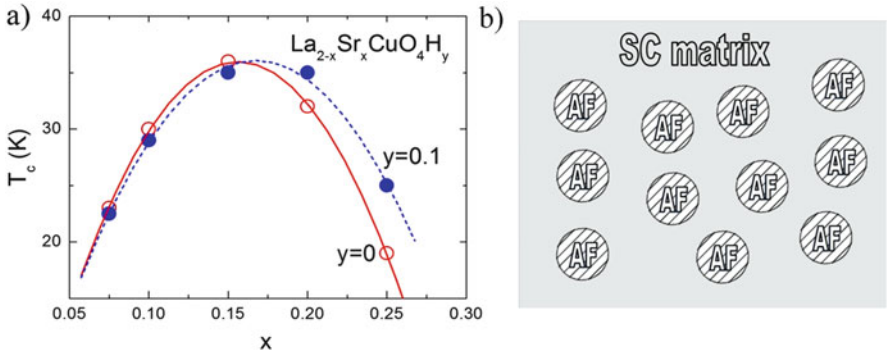

Fig. 25.1 (**a**) T_c vs. x phase diagram of the $H_yLa_{2-x}Sr_xCuO_4$ with y = 0 and 0.1 [2]. (**b**) Schematic picture of the superconducting matrix of underdoped LSCO doped with hydrogen. Hatched areas represent regions where the superconductivity is suppressed due to hole neutralization resulting in recovered antiferromagnetic order [2]

PhD thesis at the Institute of Low Temperature and Structure Research in Wroclaw, Poland with my PhD advisor Prof. Henryk Drulis. We observed that the hydrogen effect on superconducting transition was qualitatively different in underdoped and overdoped regions. In overdoped region T_c was increasing with hydrogen doping as one would expect in case of decrease of hole concentration. On the other hand, in underdoped region T_c did not change and the superconducting volume fraction was gradually decreasing with hydrogen doping [2]. This behavior is shown in Fig. 25.1a.

It was possible to understand the unusual behavior in underdoped region assuming that the hole concentration is reduced by hydrogen *inhomogeneously* by forming hole-poor clusters where superconductivity is locally suppressed (see Fig. 25.1b). The hole concentration in the rest of the material remains unchanged and so is T_c. If this is the case, one can expect that in hole-poor clusters where superconductivity is suppressed, antiferromagnetic order characteristic for the parent compound will recover. This was indeed confirmed by our subsequent Electron Paramagnetic Resonance (EPR) and Mössbauer effect measurements [3, 4].

In 1995 I successfully defended PhD thesis and was looking for the postdoc position. Again I was lucky that in 1995 a first Polish-US conference on high-T_c superconductivity took place in Wroclaw organized by Prof. Jan Klamut. As a rule only Polish and US researchers were participating in this conference. Only person not coming from these countries was Alex Müller who was invited as a special guest. During the conference first Victor Emery and afterwards Alex Müller came to my poster and this was the first time I met Alex. It was of course a great honor for me. We had quite long discussion since he was also very much interested in electronic phase separation in cuprates. Soon after finishing the conference Alex called me from Zürich and invited me to present my work at the solid state physics seminar at the Physics Institute of the University of Zürich. After the seminar I

visited laboratory of Prof. Hugo Keller and I got an offer to start a postdoc position in his lab. I was of course very happy to follow this invitation since this gave me the possibility to continue work on high-T_c superconductors and related materials together with Alex and Hugo. I spent almost 10 years first as a postdoc and later as research associate at the Physics Institute and this was an extremely interesting and important period in my research carrier. Hugo Keller created wonderful and creative atmosphere in his group with excellent PhD students. I had a great pleasure and privilege to plan research and discuss obtained results together with Hugo and Alex.

EPR Study of Manganites and Cuprates

One of the main experimental techniques I used during the work in Zürich was EPR. As a graduate from Kazan State University where EPR was discovered in 1944, I had quite good training in this method, but during the stay in Zürich I greatly profited from profound experience and knowledge of Alex in EPR. I should say that Alex is a great enthusiast of EPR. This is natural since EPR was one of his favorite experimental tools to study microscopic properties of oxides over many decades. He often says that if you can observe an EPR signal in your compound you can do a lot. I completely agree with him. In Zürich I had possibility to use EPR spectrometer which belonged to Alex when he worked at IBM Zürich research laboratory in Rüschlikon. Soon we published a common paper about EPR in colossal magnetoresistive (CMR) manganese oxides [5]. In this paper we proposed a model in which so-called bottlenecked spin relaxation takes place from the exchanged coupled Mn^{4+} ions via the Mn^{3+} Jahn-Teller ions to the lattice. This model provided explanation for the unusual temperature dependence of EPR intensity in CMR manganites, as well as on the observed oxygen isotope effects. Obtained experimental results and proposed theoretical model provided evidence for Jahn-Teller polarons in CMR manganites. As it is well known, the concept of Jahn-Teller polarons played an important role in the discovery of high-T_c superconductivity in cuprates [6]. I remember very well the reaction of Alex when we were discussing these results and their interpretation within the bottleneck model. During the discussion Alex was swinging in his chair and when the physical picture became clear, oscillations of his chair increased dramatically and almost reached a resonance. I could feel how passionate he is about physics and how much he enjoys it. In the following paper using the same model we were able to explain the temperature dependence of EPR linewidth and related it with hopping conductivity of polarons in manganites [7].

We also applied EPR to study cuprate superconductors. As an EPR probe we used Mn^{2+} ions substituted for Cu^{2+} in the CuO_2 planes. EPR experiments in strongly underdoped cuprates provided evidence of electronic phase separation with existence of hole-rich and hole-poor regions [8]. Indeed in LSCO with doping range $0 < x < 0.06$ we observed two lines with different linewidth in EPR spectra: a narrow one and a broad one. The analysis of these lines showed that the broad line is

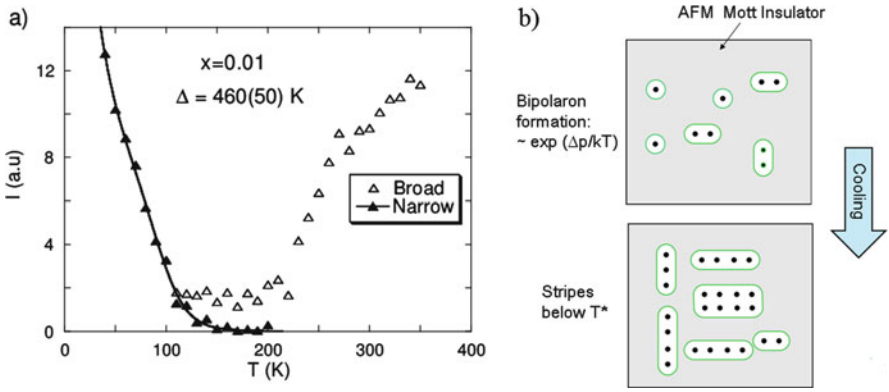

Fig. 25.2 (**a**) Temperature dependence of the narrow and broad EPR signal intensity in $La_{2-x}Sr_xCu_{0.98}Mn_{0.02}O_4$ with Sr doping x = 0.01. The solid line represents fit using the model described in [8]. (**b**) Schematic picture of hole polarons in the AF-ordered insulating matrix in CuO_2 plane at high temperatures, which form bipolarons and cluster into hole-rich metallic domains or stripes upon cooling. From [9]

due to hole-poor AF regions, while narrow line to hole-rich metallic regions. Especially interesting is that the intensity of narrow line increases exponentially with decreasing temperature (see Fig. 25.2a). This indicates that the volume fraction of metallic regions increases upon cooling. The activation energy of this process can be extracted from the temperature dependence of the narrow EPR line intensity. This activation energy is near 500 K, independent of the doping and gives the formation energy of the metallic clusters or stripes which consist of bipolarons [9].

Figure 25.2b shows schematically how individual hole polarons in the AF-ordered insulating matrix in the CuO_2 planes form bipolarons and cluster into hole-rich stripes with decreasing temperature. Very recently a remarkably similar picture was obtained experimentally by STM experiments in underdoped cuprate [10]. In our recent publication together with Alex, we review many experimental results which provide evidence that in the cuprates the superconductivity is present intrinsically in a dynamic inhomogeneous matrix [11]. In the situation shown in Fig. 25.2b, hole-rich metallic regions can be locally superconducting, but because of the small size and the absence of percolation, global phase coherence and a superconductivity cannot be achieved. However, with increasing hole doping the size and number of metallic/superconducting clusters will increase. At some doping the spreading of phase coherence by percolation occurs and macroscopic superconducting state is attained according to the model of Mihailovic, Kabanov and Müller [12].

Return to Georgia

In 2005, when I decided to return to Georgia and work at Tbilisi State University (TSU), Alex supported my decision. Moreover, he donated his EPR spectrometer to our laboratory in TSU. Spectrometer was transported from Zürich to Tbilisi with the help of Hugo Keller. It gave us a possibility to resume EPR experiments in Georgia. This spectrometer is still actively used both in research and in education of graduate students at TSU.

Alex was visiting Georgia several times. First time as a guest of Georgian Academy of Sciences in 1999. Second time he came to Georgia as a guest on my marriage party in 2000. Together with other friends from Switzerland we travelled from Tbilisi to my home town Zugdidi in west Georgia where marriage ceremony and afterwards party took place. Alex enjoyed it very much and all my family members and relatives were very happy to host such a distinguished guest. An effect was that we forgot to check the date of flight of Alex, so he arrived together with my father to airport in Tbilisi 1 day later the date of his flight. He missed the flight, but Alex did not care too much. As compensation he invited my father to drink a glass of prosecco in the nearby restaurant. Because of this delay his wife Inge was worried and she asked Hugo Keller to call Georgian Academy of Sciences to find out where is her husband (at that time Alex had no mobile phone). In Georgian Academy of Sciences they had no idea where Alex is since he was in Georgia with private visit. Finally, everything went well and Alex could depart next day to Switzerland.

"Coulomb Engineering" in Cuprates

The question about electronic phase separation in underdoped cuprates continued to be our common research interest. The size of the hole-rich clusters shown in Fig. 25.2b and therefore the percolation are controlled by Coulomb repulsion which limits the size of such clusters. During the conference of superconductivity and magnetism in Istanbul in 2012, we were discussing with Alex whether it would be possible to externally modify the Coulomb interaction and control the cluster size and percolation in underdoped cuprates. We came to idea that this could be done by increasing the dielectric constant in these compounds which would decrease the Coulomb repulsion. This looks very attractive since this would enable to increase the cluster size and attain percolation at higher temperature. As a result a bulk superconducting transition temperature T_c could be increased substantially. But how to increase the dielectric constant of a material artificially? The idea came from a discussion with my colleague Dr. Tamar Chelidze at Tbilisi State University. She pointed my attention that in semiconductor physics the possibility to modify the Coulomb interaction in a thin semiconducting layer sandwiched by insulators with a different dielectric constant was predicted by Keldysh [13]. The process which

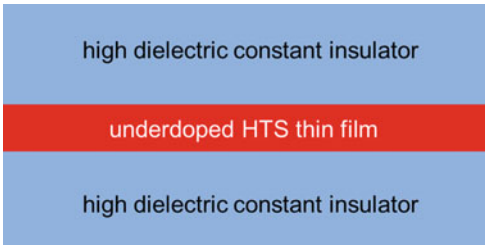

Fig. 25.3 Schematic drawing of the proposed structure where an underdoped copper-oxide high-temperature superconductor is sandwiched between high-dielectric-constant insulator layers. From [14]

one can call "Coulomb interaction engineering" was described as the effective change of the dielectric constant of a semiconductor due to the penetration of the electric field from the surrounding insulators with a different dielectric constant. This phenomenon is also called dielectric confinement effect by analogy to the quantum confinement effect. Usually, in semiconductors this effect is used for opposite purpose: to increase the Coulomb interaction which could lead to increase of exciton binding energy. Therefore semiconductor layer is brought in contact with low dielectric constant material. Following this idea, in our recent article together with Alex we proposed to create multilayer structure in which a thin film of underdoped cuprate is sandwiched between high-dielectric constant insulator layers as shown in Fig. 25.3 [14]. As a high-dielectric constant material one can take $SrTiO_3$, which is a quantum paraelectric below 4 K [15]. In that region it reaches ε values over 10,000; but at higher temperatures near 100 K, $\varepsilon = 300$ are found. The epitaxial growth of cuprate thin films on $SrTiO_3$ substrates using pulsed laser deposition has been reported by many groups. Instead of $SrTiO_3$, one can also use other perovskites with higher dielectric constants. For example, a mixed perovskite with ferri-electric properties such as $KTa_{0.9}Nb_{0.1}O_3$ has ε of 160,000 near its ferroelectric phase transition [16]. Cuprate superconductors have dielectric constants about 30. Therefore the dielectric confinement effect is expected to be significant. At present together with Alex we are actively involved in the project to create structures such as shown in Fig. 25.3 in order to test our model. Probably the effect of "Coulomb interaction engineering" also plays a role in the strong increase of T_c observed in FeSe thin films grown on $SrTiO_3$ [17].

Photostimulated Solid State Reaction

During his recent visit in Georgia in 2013 we started to collaborate with Alex Müller on a very interesting project which concerns the synthesis of cuprate superconductors and other complex oxide compounds. As it is known such compounds are usually obtained through solid state reactions. This implies continuous (for tens or hundreds of hours) heating (calcination) of well-mixed reactants in powder form in an oven at high temperatures (800–1200 °C). So it is a highly time and energy consuming process. In Tbilisi we attempted the synthesis of LSCO

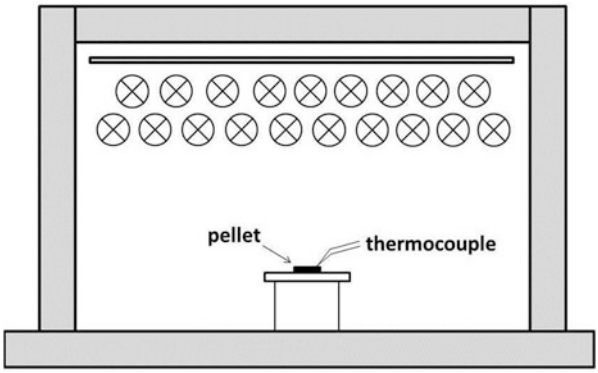

Fig. 25.4 Schematic drawing of photon irradiation setup

starting from standard precursors La_2O_3, $SrCO_3$ and CuO, but instead of using conventional furnace, we treated the pressed pellet from the mixture of these precursors in home built photon irradiation setup. Schematic drawing of this setup is shown in Fig. 25.4. It contains a bank of 19 halogen lamps, with 1 kW power each and a color temperature of 3200 K. With this setup, a maximum temperature of 1200 °C could be reached in 7 s. Light irradiation was performed in pulsed mode, with the pulse length being 20 s. The sample was mounted on a quartz plate, and its temperature was measured by a quick-response thermocouple attached to the pellet as shown in Fig. 25.4.

Using this setup the starting pellets were irradiated for periods of 20 s. After each irradiation step, the sample was allowed to cool and then irradiated again from another side for 20 s. We found that with this method superconducting LSCO samples can be synthesized in unusually short time. Figure 25.5a shows as an example the superconducting transition in LSCO ($x = 0.16$) sample which was irradiated with one 20 s pulse from both sides with total irradiation time 40 s. During the irradiation sample temperature was 1200 °C.

The superconducting volume fraction estimated from zero-field-cooled (ZFC) magnetization is about 50%, revealing the bulk nature of the superconductivity. This means that bulk superconducting LSCO samples can be obtained in only 40 s instead of several tens of hours required in a conventional furnace. Halogen lamps in our setup provide both light and heat. In order to separate effects of light irradiation from simple heating we performed following experiments. Pellets of initial precursor mixture were inserted in a conventional preheated furnace at given temperature and kept there during 2 min. Identical pellets were treated in photon irradiation setup during the same time and at the same temperature. Figure 25.5b shows the superconducting volume fraction determined from ZFC magnetization versus synthesis temperature in obtained samples. One can see that the superconducting volume fraction is negligible in furnace-prepared LSCO samples up to 1000 °C. On the other hand, in the samples prepared under light irradiation, the superconducting phase forms already at about 825 °C and increases linearly with increasing temperature. Obtained results show that the solid-state reaction rate

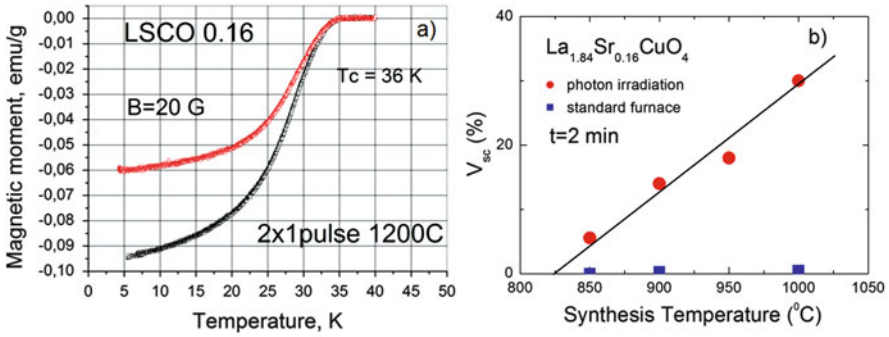

Fig. 25.5 (**a**) Temperature dependence of the zero-field-cooled (ZFC) and field-cooled (FC) magnetic moment for the $La_{1.84}Sr_{0.16}CuO_4$ sample in a magnetic field of 20 Oe. The sample was synthesized by light irradiation at $T = 1200$ °C (total irradiation time: 40 s). (**b**) Superconducting volume fraction of $La_{1.84}Sr_{0.16}CuO_4$ samples obtained by the photon irradiation and the conventional furnace-heating process at different synthesis temperatures. For all samples, the total synthesis time was 2 min. From [18]

in oxides is strongly enhanced under photon irradiation as compared with the usual heat treatment in a furnace at the same synthesis temperature. We call this process photostimulated solid-state reaction (PSSR) [18].

Naturally question arises: what is the difference between a conventional furnace heating and lamp irradiation during the solid state reaction? According to the formula of black-body radiation, at temperatures around 900 °C, the photons emitted from a conventional furnace have wavelengths larger than 1 μm and energy below 1 eV. These infrared photons mainly contribute to sample heating. Tungsten halogen lamps with color temperature above 3000 K emit photons mostly in the near infrared and visible range with energies of 0.5–2 eV. So it seems that the sample irradiation with higher energy photons can accelerate solid state reaction. If this argument is correct, increasing photon energy should make PSSR even more effective. To test this idea we installed in photon irradiation setup UV lamp in addition to halogen lamps. Experiments with modified setup showed that indeed addition of UV irradiation leads to substantial acceleration of PSSR. What are the possible mechanisms for the PSSR process? It is known that the main limiting factor for the solid state reaction rate is diffusion of atoms. Light of sufficient energy and intensity can produce several important effects which might influence the diffusion of atoms, such as creation of electron-hole pairs and change of charge state of atoms. For example, it is known that the recombination of electrons and holes in a semiconductor or insulator can release energy. This energy release can enhance defect diffusion in a semiconductor [19]. Another possible mechanism is the change of the charge state of atoms which can influence diffusion [20]. Perhaps there are also other light induced nonthermal effects which can play the role in the PSSR. Further experimental and theoretical studies are necessary for better understanding of this process.

Fig. 25.6 April 27, 2014 at the International Conference on Superconductivity and Magnetism in Antalya, Turkey. Alexander Shengelaya and Alex Müller enjoy cake and discuss during the coffee break. This cake was just presented to Alex at the conference to celebrate his 87th birthday

Subsequent experiments showed that the PSSR method works equally well for the synthesis of a broad class of oxides, such as CMR manganites, $BiFeO_3$, $CuCrO_2$ and $SrTiO_3$. Since the light penetration is limited by the sample thickness, it is expected that the PSSR method will be even more effective in the preparation of oxide thin films, which have a high technological importance. Our recent experiments showed that good quality epitaxial YBCO thin films can be obtained on $SrTiO_3$ by combined irradiation of halogen and UV lamps. The metallorganic solution of starting precursors was deposited on $SrTiO_3$ by spin coating and the whole process of thin film synthesis including pyrolysis and main reaction took only 30 min at 700 °C. In Tbilisi in collaboration with Alex Müller we continue to further develop the PSSR method and apply it to a broad class of complex oxides (Fig. 25.6).

Acknowledgments In this article I tried to show how important was the discovery of high temperature superconductivity for the beginning of my research carrier, how fortunate and privileged I was to meet subsequently Alex Müller and to collaborate with him over many years. This collaboration still continues and we hope will lead to new interesting results. For me Alex is my mentor not only in science, but also in life. I am happy and proud to be among the friends and collaborators of Alex. Together with my family and colleagues in Georgia we celebrate his 90th birthday and send him our best wishes.

References

1. N.M. Suleimanov, H. Drulis, G. Chadzynski, A. Shengelaya, E.F. Kukovitskii, R.G. Mustafin, J. Janchak, JETP Lett. **51**, 422 (1990)
2. A. Shengelaya, H. Drulis, J. Klamut, A. Zygmunt, N.M. Suleimanov, Physica C **226**, 147 (1994)
3. A. Shengelaya, J. Oleyniczak, H. Drulis, N.M. Suleimanov, Solid State Commun. **99**, 779 (1996)
4. J. Oleyniczak, A. Zaleski, A. Shengelaya, J. Klamut, Phys. Rev. B **51**, 8641 (1995)
5. A. Shengelaya, G.-m. Zhao, H. Keller, K.A. Müller, Phys. Rev. Lett. **77**, 5296 (1996)
6. J.G. Bednorz, K. A. Müller. https://www.nobelprize.org/nobel_prizes/physics/laureates/1987/bednorz-muller-lecture.pdf
7. A. Shengelaya, G.-m. Zhao, H. Keller, K.A. Müller, B.I. Kochelaev, Phys. Rev. B **61**, 5888 (2000)
8. A. Shengelaya, M. Bruun, B.I. Kochelaev, A. Safina, K. Conder, K.A. Müller, Phys. Rev. Lett. **93**, 017001 (2004)
9. K.A. Müller, J. Supercond. Nov. Magn. **27**, 2163 (2014)
10. P. Cai, W. Ruan, Y. Peng, C. Ye, X. Li, Z. Hao, X. Zhou, D.H. Lee, Y. Wang, Nat. Phys. **12**, 1047 (2016)
11. A. Shengelaya, K.A. Müller, Europhys. Lett. **109**, 27001 (2015)
12. D. Mihailovic, V.V. Kabanov, K.A. Müller, Europhys. Lett. **57**, 254 (2002)
13. L.V. Keldysh, Pis'ma Zh. Eksp, Teor. Fiz. **29**, 716 (1979) [JETP Lett. **29**, 658 (1979)].
14. A. Shengelaya, K.A. Müller, J. Supercond. Nov. Magn. **26**, 491 (2013)
15. K.A. Müller, H. Burkard, Phys. Rev. B **19**, 3593 (1979)
16. R. Kind, K.A. Müller, Comm. Phys. **1**, 223 (1976)
17. Q.-Y. Wang, Z. Li, W.-H. Zhang, Z.-C. Zhang, J.-S. Zhang, W. Li, H. Ding, Y.-B. Ou, P. Deng, K. Chang, J. Wen, C.-L. Song, K. He, J.-F. Jia, S.-H. Ji, Y.-Y. Wang, L.-L. Wang, X. Chen, X.-C. Ma, Q.-K. Xue, Chin. Phys. Lett. **29**, 037402 (2012)
18. D. Daraselia, D. Japaridze, Z. Jibuti, A. Shengelaya, K.A. Müller, J. Supercond. Nov. Magn. **26**, 2987 (2013)
19. D.V. Lang, Ann. Rev. Mater. Sci. **12**, 377 (1982)
20. A.M. Stoneham, Rep. Prog. Phys. **44**, 1251 (1981)

Chapter 26
Oxygen Isotope Effect Resulting from Polaron-Induced Superconductivity in Cuprates

Stephen Weyeneth

Copper oxides are the only compounds that show superconductivity at T_c above the boiling point of nitrogen. When not doped, these materials are antiferromagnetic insulators due to the strong correlation splitting of the $d_{x^2-y^2}$-type band into an upper empty and a lower occupied Mott–Hubbard band. When the latter is doped and holes are present, very high T_c's are found. A two-decade-long controversy resulted from the question as to whether the superconducting phenomenon still results from the electronic correlations present or whether lattice dynamics play a role. In favor of the latter, Kresin and Wolf wrote a colloquium [1] in which they review couplings from an extended lattice to phonons, plasmons, exitons and polarons, both theoretically and experimentally. For the case of polarons, i.e., a local vibronic lattice deformation, they quote a formula for the oxygen isotope coefficient $\alpha(n)$, originally derived by them [1, 2] in 1994 for lattice distortions along the c-direction:

$$\alpha(n, T_c) = \gamma(n) \frac{n}{T_c(n)} \frac{\partial T_c(n)}{\partial n}. \tag{26.1}$$

Here n denotes the superconducting carrier density. The parameter $\gamma(n)$ entering Eq. (26.1) depends only weakly on n.

Equation (26.1) resembles the formula proposed earlier by Schneider and Keller, derived by analysing the universal properties of cuprates [3, 4]. Already there, an important ingredient for mapping the experimentally obtained $\alpha(n)$ was the detailed $T_c(n)$ dependence. In the original report by Kresin and Wolf [2], the applicability of the model is discussed on the basis of the early data for $\alpha(n)$. The result of their fitting of Eq. (26.1) to the data yielded $\gamma = 0.13$. However, it is not really discussed

S. Weyeneth (✉)
Physik-Institut der Universität Zürich, Winterthuerstrasse 190, 8057 Zürich, Switzerland
e-mail: wstephen@physik.uzh.ch

A. Bussmann-Holder et al. (eds.), *High-Tc Copper Oxide Superconductors and Related Novel Materials*, Springer Series in Materials Science 255,
DOI 10.1007/978-3-319-52675-1_26

how and in which manner the gradient of $T_c(n)$ is incorporated into Eq. (26.1) during fitting.

Alex Müller and me used to discuss occasionally about scientific articles being published shortly after the discovery of superconductivity in cuprates [5]. At some afternoon, he mentioned the above work of Kresin and Wolf [1, 2] and raised the idea of using Eq. (26.1) with more recent data in order to investigate weather also lattice distortions in the ab-plane follow the same trend. This idea was the starting point of the here revisited work which we published some years ago [6].

Experimentally, it was observed by Zech et al. [7] that site-selective oxygen substitution $^{16}O \rightarrow {}^{18}O$ in optimally doped $YBa_2Cu_3O_7$ (YBCO) results in more than 80% of the oxygen isotope effects being due to the planar oxygen. This is because the hole density present was shown to reside mainly in the planar CuO_2 [8]. Accordingly, the carrier density is mainly planar $n_{//}$. Note that for the perpendicular direction $n_\perp = 0$ and therefore also $\alpha_\perp = 0$. Various groups [9–12] carefully studied $\alpha_{//}(n)$ for YBCO and doped $La_{1.85}Sr_{0.15}CuO_4$ (LSCO) as shown in Fig. 26.1, taken from [13]. In it, $\alpha_{//}(n)$ is compared with the results of a vibronic theory. The latter comprises two electronic bands present in the cuprates, a lower *t–J*-type *d*-band and a nearby, higher-lying *s*-band coupled by a linear vibronic term [8, 13, 14]. Within this model, the oxygen isotope effects on T_c result from considering in-plane bands with first t_1, second t_2, third neighbor t_3, and interplanar hopping integrals t_4 [8, 13]. The polaronic renormalizations of the second-nearest-neighbor hopping integral t_2 and the interplanar hopping term t_4 yield the correct trend for $\alpha_{//}(n)$ close to optimal doping. From Fig. 26.1 it can be seen that the agreement is

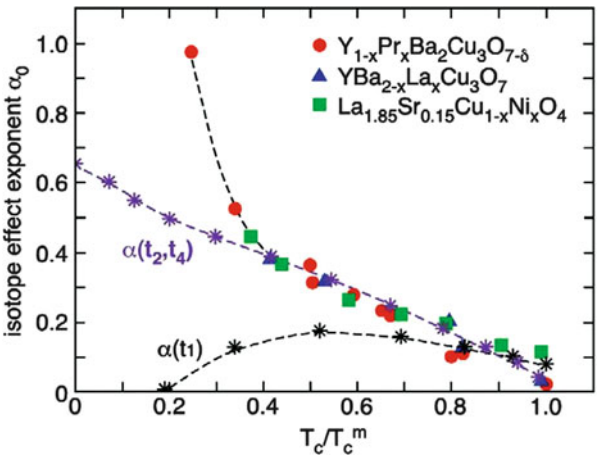

Fig. 26.1 The oxygen isotope effect exponent α as a function of $T_c/T_{c,max}$. The *black stars* refer to the calculated α when only the nearest-neighbor hopping integral (t_1) is renormalized. The *purple stars* are theoretically derived, with both the second-nearest-neighbor and the interplanar hopping integrals (t_2, t_4) renormalized. *Red, blue* and *green* data are experimental values for α for $Y_{1-x}Pr_xBa_2Cu_3O_{7-\delta}$ [9, 10], $YBa_{2-x}La_xCu_3O_{7-\delta}$ [11], and $La_{1.85}Sr_{0.15}Cu_{1-x}Ni_xO_4$ [12], respectively. The figure is taken from [13] (Color online)

rather good at and below optimal doping, but clearly deviates for very low doping. Being based on a mean-field theory, this may be expected because at very low doping individual polarons exist. A result of that theory is that the local coupling mode is of Jahn–Teller-type t_2/t_4 motion. From this we may infer that for a polaronic scenario the formal $\alpha(n)$ [see Eq. (26.1)] may also be valid for the planar polarons. Thus we identify in Eq. (26.1) $n = n_{//}$ and $\alpha(n) = \alpha_{//}(n)$, as described in the next paragraph.

The dependence of $T_c(n)$ can be approximately parameterized according to early work [14–17] as

$$\frac{T_c(n)}{T_{c,\max}} = 1 - A\left(\frac{n}{n_{\max}} - 1\right)^2 \tag{26.2}$$

$T_{c,\max}(n)$ denotes the maximum transition temperature of a given family, $n_{\max}$ the corresponding carrier density, and A an empirical constant found to be ≈2–3 [14–17]. In the inset of Fig. 26.2 the dependence in Eq. (26.1) is presented. Combining Eqs. (26.1) and (26.2), we obtain for the generic formula of $\alpha_{//}(n)$ in terms of $z = n/n_{\max}$ and $t = T_c/T_{c,\max}$:

$$\alpha_{||}(z) = 2\gamma(n)\frac{z(z-1)}{(z-1)^2 - A^{-1}} \tag{26.3}$$

and within the underdoped region:

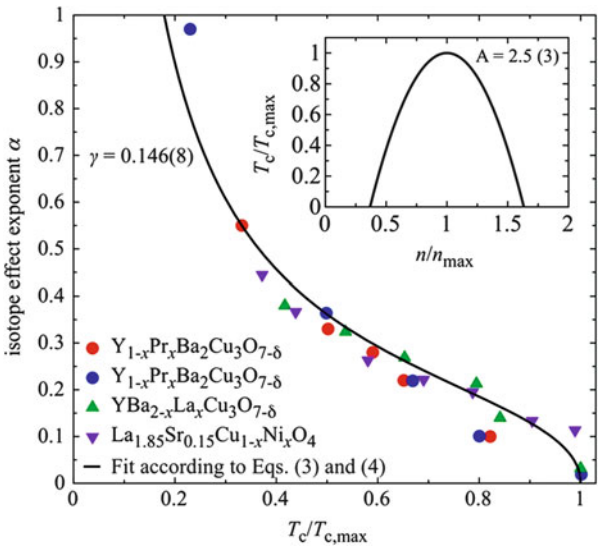

Fig. 26.2 The same data for α as in Fig. 26.1 as a function of $T_c/T_{c,\max}$ for $Y_{1-x}Pr_xBa_2Cu_3O_{7-\delta}$ [9, 10], $Y_{1-x}Pr_xBa_2Cu_3O_{7-\delta}$ [11], and $La_{1.85}Sr_{0.15}Cu_{1-x}Ni_xO_4$ [12]. Clearly, Eq. (26.3) describes the universal dependence of α rather well. We can derive a value of $\gamma = 0.146(8)$ from the fit. The inset shows the doping-dependent T_c according to Eqs. (26.3) and (26.4) using the fitted $A = 2.5(3)$. The figure is taken from [6] (Color online)

$$z = 1 - \sqrt{\frac{1-t}{A}} \tag{26.4}$$

This result can be compared with experimental data for $\alpha_{//}(n)$ from the literature. In Fig. 26.2, we depict data for $\alpha_{//}(n)$ as a function of $T_c/T_{c,max}$ for $Y_{1-x}Pr_xBa_2Cu_3O_{7-\delta}$ [9, 10], for $YBa_{2-x}La_xCu_3O_{7-\delta}$ [11], and for $La_{1.85}Sr_{0.15}Cu_{1-x}Ni_xO_4$ [12]. Clearly, Eq. (26.3) describes the universal dependence of the measured $\alpha_{//}(n)$ rather well, assuming $\gamma_{//}(n)$ to be constant. By fitting Eqs. (26.3) and (26.4) to the data, we derive a value of $A = 2.5(3)$, in good agreement with literature values [14–17], and $\gamma = 0.146(8)$, slightly larger than the value of $\gamma = 0.13$ reported in [2] based on early results for $\alpha(n)$. Globally, this calculation is similar to those previously discussed in [2, 3].

The agreement between the measured oxygen isotope effect $\alpha_{//}(n)$ as a function of doping n and the curve calculated with Eqs. (26.3) and (26.4), but with a constant parameter γ, is really remarkable. From optimal doping n_{max} down to near-vanishing superconductivity, where the measured $\alpha_{//}(n)$ exhibits a characteristic upturn, the data follow the curve obtained with Eq. (26.1) very well. This allows the conclusion that this simple expression is more generally valid than only for polarons axed along the crystallographic c-direction, for which it was originally obtained [1, 2]. It quantitatively yields the correct behavior *for polarons sited in the CuO_2 plane*. Now the vibronic theory of Bussmann-Holder and Keller [8, 13] reproduces $\alpha_{//}(n)$ quite well near optimum doping, see Fig. 26.1. In their work, the authors deduced that the *local* polaronic lattice deformation is of t_2/t_4, i.e., Jahn–Teller type. From this fact, we may assume that this is also the case in the entire range shown in Fig. 26.2. In other words, the effect of doping-dependent oxygen isotope and the theories shown in Figs. 26.1 and 26.2 are evidence of the planar polaronic origin of the high-temperature superconductivity.

The above conclusion agrees with the ones reached in the viewpoint published by Müller [18] some years ago. In this viewpoint, the possibility for superconductivity to be due to magnetic interactions was also addressed. At that time, no electronic theories were known to yield finite T_c's. Furthermore, experiments were discussed which indicated that magnetic interactions could not be responsible for the high-temperature superconductivity. However, the group of Keimer at the MPI in Stuttgart and others investigated the antiferromagnetic (AFM) peaks near the M-point of the Brillouin zone with inelastic neutron scattering [19] for a number of compounds. These peaks are very weak, and the group was able to enhance the signal by first exciting electrons from the $2p$ level of oxygen with x-rays. The signal obtained in this way quantitatively follows the temperature-dependent superconducting gap. From this, a magnetic mechanism was deduced by assuming an intrinsic homogeneous state of the material. However, as is has been pointed out recently [18] and also earlier [20] this seems not to be the case. For example, X-ray [21] and early Tm NMR [22] investigations yielded near-insulating AFM regions and metallic-like regions forming clusters. Close to a superconducting cluster or stripe, weak AFM signals exist at the border, owing to the continuous electronic

part of the wavefunction [23]. Indeed, weak spin ordering has been detected by nuclear quadrupole resonance [24]. It is thus possible that this weak AFM signal is coherent by interaction with the coherent superconducting part, and is responsible for the AFM signal.

The largest oxygen isotope effect at T_c shown in Fig. 26.1, occurring at low doping, is about $\alpha = 1.0$, i.e., much lower than those observed at the pseudogap temperature T^* reported for LSCO [25] and $HoBa_2Cu_4O_8$ [26]. For the latter, $\alpha^* = -2.2$. It is sign-inverted, as expected from Eq. (26.1), which also applies to the pseudogap isotope effect [2]. With the nearly linear $T^*(n)$, we arrive at $\gamma^* = 1.7$ from these data. The existence of an even greater α^* for copper in YBCO in terms of local lattice conformations [26] has been commented on in [8, 18]. In the latter paper, the occurrence of T^* has been assigned to the formation of intersite Jahn–Teller bipolarons [18]. Very recently, the oxygen isotope effects in the LSCO system were studied by means of Cu K-edge XANES, giving another evidence for an enormous involvement of the lattice in the formation of the pseudogap, consistent with a polaronic approach to cuprate superconductivity [28].

The isotope effect with $\alpha = 0.5$ in the classical superconductors was substantial for the acceptance of the BCS theory. The carrier-dependent $\alpha_{//}(n)$ at $T_c(n)$ quantitatively follows the Kresin–Wolf formula [Eq. (26.1)] derived for polarons along the c-direction over the entire doping range [see Fig. 26.2]. We regard this as a strong clue that, for the materials shown, superconductivity is induced by polarons, or rather bipolarons, with spin $S = 0$, but that they occur *in* the CuO_2 plane [18]. The latter follows from the agreement of the calculated planar isotope effects at $T_c(n)$ with the vibronic theory near optimum doping, see Fig. 26.1. Comparing the observed isotope effects with the vibronic theory indicates that the *local polaronic conformations* are of the t_2/t_4 Jahn–Teller type. This theory also yields the large inverted oxygen isotope effect of $\alpha^* = -2.2$ observed at the pseudogap temperature T^* and other behaviors [13]. Furthermore, already at very low doping, intersite Jahn–Teller bipolarons are formed, which cluster in probably ramified, conducting entities, such as stripes [27].

With this, I would like to that Alex Müller for various fruitful discussion and for the perpetual support at the Physics Institute of the University of Zurich. I experienced a pleasant and highly salutary time in Zurich and enjoyed our innumerable colloquies concerning physics and others.

References

1. V.Z. Kresin, S.A. Wolf, Rev. Mod. Phys. **81**, 481 (2009)
2. V.Z. Kresin, S.A. Wolf, Phys. Rev. B **49**, 3652(R) (1994)
3. T. Schneider, H. Keller, Phys. Rev. Lett. **69**, 3374 (1992)
4. T. Schneider, H. Keller, Phys. Rev. Lett. **86**, 4899 (2001)
5. J.G. Bednorz, K.A. Müller, Z. Phys B Condens. Matter **64**, 189 (1986)
6. S. Weyeneth, K.A. Müller, J. Supercond. Nov. Magn. **24**, 1235 (2011)

7. D. Zech, H. Keller, K. Conder, E. Kaldis, E. Liarokapis, N. Poulakis, K.A. Müller, Nature (London) **371**, 681 (1994)
8. A. Bussmann-Holder, H. Keller, Eur. Phys. J. B **44**, 487 (2005)
9. J.P. Franck, J. Jung, M.A.-K. Mohamed, S. Gygax, G.I. Sproule, Phys. Rev. B **44**, 5318 (1991)
10. R. Khasanov, A. Shengelaya, E. Morenzoni, K. Conder, I.M. Savic, H. Keller, J. Phys. Condens. Matter **16**, S4439 (2004)
11. H.J. Bornemann, D.E. Morris, Phys. Rev. B **44**, 5322 (1991)
12. N. Babushkina, A. Inyushkin, V. Ozhogin, A. Taldenkov, I. Kobrin, T. Vorobeva, L. Molchanova, L. Damyanets, T. Uvarova, A. Kuzakov, Physica C **185**, 901 (1991)
13. H. Keller, A. Bussmann-Holder, K.A. Müller, Mater. Today **11**(9), 38 (2008)
14. A. Bussmann-Holder, H. Keller, A.R. Bishop, A. Simon, R. Micnas, K.A. Müller, Europhys. Lett. **72**, 423 (2005)
15. M.R. Presland, J.L. Tallon, R.G. Buckley, R.S. Liu, N.E. Flower, Physica C **176**, 95 (1991)
16. J.L. Tallon, C. Bernhard, H. Shaked, R.L. Hitlerman, J.D. Jorgenen, Phys. Rev. B **51**, 12911 (R) (1995)
17. T. Schneider, in *The Physics of Superconductors*, ed. by K. Bennemann, J. B. Ketterson. (Springer, Berlin, 2004)
18. K.A. Müller, J. Phys. Condens. Matter **19**, 251002 (2007)
19. H. He, P. Bourges, Y. Sidis, C. Ulrich, L.P. Regnault, S. Paihes, N.S. Berzigiarova, N.N. Kolesnikov, B. Keimer, Science **295**, 1045 (2002)
20. D. Mihailovic, K.A. Müller, in *High-T_c Superconductivity 1996: Ten Years after the Discovery, NATO ASI Ser. E*, ed. by E. Kaldis, E. Liarokapis, K. A. Müller, vol 343 (Kluwer, Dordrecht, 1997), p. 243
21. A. Bianconi, N.L. Saini, A. Lanzara, M. Missori, T. Rosetti, H. Oyanagi, H. Yamaguchi, K. Oka, T. Ito, Phys. Rev. Lett. **76**, 3412 (1996)
22. M.A. Teplov et al., in *High-T_c Superconductivity 1996: Ten Years after the Discovery, NATO ASI. Ser. E*, ed. by E. Kaldis, E. Liarokapis, K. A. Müller, vol 343 (Kluwer, Dordrecht, 1997)
23. I. Martin, E. Kaneshita, A.R. Bishop, R.J. McQueeney, Z.G. Yu, Phys. Rev. B **70**, 224514 (2004)
24. F. Raffa, T. Ohno, M. Mali, J. Roos, D. Brinkmann, K. Conder, M. Eremin, Phys. Rev. Lett. **81**, 5912 (1998)
25. A. Lanzara, G.M. Zhao, N.L. Saini, A. Bianconi, K. Conder, H. Keller, K.A. Müller, J. Phys. Condens. Matter **11**, L541 (1999)
26. A. Furrer, in *Superconductivity in Complex Systems, Structure and Bonding Series*, ed. by K. A. Müller, A. Bussmann-Holder, vol 114 (Springer, Berlin, 2005), p. 171
27. A. Shengelaya, M. Brnun, B.J. Kochelaev, A. Safina, K. Conder, K.A. Müller, Phys. Rev. Lett. **93**, 017001 (2004)
28. M. Bendele, F. von Rohr, Z. Guguchia, E. Pomjakushina, K. Conder, A. Bianconi, A. Simon, A. Bussmann-Holder, H. Keller, Phys. Rev. B **95**, 014514 (2017)